CR-151487

REPORT NO. CASD-NSC-77-003
CONTRACT NAS9-14095

(NASA-CR-151487) SPACE SHUTTLE ORBITER REAR MOUNTED REACTION CONTROL SYSTEM JET INTERACTION STUDY Final Report (General Dynamics/Convair) 451 p HC A20/MF A01 CSCL 22B G3/16

N77-29207

Unclas
40821

SPACE SHUTTLE ORBITER REAR MOUNTED REACTION CONTROL SYSTEM JET INTERACTION STUDY

FINAL REPORT

AUG 1977
RECEIVED
NASA STI FACILITY
INPUT BRANCH

GENERAL DYNAMICS
Convair Division

REPORT NO. CASD-NSC-77-003

SPACE SHUTTLE ORBITER REAR MOUNTED REACTION CONTROL SYSTEM JET INTERACTION STUDY

FINAL REPORT

May 1977

J.R. Rausch

Prepared Under
Contract NAS9-14095

Prepared by
GENERAL DYNAMICS CONVAIR DIVISION
P.O. Box 80847
San Diego, California 92138

FOREWORD

The present study was undertaken by the Convair Division of General Dynamics under NASA contract NAS9-14095 and this report covers work undertaken from 15 June 1975 through 1 May 1977. The contract monitor was Mr. Barney Roberts of the NASA Johnson Space Center, Houston, Texas and the author wishes to acknowledge his very valuable assistance, direction and contributions to the successful completion of the study. The test data was obtained from models designed, built and tested by Rockwell International personnel at NASA Langley Research Center and at Arnold Engineering Development Center. We wish to express our appreciation to H. Dresser, J. Daileda, and J. Marroquin of Rockwell for their help and cooperation in providing test data and reports which greatly assisted in the completion of this study.

TABLE OF CONTENTS

TABLE OF CONTENTS (Continued) Page

TABLE OF CONTENTS (Continued)

LIST OF FIGURES

LIST OF FIGURES (Continued)

LIST OF FIGURES (Continued)

LIST OF FIGURES (Continued)

LIST OF FIGURES (Continued)

LIST OF TABLES

LIST OF TABLES (continued)

LIST OF TABLES (Continued)

NOMENCLATURE

Symbol	Definition
A	area (ft^2)
b	lateral-directional reference length (ft)
$\bar{c}$	wing chord reference length (ft)
C_ℓ	body axis rolling moment coefficient = (rolling moment)/q S_{ref} b
C_m	body axis pitching moment coefficient = (pitching moment)/q s_{ref} $\bar{c}$
C_N	body axis normal force coefficient = (normal force)/q S_{ref}
C_n	body axis yaw moment coefficient = (yawing moment)/q S_{ref} b
C_P	pressure coefficient = $(P - P_\infty)/q$
C_t	thrust coefficient = T/q S_{ref}
C_y	body axis side force coefficient = (side force)/q S_{ref}
C_D	nozzle discharge coefficient = measured thrust/ideal thrust
d	diameter (ft)
h	kinetic energy parameter (ft^2/sec^2)
K	force or moment amplification factor
ℓ_{ref}	longitudinal reference length (ft)
ℓ_B	body length (ft)
$\dot{m}$	mass flow (lbm/sec)
M	Mach number
n	number of jets in cluster
P	pressure (lbf/ft^2)
q	dynamic pressure (lbf/ft^2)
R	gas constant (ft^2/sec^2-°R)
r	radius (ft)
R_e	Reynolds number
S_{ref}	wing reference area (ft^2)
t	time (sec)

NOMENCLATURE (cont'd)

Symbol	Definition
T	thrust (lb)
T	temperature (°R)
V	velocity (ft/sec)
x	radial distance (ft)
α	angle of attack (deg)
β	angle of yaw (deg); also $\sqrt{M^2 - 1}$
θ_N	nozzle angle (deg)
θ	angular orientation in jet (deg)
ρ	density (lbm/ft^3)
γ	ratio of specific heat
Φ	momentum parameter (lbf) = $\gamma P M^2 A$

Subscripts

amb	ambient conditions
c	rocket chamber condition
i	initial condition or conditions at point i
j	jet exit conditions
ℓ	local condition or rolling moment
MAC	mean aerodynamic chord
M	any force or moment coefficient
m	pitching moment
n	yawing moment
N	normal force
o	total conditions
y	side force
p	peak
∞	free stream condition
interaction	increment due to plume interaction

NOMENCLATURE (cont'd)

Symbol	Definition
Subscripts (cont'd)	
impingement	increment due to plume impingement
cross coupling	increment due to combined jets interacting
thrust	thrust terms
total	sum of all terms
Superscripts	
-	mean value or averaged value
*	throat condition

SUMMARY

This report is the final technical report and documents the work performed through 1 May 1977 under NASA Contract NAS9-14095.

The space shuttle orbiter has forward mounted and rear mounted Reaction Control Systems (RCS) which are used for orbital maneuvering and also provide control during entry and abort maneuvers in the atmosphere. RCS control effectiveness is critical to orbiter flight performance and safety. The effect of interaction between the RCS jets and the flow over the vehicle in the atmosphere is the subject of this study. This report presents the analysis of test data obtained in the NASA Langley Research Center 31 inch continuous flow hypersonic tunnel at a nominal Mach number of 10.3 and the AEDC continous flow hypersonic tunnel "B" at a nominal Mach number of 6. The data was obtained with 0.01 and .0125 scale force models with aft RCS nozzles mounted both on the model and on the sting of the force model balance. The plume simulations were accomplished primarily using air in a cold gas simulation through scaled nozzles, however, various cold gas mixtures of Helium and Argon were also tested to obtain RT ratio effects. The major test parameters included: number of nozzles, tests of combined RCS controls, aerodynamic control deflections, nozzle geometry, and RCS plenum pressure.

The data shows that RCS nozzle exit momentum ratio is the primary correlating parameter for effects where the plume impinges on an adjacent surface and mass flow ratio is the parameter when the plume interaction is primarily with the external stream. An analytic model of aft mounted RCS units was developed in which the total reaction control moments are the sum of thrust, impingement, interaction, and cross-coupling terms.

1

INTRODUCTION

The space shuttle orbiter has two reaction controls systems (RCS), as shown in Figure 1-1, which are used for orbital maneuvering. The rear RCS provides control during entry until the aerodynamic surfaces have sufficient effectiveness to assume full control of the vehicle as shown in Figure 1-2. Both the front and rear RCS units are also used during abort maneuvers to separate the orbiter from the tank, to pitch it to entry attitude, and to control it until aerodynamic control is established. Thus RCS control effectiveness is critical to the space shuttle orbiter flight performance and safety.

The studies performed in References 1 to 3 and wind tunnel data on the present baseline orbiter have shown that the control effectiveness of the RCS system is appreciably changed by the presence of air flow over and around the vehicle. These RCS - flow interactions have acted in directions such that the net RCS system effectiveness is much lower than the thrust moments alone and it is critical to flight safety and performance to know what the induced RCS - flow interaction moments are caused by and to develop methods to predict them. These are the basic purposes of this study conducted under NASA contract NAS9-14095. This report is the final report of the work performed on this contract through April 1977 and documents the data analysis and analytic model development for RCS flow interference prediction. The data used for these analyses came principally from the space shuttle orbiter tests designated OA82 which was documented in Reference 2 of this contract, Test MA22 documented in Reference 4, and test OA169 documented in Reference 5. These data were obtained from tests conducted by Rockwell International personnel within NASA and AEDC test facilities, primarily the NASA-LRC 31 inch continuous flow hypersonic tunnel (CFHT) at a nominal Mach number of 10.3 and AEDC von Karman Facility tunnel "B" at Mach number of 6.0. The data was obtained at Langley with a 0.010 scale force model with the RCS nozzles mounted on the sting of the force model balance and with a .0125 scale model at AEDC where the RCS nozzles were mounted on the model as well as on the sting. The plume simulations were accomplished primarily using air in a cold gas simulation through scaled nozzles, however, various cold gas mixtures of Helium and Argon were also tested to obtain (RT) ratio effects.

This report will concentrate primarily on the data analyses and analytic model development and contains 6 parts:

a) Test Data Summary
b) Data Analysis
c) Analytic Model Development
d) Analytic Program Description
e) Full Scale Error Analysis
f) Study Conclusions

The data presented in this report is data for the aft RCS unit only.

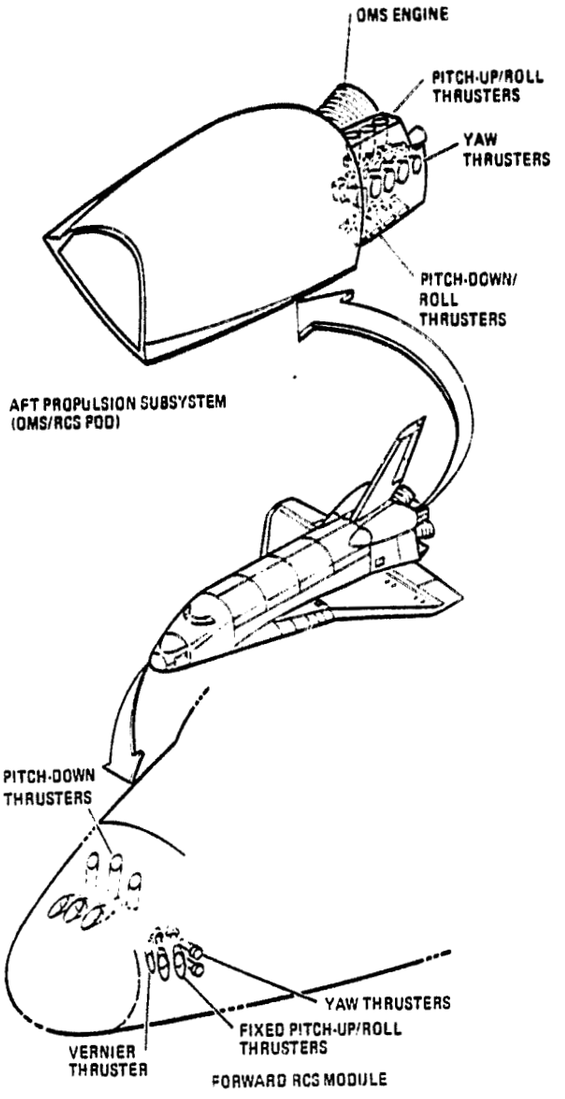

Figure 1-1. Reaction Control Subsystem Elements.

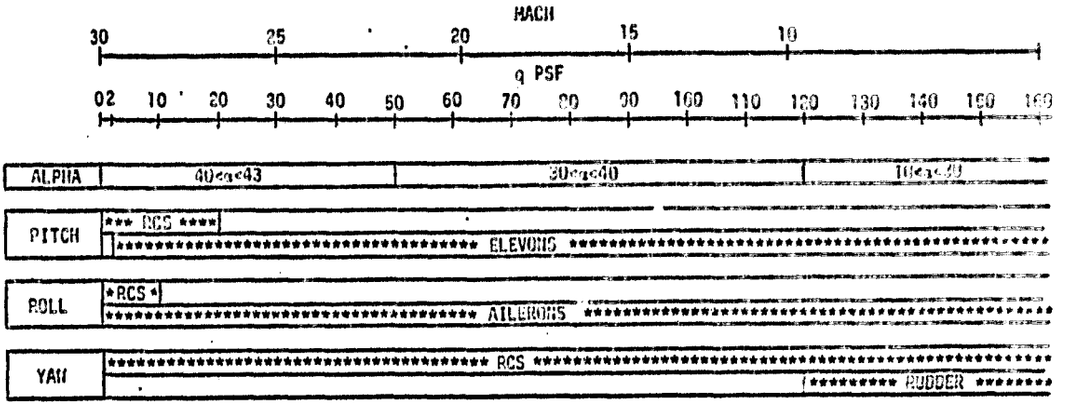

RCS AND CONTROL SURFACE UTILIZATION FOR NOMINAL ENTRY

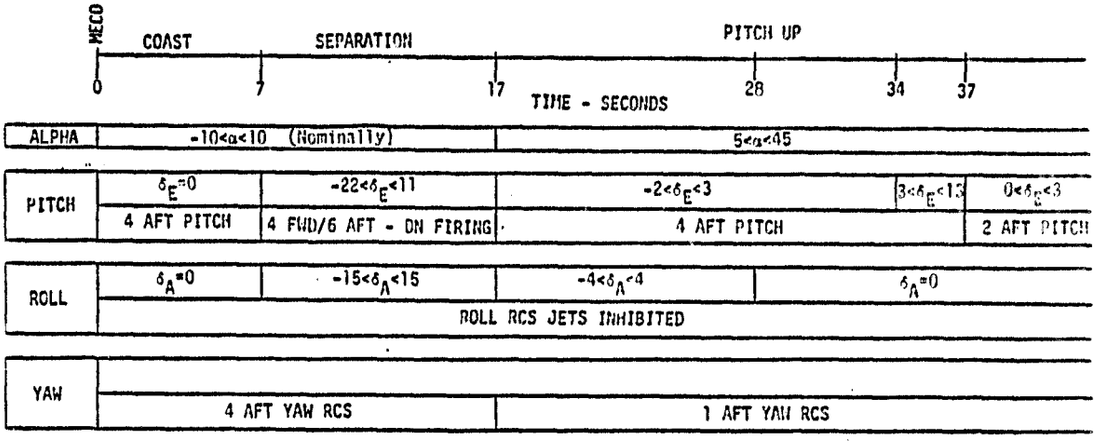

MACH RANGE: 6-8
DYNAMIC PRESSURE RANGE: 2-10 PSF
FORWARD AND AFT JETS

RCS UTILIZATION AND CONTROL SURFACE DEFLECTION FOR RTLS

Figure 1-2. RCS Operational Schedules.

2

TEST SUMMARY

2.1 REAR MOUNTED RCS DATA BASE

Data from all rear mounted RCS tests was provided to Convair by NASA-JSC for compilation and analysis under this contract. This rear mounted RCS data base represents 13 tests as summarized in Table 2-1. The PRR configuration data was obtained by General Dynamics/Convair in the test program reported in Ref. 1 and all of the remaining test data has been obtained in tests conducted by Rockwell International as part of the space shuttle orbiter development and the data for each test has been or will be reported in the DATAMAN reporting system for the shuttle. The principal sources of data for this analysis were tests designated OA82, MA22, and OA169.

2.2 CONFIGURATION AND REFERENCE DIMENSIONS

Figure 2-1 presents the Space Shuttle Vehicle 102 Orbiter configuration used in these tests. The geometry of the model is defined in detail in Ref. 6 . The model was sting mounted in all tests in an arrangement similar to the AEDC VKF tunnel B installation shown in Figures 2-2 to 2-4. The presence of the sting and of the sting mounted nozzle block used in tests OA82 and MA22 (Figure 2-5) prevented full simulation of the vehicle base geometry during all rear RCS tests. However, as much as possible the major features were maintained. Possible effects of sting mounting were shown in Ref. 2, but no further data has been obtained to clarify this issue.

All orbiter data used in this report are referenced to an axial location of 65% of body length and a vertical water line 25 inches below the fuselage reference line shown in Figure 2-1. In full scale vehicle dimension:

a) Vehicle nose station 238
b) (X) Moment ref. center station 1076.7
c) (Z) Moment ref. center waterline 375.
d) (Y) Moment ref. center butt line 0.

All data used in the analysis were reduced to coefficient form using the orbiter wing area as the reference area, the wing mean aerodynamic chord ($\bar{c}$) as the longitudinal reference length, and the wing span (b) as the lateral-directional reference length. :

a) $S_{ref} = S_{wing} = 2690$ Ft.^{2} (249.9 meters^2)
b) $\bar{c} = 39.567$ Ft. (12.06 meters)
c) $b = 78.058$ Ft. (23.79 meters)

2.3 WIND TUNNEL MODELS

2.3.1 OA82/MA22 .01 Scale Model

The .01 scale model used in tests OA82 and MA22 was an aluminum model whose geometry is defined in Ref. 6. The model was attached to a force balance mounted on a sting up through the base of the model as shown in Figure 2-5. The plenum chamber and nozzle block assembly was also mounted on the sting close to the base of the model but not attached to it. Thus the force balance measured model forces and moments and the loads induced by RCS operation but not the RCS jet moments. Grounding strips were mounted in the gap between the plenum and the model to insure that the model did not ground on the nozzles during the tests.

This model was equipped with removable nozzle blocks which were changed to test RCS jets firing in different directions, to change numbers of nozzles, and to change RCS nozzle geometry. A number of different nozzles were used throughout the tests and Tables 2-2 to 2-4 present the nozzle code numbers and a brief summary of the nozzle characteristics. All nozzles were tested using cold gas supplies located external to the tunnel and piped in through a pressure regulation system which was used to control the pressure in the plenum chamber manually during a tunnel data run. The pressure in the plenum chamber was measured by a pressure tap in the chamber connected to a pressure transducer mounted externally to the tunnel in most tests. The test gas used was air for all tests except for 12 runs on test OA82 where helium and Argon mixtures were used to vary the gas constant (R) of the test gas.

The model was equipped with elevons and a body flap which were attached to the model by metal brackets which could be changed to other pre-bent sets to obtain elevator angles of +10 degrees and -30 degrees and body flap angles of +13.75 degrees and -14.25 degrees.

The effects of elevator angle and body flap angle were tested in test MA22.

2.3.2 OA169/IA22 .0125 Scale Model

A steel model of the space shuttle orbiter was constructed for these tests using the preliminary lines for vehicle configuration 102 as the baseline. This configuration is shown in Figure 2-1 and defined in detail in Ref. 6. The model contained an internal force balance and was sting mounted through the base region of the orbiter as shown in Figure 2-4. The orbiter main engine nozzles were partially simulated on the base of model as well as the most aft side firing nozzle and all vernier nozzles on the OMS pods as shown in Figure 2-4. An external tank model was also built and was used for mated orbiter/external tank tests in OA 169 and for tank separation tests in IA22.

The elevons were mounted to the orbiter model using pre-bent brackets so that elevon settings of 0, ±10, and ±15 degrees were tested. The body flap, rudder, and speed brake were set at 0 degrees during these tests. Two umbilical doors

were provided on the model as shown in Figure 2-6 , and some RCS data was obtained with these doors either partially open or full open.

Twenty-seven (27) RCS thrusters were simulated on this model. These include 9 in the nose and 9 in each of the two rear orbital maneuvering system (OMS) as sketched in Figure 1-1. When the flow-through balance was used, the RCS simulation airflow was ducted up the support sting and entered the model through the balance. The balance flow was then ducted to 3 plenums within the model; one in front to feed the forward RCS thrusters and one for each of the rear OMS pod assemblies. All nozzles within a pod shown in Figure 1-1 are connected to the plenum and can be operated in any combination. Nine (9) ports connect the individual nozzles to the plenum and are plugged when a given nozzle is not being used on a particular run. Individual nozzle geometry is fixed and the primary test variables are numbers of nozzles operating in a given direction, thrust direction, and combinations of nozzles. The nozzles are all metric (thrust measured in balance loads) when the flow-through balance was used. An alternate method allowed the rear RCS units to be fed by a non-metric supply fixture on the sting. When this arrangement was used, the rear RCS units were non-metric also. Nozzle definitions are given Tables 2-2 to 2-4 where nozzle numbers N95, N96, and N97 are used for the 1, 2, and 3 nozzle cases respectively.

2.4 TEST SUMMARIES

2.4.1 OA82 Test Program Summary

The aft RCS test designated OA82 was performed at the NASA Langley Research Center Continuous Flow Hypersonic Tunnel (CFHT) where it carried the test number CFHT113. The test was performed at a nominal Mach number of 10.3 using a .01 scale model of 139B orbiter to obtain 6 component force and moment data using a cold gas simulation of the RCS exhaust flow. The major test variables included:

a) tunnel dynamic pressure (q = 75, 100, 125, 150, 200 PSF)
b) RCS chamber pressure (P_{0j} = 0 to 700 PSIA)
c) test gas (air, He, Argon, .85 He. 15A, .90 He. 10A)
d) RCS control direction
e) number of RCS nozzles

I	Pitch down	1, 2, 3
II	Pitch up	1, 2, 3
III	Yaw	2, 4

All aerodynamic control surfaces were kept at zero degree deflection throughout the test. The angle of attack range tested varied from -10 degrees to +35 degrees.

2.4.2 MA22 Test Program Summary

The aft RCS test designated MA22 was performed at the NASA Langley Research Center Continuous Flow Hypersonic Tunnel (CFHT) where it carried the test number CFHT 118. This test used the same model and test conditions summarized above. The major test variables included:

a) Tunnel dynamic pressure (q = 125, 150 PSIA)
b) RCS chamber pressure (P_{oj} = 0 to 700 PSIA)
c) RCS control direction (pitch up, pitch down, yaw)
d) RCS nozzle geometry (Table 2-2 to 2-4)
e) Number of RCS nozzles
f) elevator angle (δ_e = +10°, 0°, -30°)
g) body flap angle (δ_{BF} = +13.5°, 0°, -14.25°)
h) Combined RCS control directions
i) Jet off repeat runs

Air was used as the test gas for all RCS exhaust simulations in this test.

2.4.3 OA169 Test Program Summary

The test designated OA169 was performed at the Arnold Engineering Development Center von Karman Facility Continuous Flow Hypersonic Tunnel B where it carried a facility test number V41B-D8A. The test used the .0125 scale model defined in Section 2.3 and was performed at a nominal Mach number of 6.0. The primary purpose of the test was to provide data for Shuttle "Return to Launch Site" abort separation maneuvers from the external tank. The test thus included data of the forward, aft, and combined forward and aft RCS units firing both with and without the external tank attached to the orbiter. The portion of the test of interest to this part of the RCS study are those runs of rear RCS only without the external tank. The principal test parameters for the rear RCS only runs were:

a) RCS Chamber Pressure (P_{oj} = 0 to 1150 psia)
b) RCS control direction (pitch down, pitch up, yaw)
c) Number of RCS nozzles
d) combined RCS control directions
e) umbilical door position

Data was taken from -10 degrees angle of attack to +45 degrees using one sting pre-bend to obtain data from -10° to +15 and another from 15° to 45°. Nominal test conditions were:

a) Mach number = 5.89
b) $T_{o\infty}$ = 850°R
c) q_∞ = 93.6 PSF
d) R_e = 1×10^6/ft.

2.5 DATA REDUCTION PROCEDURE

The test data from all tests was reduced by the wind-tunnel personnel into body axis force and moment coefficients (C_N, C_A, C_m, C_ℓ, C_n, C_Y) with the RCS thrust forces and moments removed. Thus, the test data obtained with the non-metric RCS jets was reduced directly from measured balance data since the RCS jet thrust was not included in the balance loads. These data included all of the data on tests OA82, MA22 and some runs of OA169. The OA169 data obtained with the flow-through balance had metric jets and these data were reduced at the wind tunnel by removing thrust effects using wind tunnel static calibrations of measured thrust effects.

The net result is that all data received from the wind tunnel represented the basic vehicle aerodynamic forces and moments plus any induced loads resulting either from RCS jet impingement or from changes to the vehicle flow caused by the RCS jet plumes. Therefore, the incremental induced effects are computed by removing the basic vehicle characteristics from the jet-on data:

$$\Delta C_{M_i} = C_{M_j} - C_{M_o} \tag{1}$$

where

ΔC_{M_i} = induced force or moment increment

C_{M_j} = measured force or moment coefficient with jet on

C_{M_o} = measured force or moment coefficient with jet off.

Because the incremental values can be very small and thus sensitive to data scatter, the mean values of the jet off coefficient data were used as the best estimates of the data in the previous analyses (Reference 3). However, because of the large number of samples of data to be compiled in this analysis, the approach taken was to allow all scatter to remain in the data and to use one reference jet-off run as the base from which jet-on differences were obtained. It turned out not to be possible to use one jet-off run because of the umbilical door configurations on OA169 and thus 3 jet-off runs were used as the reference jet-off conditions:

a) Tests OA82 and MA22 used MA22 run 5 as base
b) Test OA169 high angle of attack range data used OA169 run 20 as base
c) Test OA169 low angle of attack range data used OA169 run 337 as base.

Angle of attack differences between the jet-on data and the jet-off data were accounted for by passing a 3rd degree polynominal through the jet-off base data with the nearest mean value angle of attack data as the midpoint of the curve fit and the interpolation is made to the jet-on angle of attack. Interpolation of the base line jet-off data was used since this method results in the same base value

without regard to nozzle used, jet pressure, or possible jet-on angle of attack effects. Difference data was generated and analyzed for all 6 force and moment components.

During the data analysis the induced data increment was broken into an impingement component and a flow interaction component where the interaction component was obtained by

$$\Delta C_{M_{interaction}} = C_{M_j} - C_{M_o} - C_{M_{impingement}} \tag{2}$$

where

$\Delta C_{M_{interaction}}$ = induced force or moment resulting from RCS flow/flow field interactions

$C_{M_{impingement}}$ = predicted force or moment due to plume impingement

and where the plume impingement of the model nozzles was predicted using the model to be discussed in Section 4.

Nozzle thrust was computed using the calibration data on the model nozzles given in Tables 2-2 to 2-4 while the other nozzle flow parameters were computed using ideal nozzle equations.

The discharge coefficient was computed for each test nozzle as the ratio of the calibrated thrust to the theoretical thrust as defined in Equation 3:

$$C_D = \frac{K_T P_{o_j}}{A_T P_{o_j} \sqrt{\frac{2\gamma^2}{\gamma-1}\left(\frac{2}{\gamma+1}\right)^{\frac{\gamma+1}{\gamma-1}}\left(1-\left(\frac{P_N}{P_{o_j}}\right)^{\frac{\gamma-1}{\gamma}}\right)} + A_E (P_N - P_\infty)} \tag{3}$$

where

C_D = discharge coefficient

A_T = nozzle throat area

A_E = nozzle exit area

K_T = nozzle calibration coefficient = $\frac{T_{meas}}{P_{o_j}}$

γ = exhaust gas specific heat ratio

P_{o_j} = nozzle chamber pressure

R_N = static pressure at nozzle exit

P_∞ = ambient pressure

T_{meas} = measured thrust

and this discharge coefficient was used to define an effective total pressure when computing nozzle flow parameters and impingement components.

$$P_{o_j}' = C_D \, P_{o_j} \tag{4}$$

This effective nozzle total pressure assumes that the principal reason for the difference between a real nozzle and its theoritical performance is due to a loss in total pressure. This approach was taken when the data analyses showed that it was the best method of accounting for scatter between data from different nozzles not otherwise accounted for using nozzle simulation parameters.

2.6 SUMMARY OF TEST RESULTS

2.6.1 Pitch Down Jet Induced Data

The pitch down jet data was generated primarily with the nozzle set designated N_{49} whose principal characteristics are defined in Table 2-2. This nozzle was mounted on the left side of the model as were all the other pitch nozzles used in this test except for the tests of symmetric pitch down jets. The thrust moments thus would be nose down pitch (-) and right wing down roll (+) in the body axis data sign convention.

Figure 2-7 presents the effect of supply pressure for nozzle N_{49} for freestream dynamic pressure of 125 PSF. The nominal values of the RCS thrust moments are tabulated with the run symbols on each plot. These data show that the induced pitch and roll oppose the thrust moment and they are large compared to the control moment; therefore, the total control amplification factor will be low. The lowest pressure data on Figure 2-7 cluster very close together indicating a non-linearity in the induced effects and the data shows very little sensitivity or change with angle of attack. These data are typical of the pitch down jet incremental data shown in Reference 2. Symmetric down firing jet data was primarily obtained during the OA 169 test using nozzles N95, N96, and N97 of Table 2-2 with only one other case being obtained on test OA82. Symmetric firing of the pitch down jets results in an induced moment which is greater than twice the value for one side by a significant amount indicating plume/plume flow interaction in the base region of the model around the sting mount. These data indicate that a better representation of the base region is needed for the pitch down RCS simulation. The roll jet data of Reference 2, showed that the normal force and pitching moment effects are derived primarily from the pitch down jet, the side force and yawing moment are derived from the pitch up jet, and the induced roll increment as the sum of the single jet induced effects.

2.6.2 Pitch Up Jet Induced Data

The pitch-up RCS data was generated primarily with the nozzle designated as N_{52} whose principal characteristics are defined in Table 2-3. All pitch up nozzles were mounted on the right side of the model and the nozzle sets exhausted vertically upward past the vertical fin which is approximately 9 nozzle diameters laterally from the nozzle centerlines. Figure 2-8 presents typical data of the induced forces and moments resulting from RCS jets firing upward. The pitch axis data shows some jet interaction effects at negative angle of attack where the upper surface is completely exposed to the flow but very little at higher angles of attack. The trends are much clearer in the lateral-directional data which shows strong interactions at negative angles decreasing as the angle of attack increases to approximately 10 degrees. Above this angle the induced effects become relatively insensitive to angle of attack. This data could be interpreted to show that a jet interaction type of flow occurs as long as the free stream flow is attached to the fin and when this is no longer true the interaction is primarily plume impingement on the fin where the plume shape is modified by freestream flow over the vehicle.

2.6.3 Yaw Jet Induced Data

The yaw jet data obtained in test OA82 and MA22 were obtained primarily with the nozzle set designated N_{85} whose characteristics are defined in Table 2-4. All yaw nozzles were mounted on the left side of the model and exhausted perpendicular to the fuselage centerline in a plane parallel to the wing and approximately 13 nozzle diameters above it. Figure 2-9 presents yaw RCS data at two supply pressures and these data show little flow interaction at angles of attack below 5 degrees except in yaw where there appears to be some amplification of the thrust moment due to jet interaction. At higher angles of attack, pitch up and left wing down moments are induced by the yaw jet but the effect appears to be non-linear in that the initial thrust created a larger change in moments than that caused by increasing thrust.

2.6.4 Combined Control Data

Combined control data was obtained during these tests for the following control combinations:

a) Symmetric Pitch down (left and right down firing)
b) Symmetric Pitch up (left and right up firing)
c) Symmetric roll (left down and right up)
d) Pitch up plus yaw (right up and right side yaw)
e) Pitch down plus yaw (right down plus left side yaw)

The combined control data was obtained in limited amounts only and was correlated against the sum of the individual control components to determine if there was any plume-plume interactions to be considered.

TABLE 2-1
RCS TESTS

Test Number	Test Type	Model	Scale	Facility	Data Received	Other
-	Force + Heat Transfer	PRR	.015	UPWT	Tape	Original PRR Data
OA70	Force	139B	.015	UPWT	Tape	Yaw RCS Data Only
OA73	Force	139B	.015	ARC 3.5	Tape	
OA85	Force + Limited Press.	139B	.010	CFHT	Tape	Tabulated Pressure Only
OA105	Force	"	"	"	"	
IA60	Force	"	"	"	"	Orbiter + Tank
OA83	Pressure	"	"	ARC 3.5	Plots	Plotted Data Only
LA25	Force	"	.010	CFHT	Tape	
OA82	Force	"	"	CFHT	Tape	
OA99	Force + Limited Press.	"	.0175	Vacuum	Report	Vacuum Impingement
MA22	Force	"	.010	CFHT	Tape	
OA169	Force	"	.0125	VKF "B"	Tape	Forward + Aft RCS Simulations
IA22	Force	"	.0125	VKF "B"	Tape	Orbiter + Tank

TABLE 2-2 PITCH DOWN RCS NOZZLES

Nozzle I.D	No. of Jets	Expansion Ratio	Exit Diameter	Exit Angle	$K_T = \frac{T}{P_{oj}}$	Outboard Cant	Aft Cant	Side	Test Used
N21	2	1.159	.144 in.	5°	-	20°	12°	Left	OA73
N22	"	"	"	"	-	0°	0°	"	"
N31	"	1.115	.099	"	.00692	20°	12°	"	LA25 MA22
N34	"	2.851	.0878	9°	.00266	"	"	"	LA25 MA22
N35	"	"	"	"	"	"	"	Right	LA25
N38	"	"	"	"	"	"	30°	"	"
N42	"	7.697	.129	31.75°	.00237	"	"	"	OA85
N43	"	"	"	"	.00250	"	12°	Left	OA85 MA22
N45	"	"	"	"	.0024	"	30°	"	OA85
N46	"	6.332	.117	34.5	.00222	"	12°	Right	OA85
N47	"	"	"	"	.00237	"	"	Left	OA85 MA22
N49	"	4.43	.1413	34.25	.00460	"	"	"	LA60 OA82 OA85 MA22
N50	"	"	"	"	.00412	"	"	Right	LA60 OA82 OA85
N60	"	7.7	.129	31.75	.00240	"	"	"	OA85
N79	1	4.43	.1413	34.21	.0046	"	"	Left	OA82 MA22
N83	3	"	"	"	.00452	"	"	"	OA82 MA22
N95	1	12.5	.136	12.01	.001647	20°	12°	Left	OA169
N96	2	"	"	"	.001318	"	"	"	"
N97	3	"	"	"	.0012258	"	"	"	"
N98	3	4.43	.1413	34.21	.0046	"	"	Right	OA82

TABLE 3-3 PITCH UP RCS NOZZLES

Nozzle I.D	No. of Jets	Expansion Ratio	Exit Diameter	Exit Angle	$K_T = \frac{T}{P_{0j}}$	Outboard Cant.	Aft Cant.	Side	Test Used
N23	2	1.159	.144	5°	-	0	0	Right	OA73
N32	"	1.155	.099	"	.00738	"	"	"	LA25 MA22
N36	"	2.851	.0878	9°	.00261	"	"	"	LA25 MA22
N44	"	7.697	.129	31.75°	.00245	"	"	"	OA85 MA22
N48	"	6.332	.117	34.5°	.00237	"	"	"	OA85 MA22
N52	"	4.43	.141B	34.25°	.0046	"	"	"	IA60 OA82 OA85 MA22
N78	1	"	"	34.21	.0045	"	"	"	OA82 MA22
N81	2	"	"	"	.00452	"	"	Left	OA82
N82	3	"	"	"	.00452	"	"	"	OA82 MA22
N84	2+2	"	"	"	.00443	"	"	Right Up +Yaw	OA82 MA22
N95	1	12.5	.136	12.01	.001647	"	"	Right	OA169
N96	2	"	"	"	.001318	"	"	"	"
N97	3	"	"	"	.001226	"	"	"	"

TABLE 2-4 YAW RCS NOZZLES

Nozzle I.D.	No. of Jets	Expansion Ratio	Exit Diameter	Exit Angle	$K_T = \frac{T}{P_{o_j}}$	Outboard Cant.	Aft Cant.	Side	Test Used
N19	2	10.81	.144 in.	5°	-	0	0	Left	OA70 OA73
N20	"	1.159	"	"	-	"	"	"	OA73
N33	"	"	.099	"	.00792	"	"	"	LA25 MA22
N37	"	2.85	.0878	9	.00300	"	"	"	LA25 MA22
N51	4	4.43	.1413	34.25	.00405	"	"	"	LA60 OA82 OA85 MA22
N61	2	7.697	.129	31.75	.00221	"	"	"	OA85 MA22
N85	"	4.43	.1413	34.21	.00452	"	"	"	OA82 MA22
N95	1	12.5	.136	12.01	.001647	"	"	"	OA169
N96	2	"	"	"	.001318	"	"	"	"
N97	3	"	"	"	.001226	"	"	"	"
N100	3	4.43	.1413	34.21	.00452	"	"	"	OA82

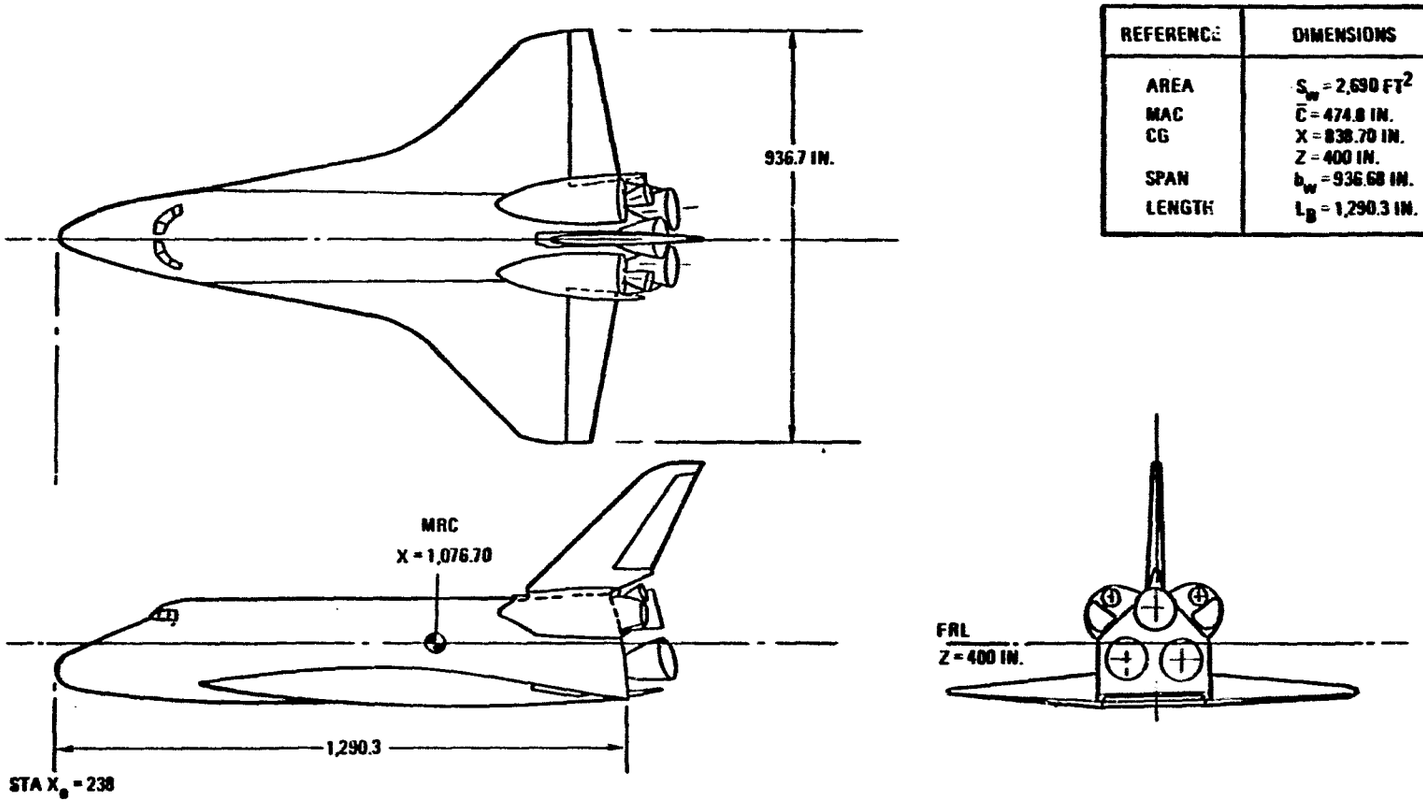

REFERENCE	DIMENSIONS
AREA	S_w = 2,690 FT^2
MAC	$\bar{C}$ = 474.8 IN.
CG	X = 838.70 IN.
	Z = 400 IN.
SPAN	b_w = 936.68 IN.
LENGTH	L_B = 1,290.3 IN.

Figure 2-1. 139B Orbiter Configuration

ORIGINAL PAGE IS
OF POOR QUALITY

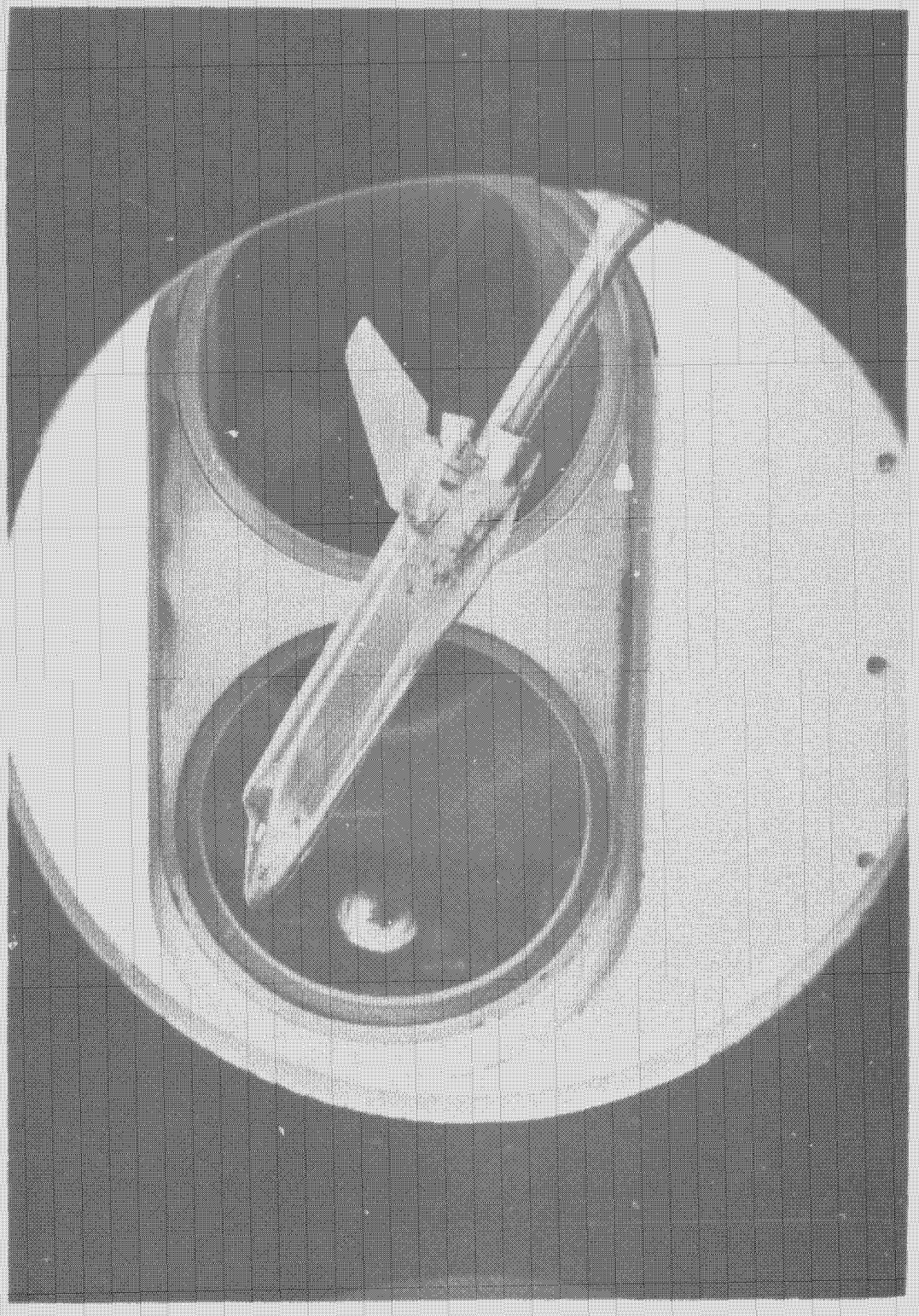

Figure 2-2. OA169 Test Installation.

ORIGINAL PAGE IS
OF POOR QUALITY

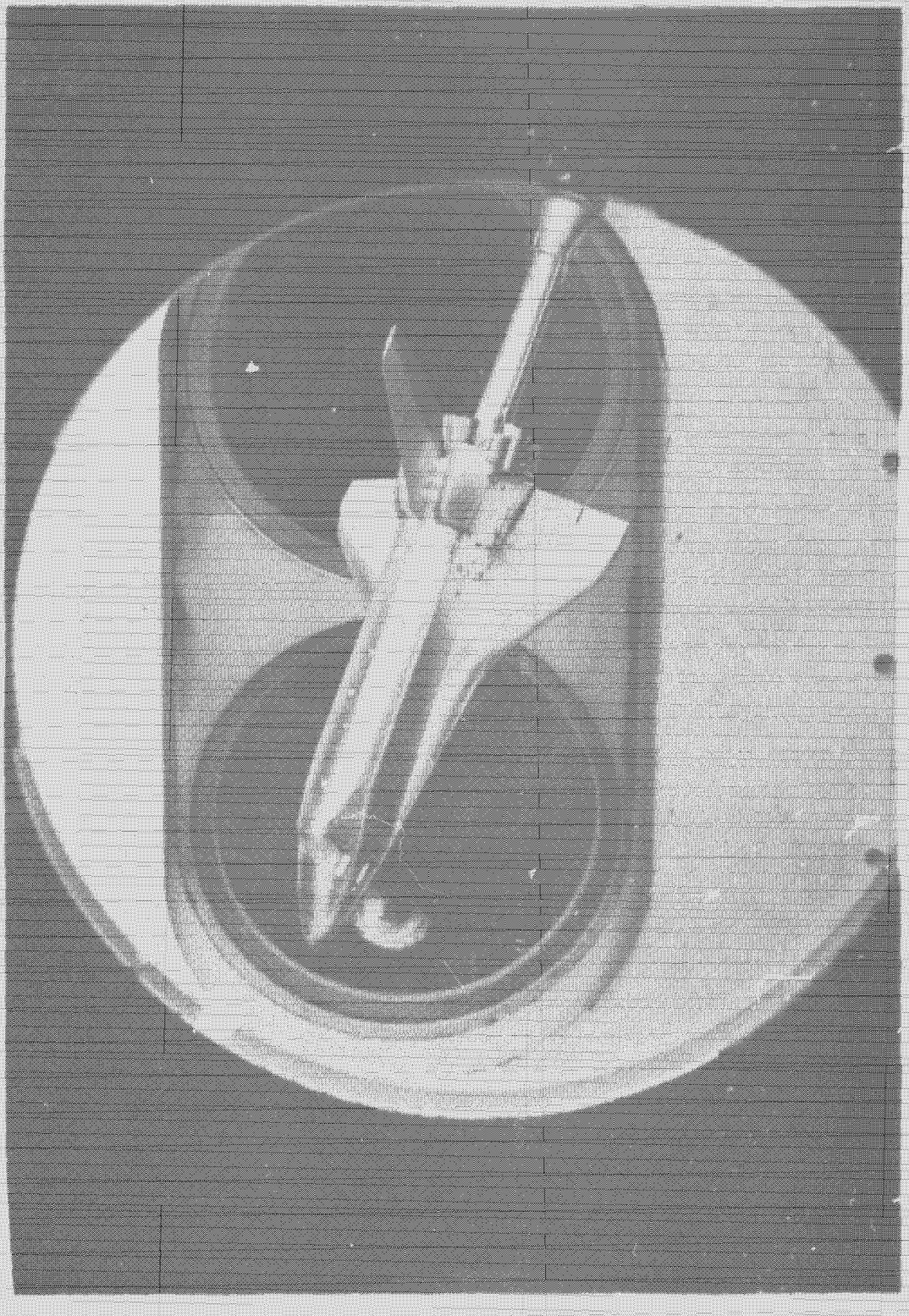

Figure 2-3. OA169 Orbiter Model.

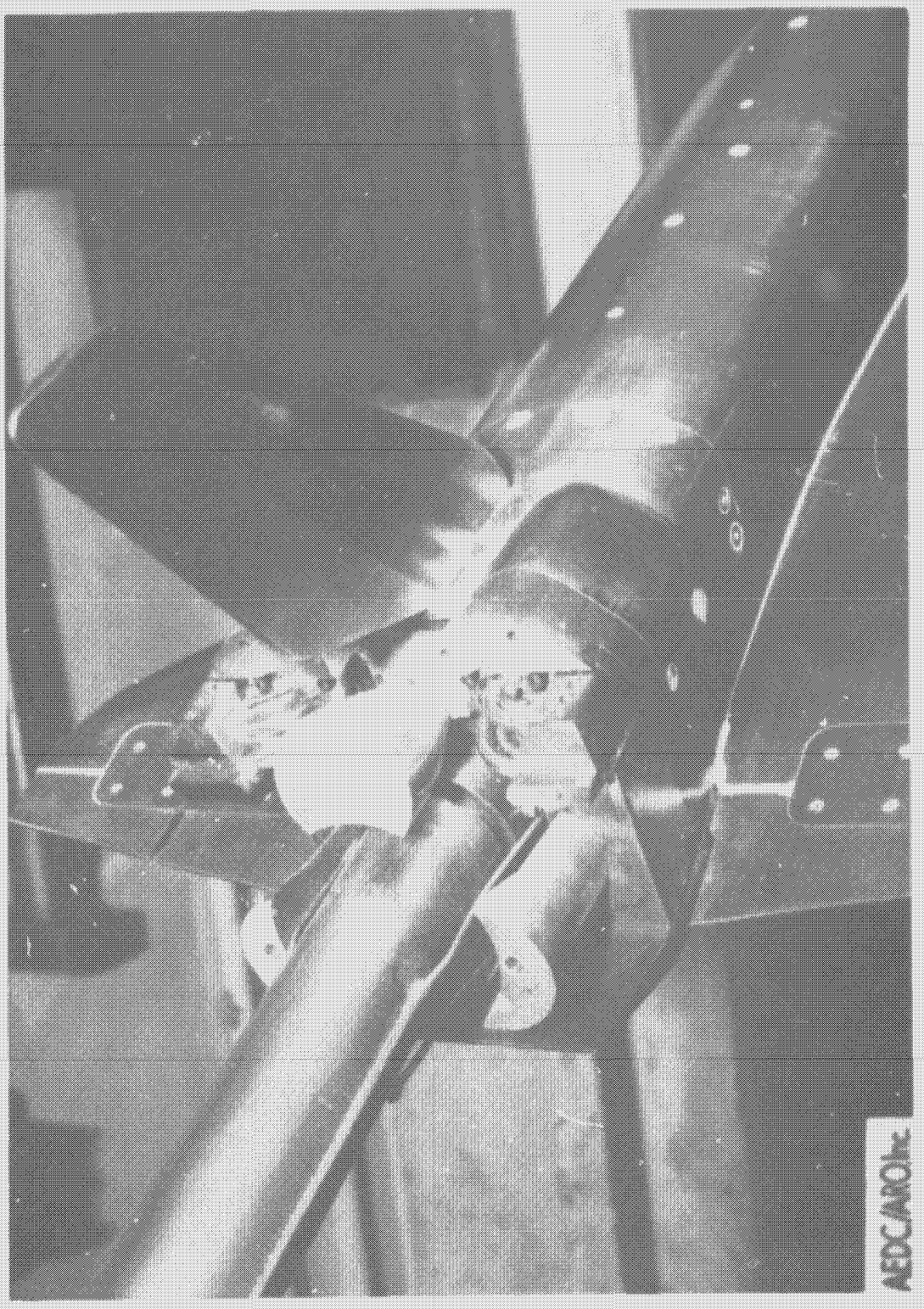

Figure 2-4. OA169 Sting Mount.

ORIGINAL PAGE IS
OF POOR QUALITY

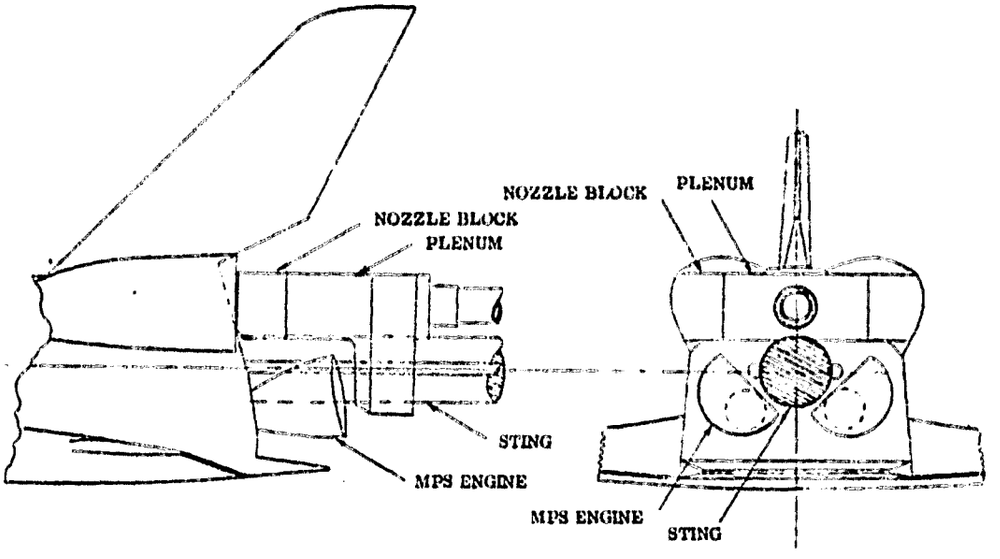

Figure 2-5. OA82/MA22 Sting Mounted RCS.

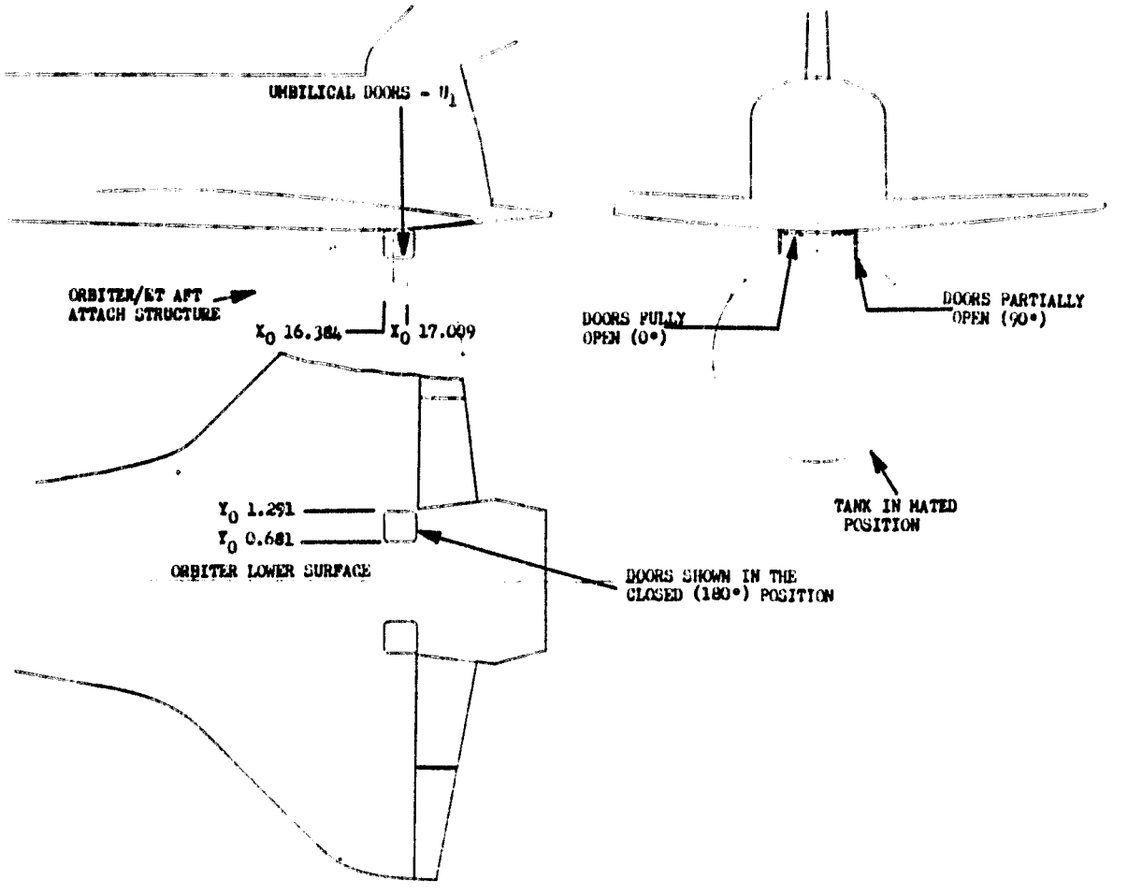

Figure 2-6. OA169 Umbilical Door Configuration.

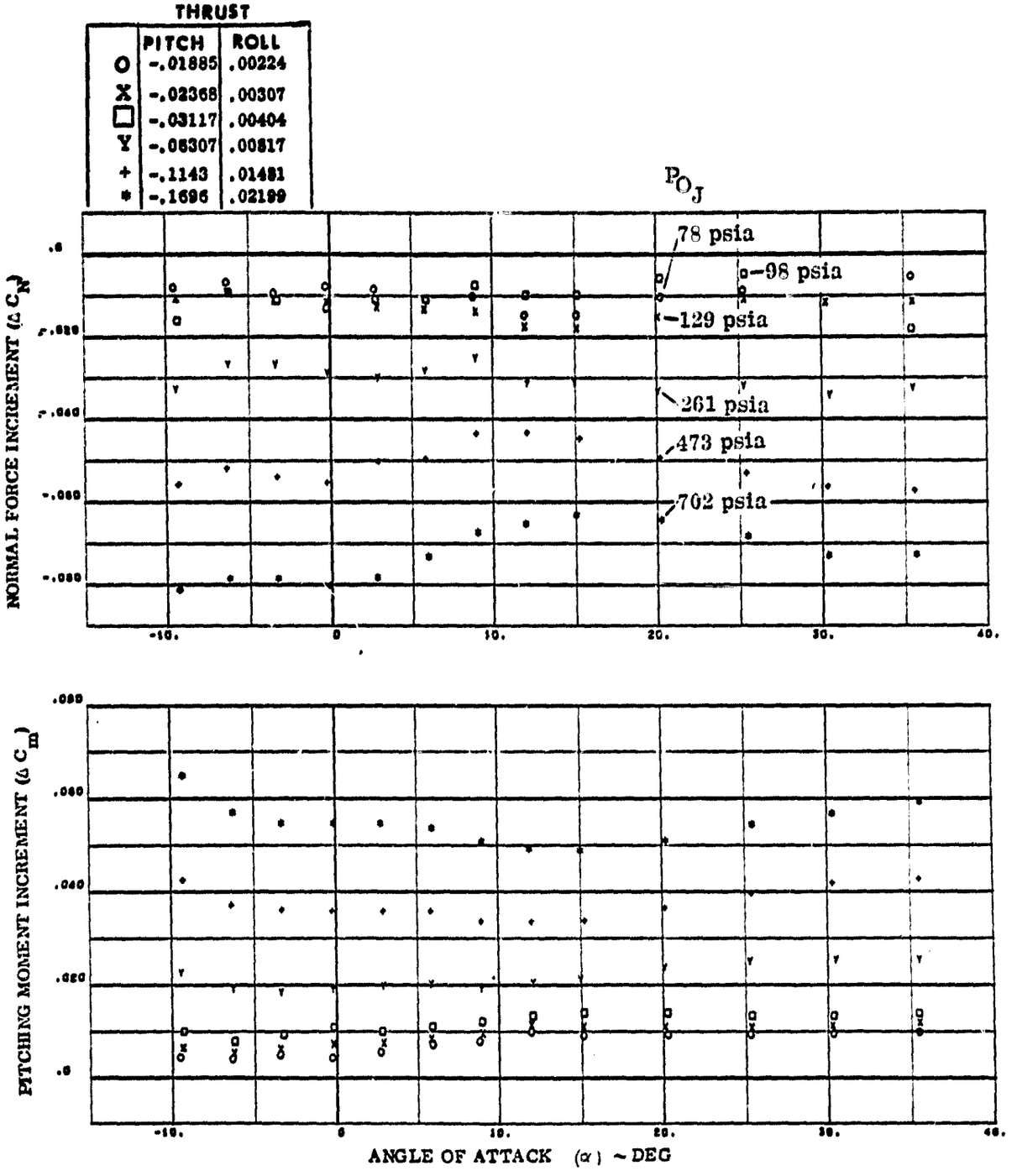

Figure 2-7a. N_{49} Effect of Supply Pressure at Q = 125 PSF.

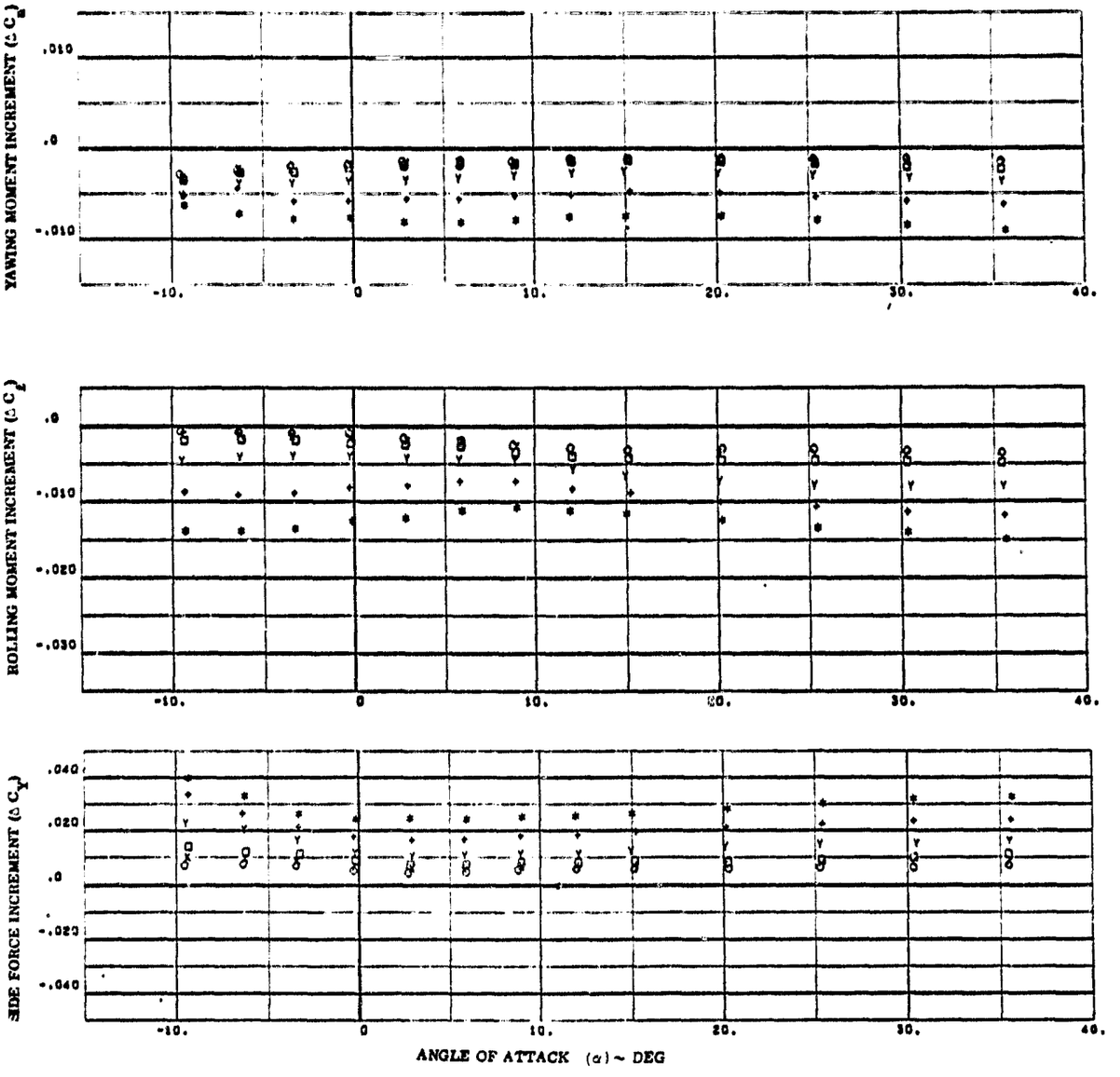

Figure 2-7b. N_{49} Effect of Supply Pressure at Q = 125 PSF.

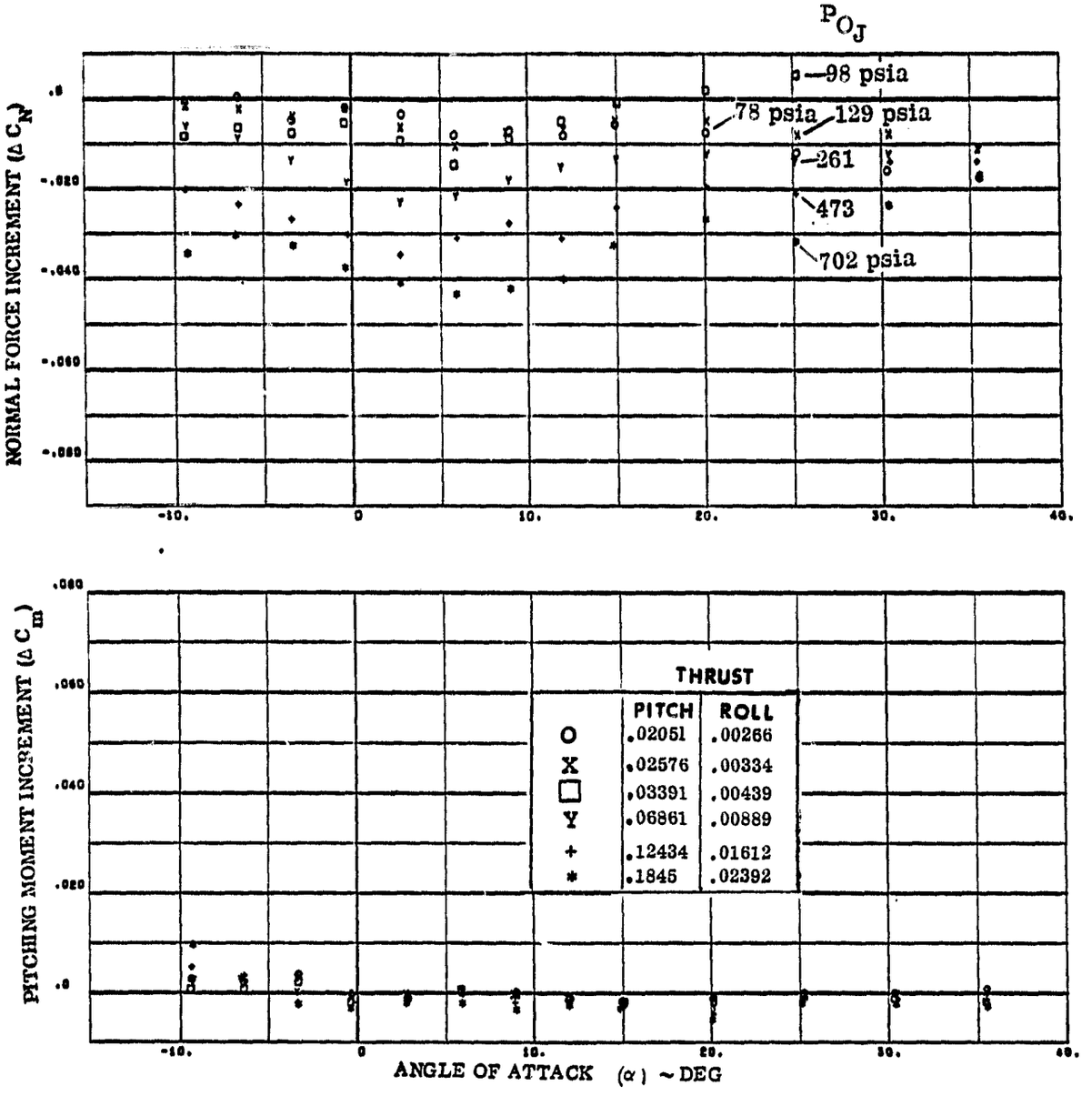

Figure 2-8a. N_{52} Effect of Supply Pressure at Q = 125 PSF.

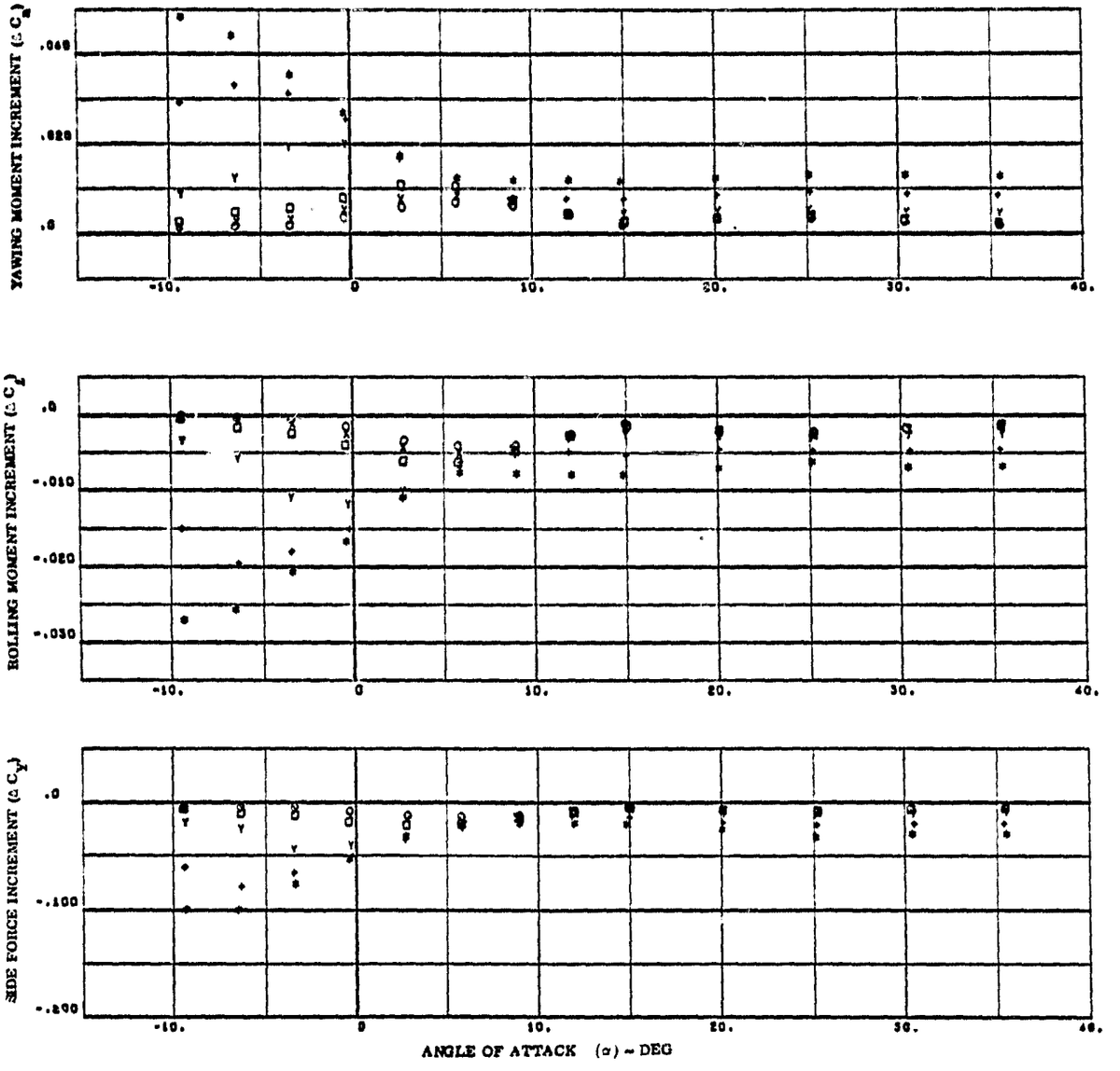

Figure 2-8b. N_{52} Effect of Supply Pressure at Q = 125 PSF.

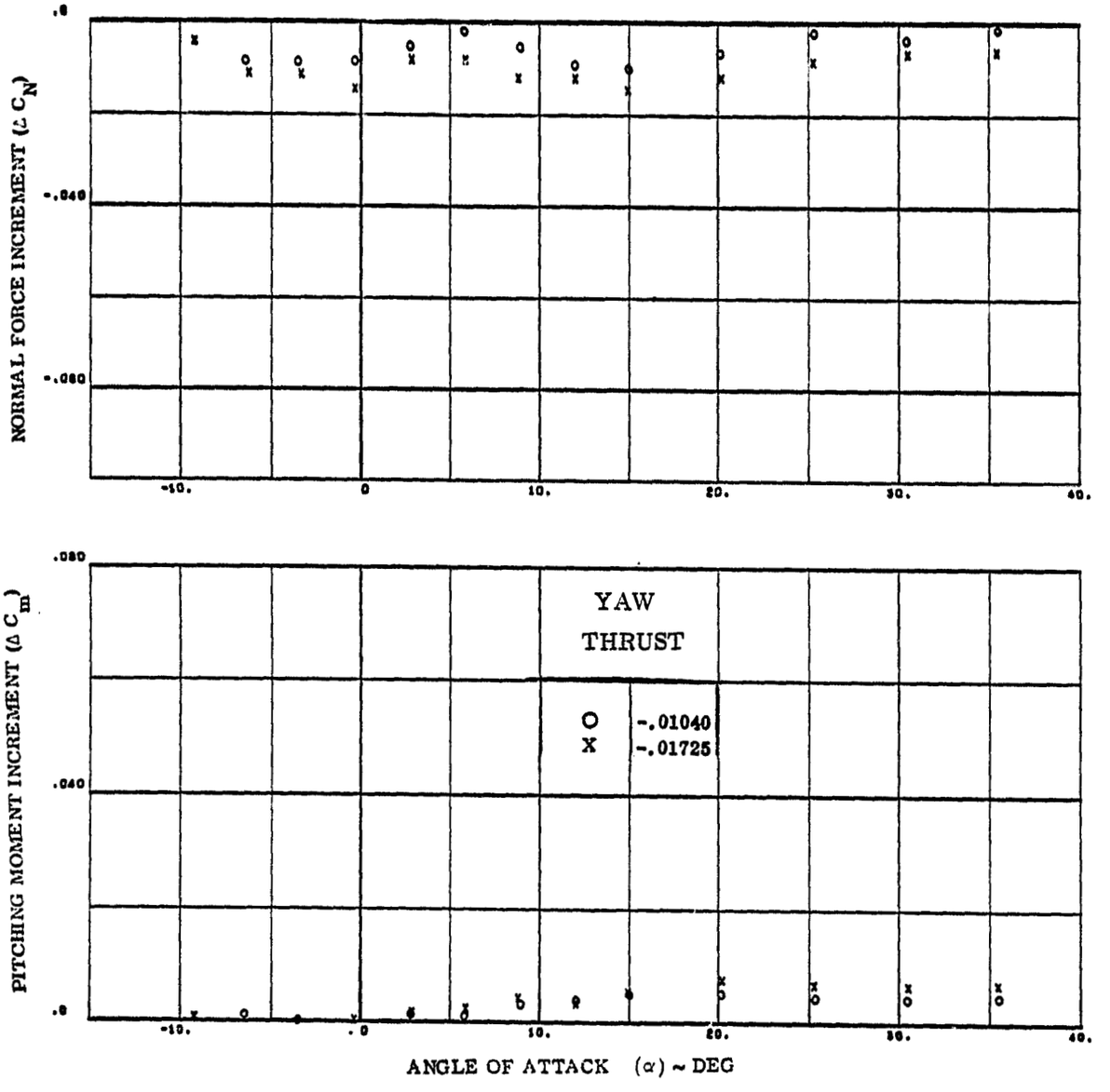

Figure 2-9a. N_{85} Effect of Supply Pressure at Q = 125 PSF.

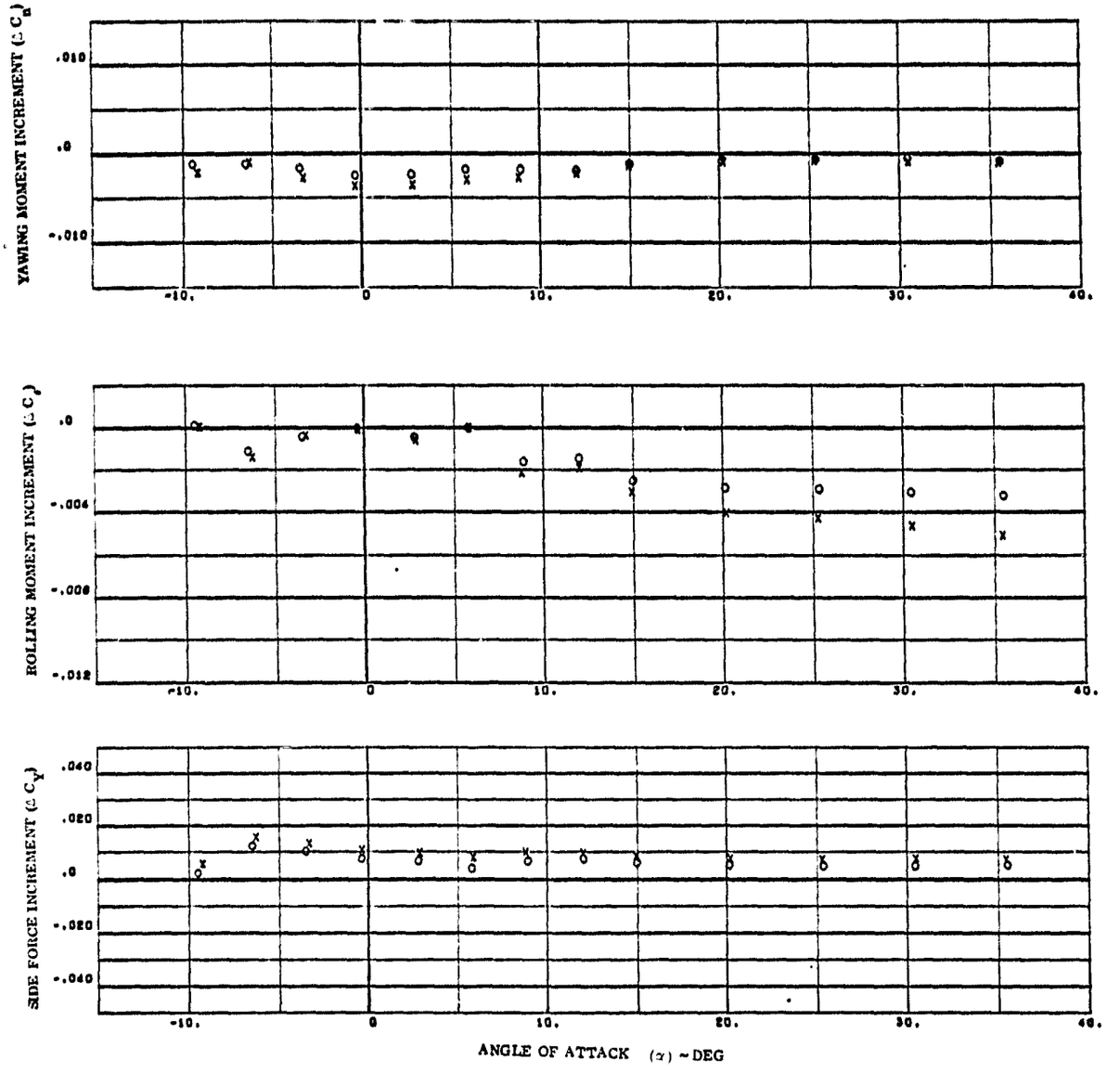

Figure 2-9b. N_{85} Effect of Supply Pressure at Q = 125 PSF.

3

DATA ANALYSIS

3.1 SUMMARY OF PREVIOUS RESULTS

The analytic model developed in Reference 3 assumes that the total control force or moment of a RCS control is the linear sum of the jet force or moment and an induced force or moment which is itself the sum of a term contributed by the direct impingement of the RCS plumes on adjacent surfaces and an interaction term which is the plume flow interacting with the external flow over the vehicle.

$$C_{M_{total}} = C_{M_{jet}} + C_{M_{impingement}} + C_{M_{interaction}} \quad (1)$$

where

$C_{M_{total}}$ = total control force or moment coefficient

$C_{M_{jet}}$ = RCS force or moment coefficient

$C_{M_{impingement}}$ = force or moment coefficient due to plume impingement on adjacent surfaces

$C_{M_{interaction}}$ = force or moment coefficient caused by plume interactions with the flow over the vehicle.

The reasons for dividing the RCS induced effects into an impingement and an interaction component are that the vehicle geometry is such that the RCS jets exhaust toward many surfaces such as the wing upper surface, the body flap, the main propulsion engines, and vertical fin. The vacuum test data (Ref. 7) showed that there is plume impingement on these surfaces; but, the analysis of Reference 3. showed that the total induced forces and moments are larger than that which is predicted by plume impingement alone and thus there exists a plume interaction with the flow field around the shuttle orbiter. In order to derive this interaction term, however, it is necessary to know or assume the impingement term and to subtract it from the total induced term. This was done in these analyses by using the analytic plume impingement model presented in Section 4 to predict the plume impingement for the model nozzle, test gas, and wind tunnel conditions and to remove it from the induced data as shown in Equation 2 of Section 2.

3.1.1 Previous Pitch Down/Roll Results

The analysis reported in Reference 3 established a number of basic facts for the left side, pitch down/roll jet data. These are:

a) Angle of attack is a relatively insensitive parameter
b) (RT) ratio effects are not important

c) Momentum ratio appeared to be the best correlating parameter
d) Number of nozzles could be accounted for by using an equivalent area in the momentum ratio parameter.

Based on the first fact, the data was broken into 2 ranges of angle of attack and correlations were made for the data below 15° and above 15°. The second fact verified that cold gas simulations are acceptable to define reaction control effects but did not eliminate mass flow ratio completely as a parameter since almost all of the data was based on one nozzle geometry and thus all nozzle parameters were directly related to each other in a constant manner. The equivalent nozzle momentum ratio was related to wing area as the reference area and the momentum ratio equation became:

$$\frac{\Phi_j}{\Phi_\infty} = \frac{\gamma_j P_j M_j^2 \Sigma A_j}{\gamma_\infty P_\infty M_\infty^2 S_{wing}} \qquad (2)$$

3.1.2 Previous Pitch Up/Roll Results

The analysis of the pitch up/roll jet data reported in Reference 3 established a number of facts about the flow interaction which include:

a) The interaction is relatively insensitive to angle of attack at high angle of attack
b) The interaction shows a peak value at low angles of attack
c) There is a region between these two angles of attack where the data appears to be independent of nozzle flow parameters
d) The equivalent nozzle momentum ratio appeared to be the primary parameter although mass flow ratio seemed to correlate better for the values of normal force and pitching moment at all angles of attack.

Figure 2-8b presents a sample of rolling moment increment data plotted as a function of angle of attack. Above 15 degrees, the data appears much like the pitch down data in that angle of attack effects are small. As angle of attack decreases below 15 degrees angle of attack, all the data appears to follow one curve until a peak value is reached and the data decays along separate curves. The peak values and the angles of attack at which they occur appear to be functions of some nozzle related parameters. The pitch up RCS data was broken into three parts for analysis based on these observations which were:

a) high angle of attack
b) peak values
c) below peak values

The division between the high angle of attack data and the other regions was arbitrarily chosen as 15 degrees and the data was averaged in this region to

obtain high angle of attack correlations. These data were treated in the same way as the pitch down data in which it was assumed that the total induced force or moment was the sum of an impingement term and an interaction term. A theoretically predicted impingement term was then subtracted from the induced terms in order to define the interaction terms for correlation with nozzle parameters. Momentum ratio as defined in Equation 2 above appeared to be the better parameter for all data except normal force and pitching moment where mass flow ratio was chosen as the parameter.

The model for predicting the effects in the low angle of attack region consisted of the following steps:

a) predict peak value as a function of nozzle parameters,
b) predict peak angle of attack from peak value,
c) if the angle of attack is above that for the peak value, predict interaction value from angle of attack vs peak value curve
d) if the angle of attack is below that for the peak, predict interaction based on a decay from peak curve fit.

The peak values of side force, rolling moment, and yawing moment showed excellent correlation with momentum ratio while the peak normal force data tended to show good agreement with mass flow ratio but the peak pitching moment showed only poor agreement with either parameter. Steps b and c listed above required curve fits of peak values versus angle of attack which were made also.

Figure 3-1 showed that the interaction data decayed to a reduced level at angles of attack below that of the peak value. A limited amount of analysis was performed in this region because the number of data points is very small particularly for the higher jet pressures where the peak value was reached at or very near the lowest value of angle of attack tested and the curves depend on the lowest pressure data where error effects become large.

A model was tentatively selected for this region which used the peak value and assumed that the interaction increment goes to zero at 20 degrees below the peak.

$$C_M = C_{M_{peak}} \left\{ \sin\left[\frac{\pi}{2} \left(\frac{\alpha - \alpha_{peak} + 20}{20} \right) \right] \right\}^2 \qquad (3)$$

where C_M = pitch up force or moment coefficient

$C_{M_{peak}}$ = peak pitch up force or moment coefficient

α = angle of attack

3.1.3 Previous Yaw Results

Very few yaw RCS data were available to analyze in Reference 3 . These data did establish the following facts about yaw RCS jet interaction:

a) The data showed moderate sensitivity to angle of attack
b) (RT) ratio effects are important and mass flow ratio appeared to be the better correlating parameter.

The data was divided into a low angle of attack model ($\alpha < 15°$) and a high angle of attack model and was averaged over each angle of attack range. The parameter which appeared to work best was mass flow ratio as defined in Equation 4 and curve fits were made using it as the parameter.

$$\frac{\dot{m}_j}{\dot{m}_\infty} = \left[\frac{\bar{q}_j}{\bar{q}_\infty} \frac{\Sigma A_j P_j}{S_{Ref} P_\infty} \left(\frac{R_\infty T_\infty}{R_j T_j} \right) \right]^{1/2} \quad (4)$$

The limited amount of data, however, showed a fair amount of scatter and confidence in the results was low.

3.1.4 Previous Combined Control Results

A very limited set of combined control results were analyzed in Reference 3 and a set of corrections were obtained which in general ratioed the combined effects to the data for the single axis controls. Cross-coupling effects were found in the following cases:

a) symmetric pitch down
b) symmetric roll
c) pitch up plus yaw on same side

3.2 PITCH DOWN/ROLL RCS INTERACTION

Section 3.1.1 briefly described the previous results obtained from data from test OA82 at Mach 10. The test labeled MA22 added considerable data to the pitch down data base particularily through the testing of a large number of nozzles ranging in expansion ratio from 1.15 to 7.7 as shown in Table 2-2. Test OA169 then added to the data base with Mach 6 data and a nozzle of an expansion ratio of 12.5. These data removed the previous limitations on nozzle simulation parameters (i.e., that they were all directly related because only one nozzle geometry was tested) and it was decided to start the analysis over again as in Reference 3 to ascertain the best interaction correlating parameter. In addition since a large body of data was available it was decided to account for angle of attack effects by eliminating the high-low model with its attendant data averaging and to curve fit all data within selected angle of attack bands. Another purpose of this approach was to obtain good estimates of the true data scatter within a given angle of attack range so that the standard deviation of error could be

computed. The data intervals were chose as 5 degrees starting from -10 degrees angle of attack to 35 degrees with a .5 degree buffer on both ends of the interval to insure all data on the end of an interval occurred in both samples. The data above 35 degrees (up to 43 degrees) were taken in one interval.

The re-analysis of the new data base confirmed the fact that the equivalent area momentum ratio described in Equation 2 was the best parameter for the pitch down-roll RCS interaction data. Considerable scatter was found between different nozzles operating at the same nominal momentum ratio and a number of second order parameters were tried to correct for this. The resolution of this problem which resulted in the greatest reduction in this kind of scatter was to account for the actual nozzle characteristics in the momentum ratio through the use of a coefficient which accounts for the actual nozzle performance ratioed to its theoretical performance. This coefficient is defined in Section 2, Equation 3 and is called a discharge coefficient in this analysis. Thus effective momentum ratio is defined:

$$\left(\frac{\Phi_j}{\Phi_\infty}\right)_{\text{eff}} = C_D \left(\frac{\Phi_j}{\Phi_\infty}\right)_{\text{theoretical}} \tag{5}$$

where C_D = discharge coefficient (Section 2, Equation 3)

$\left(\frac{\Phi_j}{\Phi_\infty}\right)_{\text{theoretical}}$ = ideal nozzle momentum ratio (Equation 2)

and any further reference to momentum ratio in this section refers to the Equation 5 definition.

All data were curve fitted with both a quadratic and cubic least square curve fit and the one with the lowest root mean square error was chosen to represent the data. The cubic curve has the general form:

$$\Delta C_M = a_o + a_1 \left(\frac{\Phi_j}{\Phi_\infty}\right) + a_2 \left(\frac{\Phi_j}{\Phi_\infty}\right)^2 + a_3 \left(\frac{\Phi_j}{\Phi_\infty}\right)^3 \tag{6}$$

where ΔC_M = any force or moment due to interaction

a_o to a_3 = curve fit constants

In addition a maximum and minimum value of momentum ratio are specified over which the equation applies. All data presented here are at zero elevon and body flap control deflection. Control deflection effects are treated incrementally and will be presented in Section 3.6 and 3.7.

3.2.1 Pitch Down Axial Force Correlations

Table 3-1 presents the coefficients for the ten (10) angle of attack intervals over which the data was curve-fitted while Figures 3-1a to 3-1j present the correlations between the curve fits and the data base. These curves show that the lowest number of points within an angle of attack interval was 99 and the greatest number was 155 both numbers are sufficiently large to insure a good statistical sample. The root-mean-square error was computed from the least square curve fit and is tabulated on each plot as the standard deviation (sigma). Also plotted are the 2 sigma error band limits around the least square curve fits to show how the data scatters within the error band.

All data shows the same trend that increasing RCS jet momentum ratio results in a decrease in axial force up to a momentum ratio (Equation 5) of approximately 0.1 which is close to the upper limit of data obtained. The best fit as measured by lowest root mean square error occurs in the 25 to 30 degree angle of attack range while the worst occurs from -10 to -5 degrees angle of attack although the values of sigma for both are close. The intercept (a_0) does not approach zero below 10 degrees angle of attack and probably represents a measure of average difference between the jet-off data and a total test base jet-off average. As such, one approach to using these curves would be to set this term to zero and in effect adjusting the data to obtain zero interaction at the no flow condition. The OA169 data can be seen on these curves to be well within the scatter of the Mach 10 data except perhaps at 15 degrees angle of attack where the OA169 data itself showed a discontinuity between the high and low range angle of attack data.

3.2.2 Pitch Down Normal Force Correlations

Table 3-2 presents the equations for the curve fits of normal force versus momentum ratio shown in Figure 3-2a to 3-2j. These curves are plotted in the same manner described for the axial force above and show that exhausting the RCS down toward the wing results in a negative normal force being generated at all angles of attack which is proportional to the equivalent nozzle effective momentum ratio. The data below 20 degrees angle of attack shows excellent correlation with a small root-mean-square errors, however, the data above 20 degrees shows increasingly more scatter with increasing angle of attack. This was shown in Reference 3 to come in part from the sizeable differences in jet-off data at high angles of attack and is seen primarily in the Mach 10 data. The Mach 6 data is well within the error band of the total data indicating no discernable

Mach effect and it is possible that a fit of the Mach 6 data only at high angles of attack would be a better curve.

3.2.3 Pitch Down Side Force Correlations

Table 3-3 presents the equations of the side force due to downward exhausting RCS nozzles while Figures 3-3a to 3-3 j present the correlating curves. All pitch down RCS data was obtained from nozzles mounted on the left side of the model so that all interaction result in a positive side force increment. The equations fit the data about equally well at all angles of attack and no Mach effects can be seen.

3.2.4 Pitch Down Pitching Moment Correlations

Table 3-4 and Figures 3-4 a to 3-4 j present the correlation of pitching moment induced by the RCS unit exhausting toward the wing. These data are for the RCS units on one side only; the symmetric pitch down case will be considered in Section 3.5. The data shown in Figures 3-4 a to 3-4 j show that exhausting RCS jets toward the wing results in a nose up pitching moment being induced on the vehicle at all angles of attack which counteracts the thrust moment being generated. The poorest correlation occurs at the lowest angle of attack but the RMS error is still close to the rest of the data. The Mach 6 data in the 10 to 15 degree angle of attack range appears to lie along a different line than the Mach 10 data but this is the only angle of attack interval where this occurs.

3.2.5 Pitch Down Rolling Moment Correlations

Table 3-5 and Figures 3-5 a to 3-5 j present the correlations of rolling moment across the ten (10) angle of attack intervals. The pitch down/roll RCS data was all taken with the jets exhausting downward on the left side of the model so that a negative rolling moment indicates the induced moments counteract the thrust moment. The curve fits appear to be uniformly consistent across the angle of attack range with the RMS error slightly larger in the lowest range and best at the highest angles of attack.

3.2.6 Pitch Down Yawing Moment Correlations

Figures 3-6 a to 3-6 j show that the yawing moment induced by pitch down jets is dependent on the jet momentum ratio only up to a momentum ratio of about .04 where it becomes constant. The scatter in the data is large relative to the small values of measured induced moment due to taking the differences between two small numbers. The curve-fit equations of Table 3-6 only apply to the maximum value and are assumed constant at this value at momentum ratios above the maximum.

3.3 PITCH UP/ROLL RCS INTERACTION

Section 3.1.2 briefly summarized the previous pitch up/roll reaction control system results and models. The additional data base obtained in test MA22 expanded the correlation of nozzle parameters since as shown in Table 2-3 a number of different nozzle geometries were tested. The OA169 data at Mach 6 added Mach number as a correlation variable as well as increasing the nozzle expansion ratio range and numbers of nozzle data to the base. The data to be reported in this section was obtained from nozzles exhausting upward past the vertical fin on the right side of the model.

The approach taken in this part of the study was similar to that of Section 3.2 basically to start over with the new data base and to reanalyze all of the data together rather than to make the data fit the old model. In this case large changes to the model have resulted from this approach. First the longitudinal data (C_N, C_A, C_m) were found not to have peak values at low angle of attack but were better correlated by the approach used for pitch down data in Section 3.2 that is to break it up into intervals by angle of attack and correlate each interval. The longitudinal data using this approach was also found to correlate better with momentum ratio than mass flow ratio as previously modeled making it consistent with the other pitch up RCS correlations. The occurance of a peak value at low angles of attack still remains in the lateral-directional data (C_Y, C_ℓ, C_n).

3.3.1 Longitudinal Data

3.3.1.1 Pitch Up Axial Force Interaction

Table 3-7 and Figures 3-7a to 3-7j present the correlations of induced axial force versus equivalent nozzle effective momentum ratio (Equation 5). These figures show a relatively small change (reduction) in axial force occurs when the jets exhausting upward are fired but good correlations are obtained at all angles of attack with momentum ratio. The smallest number of data points obtained within one interval was 77 and the largest 123. The Mach 6 data tends to scatter at the edge of the data band at low angles of attack, however, it occurs on both edges (Figures 3-7d and e) and no significant Mach effect can be ascertained.

3.3.1.2 Pitch Up Normal Force Interaction

The additional data base obtained in tests MA22 and OA169 have changed the normal force interaction from a peak model at low angle of attack correlated with mass flow ratio to a model based on momentum ratio with no peak value. Table 3-8 and Figures 3-8a to 3-8j show the correlation. If we consider the higher angles of attack first (Figures 3-8f to 3-8j), we see that only a small induced normal force results from the plumes exhausting upward and the high angle of attack data scatter largely masks it. Only the Mach 6 data appears to show any trend. In contrast at

low angles of attack while the force is small the correlation is clear for the Mach 10 data but the very limited Mach 6 data tends to show no induced normal force. The model shown in Table 3-8 was chosen to follow the data correlations up to 25 degrees and assumes no effect beyond this angle of attack. These data show that the induced force acts in the same direction as the thrust and this enhances control power.

3.3.1.3 Pitch Up Pitching Moment Interaction

Table 3-9 and Figures 3-9a to 3-9j present the induced pitching moment resulting from firing the pitch up RCS units. Figure 3-9a shows that the thrust moment is enhanced by the interaction at negative angles of attack where the upper surface is fully exposed to the flow, however, this amplification disappears at zero angle of attack (Figure 3-9b) and some very small nose down moments appear. It would seem that the only source of these small moments could be the reduction in axial force (Figures 3-7a to 3-7j) acting on the base of the missile but the effect is clouded by possible sting effects on any base flow.

3.3.2 Lateral-Directional High Angle of Attack Data

The lateral-directional data at angles above 15 degrees has been correlated with momentum ratio just as the longitudinal data. The peak value correlation for low angles will be treated in Section 3.3.3.

3.3.2.1 Pitch Up Side Force Interaction

The pitch up RCS data was obtained from RCS simulations all exhausting upward past the right side of the vertical fin thus, any interaction would expected to be with the fin and have a negative sign. Table 3-10 and Figures 3-10a to 3-10e indicate that such an interaction does occur and that it correlates well with momentum ratio as defined by Equation 5. None of these curves shows that a maximum value occurs within the range of measured data and this makes it difficult to know how far to extrapolate to the limiting low dynamic pressure case.

3.3.2.2 Pitch Up Rolling Moment Interaction

The incremental induced rolling moment data is presented in Figures 3-11a to 3-11e and the corresponding curve fits in Table 3-11. These data show that the induced moment counteracts the desired control moment from the thrust of the RCS units. The curve fits of the data again show no maximum values and it is critical to the roll control to know how far these curves can be extrapolated in the very low dynamic pressure cases.

3.3.2.3 Pitch Up Yawing Moment Interaction

Figures 3-12a to 3-12e and Table 3-12 present the yawing moment data for the pitch up RCS at high angles of attack which shows the same trends as the other

lateral-directional data. In all three lateral-directional components the curve fit routine chose to pass closer to the N82 nozzle data at the highest measured momentum ratio in preference to the N52 data at a momentum ratio of .08. The fairing of the curve in this range could be critical to roll control at high angles of attack and low dynamic pressure during entry as will be discussed further in the error analysis. The equations at present do not extrapolate the data beyond a momentum ratio of .1.

3.3.3 Lateral Directional Low Angle of Attack Correlations

Figure 3-1 showed that the reaction control system-flow field interaction exhibited a range of peak values at lower angles of attack. The analysis of Reference 3 showed that the peak value and the angle of attack at which it occurred are dependent on nozzle momentum ratio. The present analysis arrived at the same results except that considerably more data was available to give higher confidence in the fact that momentum ratio is the primary correlating parameter and new curve fits of peak value data were obtained. The model for predicting the RCS interaction lateral-directional effects in the peak value region proceeds in the following manner.

a) Predict peak force or moment coefficient as a function of momentum ratio (Table 3-13)
b) Predict the angle of attack at which the peak value occurs as a function of peak value (Table 3-14)
c) If present angle of attack is greater than peak angle, recompute interaction coefficient as a function of angle of attack (Table 3-14)
d) If present angle of attack is lower than that of the peak value, compute interaction based on decay from peak value model as a function of peak value and incremental angle below peak value. (Table 3-15).

Tables 3-13 to 3-15 summarize the coefficients for the equations used above and the momentum ratio used for peak values is defined by Equation 5.

3.3.3.1 Peak Interaction Coefficients

Figures 3-13a to 3-13c present the correlations of peak values of the side force, rolling moment, and yawing moment. Only one point was obtained on a data run so the number of samples is low compared to other data correlations discussed earlier, however, the sample size of 43 points is still large enough to be an excellent measure of the true nature of the data. The curves show very little scatter at low values of momentum ratio where the OA169 Mach 6 data shows good agreement with the Mach 10 data indicating no significant Mach effect. The yawing moment and rolling moment peak interaction curves do not reach maximum values within the measured data range so the limit of a momentum ratio of .1 is applied as a limit on these curves.

3.3.3.2 Peak Value Angle of Attack Correlations

The sample data shown in Figure 3-1 show that the angle of attack at which the peak value occurs is directly related to the peak value and through that to nozzle momentum ratio. Attempts to correlate peak value angles of attack with momentum ratio demonstrated that a better fit was obtained by fitting the peak value of coefficient against the angle of attack at which it occurred as shown in Figures 3-14a, 3-14c, and 3-14e. These curves show good correlation in which increasing momentum ratio which increases peak interaction (Figure 3-13) also causes it to occur at lower angle of attack. Better correlation would have required more data at angles of attack below -10 degrees for the higher momentum ratios and smaller intervals in angle of attack near the peak values. The curve fit of peak value versus angle of attack is fairly flat and the angle of attack interval was usually 2 degrees so that chosing the peak value and its angle of attack would be very prone to error and more scatter would have been expected.

The data tends to show and the model assumes that all data at angles of attack above the peak value but below the high angle of attack range collapse into one curve which can be described by the peak value versus angle of attack correlation. Figures 3-14b, 3-14d, and 3-14f present correlation of the available data at all momentum ratios tested from .004 to .09 starting from the peak value and terminating at 15 degrees angle of attack. The shape of these data curves shows good agreement with the peak value curves and the collapse of all curves into one is verified.

3.3.3.3 Correlations at Angles of Attack Below the Peak Value

The data sample of Figure 2-8 shows that the interaction decreases at angles of attack below that where the peak value occurs. The value of interaction at any of these angles appears to be tied to the peak value and the angle at which it occurs. The first correlation developed in Reference 3 correlated the ratio of the present value to the peak value against the incremental angle below the angle of the peak value. Figures 3-15a, 3-15b, and 3-15c present similar correlations made for this analysis of the expanded data base. A large scatter is to be expected in this analysis since the data base is primarily derived from the data where the peak value occurs at the higher angles of attack. These data were obtained at the lowest momentum ratios tested and would be expected to have the greatest scatter. Scatter results from the 4 terms in this correlation, however no other correlation was found which worked any better. In this analysis the peak value correlations of Figures 3-13 and 3-14 were used to generate the peak interaction coefficient and the angle of attack at which it occurred to help reduce the scatter. Cubic curve fits were applied to the data, whose coefficients are defined in Table 3-15. The rolling moment data (3-15c) shows that the interaction decreases until no measureable interaction occurs at approximately 15 degrees below the peak value. The Mach 6 data appears to agree with the Mach 10 data in this region also.

3.4 YAW RCS INTERACTION

Section 3.1.3 described the previous yaw reaction control system interaction results and gives the definition of mass flow ratio used in that analysis. The yaw nozzle data obtained from the nozzles defined in Table 2-4 for test MA22 resulted in a large increase in the range of nozzle parameters obtained compared to that from previous tests wh') the OA169 data added to the data base Mach 6 data and extended the data of the effects of the number of nozzles within a cluster to a large degree. All data was obtained from nozzles on the left side of the model exhausting outboard parallel to the left wing.

Analysis of the data showed that the number of nozzles was not a parameter in the correlation but that nozzle exit angle was a parameter. Mass flow ratio proved to be a better parameter than momentum ratio when modified to the following form:

$$\frac{\dot{m}_j}{\dot{m}_\infty} = \left(\frac{\gamma_j R_\infty T_\infty (C_D \; P_j \; M_j \; A_j)^2 \; \mathrm{Sin}\,(\theta_N)}{\gamma_\infty R_j T_j (P_\infty \; M_\infty \; S_{ref})^2} \right)^{1/2} \qquad (7)$$

In general the correlations worked best with the mass flow parameter given in Equation 7 above although the relationship appears to be weak for much of the longitudinal data.

3.4.1 Yaw RCS Axial Force Correlation

The previous model reported in Reference 3 did not attempt a correlation of the induced axial force due to yaw reaction control system operation. Figures 3-16a to 3-16j show that there is at best only a doubtful relationship established at the higher angles of attack. It must be pointed out that a strong one was not expected since the yaw RCS flow is away from the fuselage and its large base area. The lower angle of attack data is consistent only to the extent that low mass flow data show a slight increase in axial force. The coefficients of the equations in these figures are given in Table 3-16.

3.4.2 Yaw RCS Normal Force Correlation

The yaw jets exhaust over the upper surface of the wing so that the expected result of an interaction would be a negative normal force increment. Figures 3-17a to 3-17j shows that this does occur and that the data trends at lower angles of attack are much better defined than the axial force data. The equations of the curve fits on these figures are given in Table 3-17. The fact that number of nozzles in a yaw cluster is not a parameter is shown by the agreement between the N51 (4 nozzle) and N85 (2 nozzle) data at Mach 10 and the N95 (1 nozzle), N96 (2 nozzle), and N97 (3 nozzle) data at Mach 6. The addition of nozzle exit angle into the mass flow parameter resulted from trying to get the N33 and N37 to fit into the correlation of the other data.

The high angle of attack data shows the same problems with the scatter in the Mach 10 data noted previously in both the pitch down data (Section 3.2.2) and in the pitch up case (Section 3.3.1.2).

3.4.3 Yaw RCS Side Force Correlation

All yaw jet data was taken with jets exhausting out of the left side RCS pod of the model and the positive side load increments shown in Figure 3-18a to 3-18j indicate an interaction which enhances the side force generated by the yaw thrusters. The data scatter is worst in the negative angle of attack range but becomes very consistent at positive angles. Since this positive interaction side force is generated on the OMS pod, there must be a negative angle of attack where no force is generated and this may be the reason for the scatter at negative angles. The fact that numbers of nozzles is not a parameter and that exit angle is a parameter is confirmed by these curves. Table 3-18 gives the coefficients of the least square cubic curve fit of these data.

3.4.4 Yaw RCS Pitching Moment Correlation

Table 3-19 and Figures 3-19a to 3-19j show that a nose up pitching moment is induced by operation of the yaw reaction control units. The trend is clear at negative angles (Figure 3-19a) and again at angles above 15 degrees (Figures 3-19f to 3-19j). No correlation was found for angles of attack from -5 degrees to +15 degrees where interestingly the induced normal force showed its clearest trends. This evidently occurs because the induced moments are so low they cannot be resolved from the data scatter. The standard deviation for these data are similar to those of the pitch down data shown in Figure 3-4 so that both sets have comparible accuracy.

3.4.5 Yaw RCS Rolling Moment Correlation

Firing the yaw jets over the left wing of the orbiter results in a left wing down induced roll which is small at low angles of attack but becomes much larger with increasing angle of attack. This is shown in Figures 3-20a to 3-20j where the data above 15 degrees is fairly sensitive to angle of attack as well as the nozzle mass flow parameter defined in Equation 7. The coefficients of the curve fits are tabulated in Table 3-20.

The low level of induced roll in the lower angle of attack range is a consistent result with the pitching moment data of the preceeding section since both would arise from interactions with wing upper surface flow, thus, confirming the pitching moment results.

3.4.6 Yaw RCS Yawing Moment Correlation

Table 3-21 and Figures 3-21a to 3-21j present the induced yawing moment data resulting from yaw jets exhausting from on the left OMS pod on the model. These data show that the thrust moment is enhanced at all angles of attack but the greatest amount occurs at low angles.

3.5 COMBINED CONTROL

Combined control refers to the use of more than one cluster of RCS units operating at one time. Numbers of jets operating within one cluster has been accounted for in the analysis to this point generally through the use of the equivalent nozzle momentum ratio (Equation 5) or as in the case of the yaw RCS shown not to be a factor. Combined control includes the symmetric pitch control cases where both side jets are fired together, the pure roll case where one side is fired up and one down, and the combined pitch, roll, yaw cases.

Data was not obtained on all possible control combinations but data was obtained on the most important combinations including:

a) Symmetric pitch down
b) Symmetric pitch up
c) Pure roll
d) Combined pitch up and yaw
e) opposing pitch down and yaw

The approach taken in the analysis of these data was to compare the sum of the correlating curve fits and associated error bands from Section 3.2 to 3.5 with the combined control data. The estimated standard deviation error was computed as the square root of the sum of the squares of the individual control errors and plotted on the curves to determine whether the measured data was within the expected scatter or not.

$$\sigma_{\text{combined}} = \sqrt{(\sigma_{\text{control 1}})^2 + (\sigma_{\text{control 2}})^2} \qquad (8)$$

When a difference was taken, it was computed as the difference between a least squares curve fit of the data and the basic data curve fit.

3.5.1 Symmetric Pitch Down Correlation

One symmetric pitch down data run was obtained in test OA82 at Mach 10 and was the basis of the previous analysis of Reference 3. Ten (10) additional data runs were obtained at Mach 6 in test OA169 but only 4 were obtained in the high angle of attack range. Figures 3-22a to 3-22 l present the data correlations obtained from 15 degrees to 42.5 degrees angle of attack. Samples of the axial force correlations are shown in Figures 3-22a to 3-22d. These plots show that the Mach 6 data indicates a sizeable increase in the incremental axial force due to plume interaction occurs when both sides are fired symmetrically however, the limited Mach 10 data shows much closer agreement with the single side data. Since the region for this interaction is across the base of the model, the effect of the sting is a large unknown which(as in Reference 2) remains to be resolved.

Samples of the induced normal force are shown in Figures 3-22e to 3-22h and of the pitching moment in Figures 3-22i to 3-22l. These data also show additional force and moment are induced by pitch down jets firing on both sides of the model. Since other available data does not cover a large range of momentum ratios it was decided only to use the linear term of the differences in curve fit equations between the single side and the symmetric data. These data are tabulated in table 3-22 and show very little variation due to angle of attack. The model then uses an average value for the linear coefficient independent of angle of attack where the independent variable is the average momentum ratio of both clusters of down firing jets.

The lack of data at higher momentum ratios severly limits this model as does the unknown effect of the sting.

3.5.2 Symmetric Pitch Up RCS Correlation

Reference 3 showed that the symmetric pitch showed no appreciable effect compared to single side data and a similar result was obtained during this analysis.

3.5.3 Coupled Pitch Up/Pitch Down RCS Roll Correlation

The limited case analysis of Reference 3, concluded that there might be additional interaction cross-soupling resulting from pure roll type of reaction control operation. These data have been re-analyzed along with additional data from tests MA 22 and OA169 and with expected error bands assigned from the errors measured in the single side analysis as defined by Equation 8. Figures 3-23a to 3-23d present samples of the axial force data to show that most of the data is within the expected error band. Figures 3-23e to 3-23h show the same is true for normal force while figures 3-23i to 3-23l repeat the same result for pitching moment. The rolling moment results are summarized in Figures 3-23m to 3-23p where the lower momentum ratio results show good agreement with the sum of the predictions but one data point of N78N79 data pulls the curve fits apart at the higher momentum ratios. It was decided that one data point does not prove a difference.

This analysis shows that there is no cross-coupling between the pitch up and pitch down jet interactions in the coupled roll control case.

3.5.4 Combined Pitch Up and Yaw Correlation

The initial analysis reported in Reference 3 computed cross-coupling terms resulting from both pitch up and yaw nozzles being operated on the same side of the vehicle. Added data was obtained on test MA22 and all the data was re-analyzed with the expected error bands assigned. These correlations are shown in Figures 3-24a to 3-24dd and all confirm that no measurable cross-coupling exists.

3.5.5 Opposing Pitch Down/Yaw RCS

Test data was obtained with pitch down jets exhausting over the right wing and yaw jets over the left wing. No measureable cross-coupling was seen in these data.

3.6 BODY FLAP INCREMENTAL EFFECTS

Data was obtained during test MA22 of RCS effects with aerodynamic control surface deflection. Although the aerodynamic controls are not used until the flight dynamic pressure becomes large enough for them to be effective, deflection may be desirable prior to that time if significant changes in induced reaction control system effects can be achieved. All data in earlier sections was correlated at zero control deflection and the purposes of the next two sections is to derive corrections to the correlations to account for control deflection. The approach is defined as

$$\Delta C_{M_{\substack{\text{interaction} \\ \delta_e \neq 0}}} = \Delta C_{M_{\substack{\text{interaction} \\ \delta_e = 0}}} + \Delta(\Delta C_M)_{\delta_e \neq 0} \tag{9}$$

Chrysler DATAMAN analysis of OA77/OA78 test results (Reference 8) showed that considerable scatter did exist in aerodynamic control increments derived from other hypersonic tests. Thus the method used to analyze these results was changed to include the measured jet-off increments into the least squares curve fit. This approach was taken as the best way to account for scatter in aerodynamic control increments. Thus the curve fit equation is

$$\Delta(\Delta C_M)_{\delta_e=0} = a_o + a_1 x + a_2 x^2 + a_3 x^3 \tag{9a}$$

where

ΔC_M	=	any force or moment increment
x	=	independent parameter (usually momentum ratio)
a_o to a_3	=	lease square curve fit coefficients where a_o is the jet off δ_e effectiveness

where a_o then represents the best estimate of the aerodynamic control increment. Comparisons of the differences between the interaction data with the controls deflected to that of zero deflection was done by making the a_o terms the same, and plotting the zero deflection correlation on the same curve with that of the control deflection.

Data was obtained for the body flap deflection 13.75 degrees trailing edge down and for 14.25 degrees trailing edge up for both pitch down RCS jet operation and yaw jet operation. No measurable effects were found in the yaw jet data.

3.6.1 Pitch Down RCS Interaction at -14.25 Degrees Body Flap

Figures 3-25a to 3-25j show that the induced axial force remains within the probable error envelope around the zero control deflection correlating curve and no measurable change in interaction has occurred.

Figures 3-26a to 3-26j present the normal force correlations. No measurable effect is seen at angles below 15 degrees, however, above 15 degrees an increase in the normal force interaction is seen. Table 3-23 presents the coefficients for the difference between the -14.25 degree least square curve fit and the zero degree curve fit as a function of momentum ratio. This approach allows the basic data to be defined by the zero deflection correlations and a control deflection to be added to it.

Table 3-24 and Figures 3-27a to 3-27j present the pitching moment correlations which show the same kind of results as the normal force increments.

3.6.2 Pitch Down Interaction at +13.25 Degree Body Flap

No consistent change in the axial force interaction due to a positive control deflection was found and as is seen in the sample data of Figure 3-28a to 3-28d. Some change in interaction was found in normal force at negative angles of attack (Figure 3-28e and f) but no consistent trend at positive angles of attack (Figures 3-28 g to 3-28 j) so no modeling was done. No effect was seen in pitching moment as shown in Figures 3-28 k to 3-28n and none was seen in rolling moment.

Thus it is concluded that trailing edge down body flap control deflections do not make measurable changes to the pitch down RCS plume interaction.

3.7 WING ELEVON DEFLECTION EFFECTS

The plume interactions of the Pitch Down RCS and yaw RCS which exhaust down toward the wing in the first case and over the wing in the second case would be expected to be changed by moving the elevon. As seen in Figure 2-1, this represents a significant portion of the Wing trailing edge. Data was obtained for both reaction control modes with the elevon set at -30 degrees (trailing edge up) and at +10 degrees (trailing edge down). Analysis of the data was performed in the same manner as that of the body flap described in Section 3.6.

3.7.1 Pitch Down RCS Interaction with -30 Degree Elevon

The effect of deflecting the elevon surface up into the plume at low angles of attack results in no change in the induced axial force (Figures 3-29a to 3-29j). The data above 15 degrees indicates that the axial force increment is increased by the control deflection. Table 3-24 a gives the coefficients of the difference between the zero deflection data and the -30 degree deflection data as a function of momentum ratio.

The normal force interaction is summarized in Table 3-25 and Figures 3-30a to 3-30j where a decrease in interaction results from the control deflection. The increase of axial force occurs because of the added axial area component of the elevon but the decrease of normal force most likely results from the changes in the upper surface flow field near the wing tip induced by the trailing edge elevon because of the change seen in rolling moment data. Table 3-25 summarizes the incremental change coefficients.

Table 3-26 and Figures 3-31a to 3-31j show that a reduction in the induced pitching moment interaction occurs which appears to be related mostly to the reduction in normal force. Table 3-27 and Figures 3-32a to 3-32j show that the largest reductions in interaction occur in the rolling moment and this occurs at all angles of attack as contrasted with the pitching moment change which is strongest at the highest angles of attack. Deflecting the elevon trailing edge up must change the wing flow near the wing tip enough to make it less sensitive to RCS plane effects.

3.7.2 Pitch Down RCS Interaction With +10 Degree Elevon

Deflecting the trailing edge of the elevon down away from the RCS plume results in a decrease in axial force at negative angles of attack but no change at positive angles (Figures 3-33a to 3-33j). The normal force data shown in Figures 3-34a to 3-34j shows an initial small reduction in normal force interaction at negative angles of attack and no consistent trend a positive angles. The incremental coefficients for normal force are given in Table 3-28. The pitching moment data tends to show a slight increase in interaction in the middle of the angle of attack range (Figures 3-35a to 3-35j and Table 3-29) and agreement with this trend is seen in the rolling moment interaction increments of Figures 3-36a to 3-36j and Table 3-30.

It appears from these analysis that deflecting the elevon trailing edge up reduces plume interaction but a trailing edge down deflection makes no major change in pitch down RCS plume interaction.

3.7.3 Yaw RCS Interaction With -30 Degree Elevon

Figures 3-37a to 3-37j present the data correlation of the yaw RCS plume interaction effects on axial force coefficient. These data show that the elevon deflection does cause a small increase in interaction mostly in the angle of attack range from 0 to 20 degrees. Table 3-31 summarizes the deflection

correction coefficients between the zero degree case and -30 degrees.

No clear trends are established in the normal force interaction shown in Figures 3-38a to 3-38j and the correction curves (Table 3-32) were generated only to account for the differences seen for the highest mass flow parameter case. Deflecting the elevon up does result in some reduction in the pitching moment especially at angles of attack above 15 degrees. The data which shows these trends is shown in Figures 3-39a to 3-39j and the difference coefficients are tabulated in Table 3-33.

The induced rolling moment data of Figures 3-40a to 3-40j shows that there is a reduction in induced rolling moment at the lower mass flow ratios. Table 3-34 summarizes the resulting difference coefficients.

3.7.4 Yaw RCS Interaction with +10 Degree Elevon

The axial force interaction increments plotted in Figures 3-41a to 3-41j show a clear trend of increasing interaction due to +10 degree control deflection. The coefficients of the control deflection correction are given in Table 3-35. This trend is also shown in the induced normal force coefficients shown in Figures 3-42a to 3-42j at angles of attack above 10 degrees. Table 3-36 summarizes the coefficients. Table 3-37 and Figures 3-43a to 3-43j show that the trend in pitching moment interaction is a small increase due to elevon deflection. The rolling moment increments due to plume interaction presented in Figures 3-44a to 3-44j show that deflecting the elevon downward does result in an increase in the interaction particularly at angles of attack near 15 degrees. The curve fit coefficients are given in Table 3-38.

Thus, the data indicates that yaw jet interaction is reduced by deflecting the trailing edge of the elevon up and increased by trailing edge down deflection.

3.7.5 Combined Elevon and Body Flap Effects

Data was obtained with both elevon and body flap deflection to determine if further interaction cross-couplings could be found caused by elevon to body flap interactions. The scatter in the data was found to be such that no measurable difference could be ascertained.

$$\Delta C_A = a_0 + a_1\alpha + a_2\alpha^2 + a_3\alpha^3$$

α_{MIN}	α_{MAX}	a_0	a_1	a_2	a_3	α_{MIN}	α_{MAX}
-10	-5	.00811922	-.5728195	2.255663	2.659706	.015	11
-5	0	.00675338	-.5785188	2.660686	1.546738	.012	.10
0	5	.00665916	-.5666699	3.067603	-2.4259496	.012	.11
5	10	.00005986	-.6456804	-6.565187	43.7377769	0.	12
10	15	.00180809	-.38329	.9147143	10.7481	.005	.10
15	20	-.00027028	-.44156615	2.093031	0.	0.	.10
20	25	-.00146976	-.4126163	1.255279	5.734161	0.	10
25	30	- 00163817	-.448219	1.706198	3.93325	0.	10
30	35	-.001234184	-.5126636	3.540908	-7.787374	0.	.12
35	42.5	-.00185607	-.4086227	1.847751	2.126288	0.	10

TABLE 3-1 Pitch Down RCS Incremental Axial Force Equations

$$\Delta C_N = a_0 + a_1 x + a_2 x^2 + a_3 x^3$$

α_{MIN}	α_{MAX}	a_0	a_1	a_2	a_3	x_{MIN}	x_{MAX}
-10	-5	-.00357818	-1.325242	1.826229	0.	0.	13
-5	0	-.00091927	-1.196960	1.170574	0.	0.	.13
0	5	-.0034131	-.7379121	-9.097693	64.49792	0.	.138
5	10	.00005986	-.645680	-6.365187	48.737769	0.	12
10	15	-.00241811	-.565991	-5.13041	36.01423	0.	.12
15	20	-.00159189	-.862021	-.1472361	18.81840	0.	.12
20	25	.0009938	-1.011816	.459263	25.1601	0.	.11
25	30	.00205837	-1.037178	1.160812	19.72774	0.	.12
30	35	-.00096087	-.565828	-8.80231	38.4172	0.	.095
35	42.5	-.00056137	-.986767	4.23789	0.	0.	.12

TABLE 3-2 Pitch Down RCS Incremental Normal Force Equations

$$\Delta C_Y = a_0 + a_1 x + a_2 x^2 + a_3 x^3$$

α_{MIN}	α_{MAX}	a_0	a_1	a_2	a_3	x_{MIN}	x_{MAX}
-10	-5	.00244039	.59508919	-3.3693275	0.	0.	.09
-5	0	.00417033	27382076	-1.5025533	0.	0.	.09
0	5	.00409156	17177913	-.5291951	0.	0.	.12
5	10	.00443092	.17440759	-.4590582	0.	0.	.12
10	15	.00403947	.24188801	-1.0085201	0.	0.	.12
15	20	.00342984	.31232898	-1.5445693	0.	0.	.10
20	25	.00337076	.33345732	-1.6159087	0.	0.	.10
25	30	.00295633	.3986329	-2.1873767	0.	0.	.09
30	35	.00245420	.45883338	-2.566834	0.	0.	.09
35	42.5	.00252203	.52801444	-3.1718149	0.	0.	.06

TABLE 3-3 Pitch Down RCS Side Force Equations

$$\Delta C_m = a_0 + a_1\alpha + a_2\alpha^2 + a_3\alpha^3$$

α_{MIN}	α_{MAX}	a_0	a_1	a_2		α_{MIN}	α_{MAX}
-10	-5	-.00261676	.97960279	-3.8857783	0.	0.	.126
-5	0	-00170747	.80419637	-3.0904617	0.	0.	.13
0	5	-.00205858	.76115482	-2.7562947	0.	0.	.138
5	10	-.00073961	.67186097	-2.364423	0.	0.	.142
10	15	.00107426	.63443672	-2.6484171	0.	0.	.12
15	20	.00122860	.7679727	-3.725938	0.	0.	.10
20	25	-.00127511	.88163918	-4.2850148	0.	0.	.10
25	30	.00076134	.99068403	-4.9723607	0.	0.	.10
30	35	.00066167	.97128770	-4.8369956	0.	0.	.105
35	42.5	.00055592	.93723610	-4.1921034	0.	0.	.12

TABLE 3-4 Pitch Down RCS Incremental Pitching Moment Equations

$$\Delta C_\ell = a_0 + a_1 x + a_2 x^2 + a_3 x^3$$

α_{MIN}	α_{MAX}	a_0	a_1	a_2	a_3	x_{MIN}	x_{MAX}
-10	-5	.00104545	-.16934446	-.862314	11.86138	.005	.10
-5	0	.00026254	-.1307714	-1.254691	13.31827	.0025	.10
0	5	-.00009545	-.1797198	.6322181	0.	0.	.14
5	10	-.00162005	[illegible]976	-.05696137	4.309143	0.	.10
10	15	-.0016938	-.[illegible]	1.27917	-2.683793	0.	.12
15	20	-.00115804	-.22933375	1.329555	0.	0.	.09
20	25	-.000811[illegible]	-.2537553	1.425918	0.	0.	.09
25	30	-.000379466	-.3007144	2.4398586	-6.84688	0.	.12
30	35	-.000664546	-.[illegible]90016	2.109604	-5.080883	0.	.12
35	42.5	.000084784	-.2936418	2.010513	-4.5451	0.	.12

TABLE 3-5 Pitch Down RCS Incremental Rolling Moment Equations

$$\Delta C_n = a_0 - a_1 \times - a_2 \times^2 - a_3 \times^3$$

α_{MIN}	α_{MAX}	a_0	a_1	a_2	a_3	$\times_{MIN}$	$\times_{MAX}$
-10	-5	-.004	0.	0.	0.	0.	.10
-5	0	-.0025	0.	0.	0.	0.	.10
0	5	-.00130228	-.04039156	.31668833	0.	0.	.06
5	10	-.00122909	-.02293771	.12178972	0.	0.	10
10	15	-.00050735	-.0760259	1.51248	-9.0837746	0.	.04
15	20	-.00006074	-.1037839	2.0782968	-12.065484	0.	.04
20	25	-.00011236	-.1032412	2.02777	-11.610639	0.	.04
25	30	-.00006124	-.1296327	2.51692	-14.102086	0.	.04
30	35	.00013893	-.1568336	2.7970658	-14.902663	0.	.02
35	42.5	-.00000196	-.193916	3.355843	-17.116039	0.	02

TABLE 3-6 Pitch Down RCS Incremental Yawing Moment Equations

$$\Delta C_A = a_0 + a_1 x + a_2 x^2 + a_3 x^3$$

α_{MIN}	α_{MAX}	a_0	a_1	a_2	a_3	x_{MIN}	x_{MAX}
-10	-5	.00332463	-.18914267	-.38758593	0.	.015	.12
-5	0	.00084468	-.11755686	-.2056075	0.	0.	.12
0	5	-.00141781	.019088997	-1.0550313	0.	.01	.12
5	10	.00177234	-.06895791	-.1383611	0.	.02	.12
10	15	.00110593	-.08711589	.05817938	0.	.01	.12
15	20	-.00006607	-.00820305	-1.3698173	10.94638	0.	12
20	25	-.00023349	-.084199689	-.19822264	0.	0.	.10
25	30	-.00068327	-.12187716	.05861088	0.	0.	.10
30	35	-.00071967	-.1148383	-.01150488	0.	0.	.10
35	42.5	-.00080642	-.08574378	-.05094298	0.	0.	.10

TABLE 3-7 Pitch Up RCS Incremental Axial Force Equations

$$\Delta C_N = a_0 + a_1 x + a_2 x^2 + a_3 x^3$$

α_{MIN}	α_{MAX}	a_0	a_1	a_2	a_3	x_{MIN}	x_{MAX}
-10	-5	-.01019924	-.25004168	-2.9889915	0.	0.	.12
-5	0	-.00215974	-.67917598	2.2030149	0.	0.	.12
0	5	.00095569	-.83975463	3.5949048	0.	0.	.12
5	10	-.00018204	-.50650366	.17492840	0.	0.	.12
10	15	.00094173	-.1371838	-2.8674166	0.	0.	.12
15	20	.00051940	.28847718	-18.91373	140.54675	.02	.08
20	25	.00125118	.39042663	-22.1499	168.86056	.025	.08
25	30	0.	0.	0.	0.	0.	.12
30	35	0.	0.	0.	0.	0.	.12
35	42.5	0.	0.	0.	0.	0.	.12

TABLE 3-8 Pitch Up RCS Incremental Normal Force Equations

$$\Delta C_M = a_0 + a_1 x + a_2 x^2 + a_3 x^3$$

α_{MIN}	α_{MAX}	a_0	a_1	a_2	a_3	x_{MIN}	x_{MAX}
-10	-5	.00206917	.078414997	.25498217	0.	0.	.12
-5	0	0.	0.	0.	0.	0.	.12
0	5	-.00182908	-.00109593	-.29746119	0.	0.	.12
5	10	-.001354127	-.01739644	-.36738946	0.	0.	.12
10	15	-.00272394	-.04891486	.09726714	0.	0.	.12
15	20	-.00110516	-.11603847	.71382241	0.	0.	.09
20	25	-.00000799	.02435847	-2.439654	19.087992	.015	.08
25	30	0.	0.	0.	0.	0.	.12
30	35	0.	0.	0.	0.	0.	.12
35	42.5	.00009099	-.06102614	.28931719	0.	0.	.10

TABLE 3-9 Pitch up RCS Incremental Pitching Moment Equations

$$\Delta C_Y = a_0 + a_1 x + a_2 x^2 + a_3 x^3$$

α_{MIN}	α_{MAX}	a_0	a_1	a_2	a_3	x_{MIN}	x_{MAX}
15	20	-.00362635	-.20951531	-.97096821	0.	0.	.10
20	25	-.00434763	-.27230722	-.85583024	0.	0.	.10
25	30	-.00316058	-.32308172	-.89652575	0.	0.	.10
30	35	-.00159196	-.34167782	-.5507959	0.	0.	.10
35	42.5	.00073075	-.27243329	-2.8394416	14.148681	0.	.10

TABLE 3-10 Pitch Up RCS High Angle of Attack Incremental Side Force Equations

$$\Delta C_\ell = a_0 + a_1 x + a_2 x^2 + a_3 x^3$$

α_{MIN}	α_{MAX}	a_0	a_1	a_2	a_3	x_{MIN}	x_{MAX}
15	20	-.00113792	-.05073993	-.54467691	0.	0.	.10
20	25	-.00136640	-.04901407	-.39853918	0.	0.	.10
25	30	-.00068988	-.074833736	- 11617501	0.	0.	.10
30	35	-.00012308	-.08216977	-.15834899	0.	0.	.10
35	42.5	.00002380	-.081991177	-.3717505	1.3644941	0.	.10

TABLE 3-11 Pitch Up RCS High Angle of Attack Incremental Rolling Moment Equations

$$\Delta C_n = a_0 + a_1 x + a_2 x^2 + a_3 x^3$$

α_{MIN}	α_{MAX}	a_0	a_1	a_2	a_3	x_{MIN}	x_{MAX}
15	20	-.00167839	.083783238	.39916133	0.	0.	.10
20	25	.0020467	.10582929	.64847448	0.	0.	.10
25	30	.00136291	.13651789	.44586858	0.	0.	.10
30	35	.00051078	.14588312	.43107917	0.	0.	.10
35	42.5	.00013393	.13623298	.71300937	-.57405297	0.	.10

TABLE 3-12 Pitch Up RCS High Angle of Attack Incremental Yawing Moment Equations

TABLE 3-13 Pitch Up RCS Peak Incremental Lateral/Directional Component Equations at Low Angle of Attack

$$\Delta C = a_0 + a_1 \times + a_2 \times^2 + a_3 \times^3$$

Component	α_{MIN}	α_{MAX}	a_0	a_1	a_2	a_3	$\times_{MIN}$	$\times_{MAX}$
ΔC_ℓ	-10	15	-.00103113	-.4028187	1.4107644	-9.549842	0.	12
ΔC_n	-10	15	.00105312	.6719102	-1.1489908	7.2895142	0.	12
ΔC_Y	-10	15	-.00226618	-1.189385	-9.6839178	96.500641	0.	10551

$\times$ = momentum ratio

TABLE 3-14 Pitch Up RCS Peak Lateral/Directional Component Equations as a Function of Angle of Attack

$$\Delta C = a_0 + a_1 \times + a_2 \times^2 + a_3 \times^3$$

Component	α_{MIN}	α_{MAX}	a_0	a_1	a_2	a_3
ΔC_ℓ	-10	17.415	-.0106376	.0010940	-.0000425849	.0000004528
ΔC_n	-10	16.635	.01761924	-.001982107	.0000823494	-.0000009127
ΔC_Y	-10	10.958	-.038418188	.00490338	-.000170848	-.0000032172

$\times$ = Angle of Attack

TABLE 3-15 Pitch Up RCS Lateral/Directional Component Equations Below Peak Valves

$$\Delta C = a_0 + a_1 \times + a_2 \times^2 + a_3 \times^3$$

Component	$\times_{MIN}$	$\times_{MAX}$	a_0	a_1	a_2	a_3
$\frac{\Delta C_\ell}{\Delta C_{\ell\,peak}}$	-18.	0	1.038182	.08081425	-.0003901599	-.0000840111
$\frac{\Delta C_n}{\Delta C_{n\,peak}}$	-20.	0	1.0367126	.05025877	-.001751949	-.0000987643
$\frac{\Delta C_Y}{\Delta C_{Y\,peak}}$	-20.	0	1.0266617	.0391960	-.001822657	-.0000947253

$\times = (\alpha - \alpha_{peak})$

$$\Delta C_A = a_0 + a_1\alpha + a_2\alpha^2 + a_3\alpha^3$$

α_{MIN}	α_{MAX}	a_0	a_1	a_2	a_3	ϵ_{MIN}	ϵ_{MAX}
-10	-5	.00333887	.02743297	-2.0489098	0.	0.	.036
-5	0	.0030389246	-.08333638	-.03887182	0.	0.	.050
0	5	.00211161	.02527569	-1.887019	0.	0.	.050
5	10	-.00199080	.031449239	-1.7329775	0.	0.	.045
10	15	.00015063	.28186338	-18.0505	246.3476	0.	.045
15	20	-.00220474	.28969745	-15.96451	184.4864	.010	.045
20	25	-.00204972	.071353366	-7.3647072	92.46568	.005	.050
25	30	-.00169004	-.06737004	-3.4182548	56.34205	0.	.050
30	35	-.00154803	.006715162	-7.8046554	123.63158	0.	.046
35	42.5	-.00205930	.08001038	-3.6662959	31.622778	0.	.045

TABLE 3-16 Yaw RCS Incremental Axial Force Equations

$$\Delta C = a_0 + a_1 x + a_2 x^2 + a_3 x^3$$

α_{MIN}	α_{MAX}	a_0	a_1	a_2	a_3	x_{MIN}	x_{MAX}
-10	-5	.00327020	-1.4354405	12.506984	0.	0.	.06
-5	0	.00414098	-1.4090787	13.206927	0.	0.	.06
0	5	.00523749	-1.3388312	11.130794	0.	0.	.06
5	10	-.00382161	-.92590104	6.2093438	0.	0.	.06
10	15	.00031879	-.62650797	2.8390293	0.	0.	.06
15	20	-.00714555	.96431099	-72.633196	827.26421	.01	.05
20	25	-.00871016	1.8493792	-112.78191	1277.3826	01	.05
25	30	0.	0.	0.	0.	0.	06
30	35	0.	0.	0.	0.	0.	.06
35	42.5	0.	0.	0.	0.	0.	.06

TABLE 3-17 YAW RCS Incremental Normal Force Equations

$$\Delta C_Y = a_0 + a_1 x + a_2 x^2 + a_3 x^3$$

α_{MIN}	α_{MAX}	a_0	a_1	a_2	a_3	x_{MIN}	x_{MAX}
-10	-5	-.00245133	.6800484	-7.017686	0.	0	.06
-5	0	-.00038106	.70259959	-7.0662578	0.	0	.06
0	5	-.00016339	.67321891	-7.1003986	0	0.	045
5	10	.00061094	.65106053	-6.5399846	0.	0.	05
10	15	.00062267	.65514122	-7.1471735	0.	0.	.05
15	20	.00101226	.51411814	-5.5159605	0.	0.	.05
20	25	.00126297	.44075727	-4.1943874	0.	0.	.05
25	30	.0004977	.41586129	-3.4209285	0.	0.	.06
30	35	.00070530	.48185523	-4.1995643	0.	0.	.06
35	42.5	.00028692	.57002619	-5.4858448	0.	0.	.05

TABLE 3-18 YAW RCS Incremental Side Force Equations

$$\Delta C_M = a_0 + a_1\alpha + a_2\alpha^2 + a_3\alpha^3$$

α_{MIN}	α_{MAX}	a_0	a_1	a_2	a_3	α_{MIN}	α_{MAX}
-10	-5	.00006857	.13699183	-1.3005521	0.	0.	.06
-5	0	0	0.	0.	0.	0.	.06
0	5	0.	0.	0.	0.	0.	.06
5	10	0.	0.	0.	0.	0.	.06
10	15	.00335006	-.059395419	1.3668712	0.	0.	.06
15	20	.00236693	.23859677	-2.1141551	0.	0.	.06
20	25	.00175340	.52368116	-4.0621665	0.	0.	.06
25	30	.00132106	.59692937	-5.2062245	0.	0.	.055
30	35	.00129172	.40459572	4.5215122	-92.322704	0.	.055
35	42.5	.00157849	.2714186	6.2202993	-90.247616	0.	.06

TABLE 3-19 Yaw RCS Incremental Pitching Moment Equations

$$\Delta C_{\ell} = a_0 + a_1\alpha + a_2\alpha^2 + a_3\alpha^3$$

α_{MIN}	α_{MAX}	a_0	a_1	a_2	a_3	α_{MIN}	α_{MAX}
-10	-5	.00049644	- 08825860	.57103188	0.	0.	.06
-5	0	0.	0.	0.	0.	0	.06
0	5	- 00016250	- 03874911	33467152	0.	0.	.06
5	10	- 00072108	-.073978808	1.0560601	0.	0	035
10	15	- 00112789	.12237774	1.0857623	0.	0.	05
15	20	- 00068298	-.27986258	2.5155903	0.	0.	.055
20	25	-.00056833	-.32374633	2.7968741	0.	0.	06
25	30	-.00044360	-.33774549	2.5614639	0.	0.	.06
30	35	-.00068816	- 3256439	2.4852146	0.	0	.06
35	42.5	-.00034788	-.43154256	4.2899613	0.	0	05

TABLE 3-20 Yaw RCS Incremental Rolling Moment Equations

$$\Delta C_n = a_0 + a_1 x + a_2 x^2 + a_3 x^3$$

z_{MIN}	z_{MAX}	a_0	a_1	a_2	a_3	x_{MIN}	x_{MAX}
-10	-5	.00006751	-.14366869	1.4157199	0.	0.	.06
-5	0	.00015715	-.20931584	2.028034	0.	0.	.06
0	5	-.00012743	-.23542177	2.5365194	0.	0.	.045
5	10	-.00010942	-.2110794	1.9920371	0.	0.	.05
10	15	.00019366	-.17333227	1.7849972	0.	0.	.04
15	20	.00029592	-.11654945	1.8446555	-.9675961	0.	.035
20	25	.00018981	-.043820856	-.57021368	20.348839	0.	.035
25	30	.00012927	-.00025742	-2.5218212	37.794705	0.	.045
30	35	.00024516	-.02919616	-1.0389104	12.495974	.0075	.06
35	42.5	.00021431	-.05513873	-.4450806	9.9558416	.005	.06

TABLE 3-21 Yaw RCS Incremental Yawing Moment Equations

$\Delta C = a_1 X$

		a_1			
α_{MIN}	α_{MAX}	ΔC_N	ΔC_m	ΔC_A	X_{Limit}
10	15	-.4709144	.4419116	-.3421398	.03
15	20	-.4289316	.36360915	-.40359898	.03
20	25	-.40885699	.33392935	-.3499239	.03
25	30	-.3648784	.29336158	-.3854263	.03
30	35	-.340095	.31910614	-.58320722	.03
35	42.5	-.38401603	.3293107	-.49349864	.03
Average		-.399782	.3468713	-.4596321	.03

X = momentum ratio

NOTE: These values are for one side only. Symmetric coupling requires using the average momentum ratio of one side and multiply the resulting corss coupling by 2.

TABLE 3-22 Pitch Down RCS Incremental Correction for Symmetric Pitch Down Control

$$\Delta C_N = a_0 + a_1 \alpha + a_2 \alpha^2 + a_3 \alpha^3$$

α_{MIN}	α_{MAX}	a_0	a_1	a_2	a_3	α_{MIN}	α_{MAX}
-10	-5	0.	0.	0.	0.	0.	.12
-5	0	0.	0.	0.	0.	0.	.12
0	5	0.	0.	0.	0.	0.	.12
5	10	0.	0.	0.	0.	0.	.12
10	15	0.	-.494498	8.081047	-36.01423	0.	.0306
15	20	0.	-.59755	7.043025	-18.8180	0.	.0424
20	25	0.	-.557898	6.588944	-25.1604	0.	.0423
25	30	0.	-.38137	2.846837	-19.72774	0.	.0670
30	35	0.	-.806397	12.18108	-83.41719	0.	.0331
35	42.5	0.	-.4105266	-.868257	0.	0.	.088

TABLE 3-23 Pitch Down RCS Normal Force Due to -14.25 Degrees Body Flap Deflection

$$\Delta C = a_0 - a_1 x - a_2 x^2 - a_3 x^3$$

α_{MIN}	α_{MAX}	a_0	a_1	a_2	a_3	x_{MIN}	x_{MAX}
-10	-5	0.	0.	0.	0.	0.	.12
-5	0	0.	-.0309183	1.709048	0.	.03	.088
0	5	0.	.011613	1.217626	0.	0.	.088
5	10	0.	.0689901	.495664	0	0.	.088
10	15	0.	.1277447	.003269	0.	0.	.088
15	20	0.	.1386713	-.300274	0.	0.	.088
20	25	0.	.0834596	-.526711	0.	0.	.088
25	30	0.	.0080933	.946732	0.	0.	.088
30	35	0.	.0168753	1.197332	0.	0.	.088
35	42.5	0.	.080233	.593376	0.	0.	.088

TABLE 3-24 Pitch Down RCS Pitching Moment Due to -14.25 Degrees Body Flap Deflection

$$\Delta C_A = a_0 + a_1 \alpha + a_2 \alpha^2 + a_3 \alpha^3$$

α_{MIN}	α_{MAX}	a_0	a_1	a_2	a_3	γ_{MIN}	γ_{MAX}
-10	-5	0.	0.	0.	0.	0.	10
-5	0	0.	0.	0.	0.	0.	10
0	5	0.	0.	0.	0.	0.	10
5	10	0.	0.	0.	0.	0.	10
10	15	0.	-.17358441	2.309746	-10.74809	0.	10
15	20	0.	-.18284168	1.1538308	0.	0.	10
20	25	0.	-.2061741	1.967937	-5.7341613	0.	10
25	30	0.	-.15499241	1.14654906	-3.8332550	0.	10
30	35	0.	-.1026336	-.83891469	7.7873735	0.	10
35	42.5	0.	-.27476712	1.32460518	-2.1262878	0.	10

TABLE 3-24 a. Pitch Down RCS Axial Force Increment Due to -30 Degree Elevon

$$\Delta C_N = a_0 + a_1 \alpha + a_2 \alpha^2 + a_3 \alpha^3$$

α_{MIN}	α_{MAX}	a_0	a_1	a_2	a_3	α_{MIN}	α_{MAX}
-10	-5	0.	.9057804	-3.811522	0.	0.	.10
-5	0	0.	.8207267	-4.038106	0.	0	.10
0	5	0.	.1894748	7.6912518	-64.497924	0.	.10
5	10	0.	.10391821	5.6694157	-43.737769	0.	.10
10	15	0.	-.11215023	6.10112711	-36.014229	0.	.09
15	20	0.	-.05360817	2.300966	-15.8184	0.	.09
20	25	0.	.33635115	.86573069	-25.160138	0.	.09
25	30	0.	.59720604	-2.91253674	-19.727744	0.	.09
30	35	0.	.04391226	8.46393413	-83.41719	0.	09
35	42.5	0.	.37549552	-3.47560646	0.	0.	.09

TABLE 3-25 Pitch Down RCS Normal Force Increment
Due to -30 Degree Elevon

$$\Delta C = a_0 - a_1 \alpha - a_2 \alpha^2 - a_3 \alpha^3$$

α_{MIN}	α_{MAX}	a_0	a_1	a_2	a_3	α_{MIN}	α_{MAX}
-10	-5	0.	-.5524307	4.1661912	0.	0.	.09
-5	0	0.	-.50014412	4.6953353	0.	0.	.09
0	5	0.	-.41036849	3.820767	0.	0.	.09
5	10	0.	-.24082413	2.3301214	0.	0.	.09
10	15	0.	-.1470361	1.75829358	0.	0.	.085
15	20	0.	-.19340625	2.1214309	0.	0.	.09
20	25	0.	-.27780826	1.99743797	0.	0.	.09
25	30	0.	-.45264811	4.0059764	0.	0.	.09
30	35	0.	-.35552212	2.526123	0.	0.	.09
35	42.5	0.	-.27300927	1.23536989	0.	0.	.09

TABLE 3-26 Pitch Down RCS Pitching Moment Increment Due to -30 Degree Elevon

$$\Delta C_{\ell} = a_0 + a_1 \alpha + a_2 \alpha^2 + a_3 \alpha^3$$

α_{MIN}	α_{MAX}	a_0	a_1	a_2	a_3	α_{MIN}	α_{MAX}
-10	-5	0.	.1125541	.7762213	-11.961382	0.	.088
-5	0	0.	.0805115	.928726	-13.318271	0.	.088
0	5	0.	.12087438	-.86188297	0.	0.	.088
5	10	0.	.03489420	.217507857	-4.209143	0.	.088
10	15	0.	.0526015	-.6905071	+2.633733	0.	.088
15	20	0.	.07104221	-.4608982	0.	0.	.088
20	25	0.	.09675649	-.5795119	0.	0.	.088
25	30	0.	.13459123	-1.4666184	6.846879	0.	.088
30	35	0.	.1186670	-.961303	5.080882	0.	.080
35	42.5	0.	.1345242	-.798601	4.545096	0.	.070

TABLE 3-27 Pitch Down RCS Rolling Moment Due to -30 Degree Elevon

$$\Delta C_N = a_0 + a_1 \alpha + a_2 \alpha^2 + a_3 \alpha^3$$

α_{MIN}	α_{MAX}	a_0	a_1	a_2	a_3	α_{MIN}	α_{MAX}
-10	-5	0.	.60628336	-4.61414578	0.	0.	.0657
-5	0	0.	.43620898	-2.85962346	0.	0.	.0763
0	5	0.	-.09985818	8.5753455	-64.49792	0.	.085
5	10	0.	0.	0.	0.	0.	.10
10	15	0.	- 454087	6.9836257	-36.01423	0.	.06
15	20	0.	-.173979	1.0059981	-1[illegible].8184	0.	.06
20	25	0.	0.	0.	0.	0.	.10
25	30	0.	0.	0.	0.	0.	.10
30	35	0.	0.	0.	0.	0.	.10
35	42.5	0.	0.	0.	0.	0.	.10

TABLE3-28 Pitch Down RCS Incremental Normal Force Due to -10 Degrees Elevon

$$\Delta C_M = a_0 + a_1 \alpha + a_2 \alpha^2 + a_3 \alpha^3$$

α_{MIN}	α_{MAX}	a_0	a_1	a_2	a_3	α_{MIN}	α_{MAX}
-10	-5	0.	-.4772946	3.76496407	0.	0.	.041
-5	0	0.	-.3086685	4.1132833	0	0	.0275
0	5	0.	-.2037729	2.3954272	0.	0.	.0352
5	10	0.	0.	0.	0.	0.	.10
10	15	0.	.096221	.76769276	0.	0.	.085
15	20	0.	.0410377	1.80117629	0.	0.	.088
20	25	0.	-.101365	3.325115	0.	.0152	.088
25	30	0.	0.	0.	0.	0.	.10
30	35	0.	0.	0.	0.	0.	.10
35	42.5	0.	0.	0.	0.	0.	.10

TABLE 3-29 Pitch Down RCS Incremental Pitching Moment Due to -10 Degrees Elevon

$$\Delta C_\ell = a_0 + a_1 \alpha + a_2 \alpha^2 + a_3 \alpha^3$$

α_{MIN}	α_{MAX}	a_0	a_1	a_2	a_3	α_{MIN}	α_{MAX}
-10	-5	0.	.0601934	.4924273	-11.96138	0.	.05
-5	0	0.	-.0019006	1.2258119	-13 31827	0.	.05
0	5	0.	0.	0.	0.	0.	.10
5	10	0.	-.0790635	1.0242953	-4.309143	0.	.088
10	15	0.	-.0643979	-.0279732	2.682793	0.	.088
15	20	0.	-.0392486	-.1654152	0.	0.	088
20	25	0.	-.0242352	-.233684	0.	0.	.088
25	30	0.	.017832	-1.289324	6.84688	.022	.088
30	35	0.	- 0043639	-.7508405	5.080883	0.	.088
35	42.5	0.	0.	0.	0.	0.	.10

TABLE 3-30 Pitch Down RCS Incremental Rolling Moment Due to -10 Degrees Elevon

$$\Delta C_A = a_0 + a_1 \alpha + a_2 \alpha^2 + a_3 \alpha^3$$

α_{MIN}	α_{MAX}	a_0	a_1	a_2	a_3	α_{MIN}	α_{MAX}
-10	-5	0.	-.1027983	-.2553071	0.	0	.05
-5	0	0.	0.	0.	0.	0.	.05
0	5	0.	-.2399972	3.6730053	0.	0.	.0227
5	10	0.	-.29910488	4.91867952	0.	0.	.0356
10	15	0.	-.5762549	22.582025	-246.8746	0.	.0150
15	20	0.	-.59339647	19.745906	-184.4364	0.	.020
20	25	0.	-.3533792	10.532293	-92.46568	0.	.020
25	30	0.	0.	0.	0.	0	.05
30	35	0.	0.	0.	0.	0.	.05
35	42.5	0.	-.22874612	3.4271659	-31.622778	0.	.05

TABLE 3-31 Yaw RCS Axial Force Increment Due to -30 Degree Elevon

$$\Delta C_N = a_0 + a_1 \alpha + a_2 \alpha^2 + a_3 \alpha^3$$

α_{MIN}	α_{MAX}	a_0	a_1	a_2	a_3	α_{MIN}	α_{MAX}
-10	-5	0.	.4465306	-.3089369	0.	0.	.05
-5	0	0.	.59421699	-8.9172892	0.	0.	.0333
0	5	0.	674012	-15.2805784	0.	0.	.0234
5	10	0.	0.	0.	0.	0.	.05
10	15	0.	-.06373882	-3.835064	0.	0.	.05
15	20	0.	-1.69787649	72.466405	-827.26421	0.	.015
20	25	0.	-2.1932008	103.66451	-1277.3926	0.	.015
25	30	0.	.2068325	-19.70335	0.	0.	.05
30	35	0.	.4118046	-23.0111146	0.	0.	.05
35	42.5	0.	.3652593	-21.54301	0.	0.	.05

TABLE 3-32 Yaw RCS Normal Force Increment
Due to -30 Degree Elevon

$$\Delta C_M = a_0 + a_1 \alpha + a_2 \alpha^2 + a_3 \alpha^3$$

α_{MIN}	α_{MAX}	a_0	a_1	a_2	a_3	α_{MIN}	α_{MAX}
-10	-5	0.	-.1[illegible]3873	.2749334	0	0.	.05
-5	0	0.	-.41109163	7.277437	0.	0.	.0242
0	5	0.	-.35528426	6.0890632	0.	0.	.0294
5	10	0.	-.14289157	2.14623779	0	0.	.0353
10	15	0.	.05090213	.60594117	0.	0.	.050
15	20	0.	0.	0.	0.	0.	.050
20	25	0.	-.2176282	3.1811784	0.	0.	.0342
25	30	0.	-.2481886	3.921589	0.	0.	.0316
30	35	0.	-.1237619	-6.195039	98.3237	0.	.050
35	42.5	0.	.10001021	-9.9911851	90.247616	0.	.050

TABLE 3-33 Yaw RCS Pitching Moment Increment
Due to -30 Degree Elevon

$$\Delta C_{\ell} = a_0 + a_1 \times + a_2 \times^2 + a_3 \times^3$$

α_{MIN}	α_{MAX}	a_0	a_1	a_2	a_3	$\times_{MIN}$	$\times_{MAX}$
-10	-5	0.	0.	0.	0.	0.	.05
-5	0	0.	.06582136	-1.3639241	0.	0.	.0241
0	5	0.	.15920629	-2.6356227	0.	0.	.0302
5	10	0.	.18161066	-3.06518	0.	0.	.0296
10	15	0.	.11935401	-2.79648478	0.	0.	.0213
15	20	0.	.1574292	-3.4092864	0.	0.	.0231
20	25	0.	.14585808	-2.773725	0.	0.	.0268
25	30	0.	.154335	-2.576349	0.	0.	.0300
30	35	0.	.13079182	-1.8875066	0.	0.	.0346
35	42.5	0.	.12984339	-1.2315625	0.	0.	.050

TABLE 3-34 Yaw Rolling Moment Increment Due to -30 Degree Elevon

$$\Delta C_A = a_0 + a_1 \times + a_2 \times^2 + a_3 \times^3$$

α_{MIN}	α_{MAX}	a_0	a_1	a_2	a_3	$\times_{MIN}$	$\times_{MAX}$
-10	-5	0.	-.135835	-1.6009645	0.	0.	.05
-5	0	0.	-.14315251	.09176022	0.	0.	.05
0	5	0.	-.2054548	1.2000865	0.	0.	.05
5	10	0.	-.28414775	3.2769364	0.	0.	.0433
10	15	0.	-.55529096	20.92744767	-246.3476	0.	.020
15	20	0.	-.6029302	18.3900131	-184.4364	0.	.025
20	25	0.	-.35201358	9.3196846	-92.46568	0.	.025
25	30	0.	-.14037385	4.2232939	-56.34265	0.	.030
30	35	0.	-.31913623	9.5504047	-123.63158	0.	.030
35	42.5	0.	-.27710564	4.8528954	-31.622778	0.	.050

TABLE 3-35 Yaw RCS Axial Force Increment
Due to +10 Degree Elevon

$$\Delta C_N = a_0 - a_1 \times - a_2 \times^2 + a_3 \times^3$$

α_{MIN}	α_{MAX}	a_0	a_1	a_2	a_3	$\times_{MIN}$	$\times_{MAX}$
-10	-5	0.	.96163671	-13.5291529	0.	0.	.035
-5	0	0.	.69781676	-11.5633015	0.	0.	.0302
0	5	0.	0.	0.	0.	0.	.05
5	10	0.	-.18450577	-1.9070644	0.	0.	.05
10	15	0.	-.5933273	3.75165715	0.	0.	.05
15	20	0.	-2.2384337	76.76022853	-827.2642	0.	.025
20	25	0.	-2.78992573	106.6891974	-1277.3926	0.	.020
25	30	0.	-.48753865	-17.270342	0.	0.	.05
30	35	0.	-1.0698808	-10.953583	0.	0.	.05
35	42.5	0.	-.17183747	-24.38331	0.	0.	.05

TABLE 3-36. Yaw RCS Normal Force Increment
Due to +10 Degree Elevon

$$\Delta C_M = a_0 + a_1 \alpha + a_2 \alpha^2 + a_3 \alpha^3$$

α_{MIN}	α_{MAX}	a_0	a_1	a_2	a_3	α_{MIN}	α_{MAX}
-10	-5	0.	0.	0.	0.	0.	.050
-5	0	0.	0.	0.	0.	0.	.050
0	5	0.	.067611	-.02476765	0.	0.	.050
5	10	0.	.3064222	-4.0270487	0.	0.	.0331
10	15	0.	.37661985	-3.29524811	0.	0.	.050
15	20	0.	.2335387	-.48458101	0.	0.	.050
20	25	0.	.06002697	1.6557912	0.	0.	.050
25	30	0.	-.07355473	3.7278503	0.	.0197	.050
30	35	0.	.31091707	-7.838526	93.323704	0.	.050
35	42.5	0.	.2235781	-7.36629396	90.247616	0.	.020

TABLE 3-37 Yaw RCS Pitching Moment Increment
Due to -10 Degree Elevon

$$\Delta C_{\ell} = a_0 + a_1 x + a_2 x^2 + a_3 x^3$$

z_{MIN}	z_{MAX}	a_0	a_1	a_2	a_3	x_{MIN}	x_{MAX}
-10	-5	0.	.06512174	-1.93635	0.	.0336	.05
-5	0	0.	-.02722243	-.8984637	0.	0.	.05
0	5	0.	-.01513778	-.38125675	0.	0.	.05
5	10	0.	-.02975537	.13622365	0.	0.	.05
10	15	0.	-.06301387	-.14601042	0.	0.	.05
15	20	0.	.00605219	1.7533041	0.	.00345	.05
20	25	0.	-.0126222	-1.2510286	0.	0.	.05
25	30	0.	-.01733437	-.97838524	0.	0.	.05
30	35	0.	-.0514681	-.07905334	0.	0.	.05
35	42.5	0.	.0253333	-1.254912	0.	.0202	.05

TABLE 3-38 Yaw RCS Rolling Moment Increment Due to +10 Degree Elevon

SYMBOLS	NOZZLE NUMBER	TEST NUMBER
○	N49	OA82, MA22
×	N79	OA82, MA22
□	N83	OA82, MA22
+	N31	MA22
✱	N34	MA22
◇	N43	MA22
▷	N47	MA22
C	N95	OA169
V	N98	OA169
H	N97	OA169

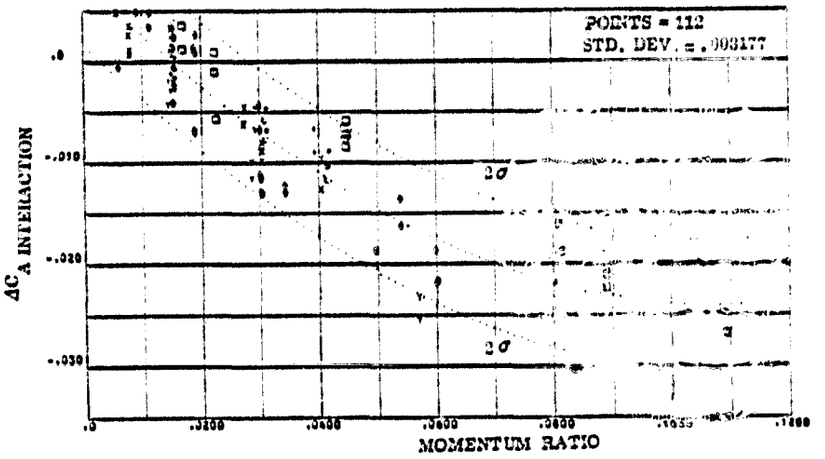

FIGURE 3-1 a. PITCH DOWN AXIAL FORCE CORRELATION FROM -10 → -5 DEGREES ANGLE OF ATTACK

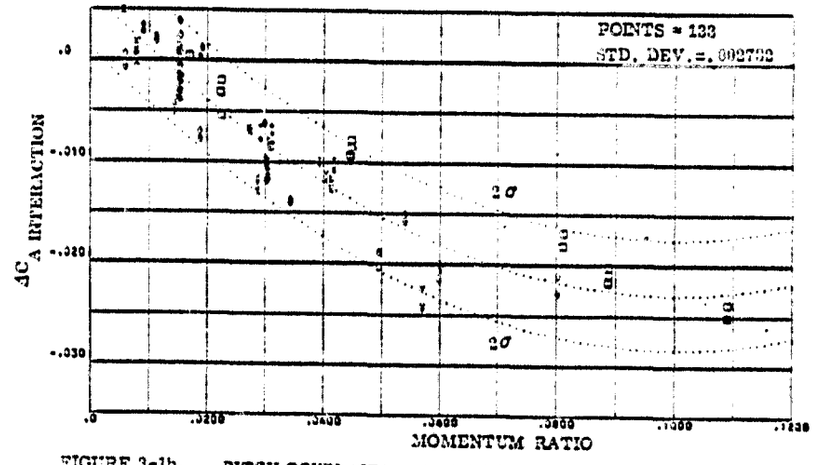

FIGURE 3-1b. PITCH DOWN AXIAL FORCE CORRELATION FROM -5 → 0 DEGREES ANGLE OF ATTACK

SYMBOLS	NOZZLE NUMBER	TEST NUMBER
0	N49	OA82, MA22
⊠	N79	OA82, MA22
□	N83	OA82, MA22
Y	N31	MA22
+	N34	MA22
*	N43	MA22
E	N47	MA22
C	N95	OA169
V	N96	OA169
H	N97	OA169

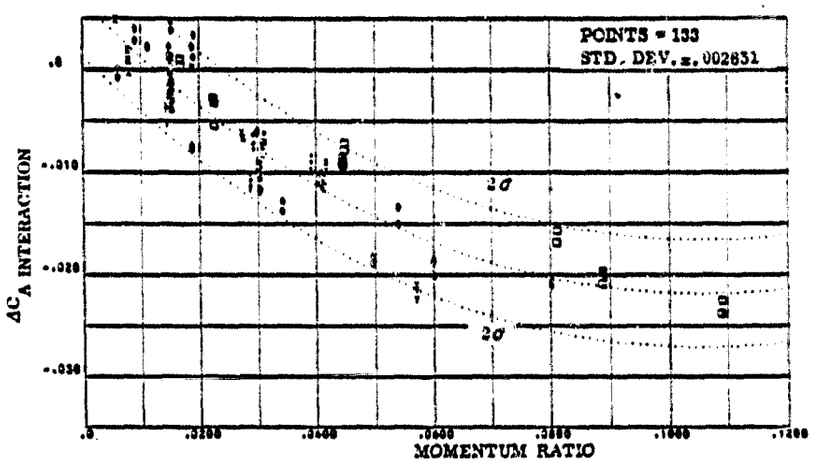

FIGURE 3-1c. PITCH DOWN AXIAL FORCE CORRELATION FROM 0–5 DEGREES ANGLE OF ATTACK

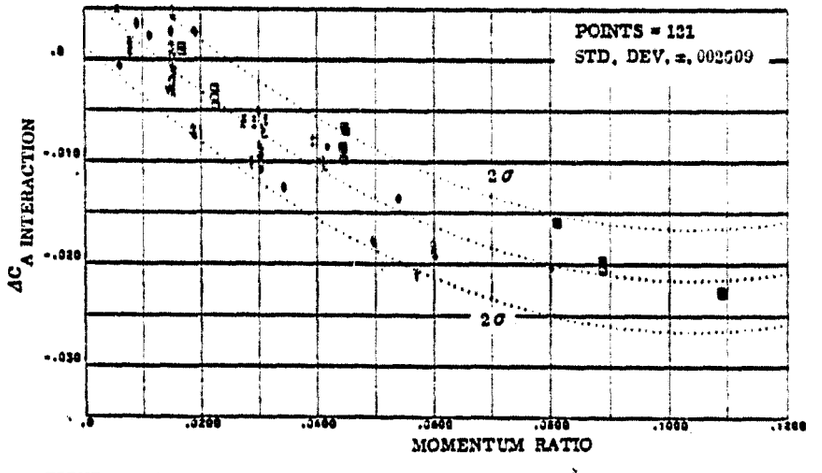

FIGURE 3-1d. PITCH DOWN AXIAL FORCE CORRELATION FROM 5–10 DEGREES ANGLE OF ATTACK

SYMBOLS	NOZZLE NUMBER	TEST NUMBER
○	N49	OA82, MA22
K	N79	OA82, MA22
□	N83	OA82, MA22
Y	N31	MA22
+	N34	MA22
*	N43	MA22
▲	N47	MA22
C	N95	OA169
V	N96	OA169
H	N97	OA169

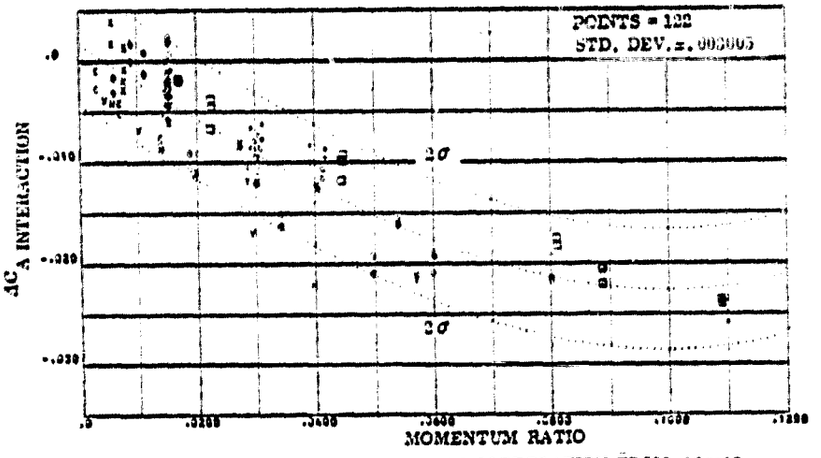

FIGURE 3-1e. PITCH DOWN AXIAL FORCE CORRELATION FROM 10°-15° DEGREES ANGLE OF ATTACK

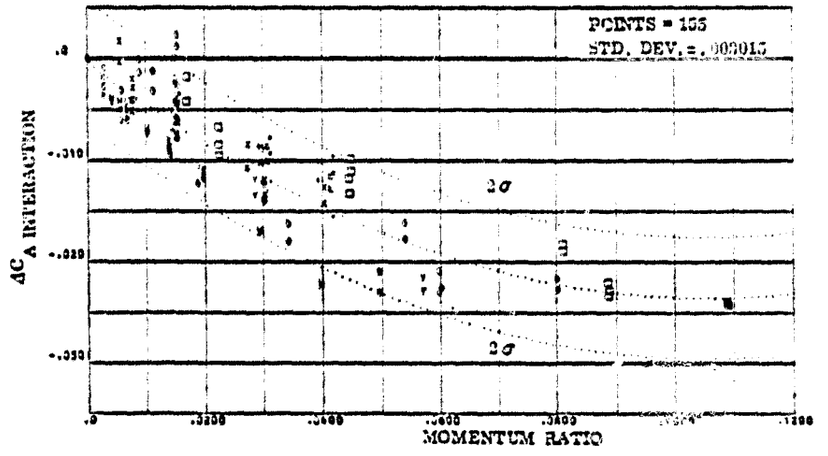

FIGURE 3-1f. PITCH DOWN AXIAL FORCE CORRELATION FROM 15°-20° DEGREES ANGLE OF ATTACK

SYMBOLS	NOZZLE NUMBER	TEST NUMBER
◊	N49	OA82, MA22
X	N79	OA82, MA22
□	N83	OA82, MA22
Y	N31	MA22
+	N34	MA22
*	N43	MA22
E	N47	MA22
C	N95	OA169
V	N96	OA169
H	N97	OA169

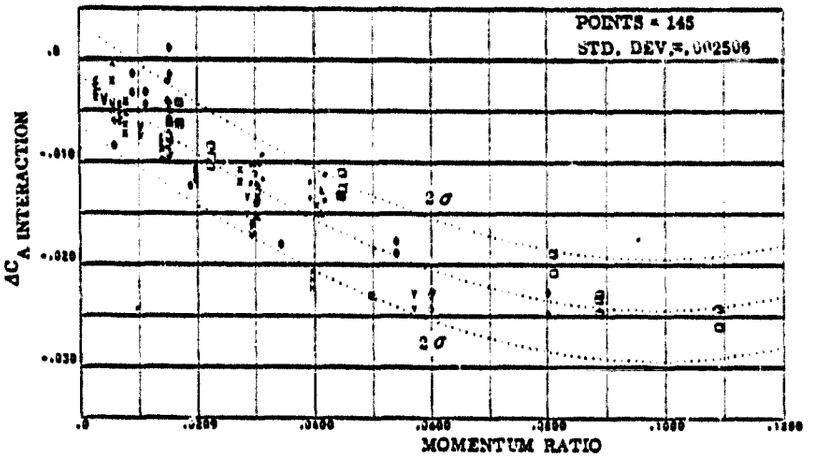

FIGURE 3-1g. PITCH DOWN AXIAL FORCE CORRELATION FROM 20=25 DEGREES ANGLE OF ATTACK

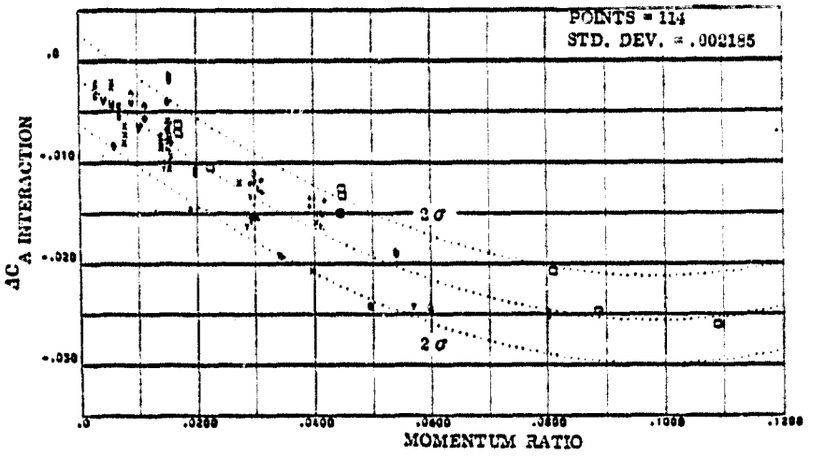

FIGURE 3-1 h. PITCH DOWN AXIAL FORCE CORRELATION FROM 25=30 DEGREES ANGLE OF ATTACK

SYMBOLS	NOZZLE NUMBER	TEST NUMBER
○	N49	OA82, MA22
×	N79	OA82, MA22
□	N83	OA82, MA22
▽	N31	MA22
+	N34	MA22
✱	N43	MA22
▷	N47	MA22
C	N95	OA169
V	N96	OA169
H	N97	OA169

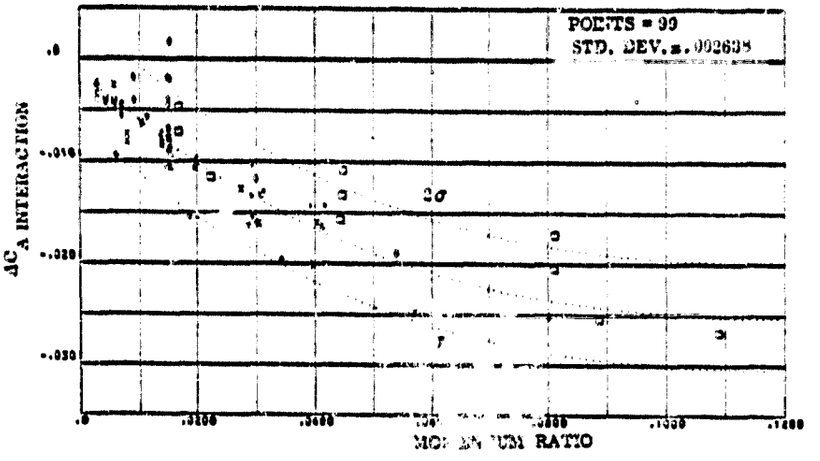

FIGURE 3-11. PITCH DOWN AXIAL FORCE CORRELATION FROM 30–35 DEGREES ANGLE OF ATTACK

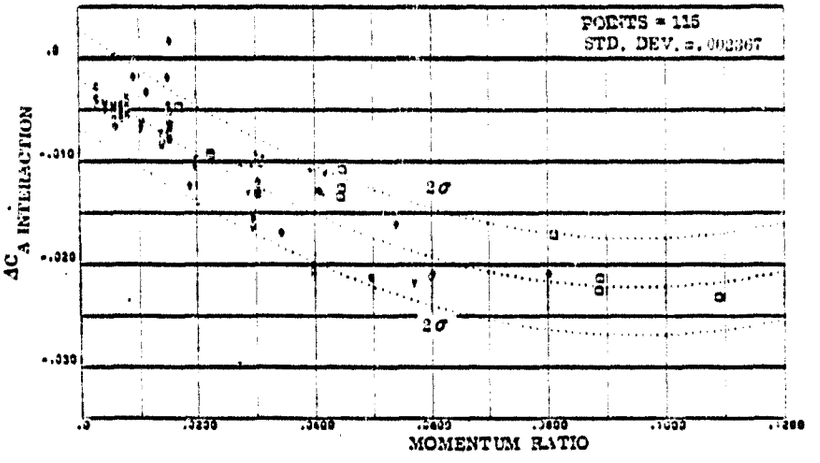

FIGURE 3-12. PITCH DOWN AXIAL FORCE CORRELATION FROM 35–MAX. DEGREES ANGLE OF ATTACK

SYMBOLS	NOZZLE NUMBER	TEST NUMBER
◊	N49	OA82, MA22
X	N79	OA82, MA22
⊡	N83	OA82, MA22
Y	N31	MA22
+	N34	MA22
*	N43	MA22
E	N47	MA22
C	N85	OA169
V	N86	OA169
H	N87	OA169

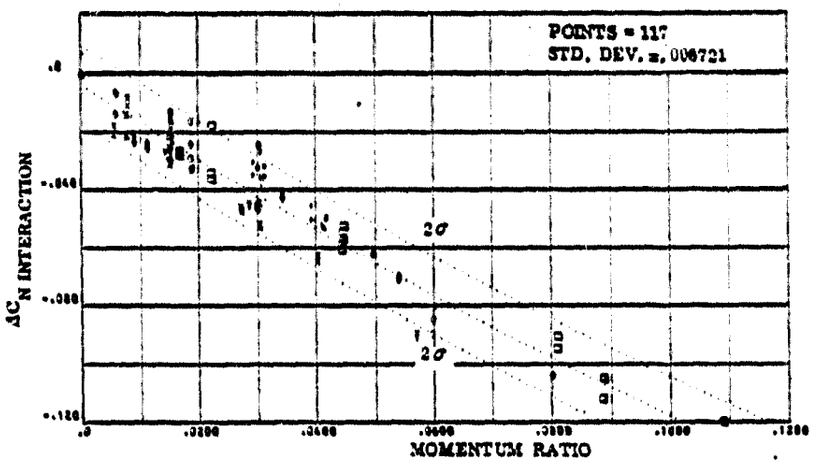

FIGURE 3-2a. PITCH DOWN NORMAL FORCE CORRELATION FROM -10 TO -5 DEGREES ANGLE OF ATTACK

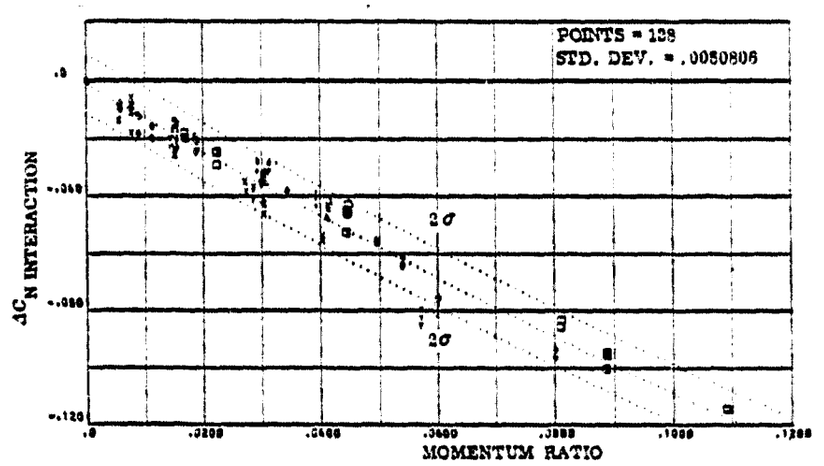

FIGURE 3-2 b. PITCH DOWN NORMAL FORCE CORRELATION FROM -5 TO 0 DEGREES ANGLE OF ATTACK

SYMBOLS	NOZZLE NUMBER	TEST NUMBER
○	N49	OA82, MA22
⊠	N79	OA82, MA22
⊞	N83	OA82, MA22
✳	N31	MA22
✚	N34	MA22
✱	N43	MA22
⊡	N47	MA22
G	N96	OA169
V	N96	OA169
H	N97	OA169

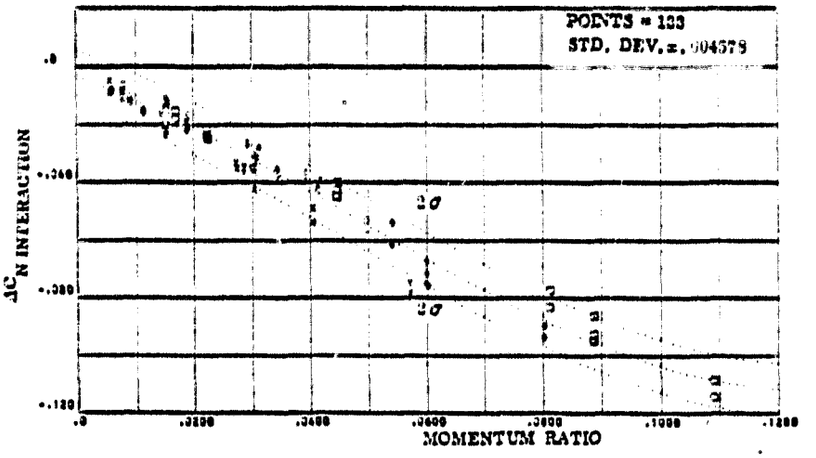

FIGURE 3-2c. PITCH DOWN NORMAL FORCE CORRELATION FROM 0=5 DEGREES ANGLE OF ATTACK

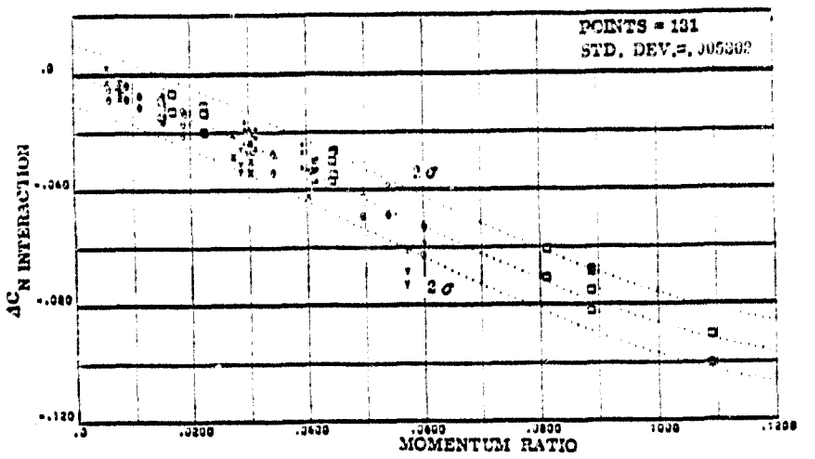

FIGURE 3-2d. PITCH DOWN NORMAL FORCE CORRELATION FROM 5=10 DEGREES ANGLE OF ATTACK

SYMBOLS	NOZZLE NUMBER	TEST NUMBER
○	N49	OA82, MA22
⊠	N79	OA82, MA22
□	N83	OA82, MA22
◇	N31	MA22
+	N34	MA22
✱	N43	MA22
⊞	N47	MA22
▽	N95	OA169
▽	N96	OA169
H	N97	OA169

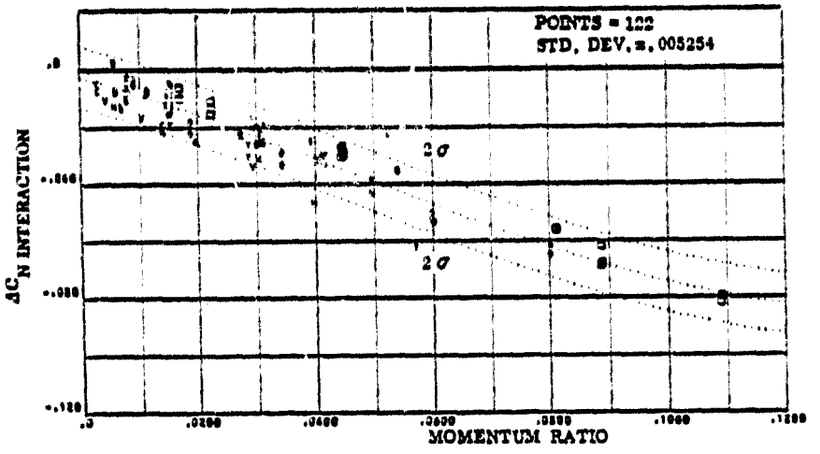

FIGURE 3-2 6. PITCH DOWN NORMAL FORCE CORRELATION FROM 10—15 DEGREES ANGLE OF ATTACK

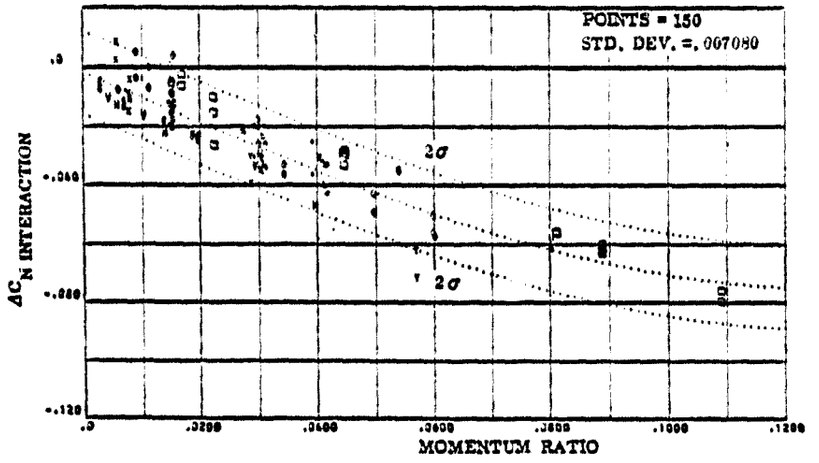

FIGURE 3-21. PITCH DOWN NORMAL FORCE CORRELATION FROM 15—20 DEGREES ANGLE OF ATTACK

SYMBOLS	NOZZLE NUMBER	TEST NUMBER
○	N49	OA82, MA22
✕	N79	OA82, MA22
□	N83	OA82, MA22
▽	N31	MA22
+	N34	MA22
*	N43	MA22
▲	N47	MA22
C	N95	OA169
V	N96	OA169
H	N97	OA169

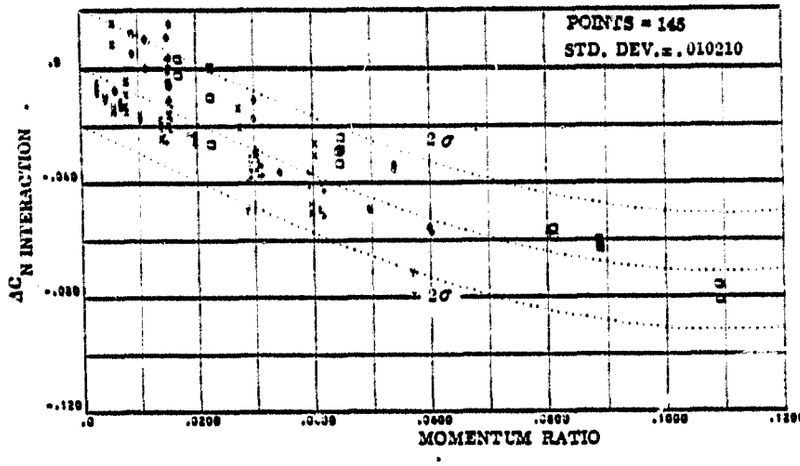

FIGURE 3-25. PITCH DOWN NORMAL FORCE CORRELATION FROM 20→25 DEGREES ANGLE OF ATTACK

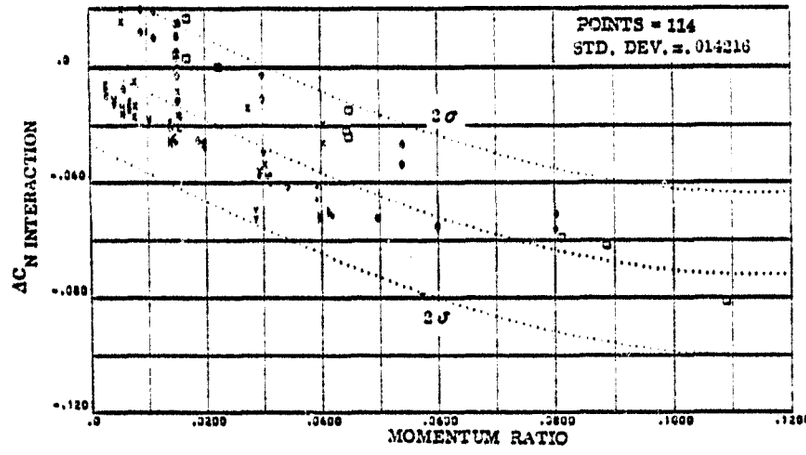

FIGURE 3-26. PITCH DOWN NORMAL FORCE CORRELATION FROM 25→30 DEGREES ANGLE OF ATTACK

SYMBOLS	NOZZLE NUMBER	TEST NUMBER
0	N49	OA82, MA22
M	N79	OA82, MA22
◇□	N83	OA82, MA22
◇	N31	MA22
+	N34	MA22
*	N43	MA22
F	N47	MA22
C	N95	OA169
V	N96	OA169
H	N97	OA169

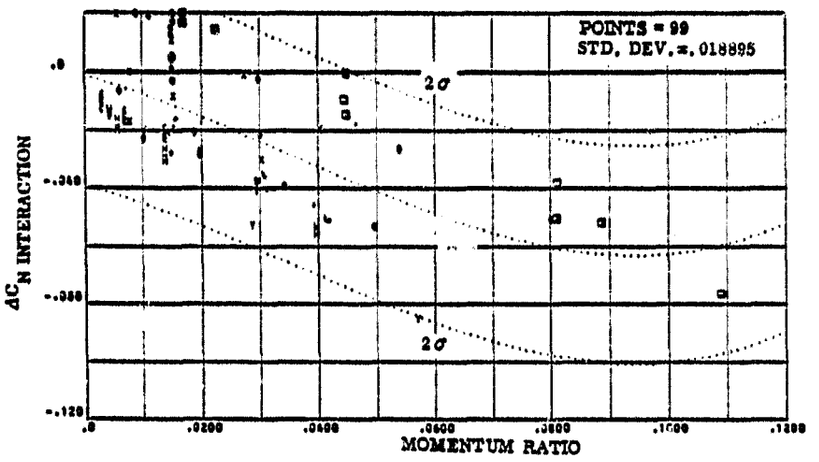

FIGURE 3-21. PITCH DOWN NORMAL FORCE CORRELATION FROM 30→35 DEGREES ANGLE OF ATTACK

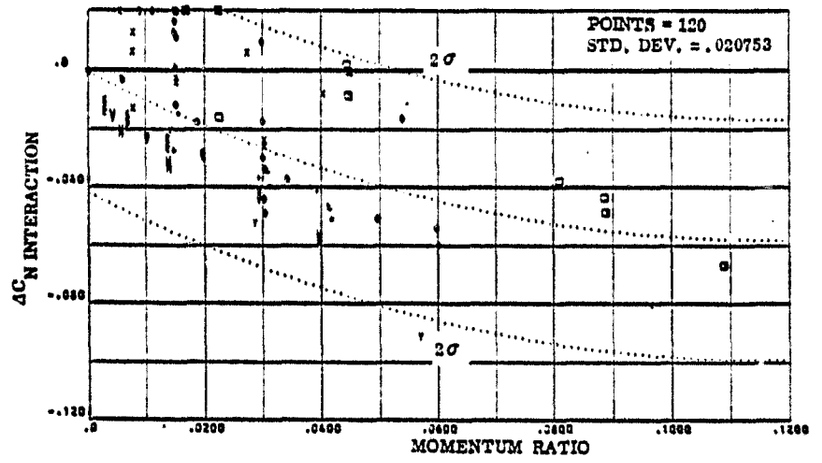

FIGURE 3-2 j. PITCH DOWN NORMAL FORCE CORRELATION FROM 35→MAX. DEGREES ANGLE OF ATTACK

SYMBOLS	NOZZLE NUMBER	TEST NUMBER
○	N49	OA82, MA22
⊠	N79	OA82, MA22
□	N83	OA82, MA22
▽	N31	MA22
+	N34	MA22
*	N43	MA22
L	N47	MA22
C	N95	OA169
V	N96	OA169
H	N97	OA169

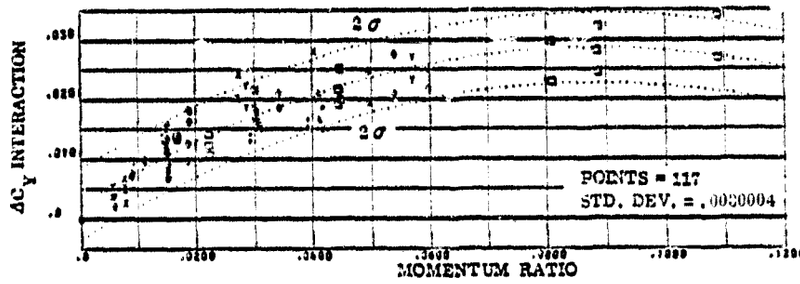

FIGURE 3-3 a. PITCH DOWN SIDE FORCE CORRELATION FROM -10=-5 DEGREES ANGLE OF ATTACK

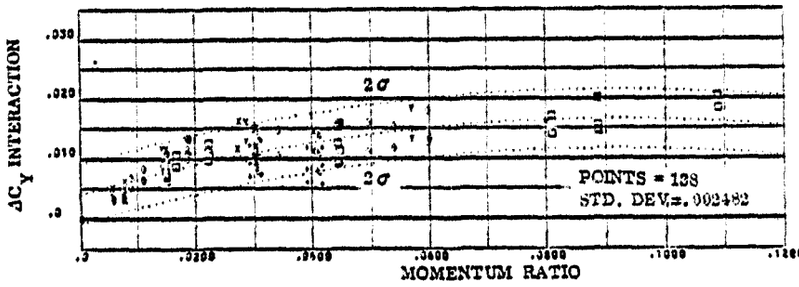

FIGURE 3-3 b. PITCH DOWN SIDE FORCE CORRELATION FROM -5=0 DEGREES ANGLE OF ATTACK

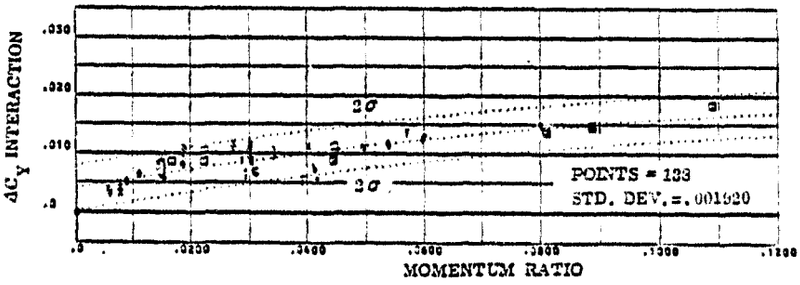

FIGURE 3-3 c. PITCH DOWN SIDE FORCE CORRELATION FROM 0=5 DEGREES ANGLE OF ATTACK

SYMBOLS	NOZZLE NUMBER	TEST NUMBER
O	N49	OA82, MA22
⊠	N79	OA82, MA22
□	N83	OA82, MA22
Y	N31	MA22
+	N34	MA22
*	N43	MA22
L	N47	MA22
C	N95	OA169
V	N96	OA169
H	N97	OA169

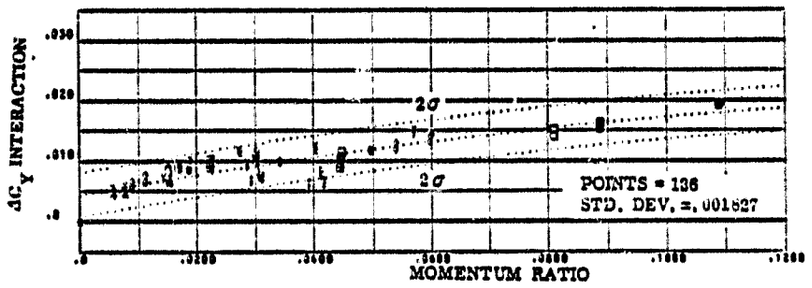

FIGURE 3-3d. PITCH DOWN SIDE FORCE CORRELATION FROM 5→10 DEGREES ANGLE OF ATTACK

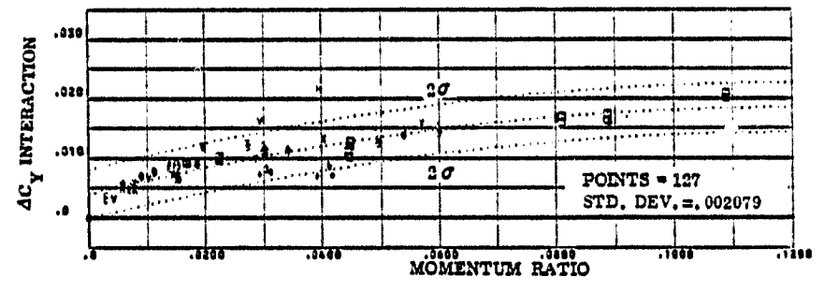

FIGURE 3-3e. PITCH DOWN SIDE FORCE CORRELATION FROM 10→15 DEGREES ANGLE OF ATTACK

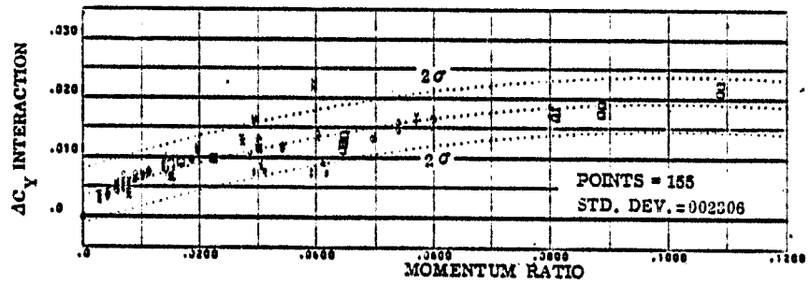

FIGURE 3-3f. PITCH DOWN SIDE FORCE CORRELATION FROM 15→20 DEGREES ANGLE OF ATTACK

SYMBOLS	NOZZLE NUMBER	TEST NUMBER
○	N42	OA82, MA22
⊠	N79	OA82, MA22
□	N83	OA82, MA22
▽	N31	MA22
+	N34	MA22
*	N43	MA22
▷	N47	MA22
C	N95	OA169
V	N96	OA169
H	N97	OA169

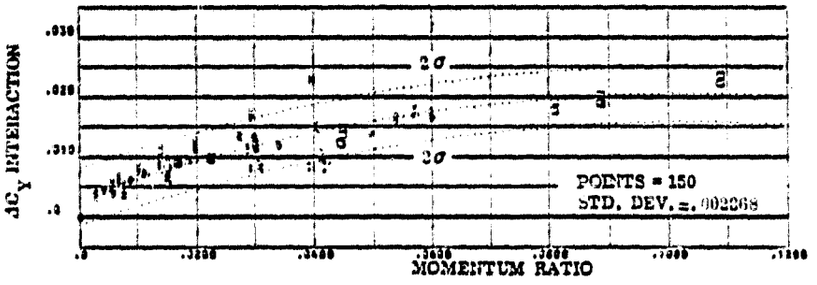

FIGURE 3-3 g. PITCH DOWN SIDE FORCE CORRELATION FROM 20→25 DEGREES ANGLE OF ATTACK

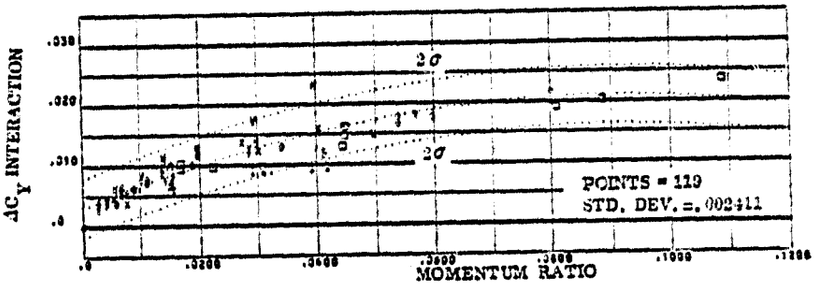

FIGURE 3-3 h. PITCH DOWN SIDE FORCE CORRELATION FROM 25→30 DEGREES ANGLE OF ATTACK

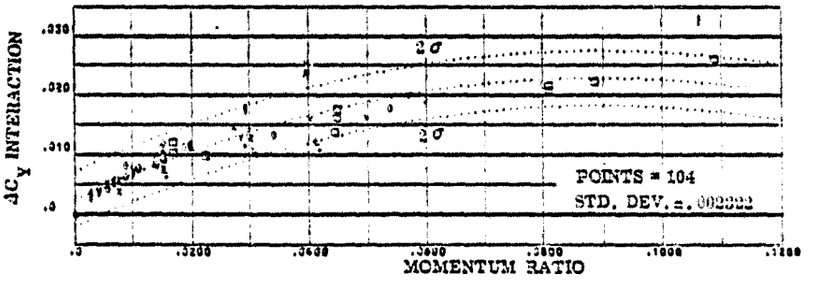

FIGURE 3-3 i. PITCH DOWN SIDE FORCE CORRELATION FROM 30→35 DEGREES ANGLE OF ATTACK

SYMBOLS	NOZZLE NUMBER	TEST NUMBER
.0	N49	OA82, MA22
X	N79	OA82, MA22
□	N83	OA82, MA22
Y	N31	MA22
+	N34	MA22
*	N43	MA22
◇	N47	MA22
C	N95	OA169
V	N96	OA169
H	N97	OA169

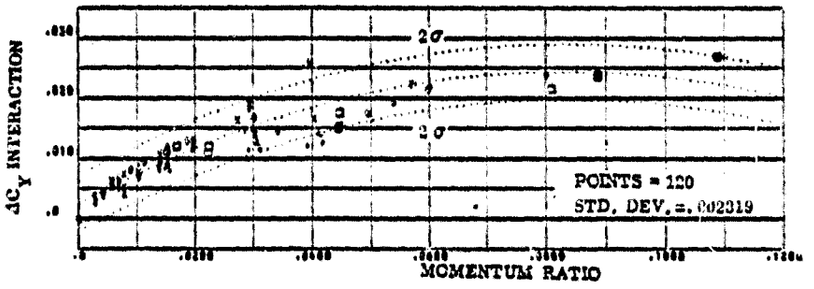

FIGURE 3-3 j. PITCH DOWN SIDE FORCE CORRELATION FROM 36° MAX. DEGREES ANGLE OF ATTACK

SYMBOLS	NOZZLE NUMBER	TEST NUMBER
○	N49	OA82, MA22
⊠	N79	OA82, MA22
▽	N83	OA82, MA22
▽	N31	MA22
+	N34	MA22
✱	N43	MA22
▷	N47	MA22
○	N95	OA169
▽	N96	OA169
⊠	N97	OA169

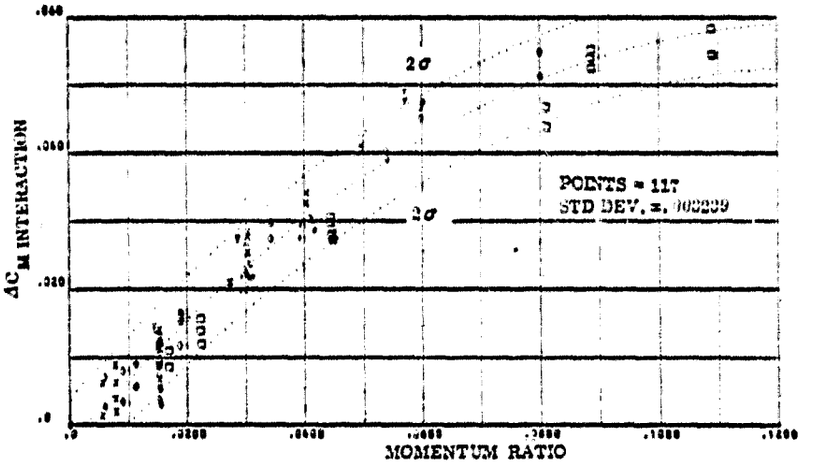

FIGURE 3-4 a. PITCH DOWN PITCHING MOMENT CORRELATION FROM -10 TO -5 DEGREES ANGLE OF ATTACK

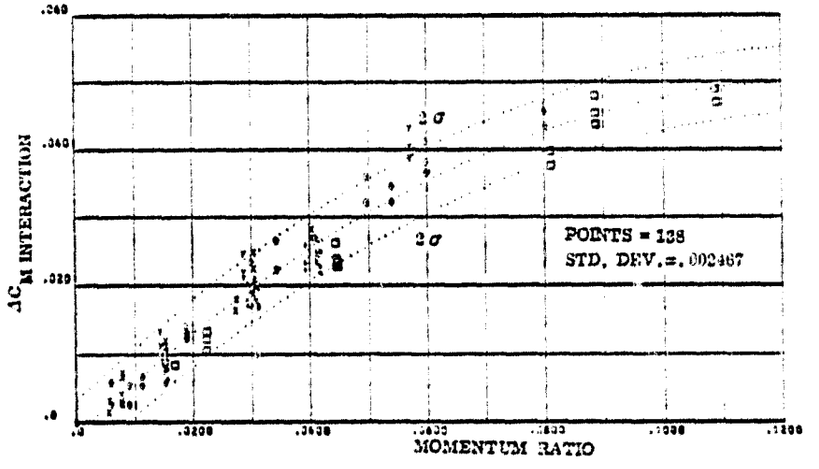

FIGURE 3-4 b. PITCH DOWN PITCHING MOMENT CORRELATION FROM -5 TO 0 DEGREES ANGLE OF ATTACK

SYMBOLS	NOZZLE NUMBER	TEST NUMBER
O	N49	OA82, MA22
X	N79	OA82, MA22
□	N83	OA82, MA22
◇	N31	MA22
+	N34	MA22
*	N43	MA22
▷	N47	MA22
G	N96	OA169
V	N98	OA169
H	N97	OA169

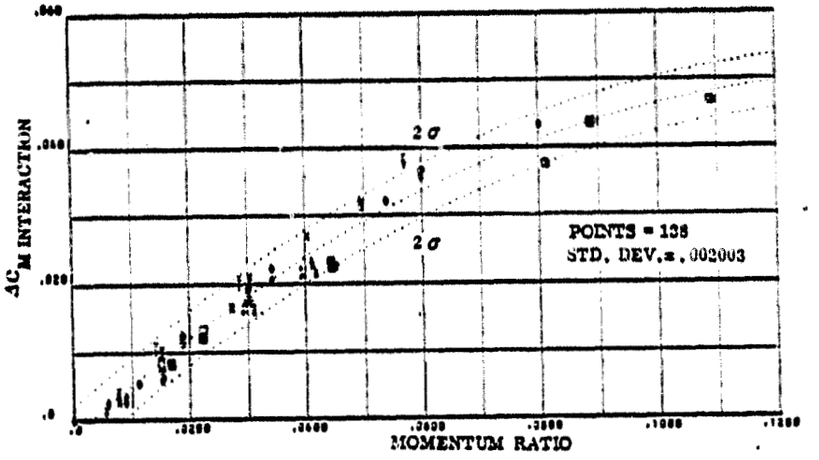

FIGURE 3-4c. PITCH DOWN PITCHING MOMENT CORRELATION FROM 0-5 DEGREES ANGLE OF ATTACK

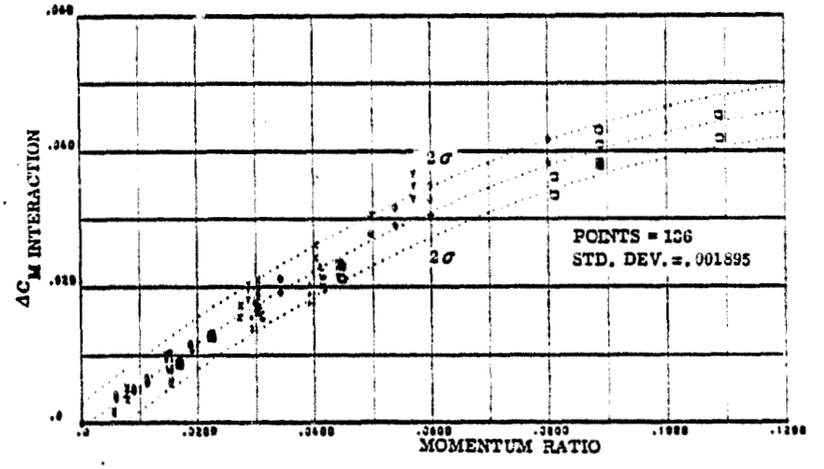

FIGURE 3-4 d. PITCH DOWN PITCHING MOMENT CORRELATION FROM 5-10 DEGREES ANGLE OF ATTACK

SYMBOLS	NOZZLE NUMBER	TEST NUMBER
○	N49	OA82, MA22
×	N79	OA82, MA22
□	N83	OA82, MA22
+	N81	MA22
◇	N84	MA22
*	N43	MA22
▽	N47	MA22
G	N95	OA169
▷	N96	OA169
H	N97	OA169

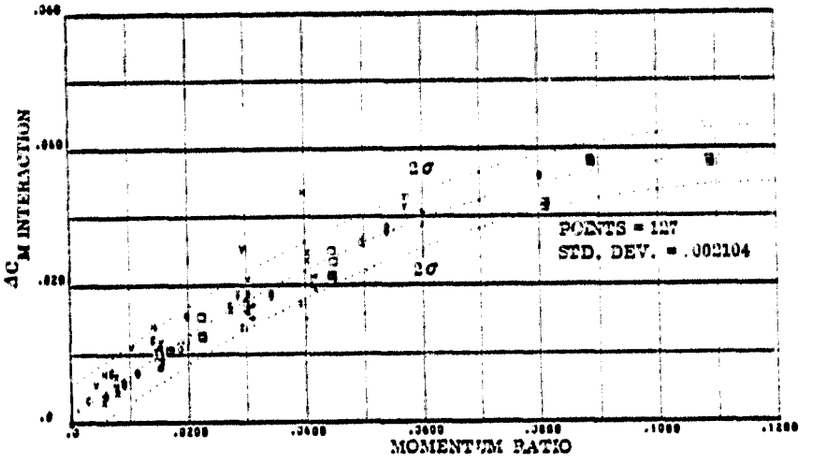

FIGURE 3-4 e. PITCH DOWN PITCHING MOMENT CORRELATION FROM 10-15 DEGREES ANGLE OF ATTACK

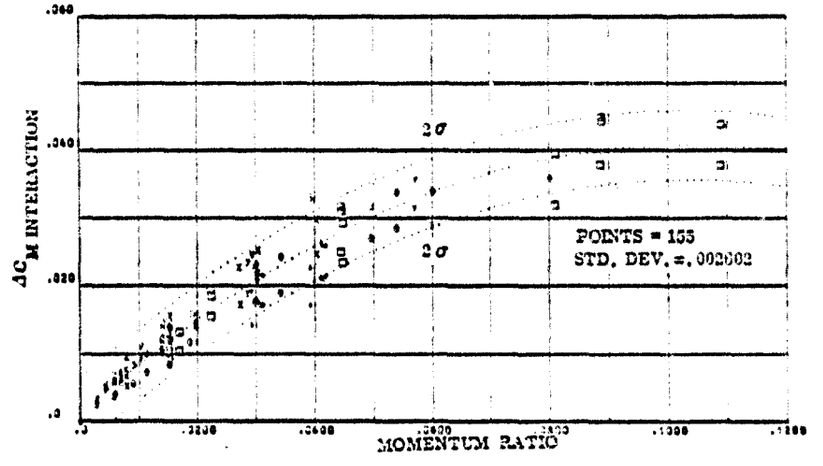

FIGURE 3-4 f. PITCH DOWN PITCHING MOMENT CORRELATION FROM 15-20 DEGREES ANGLE OF ATTACK

SYMBOLS	NOZZLE NUMBER	TEST NUMBER
○	N49	OA82, MA22
✕	N79	OA82, MA22
□	N83	OA82, MA22
▽	N31	MA22
+	N34	MA22
*	N43	MA22
▷	N47	MA22
○	N95	OA169
▽	N96	OA169
▷	N97	OA169

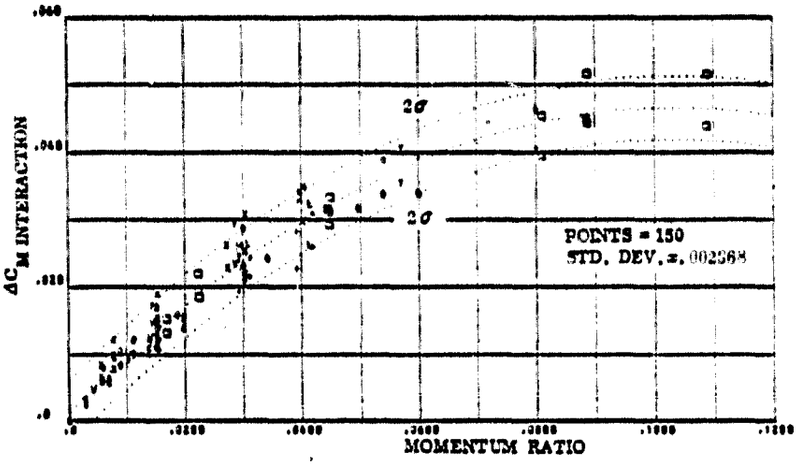

FIGURE 3-4 g. PITCH DOWN PITCHING MOMENT CORRELATION FROM 20-25 DEGREES ANGLE OF ATTACK

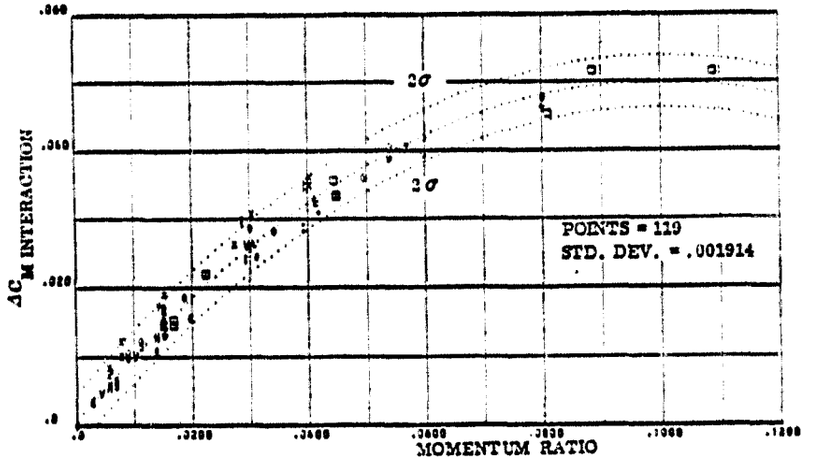

FIGURE 3-4 h. PITCH DOWN PITCHING MOMENT CORRELATION FROM 25-30 DEGREES ANGLE OF ATTACK

SYMBOLS	NOZZLE NUMBER	TEST NUMBER
○	N49	OA42, MA22
X	N79	OA42, MA22
□	N83	OA42, MA22
+	N31	MA22
◇	N34	MA22
*	N43	MA22
△	N47	MA22
C	N35	OA169
▽	N36	OA169
H	N37	OA169

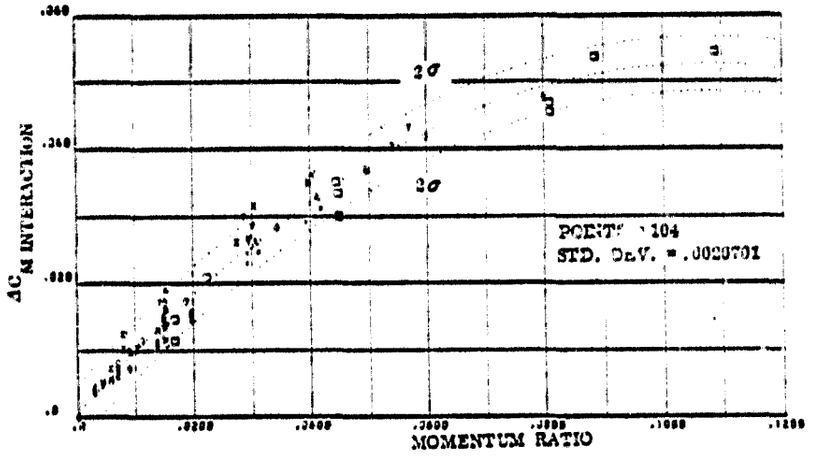

FIGURE 3-41. PITCH DOWN PITCHING MOMENT CORRELATION FROM 30-35 DEGREES ANGLE OF ATTACK

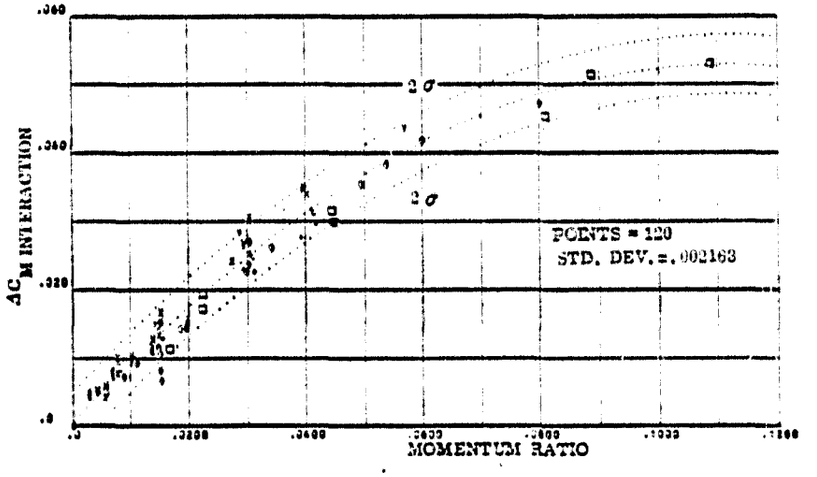

FIGURE 3-42. PITCH DOWN PITCHING MOMENT CORRELATION FROM 35-MAX. DEGREES ANGLE OF ATTACK

SYMBOLS	NOZZLE NUMBER	TEST NUMBER
○	N49	OA82, MA22
⊠	N79	OA82, MA22
⊞	N83	OA82, MA22
×	N31	MA22
+	N34	MA22
*	N43	MA22
E	N47	MA22
C	N95	OA169
V	N96	OA169
H	N97	OA169

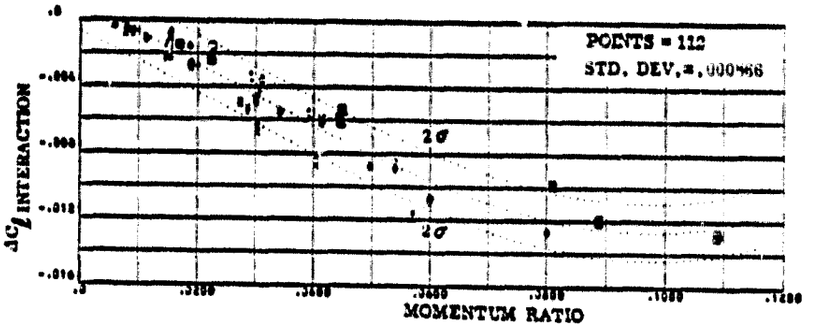

FIGURE 3-5 a. PITCH DOWN ROLLING MOMENT CORRELATION FROM -10 to -5 DEGREES ANGLE OF ATTACK

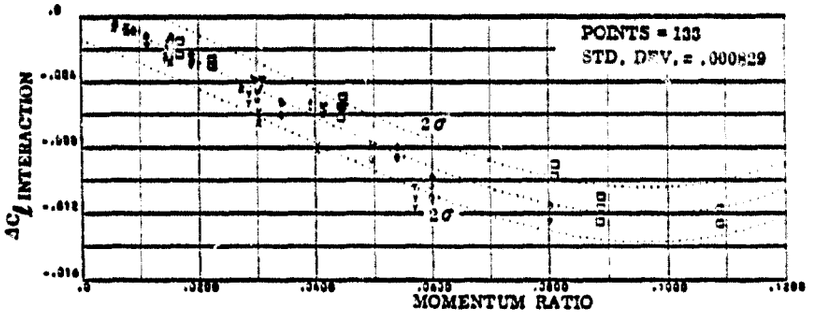

FIGURE 3-5 b. PITCH DOWN ROLLING MOMENT CORRELATION FROM -5 to 0 DEGREES ANGLE OF ATTACK

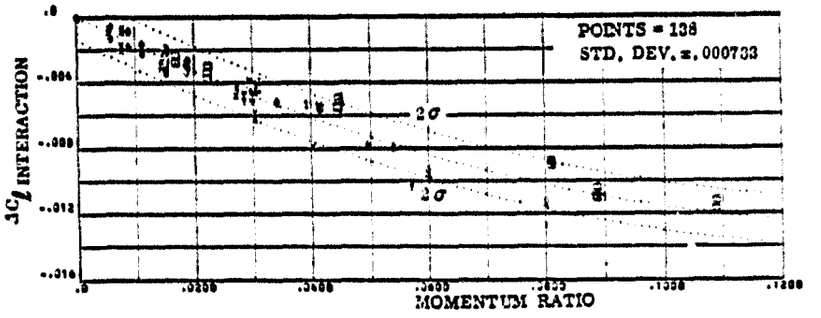

FIGURE 3-5c. PITCH DOWN ROLLING MOMENT CORRELATION FROM 0 to 5 DEGREES ANGLE OF ATTACK

SYMBOLS	NOZZLE NUMBER	TEST NUMBER
○	N49	OA82, MA22
×	N79	OA82, MA22
□	N83	OA82, MA22
▽	N31	MA22
+	N34	MA22
✱	N43	MA22
▷	N47	MA22
○	N95	OA169
▽	N96	OA169
H	N97	OA169

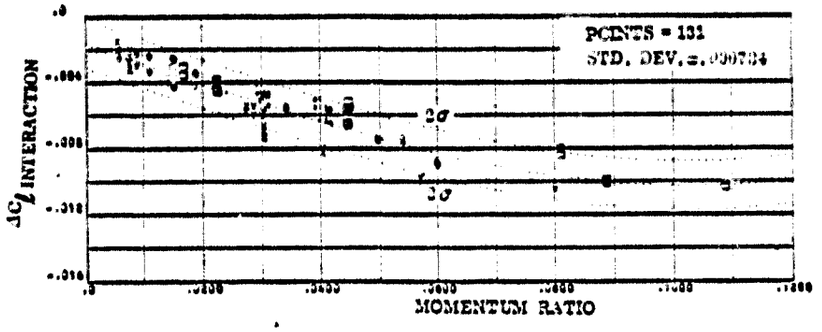

FIGURE 3-5d. PITCH DOWN ROLLING MOMENT CORRELATION FROM 5→10 DEGREES ANGLE OF ATTACK

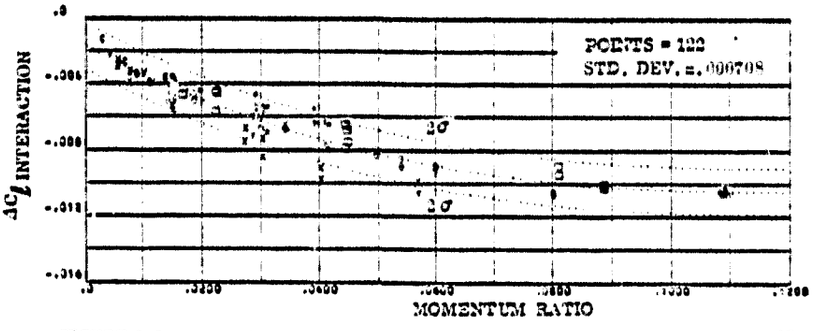

FIGURE 3-5e. PITCH DOWN ROLLING MOMENT CORRELATION FROM 10→15 DEGREES ANGLE OF ATTACK

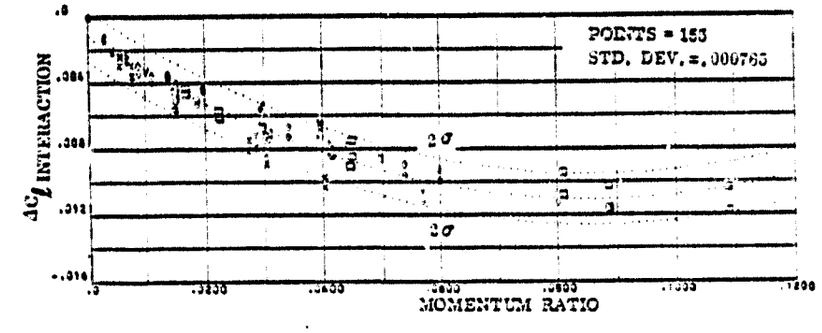

FIGURE 3-5f. PITCH DOWN ROLLING MOMENT CORRELATION FROM 15→20 DEGREES ANGLE OF ATTACK

SYMBOLS	NOZZLE NUMBER	TEST NUMBER
○	N49	OA82, MA22
⊠	N79	OA82, MA22
□	N83	OA82, MA22
▽	N31	MA22
+	N34	MA22
✱	N43	MA22
⊞	N47	MA22
○	N95	OA169
▽	N96	OA169
⊞	N97	OA169

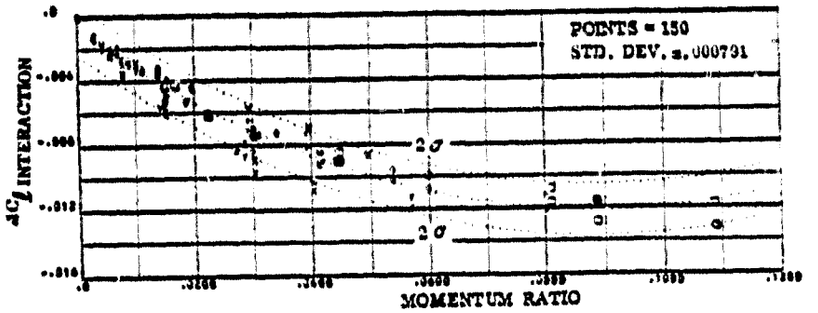

FIGURE 3-5 g. PITCH DOWN ROLLING MOMENT CORRELATION FROM 20–25 DEGREES ANGLE OF ATTACK

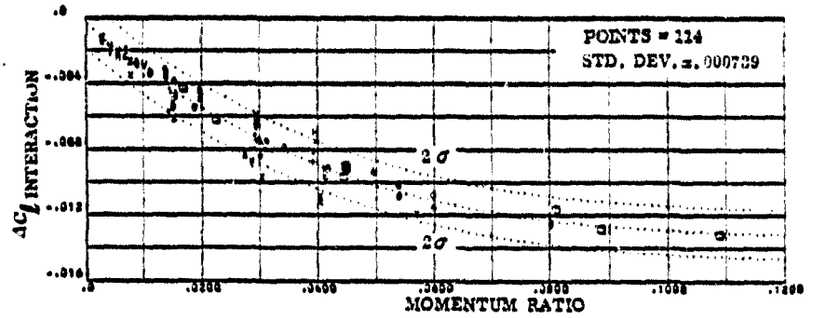

FIGURE 3-5 h. PITCH DOWN ROLLING MOMENT CORRELATION FROM 25–30 DEGREES ANGLE OF ATTACK

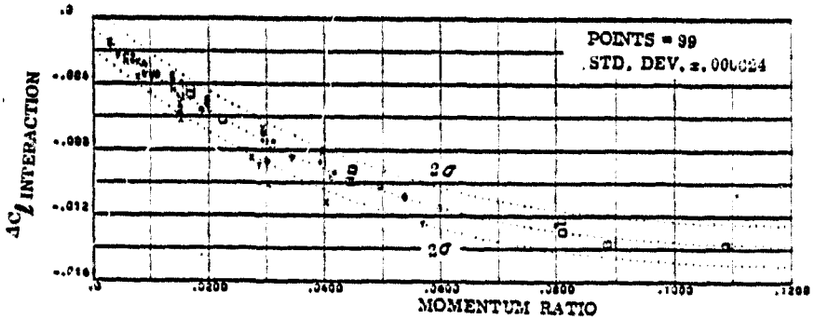

FIGURE 3-5 i. PITCH DOWN ROLLING MOMENT CORRELATION FROM 30–35 DEGREES ANGLE OF ATTACK

SYMBOLS	NOZZLE NUMBER	TEST NUMBER
○	N49	OA82, MA22
□	N79	OA82, MA22
△	N83	OA82, MA22
+	N31	MA22
◇	N34	MA22
*	N43	MA22
▷	N47	MA22
⊂	N95	OA169
▽	N96	OA169
H	N97	OA169

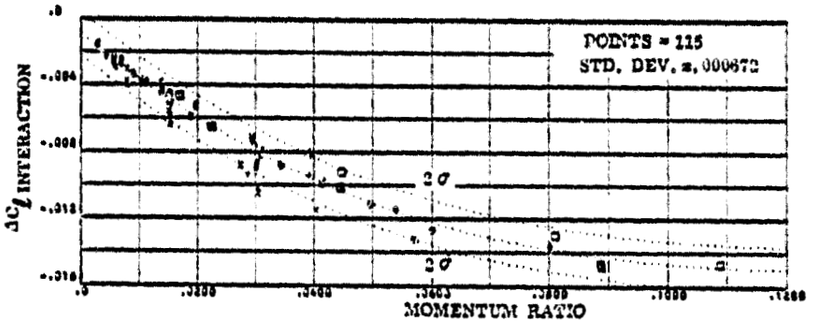

FIGURE 3-51. PITCH DOWN ROLLING MOMENT CORRELATION FROM 35°-MAX. DEGREES ANGLE OF ATTACK

SYMBOLS	NOZZLE NUMBER	TEST NUMBER
○	N49	OA82, MA22
×	N79	OA82, MA22
□	N83	OA82, MA22
▽	N31	MA22
+	N34	MA22
*	N43	MA22
▷	N47	MA22
C	N96	OA169
V	N96	OA169
H	N97	OA169

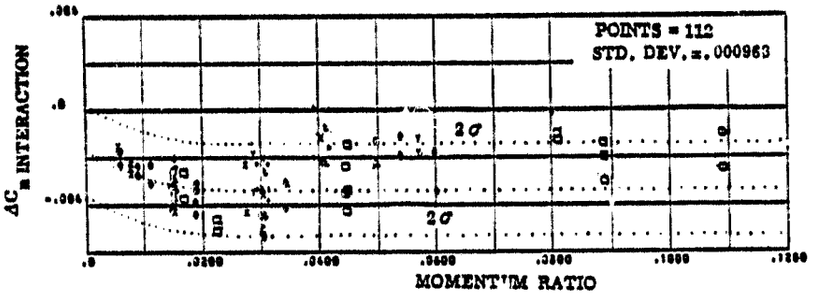

FIGURE 3-6a. PITCH DOWN YAWING MOMENT CORRELATION FROM -10 to -5 DEGREES ANGLE OF ATTACK

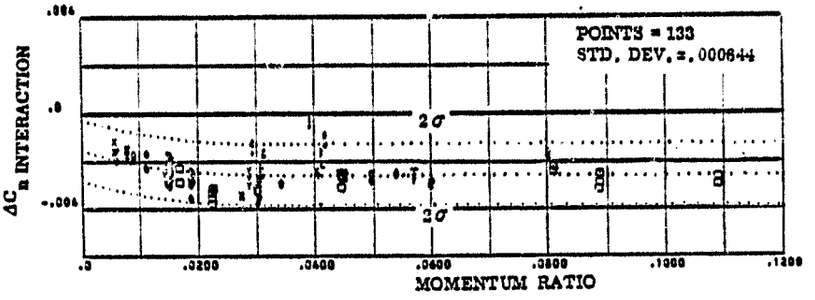

FIGURE 3-6b. PITCH DOWN YAWING MOMENT CORRELATION FROM -5 to 0 DEGREES ANGLE OF ATTACK

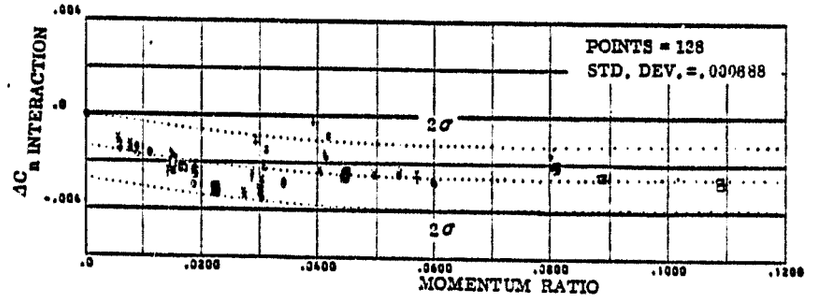

FIGURE 3-6c. PITCH DOWN YAWING MOMENT CORRELATION FROM 0 to 5 DEGREES ANGLE OF ATTACK

SYMBOLS	NOZZLE NUMBER	TEST NUMBER
○	N49	OA82, MA22
⊠	N79	OA82, MA22
▽	N83	OA82, MA22
+	N31	MA22
✱	N34	MA22
E	N43	MA22
C	N47	MA22
V	N95	OA169
H	N96	OA169
	N97	OA169

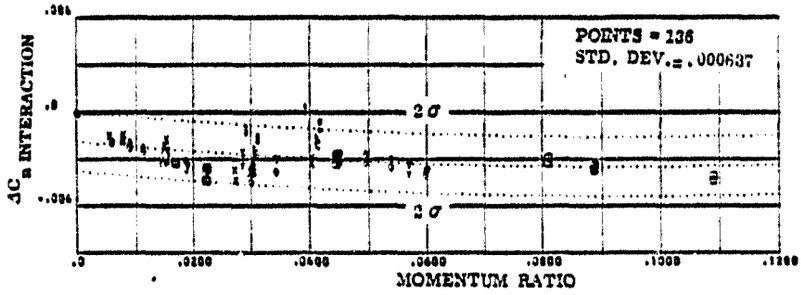

FIGURE 3-6d. PITCH DOWN YAWING MOMENT CORRELATION FROM 5→10 DEGREES ANGLE OF ATTACK

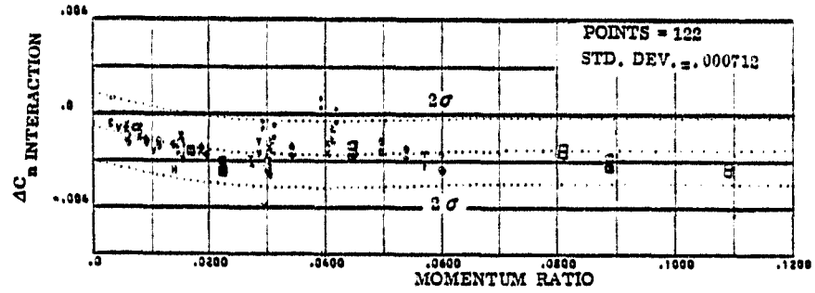

FIGURE 3-6e. PITCH DOWN YAWING MOMENT CORRELATION FROM 10→15 DEGREES ANGLE OF ATTACK

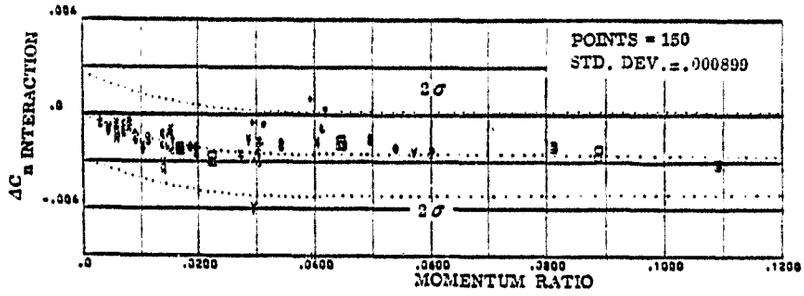

FIGURE 3-6f. PITCH DOWN YAWING MOMENT CORRELATION FROM 15→20 DEGREES ANGLE OF ATTACK

SYMBOLS	NOZZLE NUMBER	TEST NUMBER
○	N49	OA82, MA22
X	N79	OA82, MA22
□	N83	OA82, MA22
V	N31	MA22
+	N34	MA22
*	N43	MA22
E	N47	MA22
C	N95	OA169
V	N96	OA169
H	N97	OA169

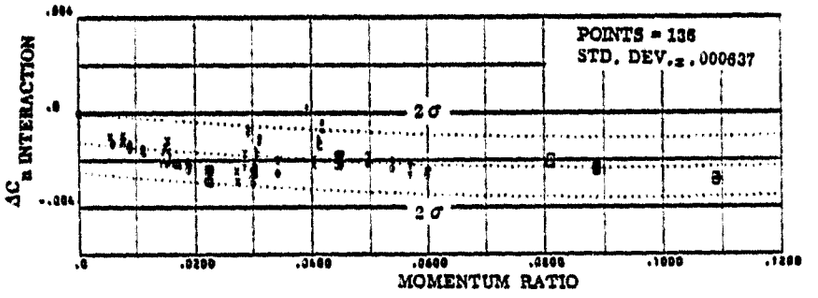

FIGURE 3-6d. PITCH DOWN YAWING MOMENT CORRELATION FROM 5→10 DEGREES ANGLE OF ATTACK

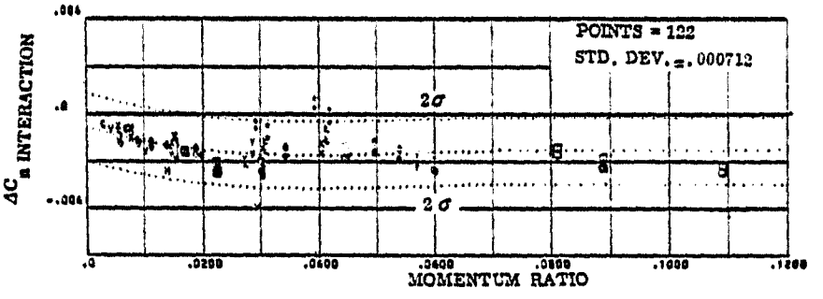

FIGURE 3-6e. PITCH DOWN YAWING MOMENT CORRELATION FROM 10→15 DEGREES ANGLE OF ATTACK

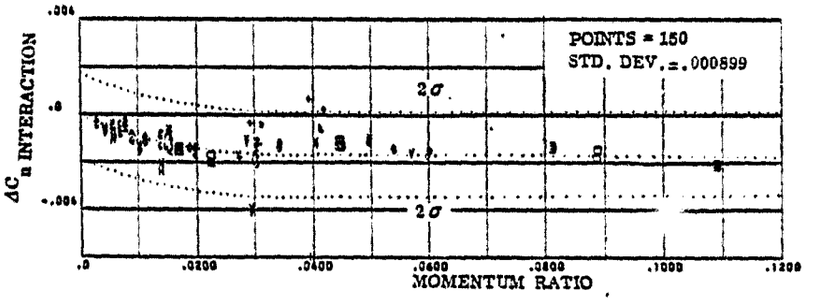

FIGURE 3-6f. PITCH DOWN YAWING MOMENT CORRELATION FROM 15→20 DEGREES ANGLE OF ATTACK

SYMBOLS	NOZZLE NUMBER	TEST NUMBER
O	N49	OA82, MA22
X	N79	OA82, MA22
□	N83	OA82, MA22
Y	N31	MA22
+	N34	MA22
*	N43	MA22
E	N47	MA22
C	N95	OA169
V	N96	OA169
H	N97	OA169

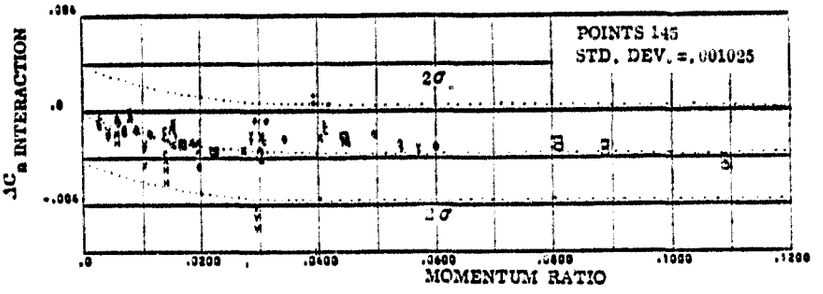

FIGURE 3-6 g. PITCH DOWN YAWING MOMENT CORRELATION FROM 30→25 DEGREES ANGLE OF ATTACK

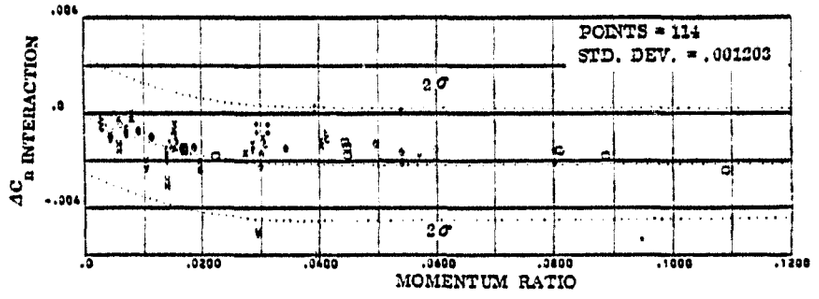

FIGURE 3-6 h. PITCH DOWN YAWING MOMENT CORRELATION FROM 25→30 DEGREES ANGLE OF ATTACK

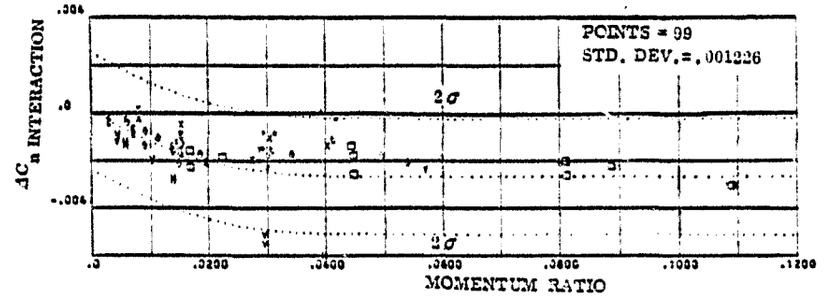

FIGURE 3-6 i. PITCH DOWN YAWING MOMENT CORRELATION FROM 30→35 DEGREES ANGLE OF ATTACK

SYMBOLS	NOZZLE NUMBER	TEST NUMBER
○	N49	OA82, MA22
✕	N79	OA82, MA22
□	N83	OA82, MA22
▽	N31	MA22
+	N34	MA22
*	N43	MA22
△	N47	MA22
G	N95	OA169
V	N96	OA169
H	N97	OA169

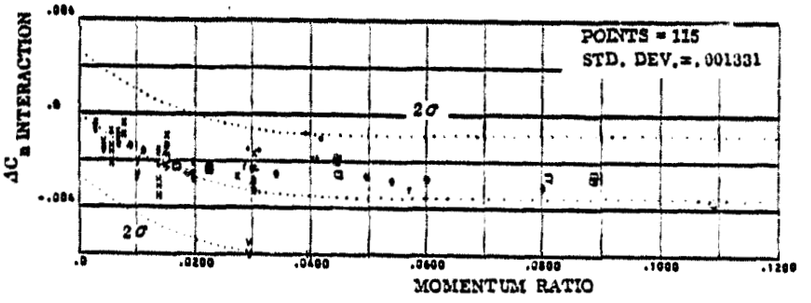

FIGURE 3-6j. PITCH DOWN YAWING MOMENT CORRELATION FROM 35→MAX. DEGREES ANGLE OF ATTACK

SYMBOLS	NOZZLE NUMBER	TEST NUMBER
0	N62	OA82, MA22
X	N78	OA82, MA22
□	N82	OA82, MA22
Y	N31	MA22
+	N36	MA22
*	N44	MA22
E	N48	MA22
¢	N95	OA169
V	N96	OA169
H	N97	OA169

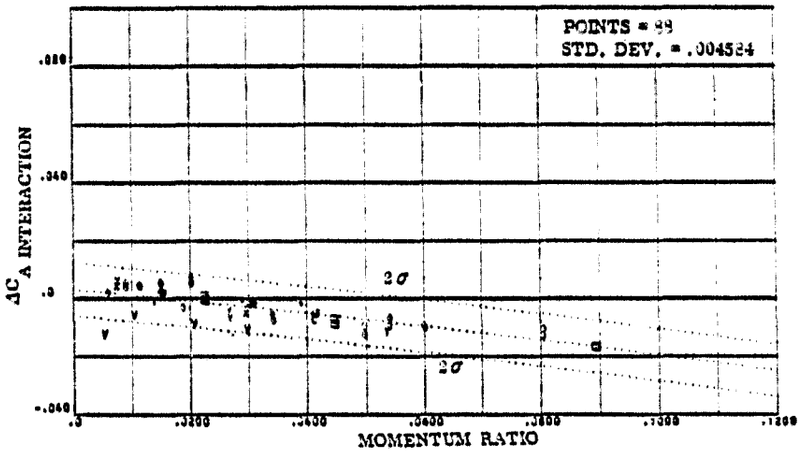

FIGURE 3-7 a. PITCH UP AXIAL FORCE CORRELATION FROM -10 ⟹ -5 DEGREES ANGLE OF ATTACK

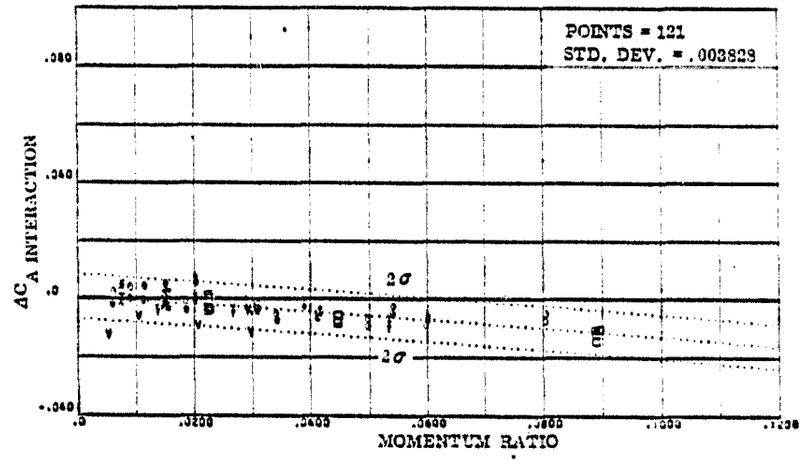

FIGURE 3-7b. PITCH UP AXIAL FORCE CORRELATION FROM -5 ⟹ 0 DEGREES ANGLE OF ATTACK

SYMBOLS	NOZZLE NUMBER	TEST NUMBER
0	N62	OA62, MA22
×	N78	OA62, MA22
□	N82	OA62, MA22
Y	N31	MA22
+	N36	MA22
*	N44	MA22
L	N48	MA22
‹	N95	OA169
V	N96	OA169
H	N97	OA169

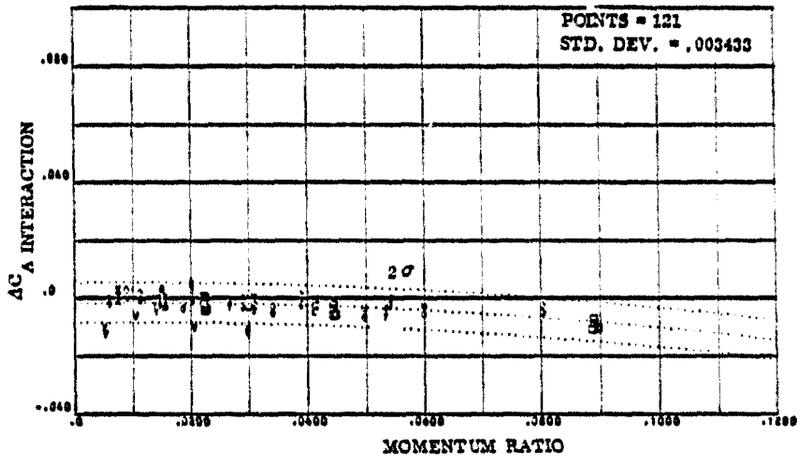

FIGURE 3-7 c. PITCH UP AXIAL FORCE CORRELATION FROM 0–5 DEGREES ANGLE OF ATTACK

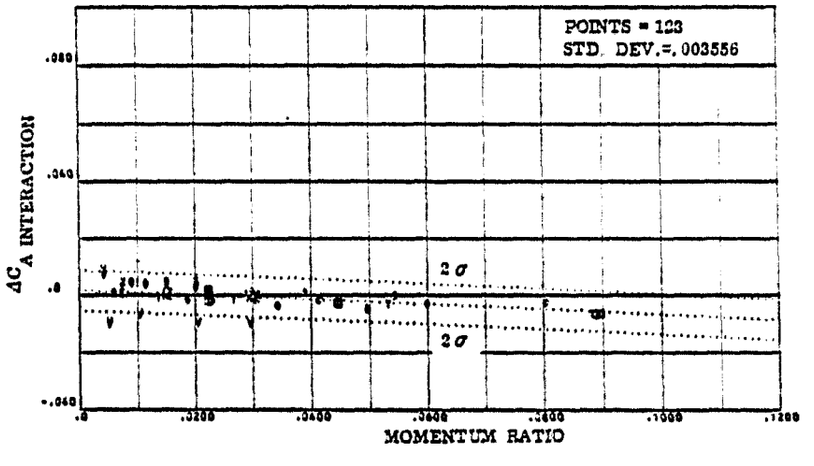

FIGURE 3-7 d. PITCH UP AXIAL FORCE CORRELATION FROM 5–10 DEGREES ANGLE OF ATTACK

SYMBOLS	NOZZLE NUMBER	TEST NUMBER
○	N52	OA82, MA22
×	N79	OA82, MA22
□	N82	OA82, MA22
▽	N31	MA22
+	N36	MA22
*	N44	MA22
▷	N48	MA22
◁	N95	OA169
V	N96	OA169
H	N97	OA169

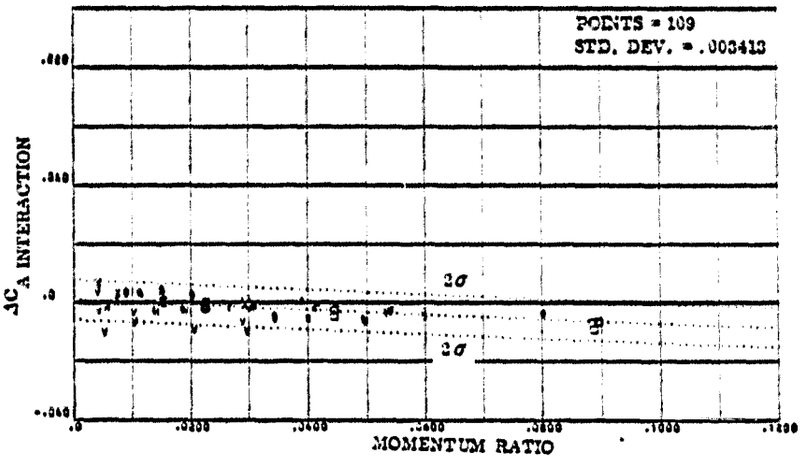

FIGURE 3-7e. PITCH UP AXIAL FORCE CORRELATION FROM 10→15 DEGREES ANGLE OF ATTACK

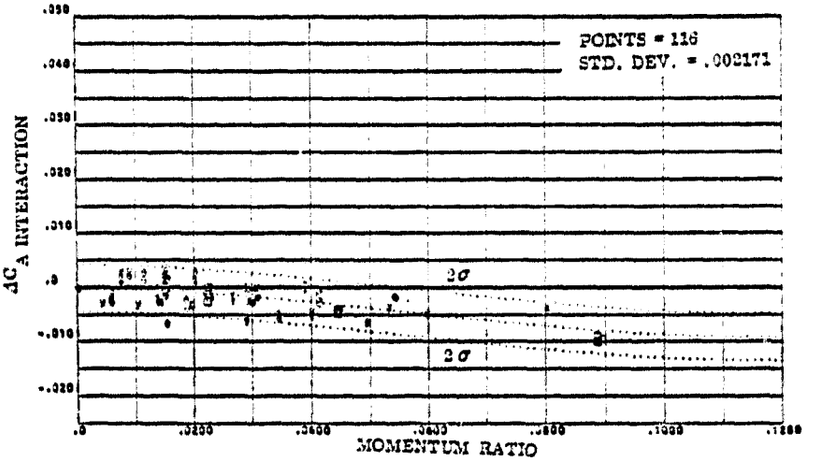

FIGURE 3-7f. PITCH UP AXIAL FORCE CORRELATION FROM 15→20 DEGREES ANGLE OF ATTACK

SYMBOLS	NOZZLE NUMBER	TEST NUMBER
0	N52	OA62, MA22
X	N78	OA62, MA22
□	N82	OA62, MA22
Y	N31	MA22
+	N36	MA22
*	N44	MA22
E	N48	MA22
◇	N95	OA169
V	N96	OA169
H	N97	OA169

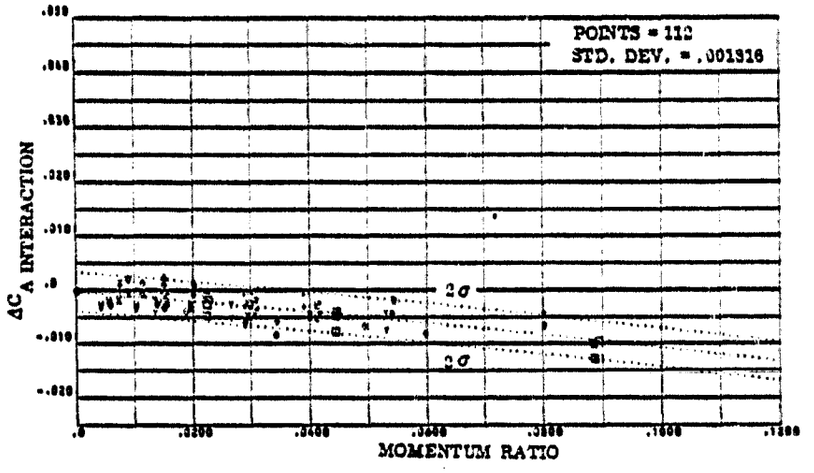

FIGURE 3-7g. PITCH UP AXIAL FORCE CORRELATION FROM 20→25 DEGREES ANGLE OF ATTACK

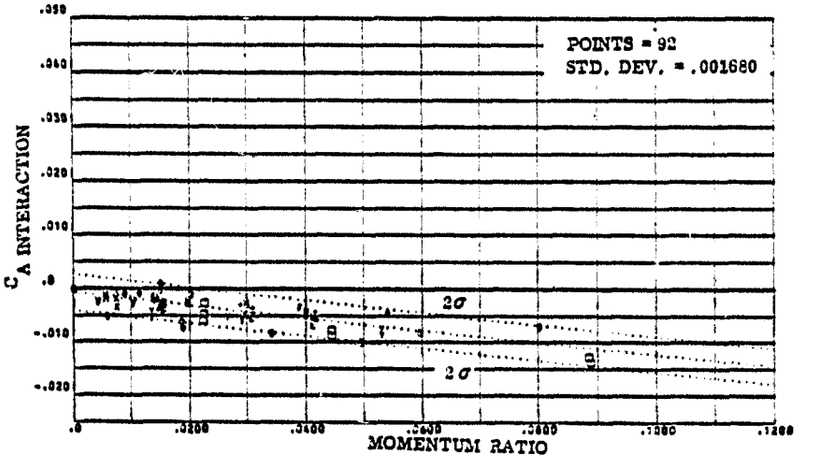

FIGURE 3-7 h. PITCH UP AXIAL FORCE CORRELATION FROM 25→30 DEGREES ANGLE OF ATTACK

SYMBOLS	NOZZLE NUMBER	TEST NUMBER
0	N52	OA82, MA22
X	N78	OA82, MA22
□	N82	OA82, MA22
Y	N31	MA22
+	N36	MA22
*	N44	MA22
L	N48	MA22
◐	N95	OA169
V	N96	OA169
H	N97	OA169

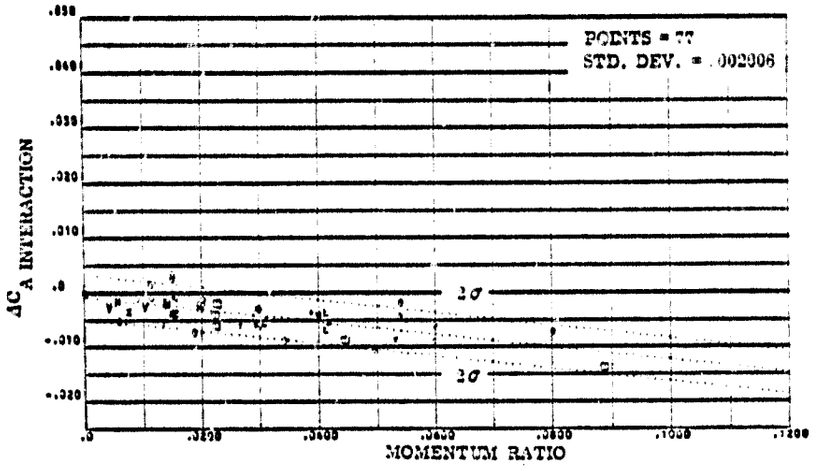

FIGURE 3-71. PITCH UP AXIAL FORCE CORRELATION FROM 30→35 DEGREES ANGLE OF ATTACK

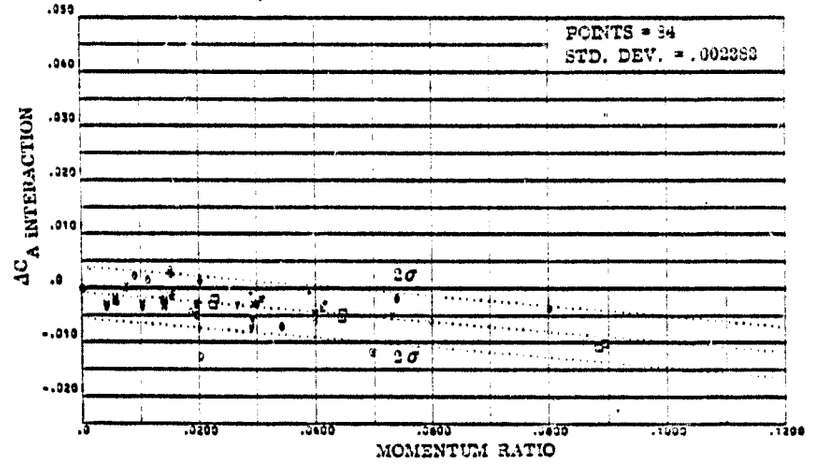

FIGURE 3-71. PITCH UP AXIAL FORCE CORRELATION FROM 35→MAX. DEGREES ANGLE OF ATTACK

SYMBOLS	NOZZLE NUMBER	TEST NUMBER
0	N62	OA62, MA22
X	N78	OA62, MA22
□	N82	OA62, MA22
Y	N31	MA22
+	N36	MA22
*	N44	MA22
L	N48	MA22
◐	N95	OA169
V	N96	OA169
H	N97	OA169

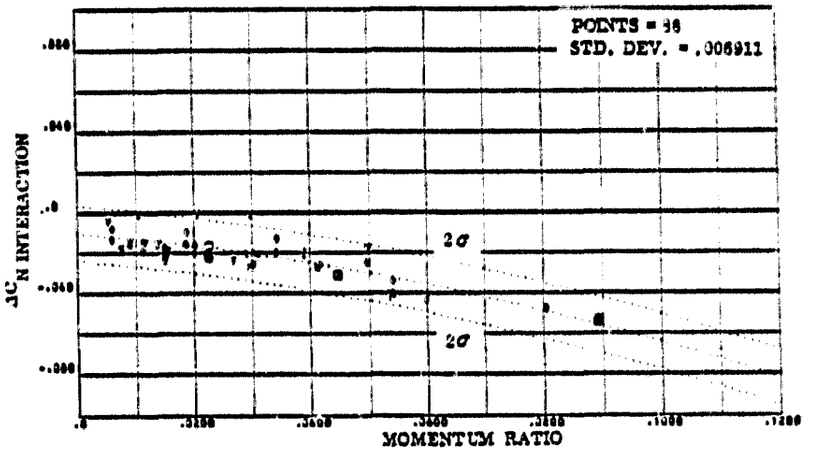

FIGURE 3-8 a. PITCH UP NORMAL FORCE CORRELATION FROM -10 TO -5 DEGREES ANGLE OF ATTACK

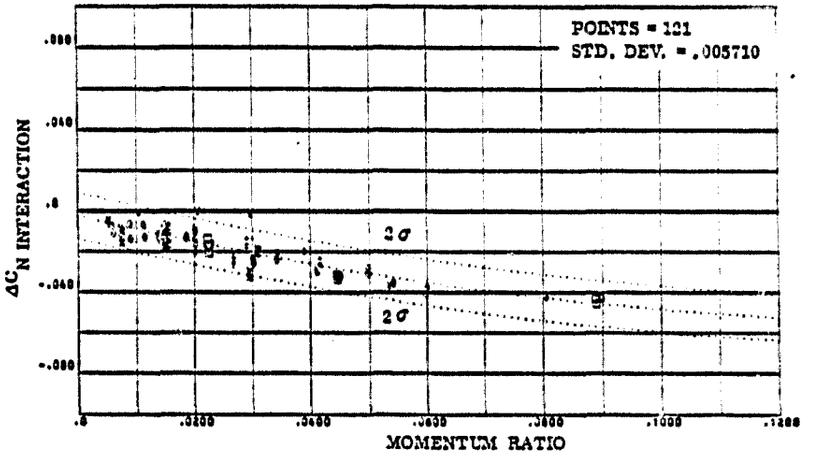

FIGURE 3-8 b. PITCH UP NORMAL FORCE CORRELATION FROM -5 TO 0 DEGREES ANGLE OF ATTACK

SYMBOLS	NOZZLE NUMBER	TEST NUMBER
0	N52	OA42, MA22
K	N70	OA82, MA22
□	N82	OA82, MA22
V	N31	MA22
+	N36	MA22
*	N44	MA22
E	N48	MA22
◇	N95	OA169
V	N96	OA169
H	N97	OA169

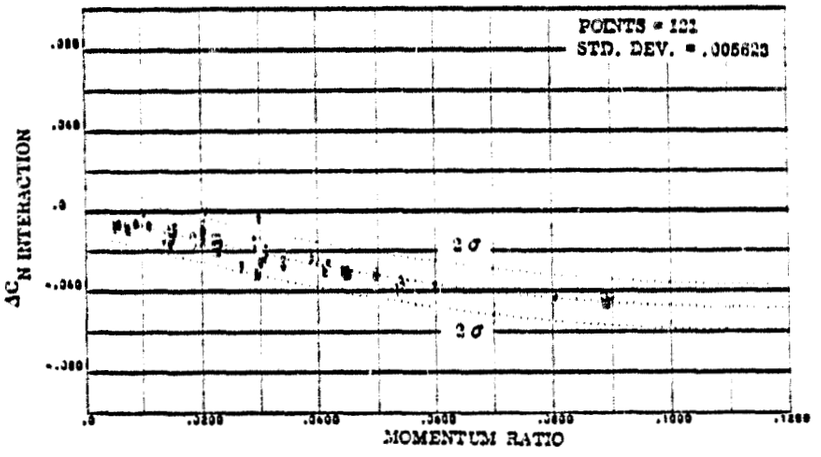

FIGURE 3-8 c. PITCH UP NORMAL FORCE CORRELATION FROM 0-5 DEGREES ANGLE OF ATTACK

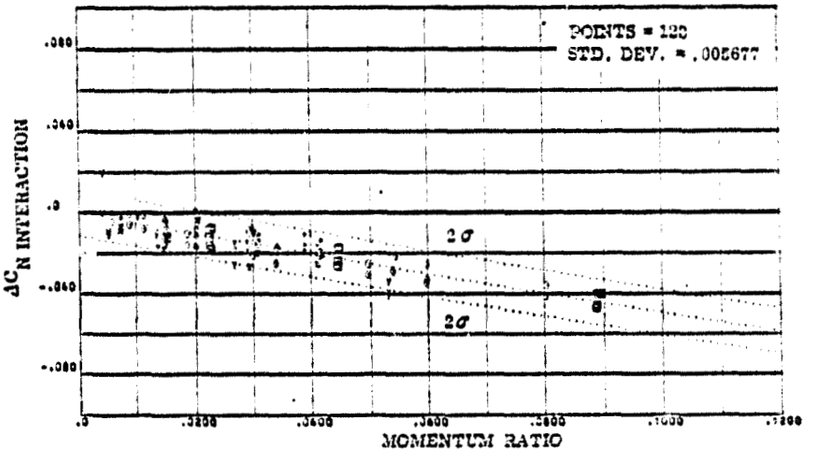

FIGURE 3-8 d. PITCH UP NORMAL FORCE CORRELATION FROM 5-10 DEGREES ANGLE OF ATTACK

SYMBOLS	NOZZLE NUMBER	TEST NUMBER
0	N52	OA82, MA22
X	N78	OA82, MA22
□	N82	OA82, MA22
Y	N31	MA22
+	N36	MA22
#	N44	MA22
L	N48	MA22
‹	N95	OA169
V	N96	OA169
H	N97	OA169

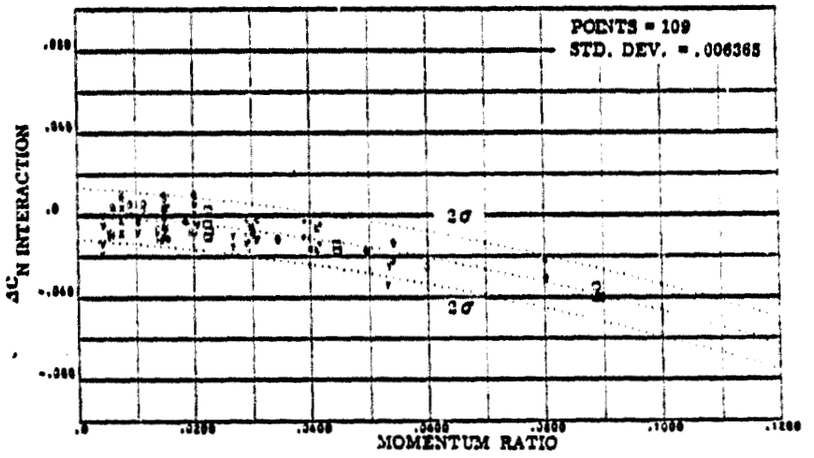

FIGURE 3-4 e. PITCH UP NORMAL FORCE CORRELATION FROM 10→15 DEGREES ANGLE OF ATTACK

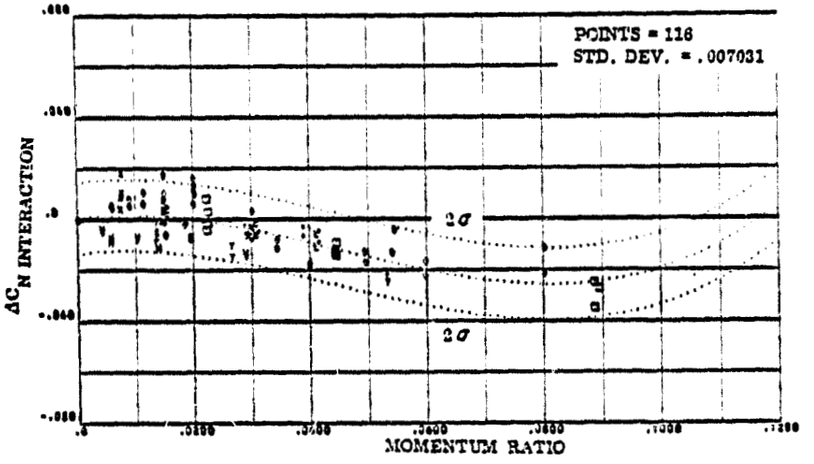

FIGURE 3-4 f. PITCH UP NORMAL FORCE CORRELATION FROM 15→20 DEGREES ANGLE OF ATTACK

SYMBOLS	NOZZLE NUMBER	TEST NUMBER
O	N52	OA82, MA22
X	N79	OA82, MA22
□	N82	OA82, MA22
+	N31	MA22
✱	N36	MA22
▷	N44	MA22
◁	N48	MA22
◇	N95	OA169
▽	N96	OA169
H	N97	OA169

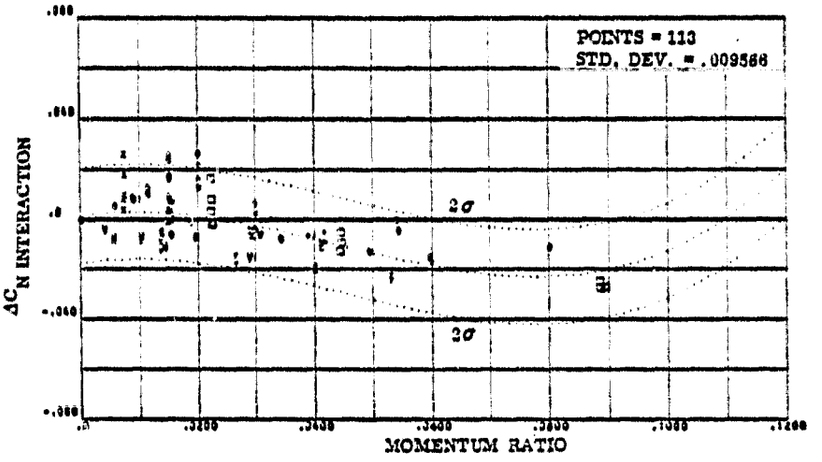

FIGURE 3-8 g. PITCH UP NORMAL FORCE CORRELATION FROM 20-25 DEGREES ANGLE OF ATTACK

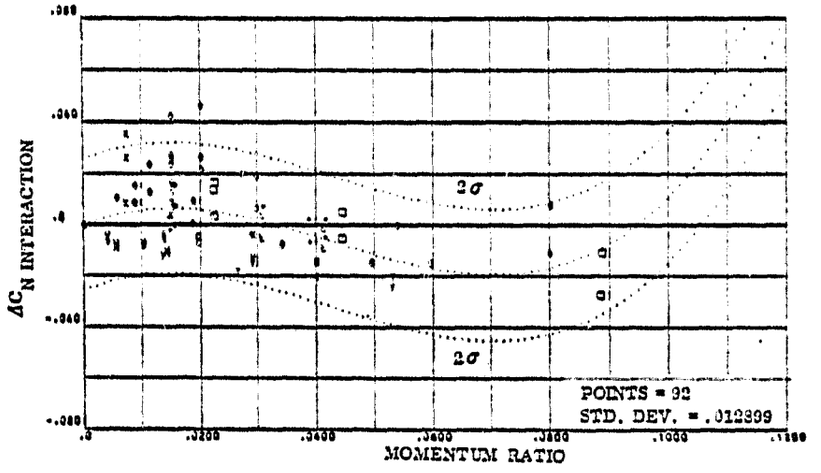

FIGURE 3-8 h. PITCH UP NORMAL FORCE CORRELATION FROM 25-30 DEGREES ANGLE OF ATTACK

SYMBOLS	NOZZLE NUMBER	TEST NUMBER
0	N52	OA82, MA22
×	N78	OA82, MA22
□	N82	OA82, MA22
Y	N31	MA22
+	N36	MA22
*	N44	MA22
⅄	N48	MA22
◇	N95	OA169
V	N96	OA169
R	N97	OA169

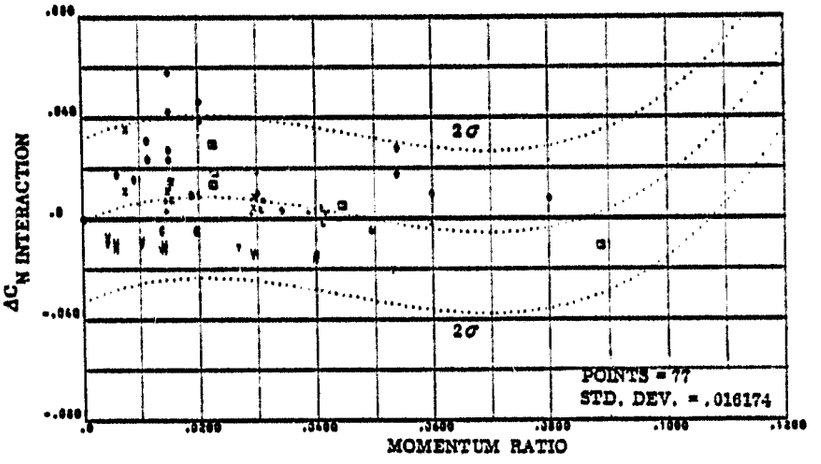

FIGURE 3-8 i. PITCH UP NORMAL FORCE CORRELATION FROM 30→35 DEGREES ANGLE OF ATTACK

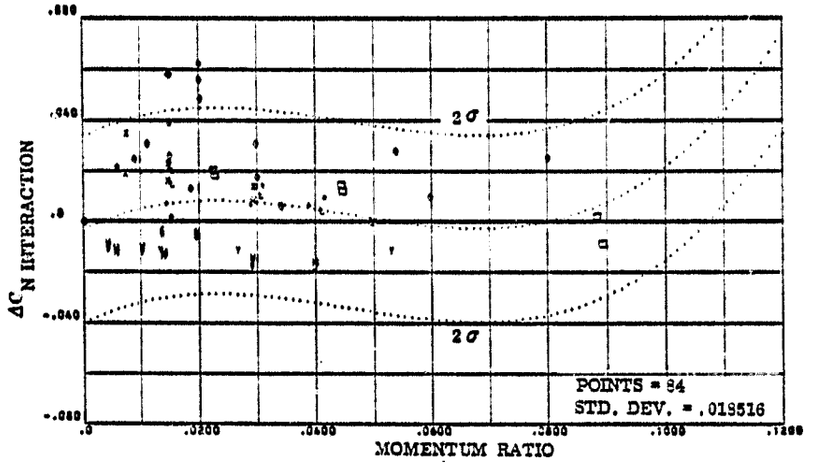

FIGURE 3-8 j. PITCH UP NORMAL FORCE CORRELATION FROM 35→MAX. DEGREES ANGLE OF ATTACK

SYMBOLS	NOZZLE NUMBER	TEST NUMBER
0	N52	OA82, MA22
X	N78	OA82, MA22
□	N82	OA82, MA22
Y	N31	MA22
+	N36	MA22
*	N44	MA22
L	N46	MA22
¢	N95	OA169
V	N96	OA169
H	N97	OA169

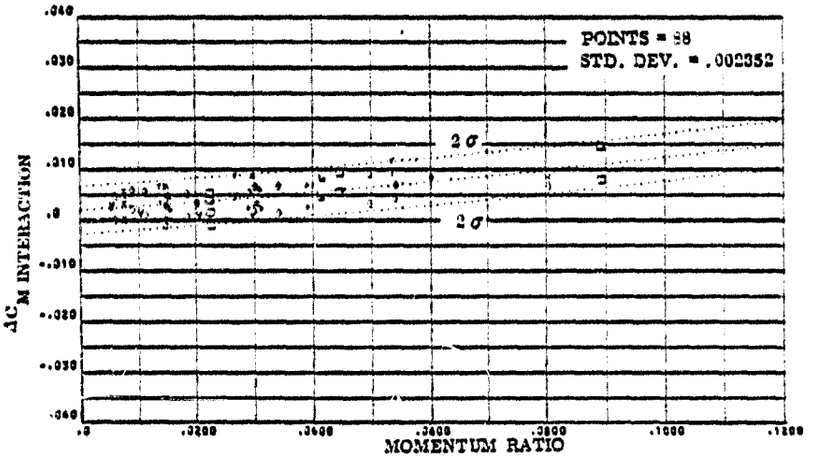

FIGURE 3-9a. PITCH UP PITCHING MOMENT CORRELATION FROM -10 TO -5 DEGREES ANGLE OF ATTACK

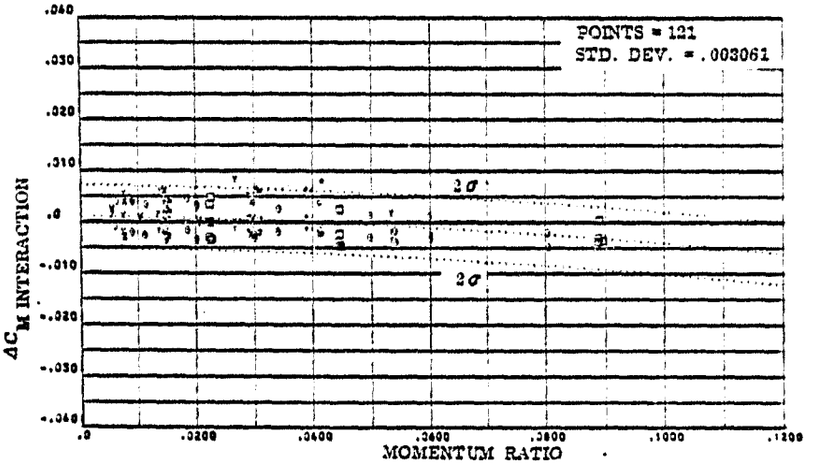

FIGURE 3-9b. PITCH UP PITCHING MOMENT CORRELATION FROM -5 TO 0 DEGREES ANGLE OF ATTACK

SYMBOLS	NOZZLE NUMBER	TEST NUMBER
0	N52	OA82, MA22
X	N78	OA82, MA22
□	N82	OA82, MA22
Y	N31	MA2[illegible]
+	N36	MA22
*	N44	MA22
E	N48	MA22
◐	N95	OA169
V	N96	OA169
H	N97	OA169

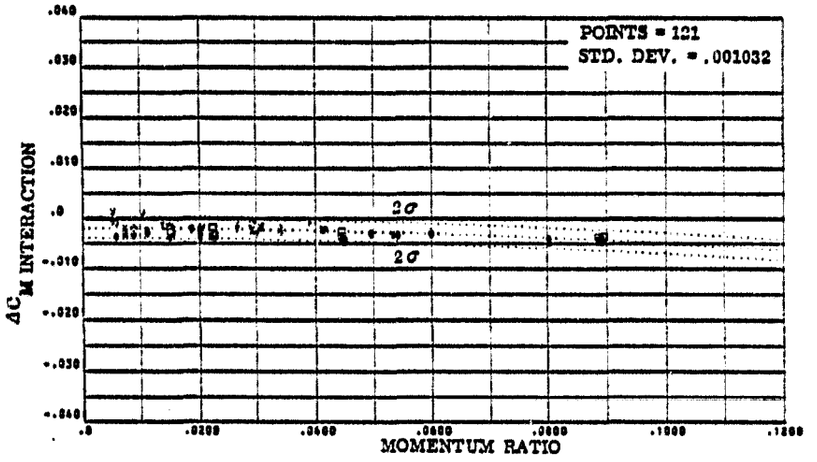

FIGURE 3-9c. PITCH UP PITCHING MOMENT CORRELATION FROM 0→5 DEGREES ANGLE OF ATTACK

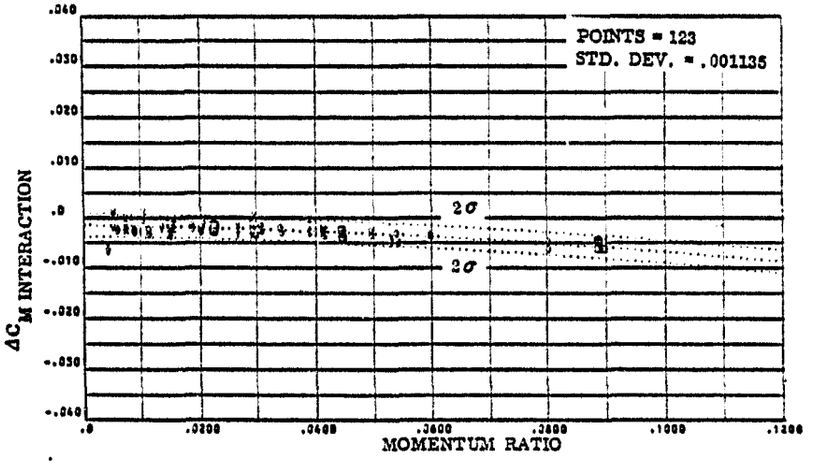

FIGURE 3-9d. PITCH UP PITCHING MOMENT CORRELATION FROM 5→10 DEGREES ANGLE OF ATTACK

SYMBOLS	NOZZLE NUMBER	TEST NUMBER
0	N52	OA52, MA22
×	N79	OA52, MA22
□	N62	OA52, MA22
▽	N31	MA22
+	N36	MA22
*	N44	MA22
L	N48	MA22
◐	N95	OA169
V	N96	OA169
H	N97	OA169

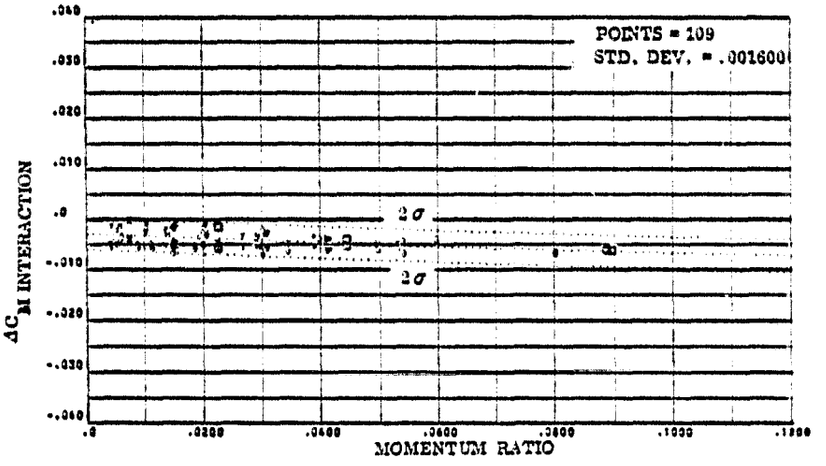

FIGURE 3-9e. PITCH UP PITCHING MOMENT CORRELATION FROM 10→15 DEGREES ANGLE OF ATTACK

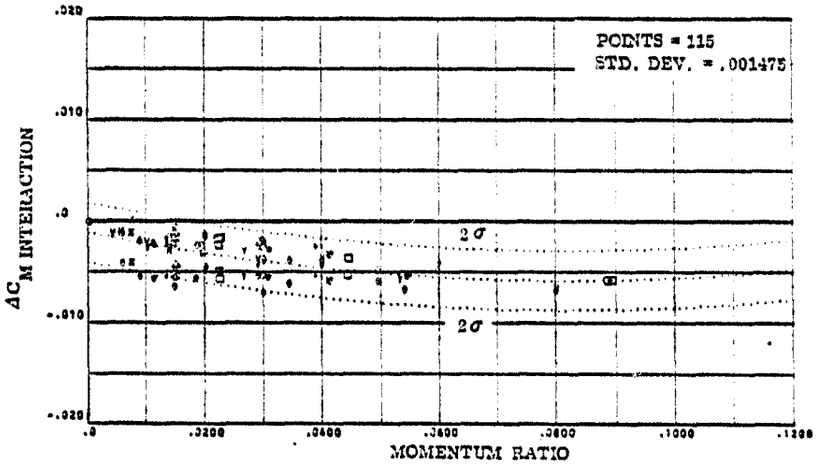

FIGURE 3-9f. PITCH UP PITCHING MOMENT CORRELATION FROM 15→20 DEGREES ANGLE OF ATTACK

SYMBOLS	NOZZLE NUMBER	TEST NUMBER
0	N52	OA82, MA22
X	N78	OA82, MA22
□	N82	OA82, MA22
Y	N31	MA22
+	N36	MA22
*	N44	MA22
◺	N48	MA22
◖	N95	OA169
V	N96	OA169
H	N97	OA169

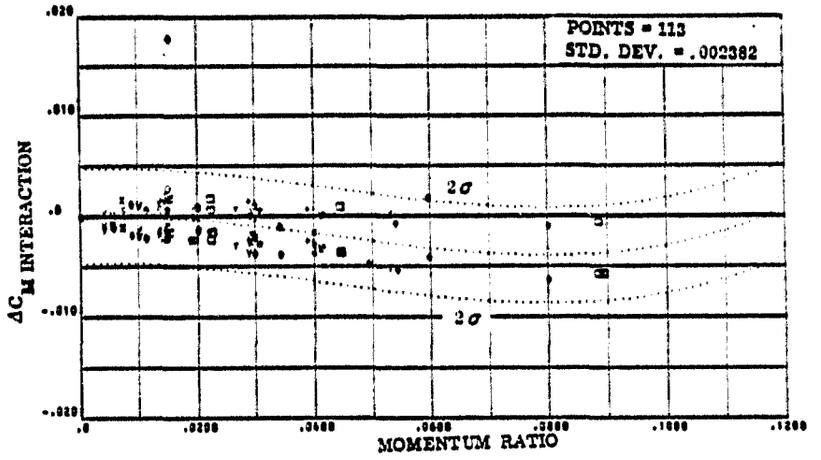

FIGURE 3-9g. PITCH UP PITCHING MOMENT CORRELATION FROM 20→25 DEGREES ANGLE OF ATTACK

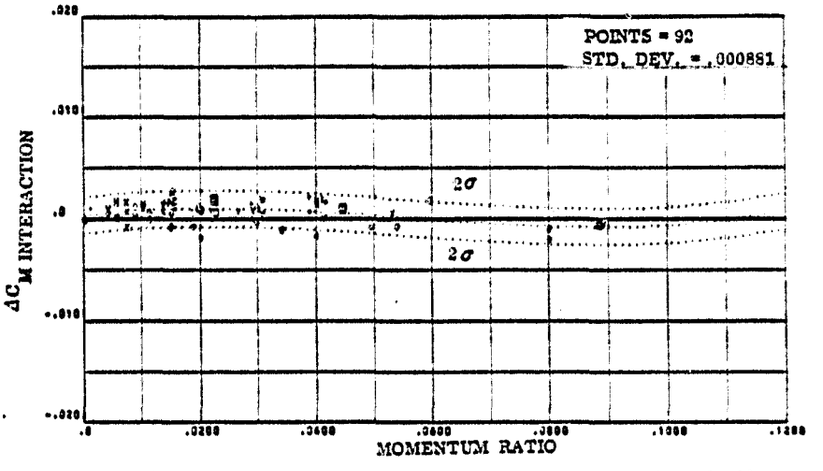

FIGURE 3-9h. PITCH UP PITCHING MOMENT CORRELATION FROM 25→30 DEGREES ANGLE OF ATTACK

SYMBOLS	NOZZLE NUMBER	TEST NUMBER
0	N52	OA82, MA22
X	N78	OA82, MA22
□	N82	OA82, MA22
Y	N31	MA22
+	N36	MA22
*	N44	MA22
L	N48	MA22
¢	N95	OA169
V	N96	OA169
R	N97	OA169

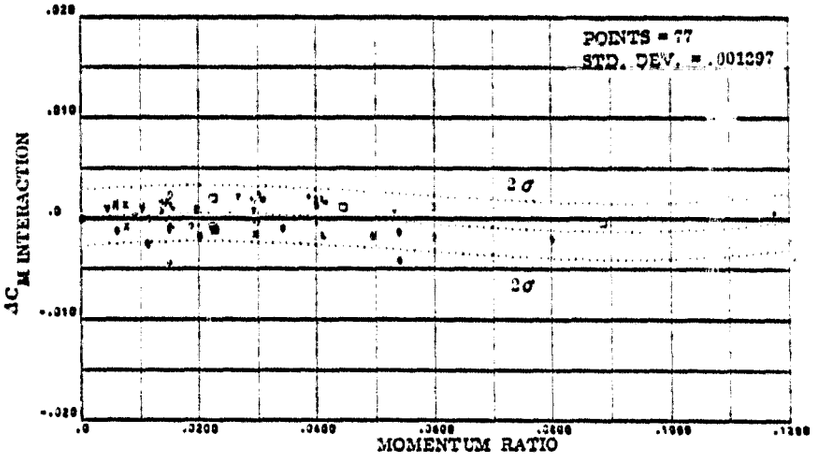

FIGURE 3-91. PITCH UP PITCHING MOMENT CORRELATION FROM 30→35 DEGREES ANGLE OF ATTACK

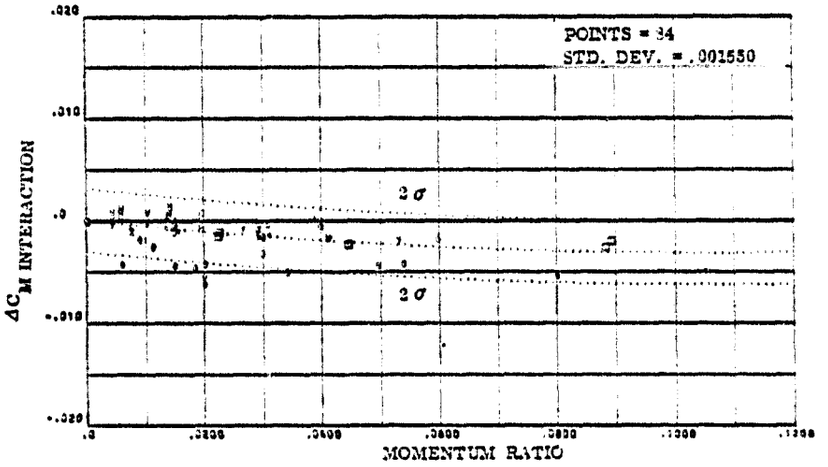

FIGURE 3-91. PITCH UP PITCHING MOMENT CORRELATION FROM 35→MAX. DEGREES ANGLE OF ATTACK

SYMBOLS	NOZZLE NUMBER	TEST NUMBER
0	N52	OA82, MA22
X	N78	OA82, MA22
□	N82	OA82, MA22
Y	N31	MA22
+	N36	MA22
*	N44	MA22
L	N48	MA22
◇	N85	OA169
V	N86	OA169
H	N87	OA169

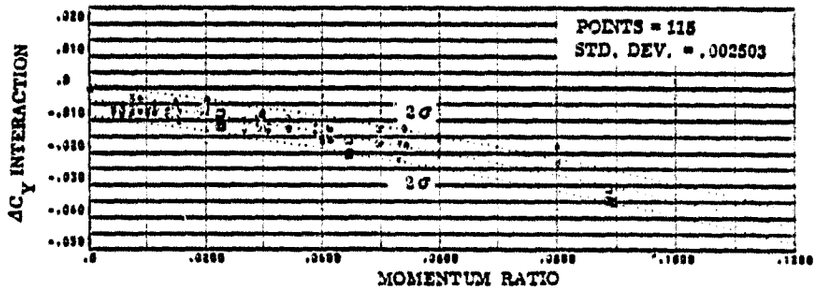

FIGURE 3-10a. PITCH UP SIDE FORCE CORRELATION FROM 15–20 DEGREES ANGLE OF ATTACK

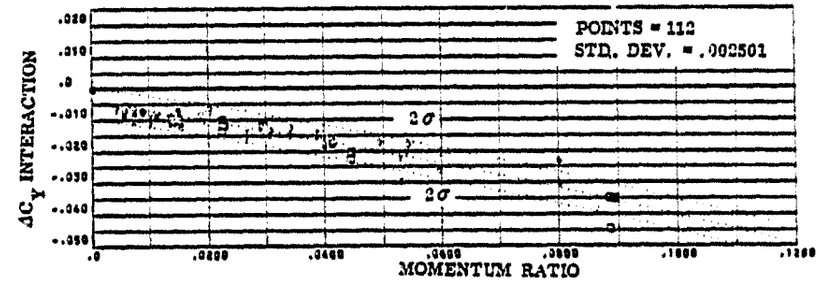

FIGURE 3-10b. PITCH UP SIDE FORCE CORRELATION FROM 20–25 DEGREES ANGLE OF ATTACK

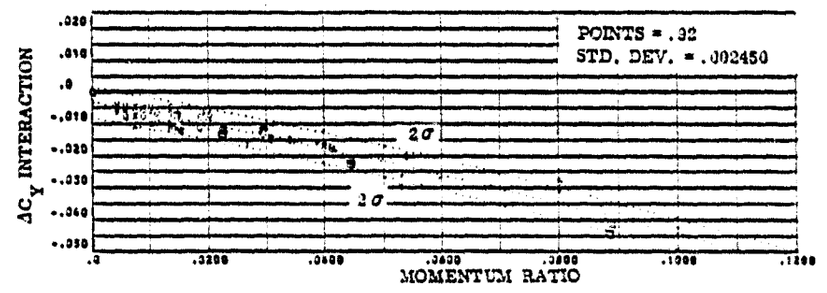

FIGURE 3-10c. PITCH UP SIDE FORCE CORRELATION FROM 25–30 DEGREES ANGLE OF ATTACK

SYMBOLS	NOZZLE NUMBER	TEST NUMBER
○	N52	OA82, MA22
×	N78	OA82, MA22
□	N82	OA82, MA22
▽	N31	MA22
+	N36	MA22
*	N44	MA22
◇	N48	MA22
◇	N95	OA169
V	N96	OA169
H	N97	OA169

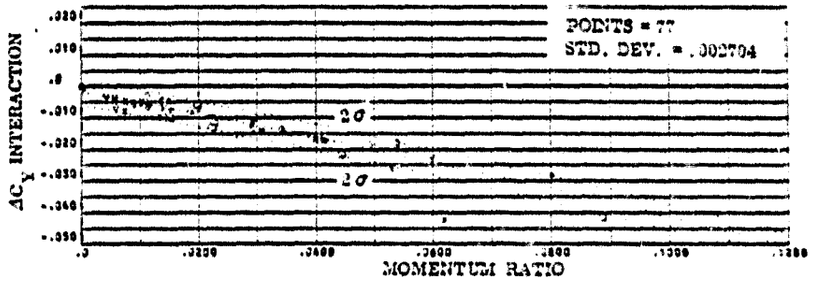

FIGURE 3-10d. PITCH UP SIDE FORCE CORRELATION FROM 30°-35° DEGREES ANGLE OF ATTACK

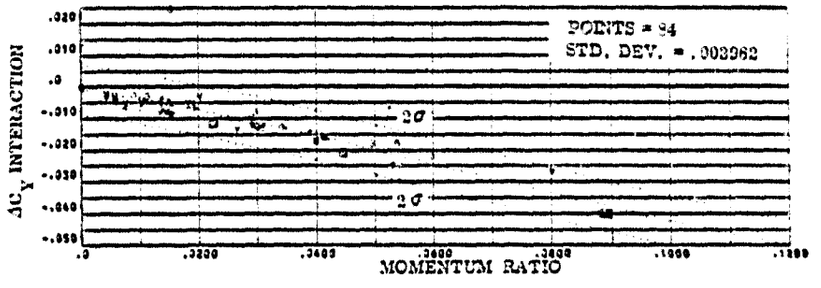

FIGURE 3-10e. PITCH UP SIDE FORCE CORRELATION FROM 35°-MAX. DEGREES ANGLE OF ATTACK

SYMBOLS	NOZZLE NUMBER	TEST NUMBER
0	N52	OA82, MA22
X	N78	OA82, MA22
□	N82	OA82, MA22
Y	N31	MA22
+	N36	MA22
*	N44	MA22
L	N48	MA22
‹	N95	OA169
V	N96	OA169
H	N97	OA169

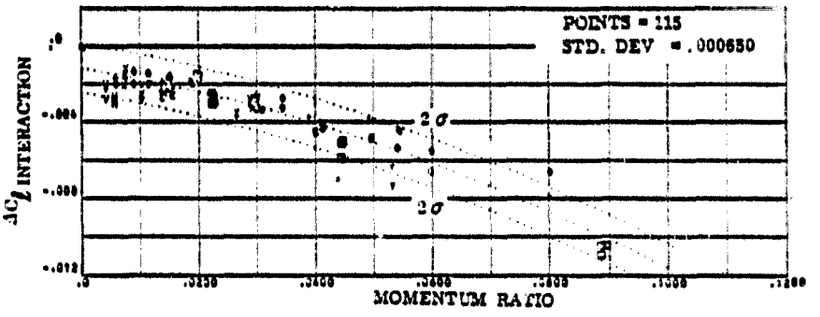

FIGURE 3-11 a. PITCH UP ROLLING MOMENT CORRELATION FROM 15→20 DEGREES ANGLE OF ATTACK

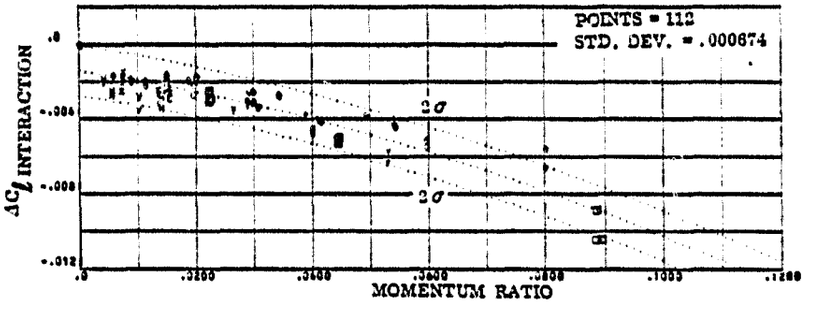

FIGURE 3-11 b. PITCH UP ROLLING MOMENT CORRELATION FROM 20→25 DEGREES ANGLE OF ATTACK

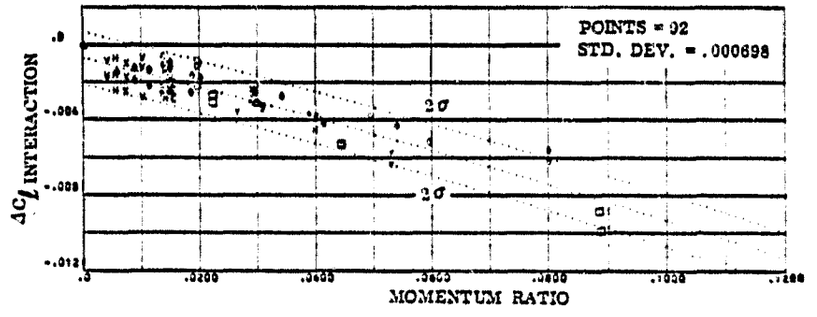

FIGURE 3-11c. PITCH UP ROLLING MOMENT CORRELATION FROM 25→30 DEGREES ANGLE OF ATTACK

SYMBOLS	NOZZLE NUMBER	TEST NUMBER
0	N52	OA82, MA22
X	N78	OA82, MA22
□	N82	OA82, MA22
+	N31	MA22
+	N36	MA22
*	N44	MA22
E	N48	MA22
◇	N95	OA169
V	N96	OA169
H	N97	OA169

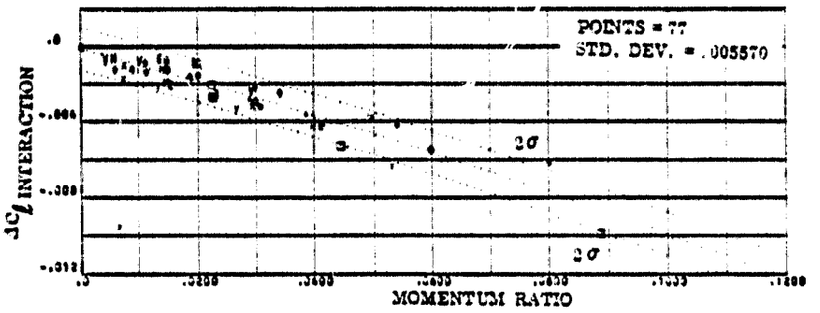

FIGURE 3-11d. PITCH UP ROLLING MOMENT CORRELATION FROM 30–35 DEGREES ANGLE OF ATTACK

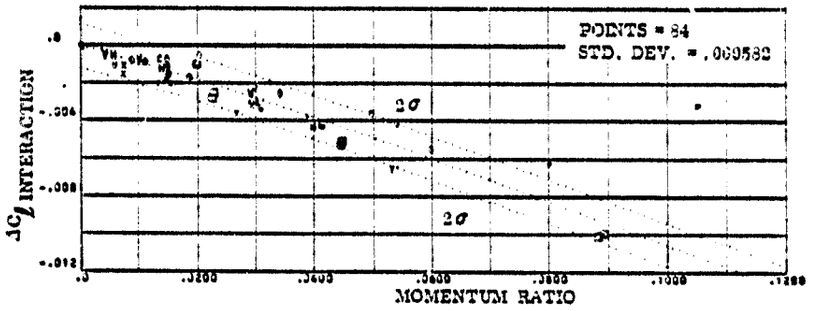

FIGURE 3-11e. PITCH UP ROLLING MOMENT CORRELATION FROM 35–MAX. DEGREES ANGLE OF ATTACK

SYMBOLS	NOZZLE NUMBER	TEST NUMBER
0	N52	OA62, MA22
✖	N76	OA62, MA22
□	N82	OA62, MA22
▼	N31	MA22
+	N36	MA22
*	N44	MA22
L	N48	MA22
◐	N95	OA169
V	N96	OA169
H	N97	OA169

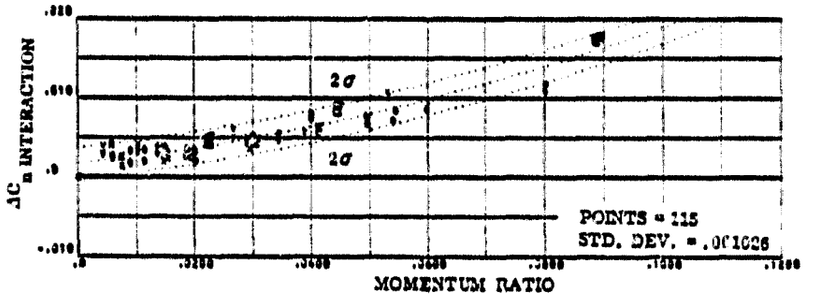

FIGURE 3-12a. PITCH UP YAWING MOMENT CORRELATION FROM 15=20 DEGREES ANGLE OF ATTACK

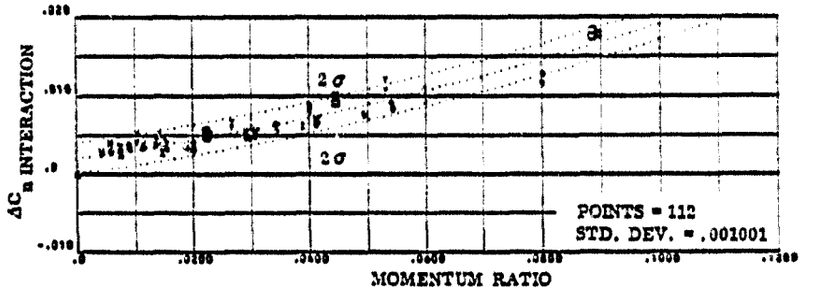

FIGURE 3-12 b. PITC P YAWING MOMENT CORRELATION FROM 20=25 DEGREES ANGLE OF ATTACK

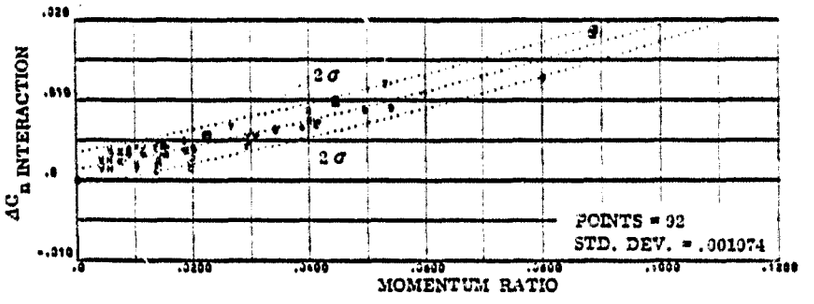

FIGURE 3-12c. PITCH UP YAWING MOMENT CORRELATION FROM 25=30 DEGREES ANGLE OF ATTACK

SYMBOLS	NOZZLE NUMBER	TEST NUMBER
0	N52	OA82, MA22
×	N78	OA82, MA22
□	N82	OA82, MA22
▽	N31	MA22
+	N36	MA22
*	N44	MA22
L	N48	MA22
◁	N95	OA169
V	N96	OA169
R	N97	OA169

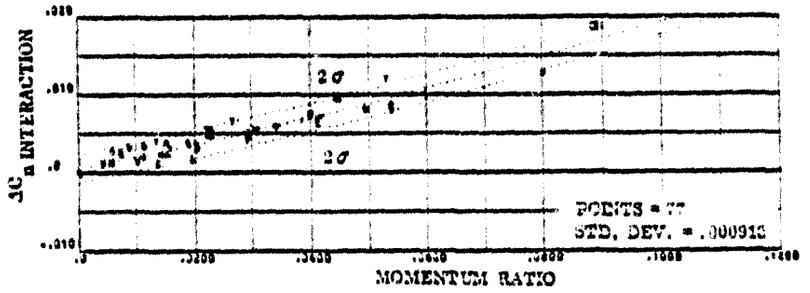

FIGURE 3-12d. PITCH UP YAWING MOMENT CORRELATION FROM 30→35 DEGREES ANGLE OF ATTACK

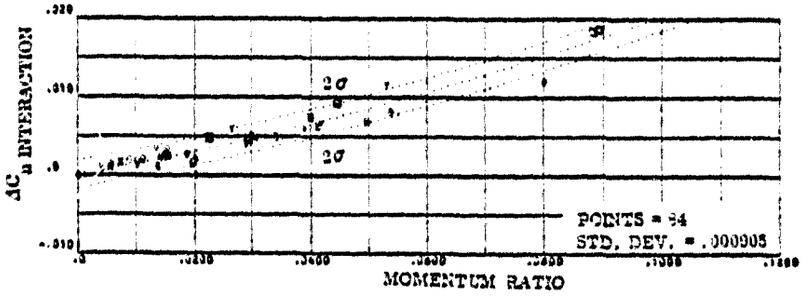

FIGURE 3-12e. PITCH UP YAWING MOMENT CORRELATION FROM 35→MAX, DEGREES ANGLE OF ATTACK

SYMBOLS	NOZZLE NUMBER	TEST NUMBER
0	N62	OA62, MA22
X	N76	OA62, MA22
□	N82	OA62, MA22
Y	N31	MA22
+	N36	MA22
*	N44	MA22
▷	N48	MA22
◁	N95	OA169
V	N96	OA169
H	N97	OA169

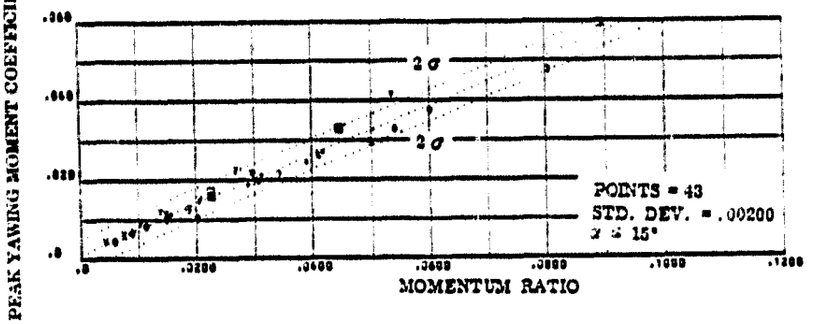

FIGURE 3-13 a. PITCH UP RCS PEAK YAWING MOMENT AT LOW ANGLES OF ATTACK

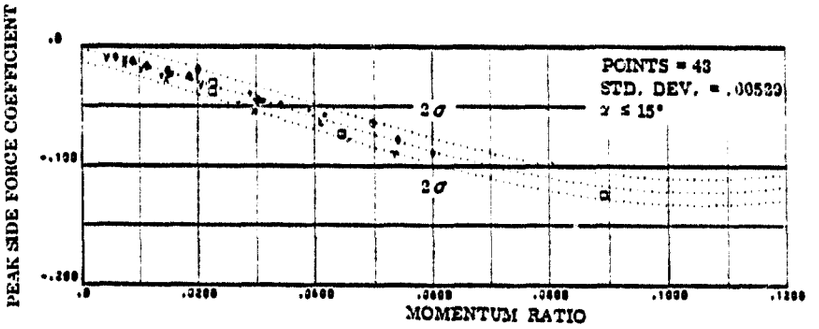

FIGURE 3-13b. PITCH UP RCS PEAK SIDE FORCE AT LOW ANGLES OF ATTACK

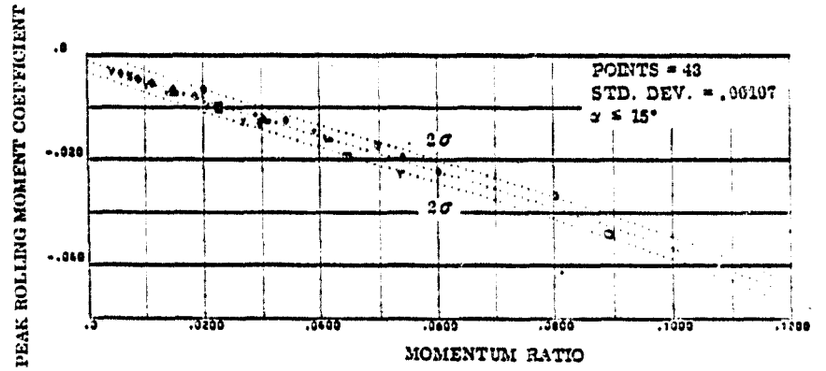

FIGURE 3-13 c. PITCH UP RCS PEAK ROLLING MOMENT AT LOW ANGLES OF ATTACK

SYMBOLS	NOZZLE NUMBER	TEST NUMBER
O	N52	OA82, MA22
X	N78	OA82, MA22
□	N82	OA82, MA22
Y	N31	MA22
+	N36	MA22
*	N44	MA22
▷	N48	MA22
◁	N95	OA169
V	N96	OA169
H	N97	OA168

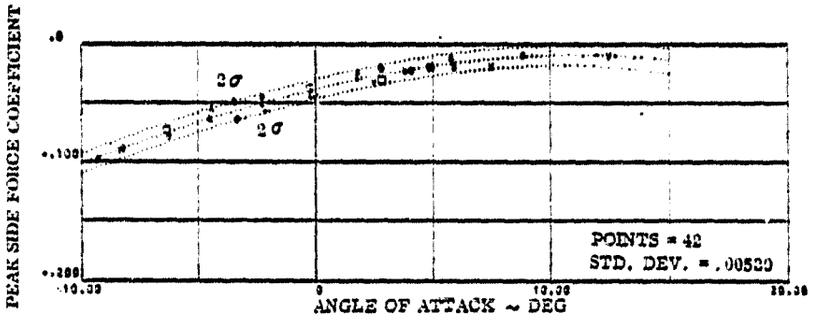

FIGURE 3-14a. PITCH UP RCS PEAK SIDE FORCE CORRELATION WITH ANGLE OF ATTACK

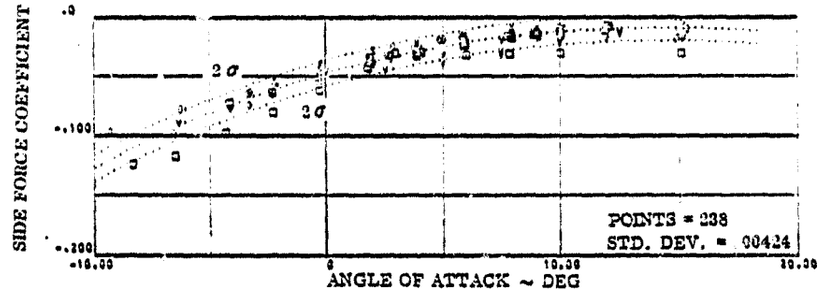

FIGURE 3-14b. PITCH UP RCS SIDE FORCE VARIATION FROM PEAK VALUE TO 15 DEGREES ANGLE OF ATTACK

SYMBOLS	NOZZLE NUMBER	TEST NUMBER
0	N82	OA82, MA22
✕	N78	OA82, MA22
□	N82	OA82, MA22
▽	N31	MA22
+	N36	MA22
*	N44	MA22
▷	N48	MA22
◇	N95	OA169
V	N96	OA169
H	N97	OA169

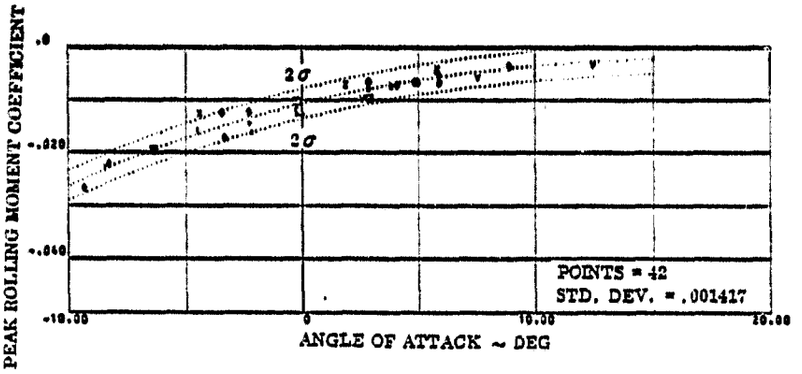

FIGURE 3-14c. PITCH UP RCS PEAK ROLLING MOMENT CORRELATION WITH ANGLE OF ATTACK

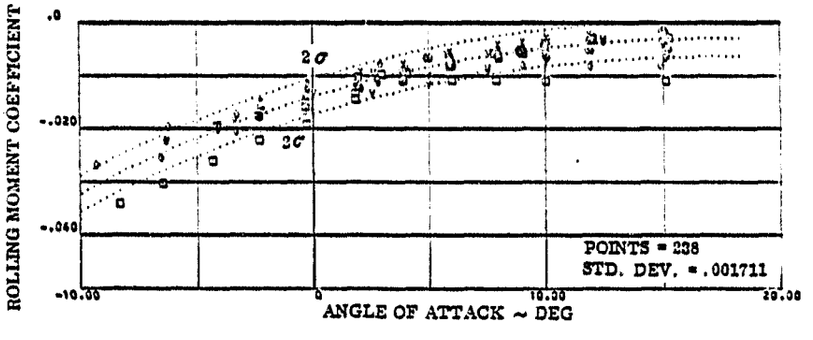

FIGURE 3-14d. PITCH UP RCS ROLLING MOMENT VARIATION FROM PEAK VALUE TO 15 DEGREES ANGLE OF ATTACK

SYMBOLS	NOZZLE NUMBER	TEST NUMBER
0	N52	OA82, MA22
X	N78	OA82, MA22
□	N82	OA82, MA22
Y	N31	MA22
+	N36	MA22
*	N44	MA22
L	N48	MA22
◇	N95	OA169
V	N96	OA169
H	N97	OA169

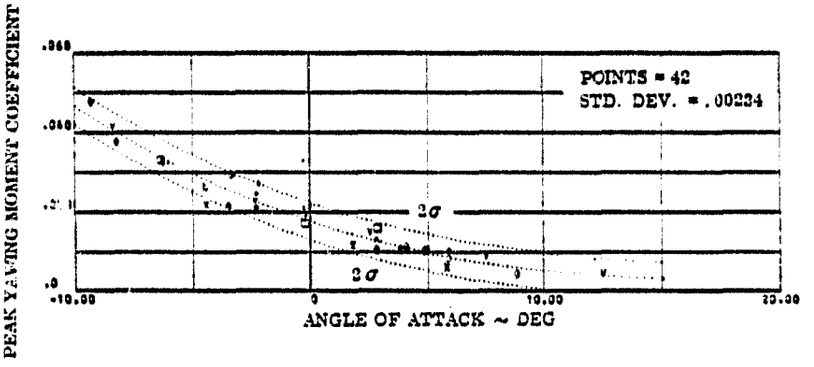

FIGURE 3-14e. PITCH UP RCS PEAK YAWING MOMENT CORRELATION WITH ANGLE OF ATTACK

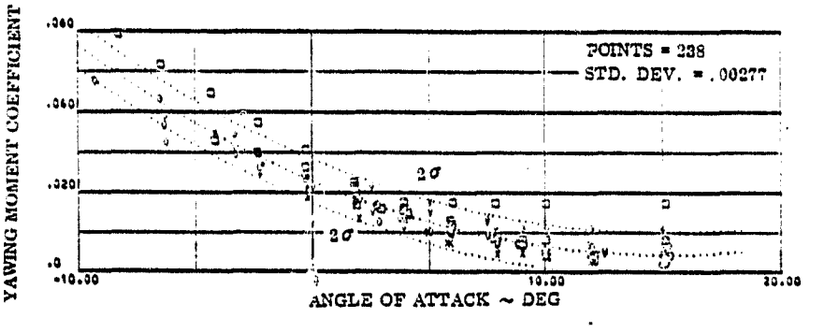

FIGURE 3-14f. PITCH UP RCS YAWING MOMENT VARIATION FROM PEAK VALUE TO 15 DEGREES ANGLE OF ATTACK

SYMBOLS	NOZZLE NUMBER	TEST NUMBER
0	N52	OA82, MA22
X	N78	OA82, MA22
□	N82	OA82, MA22
Y	N31	MA22
+	N36	MA22
*	N44	MA22
⊵	N48	MA22
◁	N95	OA169
V	N96	OA169
H	N97	OA169

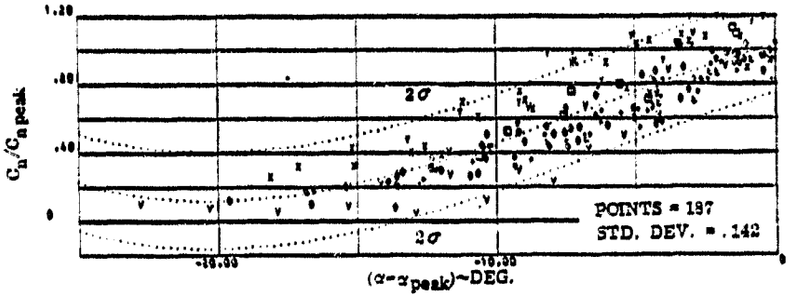

FIGURE 3-15a. PITCH UP RCS YAWING MOMENT CORRELATION AT ANGLES BELOW PEAK VALUES

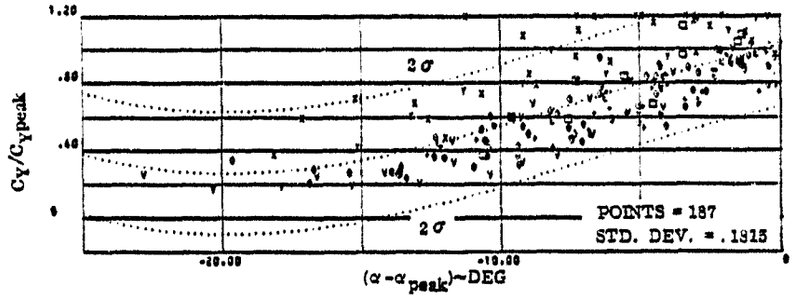

FIGURE 3-15b. PITCH UP RCS SIDE FORCE CORRELATION AT ANGLES BELOW PEAK VALUES

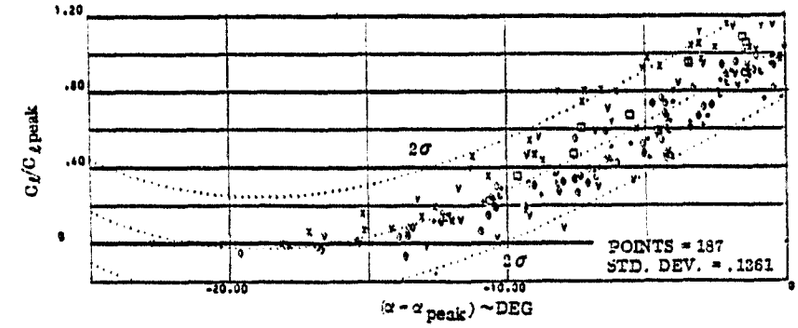

FIGURE 3-15c. PITCH UP RCS ROLLING MOMENT CORRELATION AT ANGLES BELOW PEAK VALUES

SYMBOLS	NOZZLE NUMBER	TEST NUMBER
0	N51	OA82, MA22
X	N61	MA22
□	N85	OA82, MA22
Y	N33	MA22
+	N37	MA22
C	N95	OA169
V	N96	OA169
H	N97	OA169

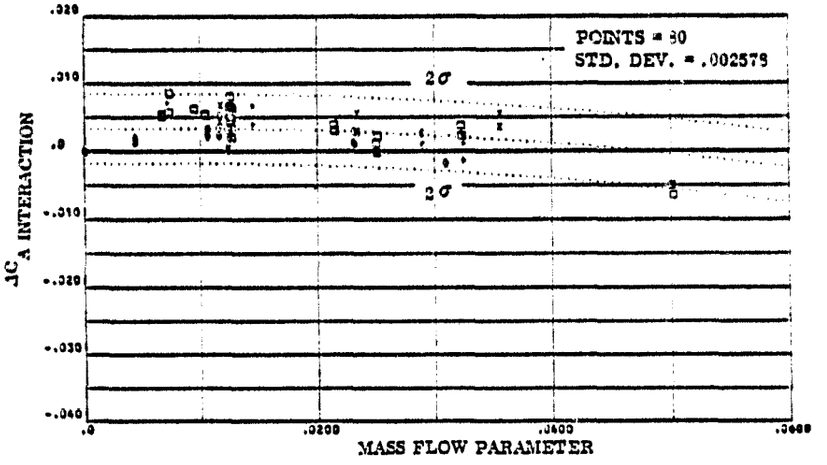

FIGURE 3-16 a. YAW R.C.S AXIAL FORCE CORRELATION FROM -10 to -5 DEGREES ANGLE OF ATTACK

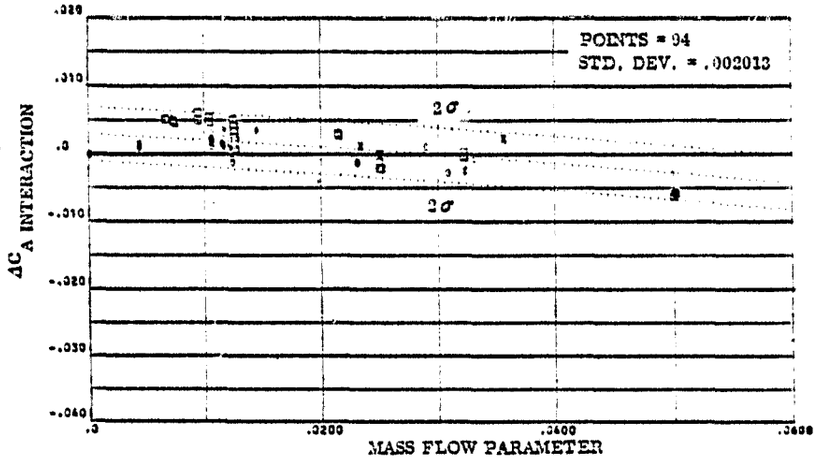

FIGURE 3-16 b. YAW R.C.S AXIAL FORCE CORRELATION FROM -5 to 0 DEGREES ANGLE OF ATTACK

SYMBOLS	NOZZLE NUMBER	TEST NUMBER
0	N61	OA62, MA22
×	N61	MA22
□	N65	OA62, MA22
▽	N33	MA22
+	N37	MA22
C	N95	OA169
V	N96	OA169
H	N97	OA169

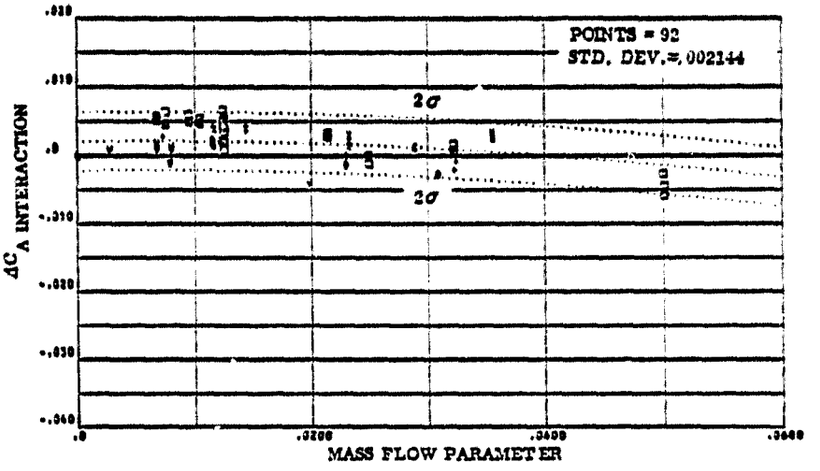

FIGURE 3-16 c. YAW R.C.S AXIAL FORCE CORRELATION FROM 0–5 DEGREES ANGLE OF ATTACK

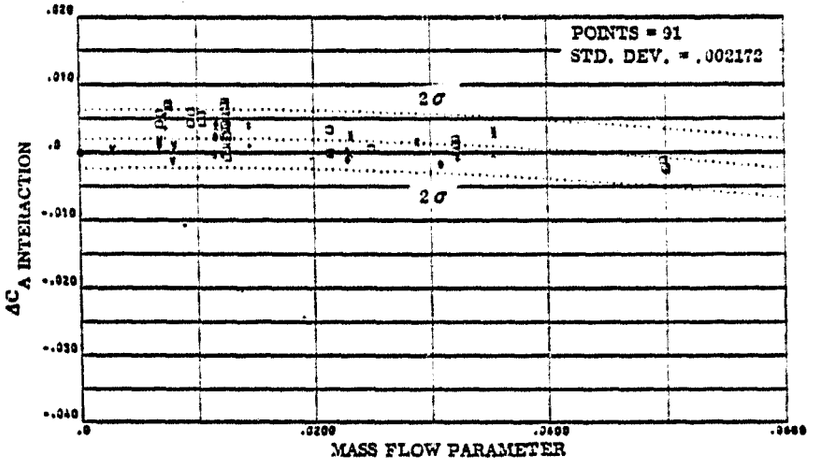

FIGURE 3-16 d. YAW R.C.S AXIAL FORCE CORRELATION FROM 5–10 DEGREES ANGLE OF ATTACK

SYMBOLS	NOZZLE NUMBER	TEST NUMBER
O	N61	OA82, MA22
X	N61	MA22
□	N85	OA82, MA22
Y	N33	MA22
+	N37	MA22
C	N95	OA169
V	N96	OA169
H	N97	OA169

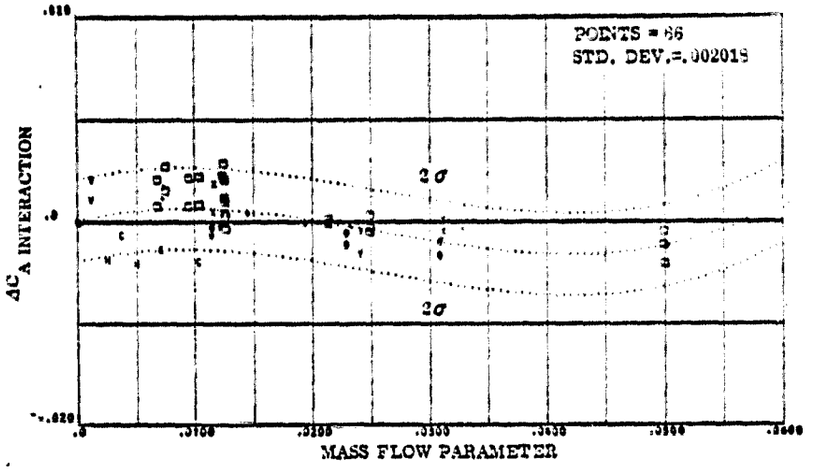

FIGURE 3-16 e. YAW R.C.S AXIAL FORCE CORRELATION FROM 10—15 DEGREES ANGLE OF ATTACK

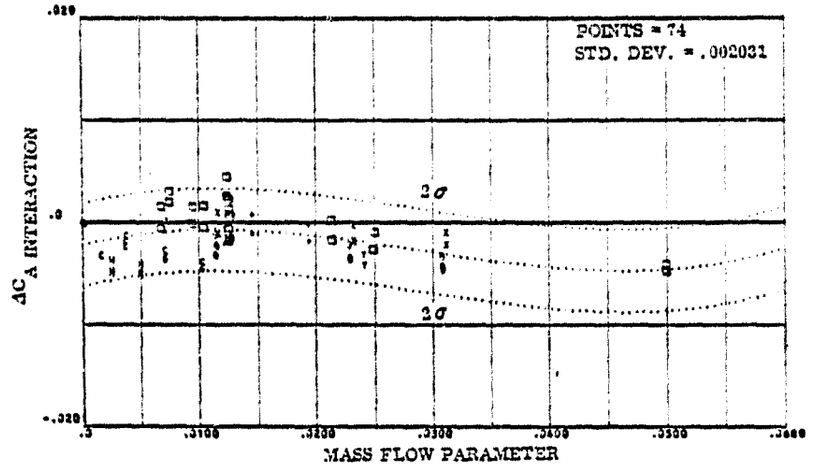

FIGURE 3-16 f. YAW R.C.S AXIAL FORCE CORRELATION FROM 15—20 DEGREES ANGLE OF ATTACK

SYMBOLS	NOZZLE NUMBER	TEST NUMBER
0	N61	OA82, MA22
⋈	N61	MA22
□	N65	OA82, MA22
+	N33	MA22
◇	N37	MA22
C	N95	OA169
V	N96	OA169
H	N97	OA169

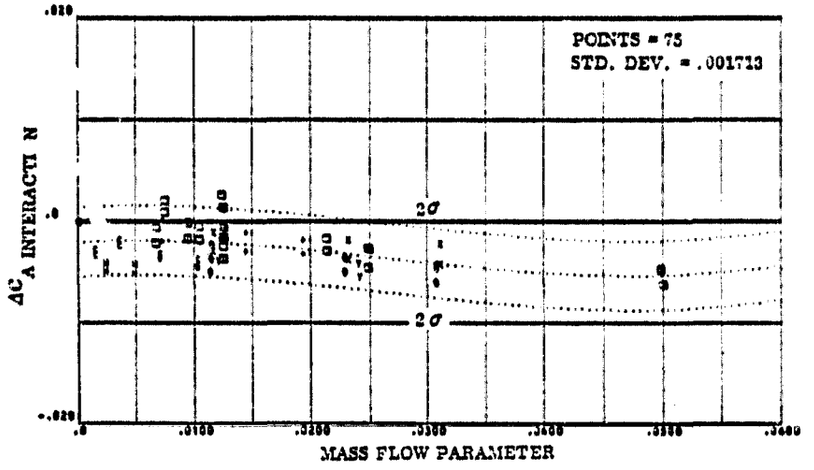

FIGURE 3-16 g. YAW R.C.S AXIAL FORCE CORRELATION FROM 20→25 DEGREES ANGLE OF ATTACK

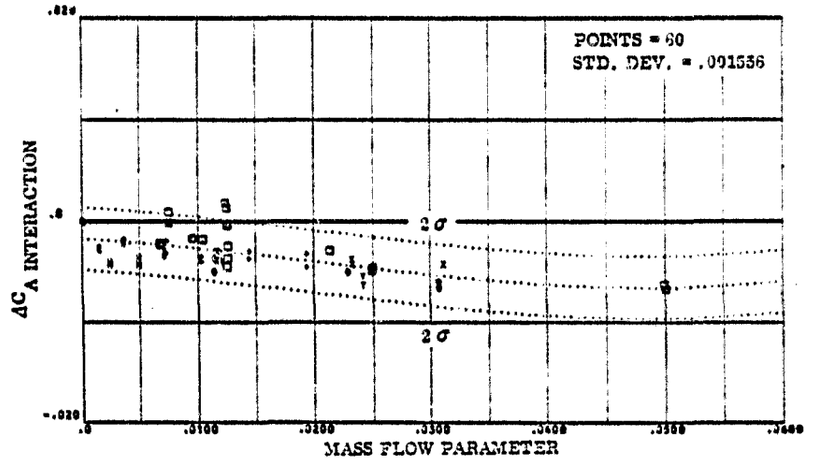

FIGURE 3-16 h. YAW R.C.S AXIAL FORCE CORRELATION FROM 25→30 DEGREES ANGLE OF ATTACK

SYMBOLS	NOZZLE NUMBER	TEST NUMBER
0	N31	OA82, MA22
X	N61	MA22
□	N85	OA82, MA22
▽	N33	MA22
+	N37	MA22
C	N35	OA169
V	N96	OA169
H	N97	OA169

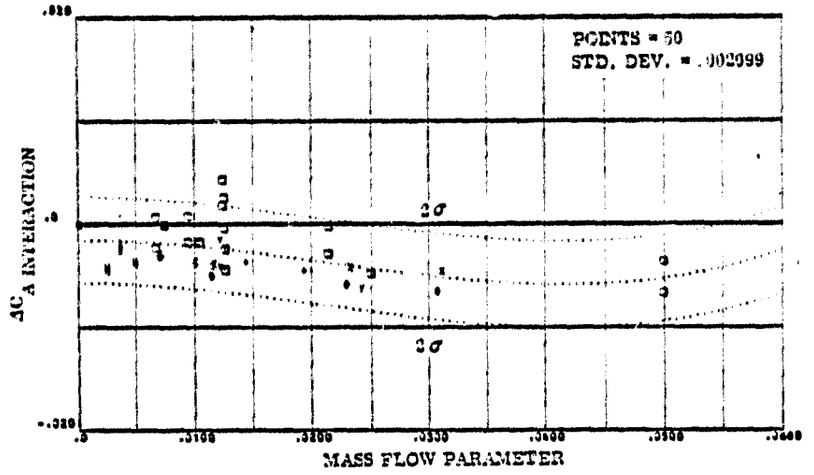

FIGURE 3-16 i. YAW R.C.S AXIAL FORCE CORRELATION FROM 30→35 DEGREES ANGLE OF ATTACK

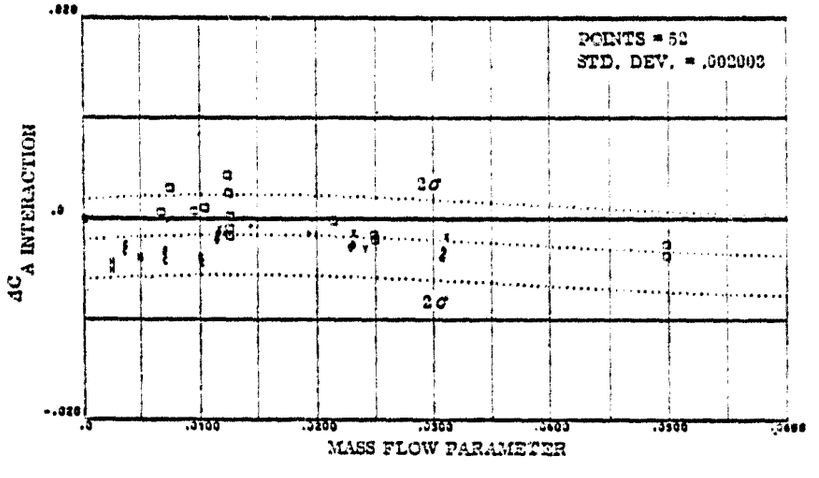

FIGURE 3-16 j. YAW R.C.S AXIAL FORCE CORRELATION FROM 35→MAX. DEGREES ANGLE OF ATTACK

SYMBOLS	NOZZLE NUMBER	TEST NUMBER
0	N61	OA82, MA22
×	N61	MA22
□	N85	OA82, MA22
Y	N33	MA22
+	N37	MA22
C	N95	OA169
V	N96	OA169
H	N97	OA169

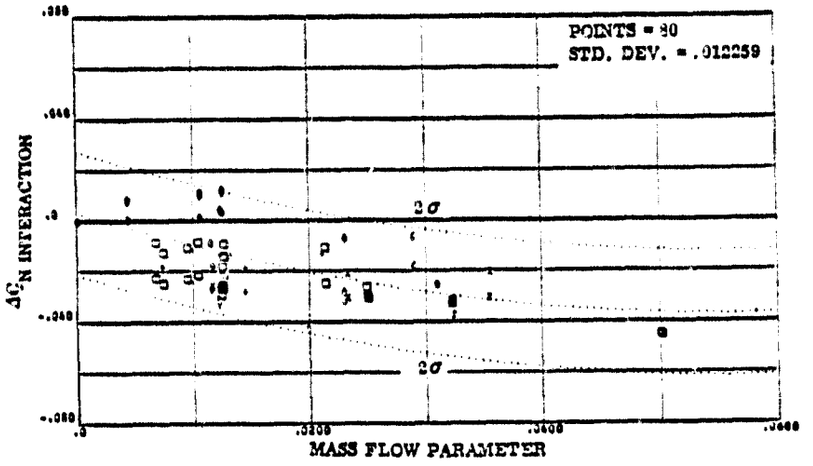

FIGURE 3-17a. YAW R.C.S. NORMAL FORCE CORRELATION FROM -10 — -5 DEGREES ANGLE OF ATTACK

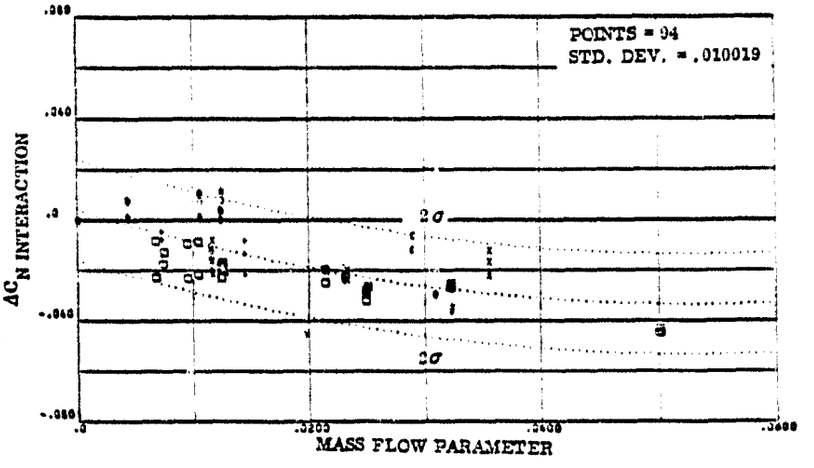

FIGURE 3-17b. YAW R.C.S. NORMAL FORCE CORRELATION FROM -5 — 0 DEGREES ANGLE OF ATTACK

SYMBOLS	NOZZLE NUMBER	TEST NUMBER
○ •	N51	OA82, MA22
X	N61	MA22
□	N85	OA82, MA22
Y	N33	MA22
+	N37	MA22
C	N95	OA169
V	N96	OA169
H	N97	OA169

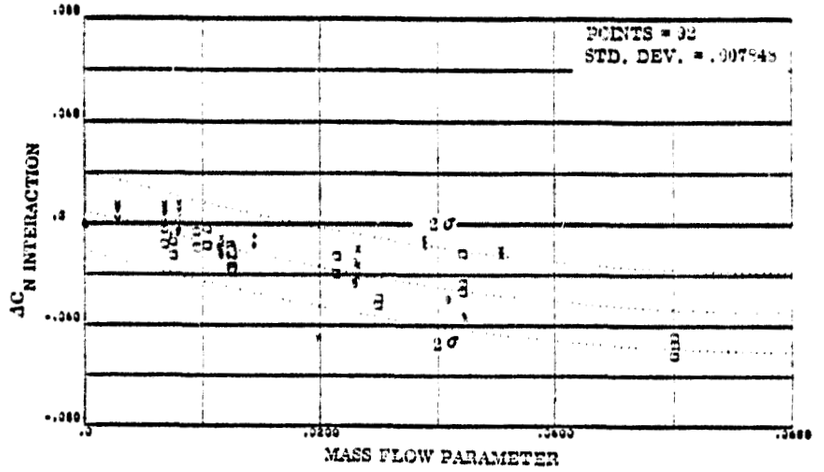

FIGURE 3-17c. YAW R.C.S. NORMAL FORCE CORRELATION FROM 0→5 DEGREES ANGLE OF ATTACK

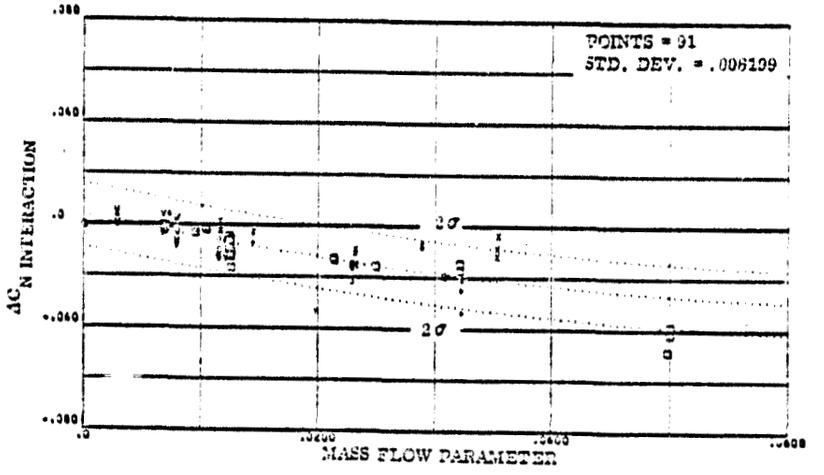

FIGURE 3-17d. YAW R.C.S. NORMAL FORCE CORRELATION FROM 5→10 DEGREES ANGLE OF ATTACK

SYMBOLS	NOZZLE NUMBER	TEST NUMBER
0	N81	OA82, MA22
⊠	N61	MA22
□	N85	OA82, MA22
Y	N33	MA22
+	N37	MA22
C	N95	OA169
V	N96	OA169
H	N97	OA169

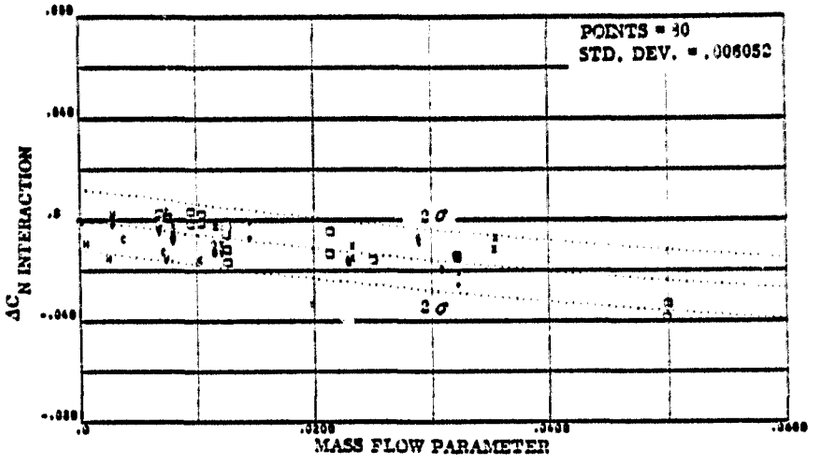

FIGURE 3-17e. YAW R.C.S. NORMAL FORCE CORRELATION FROM 10→15 DEGREES ANGLE OF ATTACK

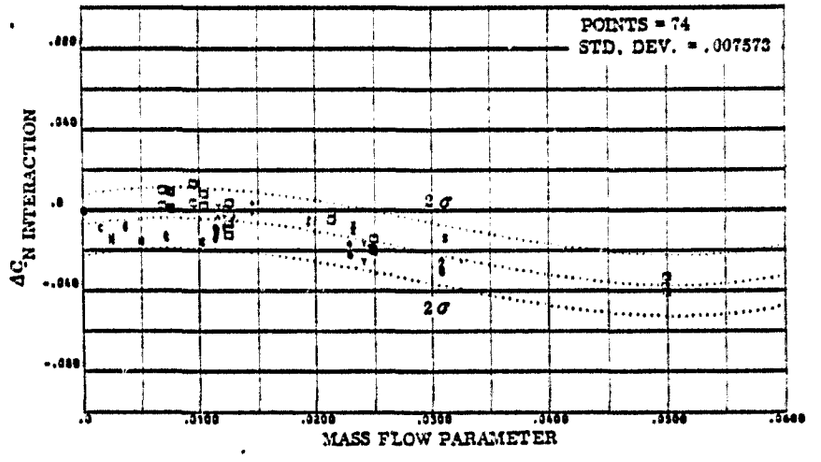

FIGURE 3-17f. YAW R.C.S. NORMAL FORCE CORRELATION FROM 15→20 DEGREES ANGLE OF ATTACK

SYMBOLS	NOZZLE NUMBER	TEST NUMBER
○	N57	OA92, MA22
⊠	N61	MA22
⊞	N86	OA92, MA22
+	N33	MA22
◇	N37	MA22
▽	N95	OA169
⊟	N96	OA169
H	N97	OA169

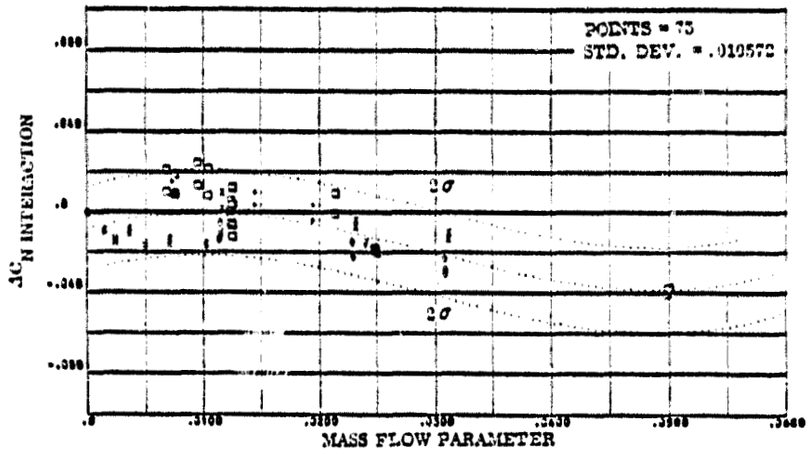

FIGURE 3-17g. YAW R.C.S. NORMAL FORCE CORRELATION FROM 20→25 DEGREES ANGLE OF ATTACK

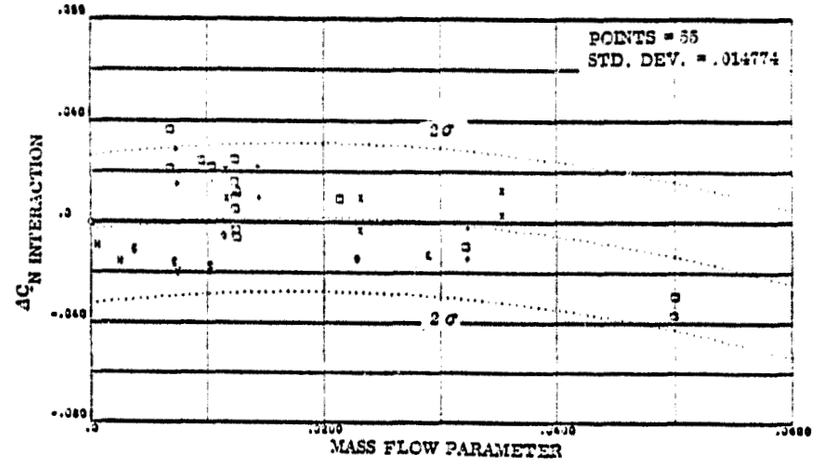

FIGURE 3-17h. YAW R.C.S. NORMAL FORCE CORRELATION FROM 25→30 DEGREES ANGLE OF ATTACK

SYMBOLS	NOZZLE NUMBER	TEST NUMBER
0	N61	OA62, MA22
⋈	N61	MA22
□	N65	OA62, MA22
✕	N33	MA22
+	N37	MA22
⊂	N95	OA169
∨	N96	OA169
H	N97	OA169

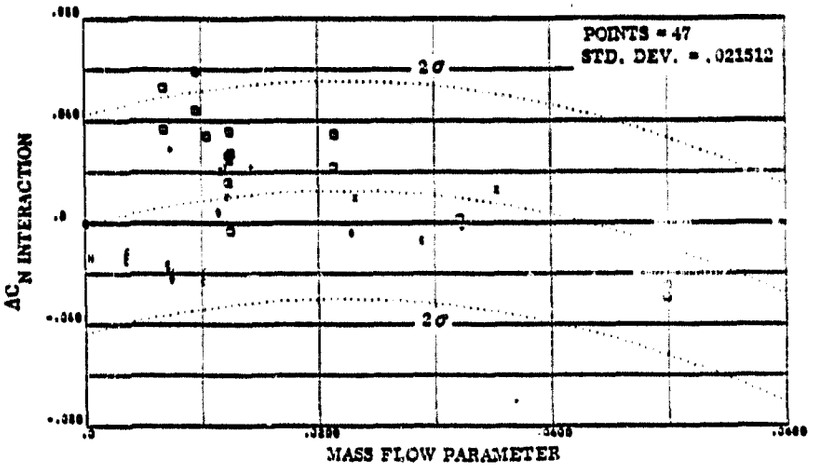

FIGURE 3-17i. YAW R.C.S. NORMAL FORCE CORRELATION FROM 30→35 DEGREES ANGLE OF ATTACK

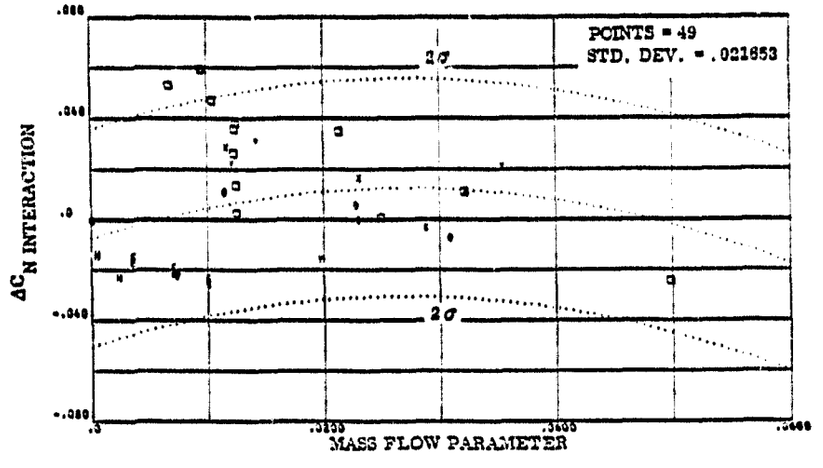

FIGURE 3-17j. YAW R.C.S. NORMAL FORCE CORRELATION FROM 35→MAX. DEGREES ANGLE OF ATTACK

SYMBOLS	NOZZLE NUMBER	TEST NUMBER
0	N51	OA82, MA22
X	N61	MA22
□	N85	OA82, MA22
Y	N33	MA22
+	N37	MA22
C	N95	OA169
V	N96	OA169
H	N97	OA169

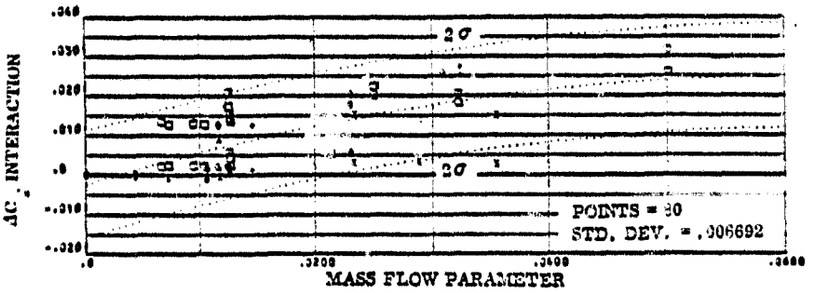

FIGURE 3-18a. YAW R.C.S. SIDE FORCE CORRELATION FROM -10→-5 DEGREES ANGLE OF ATTACK

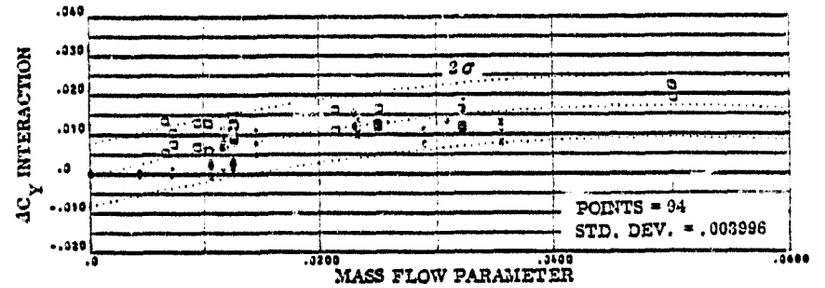

FIGURE 3-18b. YAW R.C.S. SIDE FORCE CORRELATION FROM -5→0 DEGREES ANGLE OF ATTACK

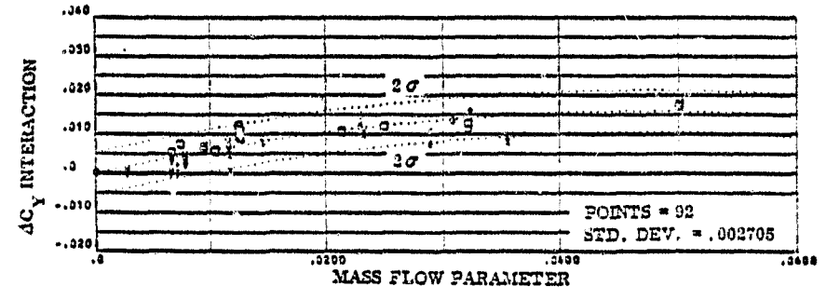

FIGURE 3-18c. YAW R.C.S. SIDE FORCE CORRELATION FROM 0→5 DEGREES ANGLE OF ATTACK

SYMBOLS	NOZZLE NUMBER	TEST NUMBER
0	N51	OA82, MA22
X	N61	MA22
□	N85	OA82, MA22
Y	N33	MA22
+	N37	MA22
C	N95	OA169
V	N96	OA169
H	N97	OA169

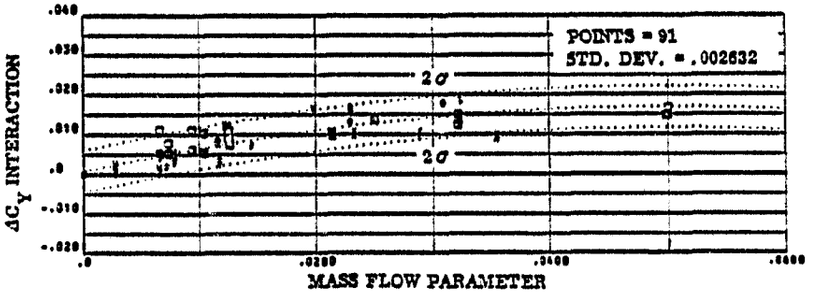

FIGURE 3-18d. YAW R.C.S. SIDE FORCE CORRELATION FROM 5→10 DEGREES ANGLE OF ATTACK

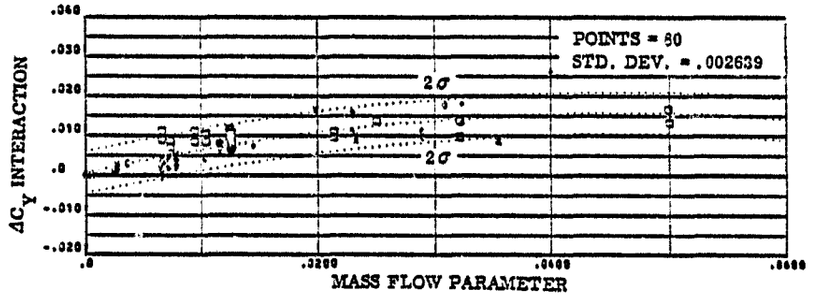

FIGURE 3-18e. YAW R.C.S. SIDE FORCE CORRELATION FROM 10→15 DEGREES ANGLE OF ATTACK

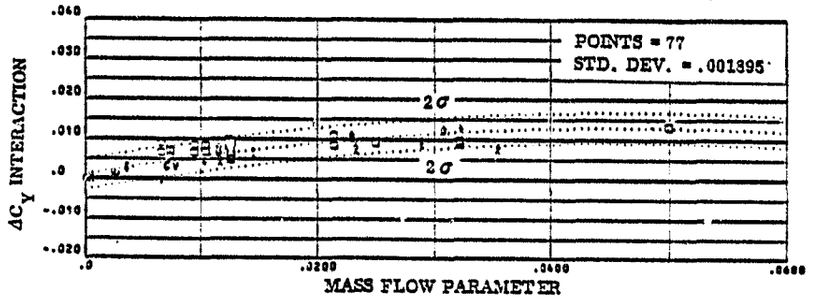

FIGURE 3-18f. YAW R.C.S. SIDE FORCE CORRELATION FROM 15→20 DEGREES ANGLE OF ATTACK

SYMBOLS	NOZZLE NUMBER	TEST NUMBER
0	N51	OA82, MA22
X	N61	MA22
□	N85	OA82, MA22
Y	N33	MA22
+	N37	MA22
C	N95	OA169
V	N96	OA169
H	N97	OA169

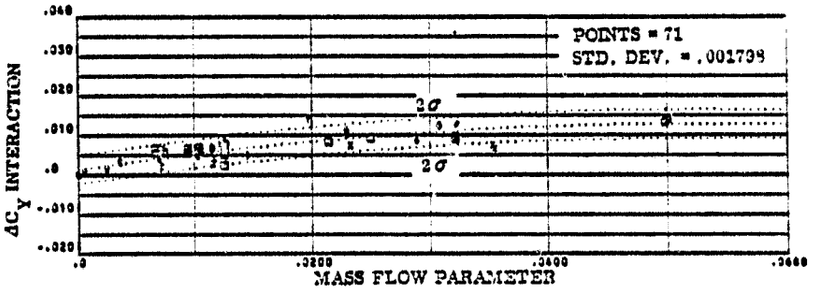

FIGURE 3-18g. YAW R.C.S. SIDE FORCE CORRELATION FROM 20-25 DEGREES ANGLE OF ATTACK

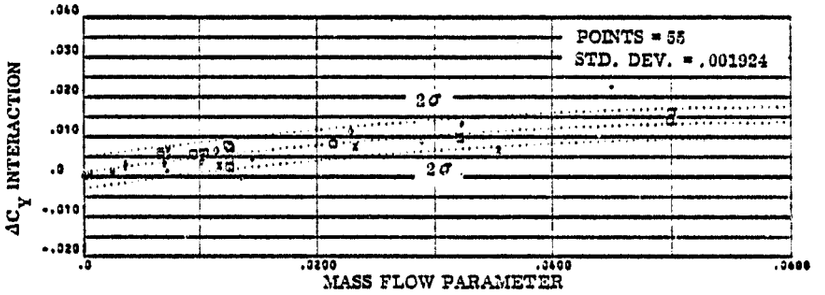

FIGURE 3-18h. YAW R.C.S. SIDE FORCE CORRELATION FROM 25-30 DEGREES ANGLE OF ATTACK

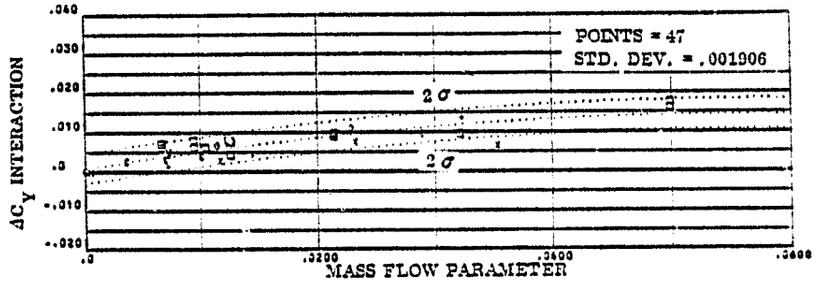

FIGURE 3-18i. YAW R.C.S. SIDE FORCE CORRELATION FROM 30-35 DEGREES ANGLE OF ATTACK

SYMBOLS	NOZZLE NUMBER	TEST NUMBER
0	N61	OA82, MA22
X	N61	MA22
□	N85	OA82, MA22
Y	N83	MA22
+	N87	MA22
C	N95	OA169
V	N96	OA169
H	N97	OA169

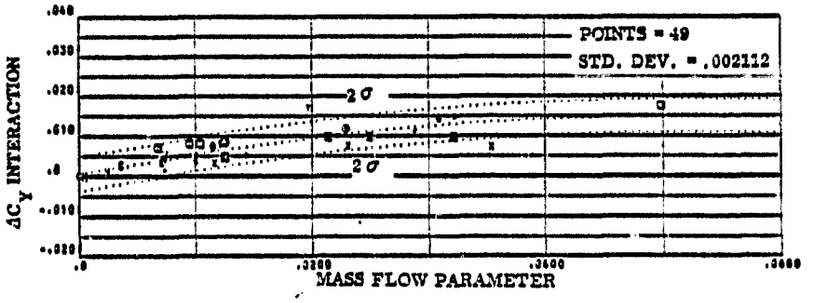

FIGURE 3-18j. YAW R.C.S. SIDE FORCE CORRELATION FROM 35►MAX. DEGREES ANGLE OF ATTACK

SYMBOLS	NOZZLE NUMBER	TEST NUMBER
○	N51	OA82, MA22
□	N61	MA22
◇	N85	OA82, MA22
+	N33	MA22
⊙	N37	MA22
△	N95	OA169
▽	N96	OA169
☒	N97	OA169

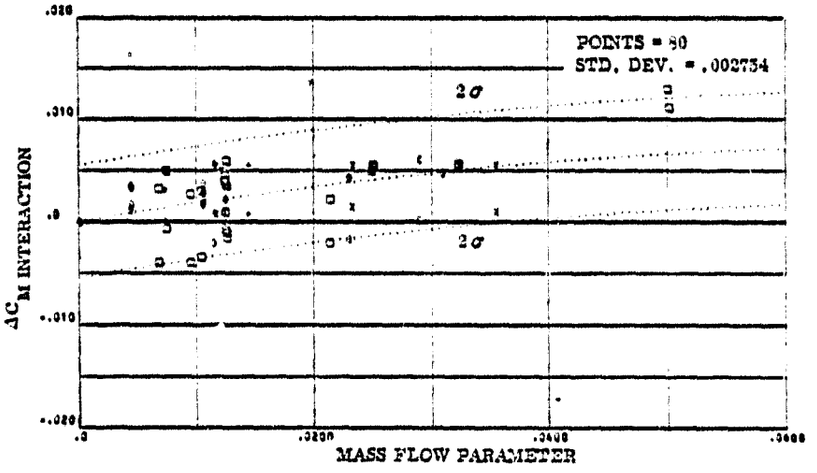

FIGURE 3-19 a. YAW R.C.S. PITCHING MOMENT CORRELATION FROM -10→-5 DEGREES ANGLE OF ATTACK

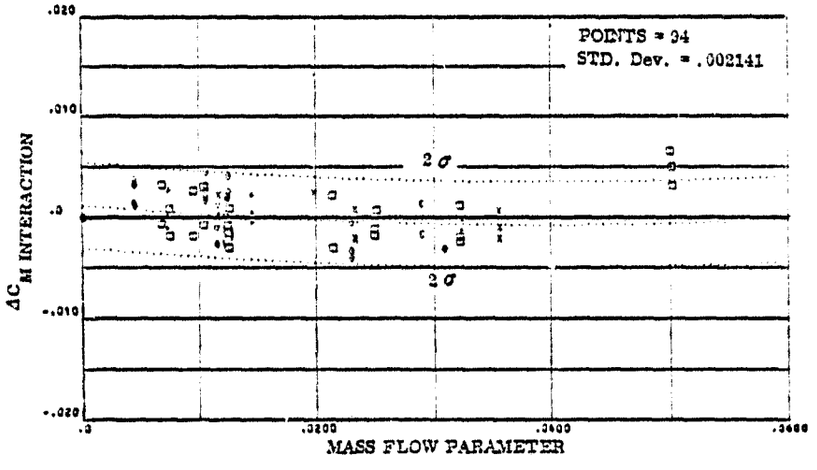

FIGURE 3-19 b. YAW R.C.S. PITCHING MOMENT CORRELATION FROM -5→0 DEGREES ANGLE OF ATTACK

SYMBOLS	NOZZLE NUMBER	TEST NUMBER
0 •	N61	OA82, MA22
⊠	N61	MA22
□	N85	OA82, MA22
Y	N33	MA22
+	N37	MA22
C	N95	OA169
V	N96	OA169
H	N97	OA169

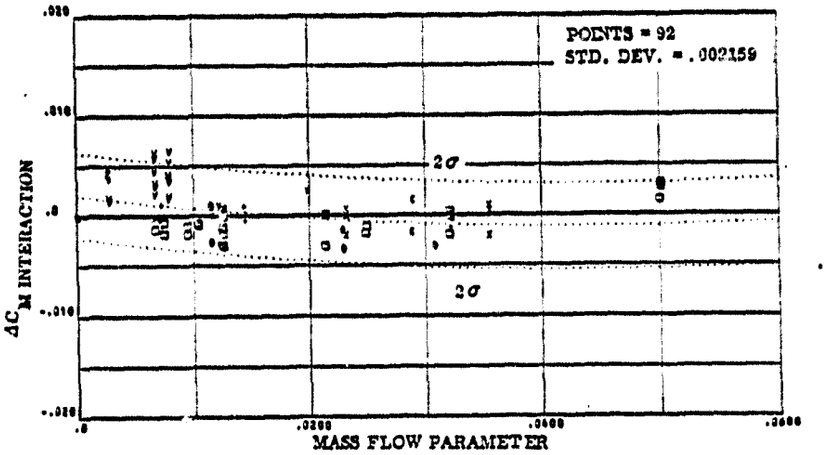

FIGURE 3-19c. YAW R.C.S. PITCHING MOMENT CORRELATION FROM 0→5 DEGREES ANGLE OF ATTACK

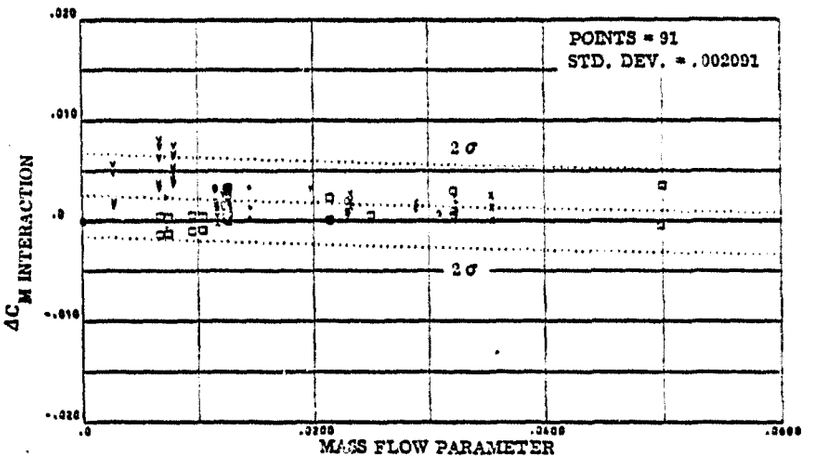

FIGURE 3-19d. YAW R.C.S. PITCHING MOMENT CORRELATION FROM 5→10 DEGREES ANGLE OF ATTACK

SYMBOLS	NOZZLE NUMBER	TEST NUMBER
0 •	N51	OA32, MA22
×□	N61	MA22
▽△	N85	OA32, MA22
+	N33	MA22
○	N37	MA22
◇	N95	OA169
⊟	N96	OA169
H	N97	OA169

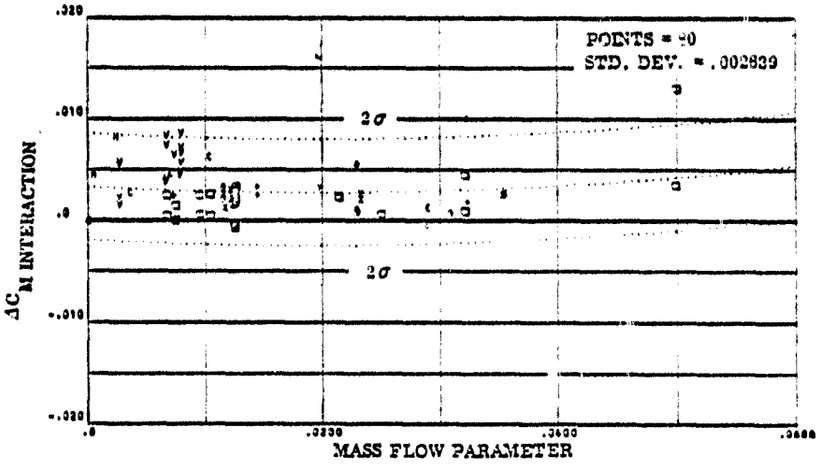

FIGURE 3-19e. YAW R.C.S. PITCHING MOMENT CORRELATION FROM 10—15 DEGREES ANGLE OF ATTACK

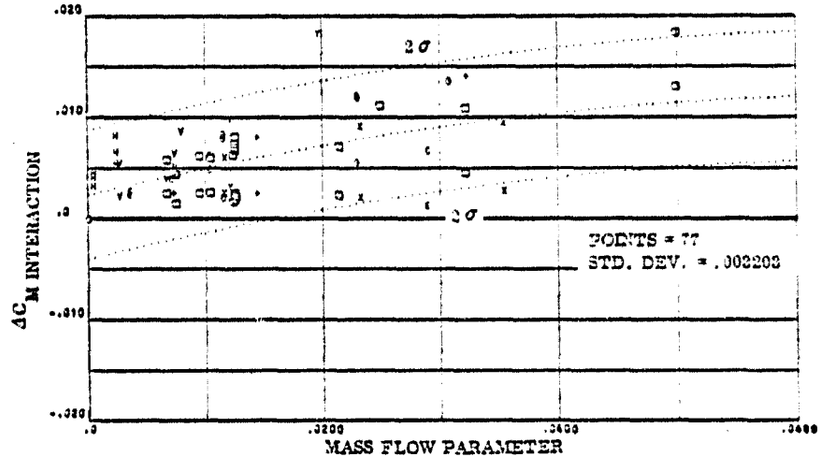

FIGURE 3-19f. YAW R.C.S. PITCHING MOMENT CORRELATION FROM 15—20 DEGREES ANGLE OF ATTACK

SYMBOLS	NOZZLE NUMBER	TEST NUMBER
0	N61	OA82, MA22
X	N61	MA22
□	N85	OA82, MA22
Y	N33	MA22
+	N37	MA22
C	N95	OA169
V	N96	OA169
H	N97	OA169

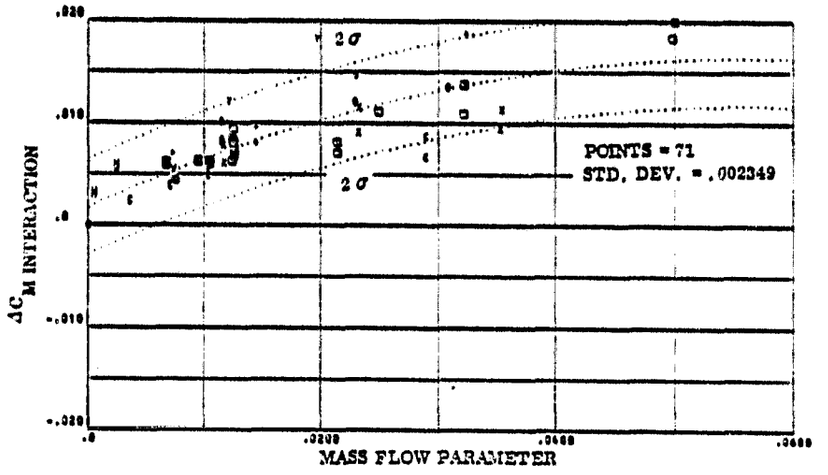

FIGURE 3-19g. YAW R.C.S. PITCHING MOMENT CORRELATION FROM 20=25 DEGREES ANGLE OF ATTACK

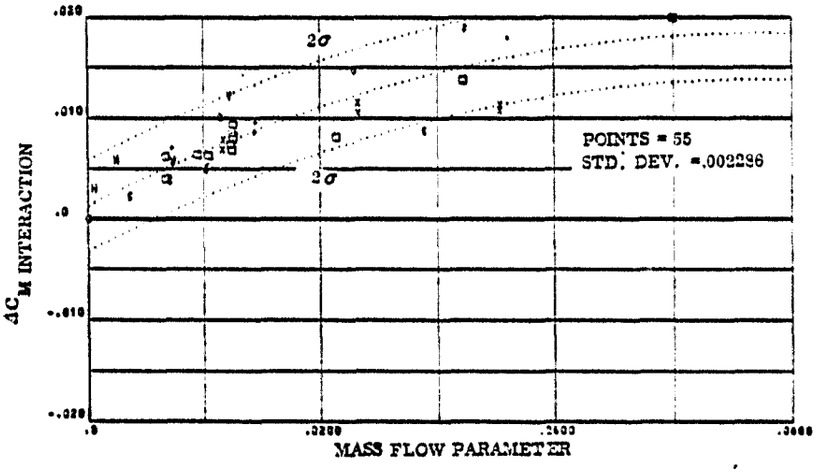

FIGURE 3-19h. YAW R.C.S. PITCHING MOMENT CORRELATION FROM 25=30 DEGREES ANGLE OF ATTACK

SYMBOLS	NOZZLE NUMBER	TEST NUMBER
◇	N51	OA82, MA22
X	N61	MA22
□	N85	OA82, MA22
Y	N33	MA22
+	N37	MA22
C	N95	OA169
V	N96	OA169
H	N97	OA169

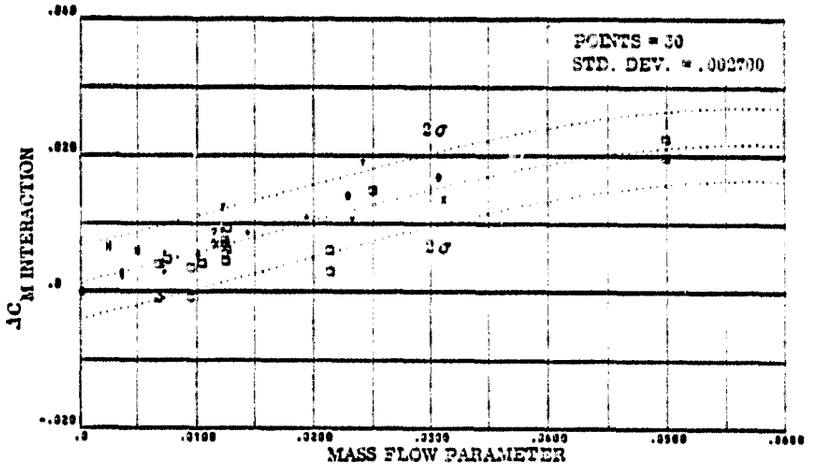

FIGURE 3-19i. YAW R.C.S. PITCHING MOMENT CORRELATION FROM 30-35 DEGREES ANGLE OF ATTACK

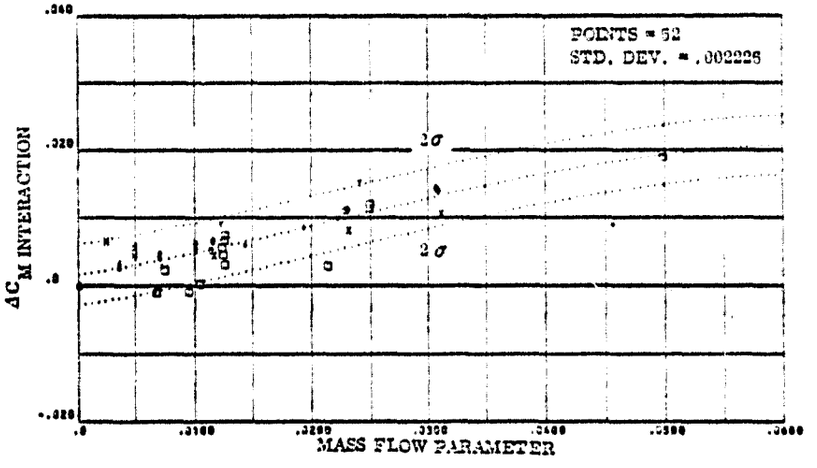

FIGURE 3-19j. YAW R.C.S. PITCHING MOMENT CORRELATION FROM 35-MAX. DEGREES ANGLE OF ATTACK

SYMBOLS	NOZZLE NUMBER	TEST NUMBER
○	N51	OA82, MA22
✕	N61	MA22
□	N65	OA82, MA22
▽	N33	MA22
+	N37	MA22
C	N95	OA169
V	N96	OA169
H	N97	OA169

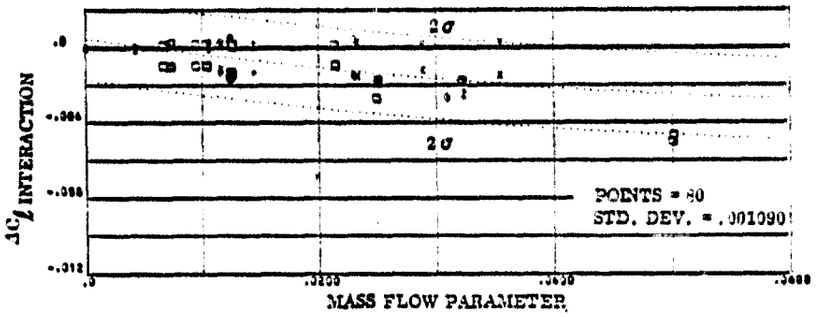

FIGURE 3-20a. YAW R.C.S. ROLLING MOMENT CORRELATION FROM -10=-5 DEGREES ANGLE OF ATTACK

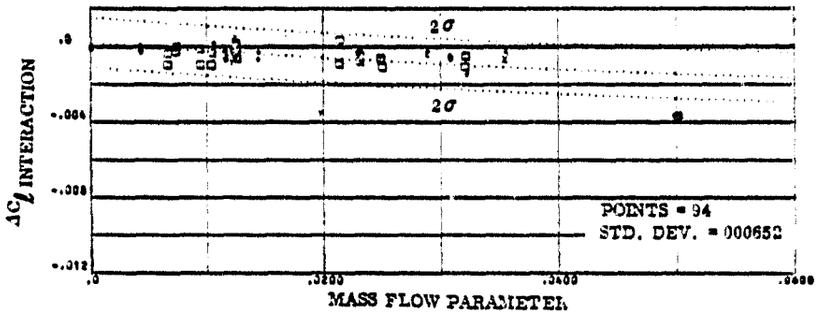

FIGURE 3-20b. YAW R.C.S. ROLLING MOMENT CORRELATION FROM -5=0 DEGREES ANGLE OF ATTACK

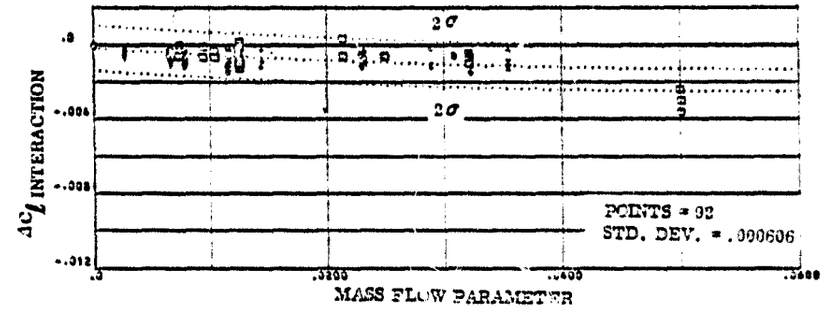

FIGURE 3-20c. YAW R.C.S. ROLLING MOMENT CORRELATION FROM 0=5 DEGREES ANGLE OF ATTACK

SYMBOLS	NOZZLE NUMBER	TEST NUMBER
○	N51	OA82, MA22
✕	N61	MA22
□	N85	OA82, MA22
+	N33	MA22
+	N37	MA22
○	N95	OA169
▽	N96	OA169
H	N97	OA169

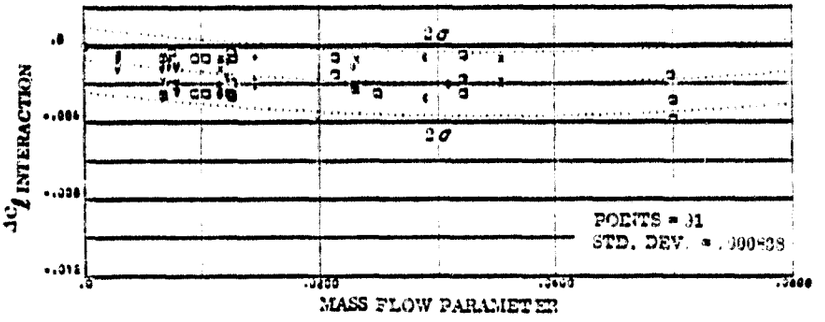

FIGURE 3-20d. YAW R.C.S. ROLLING MOMENT CORRELATION FROM 5→10 DEGREES ANGLE OF ATTACK

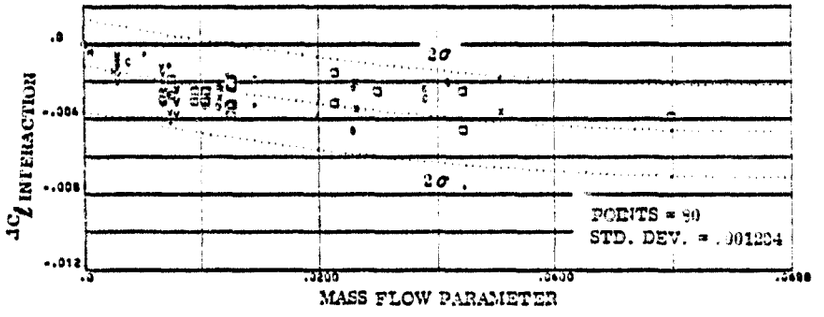

FIGURE 3-20e. YAW R.C.S. ROLLING MOMENT CORRELATION FROM 10→15 DEGREES ANGLE OF ATTACK

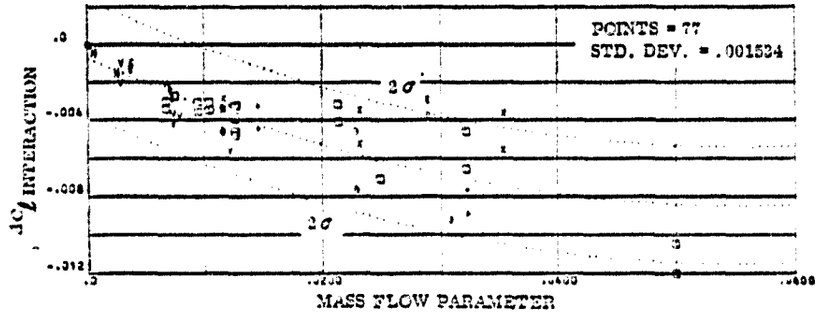

FIGURE 3-20f. YAW R.C.S. ROLLING MOMENT CORRELATION FROM 15→20 DEGREES ANGLE OF ATTACK

SYMBOLS	NOZZLE NUMBER	TEST NUMBER
0 ·	N51	OA62, MA22
X	N61	MA22
□	N65	OA62, MA22
Y	N33	MA22
+	N37	MA22
C	N95	OA169
V	N96	OA169
H	N97	OA169

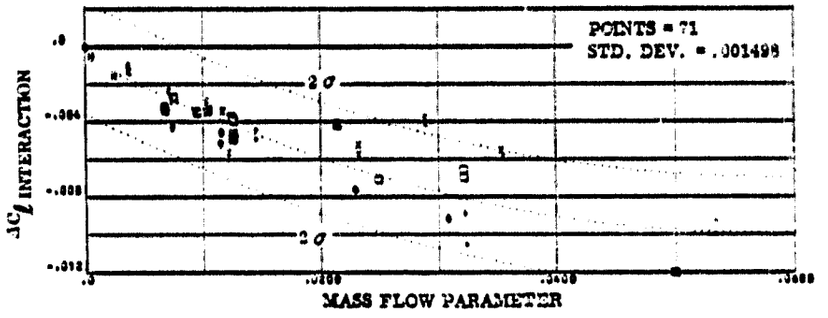

FIGURE 3-20g. YAW R.C.S. ROLLING MOMENT CORRELATION FROM 20→25 DEGREES ANGLE OF ATTACK

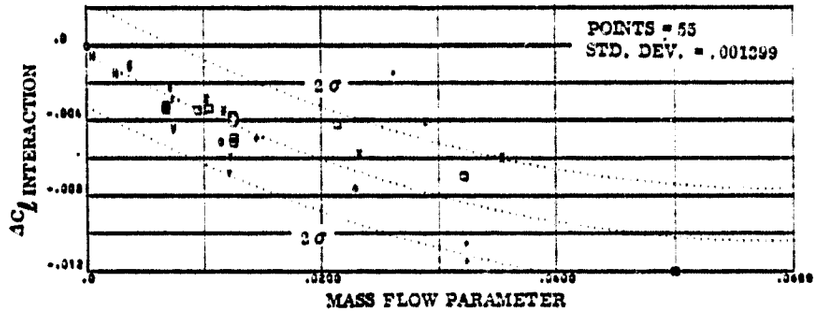

FIGURE 3-20h. YAW R.C.S. ROLLING MOMENT CORRELATION FROM 25→30 DEGREES ANGLE OF ATTACK

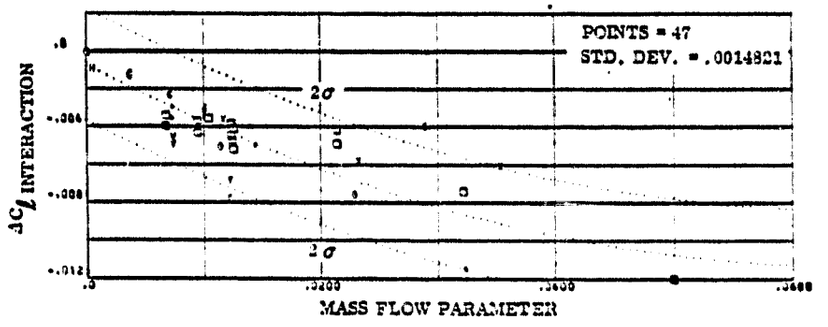

FIGURE 3-20i. YAW R.C.S. ROLLING MOMENT CORRELATION FROM 30→35 DEGREES ANGLE OF ATTACK

SYMBOLS	NOZZLE NUMBER	TEST NUMBER
○	N61	OA82, MA22
×	N61	MA22
□	N85	OA82, MA22
▽	N33	MA22
+	N37	MA22
◇	N95	OA169
▽	N96	OA169
H	N97	OA169

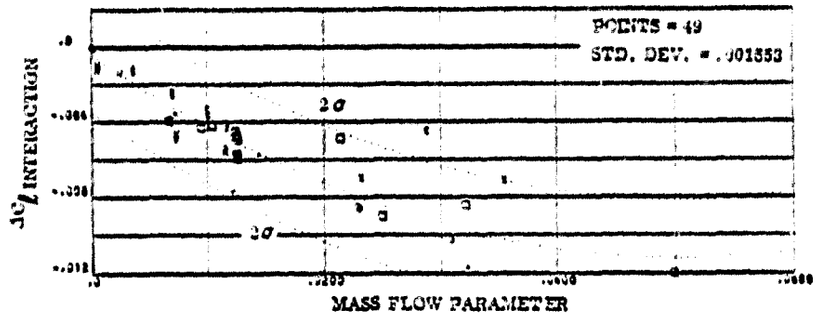

FIGURE 3-20. YAW R.C.S. ROLLING MOMENT CORRELATION FROM 35°-MAX. DEGREES ANGLE OF ATTACK

SYMBOLS	NOZZLE NUMBER	TEST NUMBER
0	N51	OA82, MA22
×	N61	MA22
□	N55	OA82, MA22
▽	N53	MA22
+	N57	MA22
C	N95	OA169
V	N96	OA169
H	N97	OA169

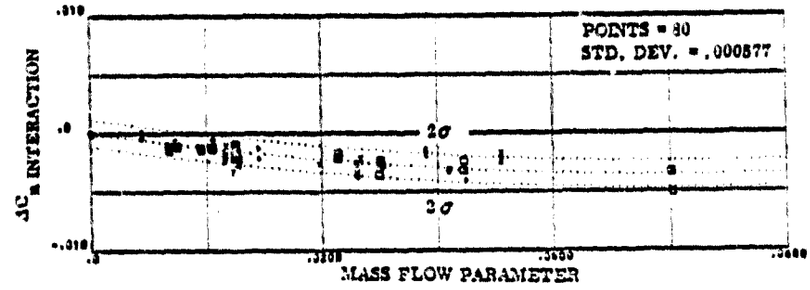

FIGURE 3-21a. YAW R.C.S. YAWING MOMENT CORRELATION FROM -10 ⟵ -5 DEGREES ANGLE OF ATTACK

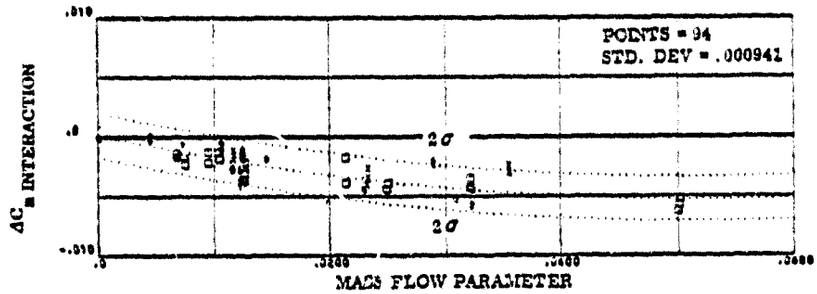

FIGURE 3-21b. YAW R.C.S. YAWING MOMENT CORRELATION FROM -5 ⟵ 0 DEGREES ANGLE OF ATTACK

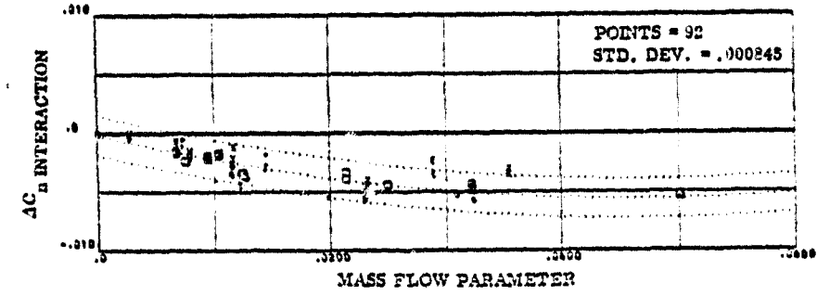

FIGURE 3-21c. YAW R.C.S. YAWING MOMENT CORRELATION FROM 0 ⟵ 5 DEGREES ANGLE OF ATTACK

SYMBOLS	NOZZLE NUMBER	TEST NUMBER
O	N51	OA82, MA22
X	N61	MA22
□	N85	OA82, MA22
+	N36	MA22
◇	N37	MA22
C	N95	OA169
V	N96	OA169
H	N97	OA169

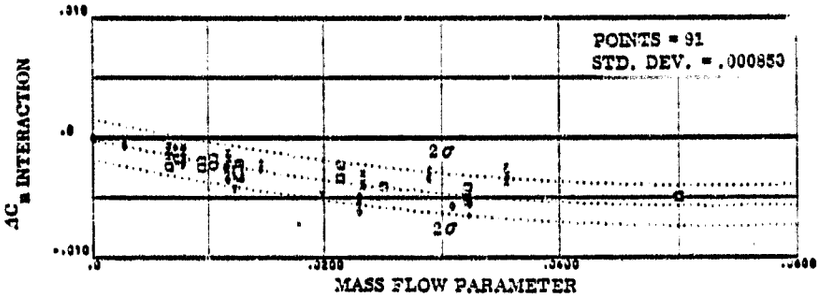

FIGURE 3-21d. YAW R.C.S. YAWING MOMENT CORRELATION FROM 5→10 DEGREES ANGLE OF ATTACK

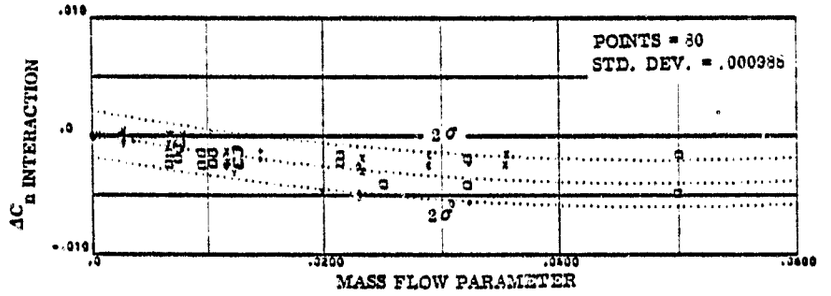

FIGURE 3-21e. YAW R.C.S. YAWING MOMENT CORRELATION FROM 10→15 DEGREES ANGLE OF ATTACK

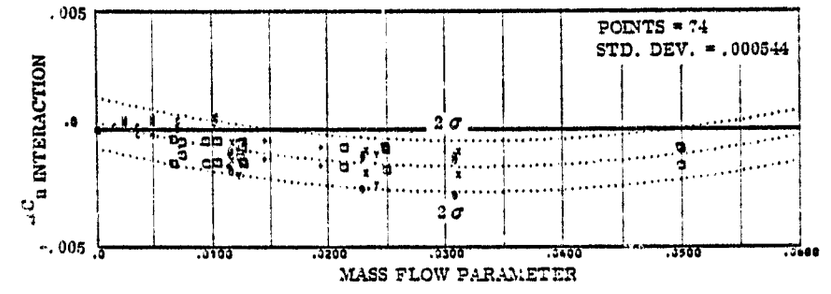

FIGURE 3-21f. YAW R.C.S. YAWING MOMENT CORRELATION FROM 15→20 DEGREES ANGLE OF ATTACK

SYMBOLS	NOZZLE NUMBER	TEST NUMBER
0	N61	OA82, MA22
×	N61	MA22
□	N85	OA82, MA22
Y	N33	MA22
+	N37	MA22
C	N95	OA169
V	N96	OA169
H	N97	OA169

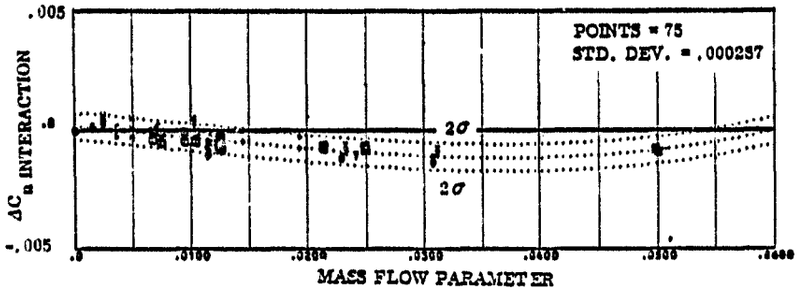

FIGURE 3-21g. YAW R.C.S.YAWING MOMENT CORRELATION FROM 20→25 DEGREES ANGLE OF ATTACK

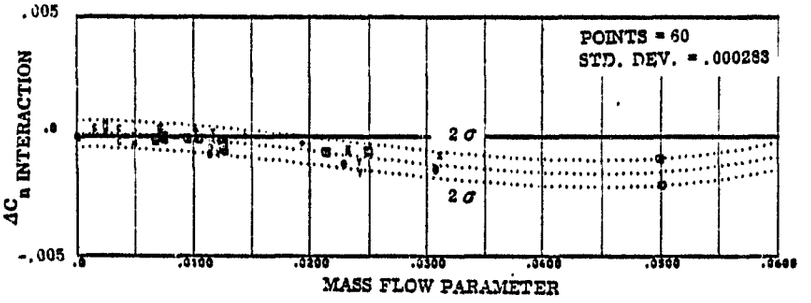

FIGURE 3-21h. YAW R.C.S.YAWING MOMENT CORRELATION FROM 25→30 DEGREES ANGLE OF ATTACK

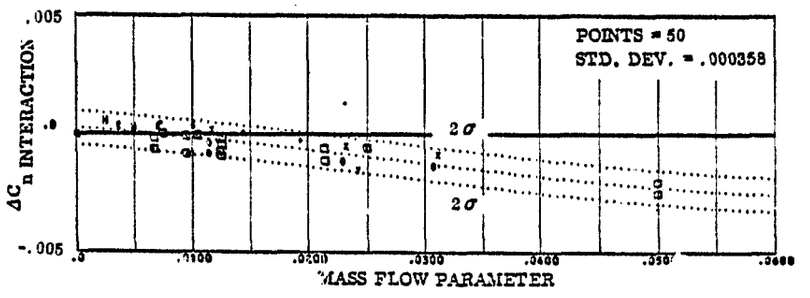

FIGURE 3-21i. YAW R.C.S.YAWING MOMENT CORRELATION FROM 30→35 DEGREES ANGLE OF ATTACK

SYMBOLS	NOZZLE NUMBER	TEST NUMBER
0	N31	OA82, MA22
X	N61	MA22
□	N65	OA82, MA22
Y	N33	MA22
+	N37	MA22
C	N95	OA169
V	N96	OA169
H	N97	OA169

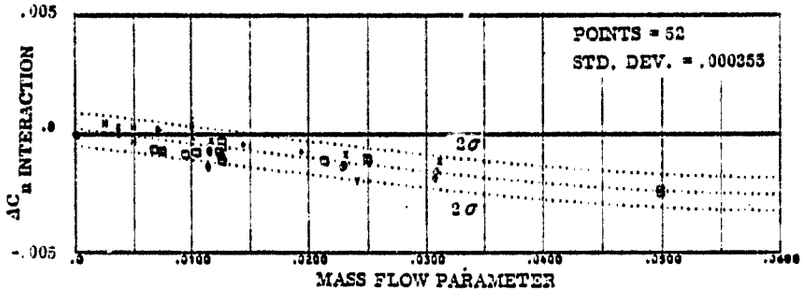

FIGURE 3-21 j. YAW R.C.S. YAWING MOMENT CORRELATION FROM 35►MAX. DEGREES ANGLE OF ATTACK

NOTE: PLOTTED DATA IS COMPUTED DATA DIVIDED BY 2.

SYMBOL	NOZZLE NUMBER	TEST NUMBER
□	N49, N50	OA 82
V	N96	OA 169

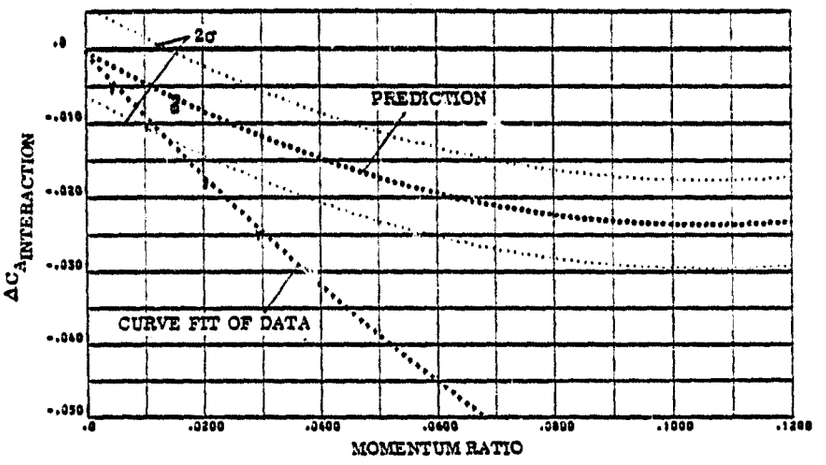

FIGURE 3-22 a. : SYMMETRIC PITCH DOWN RCS INTERACTIONS FROM 15 TO 20 DEGREES ANGLE OF ATTACK; AXIAL FORCE

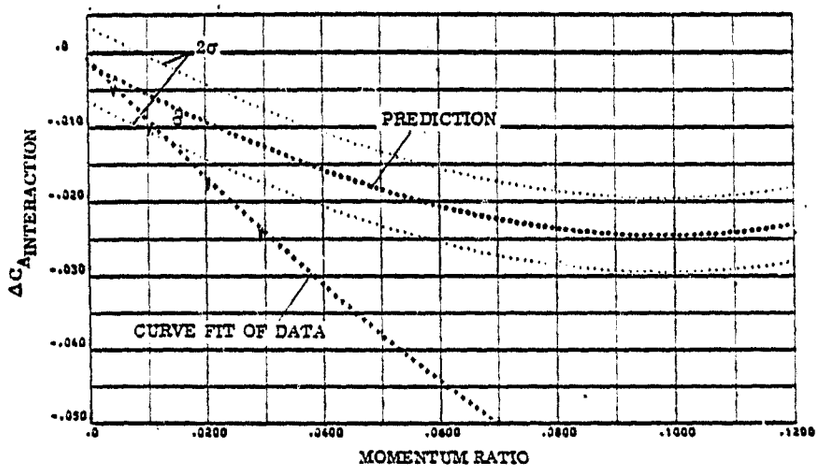

FIGURE 3-22 b. : SYMMETRIC PITCH DOWN RCS INTERACTIONS FROM 20 TO 25 DEGREES ANGLE OF ATTACK; AXIAL FORCE

NOTE: PLOTTED DATA IS COMPUTED DATA DIVIDED BY 2.

SYMBOL	NOZZLE NUMBER	TEST NUMBER
□	N49, N50	OA 82
V	N96	OA 169

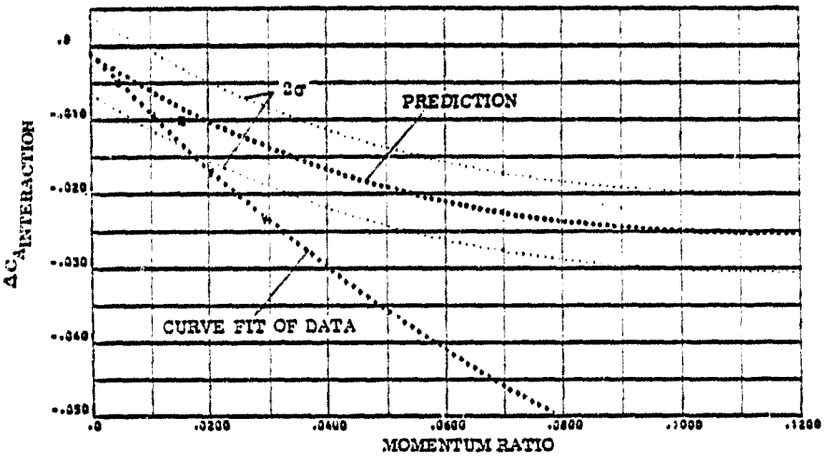

FIGURE 3-22 c. : SYMMETRIC PITCH DOWN RCS INTERACTIONS FROM 15 TO 20 DEGREES ANGLE OF ATTACK; AXIAL FORCE

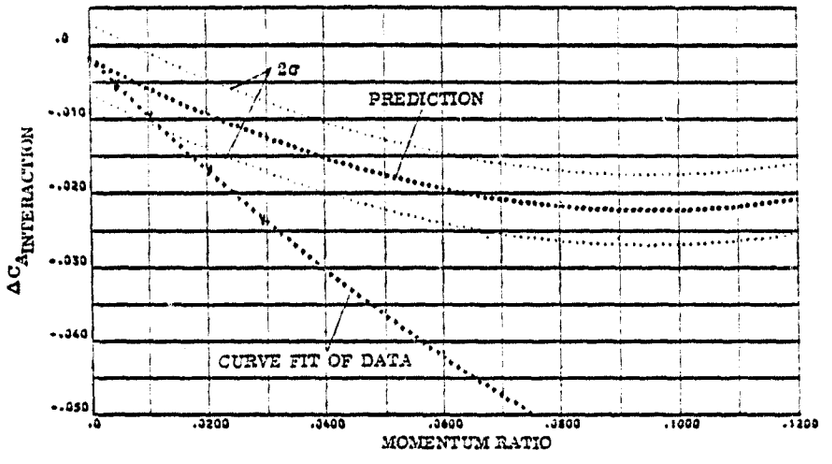

FIGURE 3-22d. : SYMMETRIC PITCH DOWN RCS INTERACTIONS FROM 20 TO 25 DEGREES ANGLE OF ATTACK; AXIAL FORCE

NOTE: PLOTTED DATA IS COMPUTED DATA DIVIDED BY 2.

SYMBOL	NOZZLE NUMBER	TEST NUMBER
□	N49, N50	OA 82
V	N96	OA 169

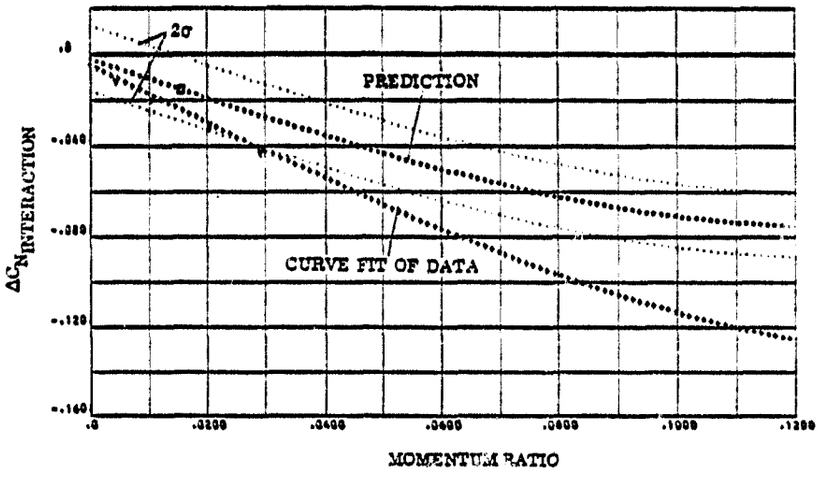

FIGURE 3-22e. : SYMMETRIC PITCH DOWN RCS INTERACTIONS FROM 15 TO 20 DEGREES ANGLE OF ATTACK; NORMAL FORCE

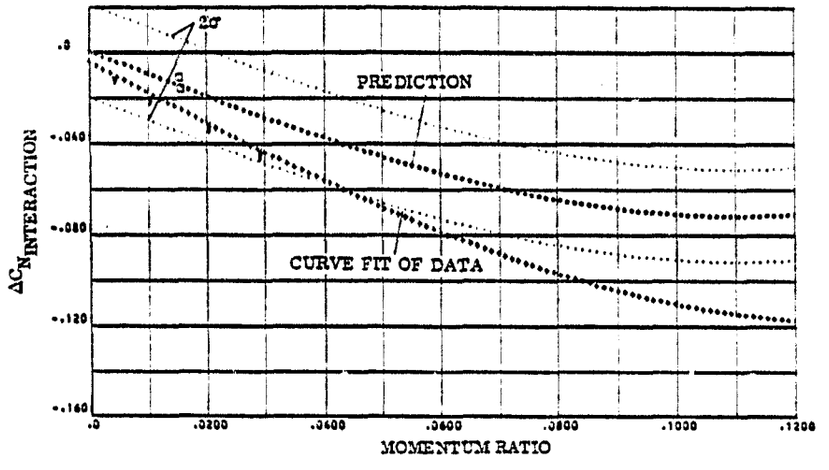

FIGURE 3-22f. : SYMMETRIC PITCH DOWN RCS INTERACTIONS FROM 20 TO 25 DEGREES ANGLE OF ATTACK; NORMAL FORCE

NOTE: PLOTTED DATA IS COMPUTED DATA DIVIDED BY 2.

SYMBOL	NOZZLE NUMBER	TEST NUMBER
□	N49, N50	OA 82
V	N96	OA 169

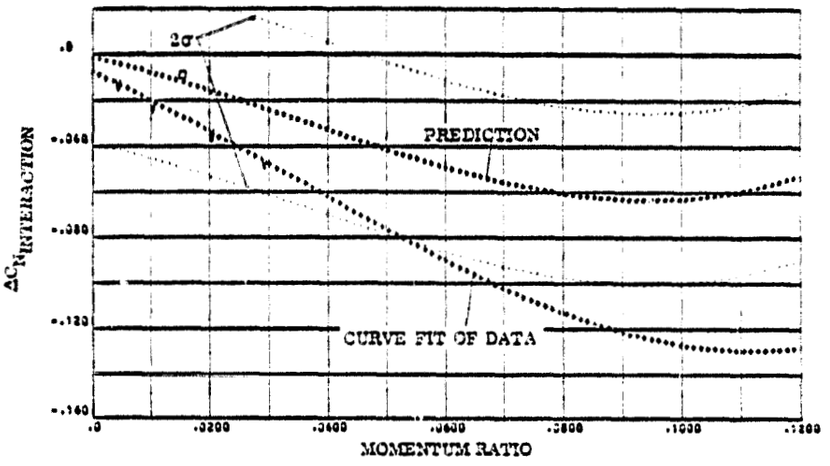

FIGURE 3-22q. : SYMMETRIC PITCH DOWN RCS INTERACTIONS FROM 30 TO 35 DEGREES ANGLE OF ATTACK; NORMAL FORCE

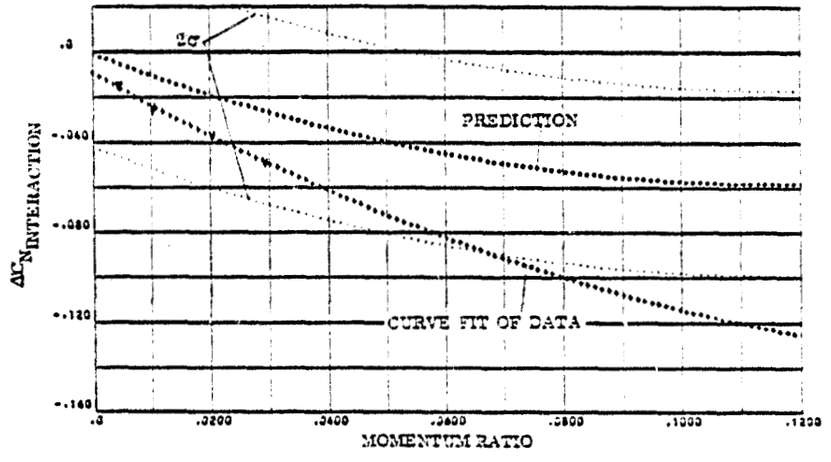

FIGURE 3-22r. : SYMMETRIC PITCH DOWN RCS INTERACTIONS FROM 35 TO 42.5 DEGREES ANGLE OF ATTACK; NORMAL FORCE

NOTE: PLOTTED DATA IS COMPUTED DATA DIVIDED BY 2.

SYMBOL	NOZZLE NUMBER	TEST NUMBER
□	N49, N50	OA 82
V	N96	OA 169

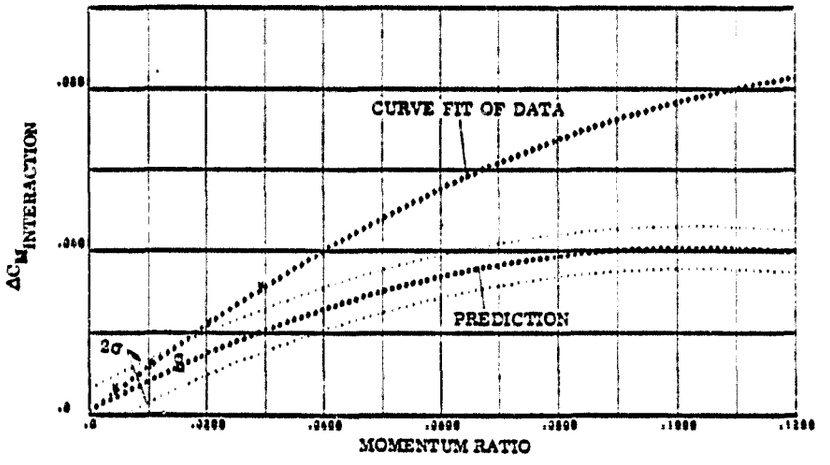

FIGURE 3-22 i. : SYMMETRIC PITCH DOWN RCS INTERACTIONS FROM 15 TO 20 DEGREES ANGLE OF ATTACK; PITCHING MOMENT

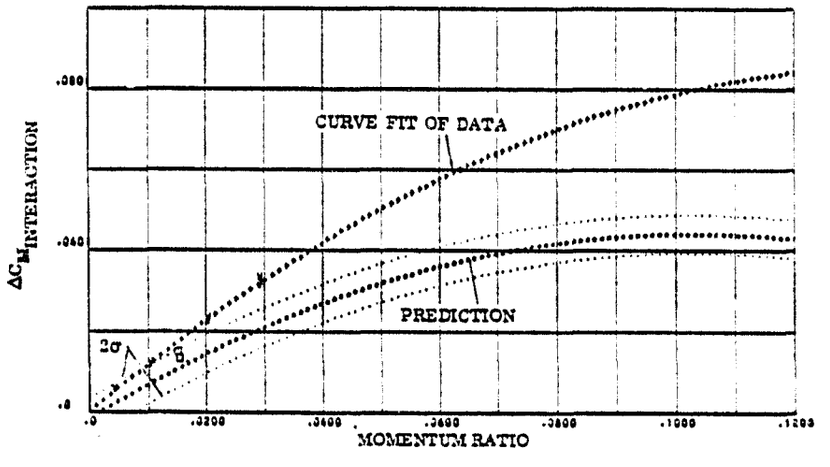

FIGURE 3-22 j. : SYMMETRIC PITC.. DOWN RCS INTERACTIONS FROM 20 TO 25 DEGREES ANGLE OF ATTACK; PITCHING MOMENT

NOTE: PLOTTED DATA IS COMPUTED DATA DIVIDED BY 2.

SYMBOL	NOZZLE NUMBER	TEST NUMBER
□	N49, N50	OA 32
V	N96	OA 169

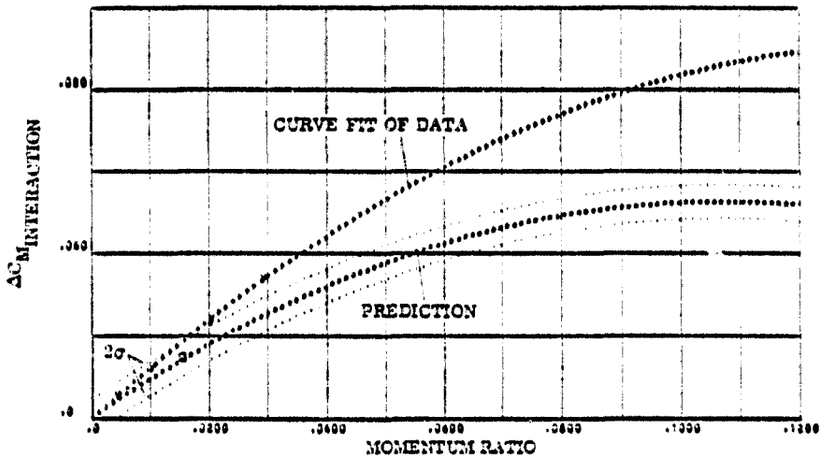

FIGURE 3-22k: SYMMETRIC PITCH DOWN RCS INTERACTIONS FROM 30 TO 35 DEGREES ANGLE OF ATTACK; PITCHING MOMENT

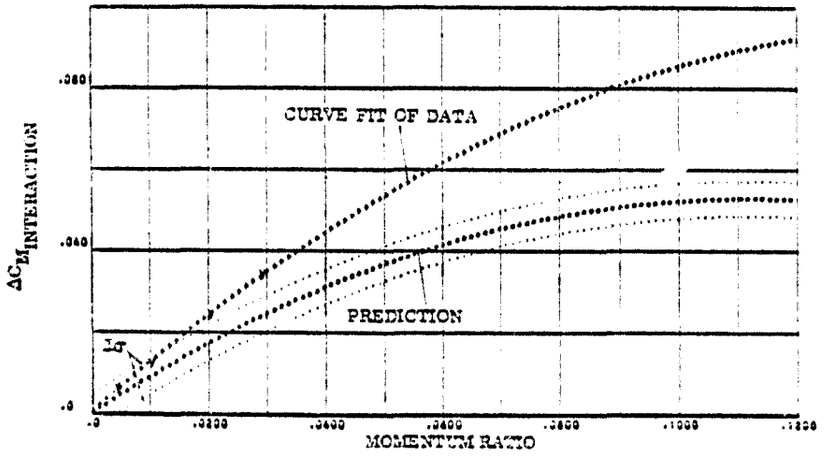

FIGURE 3-22l: SYMMETRIC PITCH DOWN RCS INTERACTIONS FROM 35 TO 42.5 DEGREES ANGLE OF ATTACK; PITCHING MOMENT

SYMBOL	NOZZLE NUMBER	TEST NUMBER
0	N49, N52	OA 82
X	N79, N78	MA 22
V	N96	OA 169

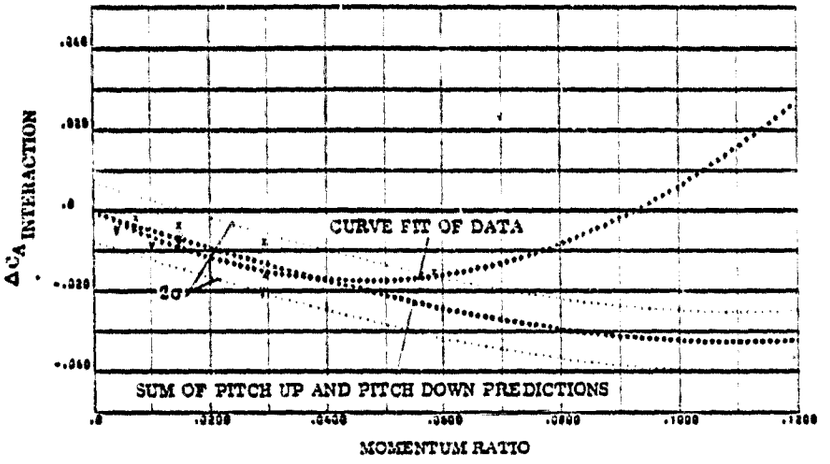

FIGURE 3-23 a. : SYMMETRIC ROLL RCS INTERACTIONS FROM 15 TO 20 DEGREES ANGLE OF ATTACK; AXIAL FORCE

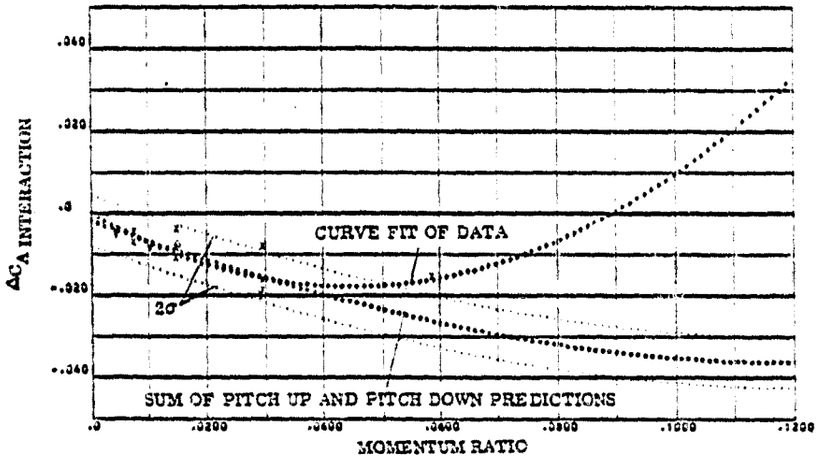

FIGURE 3-23 b. : SYMMETRIC ROLL RCS INTERACTIONS FROM 20 TO 25 DEGREES ANGLE OF ATTACK; AXIAL FORCE

SYMBOL	NOZZLE NUMBER	TEST NUMBER
0	N49, N52	OA 82
X	N73, N78	MA 22
V	N96	OA 189

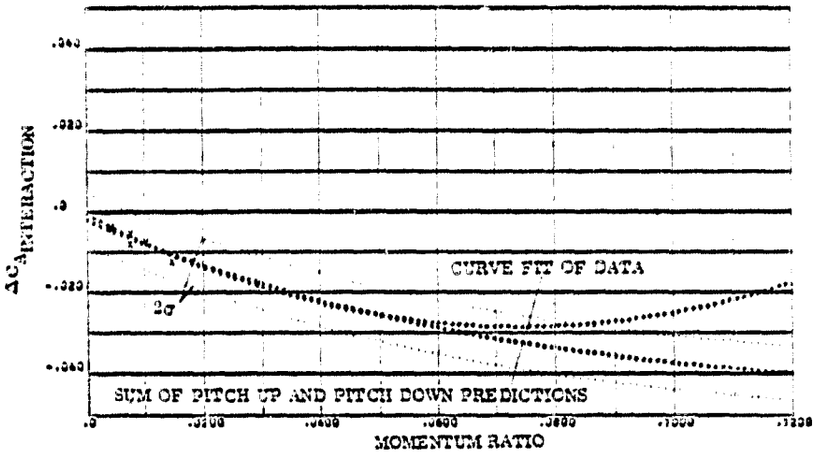

FIGURE 3-23c. : SYMMETRIC ROLL RCS INTERACTIONS FROM 30 TO 35 DEGREES ANGLE OF ATTACK; AXIAL FORCE

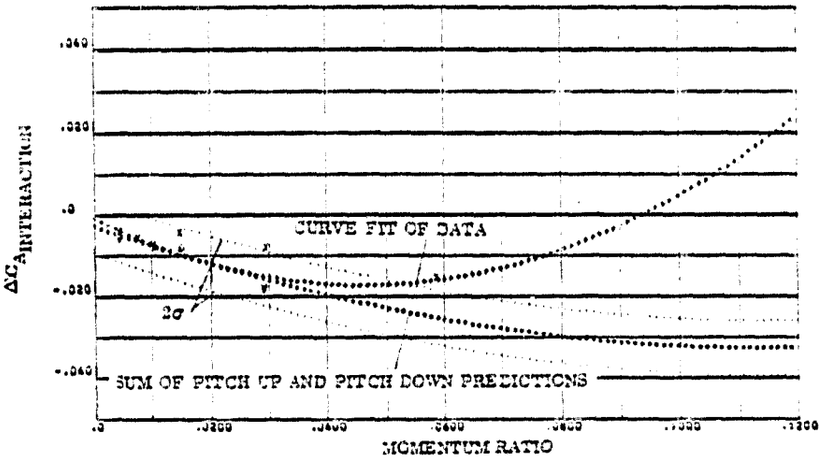

FIGURE 3-23d. : SYMMETRIC ROLL RCS INTERACTIONS FROM 35 TO 42.5 DEGREES ANGLE OF ATTACK; AXIAL FORCE

SYMBOL	NOZZLE NUMBER	TEST NUMBER
0	N49, N52	OA 82
X	N79, N78	MA 22
V	N96	OA 169

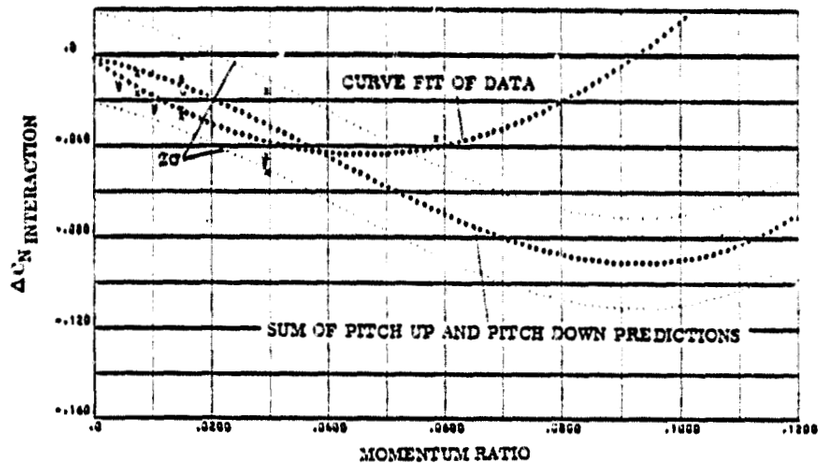

FIGURE 3-23e. : SYMMETRIC ROLL RCS INTERACTIONS FROM 15 TO 20 DEGREES ANGLE OF ATTACK; NORMAL FORCE

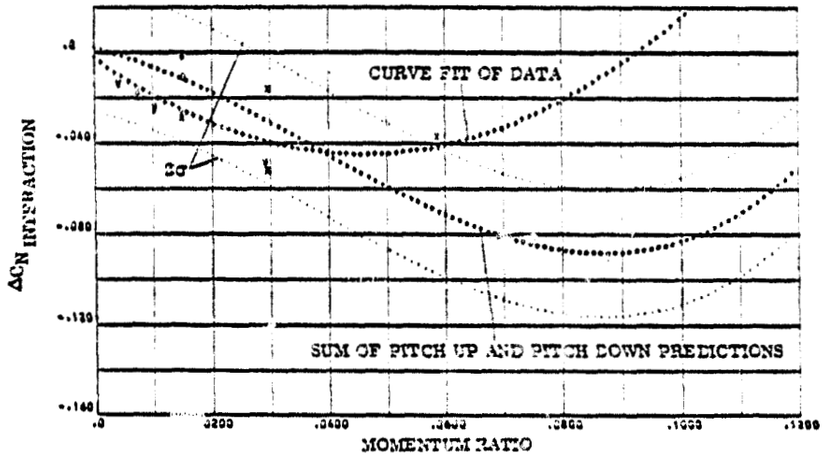

FIGURE 3-23f. : SYMMETRIC ROLL RCS INTERACTIONS FROM 20 TO 25 DEGREES ANGLE OF ATTACK; NORMAL FORCE

SYMBOL	NOZZLE NUMBER	TEST NUMBER
0	N49, N52	OA 82
X	N79, N78	MA 22
V	N36	OA 169

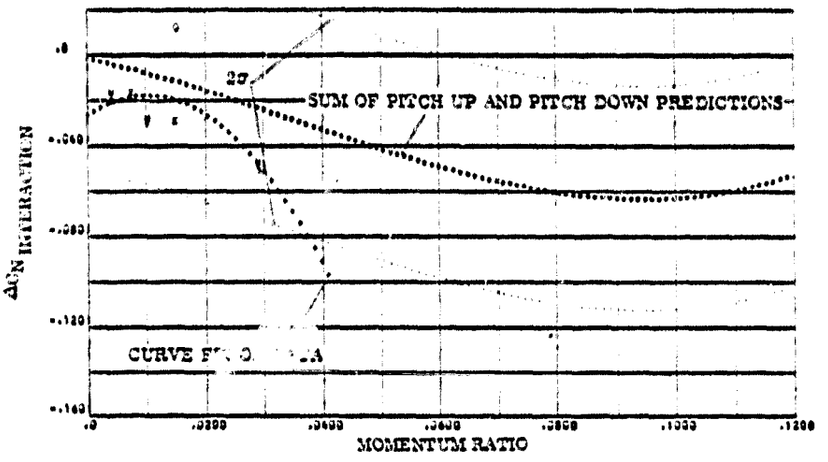

FIGURE 3-23g. : SYMMETRIC ROLL RCS INTERACTIONS FROM 30 TO 35 DEGREES ANGLE OF ATTACK;

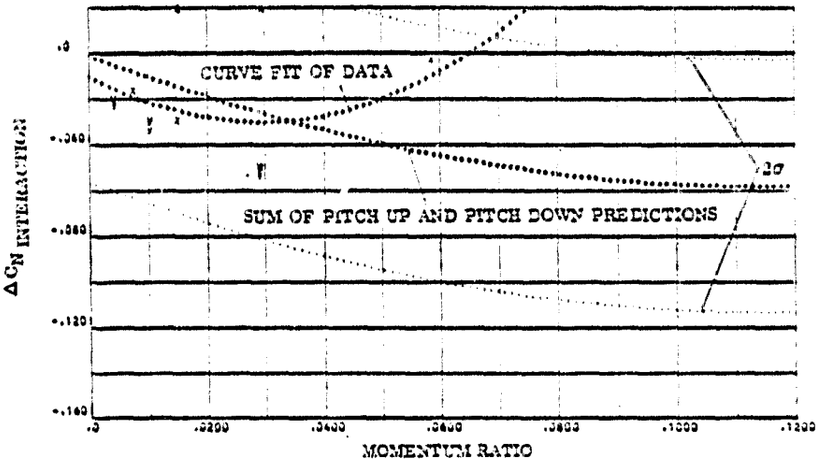

FIGURE 3-23 h. : SYMMETRIC ROLL RCS INTERACTIONS FROM 35 TO 42.5 DEGREES ANGLE OF ATTACK;

SYMBOL	NOZZLE NUMBER	TEST NUMBER
0	N49, N52	OA 82
X	N79, N78	MA 22
V	N96	OA 169

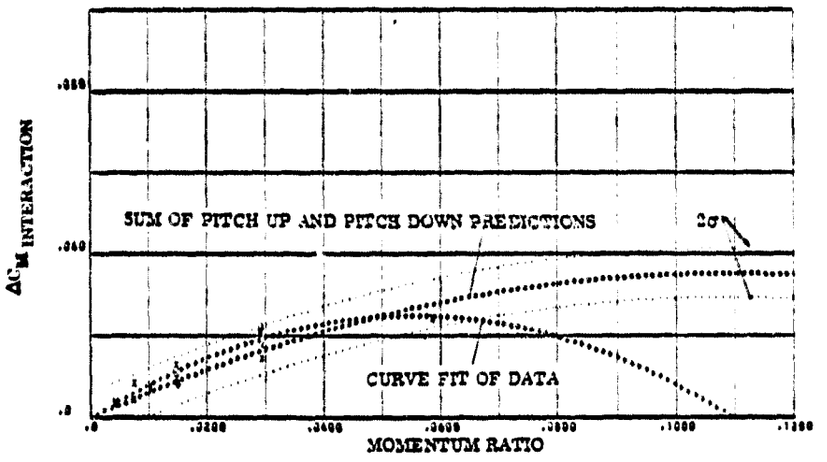

FIGURE 3-231. : SYMMETRIC ROLL RCS INTERACTIONS FROM 15 TO 20 DEGREES ANGLE OF ATTACK; PITCHING MOMENT

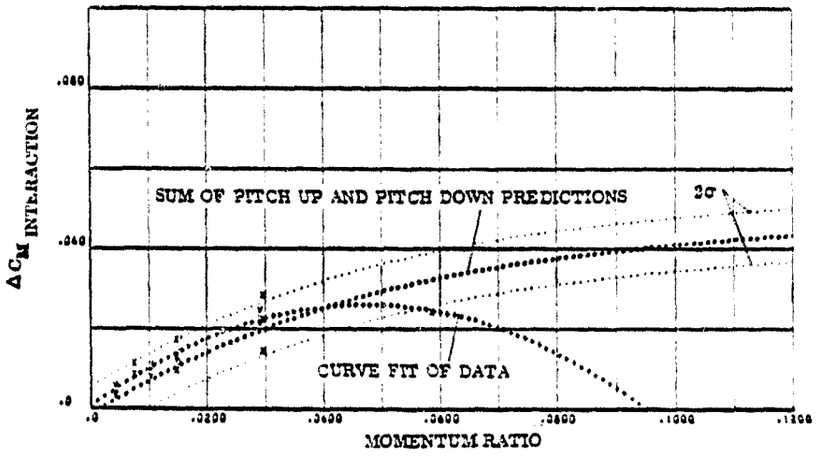

FIGURE 3-231. : SYMMETRIC ROLL RCS INTERACTIONS FROM 20 TO 25 DEGREES ANGLE OF ATTACK; PITCHING MOMENT

SYMBOL	NOZZLE NUMBER	TEST NUMBER
0	N49, N52	OA 92
X	N73, N75	MA 22
V	N96	OA 169

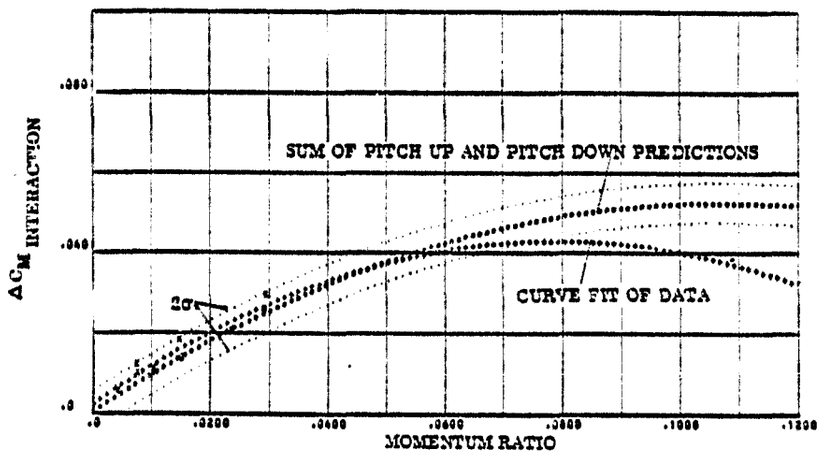

FIGURE 3-231k : SYMMETRIC ROLL RCS INTERACTIONS FROM 30 TO 35 DEGREES ANGLE OF ATTACK; PITCHING MOMENT

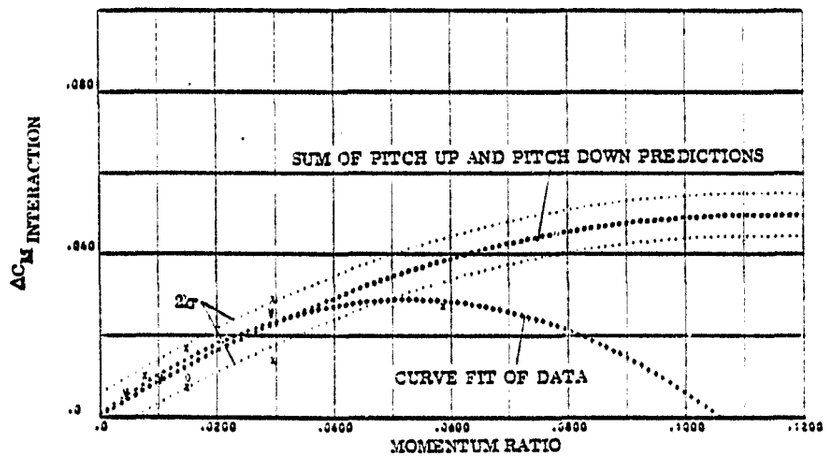

FIGURE 3-231 : SYMMETRIC ROLL RCS INTERACTIONS FROM 35 TO 42.5 DEGREES ANGLE OF ATTACK; PITCHING MOMENT

SYMBOL	NOZZLE NUMBER	TEST NUMBER
0	N49, N52	OA 32
X	N79, N78	MA 22
V	N96	OA 169

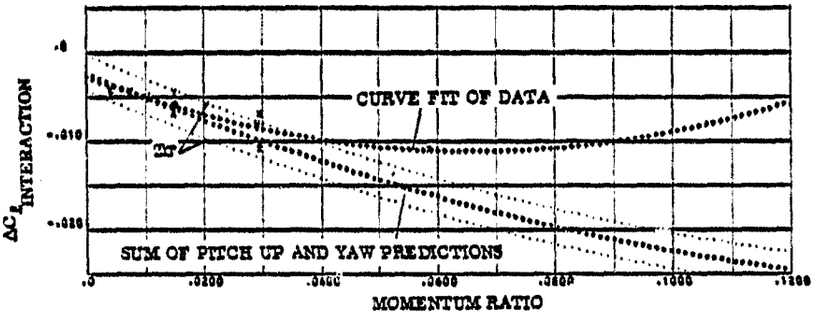

FIGURE 3-23m: SYMMETRIC ROLL RCS INTERACTIONS FROM 15 TO 20 DEGREES ANGLE OF ATTACK; ROLLING MOMENT

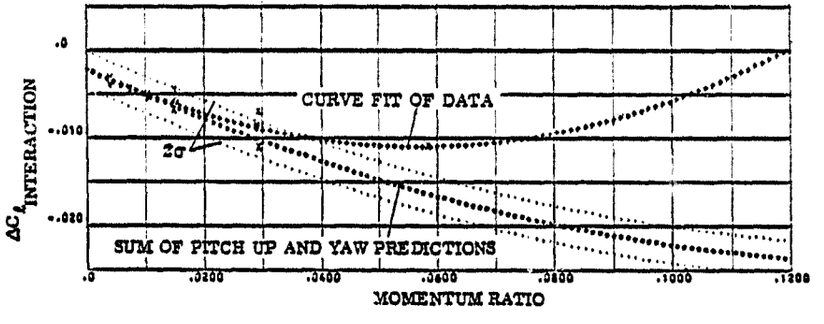

FIGURE 3-23n : SYMMETRIC ROLL RCS INTERACTIONS FROM 20 TO 25 DEGREES ANGLE OF ATTACK; ROLLING MOMENT

SYMBOL	NOZZLE NUMBER	TEST NUMBER
0	N49, N52	OA 82
X	N79, N78	MA 22
V	N96	OA 169

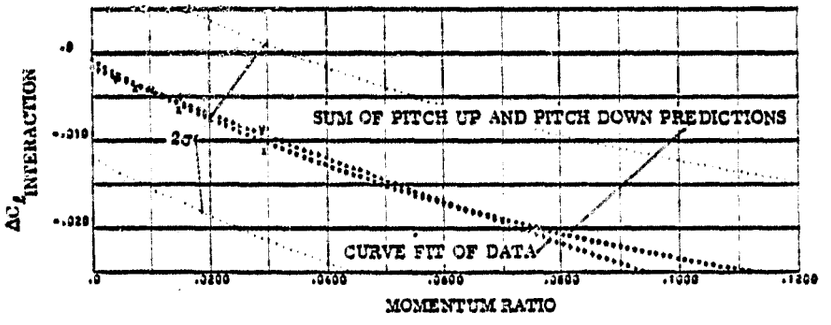

FIGURE 3-23o : SYMMETRIC ROLL RCS INTERACTIONS FROM 30 TO 35 DEGREES ANGLE OF ATTACK; ROLLING MOMENT

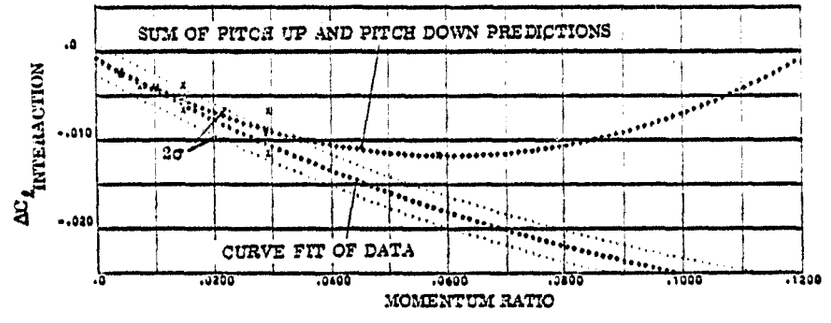

FIGURE 3-23p : SYMMETRIC ROLL RCS INTERACTIONS FROM 35 TO 42.5 DEGREES ANGLE OF ATTACK; ROLLING MOMENT

SYMBOL	NOZZLE NUMBER	TEST NUMBER
0	N84	OA 82, MA 22

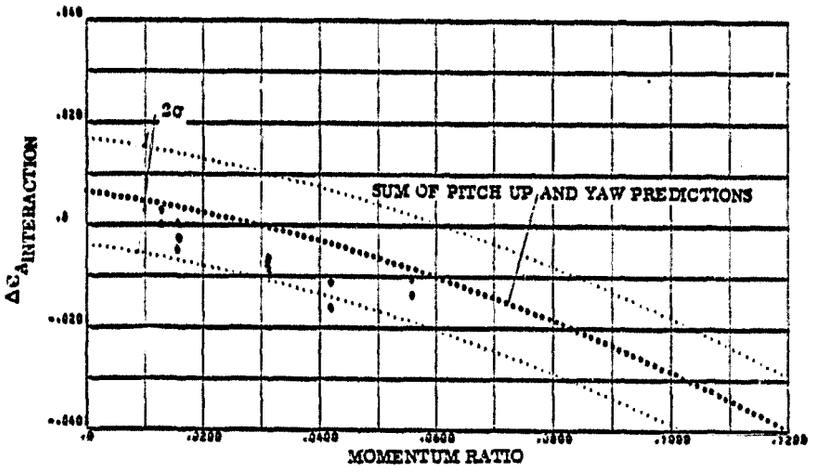

FIGURE 3-24a. : PITCH UP PLUS YAW RCS COMBINED CONTROL INTERACTIONS FROM -10 TO -5 DEGREES ANGLE OF ATTACK; AXIAL FORCE

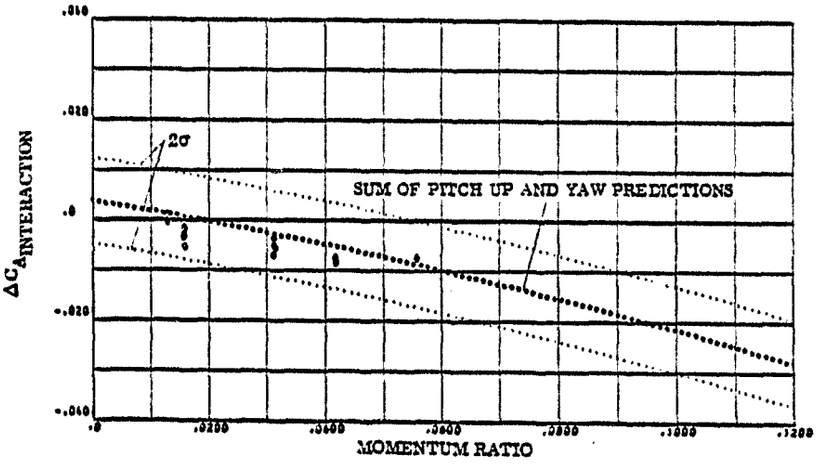

FIGURE 3-24b. : PITCH UP PLUS YAW RCS COMBINED CONTROL INTERACTIONS FROM -5 TO 0 DEGREES ANGLE OF ATTACK; AXIAL FORCE

SYMBOL	NOZZLE NUMBER	TEST NUMBER
0	N84	OA 82, MA 22

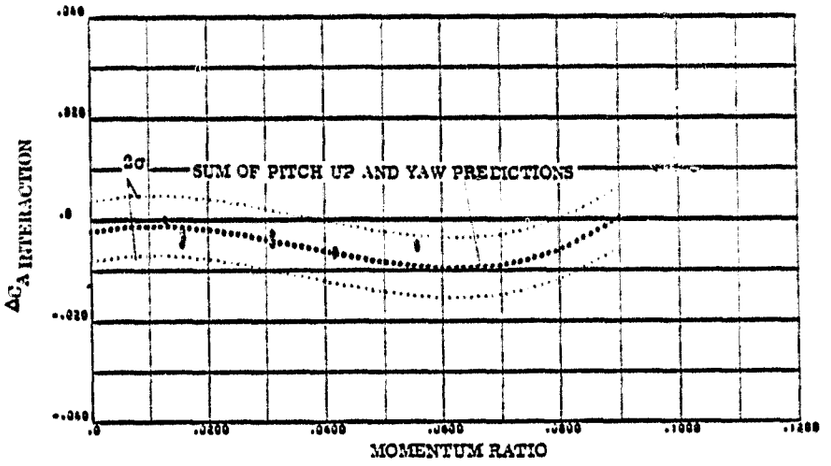

FIGURE 3-24c. : PITCH UP PLUS YAW RCS COMBINED CONTROL INTERACTIONS FROM 15 TO 20 DEGREES ANGLE OF ATTACK; AXIAL FORCE

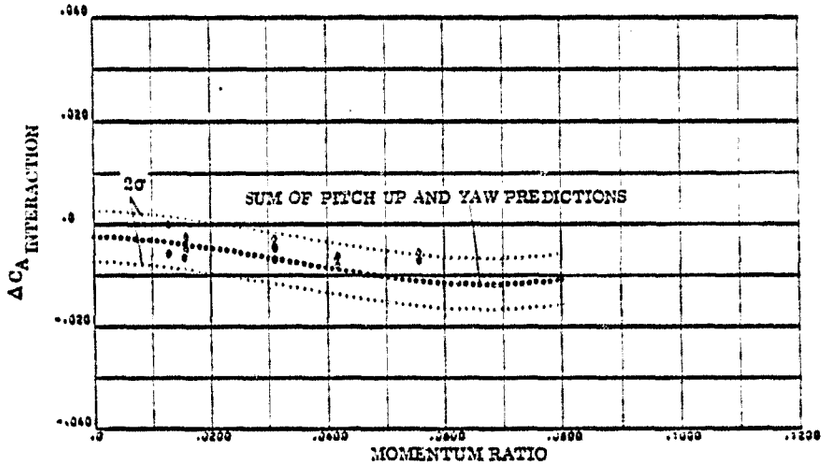

FIGURE 3-24d. : PITCH UP PLUS YAW RCS COMBINED CONTROL INTERACTIONS FROM 20 TO 25 DEGREES ANGLE OF ATTACK; AXIAL FORCE

SYMBOL	NOZZLE NUMBER	TEST NUMBER
0	N84	OA 82, MA 22

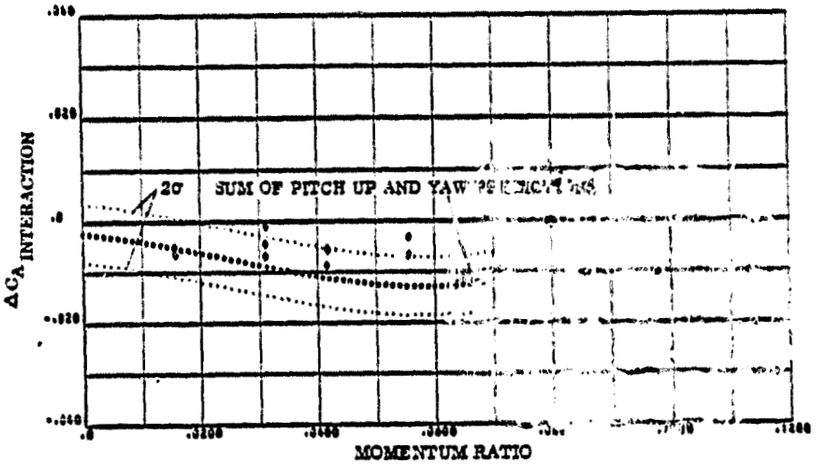

FIGURE 3-24e. : PITCH UP PLUS YAW RCS COMBINED CONTROL INTERACTIONS FROM 30 TO 35 DEGREES ANGLE OF ATTACK; AXIAL FORCE

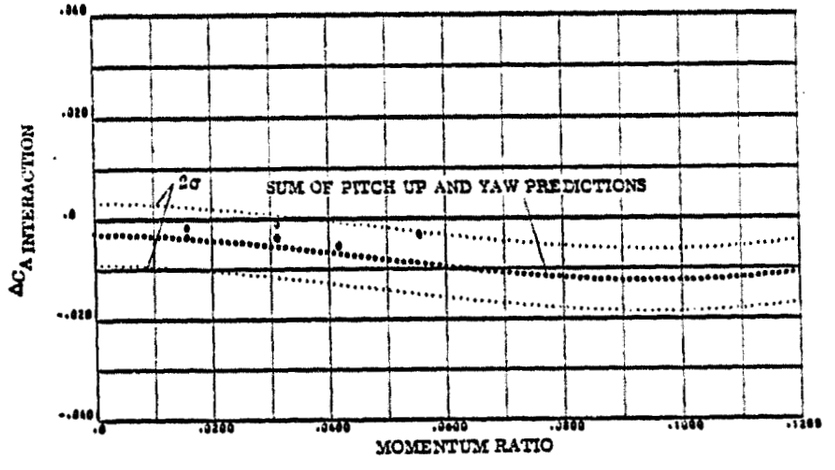

FIGURE 3-24f. : PITCH UP PLUS YAW RCS COMBINED CONTROL INTERACTIONS FROM 35 TO 42.5 DEGREES ANGLE OF ATTACK; AXIAL FORCE

SYMBOL	NOZZLE NUMBER	TEST NUMBER
0	N84	OA 82, MA 22

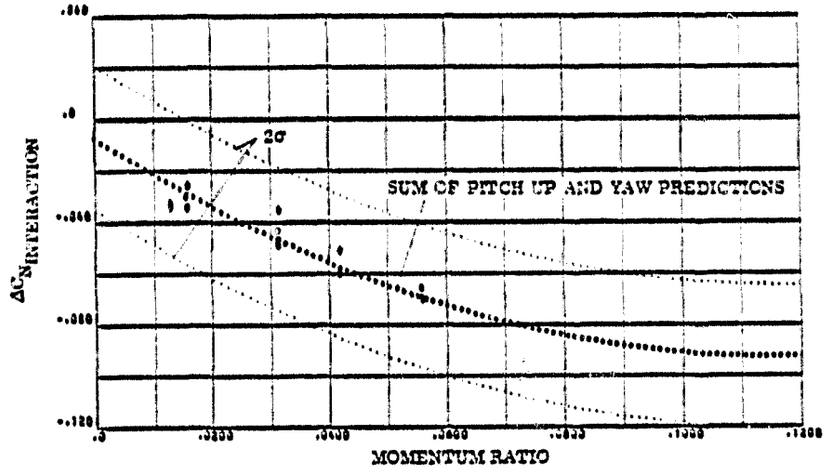

FIGURE 3-24g. : PITCH UP PLUS YAW RCS COMBINED CONTROL INTERACTIONS FROM -10 TO -5 DEGREES ANGLE OF ATTACK: NORMAL FORCE

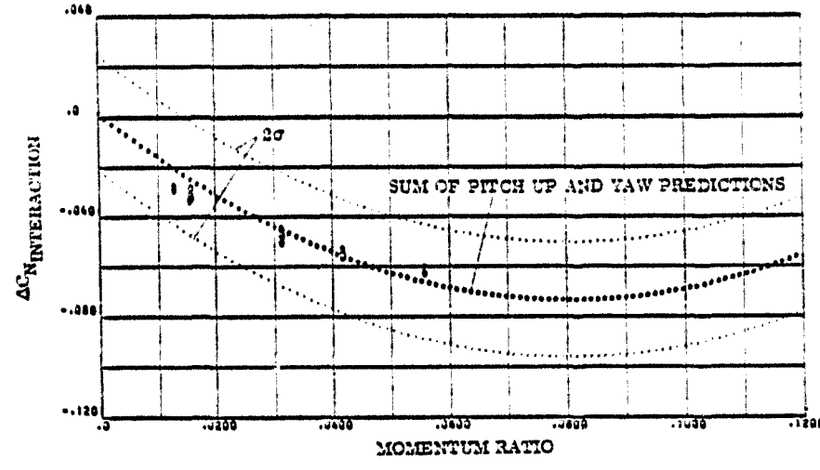

FIGURE 3-24h. : PITCH UP PLUS YAW RCS COMBINED CONTROL INTERACTIONS FROM -5 TO 0 DEGREES ANGLE OF ATTACK: NORMAL FORCE

SYMBOL	NOZZLE NUMBER	TEST NUMBER
0	N04	OA 82, MA 22

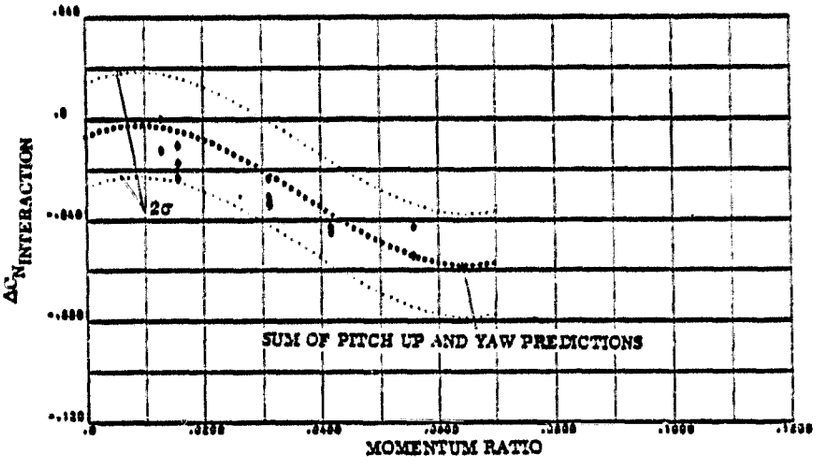

FIGURE 3-241. : PITCH UP PLUS YAW RCS COMBINED CONTROL INTERACTIONS FROM 15 TO 20 DEGREES ANGLE OF ATTACK; NORMAL FORCE

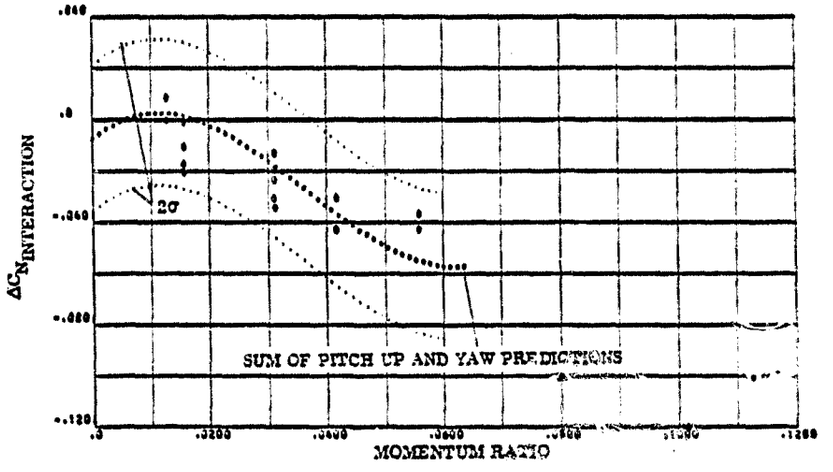

FIGURE 3-242. : PITCH UP PLUS YAW RCS COMBINED CONTROL INTERACTIONS FROM 20 TO 25 DEGREES ANGLE OF ATTACK; NORMAL FORCE

SYMBOL	NOZZLE NUMBER	TEST NUMBER
0	N84	OA 32, MA 22

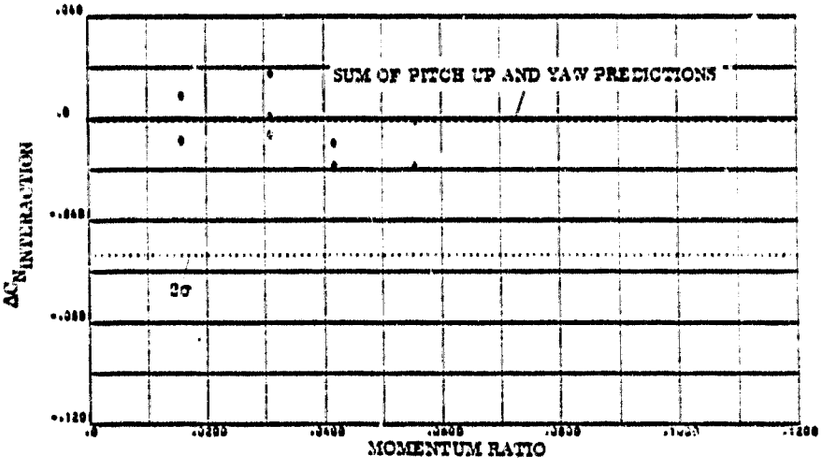

FIGURE 3-24k: PITCH UP PLUS YAW RCS COMBINED CONTROL INTERACTIONS FROM 30 TO 35 DEGREES ANGLE OF ATTACK; NORMAL FORCE

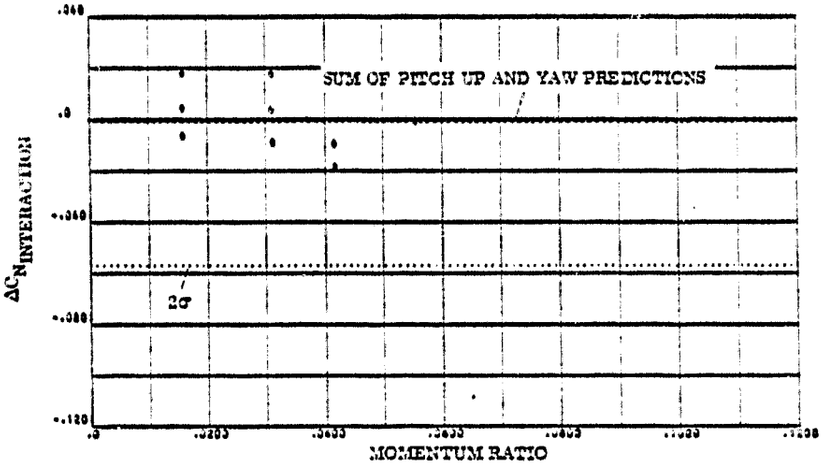

FIGURE 3-24l: PITCH UP PLUS YAW RCS COMBINED CONTROL INTERACTIONS FROM 35 TO 42.5 DEGREES ANGLE OF ATTACK; NORMAL FORCE

SYMBOL	NOZZLE NUMBER	TEST NUMBER.
0	N84	OA 82, MA 22

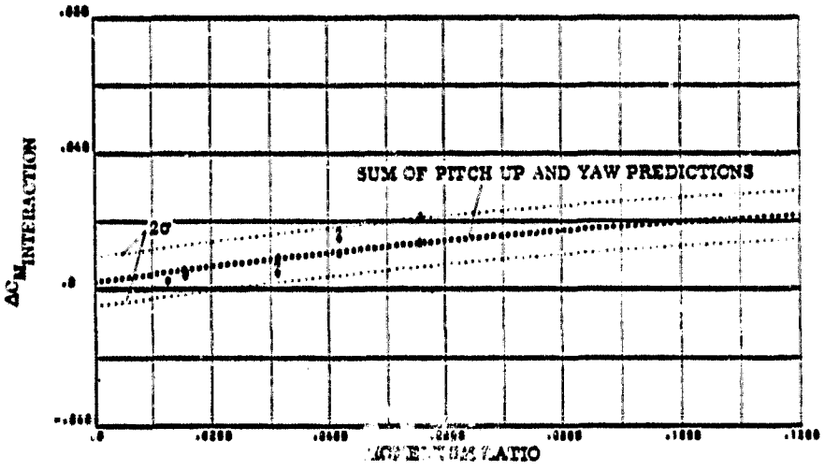

FIGURE 3-24m : PITCH UP PLUS YAW RCS COMBINED CONTROL INTERACTIONS FROM -10 TO -5 DEGREES ANGLE OF ATTACK; PITCHING MOMENT

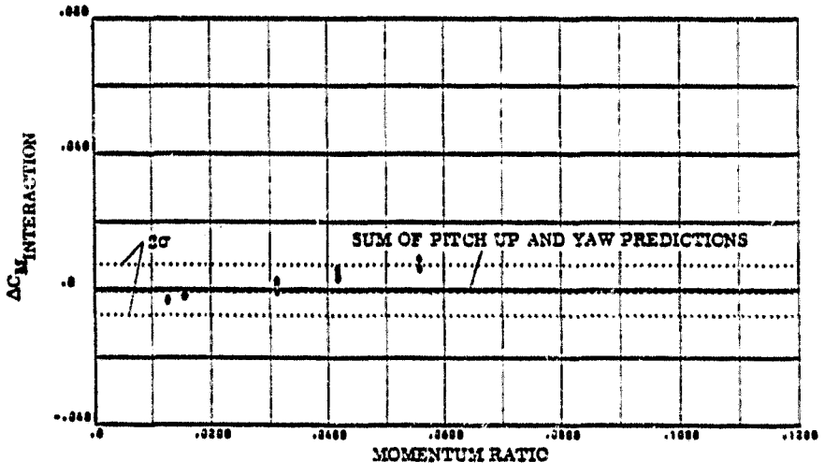

FIGURE 3-24n : PITCH UP PLUS YAW RCS COMBINED CONTROL INTERACTIONS FROM -5 TO 0 DEGREES ANGLE OF ATTACK; PITCHING MOMENT

SYMBOL	NOZZLE NUMBER	TEST NUMBER
0	N94	OA 42, MA 22

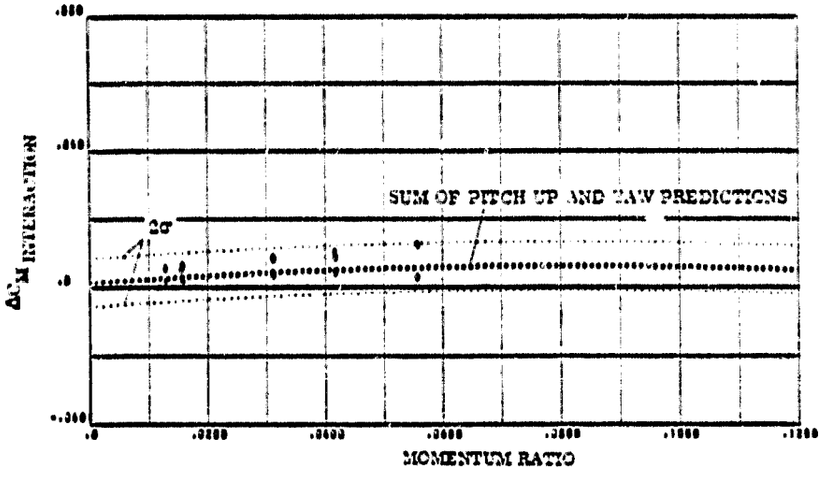

FIGURE 3-24o : PITCH UP PLUS YAW RCS COMBINED CONTROL INTERACTIONS FROM 15 TO 20 DEGREES ANGLE OF ATTACK; PITCHING MOMENT

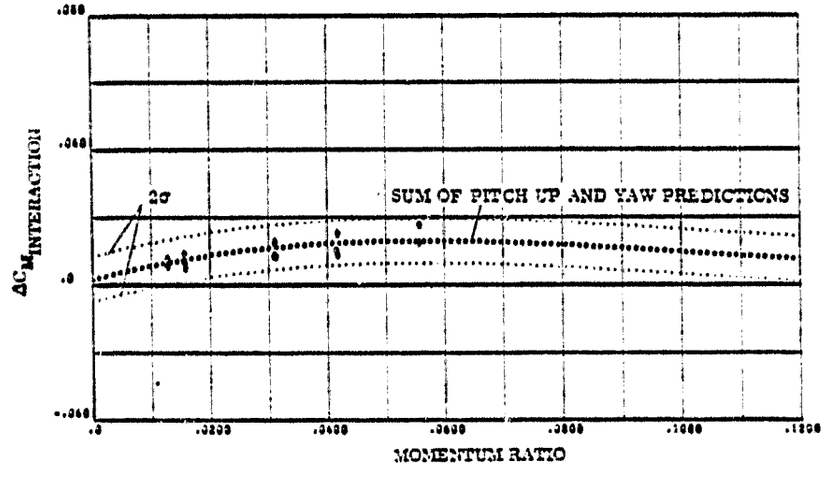

FIGURE 3-24p : PITCH UP PLUS YAW RCS COMBINED CONTROL INTERACTIONS FROM 20 TO 25 DEGREES ANGLE OF ATTACK; PITCHING MOMENT

SYMBOL	NOZZLE NUMBER	TEST NUMBER
0	N84	OA 82, MA 22

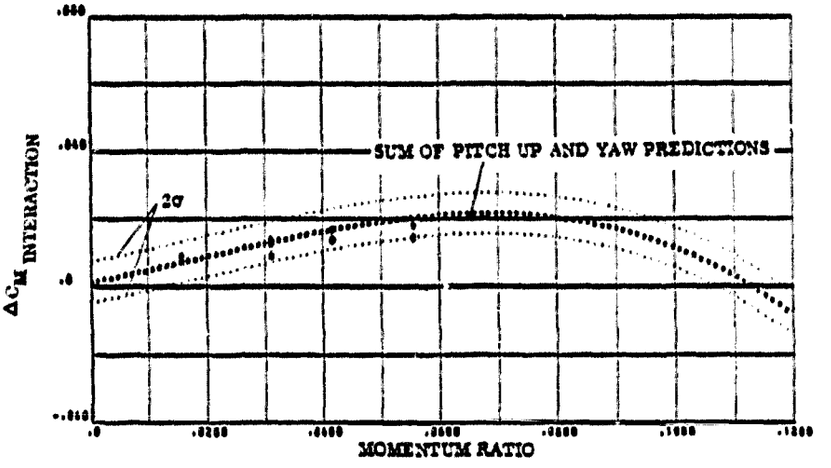

FIGURE 3-24q : PITCH UP PLUS YAW RCS COMBINED CONTROL INTERACTIONS FROM 30 TO 35 DEGREES ANGLE OF ATTACK; PITCHING MOMENT

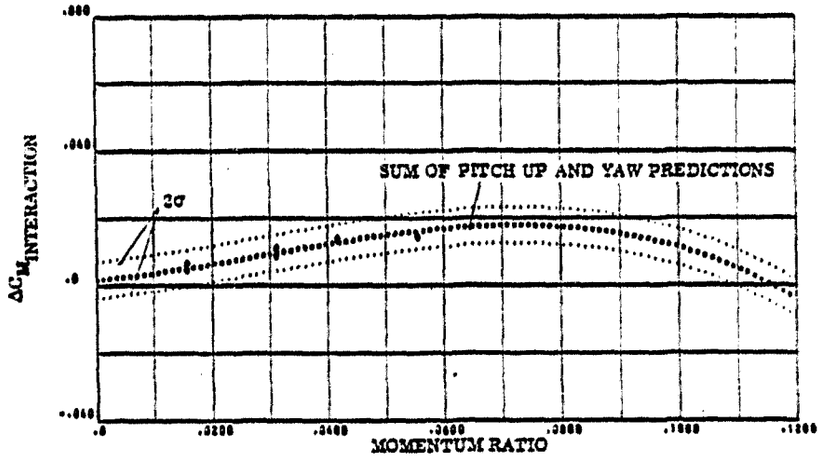

FIGURE 3-24r : PITCH UP PLUS YAW RCS COMBINED CONTROL INTERACTIONS FROM 35 TO 42.5 DEGREES ANGLE OF ATTACK; PITCHING MOMENT

SYMBOL	NOZZLE NUMBER	TEST NUMBER
0	N84	OA 82, MA 22

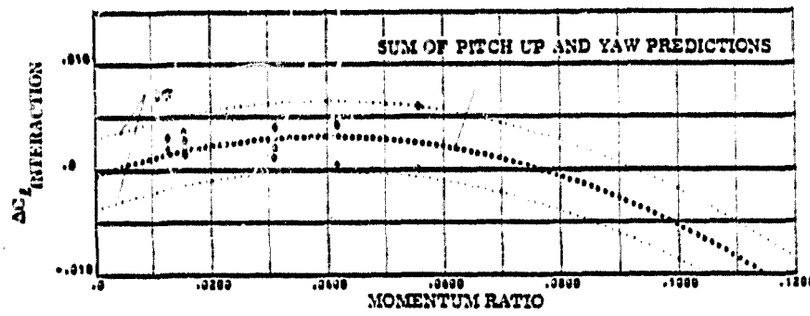

FIGURE 3-34 s : PITCH UP PLUS YAW RCS COMBINED CONTROL INTERACTIONS FROM 15 TO 20 DEGREES ANGLE OF ATTACK; ROLLING MOMENT

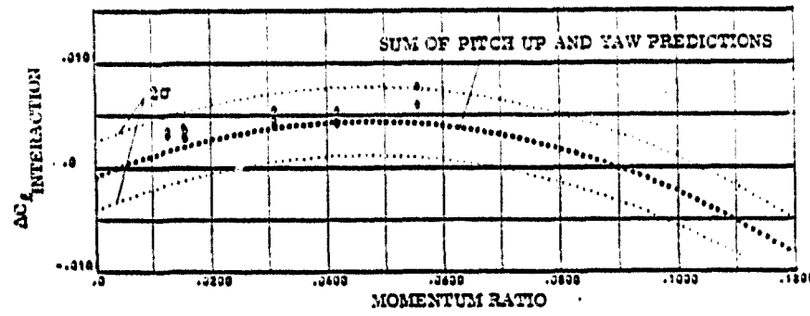

FIGURE 3-34t : PITCH UP PLUS YAW RCS COMBINED CONTROL INTERACTIONS FROM 20 TO 25 DEGREES ANGLE OF ATTACK; ROLLING MOMENT

SYMBOL	NOZZLE NUMBER	TEST NUMBER
0	N84	OA 82, MA 22

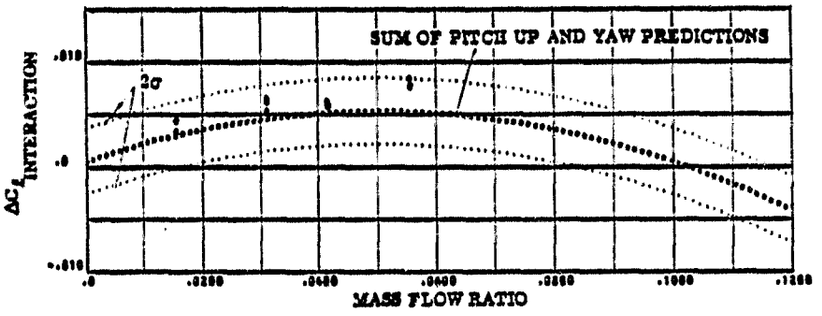

FIGURE 3-24u : PITCH UP PLUS YAW RCS COMBINED CONTROL INTERACTIONS FROM 30 TO 35 DEGREES ANGLE OF ATTACK; ROLLING MOMENT

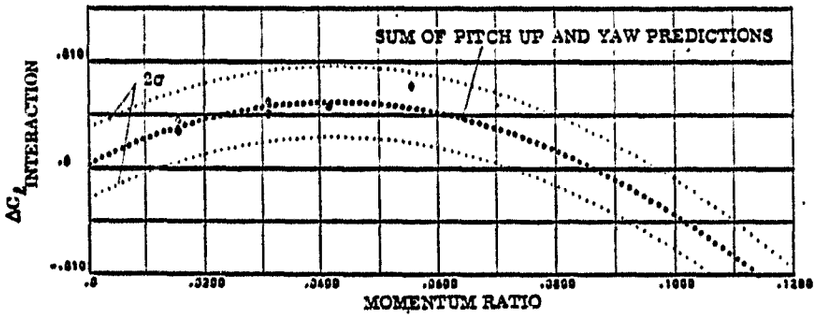

FIGURE 3-24v : PITCH UP PLUS YAW RCS COMBINED CONTROL INTERACTIONS FROM 35 TO 42.5 DEGREES ANGLE OF ATTACK; ROLLING MOMENT

SYMBOL	NOZZLE NUMBER	TEST NUMBER
0	N84	OA 82, MA 22

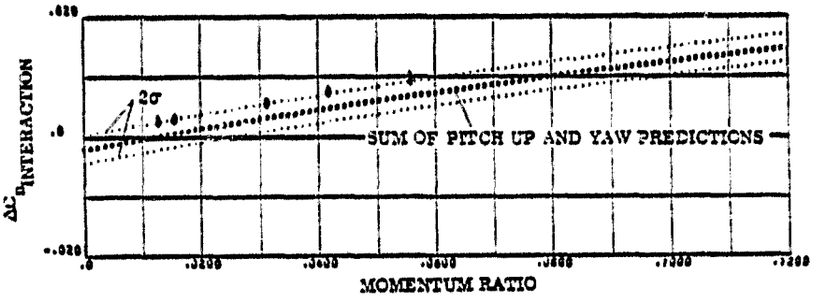

FIGURE 3-24w: PITCH UP PLUS YAW RCS COMBINED CONTROL INTERACTIONS FROM 15 TO 20 DEGREES ANGLE OF ATTACK: YAWING MOMENT

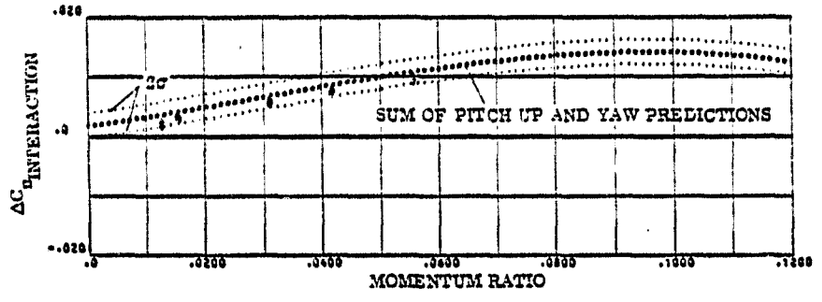

FIGURE 3-24x: PITCH UP PLUS YAW RCS COMBINED CONTROL INTERACTIONS FROM 20 TO 25 DEGREES ANGLE OF ATTACK: YAWING MOMENT

SYMBOL	NOZZLE NUMBER	TEST NUMBER
0	N84	OA 82, MA 22

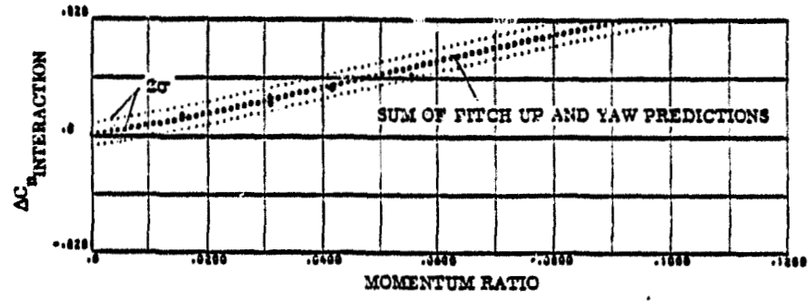

FIGURE 3-24y : PITCH UP PLUS YAW RCS COMBINED CONTROL INTERACTIONS FROM 30 TO 35 DEGREES ANGLE OF ATTACK; YAWING MOMENT

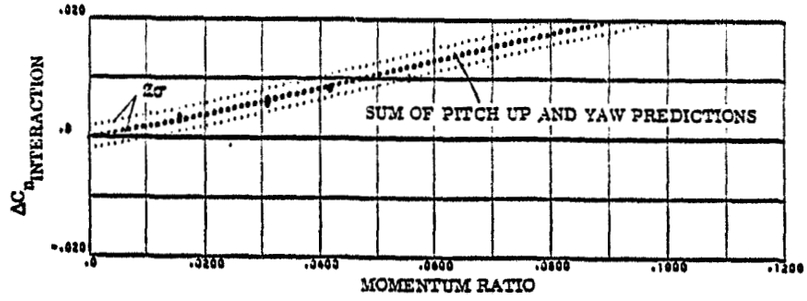

FIGURE 3-24z : PITCH UP PLUS YAW RCS COMBINED CONTROL INTERACTIONS FROM 35 TO 42.5 DEGREES ANGLE OF ATTACK; YAWING MOMENT

SYMBOL	NOZZLE NUMBER	TEST NUMBER
0	N34	OA 82, MA 22

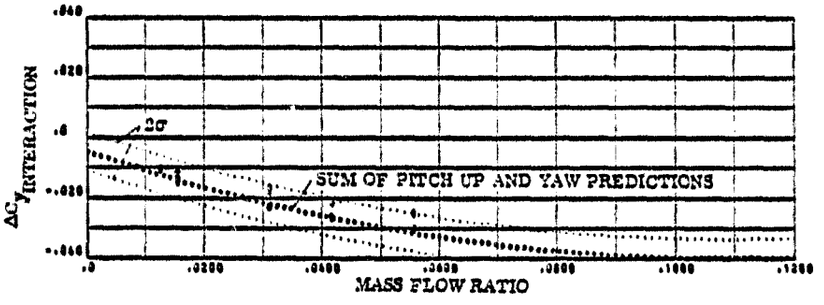

FIGURE3-24aa: PITCH UP PLUS YAW RCS COMBINED CONTROL INTERACTIONS FROM 15 TO 20 DEGREES ANGLE OF ATTACK; SIDE FORCE

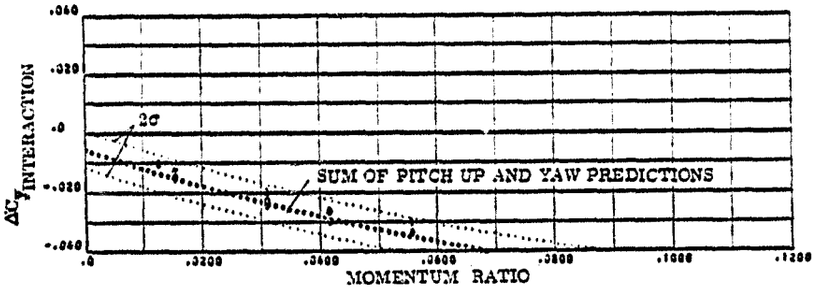

FIGURE3-24bb: PITCH UP PLUS YAW RCS COMBINED CONTROL INTERACTIONS FROM 20 TO 25 DEGREES ANGLE OF ATTACK; SIDE FORCE

SYMBOL	NOZZLE NUMBER	TEST NUMBER
0	N64	OA 82, MA 22

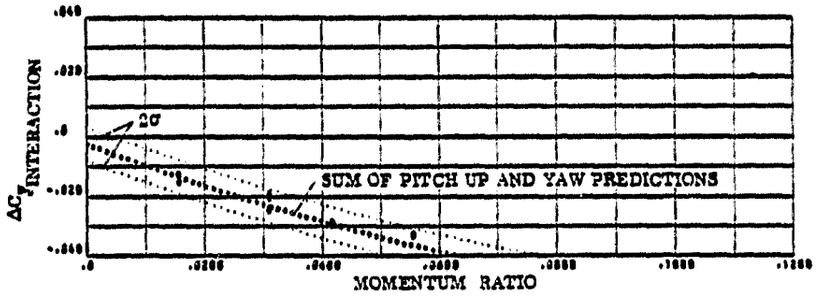

FIGURE 3-24cc: PITCH UP PLUS YAW RCS COMBINED CONTROL INTERACTIONS FROM 30 TO 35 DEGREES ANGLE OF ATTACK; SIDE FORCE

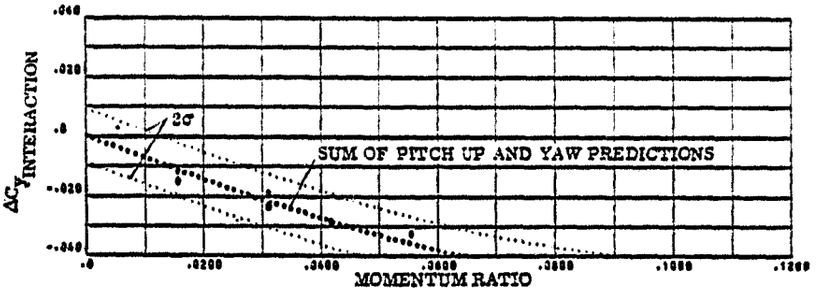

FIGURE 3-24dd: PITCH UP PLUS YAW RCS COMBINED CONTROL INTERACTIONS FROM 35 TO 42.5 DEGREES ANGLE OF ATTACK; SIDE FORCE

SYMBOLS	NOZZLE NUMBER	TEST NUMBER
0	N49	MA 22
X	N79	MA 22
□	N83	MA 22

$\delta_e = 0, \delta_{BF} = -14.25$

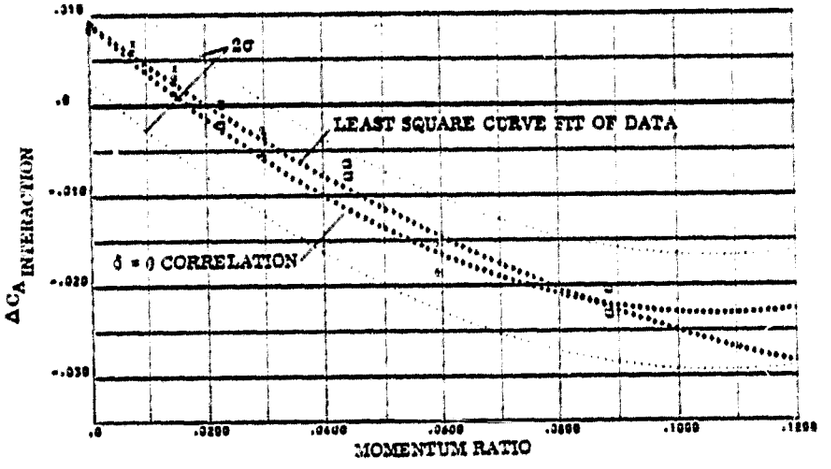

FIGURE 3-25a. : PITCH DOWN RCS INCREMENTAL EFFECTS DUE TO -14.25 DEGREE BODY FLAP DEFLECTION FROM -10 TO -5 DEGREES ANGLE OF ATTACK; AXIAL FORCE

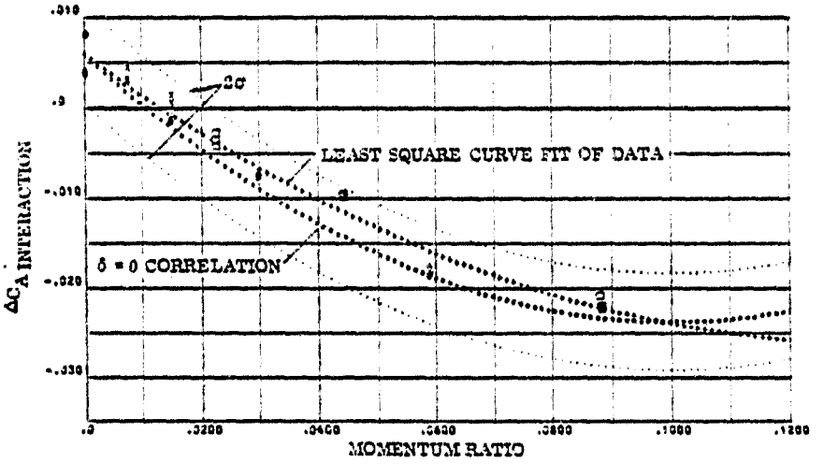

FIGURE 3-25b. : PITCH DOWN RCS INCREMENTAL EFFECTS DUE TO -14.25 DEGREE BODY FLAP DEFLECTION FROM -5 TO 0 DEGREES ANGLE OF ATTACK; AXIAL FORCE

SYMBOLS	NOZZLE NUMBER	TEST NUMBER
0	N49	MA 22
X	N79	MA 22
□	N83	MA 22

$\delta_e = 0, \delta_{BF} = -14.25$

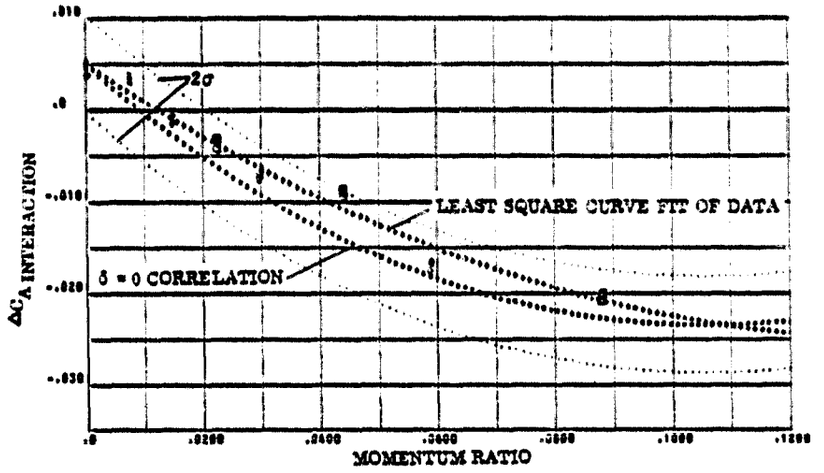

FIGURE 3-25c. : PITCH DOWN RCS INCREMENTAL EFFECTS DUE TO -14.25 DEGREE BODY FLAP DEFLECTION FROM 0 TO 5 DEGREES ANGLE OF ATTACK; AXIAL FORCE

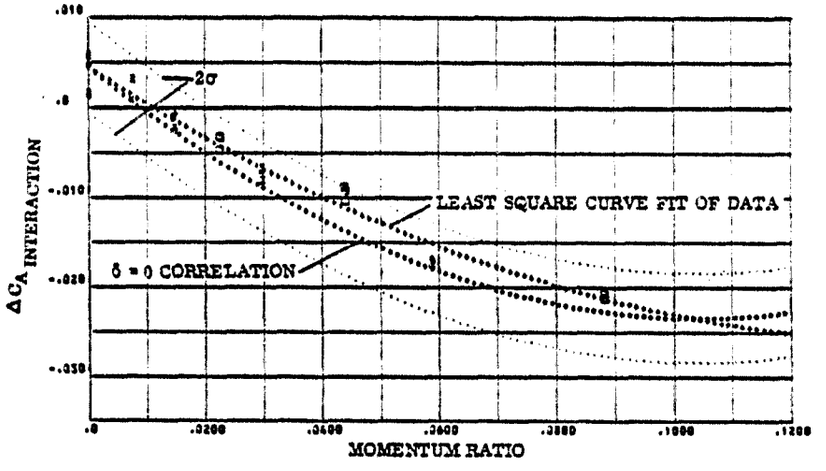

FIGURE 3-25d. : PITCH DOWN RCS INCREMENTAL EFFECTS DUE TO -14.25 DEGREE BODY FLAP DEFLECTION FROM 5 TO 10 DEGREES ANGLE OF ATTACK; AXIAL FORCE

SYMBOLS	NOZZLE NUMBER	TEST NUMBER
0	N49	MA 22
X	N79	MA 22
□	N83	MA 22

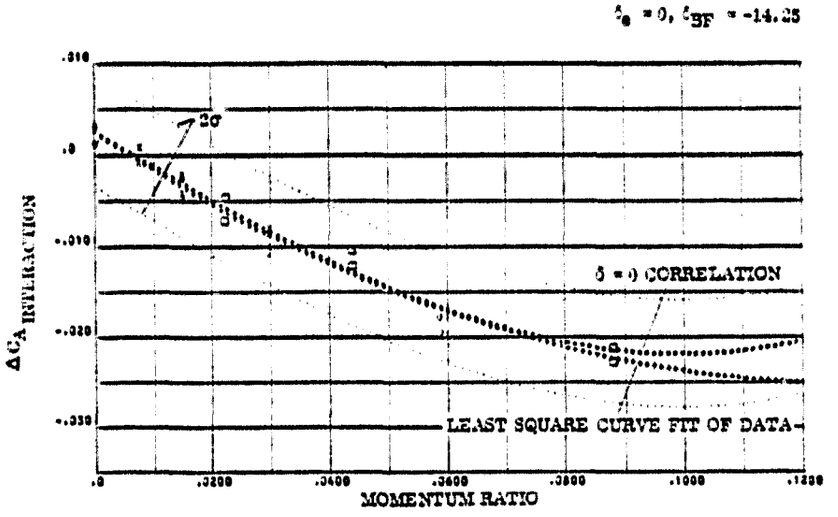

FIGURE 3-25e. : PITCH DOWN RCS INCREMENTAL EFFECTS DUE TO -14.25 DEGREE BODY FLAP DEFLECTION FROM 10 TO 15 DEGREES ANGLE OF ATTACK; AXIAL FORCE

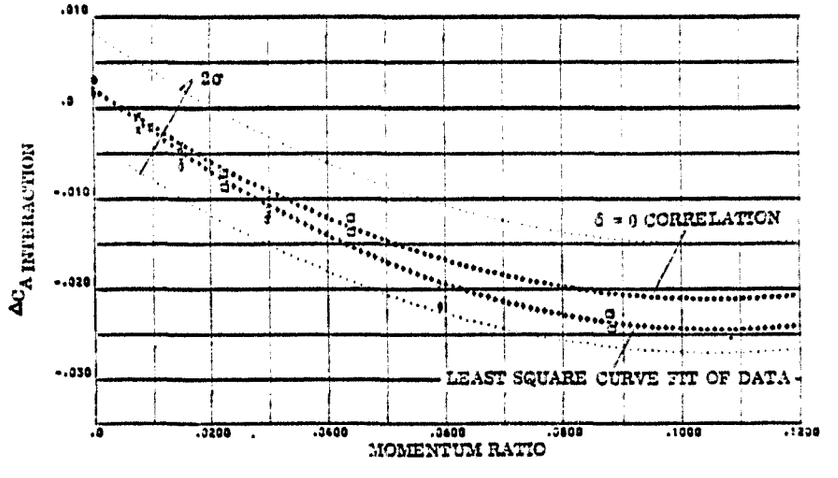

FIGURE 3-25f. : PITCH DOWN RCS INCREMENTAL EFFECTS DUE TO -14.25 DEGREE BODY FLAP DEFLECTION FROM 15 TO 20 DEGREES ANGLE OF ATTACK; AXIAL FORCE

SYMBOLS	NOZZLE NUMBER	TEST NUMBER
0	N49	MA 22
X	N79	MA 22
□	N83	MA 22

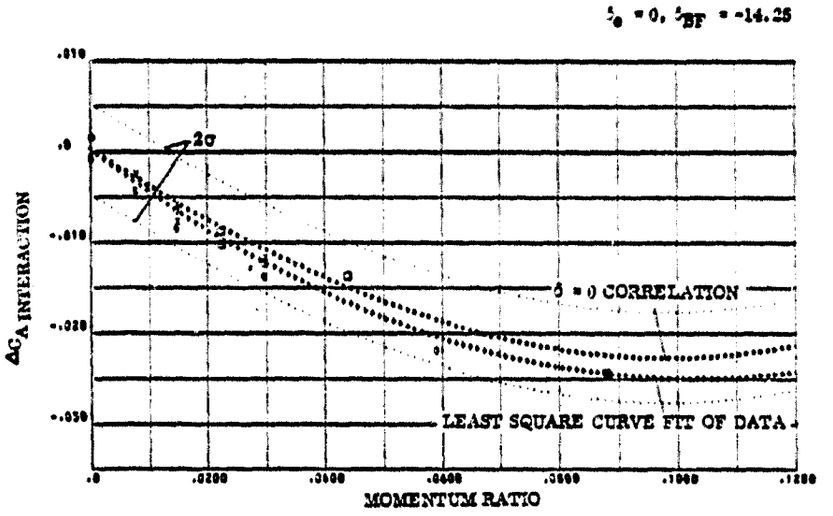

FIGURE 3-25 g. : PITCH DOWN RCS INCREMENTAL EFFECTS DUE TO -14.25 DEGREE BODY FLAP DEFLECTION FROM 20 TO 25 DEGREES ANGLE OF ATTACK; AXIAL FORCE

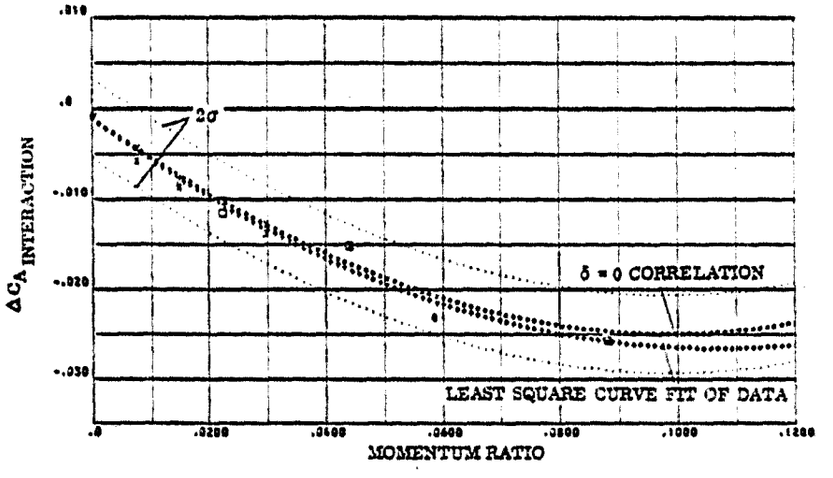

FIGURE 3-25 h. : PITCH DOWN RCS INCREMENTAL EFFECTS DUE TO -14.25 DEGREE BODY FLAP DEFLECTION FROM 25 TO 30 DEGREES ANGLE OF ATTACK; AXIAL FORCE

SYMBOLS	NOZZLE NUMBER	TEST NUMBER
○	N49	MA 22
X	N79	MA 22
□	N83	MA 22

$\delta_e = 0, \delta_{BF} = -14.25$

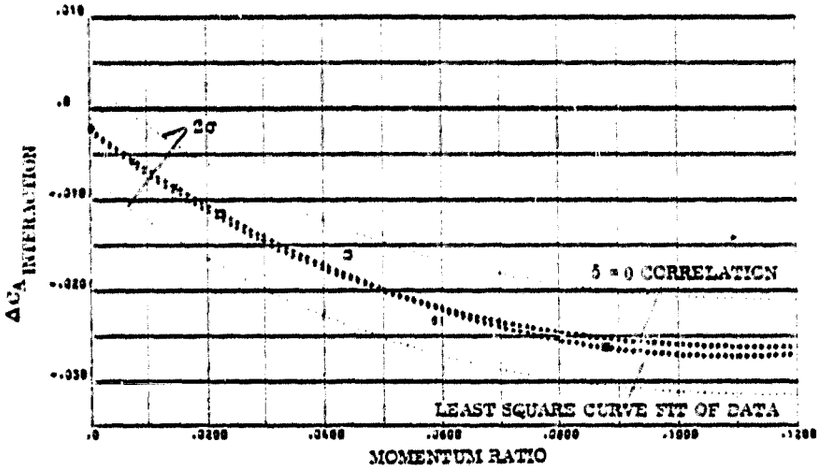

FIGURE 3-251. : PITCH DOWN RCS INCREMENTAL EFFECTS DUE TO -14.25 DEGREE BODY FLAP DEFLECTION FROM 30 TO 35 DEGREES ANGLE OF ATTACK; AXIAL FORCE

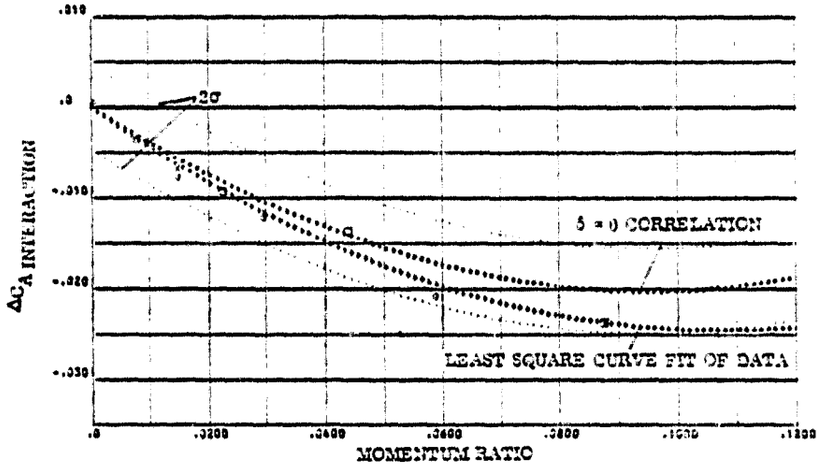

FIGURE 3-251. : PITCH DOWN RCS INCREMENTAL EFFECTS DUE TO -14.25 DEGREE BODY FLAP DEFLECTION FROM 35 TO 42.5 DEGREES ANGLE OF ATTACK; AXIAL FORCE

SYMBOLS	NOZZLE NUMBER	TEST NUMBER
○	N48	MA 22
⊠	N79	MA 22
□	N83	MA 22

$\delta_e = 0$, $\delta_{BF} = -14.25$

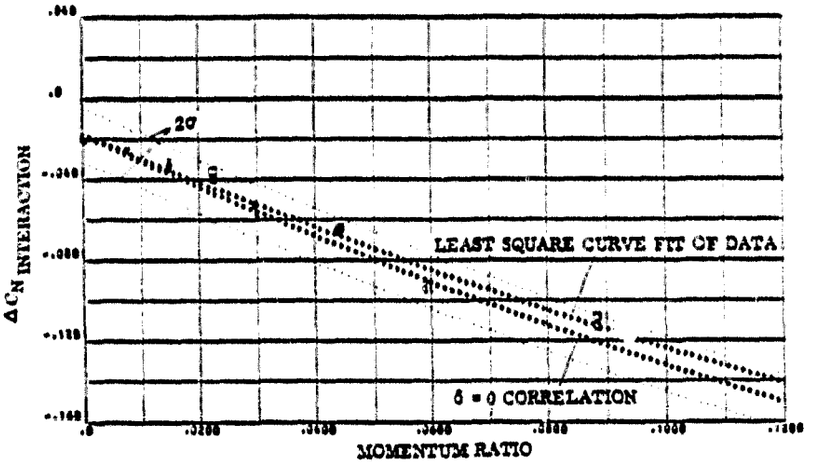

FIGURE 3-26a. : PITCH DOWN RCS INCREMENTAL EFFECTS DUE TO -14.25 DEGREE BODY FLAP DEFLECTION FROM -10 TO -5 DEGREES ANGLE OF ATTACK; NORMAL FORCE

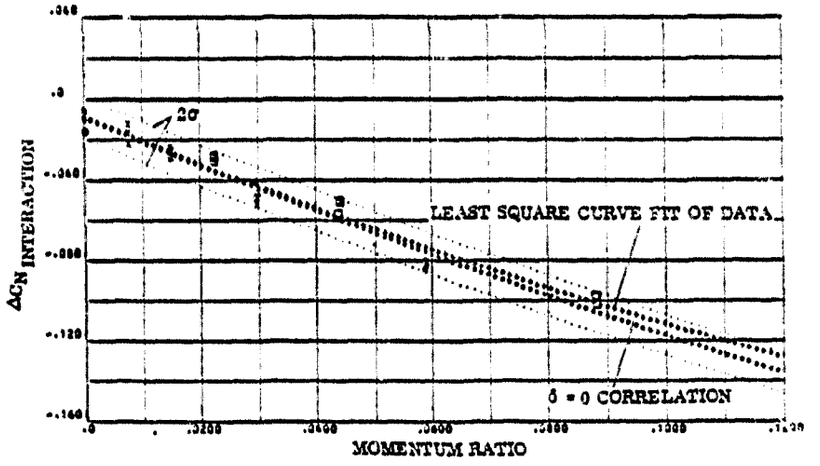

FIGURE 3-26b. : PITCH DOWN RCS INCREMENTAL EFFECTS DUE TO -14.25 DEGREE BODY FLAP DEFLECTION FROM -5 TO 0 DEGREES ANGLE OF ATTACK; NORMAL FORCE

SYMBOLS	NOZZLE NUMBER	TEST NUMBER
0	N49	MA 22
X	N79	MA 22
□	N83	MA 22

$\delta_\phi = 0, \ \delta_{BF} = -14.25$

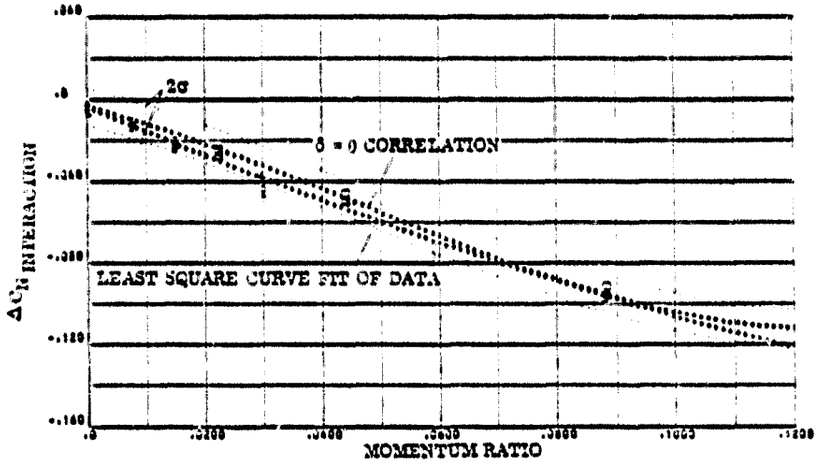

FIGURE 3-26c. : PITCH DOWN RCS INCREMENTAL EFFECTS DUE TO -14.25 DEGREE BODY FLAP DEFLECTION FROM 0 TO 5 DEGREES ANGLE OF ATTACK; NORMAL FORCE

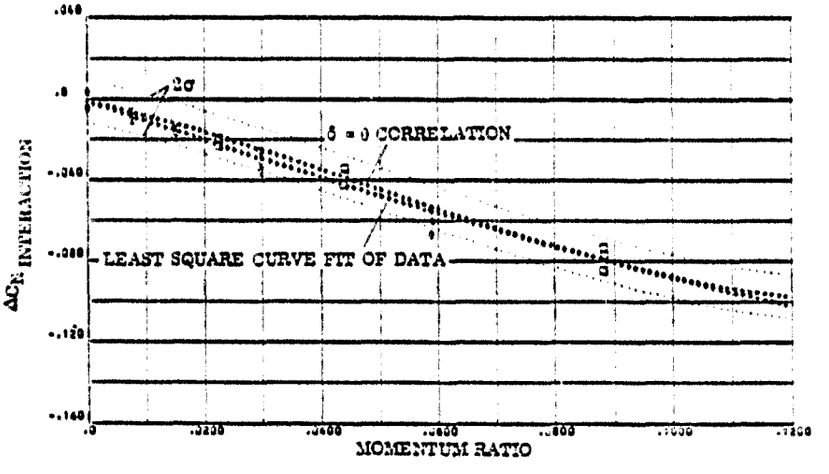

FIGURE 3-26d. : PITCH DOWN RCS INCREMENTAL EFFECTS DUE TO -14.25 DEGREE BODY FLAP DEFLECTION FROM 5 TO 10 DEGREES ANGLE OF ATTACK; NORMAL FORCE

SYMBOLS	NOZZLE NUMBER	TEST NUMBER
0	N49	MA 22
×	N79	MA 22
□	N83	MA 22

$\delta_e = 0, \delta_{BF} = -14.25$

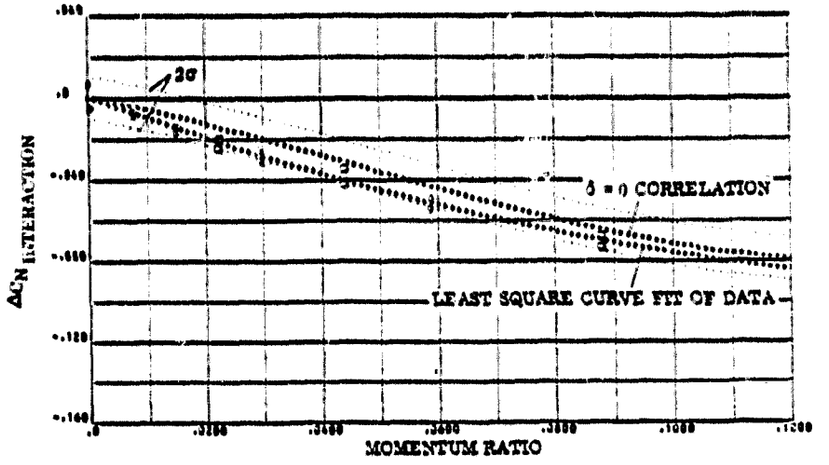

FIGURE 3-26e. : PITCH DOWN RCS INCREMENTAL EFFECTS DUE TO -14.25 DEGREE BODY FLAP DEFLECTION FROM 10 TO 15 DEGREES ANGLE OF ATTACK; NORMAL FORCE

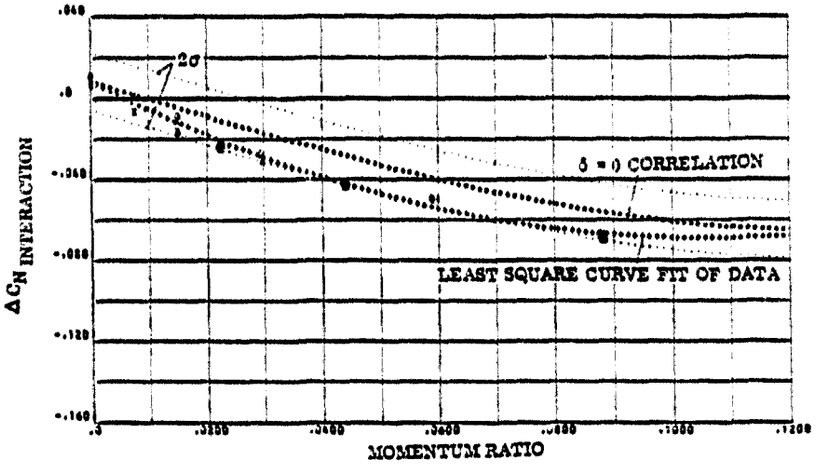

FIGURE 3-26f. : PITCH DOWN RCS INCREMENTAL EFFECTS DUE TO -14.25 DEGREE BODY FLAP DEFLECTION FROM 15 TO 20 DEGREES ANGLE OF ATTACK; NORMAL FORCE

SYMBOLS	NOZZLE NUMBER	TEST NUMBER
0	N49	MA 22
X	N79	MA 22
□	N83	MA 22

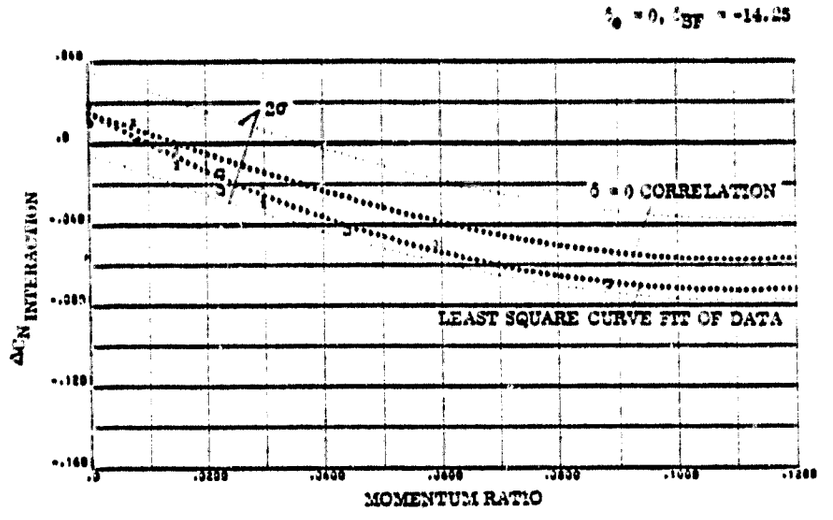

FIGURE 3-26g. : PITCH DOWN RCS INCREMENTAL EFFECTS DUE TO -14.25 DEGREE BODY FLAP DEFLECTION FROM 20 TO 25 DEGREES ANGLE OF ATTACK; NORMAL FORCE

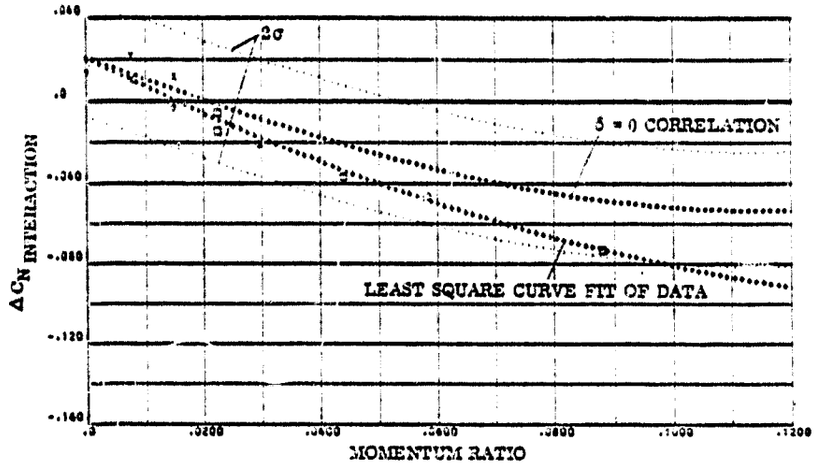

FIGURE 3-26h. : PITCH DOWN RCS INCREMENTAL EFFECTS DUE TO -14.25 DEGREE BODY FLAP DEFLECTION FROM 25 TO 30 DEGREES ANGLE OF ATTACK; NORMAL FORCE

SYMBOLS	NOZZLE NUMBER	TEST NUMBER
0	N49	MA 22
X	N79	MA 22
□	N83	MA 22

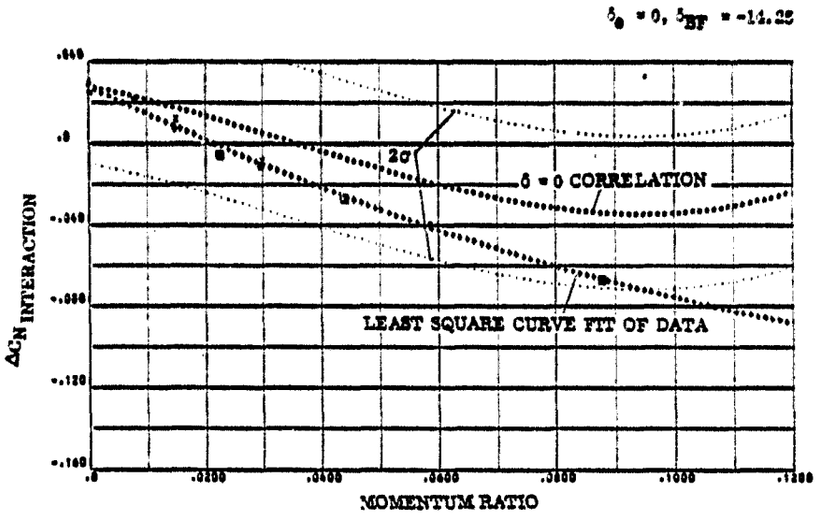

FIGURE 3-26i. : PITCH DOWN RCS INCREMENTAL EFFECTS DUE TO -14.25 DEGREE BODY FLAP DEFLECTION FROM 30 TO 35 DEGREES ANGLE OF ATTACK; NORMAL FORCE

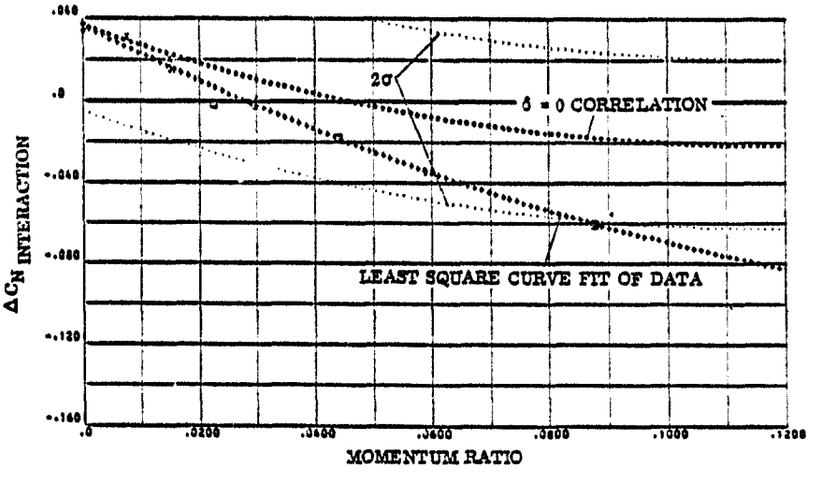

FIGURE 3-26j. : PITCH DOWN RCS INCREMENTAL EFFECTS DUE TO -14.25 DEGREE BODY FLAP DEFLECTION FROM 35 TO 42.5 DEGREES ANGLE OF ATTACK; NORMAL FORCE

SYMBOLS	NOZZLE NUMBER	TEST NUMBER
○	N49	MA 22
×	N79	MA 22
□	N83	MA 22

$\delta_e = 0, \delta_{BF} = -14.25$

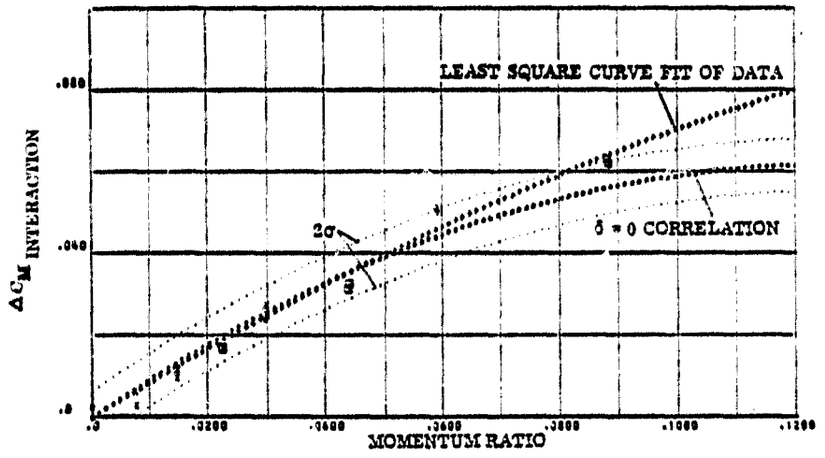

FIGURE 3-27a. : PITCH DOWN RCS INCREMENTAL EFFECTS DUE TO -14.25 DEGREE BODY FLAP DEFLECTION FROM -10 TO -5 DEGREES ANGLE OF ATTACK; PITCHING MOMENT

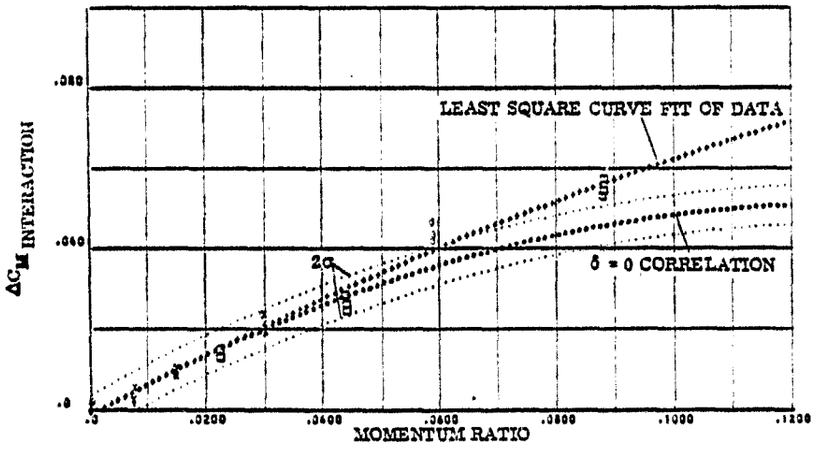

FIGURE 3-27b. : PITCH DOWN RCS INCREMENTAL EFFECTS DUE TO -14.25 DEGREE BODY FLAP DEFLECTION FROM -5 TO 0 DEGREES ANGLE OF ATTACK; PITCHING MOMENT

SYMBOLS	NOZZLE NUMBER	TEST NUMBER
○	N49	MA 22
×	N79	MA 22
□	N83	MA 22

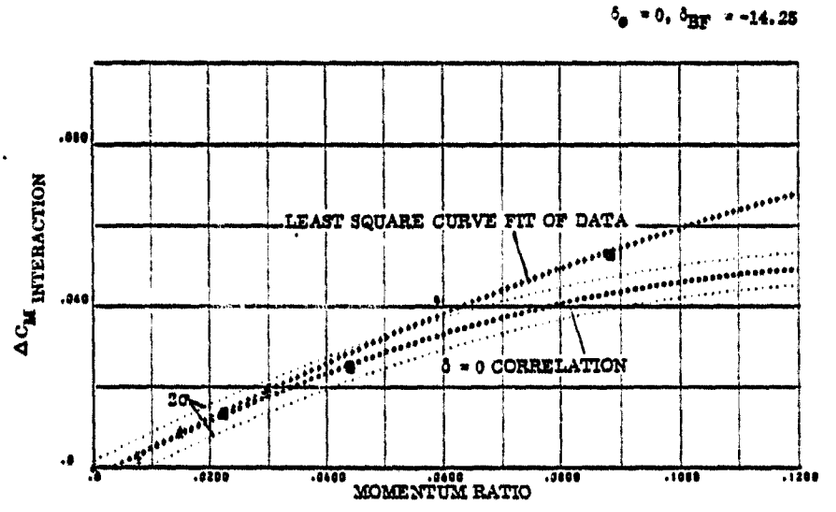

FIGURE 3-27c. : PITCH DOWN RCS INCREMENTAL EFFECTS DUE TO -14.25 DEGREE BODY FLAP DEFLECTION FROM 0 TO 5 DEGREES ANGLE OF ATTACK; PITCHING MOMENT

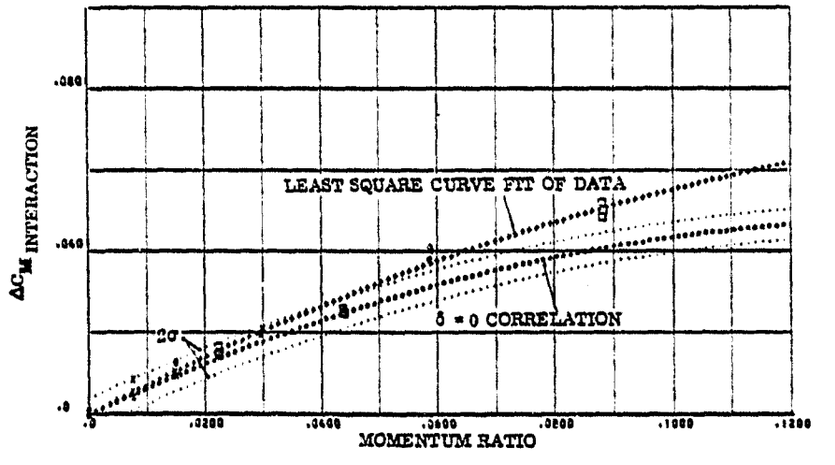

FIGURE 3-27d. : PITCH DOWN RCS INCREMENTAL EFFECTS DUE TO -14.25 DEGREE BODY FLAP DEFLECTION FROM 5 TO 10 DEGREES ANGLE OF ATTACK; PITCHING MOMENT

SYMBOLS	NOZZLE NUMBER	TEST NUMBER
0	N49	MA 22
X	N79	MA 22
□	N83	MA 22

$\delta_e = 0, \delta_{BF} = -14.25$

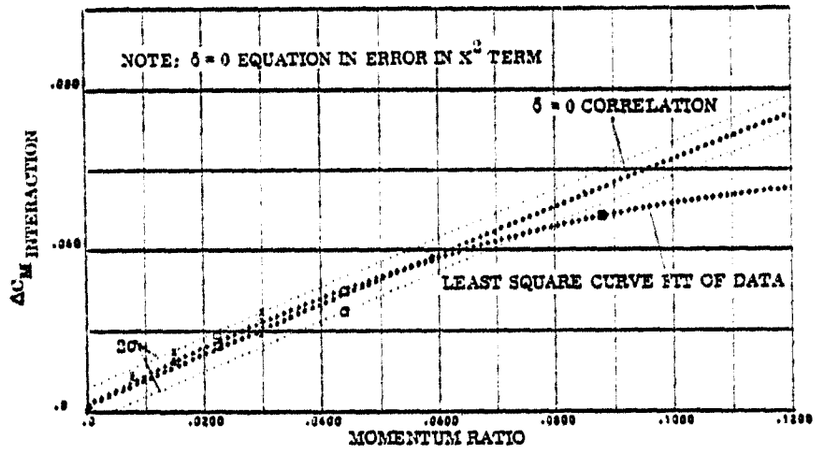

FIGURE 3-27e. : PITCH DOWN RCS INCREMENTAL EFFECTS DUE TO -14.25 DEGREE BODY FLAP DEFLECTION FROM 10 TO 15 DEGREES ANGLE OF ATTACK; PITCHING MOMENT

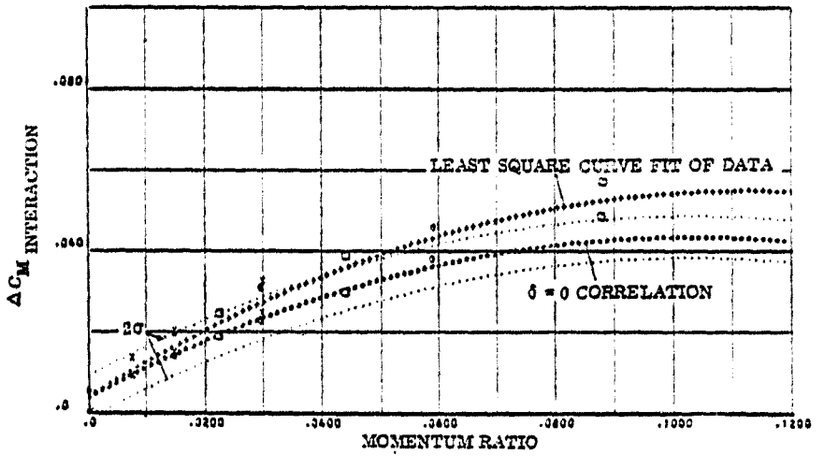

FIGURE 3-27 f. : PITCH DOWN RCS INCREMENTAL EFFECTS DUE TO -14.25 DEGREE BODY FLAP DEFLECTION FROM 15 TO 20 DEGREES ANGLE OF ATTACK; PITCHING MOMENT

SYMBOLS	NOZZLE NUMBER	TEST NUMBER
0	N49	MA 22
X	N79	MA 22
□	N83	MA 22

$\delta_e = 0$, $\delta_{BF} = -14.25$

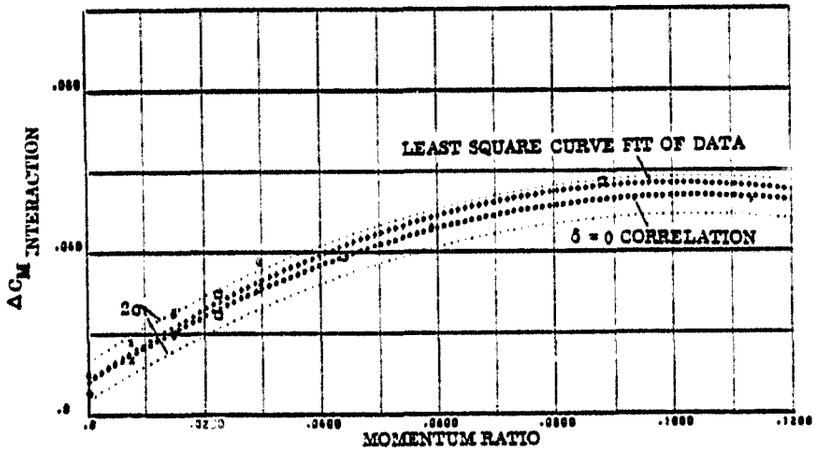

FIGURE 3-27g. : PITCH DOWN RCS INCREMENTAL EFFECTS DUE TO -14.25 DEGREE BODY FLAP DEFLECTION FROM 20 TO 25 DEGREES ANGLE OF ATTACK; PITCHING MOMENT

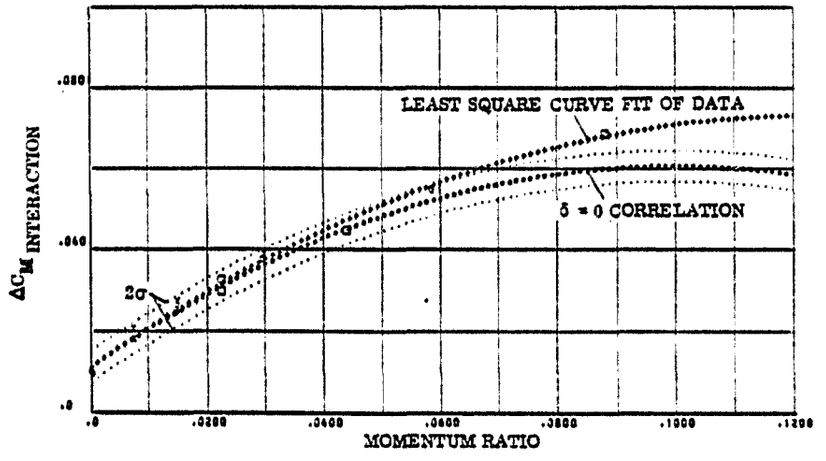

FIGURE 3-27h. : PITCH DOWN RCS INCREMENTAL EFFECTS DUE TO -14.25 DEGREE BODY FLAP DEFLECTION FROM 25 TO 30 DEGREES ANGLE OF ATTACK; PITCHING MOMENT

SYMBOLS	NOZZLE NUMBER	TEST NUMBER
0	N49	MA 22
X	N79	MA 22
□	N83	MA 22

$\delta_e = 0, \delta_{BF} = -14.25$

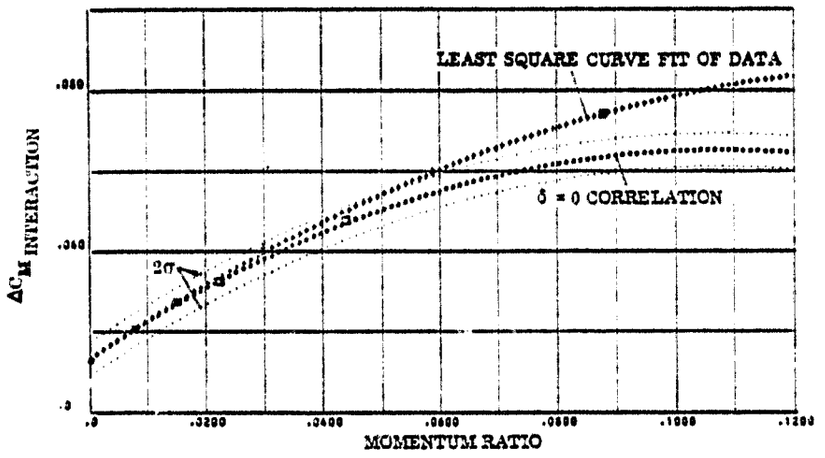

FIGURE 3-27i. : PITCH DOWN RCS INCREMENTAL EFFECTS DUE TO -14.25 DEGREE BODY FLAP DEFLECTION FROM 30 TO 35 DEGREES ANGLE OF ATTACK; PITCHING MOMENT

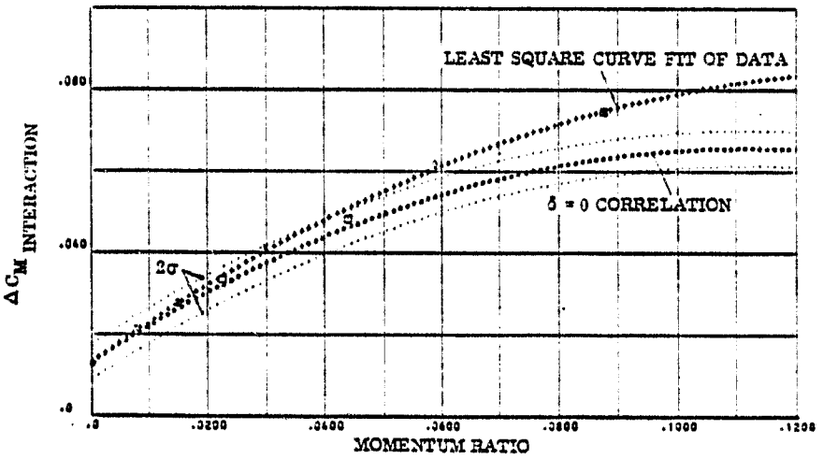

FIGURE 3-27j. : PITCH DOWN RCS INCREMENTAL EFFECTS DUE TO -14.25 DEGREE BODY FLAP DEFLECTION FROM 35 TO 42.5 DEGREES ANGLE OF ATTACK; PITCHING MOMENT

SYMBOLS	NOZZLE NUMBER	TEST NUMBER
○	N49	MA 22
×	N79	MA 22
□	N83	MA 22

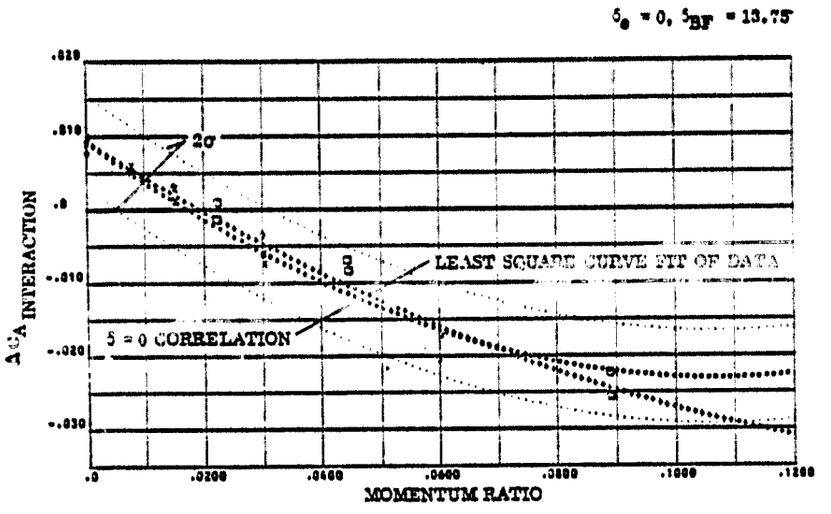

FIGURE 3-28a. : PITCH DOWN RCS INCREMENTAL EFFECTS DUE TO +13.75 DEGREE BODY FLAP DEFLECTION FROM -10 TO -5 DEGREES ANGLE OF ATTACK; AXIAL FORCE

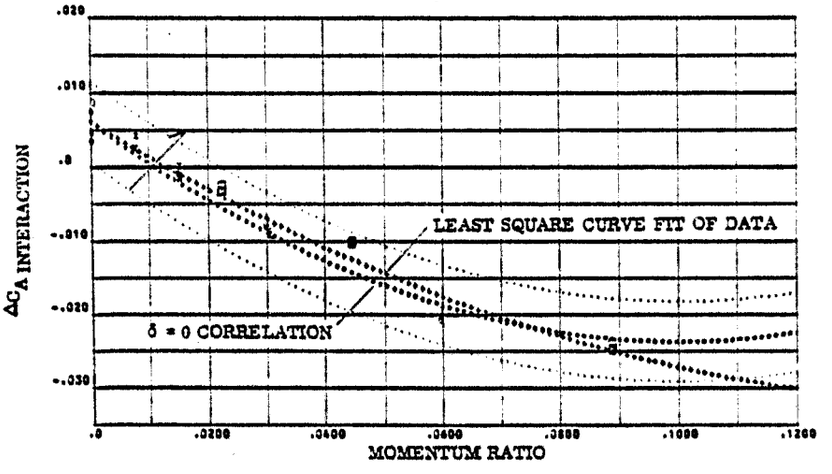

FIGURE 3-28 b. : PITCH DOWN RCS INCREMENTAL EFFECTS DUE TO +13.75 DEGREE BODY FLAP DEFLECTION FROM -5 TO 0 DEGREES ANGLE OF ATTACK; AXIAL FORCE

SYMBOLS	NOZZLE NUMBER	TEST NUMBER
0	N49	MA 22
X	N79	MA 22
□	N83	MA 22

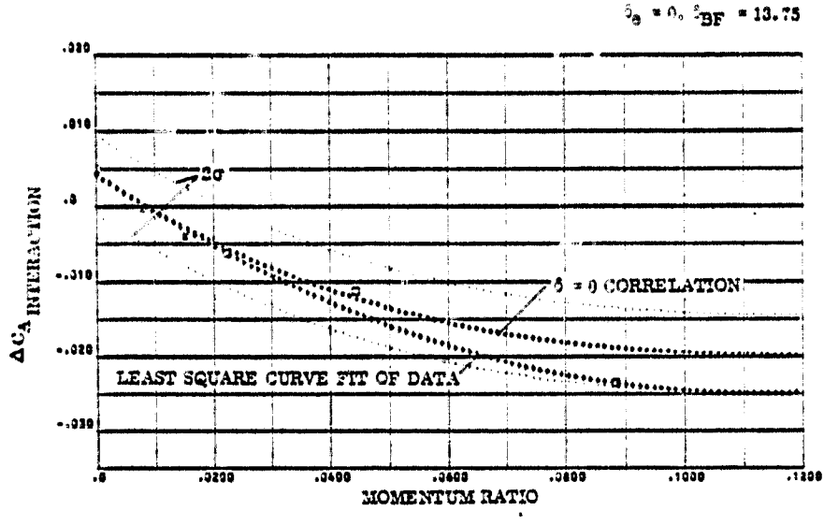

FIGURE 3-28c. : PITCH DOWN RCS INCREMENTAL EFFECTS DUE TO +13.75 DEGREE BODY FLAP DEFLECTION FROM 30 TO 35 DEGREES ANGLE OF ATTACK; AXIAL FORCE

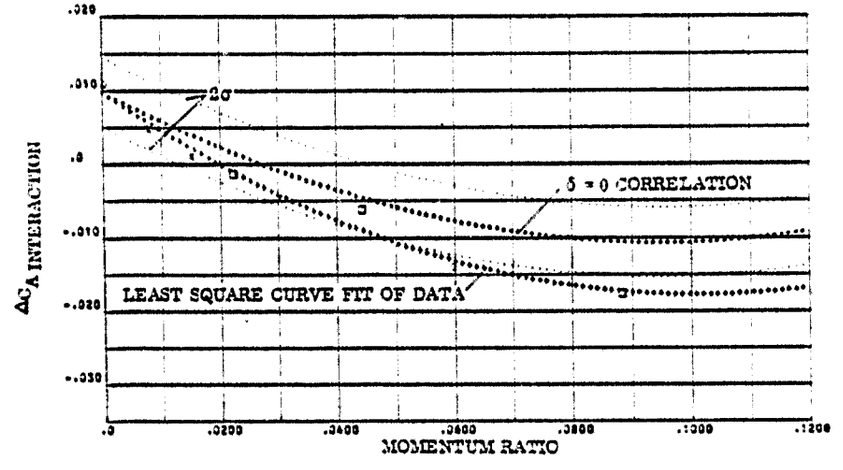

FIGURE 3-28d. : PITCH DOWN RCS INCREMENTAL EFFECTS DUE TO +13.75 DEGREE BODY FLAP DEFLECTION FROM 35 TO 42.5 DEGREES ANGLE OF ATTACK; AXIAL FORCE

SYMBOLS	NOZZLE NUMBER	TEST NUMBER
0	N49	MA 22
X	N79	MA 22
□	N83	MA 22

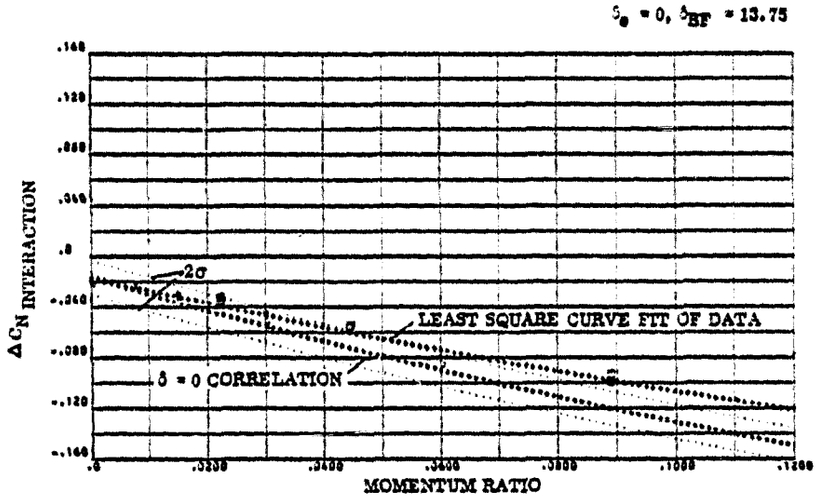

FIGURE 3-28e. : PITCH DOWN RCS INCREMENTAL EFFECTS DUE TO +13.75 DEGREE BODY FLAP DEFLECTION FROM -10 TO -5 DEGREES ANGLE OF ATTACK; NORMAL FORCE

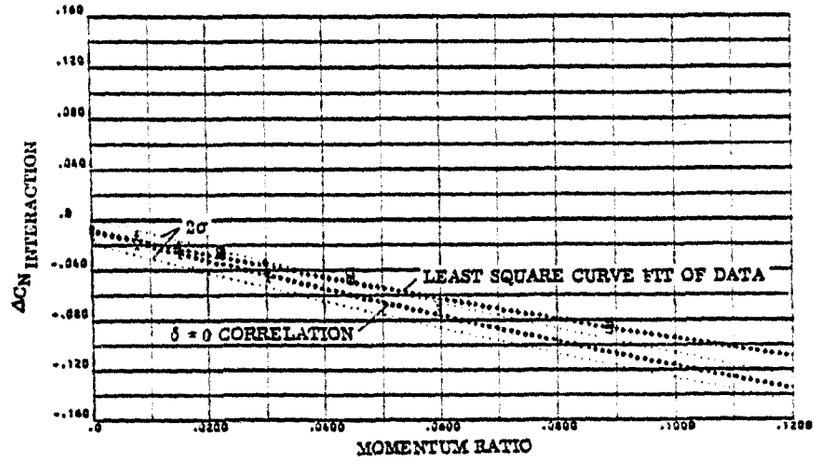

FIGURE 3-28f. : PITCH DOWN RCS INCREMENTAL EFFECTS DUE TO +13.75 DEGREE BODY FLAP DEFLECTION FROM -5 TO 0 DEGREES ANGLE OF ATTACK; NORMAL FORCE

SYMBOLS	NOZZLE NUMBER	TEST NUMBER
0	N49	MA 22
X	N79	MA 22
□	N83	MA 22

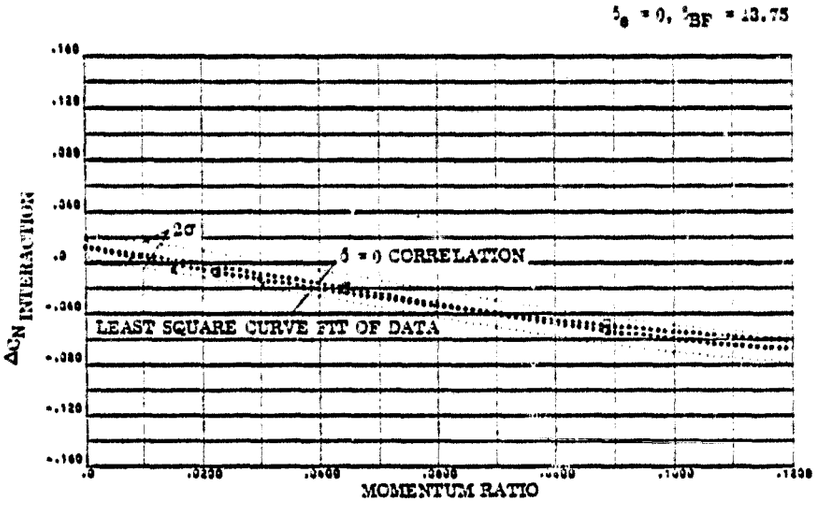

FIGURE 3-28g. : PITCH DOWN RCS INCREMENTAL EFFECTS DUE TO +13.75 DEGREE BODY FLAP DEFLECTION FROM 10 TO 15 DEGREES ANGLE OF ATTACK; NORMAL FORCE

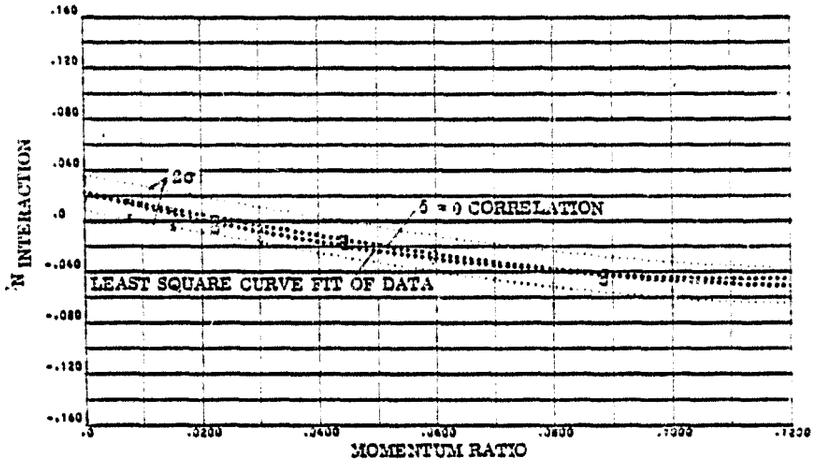

FIGURE 3-28h. : PITCH DOWN RCS INCREMENTAL EFFECTS DUE TO +13.75 DEGREE BODY FLAP DEFLECTION FROM 15 TO 20 DEGREES ANGLE OF ATTACK; NORMAL FORCE

SYMBOLS	NOZZLE NUMBER	TEST NUMBER
0	N49	MA 22
X	N79	MA 22
□	N83	MA 12

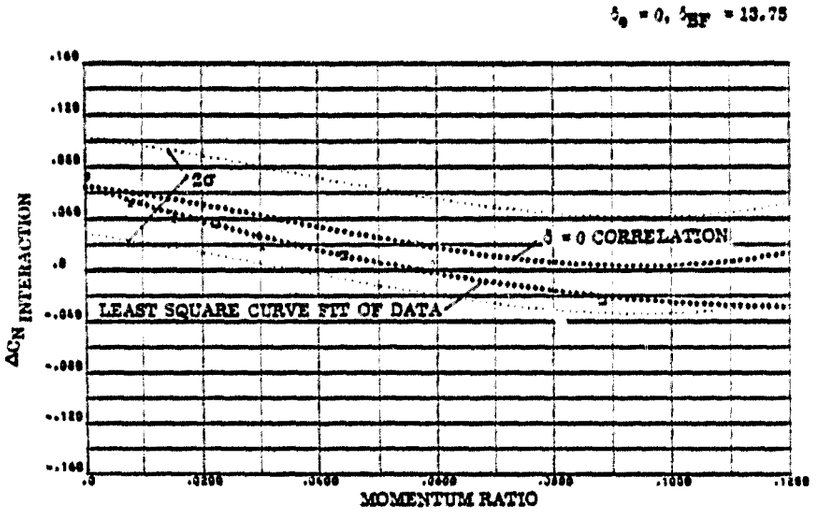

FIGURE 3-28i. : PITCH DOWN RCS INCREMENTAL EFFECTS DUE TO 0 DEGREE BODY FLAP DEFLECTION FROM 30 TO 35 DEGREES ANGLE OF ATTACK; NORMAL FORCE

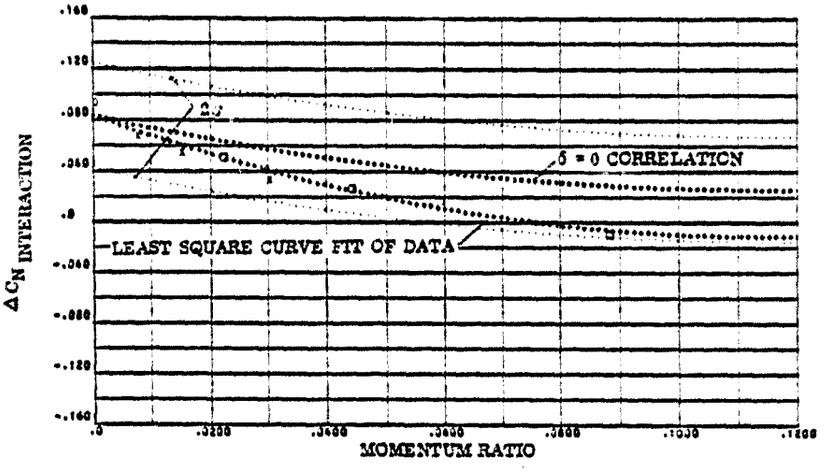

FIGURE 3-28j. : PITCH DOWN RCS INCREMENTAL EFFECTS DUE TO +13.75 DEGREE BODY FLAP DEFLECTION FROM 35 TO 42.5 DEGREES ANGLE OF ATTACK; NORMAL FORCE

SYMBOLS	NOZZLE NUMBER	TEST NUMBER
○	N49	MA 22
X	N79	MA 22
□	N83	MA 22

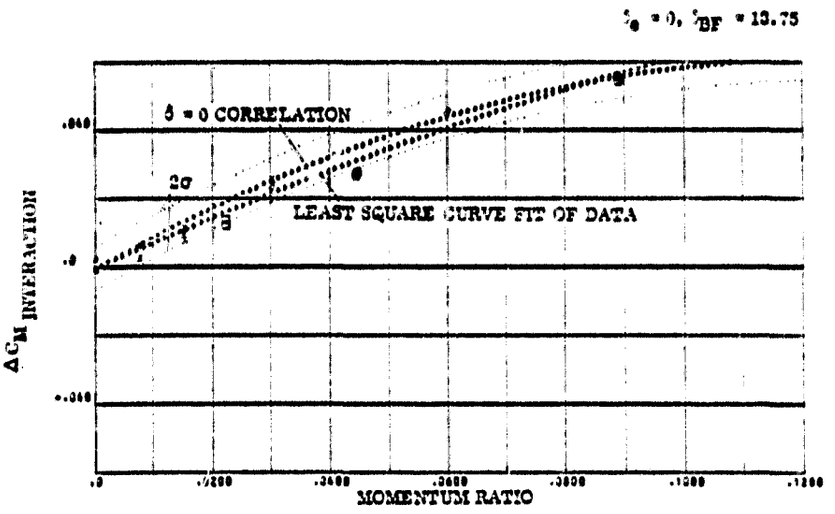

FIGURE 3-28k : PITCH DOWN RCS INCREMENTAL EFFECTS DUE TO +13.75 DEGREE BODY FLAP DEFLECTION FROM -10 TO -5 DEGREES ANGLE OF ATTACK; PITCHING MOMENT

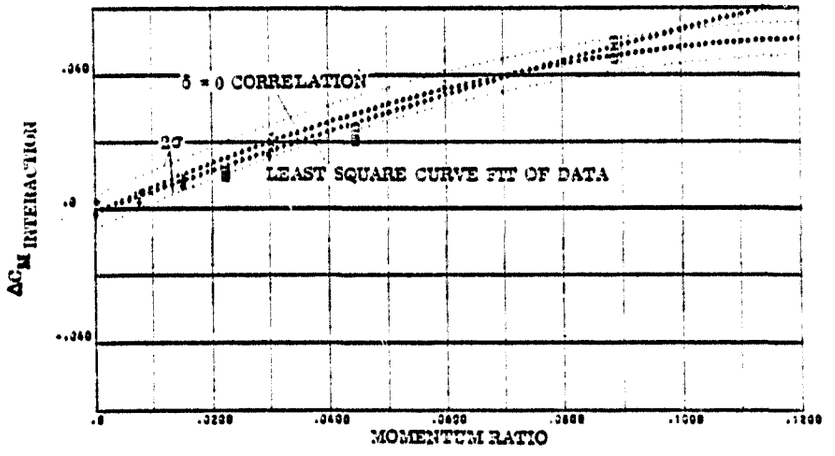

FIGURE 3-28l : PITCH DOWN RCS INCREMENTAL EFFECTS DUE TO +13.75 DEGREE BODY FLAP DEFLECTION FROM -5 TO 0 DEGREES ANGLE OF ATTACK; PITCHING MOMENT

SYMBOLS	NOZZLE NUMBER	TEST NUMBER
0	N49	MA 22
×	N79	MA 22
□	N83	MA 22

$\delta_e = 0, \delta_{BF} = 13.75$

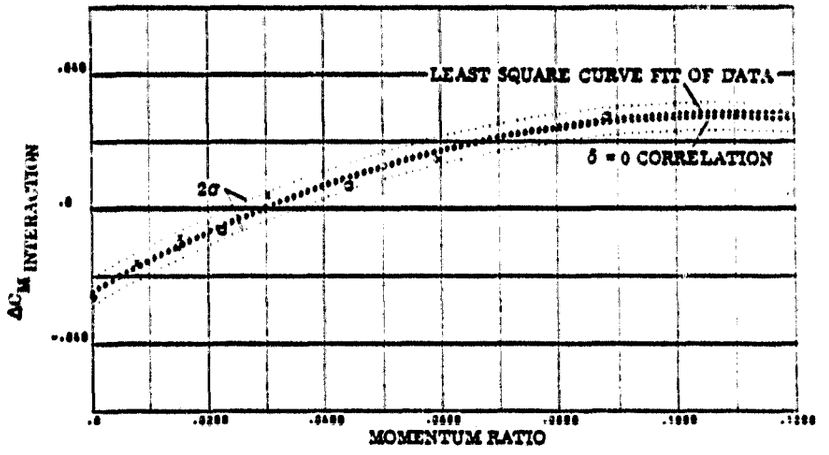

FIGURE 3-28m : PITCH DOWN RCS INCREMENTAL EFFECTS DUE TO +13.75 DEGREE BODY FLAP DEFLECTION FROM 30 TO 35 DEGREES ANGLE OF ATTACK; PITCHING MOMENT

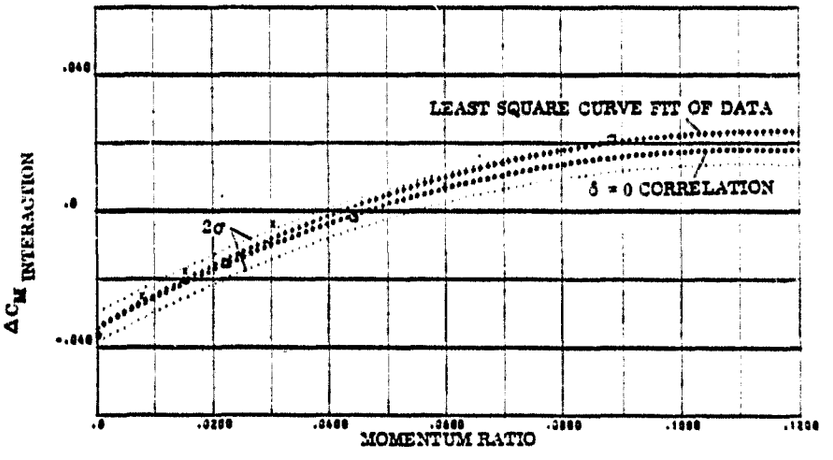

FIGURE 3-28n : PITCH DOWN RCS INCREMENTAL EFFECTS DUE TO +13.75 DEGREE BODY FLAP DEFLECTION FROM 35 TO 42.5 DEGREES ANGLE OF ATTACK; PITCHING MOMENT

SYMBOLS	NOZZLE NUMBER	TEST NUMBER
○	N49	MA 22
X	N79	MA 22
□	N83	MA 22

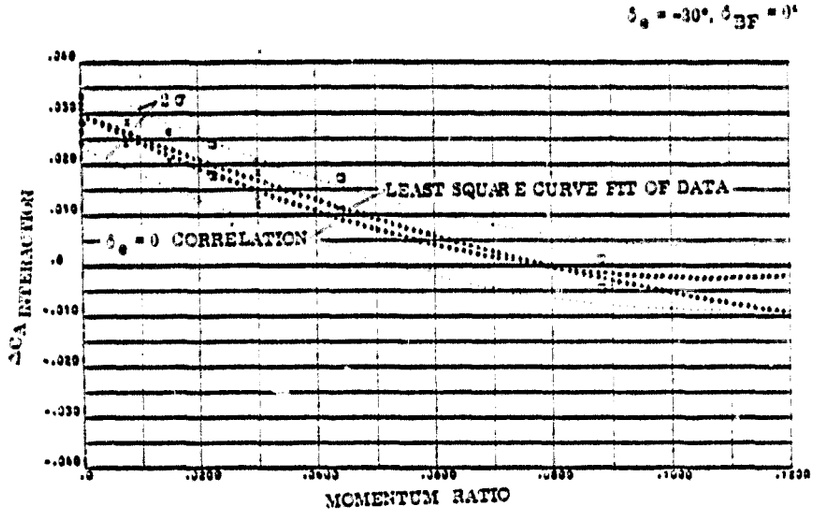

FIGURE 3-29a. : PITCH DOWN RCS INCREMENTAL EFFECTS DUE TO -30 DEGREE ELEVON DEFLECTION FROM -10 TO -5 DEGREES ANGLE OF ATTACK : AXIAL FORCE

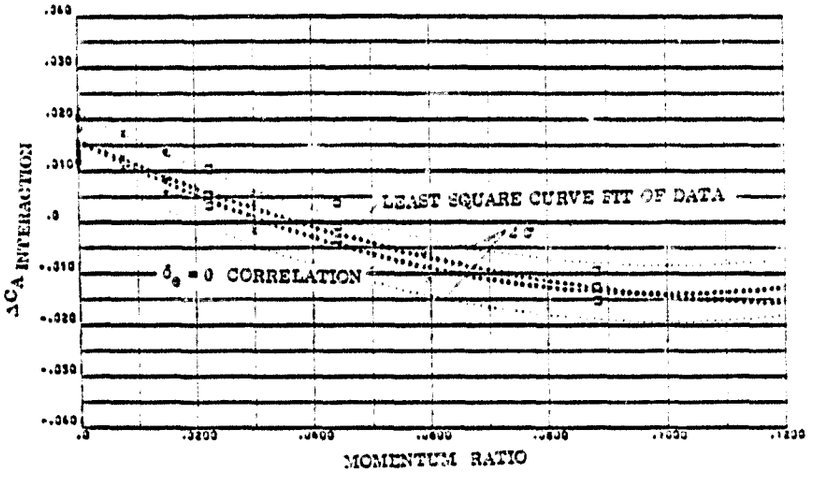

FIGURE 3-29b. : PITCH DOWN RCS INCREMENTAL EFFECTS DUE TO -30 DEGREE ELEVON DEFLECTION FROM -5 TO 0 DEGREES ANGLE OF ATTACK : AXIAL FORCE

SYMBOLS	NOZZLE NUMBER	TEST NUMBER
○	N49	MA 22
X	N79	MA 22
□	N83	MA 22

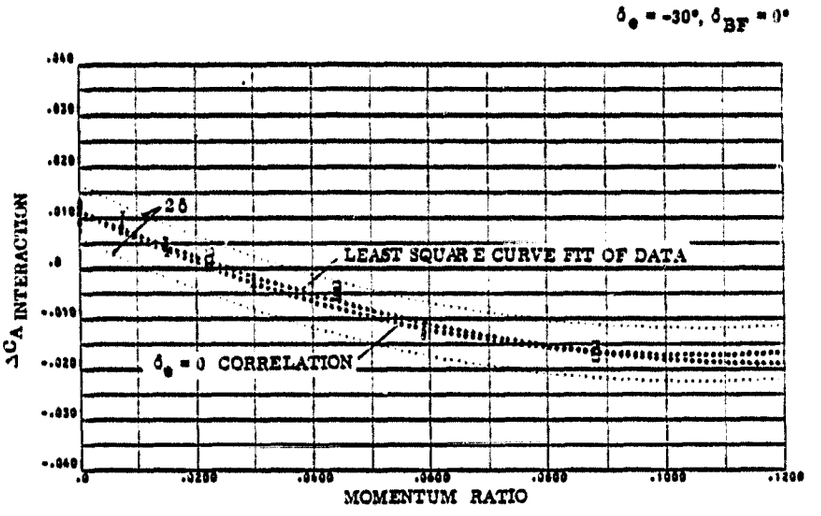

FIGURE 3-29c. : PITCH DOWN RCS INCREMENTAL EFFECTS DUE TO -30 DEGREE ELEVON DEFLECTION FROM 0 TO 5 DEGREES ANGLE OF ATTACK; AXIAL FORCE

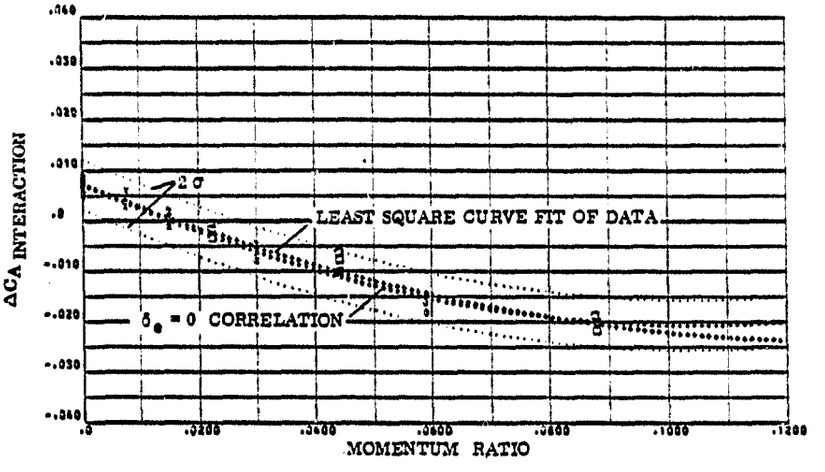

FIGURE 3-29d. : PITCH DOWN RCS INCREMENTAL EFFECTS DUE TO -30 DEGREE ELEVON DEFLECTION FROM 5 TO 10 DEGREES ANGLE OF ATTACK; AXIAL FORCE

SYMBOLS	NOZZLE NUMBER	TEST NUMBER
0	N49	MA 22
X	N79	MA 22
□	N83	MA 22

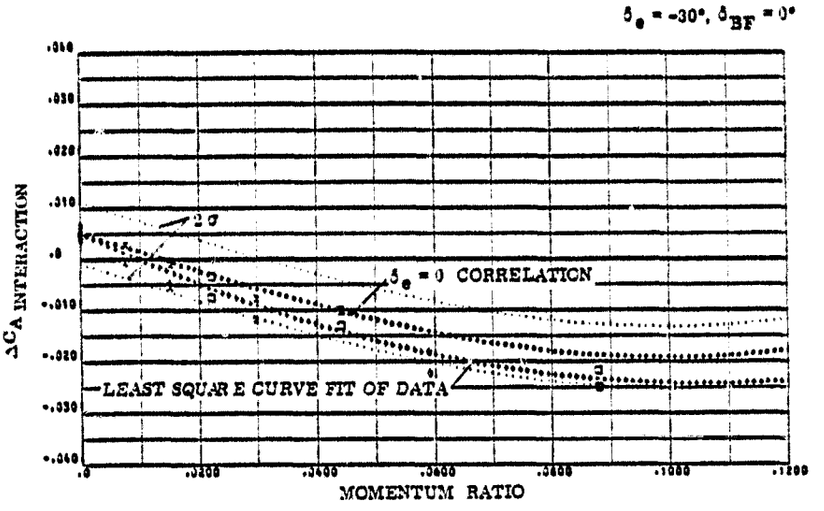

FIGURE 3-29e. : PITCH DOWN RCS INCREMENTAL EFFECTS DUE TO -30 DEGREE ELEVON DEFLECTION FROM 10 TO 15 DEGREES ANGLE OF ATTACK; AXIAL FORCE

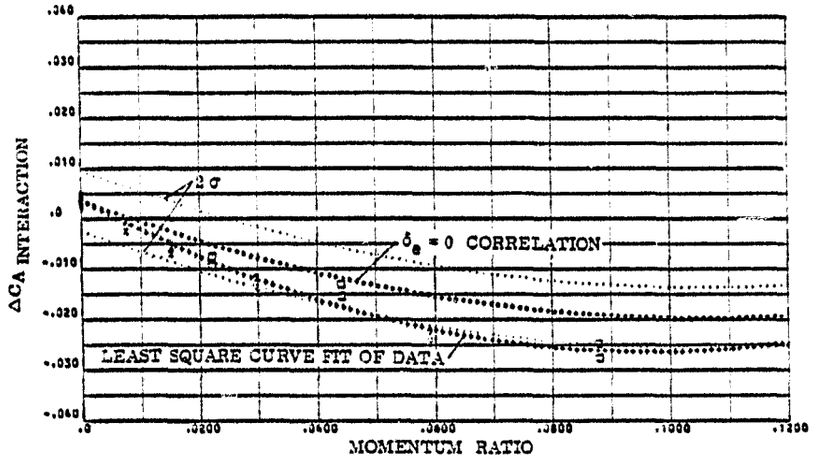

FIGURE 3-29 f. : PITCH DOWN RCS INCREMENTAL EFFECTS DUE TO -30 DEGREE ELEVON DEFLECTION FROM 15 TO 20 DEGREES ANGLE OF ATTACK; AXIAL FORCE

SYMBOLS	NOZZLE NUMBER	TEST NUMBER
0	N49	MA 22
X	N79	MA 22
□	N83	MA 22

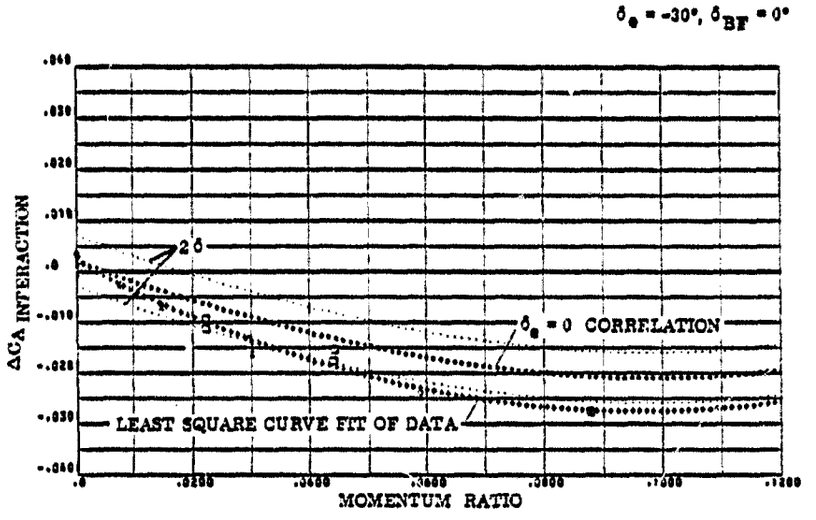

FIGURE 3-29g. : PITCH DOWN RCS INCREMENTAL EFFECTS DUE TO -30 DEGREE ELEVON DEFLECTION FROM 20 TO 25 DEGREES ANGLE OF ATTACK; AXIAL FORCE

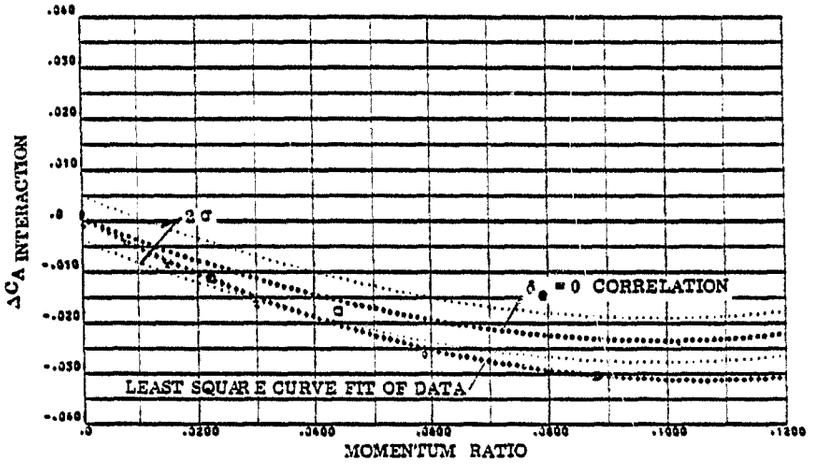

FIGURE 3-29h. : PITCH DOWN RCS INCREMENTAL EFFECTS DUE TO -30 DEGREE ELEVON DEFLECTION FROM 25 TO 30 DEGREES ANGLE OF ATTACK; AXIAL FORCE

SYMBOLS	NOZZLE NUMBER	TEST NUMBER
○	N49	MA 22
X	N79	MA 22
□	N93	MA 22

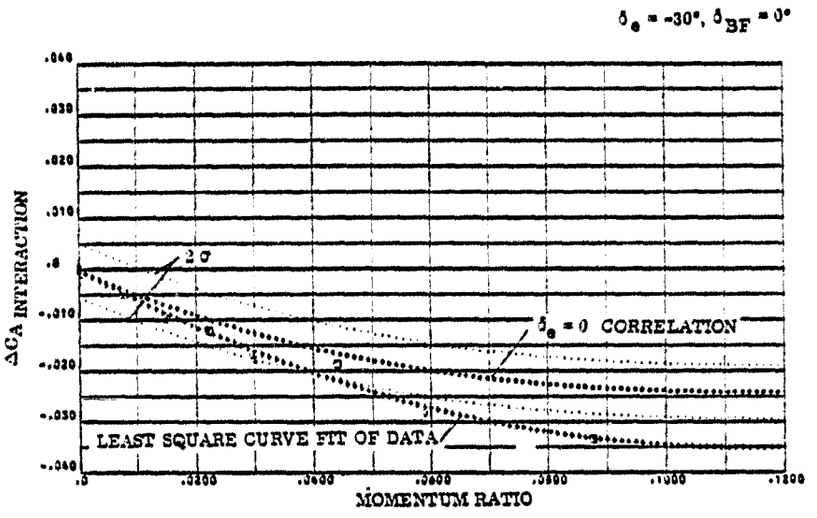

FIGURE 3-29i. : PITCH DOWN RCS INCREMENTAL EFFECTS DUE TO -30 DEGREE ELEVON DEFLECTION FROM 30 TO 35 DEGREES ANGLE OF ATTACK : AXIAL FORCE

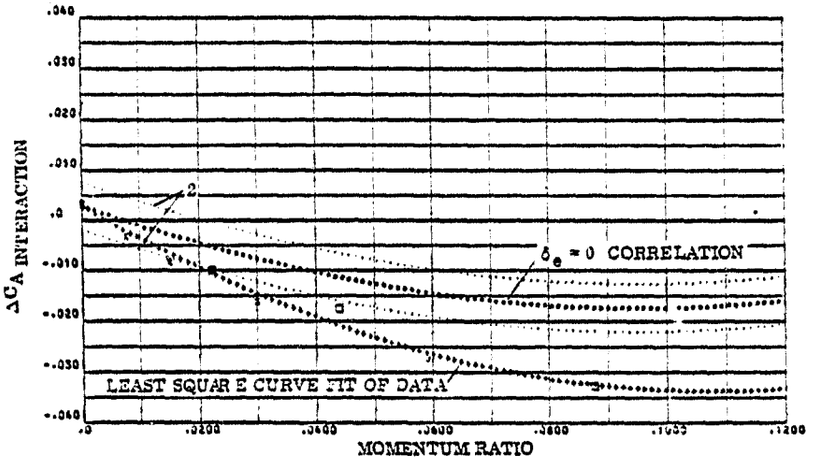

FIGURE 3-29j. : PITCH DOWN RCS INCREMENTAL EFFECTS DUE TO -30 DEGREE ELEVON DEFLECTION FROM 35 TO42.5DEGREES ANGLE OF ATTACK : AXIAL FORCE

SYMBOLS	NOZZLE NUMBER	TEST NUMBER
○	N49	MA 22
X	N79	MA 22
□	N83	MA 22

$\delta_e = -30°, \delta_{BF} = 0°$

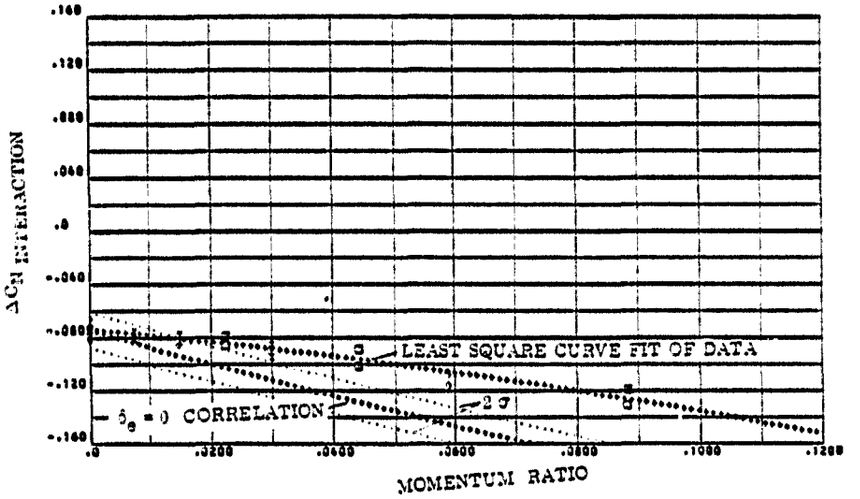

FIGURE 3-30a. : PITCH DOWN RCS INCREMENTAL EFFECTS DUE TO -30 DEGREE ELEVON DEFLECTION FROM -10 TO -5 DEGREES ANGLE OF ATTACK : NORMAL FORCE

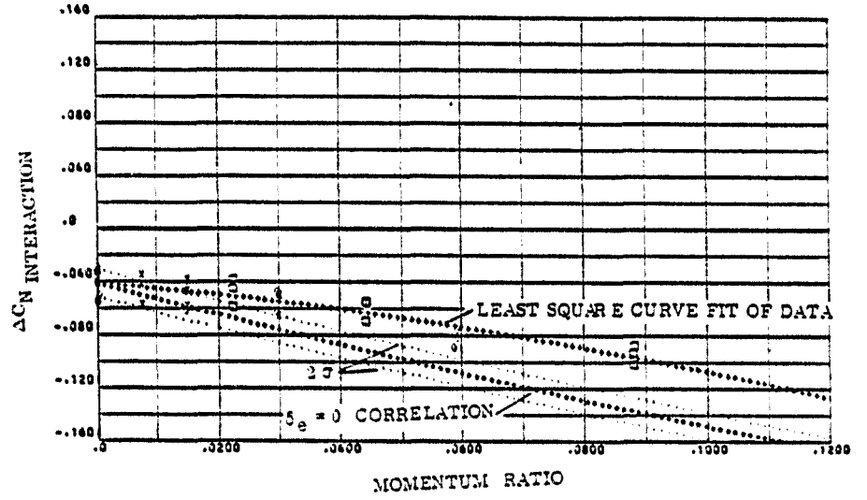

FIGURE 3-30b. : PITCH DOWN RCS INCREMENTAL EFFECTS DUE TO -30 DEGREE ELEVON DEFLECTION FROM -5 TO 0 DEGREES ANGLE OF ATTACK : NORMAL FORCE

SYMBOLS	NOZZLE NUMBER	TEST NUMBER
○	2149	MA 22
☆	2170	MA 22
□	2130	MA 22

$\delta_e = -30°$, $\delta_{BF} = 0°$

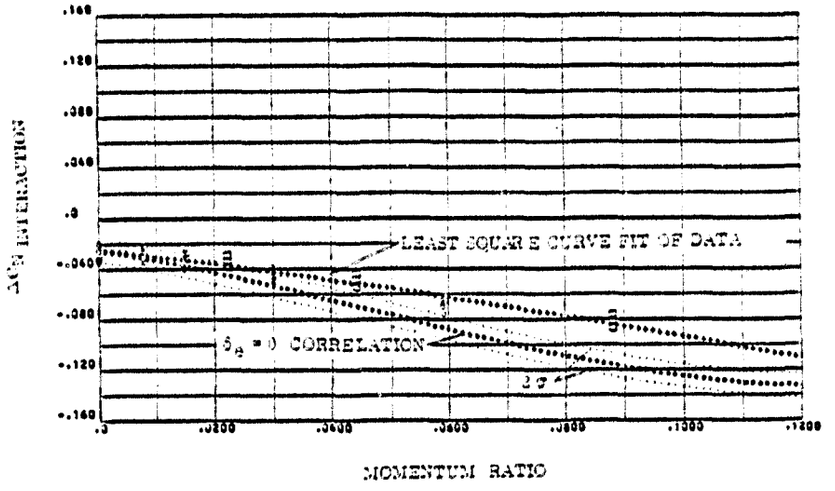

FIGURE 3-30c. : PITCH DOWN RCS INCREMENTAL EFFECTS DUE TO -30 DEGREE ELEVON DEFLECTION FROM 0 TO 5 DEGREES ANGLE OF ATTACK : NORMAL FORCE

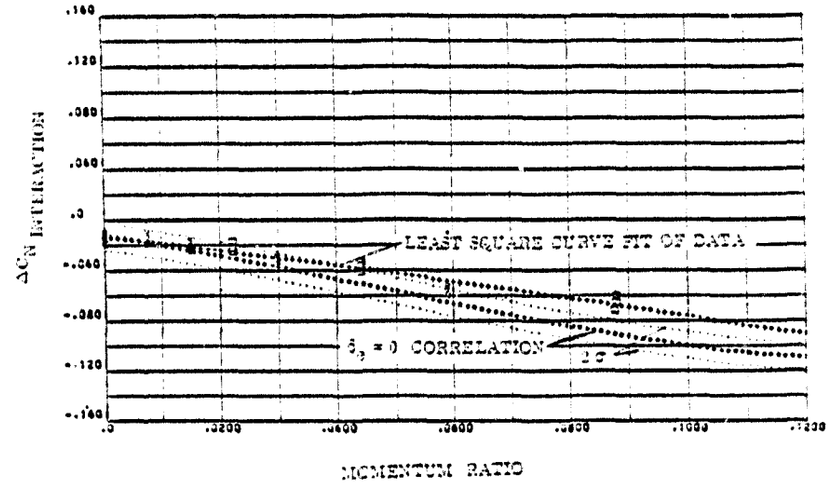

FIGURE 3-30d. : PITCH DOWN RCS INCREMENTAL EFFECTS DUE TO -30 DEGREE ELEVON DEFLECTION FROM 5 TO 10 DEGREES ANGLE OF ATTACK : NORMAL FORCE

SYMBOLS	NOZZLE NUMBER	TEST NUMBER
○	N49	MA 22
X	N79	MA 22
□	N83	MA 22

$\delta_e = -30°, \delta_{BF} = 0°$

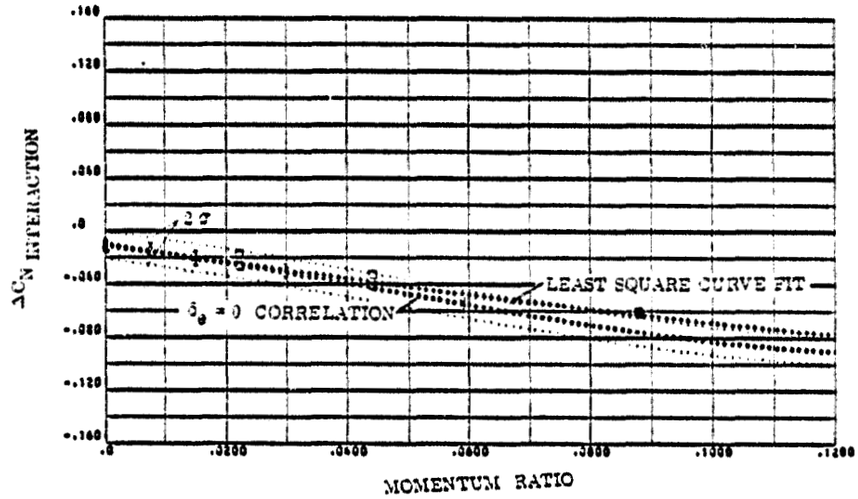

FIGURE 3-30e. : PITCH DOWN RCS INCREMENTAL EFFECTS DUE TO -30 DEGREE ELEVON DEFLECTION FROM 10 TO 15 DEGREES ANGLE OF ATTACK : NORMAL FORCE

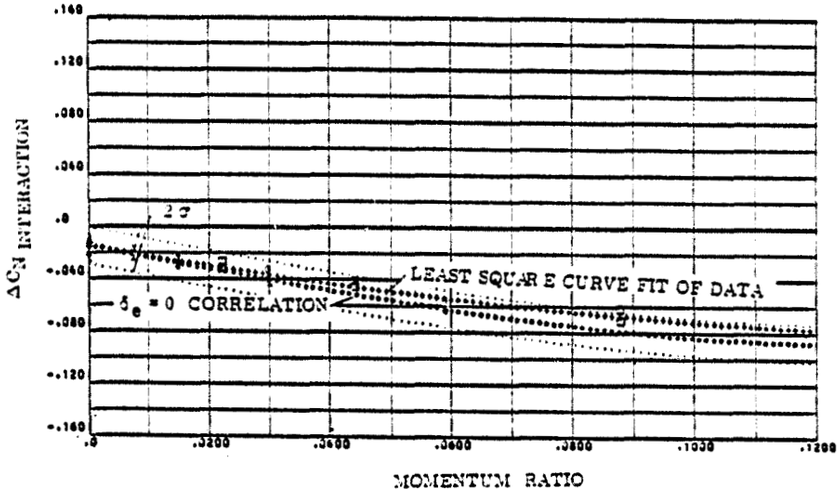

FIGURE 3-30f. : PITCH DOWN RCS INCREMENTAL EFFECTS DUE TO -30 DEGREE ELEVON DEFLECTION FROM 15 TO 20 DEGREES ANGLE OF ATTACK : NORMAL FORCE

SYMBOLS	NOZZLE NUMBER	TEST NUMBER
○	340	OA 22
◇	370	OA 22
□	380	OA 22

$\delta_e = -30°$ $\delta_{SF} = 0°$

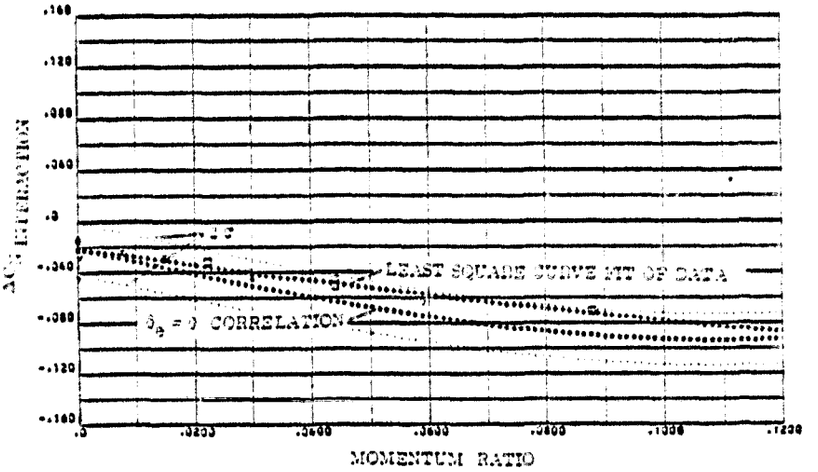

FIGURE 3-30g. : PITCH DOWN RCS INCREMENTAL EFFECTS DUE TO -30 DEGREE ELEVON DEFLECTION FROM 15 TO 25 DEGREES ANGLE OF ATTACK : NORMAL FORCE

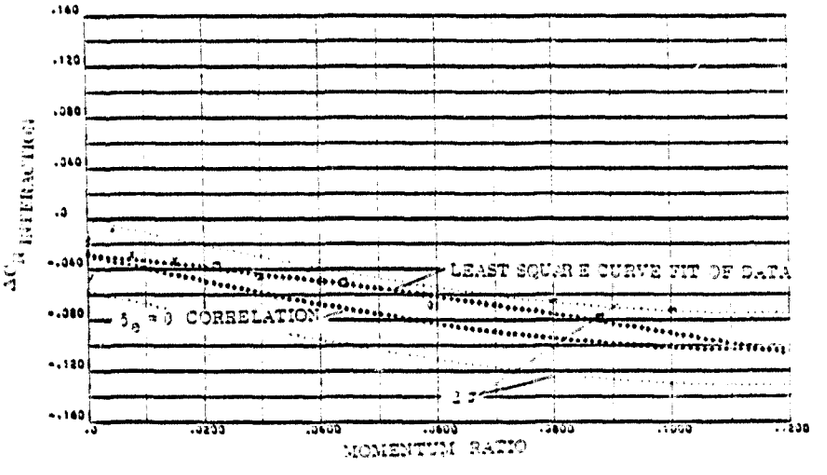

FIGURE 3-30h. PITCH DOWN RCS INCREMENTAL EFFECTS DUE TO -30 DEGREE ELEVON DEFLECTION FROM 25 TO 30 DEGREES ANGLE OF ATTACK : NORMAL FORCE

SYMBOLS	NOZZLE NUMBER	TEST NUMBER
○	2449	MA 32
✕	2479	MA 32
□	2450	MA 32

$\delta_e = -30°$, $\delta_{BF} = 0°$

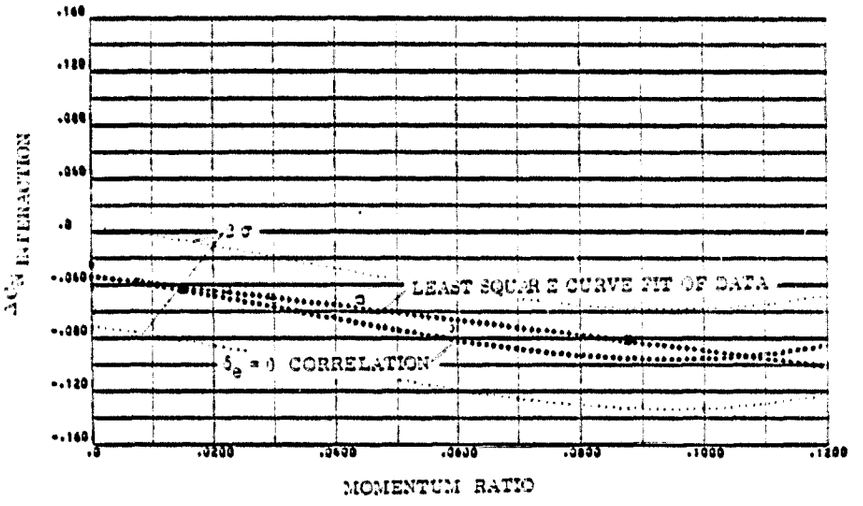

FIGURE 3-30i. : PITCH DOWN RCS INCREMENTAL EFFECTS DUE TO -30 DEGREE ELEVON DEFLECTION FROM 30 TO 35 DEGREES ANGLE OF ATTACK : NORMAL FORCE

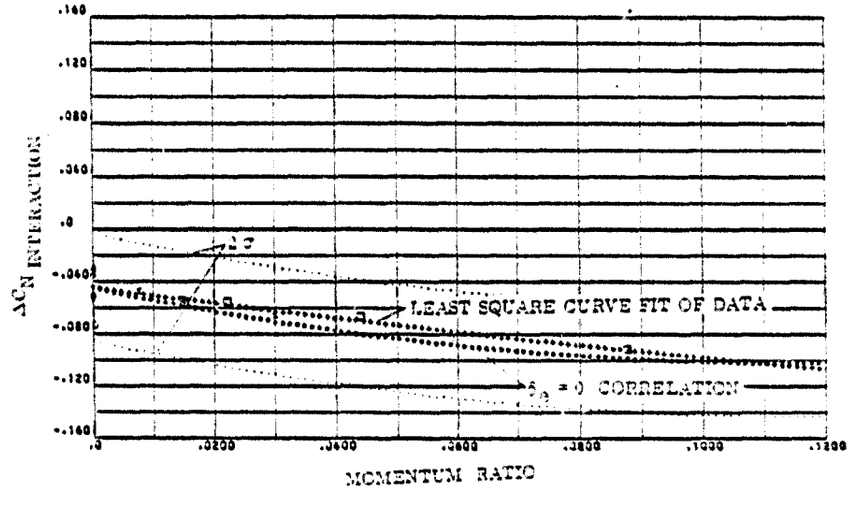

FIGURE 3-30j. : PITCH DOWN RCS INCREMENTAL EFFECTS DUE TO -30 DEGREE ELEVON DEFLECTION FROM 35 TO42.5DEGREES ANGLE OF ATTACK : NORMAL FORCE

SYMBOLS	DOUBLE NUMBER	TEST NUMBER
	1249	OMA 32
	1273	OMA 32
	1285	OMA 32

$\delta_e = -30°$, $\delta_{BT} = 0°$

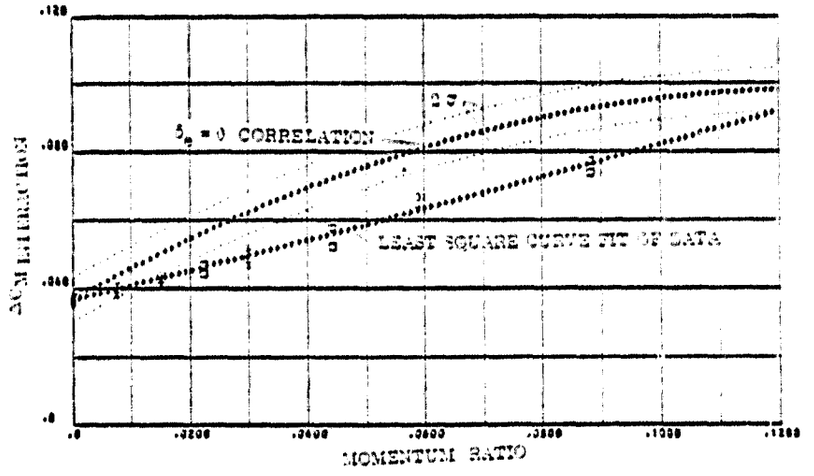

FIGURE 3-31a. : PITCH DOWN RCS INCREMENTAL EFFECTS DUE TO -30 DEGREE ELEVON DEFLECTION FROM -10 TO -5 DEGREES ANGLE OF ATTACK: PITCHING MOMENT

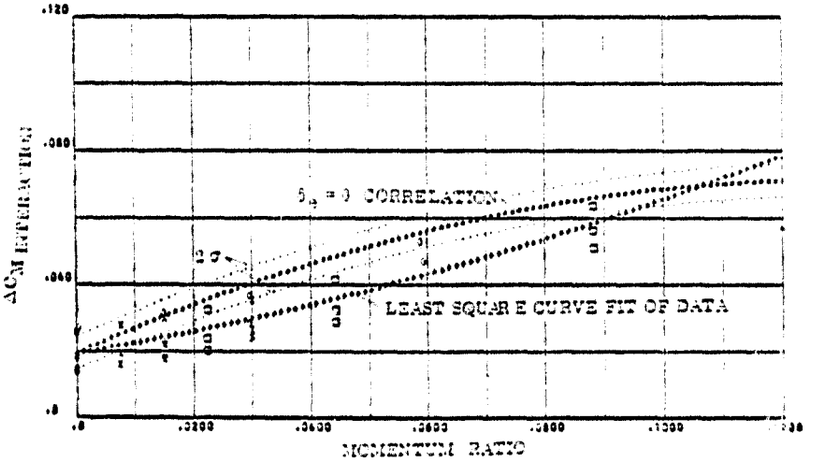

FIGURE 3-31b. PITCH DOWN RCS INCREMENTAL EFFECTS DUE TO -30 DEGREE ELEVON DEFLECTION FROM -5 TO 0 DEGREES ANGLE OF ATTACK: PITCHING MOMENT

SYMBOLS	NOZZLE NUMBER	TEST NUMBER
○	N49	MA 32
✕	N70	MA 32
□	N48	MA 32

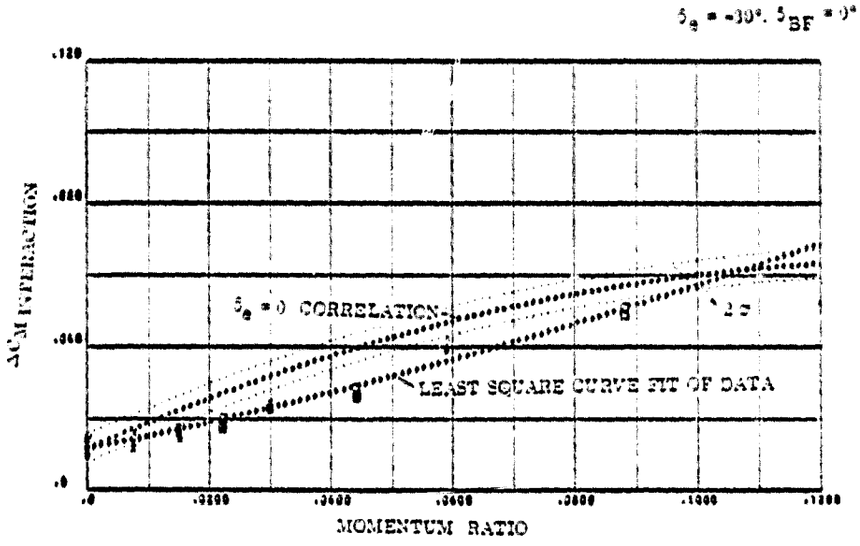

FIGURE 3-31c. : PITCH DOWN RCS INCREMENTAL EFFECTS DUE TO -30 DEGREE ELEVON DEFLECTION FROM 0 TO 5 DEGREES ANGLE OF ATTACK : PITCHING MOMENT

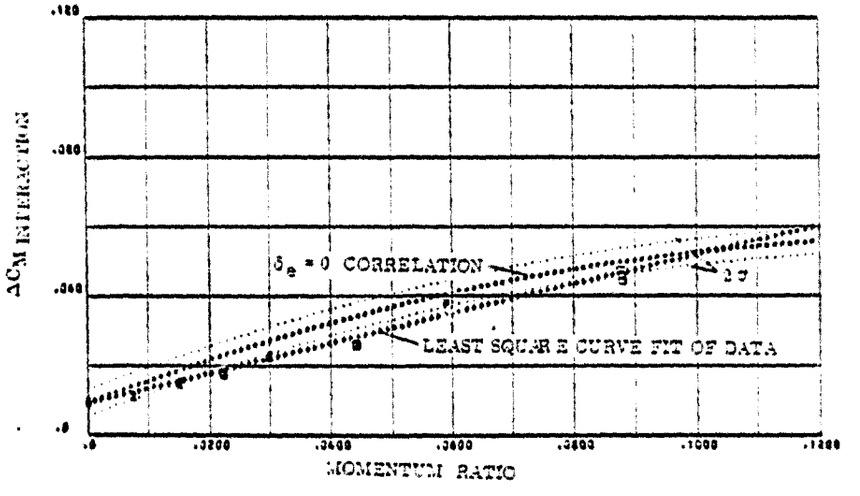

FIGURE 3-31d. : PITCH DOWN RCS INCREMENTAL EFFECTS DUE TO -30 DEGREE ELEVON DEFLECTION FROM 5 TO 10 DEGREES ANGLE OF ATTACK : PITCHING MOMENT

SYMBOLS	MODEL NUMBER	TEST NUMBER
○	1949	OA 33
△	1979	OA 32
□	1949	OA 30

δ_e = -30°, δ_{DF} = 0°

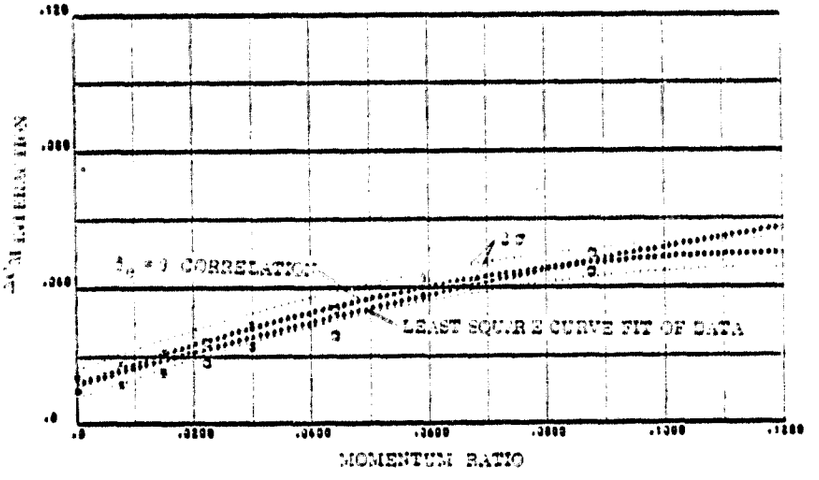

FIGURE 3-31e : PITCH DOWN RCS INCREMENTAL EFFECTS DUE TO -30 DEGREE ELEVON DEFLECTION FROM 10 TO 15 DEGREES ANGLE OF ATTACK : PITCHING MOMENT

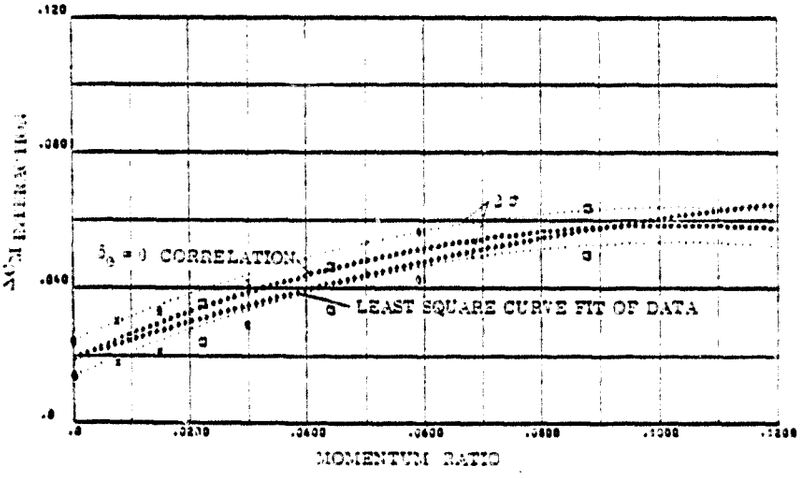

FIGURE 3-31f. : PITCH DOWN RCS INCREMENTAL EFFECTS DUE TO -30 DEGREE ELEVON DEFLECTION FROM 15 TO 20 DEGREES ANGLE OF ATTACK : PITCHING MOMENT

SYMBOLS	NOZZLE NUMBER	TEST NUMBER
○	[illegible]49	[illegible]A 32
△	[illegible]70	[illegible]A 32
□	[illegible]82	[illegible]A 32

$\delta_e = -30°$, $\delta_{BF} = 0°$

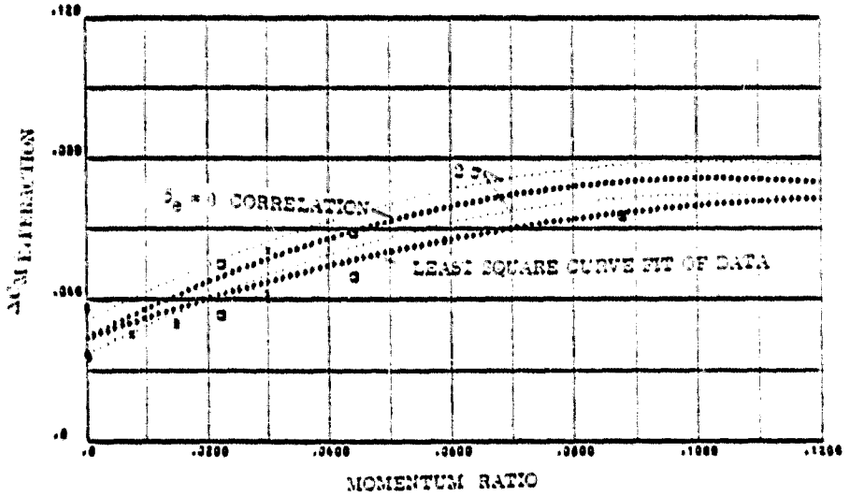

FIGURE 3-31g. : PITCH DOWN RCS INCREMENTAL EFFECTS DUE TO -30 DEGREE ELEVON DEFLECTION FROM 20 TO 25 DEGREES ANGLE OF ATTACK : PITCHING MOMENT

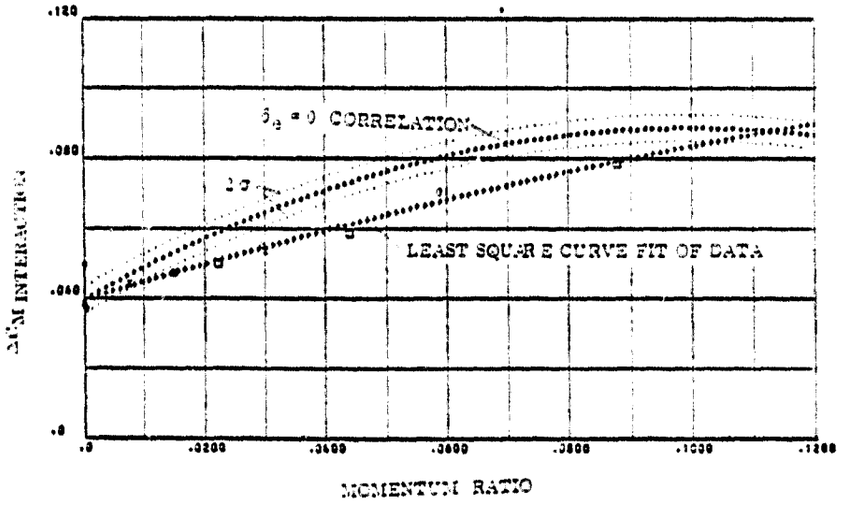

FIGURE 3-31h. : PITCH DOWN RCS INCREMENTAL EFFECTS DUE TO -30 DEGREE ELEVON DEFLECTION FROM 25 TO 30 DEGREES ANGLE OF ATTACK : PITCHING MOMENT

SYMBOLS	NOZZLE NUMBER	TEST NUMBER
○	349	33, 32
△	373	31, 33
□	389	33, 32

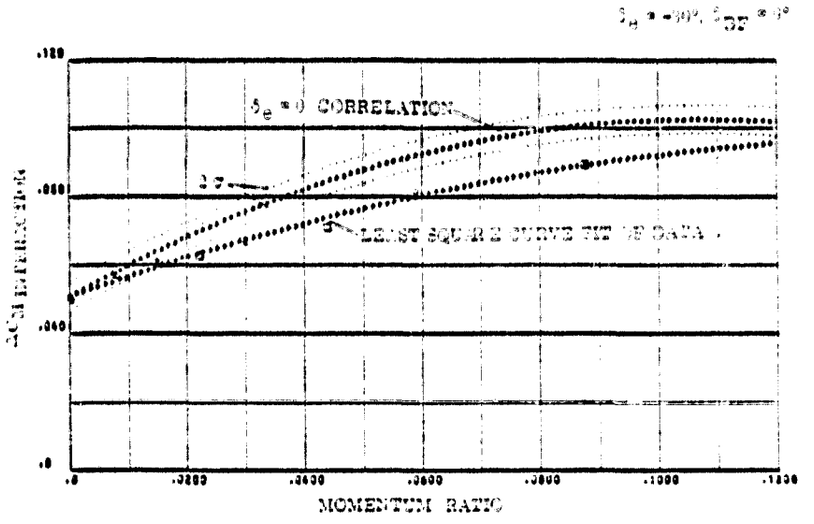

FIGURE 3-311. PITCH DOWN RCS INCREMENTAL EFFECTS DUE TO -30 DEGREE ELEVON DEFLECTION FROM 30 TO 35 DEGREES ANGLE OF ATTACK PITCHING MOMENT

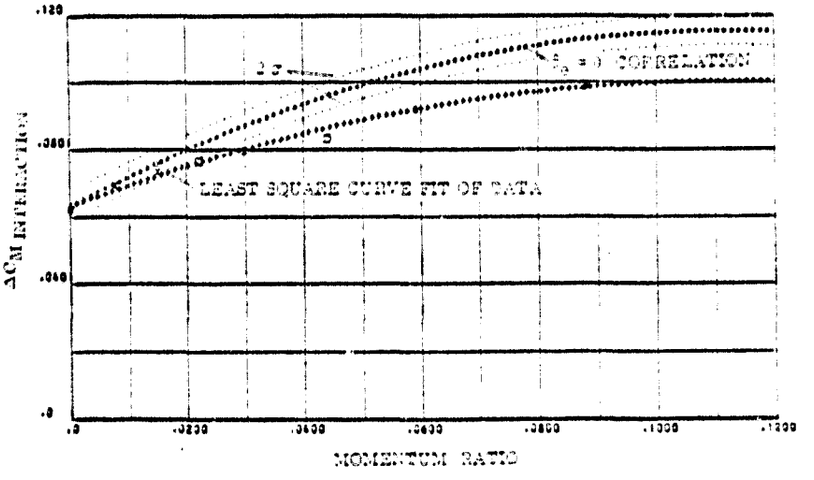

FIGURE 3-312. PITCH DOWN RCS INCREMENTAL EFFECTS DUE TO -30 DEGREE ELEVON DEFLECTION FROM 35 TO 42.5 DEGREES ANGLE OF ATTACK PITCHING MOMENT

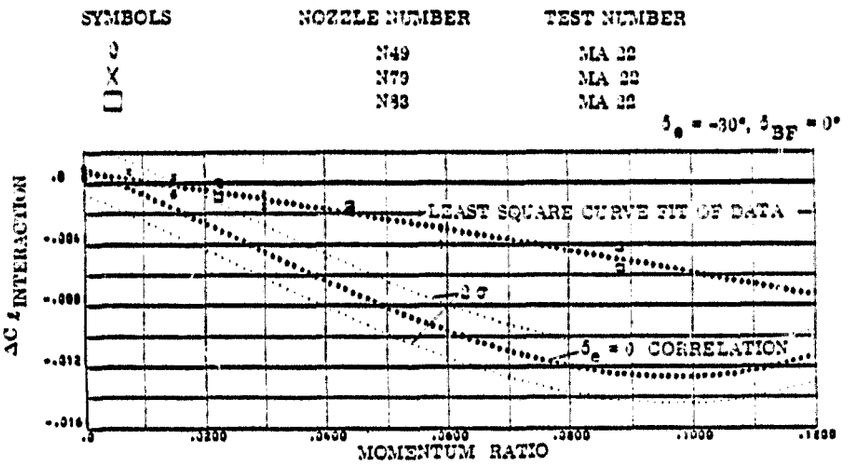

FIGURE 3-32a. : PITCH DOWN RCS INCREMENTAL EFFECTS DUE TO -30 DEGREE ELEVON DEFLECTION FROM -10 TO -5 DEGREES ANGLE OF ATTACK : ROLLING MOMENT

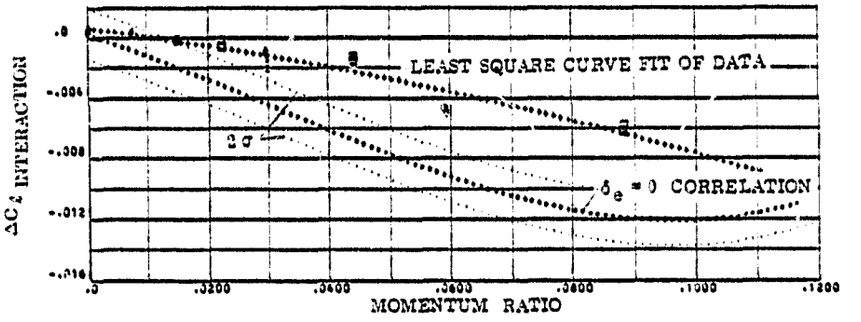

FIGURE 3-32b. : PITCH DOWN RCS INCREMENTAL EFFECTS DUE TO -30 DEGREE ELEVON DEFLECTION FROM -5 TO 0 DEGREES ANGLE OF ATTACK : ROLLING MOMENT

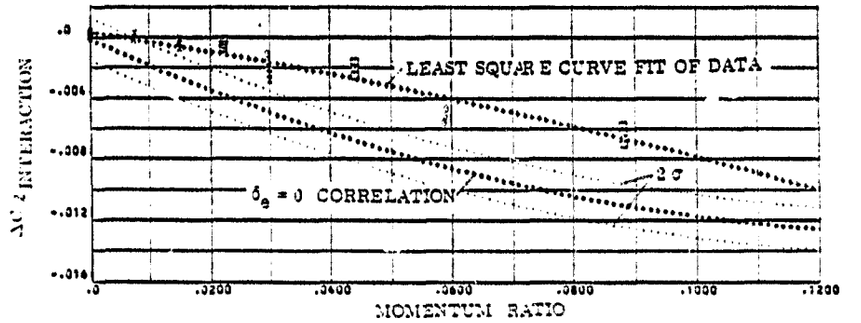

FIGURE 3-32c. : PITCH DOWN RCS INCREMENTAL EFFECTS DUE TO -30 DEGREE ELEVON DEFLECTION FROM 0 TO 5 DEGREES ANGLE OF ATTACK : ROLLING MOMENT

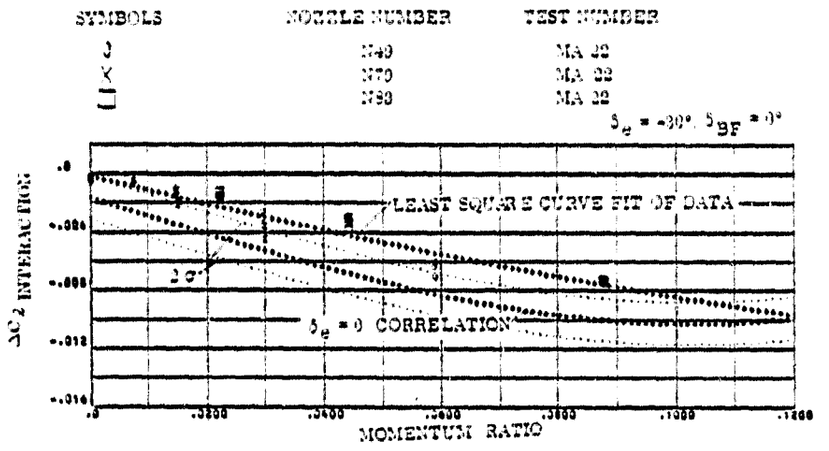

FIGURE 3-32 d. : PITCH DOWN RCS INCREMENTAL EFFECTS DUE TO -30 DEGREE ELEVON DEFLECTION FROM 5 TO 10 DEGREES ANGLE OF ATTACK ; ROLLING MOMENT

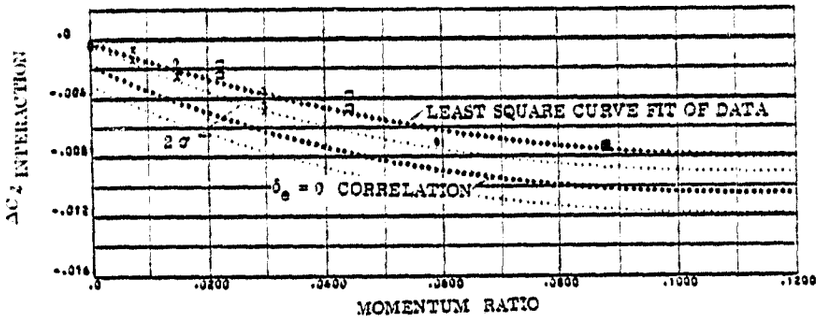

FIGURE 3-32e. : PITCH DOWN RCS INCREMENTAL EFFECTS DUE TO -30 DEGREE ELEVON DEFLECTION FROM 10 TO 15 DEGREES ANGLE OF ATTACK ; ROLLING MOMENT

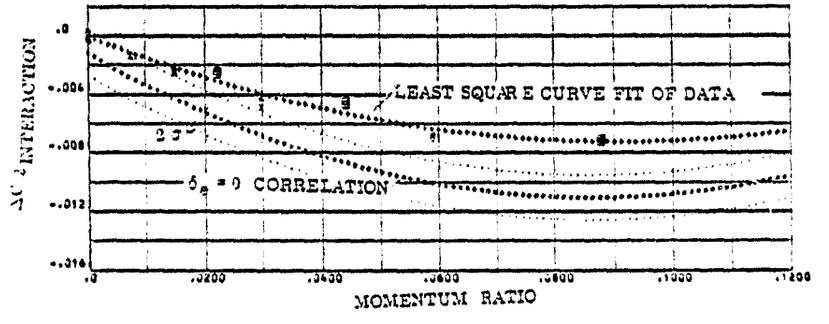

FIGURE 3-32f. : PITCH DOWN RCS INCREMENTAL EFFECTS DUE TO -30 DEGREE ELEVON DEFLECTION FROM 15 TO 20 DEGREES ANGLE OF ATTACK ; ROLLING MOMENT

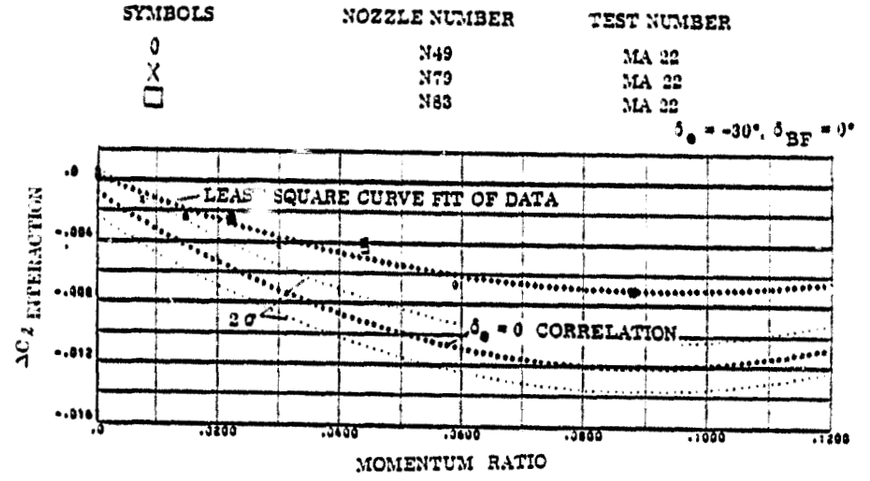

FIGURE 3-32 g : PITCH DOWN RCS INCREMENTAL EFFECTS DUE TO -30 DEGREE ELEVON DEFLECTION FROM 20 TO 25 DEGREES ANGLE OF ATTACK : ROLLING MOMENT

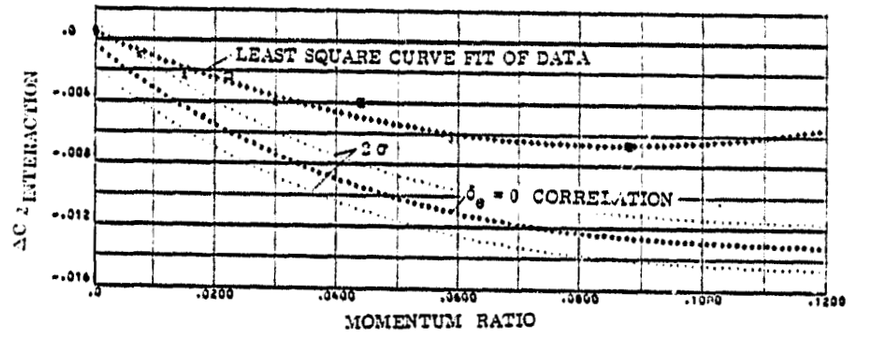

FIGURE 3-32 h. : PITCH DOWN RCS INCREMENTAL EFFECTS DUE TO -30 DEGREE ELEVON DEFLECTION FROM 25 TO 30 DEGREES ANGLE OF ATTACK : ROLLING MOMENT

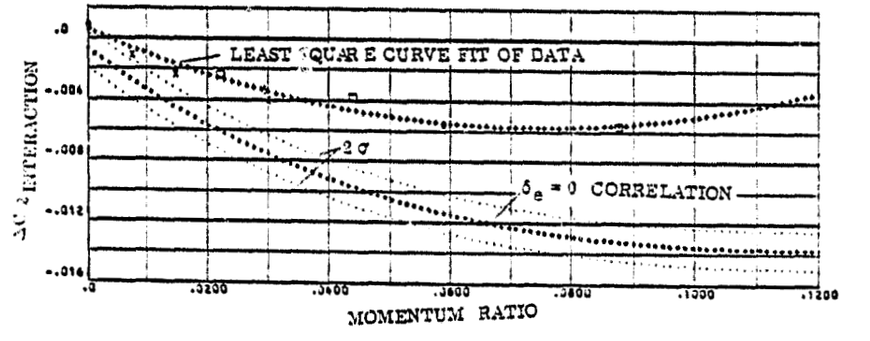

FIGURE 3-32 i. : PITCH DOWN RCS INCREMENTAL EFFECTS DUE TO -30 DEGREE ELEVON DEFLECTION FROM 30 TO 35 DEGREES ANGLE OF ATTACK : ROLLING MOMENT

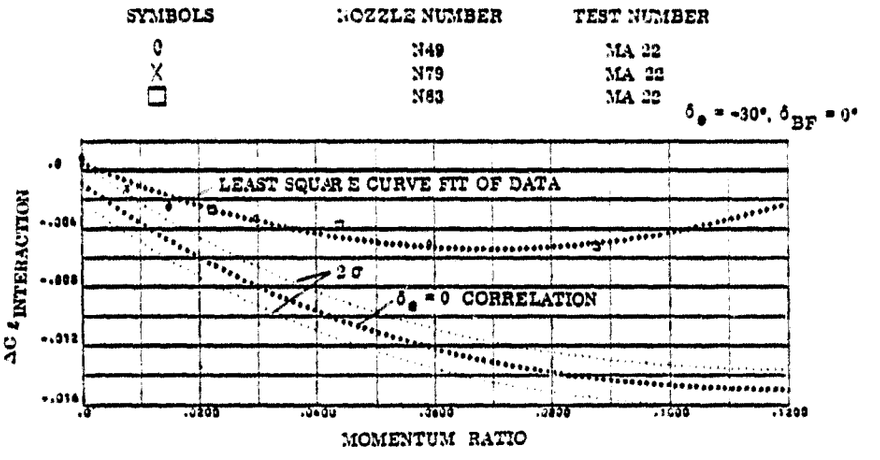

FIGURE 3-32 j. : PITCH DOWN RCS INCREMENTAL EFFECTS DUE TO -30 DEGREE ELEVON DEFLECTION FROM 35 TO 42.5 DEGREES ANGLE OF ATTACK ; ROLLING MOMENT

SYMBOLS	NOZZLE NUMBER	TEST NUMBER
0	N49	MA 22
X	N79	MA 22
□	N83	MA 22

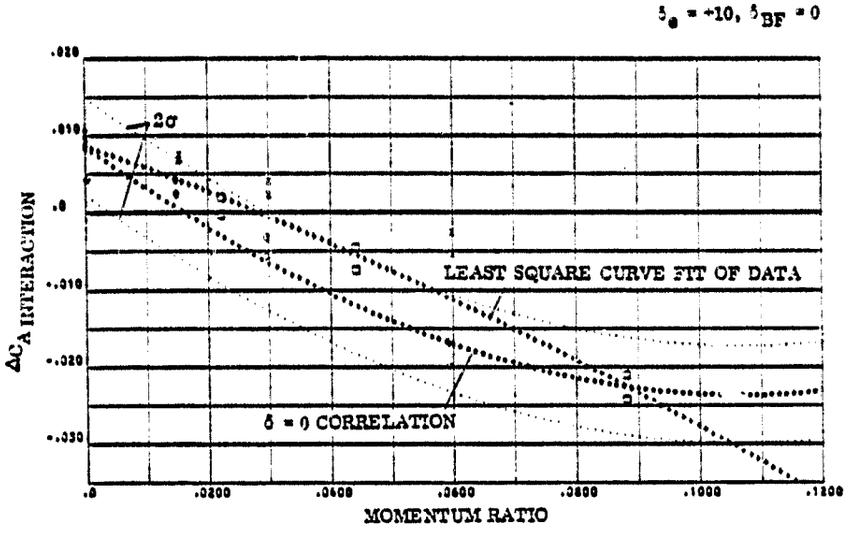

FIGURE 3-33a. : PITCH DOWN RCS INCREMENTAL EFFECTS DUE TO +10 DEGREE ELEVON DEFLECTION FROM -10 TO -5 DEGREES ANGLE OF ATTACK; AXIAL FORCE

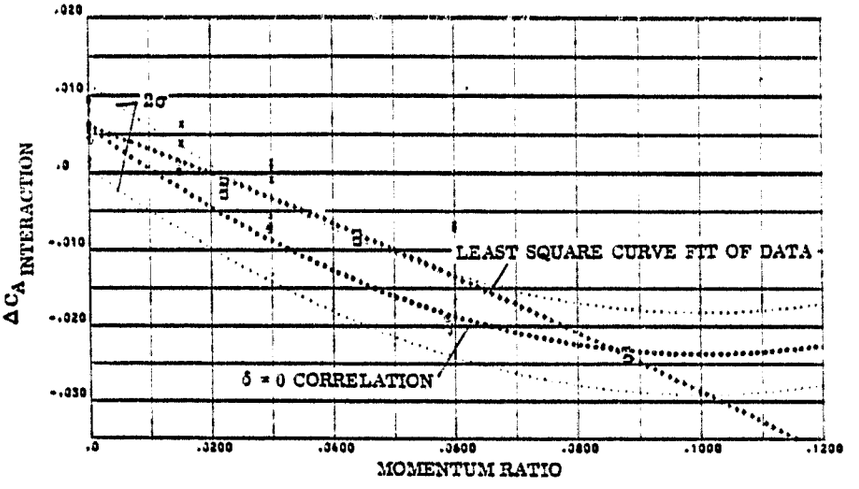

FIGURE 3-33b. : PITCH DOWN RCS INCREMENTAL EFFECTS DUE TO +10 DEGREE ELEVON DEFLECTION FROM -5 TO 0 DEGREES ANGLE OF ATTACK; AXIAL FORCE

SYMBOLS	NOZZLE NUMBER	TEST NUMBER
0	N49	MA 22
X	N79	MA 22
□	N83	MA 22

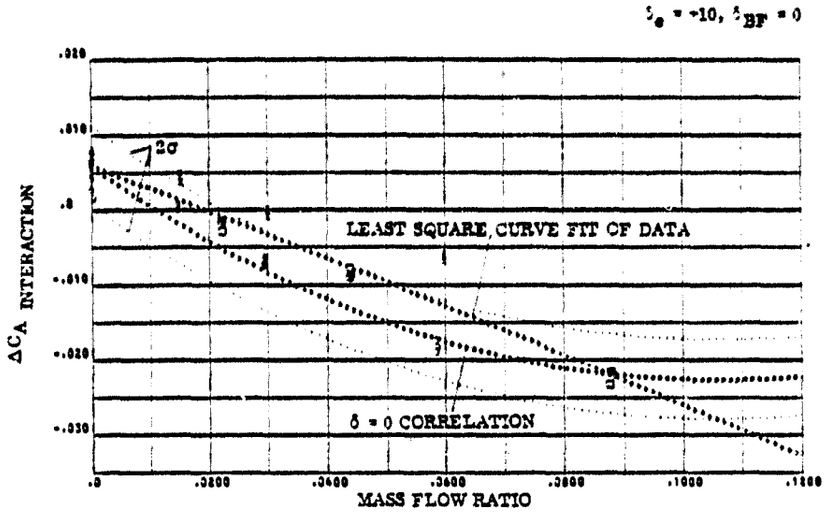

FIGURE 3-33c. : PITCH DOWN RCS INCREMENTAL EFFECTS DUE TO +10 DEGREE ELEVON DEFLECTION FROM 0 TO 5 DEGREES ANGLE OF ATTACK; AXIAL FORCE

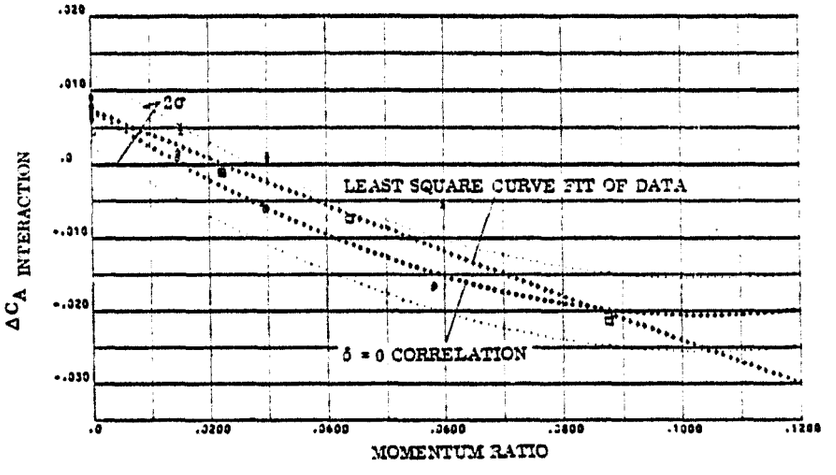

FIGURE 3-33d. : PITCH DOWN RCS INCREMENTAL EFFECTS DUE TO +10 DEGREE ELEVON DEFLECTION FROM 5 TO 10 DEGREES ANGLE OF ATTACK; AXIAL FORCE

SYMBOLS	NOZZLE NUMBER	TEST NUMBER
0	N49	MA 22
X	N79	MA 22
□	N83	MA 22

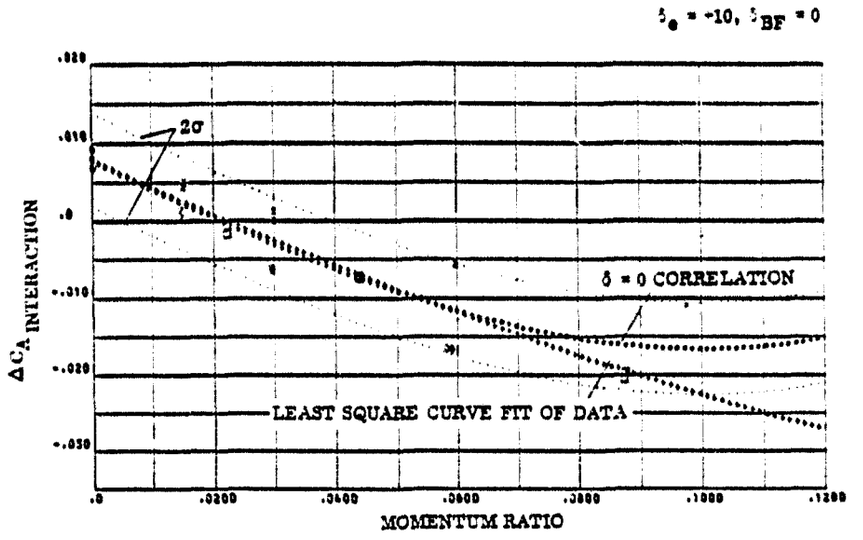

FIGURE 3-33 e. : PITCH DOWN RCS INCREMENTAL EFFECTS DUE TO +10 DEGREE ELEVON DEFLECTION FROM 10 TO 15 DEGREES ANGLE OF ATTACK; AXIAL FORCE

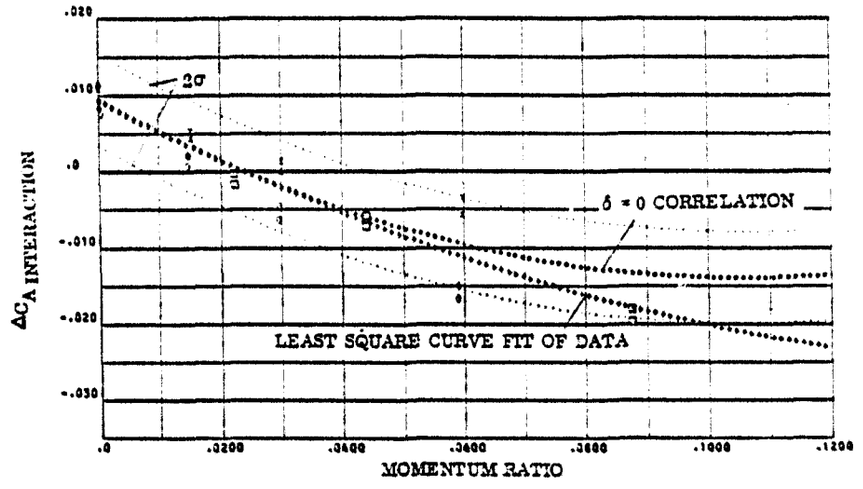

FIGURE 3-33 f. : PITCH DOWN RCS INCREMENTAL EFFECTS DUE TO +10 DEGREE ELEVON DEFLECTION FROM 15 TO 20 DEGREES ANGLE OF ATTACK; AXIAL FORCE

SYMBOLS	NOZZLE NUMBER	TEST NUMBER
0	N49	MA 22
X	N79	MA 22
□	N83	MA 22

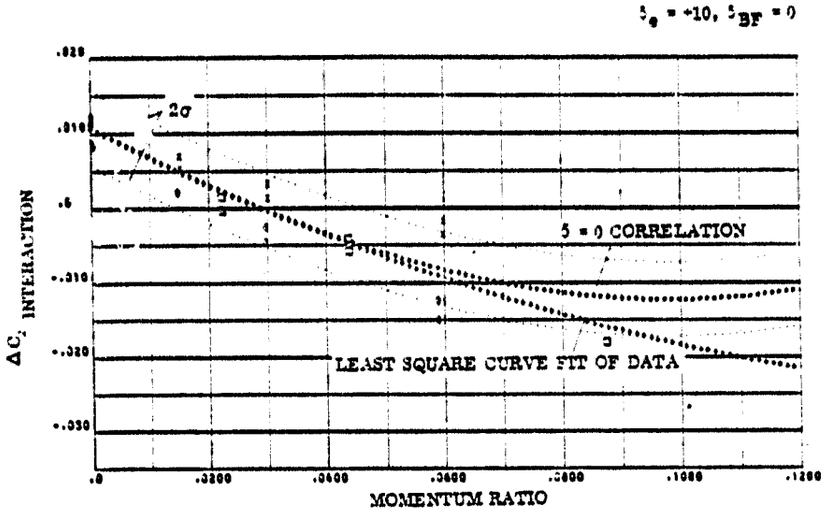

FIGURE 3-33g. : PITCH DOWN RCS INCREMENTAL EFFECTS DUE TO +10 DEGREE ELEVON DEFLECTION FROM TO 25 DEGREES ANGLE OF ATTACK; AXIAL FORCE

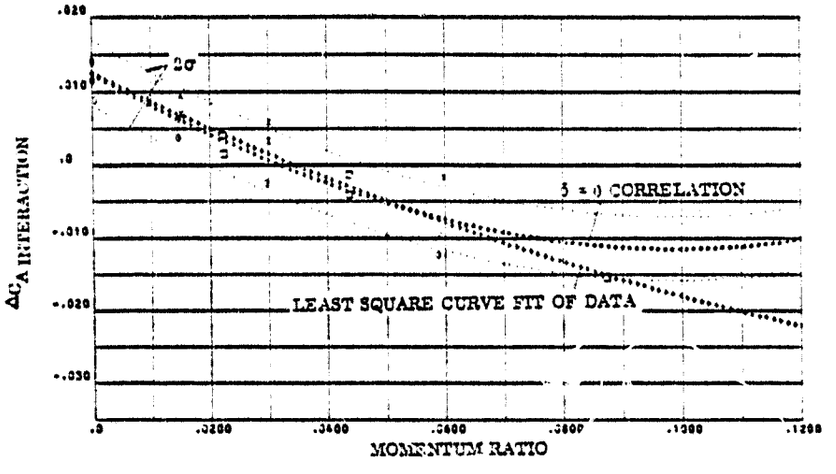

FIGURE 3-33h. : PITCH DOWN RCS INCREMENTAL EFFECTS DUE TO -10 DEGREE ELEVON DEFLECTION FROM 20 TO 25 DEGREES ANGLE OF ATTACK; AXIAL FORCE

SYMBOLS	NOZZLE NUMBER	TEST NUMBER
○	N49	MA 22
X	N79	MA 22
□	N83	MA 22

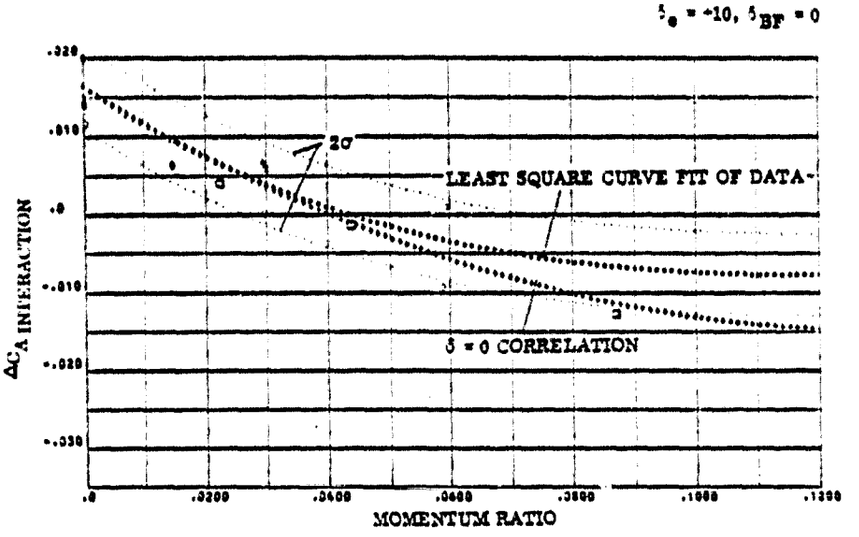

FIGURE 3-331. : PITCH DOWN RCS INCREMENTAL EFFECTS DUE TO +10 DEGREE ELEVON DEFLECTION FROM 30 TO 35 DEGREES ANGLE OF ATTACK; AXIAL FORCE

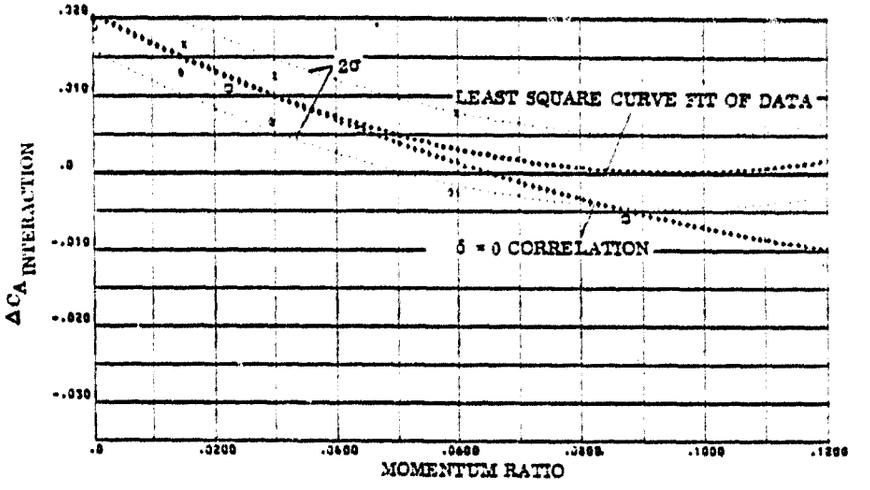

FIGURE 3-332. : PITCH DOWN RCS INCREMENTAL EFFECTS DUE TO +10 DEGREE ELEVON DEFLECTION FROM 35 TO 42.3 DEGREES ANGLE OF ATTACK; AXIAL FORCE

SYMBOLS	NOZZLE NUMBER	TEST NUMBER
0	N49	MA 22
X	N79	MA 22
□	N83	MA 22

$\delta_e = +10, \delta_{BF} = 0$

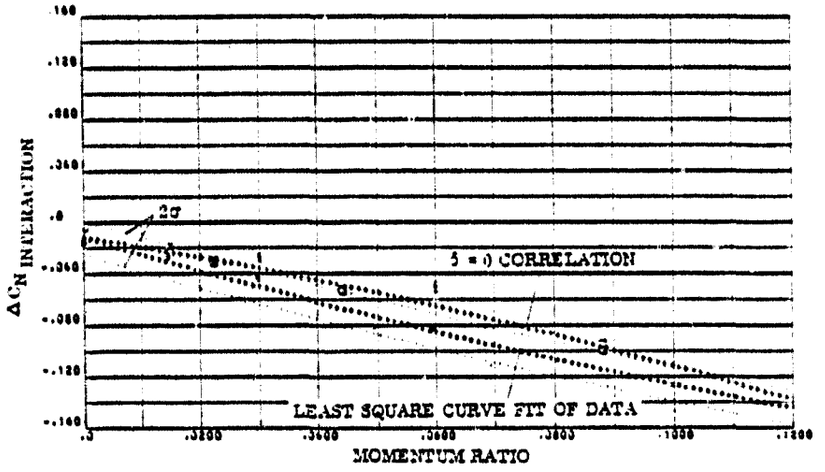

FIGURE 3-34a. : PITCH DOWN RCS INCREMENTAL EFFECTS DUE TO +10 DEGREE ELEVON DEFLECTION FROM -10 TO -5 DEGREES ANGLE OF ATTACK; NORMAL FORCE

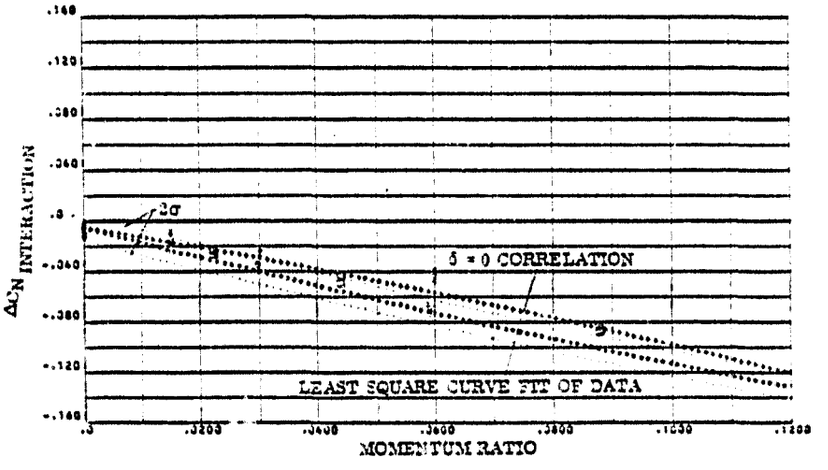

FIGURE 3-34b. : PITCH DOWN RCS INCREMENTAL EFFECTS DUE TO +10 DEGREE ELEVON DEFLECTION FROM -5 TO 0 DEGREES ANGLE OF ATTACK; NORMAL FORCE

SYMBOLS	NOZZLE NUMBER	TEST NUMBER
○	N49	MA 22
×	N79	MA 22
□	N83	MA 22

$\delta_e = +10, \delta_{BF} = 0$

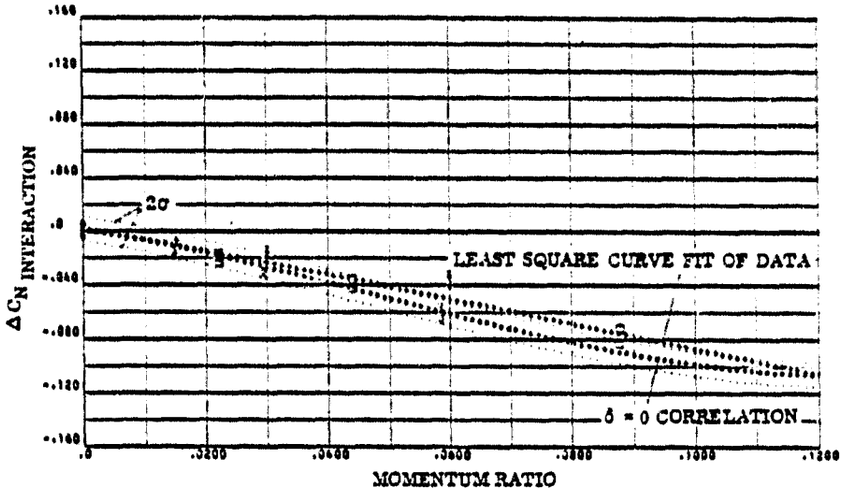

FIGURE 3-34c. : PITCH DOWN RCS INCREMENTAL EFFECTS DUE TO +10 DEGREE ELEVON DEFLECTION FROM 0 TO 5 DEGREES ANGLE OF ATTACK; NORMAL FORCE

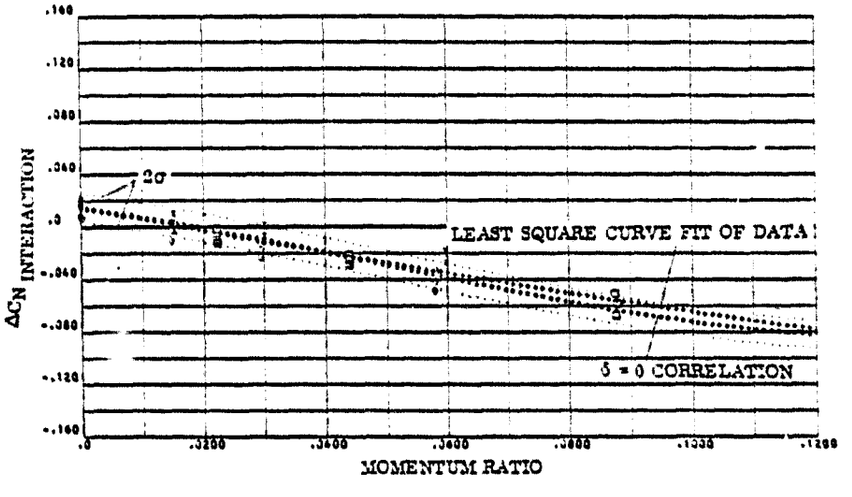

FIGURE 3-34d. : PITCH DOWN RCS INCREMENTAL EFFECTS DUE TO +10 DEGREE ELEVON DEFLECTION FROM 5 TO 10 DEGREES ANGLE OF ATTACK; NORMAL FORCE

SYMBOLS	NOZZLE NUMBER	TEST NUMBER
0	N49	MA 22
X	N79	MA 22
□	N83	MA 22

$\delta_e = +10, \delta_{BF} = 0$

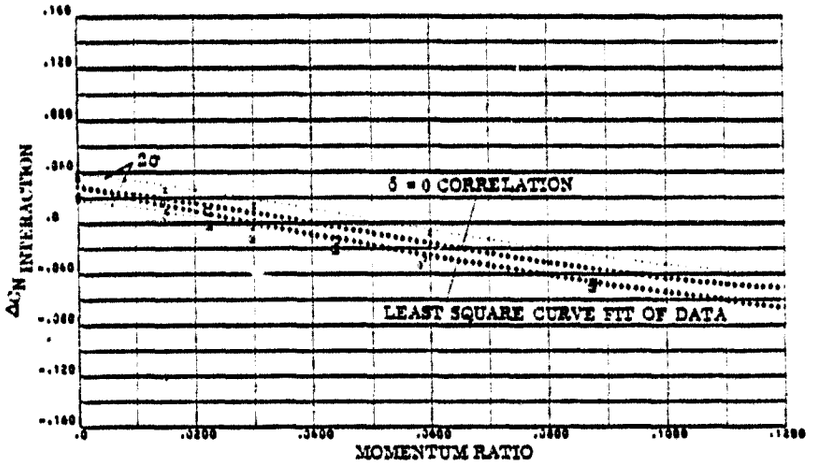

FIGURE 3-34e. : PITCH DOWN RCS INCREMENTAL EFFECTS DUE TO +10 DEGREE ELEVON DEFLECTION FROM 10 TO 15 DEGREES ANGLE OF ATTACK; NORMAL FORCE

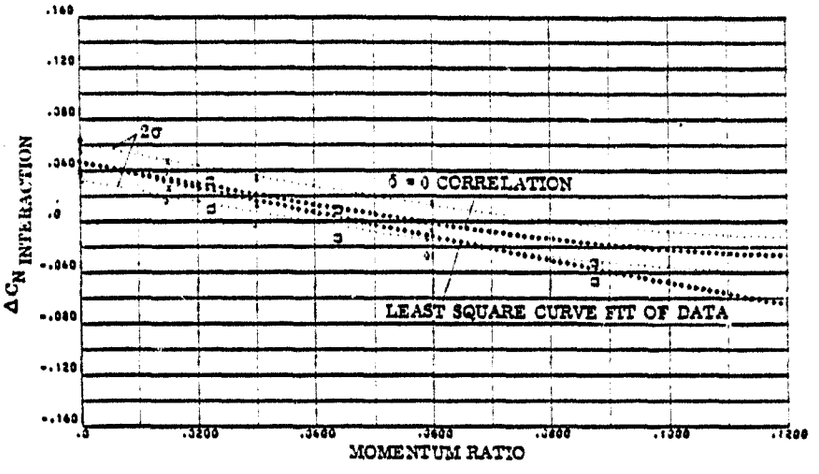

FIGURE 3-34f. : PITCH DOWN RCS INCREMENTAL EFFECTS DUE TO +10 DEGREE ELEVON DEFLECTION FROM 15 TO 20 DEGREES ANGLE OF ATTACK; NORMAL FORCE

SYMBOLS	NOZZLE NUMBER	TEST NUMBER
0	N49	MA 22
X	N79	MA 22
□	N83	MA 22

$\delta_e = +10, \delta_{BF} = 0$

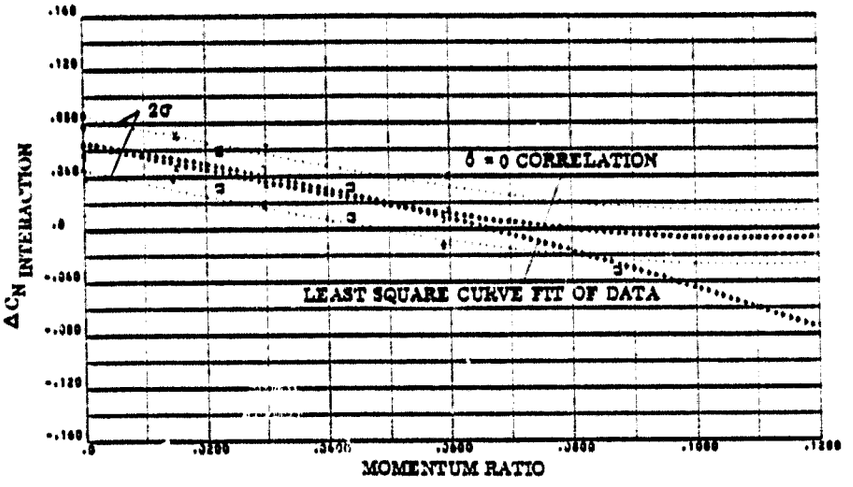

FIGURE 3-34g. : PITCH DOWN RCS INCREMENTAL EFFECTS DUE TO +10 DEGREE ELEVON DEFLECTION FROM 20 TO 25 DEGREES ANGLE OF ATTACK; NORMAL FORCE

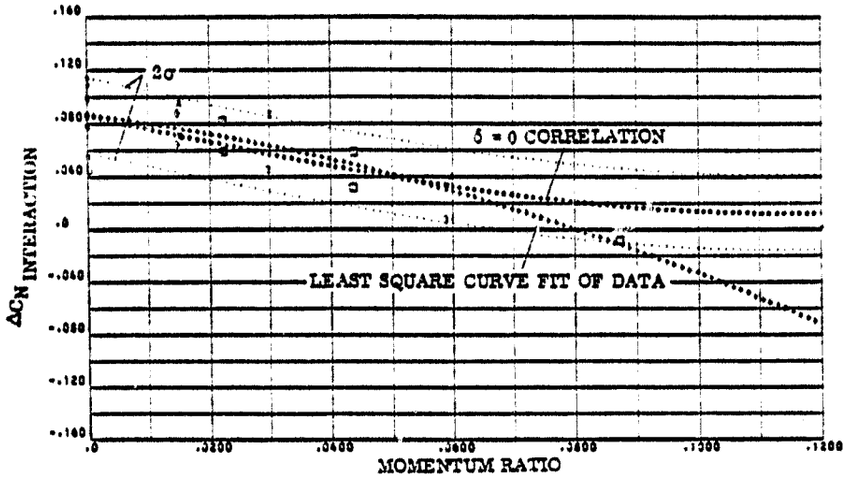

FIGURE 3-34h. : PITCH DOWN RCS INCREMENTAL EFFECTS DUE TO +10 DEGREE ELEVON DEFLECTION FROM 25 TO 30 DEGREES ANGLE OF ATTACK; NORMAL FORCE

SYMBOLS	NOZZLE NUMBER	TEST NUMBER
○	N49	MA 22
×	N79	MA 22
□	N83	MA 22

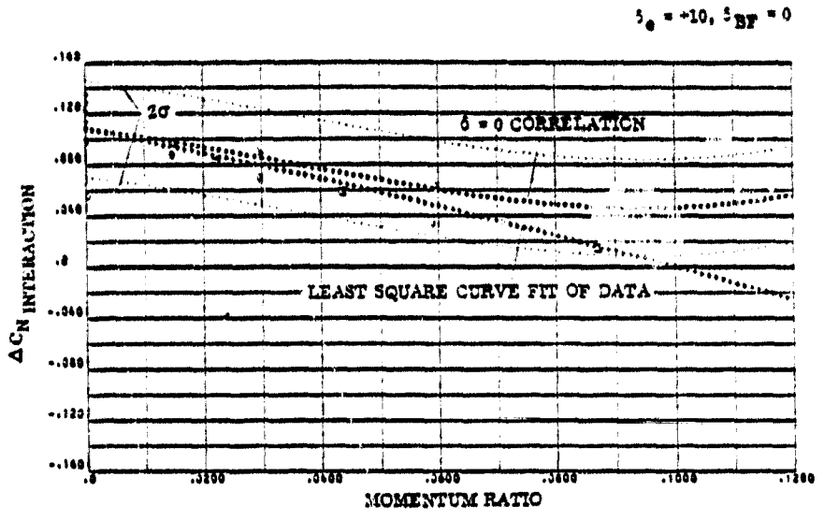

FIGURE 3-341. : PITCH DOWN RCS INCREMENTAL EFFECTS DUE TO +10 DEGREE ELEVON DEFLECTION FROM 30 TO 35 DEGREES ANGLE OF ATTACK; NORMAL FORCE

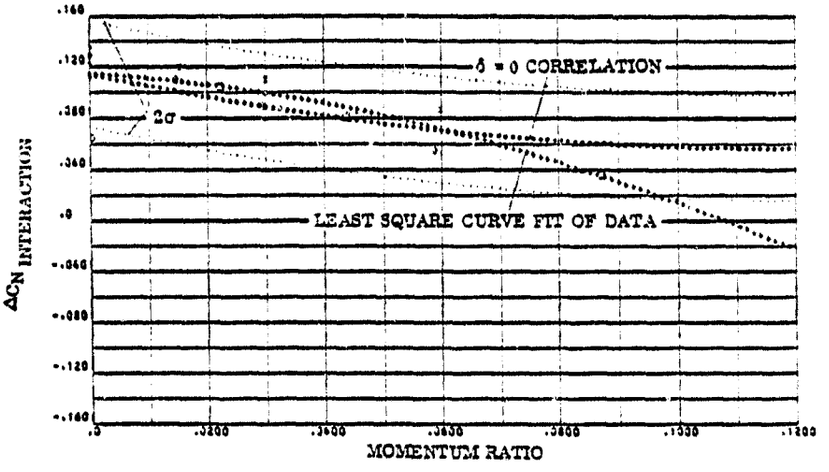

FIGURE 3-341. : PITCH DOWN RCS INCREMENTAL EFFECTS DUE TO +10 DEGREE ELEVON DEFLECTION FROM 35 TO 42.5 DEGREES ANGLE OF ATTACK; NORMAL FORCE

SYMBOLS	NOZZLE NUMBER	TEST NUMBER
0	N49	MA 22
X	N79	MA 22
□	N83	MA 22

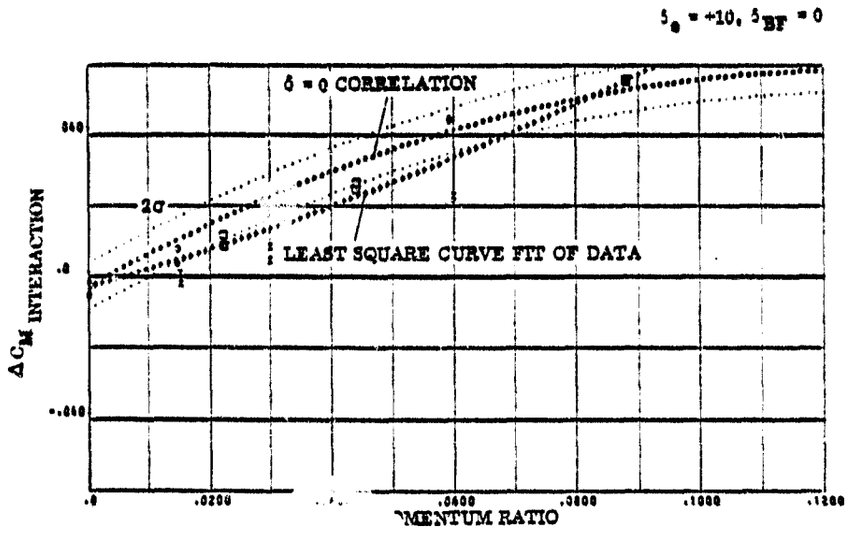

FIGURE 3-35a. : PITCH DOWN RCS INCREMENTAL EFFECTS DUE TO +10 DEGREE ELEVON DEFLECTION FROM -10 TO -5 DEGREES ANGLE OF ATTACK; PITCHING MOMENT

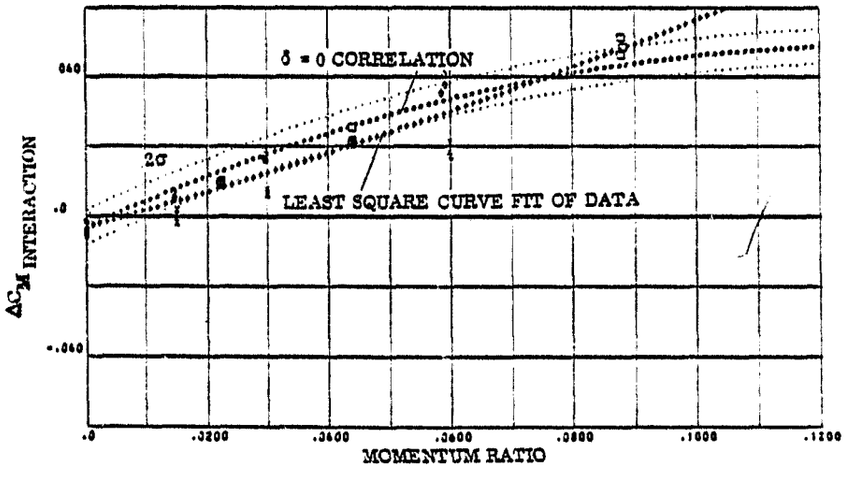

FIGURE 3-35b. : PITCH DOWN RCS INCREMENTAL EFFECTS DUE TO +10 DEGREE ELEVON DEFLECTION FROM -5 TO 0 DEGREES ANGLE OF ATTACK; PITCHING MOMENT

SYMBOLS	NOZZLE NUMBER	TEST NUMBER
0	N49	MA 22
×	N79	MA 22
□	N83	MA 22

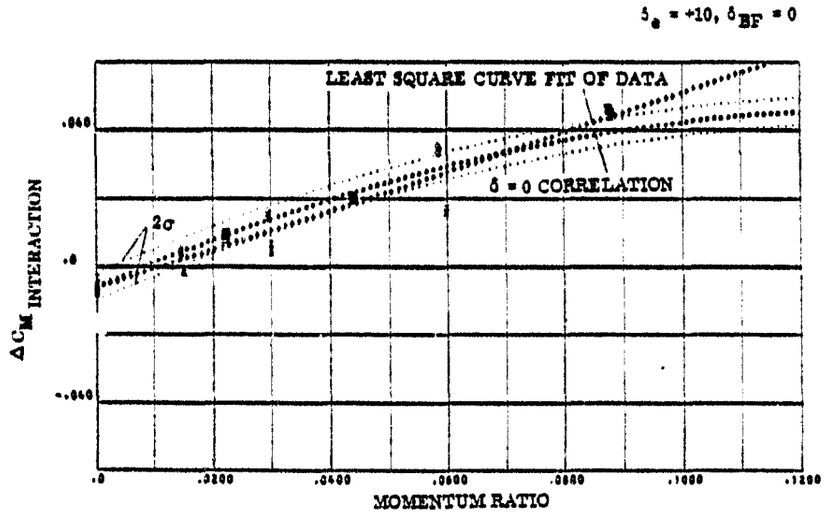

FIGURE 3-35c. : PITCH DOWN RCS INCREMENTAL EFFECTS DUE TO +10 DEGREE ELEVON DEFLECTION FROM 0 TO 5 DEGREES ANGLE OF ATTACK; PITCHING MOMENT

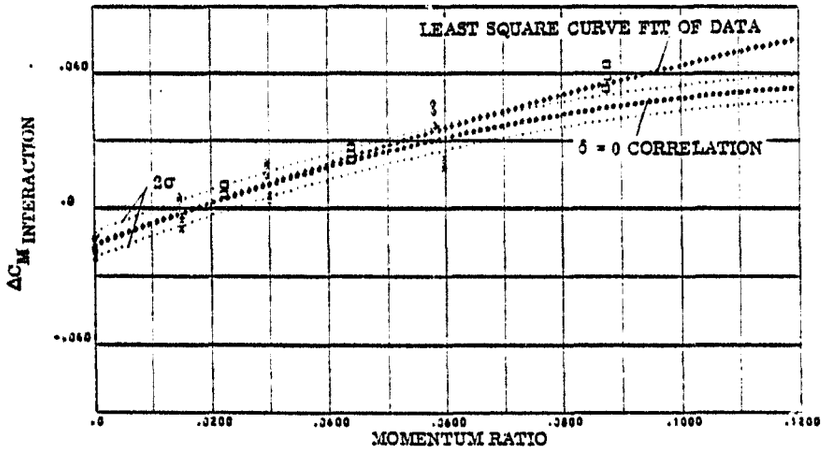

FIGURE 3-35d. : PITCH DOWN RCS INCREMENTAL EFFECTS DUE TO +10 DEGREE ELEVON DEFLECTION FROM 5 TO 10 DEGREES ANGLE OF ATTACK; PITCHING MOMENT

SYMBOLS	NOZZLE NUMBER	TEST NUMBER
0	N49	MA 22
X	N79	MA 22
□	N83	MA 22

$\delta_e = +10, \delta_{BF} = 0$

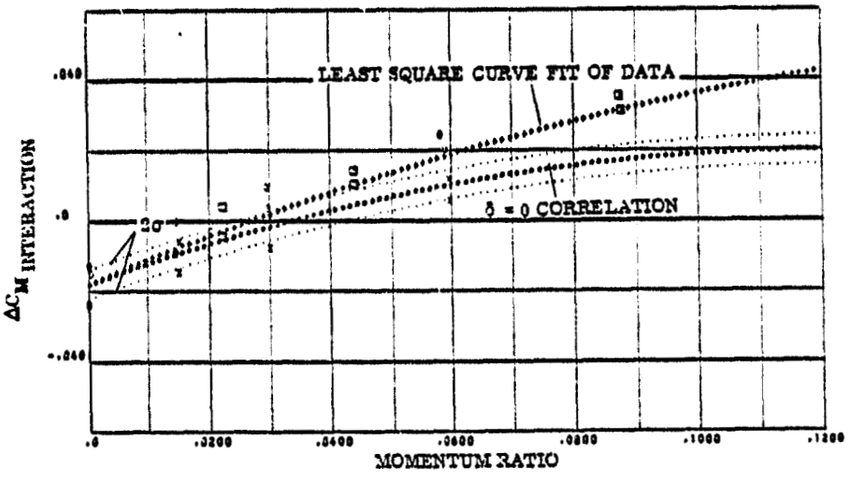

FIGURE 3-35e. : PITCH DOWN RCS INCREMENTAL EFFECTS DUE TO +10 DEGREE ELEVON DEFLECTION FROM 10 TO 15 DEGREES ANGLE OF ATTACK; PITCHING MOMENT

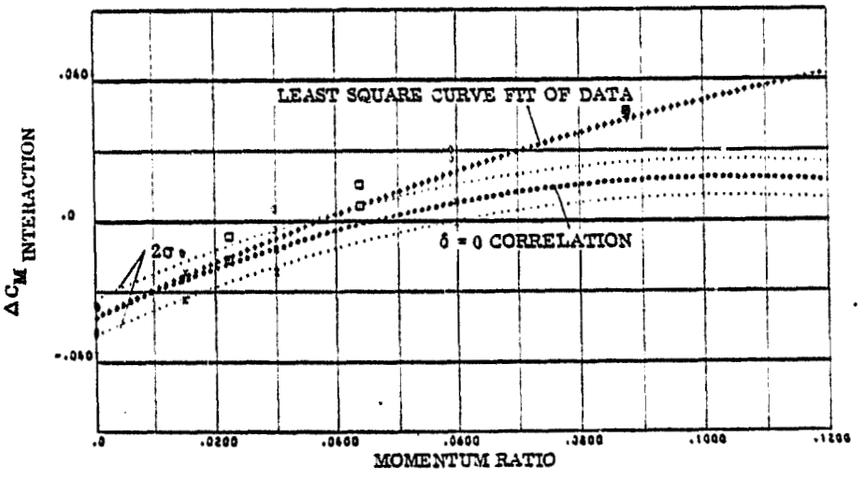

FIGURE 3-35f. : PITCH DOWN RCS INCREMENTAL EFFECTS DUE TO +10 DEGREE ELEVON DEFLECTION FROM 15 TO 20 DEGREES ANGLE OF ATTACK; PITCHING MOMENT

SYMBOLS	NOZZLE NUMBER	TEST NUMBER
0	N49	MA 22
X	N79	MA 22
□	N83	MA 22

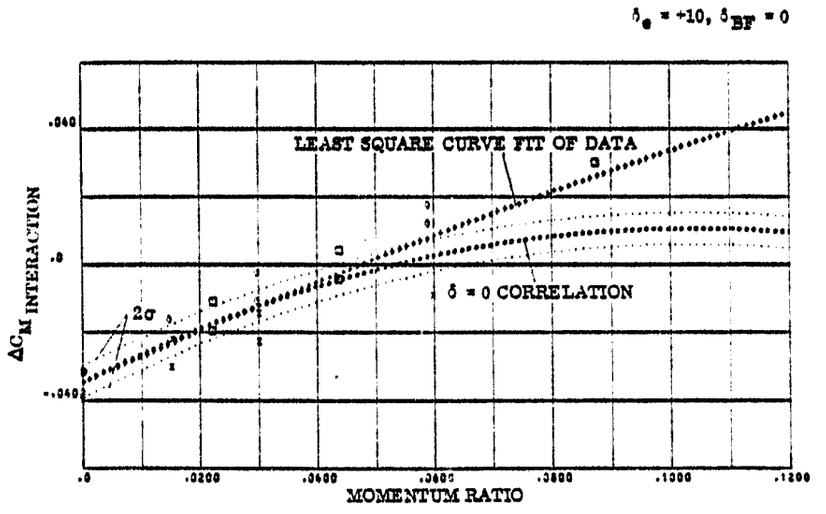

FIGURE 3-35g. : PITCH DOWN RCS INCREMENTAL EFFECTS DUE TO +10 DEGREE ELEVON DEFLECTION FROM 20 TO 25 DEGREES ANGLE OF ATTACK; PITCHING MOMENT

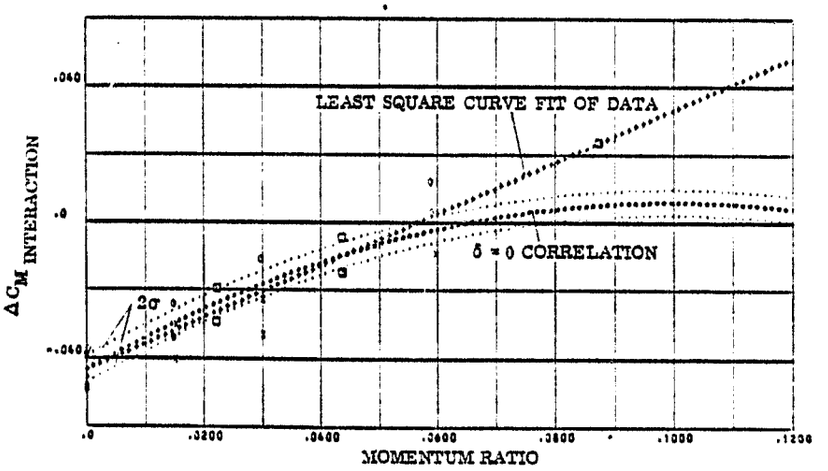

FIGURE 3-35h. : PITCH DOWN RCS INCREMENTAL EFFECTS DUE TO +10 DEGREE ELEVON DEFLECTION FROM 25 TO 30 DEGREES ANGLE OF ATTACK; PITCHING MOMENT

SYMBOLS	NOZZLE NUMBER	TEST NUMBER
0	N49	MA 22
X	N79	MA 22
□	N83	MA 22

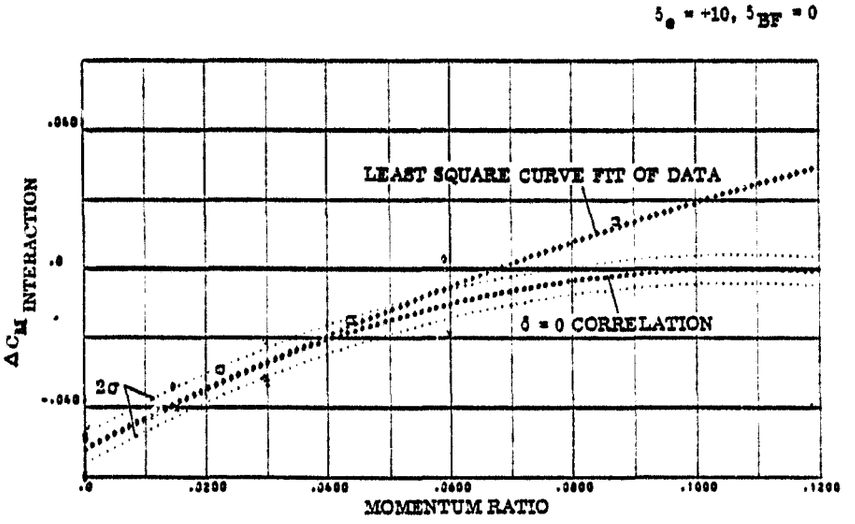

FIGURE 3-35i. : PITCH DOWN RCS INCREMENTAL EFFECTS DUE TO +10 DEGREE ELEVON DEFLECTION FROM 30 TO 35 DEGREES ANGLE OF ATTACK; PITCHING MOMENT

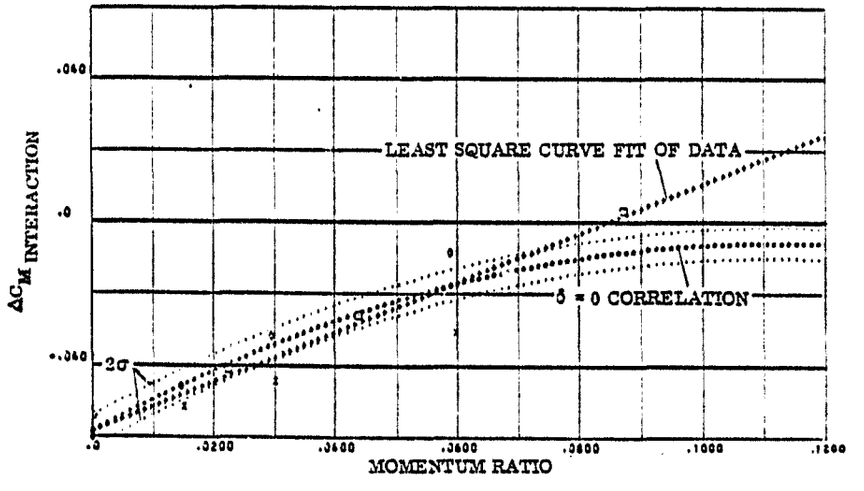

FIGURE 3-35j. : PITCH DOWN RCS INCREMENTAL EFFECTS DUE TO +10 DEGREE ELEVON DEFLECTION FROM 35 TO 42.5 DEGREES ANGLE OF ATTACK; PITCHING MOMENT

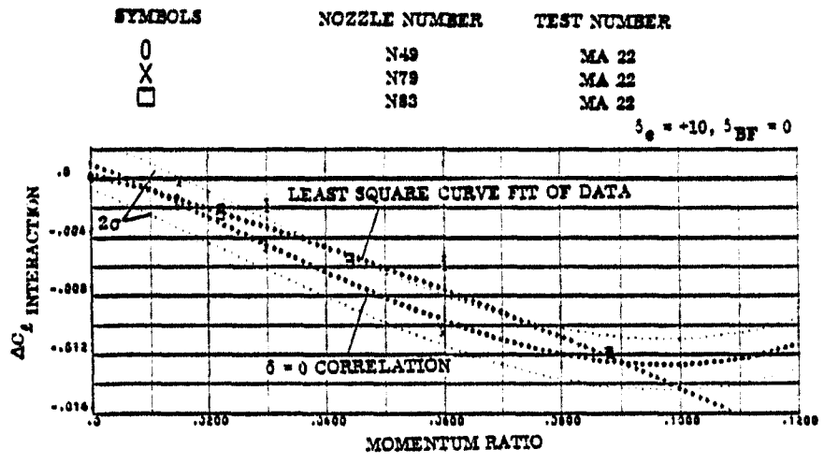

FIGURE 3-36a. : PITCH DOWN RCS INCREMENTAL EFFECTS DUE TO +10 DEGREE ELEVON DEFLECTION FROM -10 TO -5 DEGREES ANGLE OF ATTACK; ROLLING MOMENT

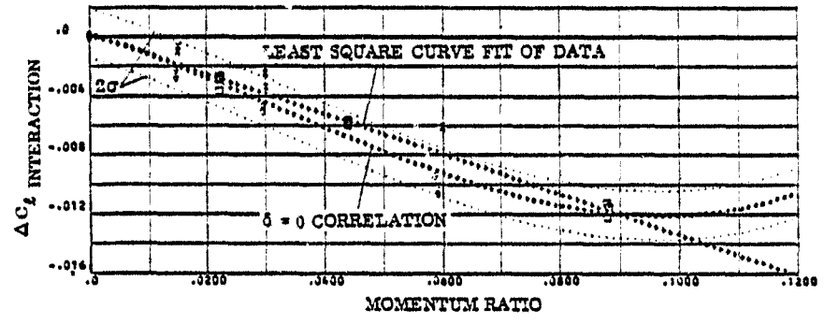

FIGURE 3-36b. : PITCH DOWN RCS INCREMENTAL EFFECTS DUE TO +10 DEGREE ELEVON DEFLECTION FROM -5 TO 0 DEGREES ANGLE OF ATTACK; ROLLING MOMENT

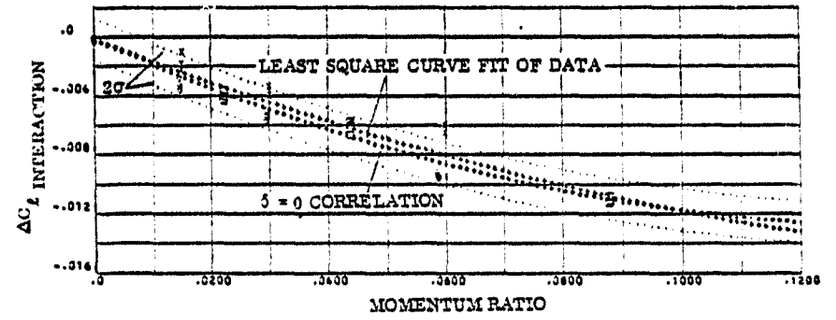

FIGURE 3-36c. : PITCH DOWN RCS INCREMENTAL EFFECTS DUE TO +10 DEGREE ELEVON DEFLECTION FROM 0 TO 5 DEGREES ANGLE OF ATTACK; ROLLING MOMENT

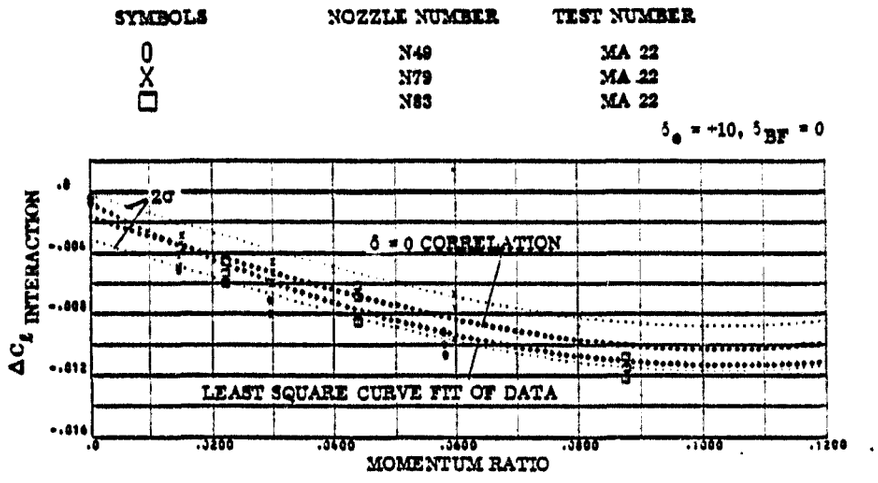

FIGURE 3-36d. : PITCH DOWN RCS INCREMENTAL EFFECTS DUE TO +10 DEGREE ELEVON DEFLECTION FROM 5 TO 10 DEGREES ANGLE OF ATTACK; ROLLING MOMENT

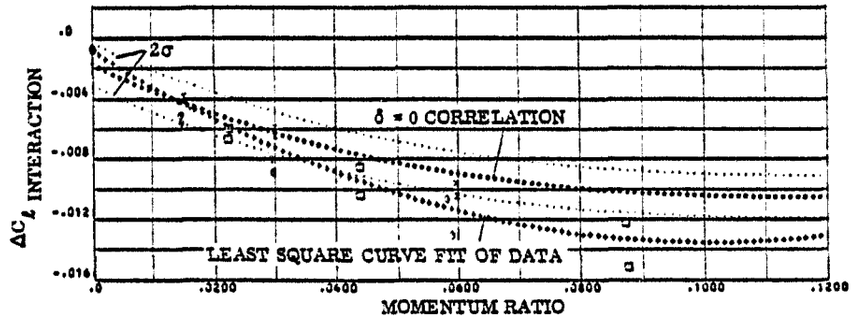

FIGURE 3-36e : PITCH DOWN RCS INCREMENTAL EFFECTS DUE TO +10 DEGREE ELEVON DEFLECTION FROM 10 TO 15 DEGREES ANGLE OF ATTACK; ROLLING MOMENT

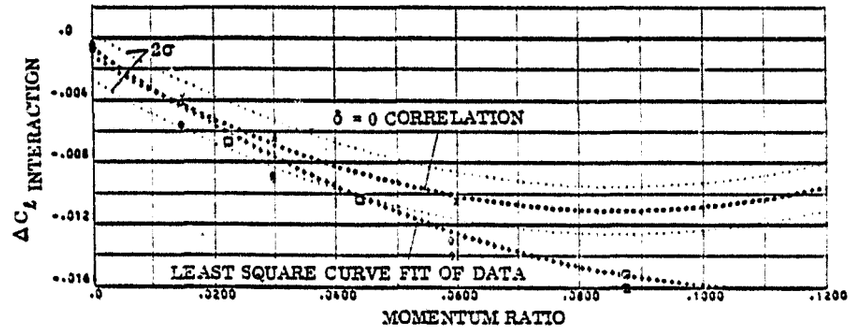

FIGURE 3-36f. : PITCH DOWN RCS INCREMENTAL EFFECTS DUE TO +10 DEGREE ELEVON DEFLECTION FROM 15 TO 20 DEGREES ANGLE OF ATTACK; ROLLING MOMENT

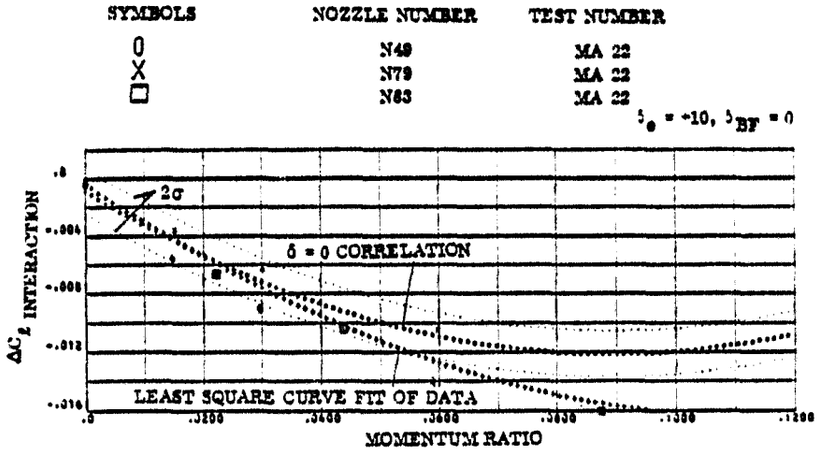

FIGURE 3-36g. : PITCH DOWN RCS INCREMENTAL EFFECTS DUE TO +10 DEGREE ELEVON DEFLECTION FROM 20 TO 25 DEGREES ANGLE OF ATTACK; ROLLING MOMENT

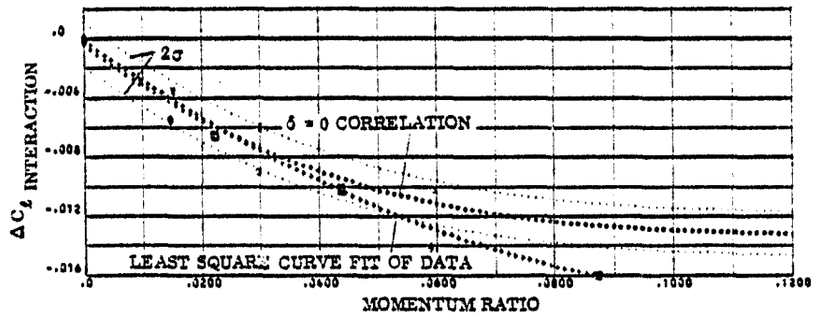

FIGURE 3-36h. : PITCH DOWN RCS INCREMENTAL EFFECTS DUE TO +10 DEGREE ELEVON DEFLECTION FROM 25 TO 30 DEGREES ANGLE OF ATTACK; ROLLING MOMENT

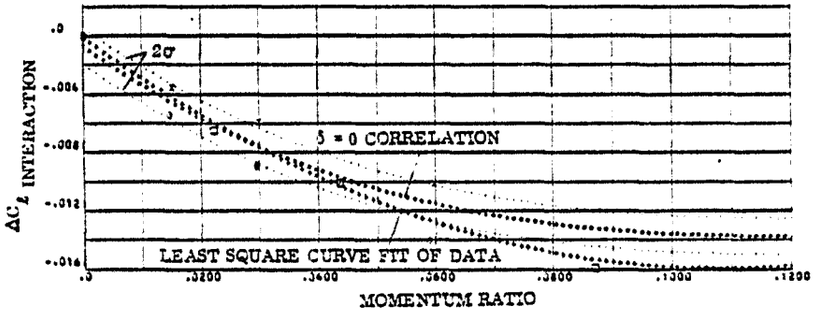

FIGURE 3-36i. : PITCH DOWN RCS INCREMENTAL EFFECTS DUE TO +10 DEGREE ELEVON DEFLECTION FROM 30 TO 35 DEGREES ANGLE OF ATTACK; ROLLING MOMENT

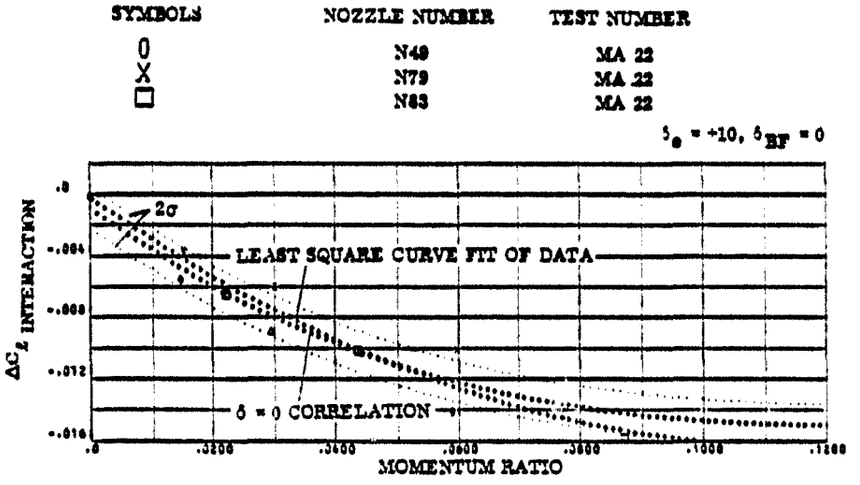

FIGURE 3-36 j. : PITCH DOWN RCS INCREMENTAL EFFECTS DUE TO +10 DEGREE ELEVON DEFLECTION FROM 35 TO 42.5 DEGREES ANGLE OF ATTACK; ROLLING MOMENT

SYMBOLS	NOZZLE NUMBER	TEST NUMBER
0	N61	MA 22
□	N85	MA 22

δ_e = -30, δ_{BF} = 0

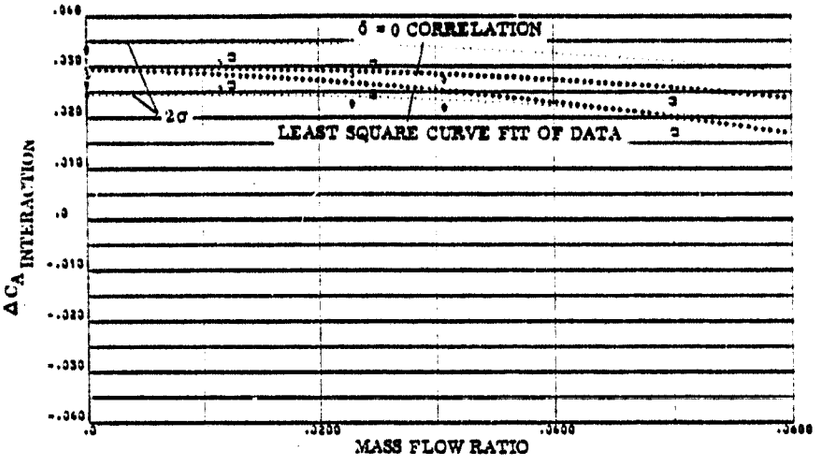

FIGURE 3-37 a. : YAW RCS INCREMENTAL EFFECTS DUE TO -30 DEGREE ELEVON DEFLECTION FROM -10 TO -5 DEGREES ANGLE OF ATTACK; AXIAL FORCE

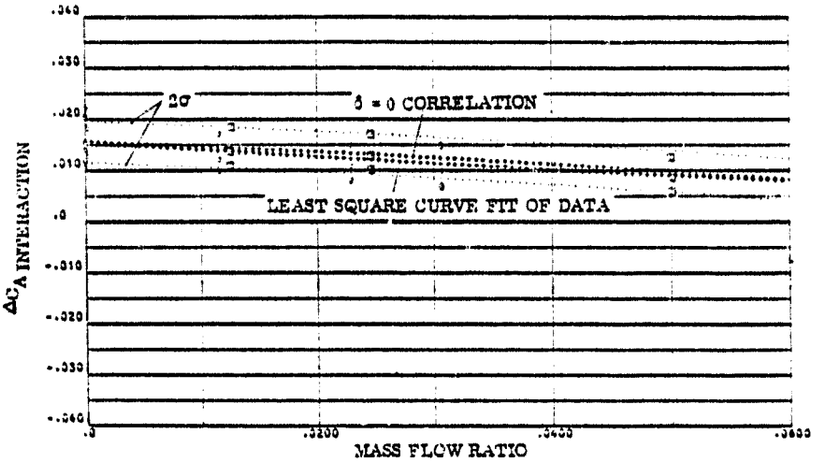

FIGURE 3-37 b. : YAW RCS INCREMENTAL EFFECTS DUE TO -30 DEGREE ELEVON DEFLECTION FROM -5 TO 0 DEGREES ANGLE OF ATTACK; AXIAL FORCE

SYMBOLS	NOZZLE NUMBER	TEST NUMBER
0	N61	MA 22
□	N66	MA 22

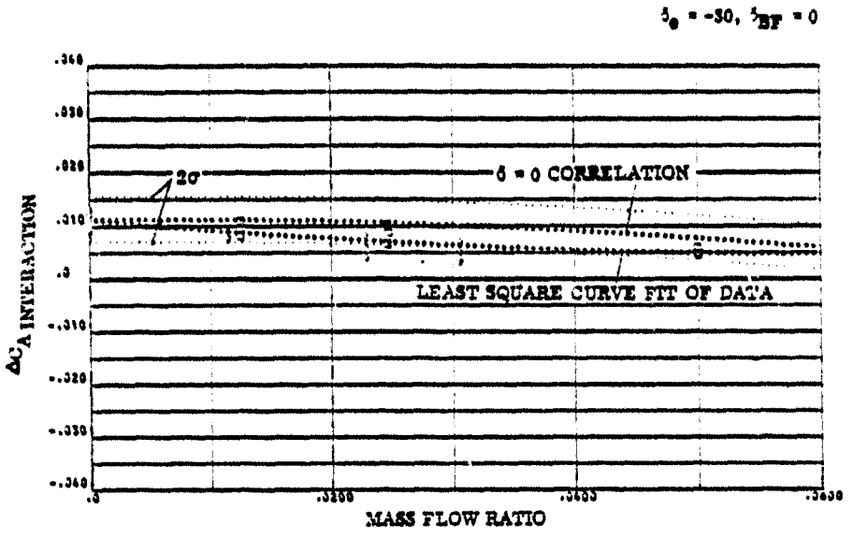

FIGURE 3-37c. : YAW RCS INCREMENTAL EFFECTS DUE TO -30 DEGREE ELEVON DEFLECTION FROM 0 TO 5 DEGREES ANGLE OF ATTACK; AXIAL FORCE

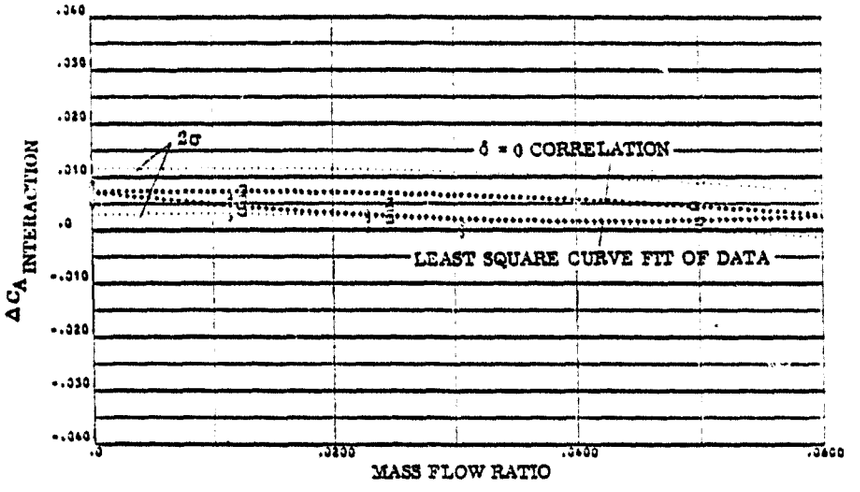

FIGURE 3-37d. : YAW RCS INCREMENTAL EFFECTS DUE TO -30 DEGREE ELEVON DEFLECTION FROM 5 TO 10 DEGREES ANGLE OF ATTACK; AXIAL FORCE

SYMBOLS	NOZZLE NUMBER	TEST NUMBER
0	N51	MA 22
□	N55	MA 22

$\delta_e = -30, \delta_{BF} = 0$

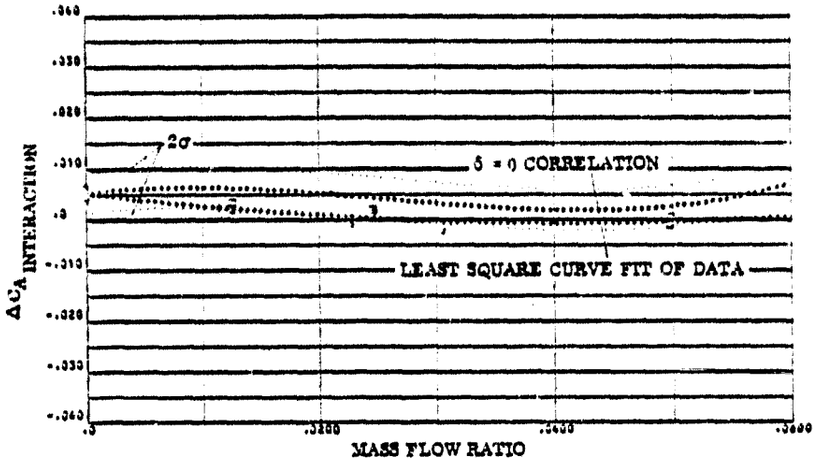

FIGURE 3-37e. : YAW RCS INCREMENTAL EFFECTS DUE TO -30 DEGREE ELEVON DEFLECTION FROM 10 TO 15 DEGREES ANGLE OF ATTACK; AXIAL FORCE

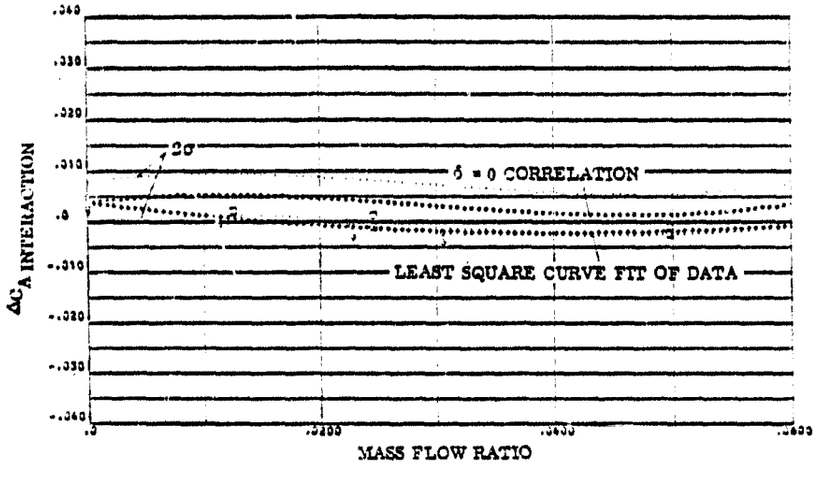

FIGURE 3-37f. : YAW RCS INCREMENTAL EFFECTS DUE TO -30 DEGREE ELEVON DEFLECTION FROM 15 TO 20 DEGREES ANGLE OF ATTACK; AXIAL FORCE

SYMBOLS	NOZZLE NUMBER	TEST NUMBER
0	N61	MA 22
□	N66	MA 22

$\delta_e = -30,\ \delta_{BF} = 0$

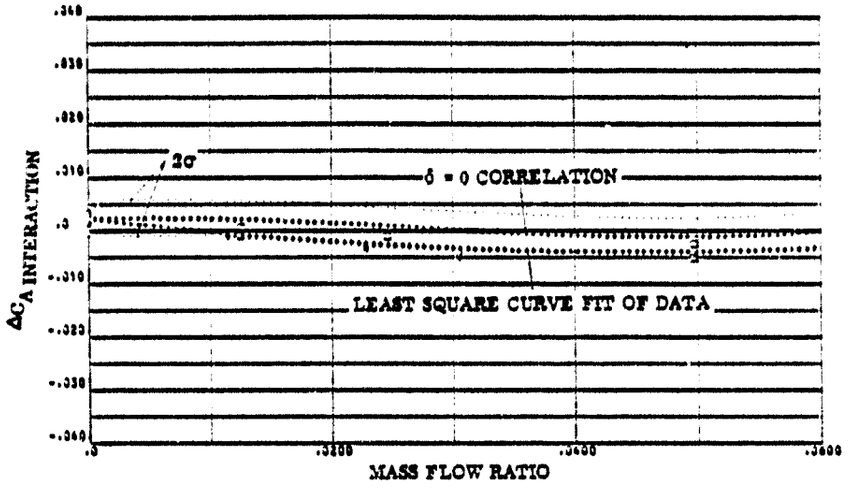

FIGURE 3-37g. : YAW RCS INCREMENTAL EFFECTS DUE TO -30 DEGREE ELEVON DEFLECTION FROM 20 TO 25 DEGREES ANGLE OF ATTACK; AXIAL FORCE

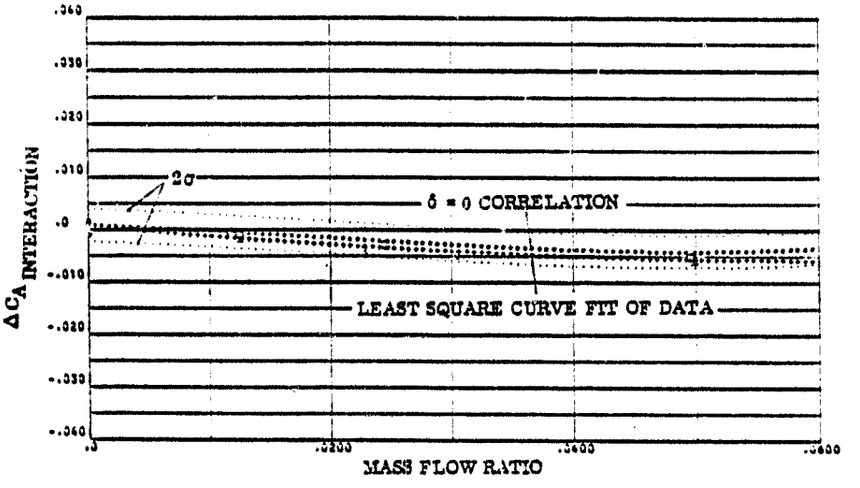

FIGURE 3-37h. : YAW RCS INCREMENTAL EFFECTS DUE TO -30 DEGREE ELEVON DEFLECTION FROM 25 TO 30 DEGREES ANGLE OF ATTACK; AXIAL FORCE

SYMBOLS	NOZZLE NUMBER	TEST NUMBER
0	N51	MA 22
□	N86	MA 22

$\delta_e = -30$, $\delta_{BF} = 0$

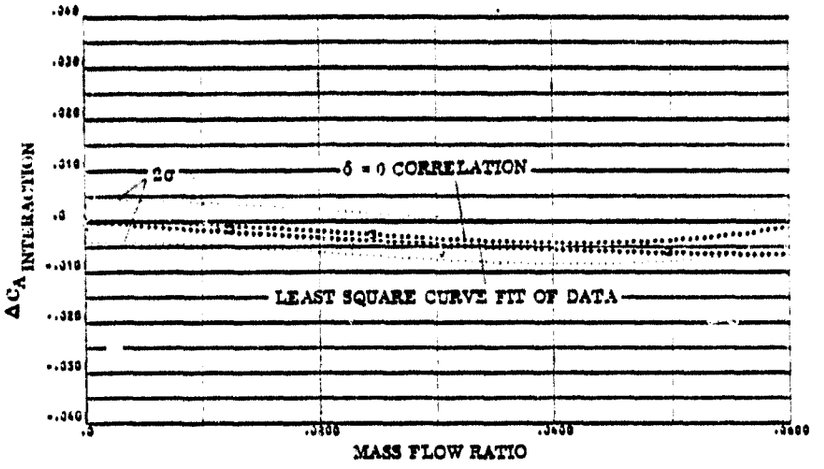

FIGURE 3-371. : YAW RCS INCREMENTAL EFFECTS DUE TO -30 DEGREE ELEVON DEFLECTION FROM 30 TO 35 DEGREES ANGLE OF ATTACK; AXIAL FORCE

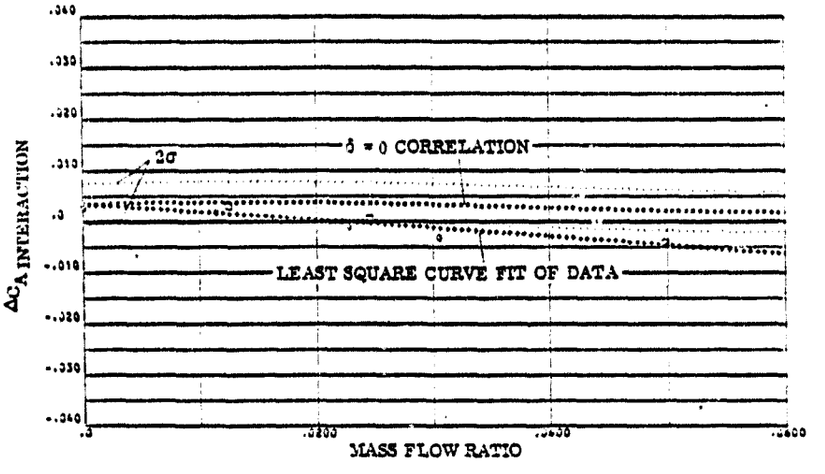

FIGURE 3-371. : YAW RCS INCREMENTAL EFFECTS DUE TO -30 DEGREE ELEVON DEFLECTION FROM 35 TO 42.5 DEGREES ANGLE OF ATTACK; AXIAL FORCE

SYMBOLS	NOZZLE NUMBER	TEST NUMBER
○	N61	MA 22
□	N65	MA 22

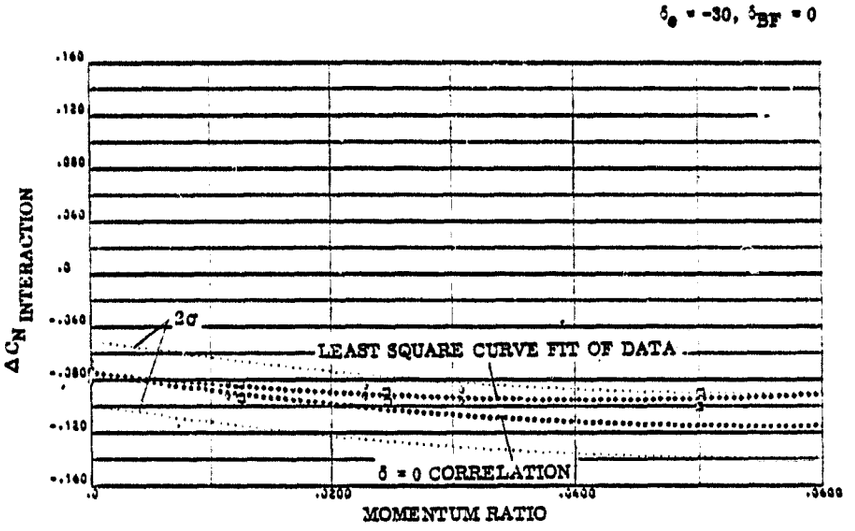

FIGURE 3-38a. : YAW RCS INCREMENTAL EFFECTS DUE TO -30 DEGREE ELEVON DEFLECTION FROM -10 TO -5 DEGREES ANGLE OF ATTACK; NORMAL FORCE

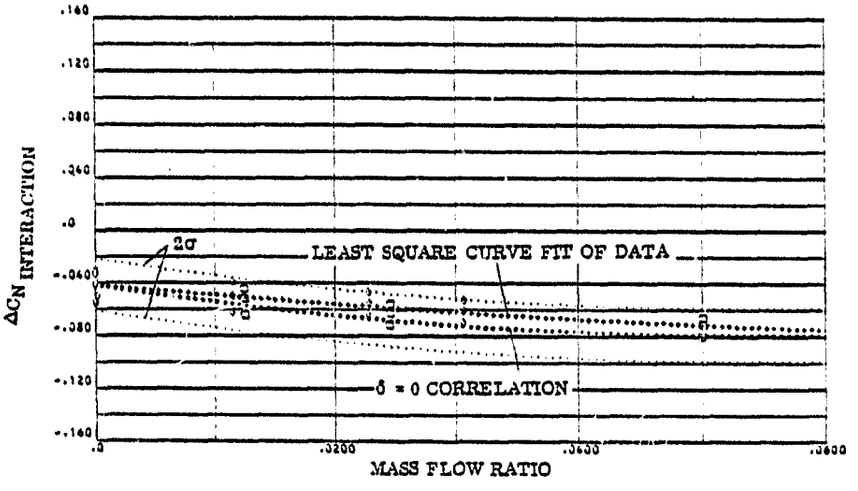

FIGURE 3-38b. : YAW RCS INCREMENTAL EFFECTS DUE TO -30 DEGREE ELEVON DEFLECTION FROM -5 TO 0 DEGREES ANGLE OF ATTACK; NORMAL FORCE

SYMBOLS	NOZZLE NUMBER	TEST NUMBER
0	N51	MA 22
□	N85	MA 22

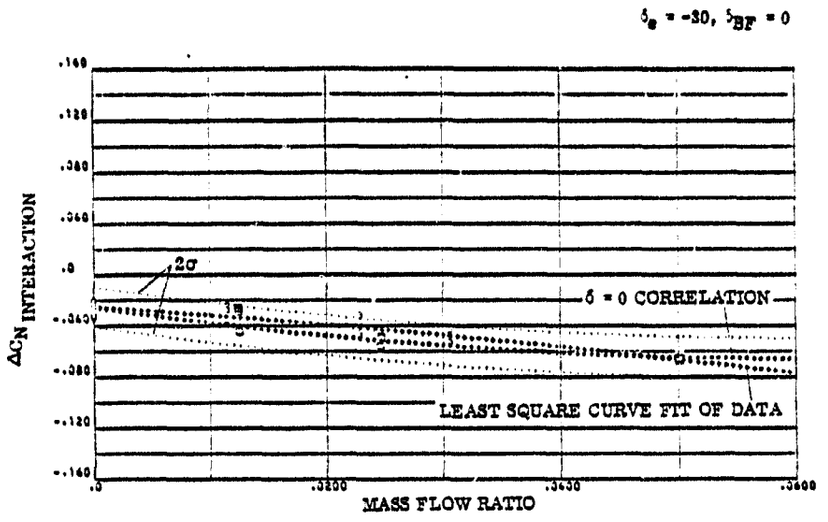

FIGURE 3-38c. : YAW RCS INCREMENTAL FFFECTS DUE TO -30 DEGREE ELEVON DEFLECTION FROM 0 TO 5 DEGREES ANGLE OF ATTACK; NORMAL FORCE

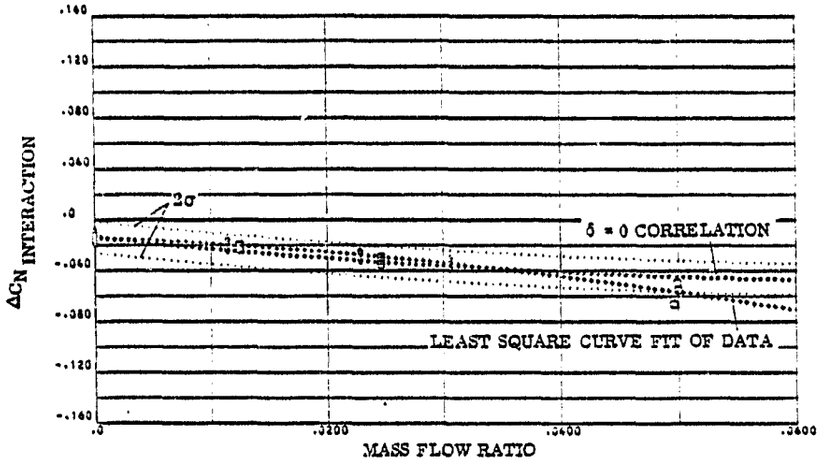

FIGURE 3-38d. : YAW RCS INCREMENTAL EFFECTS DUE TO -30 DEGREE ELEVON DEFLECTION FROM 5 TO 10 DEGREES ANGLE OF ATTACK; NORMAL FORCE

SYMBOLS	NOZZLE NUMBER	TEST NUMBER
○	N61	MA 22
□	N85	MA 22

$\delta_e = -30$, $\delta_{BF} = 0$

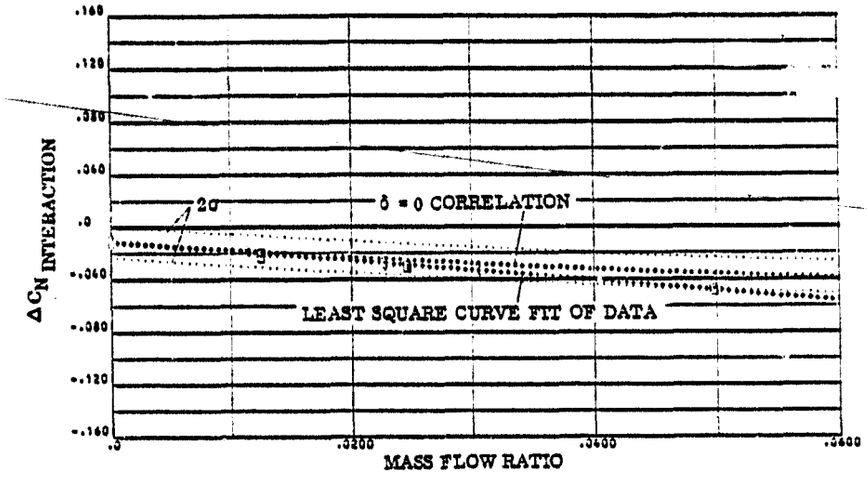

FIGURE 3-38e. : YAW RCS INCREMENTAL EFFECTS DUE TO -30 DEGREE ELEVON DEFLECTION FROM 10 TO 15 DEGREES ANGLE OF ATTACK; NORMAL FORCE

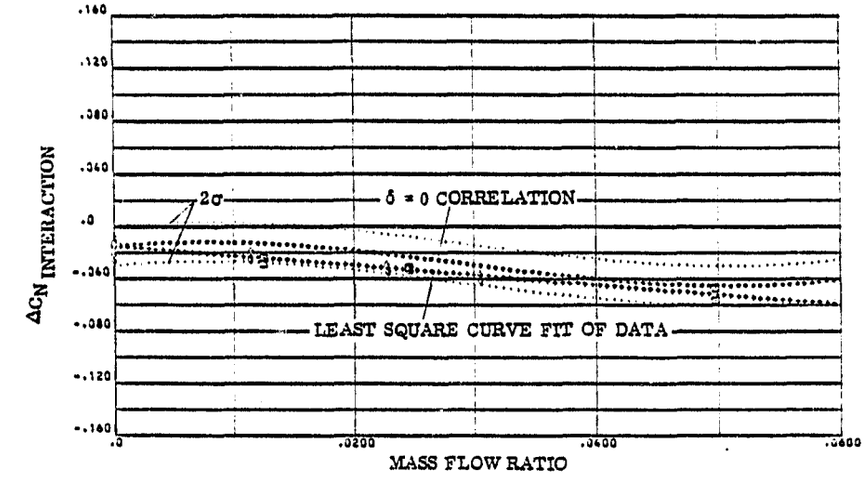

FIGURE 3-38 f. : YAW RCS INCREMENTAL EFFECTS DUE TO -30 DEGREE ELEVON DEFLECTION FROM 15 TO 20 DEGREES ANGLE OF ATTACK; NORMAL FORCE

SYMBOLS	NOZZLE NUMBER	TEST NUMBER
0	N61	MA 22
□	N65	MA 22

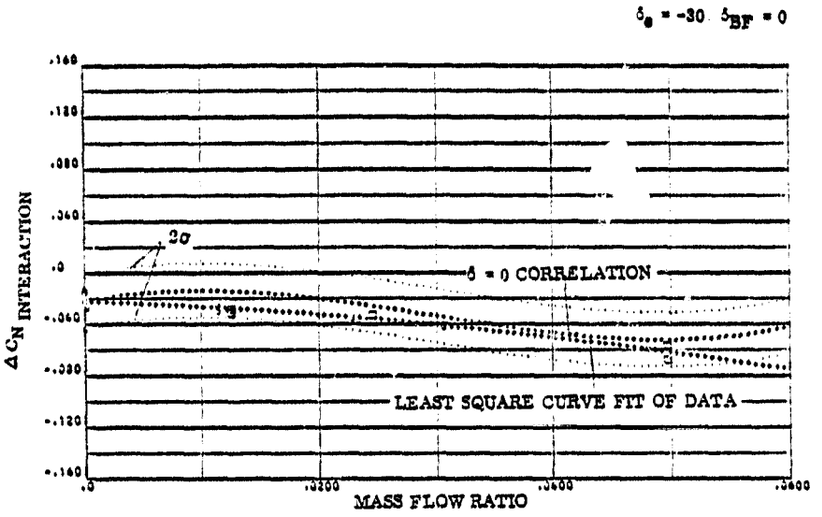

FIGURE 3-38g. : YAW RCS INCREMENTAL EFFECTS DUE TO -30 DEGREE ELEVON DEFLECTION FROM 20 TO 25 DEGREES ANGLE OF ATTACK; NORMAL FORCE

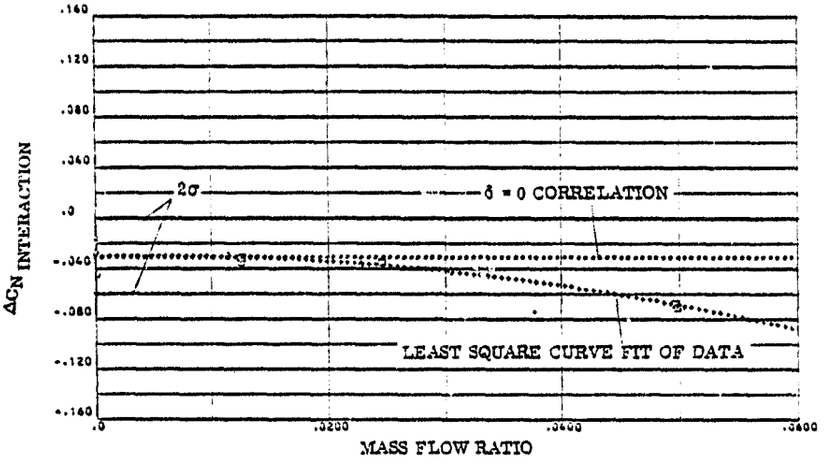

FIGURE 3-38h. : YAW RCS INCREMENTAL EFFECTS DUE TO -30 DEGREE ELEVON DEFLECTION FROM 25 TO 30 DEGREES ANGLE OF ATTACK; NORMAL FORCE

SYMBOLS	NOZZLE NUMBER	TEST NUMBER
0	N51	MA 22
□	N86	MA 22

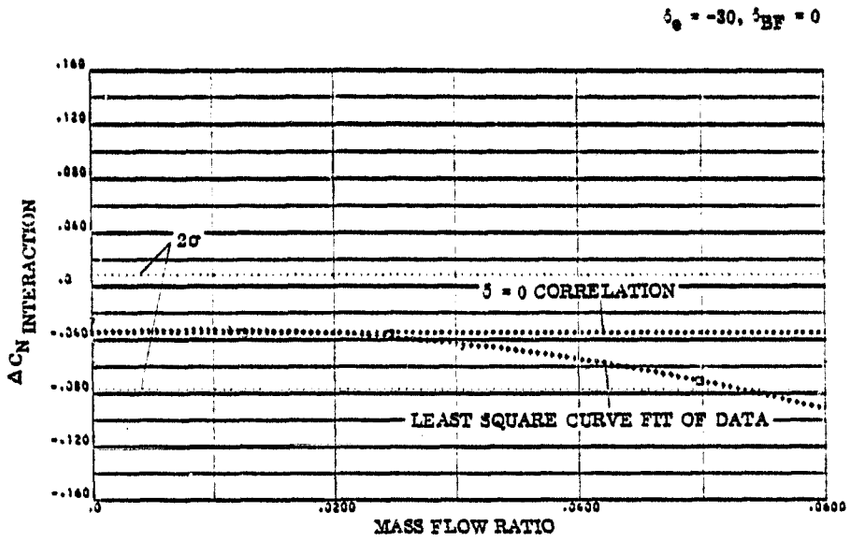

FIGURE 3-38 i. : YAW RCS INCREMENTAL EFFECTS DUE TO -30 DEGREE ELEVON DEFLECTION FROM 30 TO 35 DEGREES ANGLE OF ATTACK; NORMAL FORCE

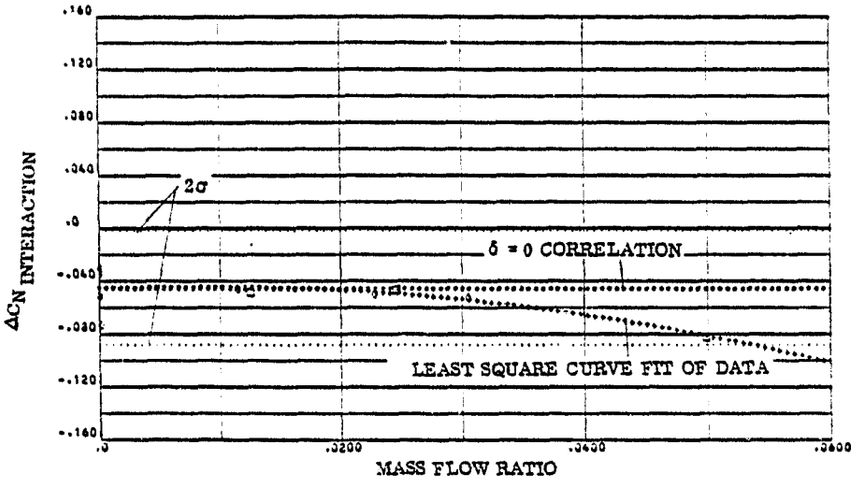

FIGURE 3-38 j. : YAW RCS INCREMENTAL EFFECTS DUE TO -30 DEGREE ELEVON DEFLECTION FROM 35 TO 42.5 DEGREES ANGLE OF ATTACK; NORMAL FORCE

SYMBOLS	NOZZLE NUMBER	TEST NUMBER
0	N51	MA 22
□	N86	MA 22

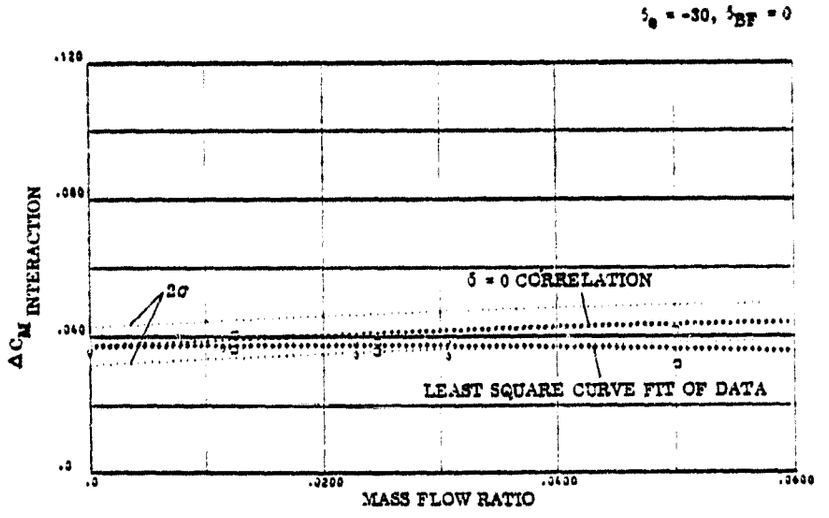

FIGURE 3-39a. : YAW RCS INCREMENTAL EFFECTS DUE TO -30 DEGREE ELEVON DEFLECTION FROM -10 TO -5 DEGREES ANGLE OF ATTACK; PITCHING MOMENT

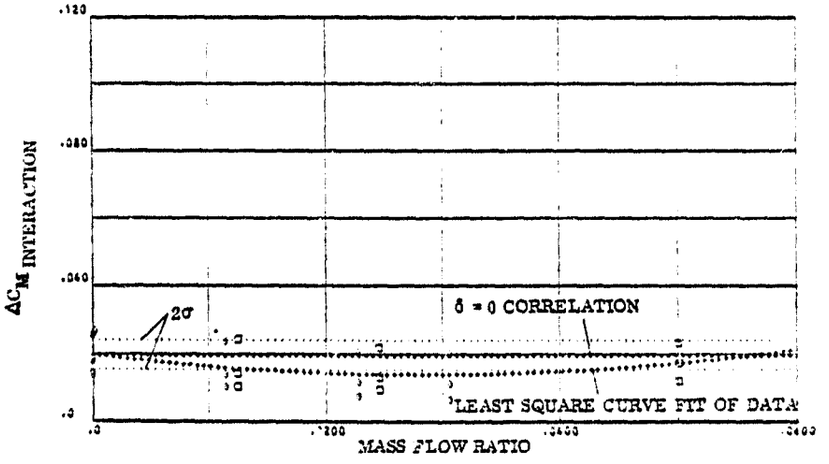

FIGURE 3-39b. : YAW RCS INCREMENTAL EFFECTS DUE TO -30 DEGREE ELEVON DEFLECTION FROM -5 TO 0 DEGREES ANGLE OF ATTACK; PITCHING MOMENT

SYMBOLS	NOZZLE NUMBER	TEST NUMBER
0	N51	MA 22
□	N85	MA 22

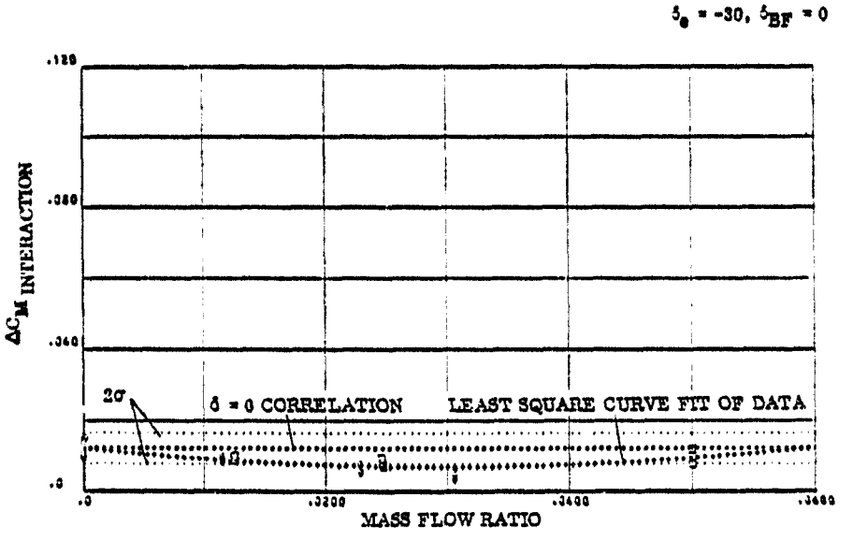

FIGURE 3-39c. : YAW RCS INCREMENTAL EFFECTS DUE TO DEGREE ELEVON DEFLECTION FROM 0 TO 5 DEGREES ANGLE OF ATTACK; PITCHING MOMENT

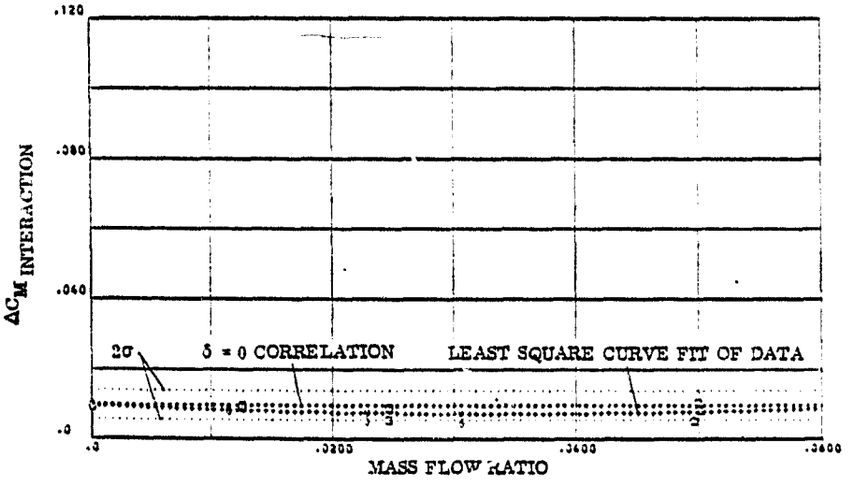

FIGURE 3-39d. : YAW RCS INCREMENTAL EFFECTS DUE TO DEGREE ELEVON DEFLECTION FROM 5 TO 10 DEGREES ANGLE OF ATTACK; PITCHING MOMENT

SYMBOLS	NOZZLE NUMBER	TEST NUMBER
0	N51	MA 22
□	N86	MA 22

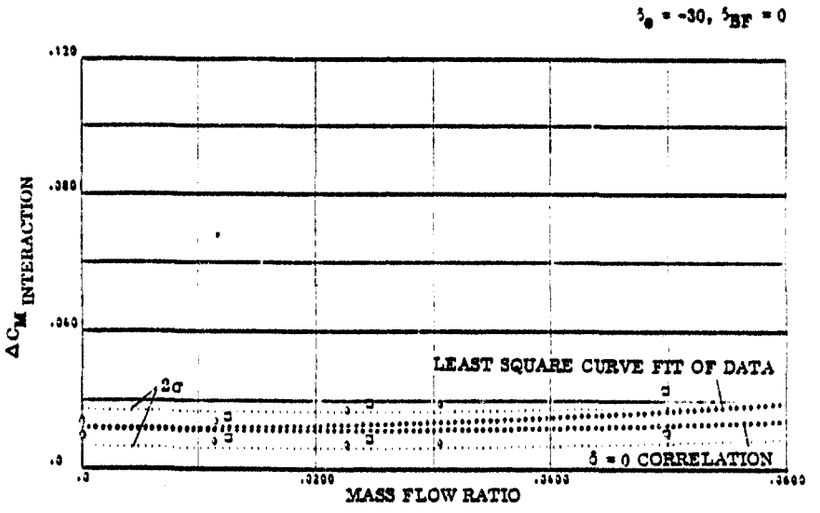

FIGURE 3-39e. : YAW RCS INCREMENTAL EFFECTS DUE TO -30 DEGREE ELEVON DEFLECTION FROM 10 TO 15 DEGREES ANGLE OF ATTACK; PITCHING MOMENT

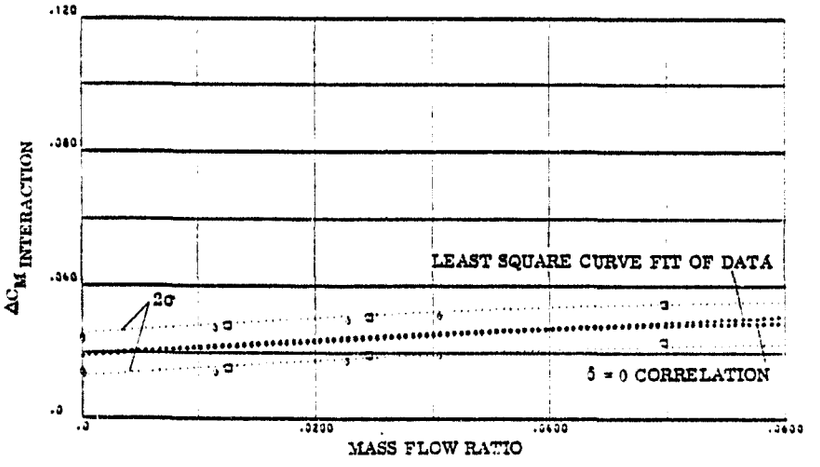

FIGURE 3-39f. : YAW RCS INCREMENTAL EFFECTS DUE TO -30 DEGREE ELEVON DEFLECTION FROM 15 TO 20 DEGREES ANGLE OF ATTACK; PITCHING MOMENT

SYMBOLS	NOZZLE NUMBER	TEST NUMBER
0	N61	MA 22
□	N66	MA 22

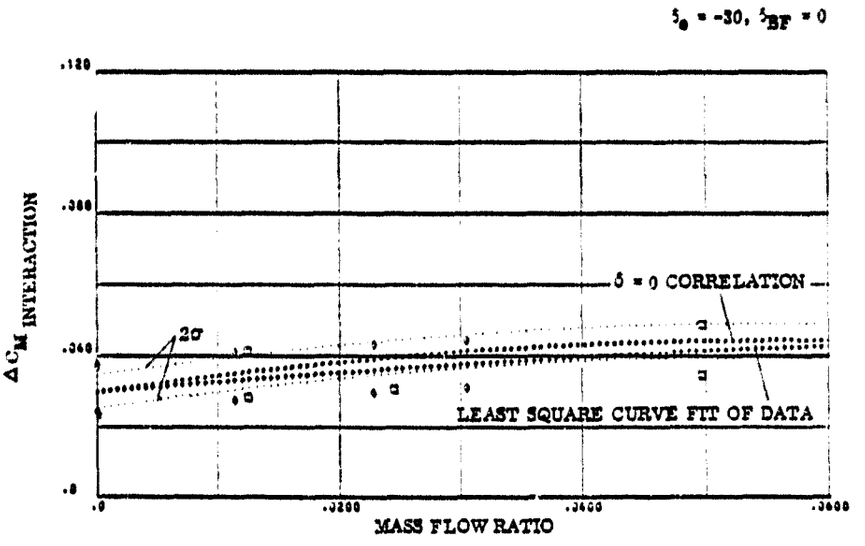

FIGURE 3-39g. : YAW RCS INCREMENTAL EFFECTS DUE TO -30 DEGREE ELEVON DEFLECTION FROM 20 TO 25 DEGREES ANGLE OF ATTACK; PITCHING MOMENT

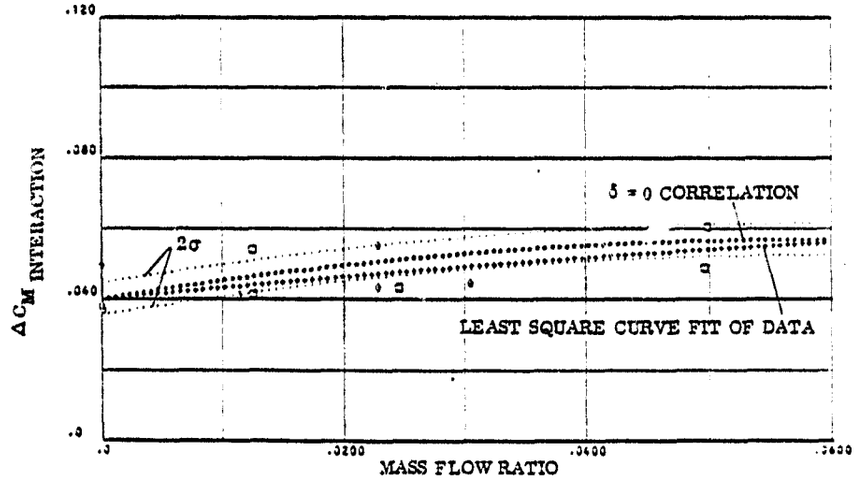

FIGURE 3-39h. : YAW RCS INCREMENTAL EFFECTS DUE TO -30 DEGREE ELEVON DEFLECTION FROM 25 TO 30 DEGREES ANGLE OF ATTACK; PITCHING MOMENT

SYMBOLS	NOZZLE NUMBER	TEST NUMBER
0	N51	MA 22
□	N85	MA 22

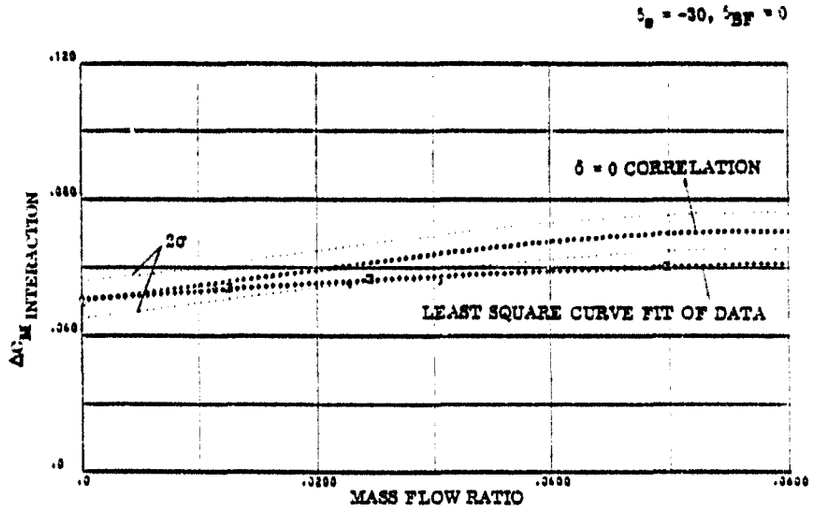

FIGURE 3-391. : YAW RC3 INCREMENTAL EFFECTS DUE TO -30 DEGREE ELEVON DEFLECTION FROM 30 TO 35 DEGREES ANGLE OF ATTACK; PITCHING MOMENT

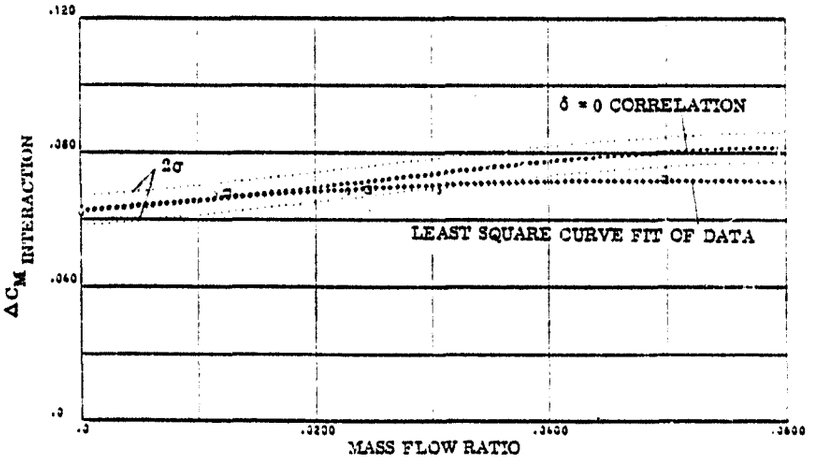

FIGURE 3-391. : YAW RCS INCREMENTAL EFFECTS DUE TO -30 DEGREE ELEVON DEFLECTION FROM 35 TO 42.5 DEGREES ANGLE OF ATTACK; PITCHING MOMENT

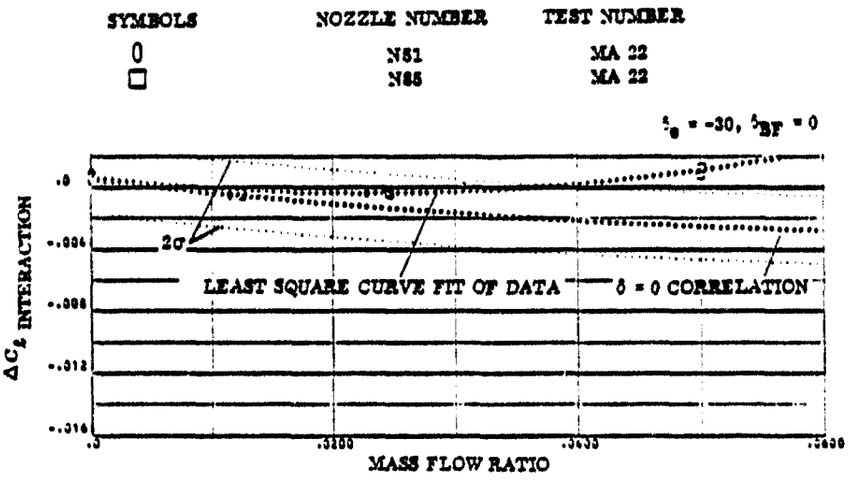

FIGURE 3-40a. : YAW RCS INCREMENTAL EFFECTS DUE TO -30 DEGREE ELEVON DEFLECTION FROM -10 TO -5 DEGREES ANGLE OF ATTACK; ROLLING MOMENT

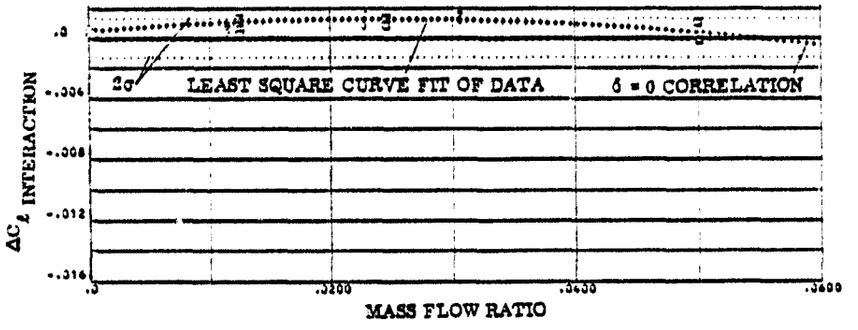

FIGURE 3-40b. : YAW RCS INCREMENTAL EFFECTS DUE TO -30 DEGREE ELEVON DEFLECTION FROM -5 TO 0 DEGREES ANGLE OF ATTACK; ROLLING MOMENT

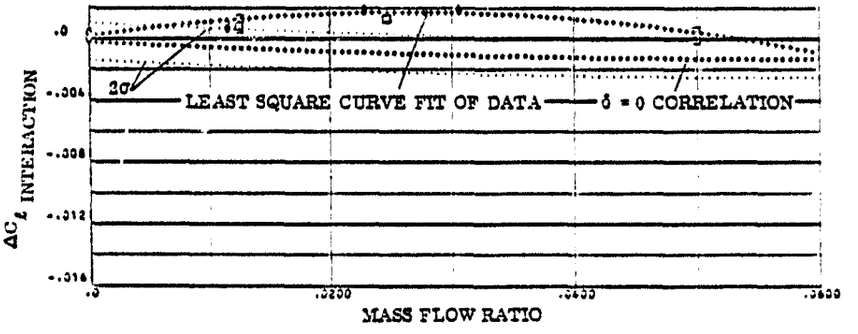

FIGURE 3-40c. : YAW RCS INCREMENTAL EFFECTS DUE TO -30 DEGREE ELEVON DEFLECTION FROM 0 TO 5 DEGREES ANGLE OF ATTACK; ROLLING MOMENT

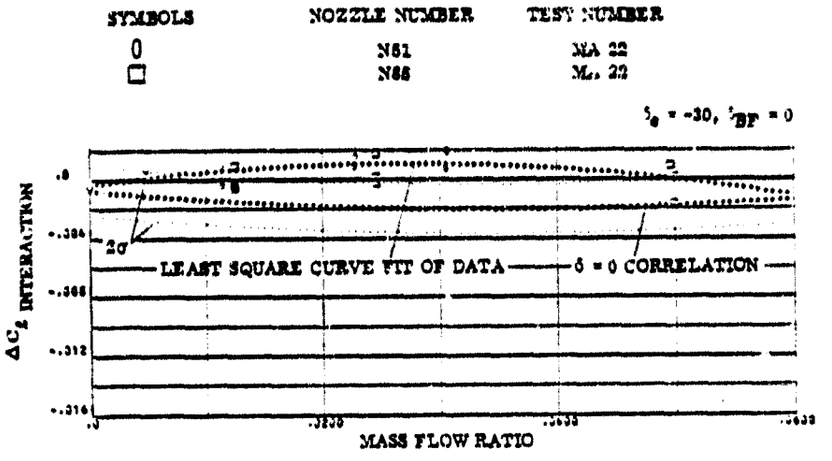

FIGURE 3-40d. : YAW RCS INCREMENTAL EFFECTS DUE TO -30 DEGREE ELEVON DEFLECTION FROM 5 TO 10 DEGREES ANGLE OF ATTACK; ROLLING MOMENT

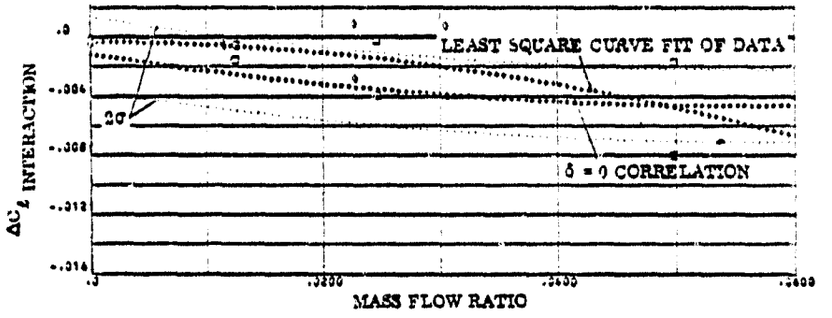

FIGURE 3-40e. : YAW RCS INCREMENTAL EFFECTS DUE TO -30 DEGREE ELEVON DEFLECTION FROM 10 TO 15 DEGREES ANGLE OF ATTACK; ROLLING MOMENT

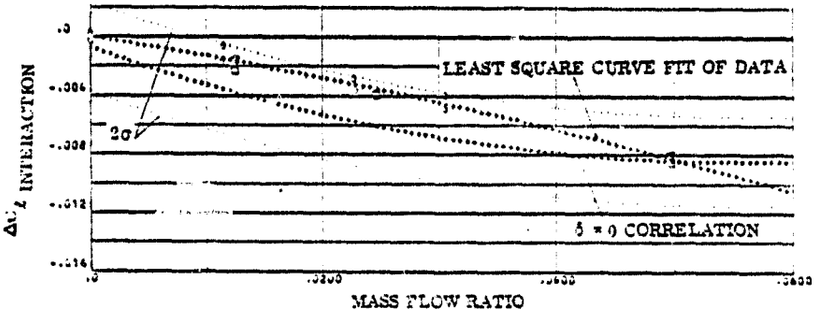

FIGURE 3-40f. : YAW RCS INCREMENTAL EFFECTS DUE TO -30 DEGREE ELEVON DEFLECTION FROM 15 TO 20 DEGREES ANGLE OF ATTACK; ROLLING MOMENT

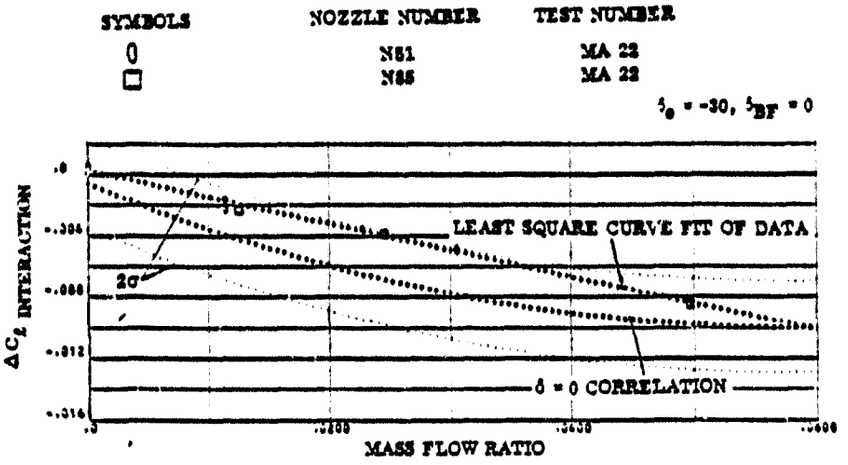

FIGURE 3-40g. : YAW RCS INCREMENTAL EFFECTS DUE TO -30 DEGREE ELEVON DEFLECTION FROM 20 TO 25 DEGREES ANGLE OF ATTACK; ROLLING MOMENT

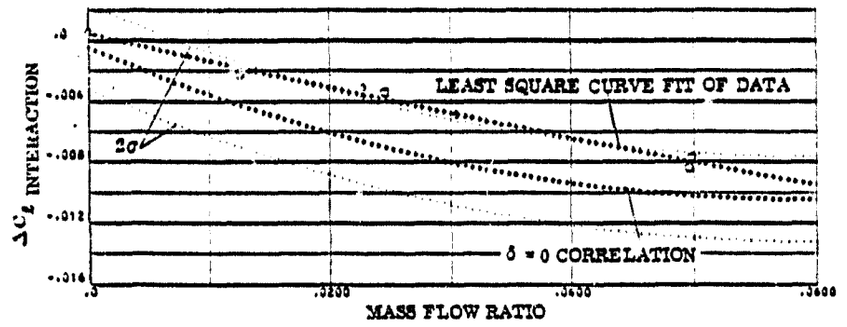

FIGURE 3-40h. : YAW RCS INCREMENTAL EFFECTS DUE TO -30 DEGREE ELEVON DEFLECTION FROM 25 TO 30 DEGREES ANGLE OF ATTACK; ROLLING MOMENT

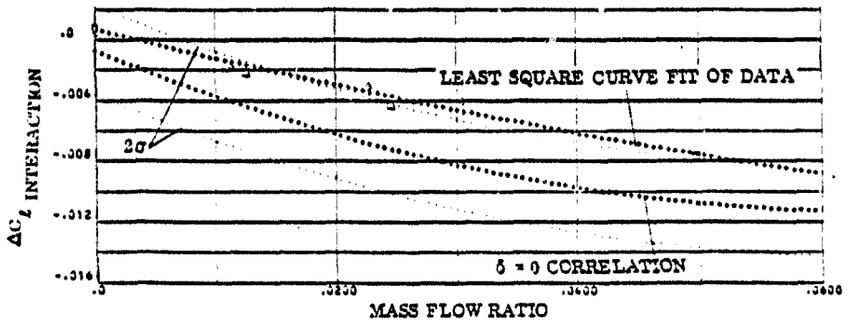

FIGURE 3-40i. : YAW RCS INCREMENTAL EFFECTS DUE TO -30 DEGREE ELEVON DEFLECTION FROM 30 TO 35 DEGREES ANGLE OF ATTACK; ROLLING MOMENT

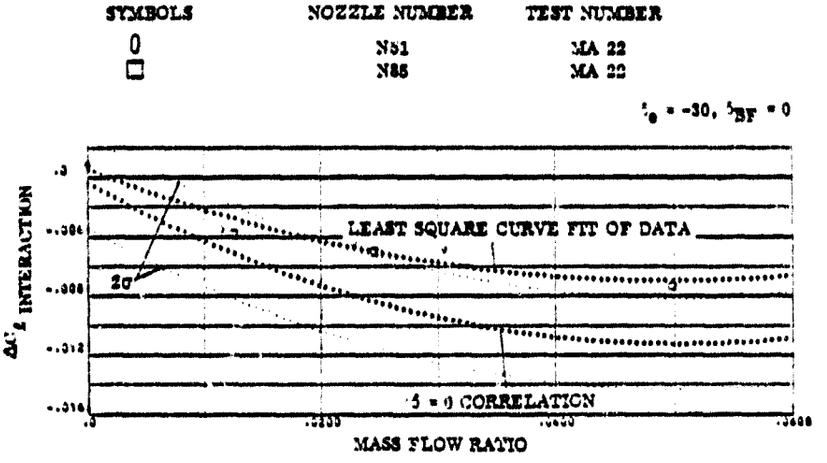

FIGURE 3-40j. : YAW RCS INCREMENTAL EFFECTS DUE TO -30 DEGREE ELEVON DEFLECTION FROM 35 TO 42.5 DEGREES ANGLE OF ATTACK; ROLLING MOMENT

SYMBOLS	NOZZLE NUMBER	TEST NUMBER
0	N51	MA 22
□	N85	MA 22

$\delta_e = +10, \delta_{BF} = 0$

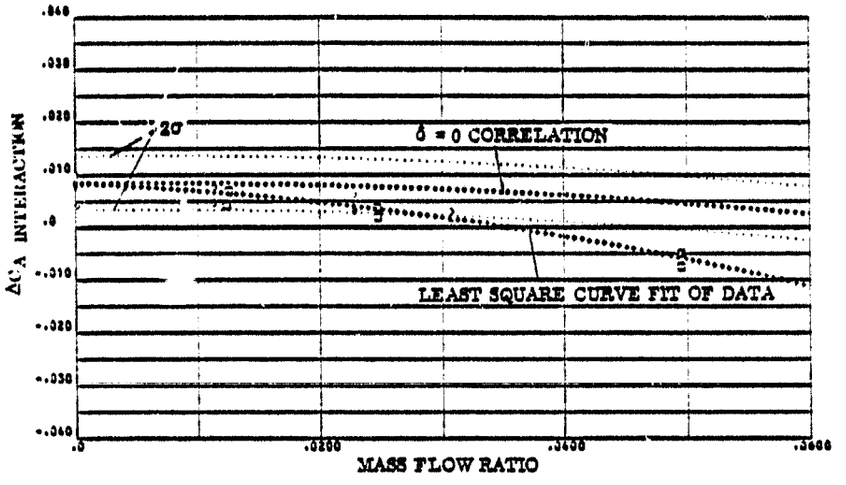

FIGURE 3-41a. : YAW RCS INCREMENTAL EFFECTS DUE TO +10 DEGREE ELEVON DEFLECTION FROM -10 TO -5 DEGREES ANGLE OF ATTACK; AXIAL FORCE

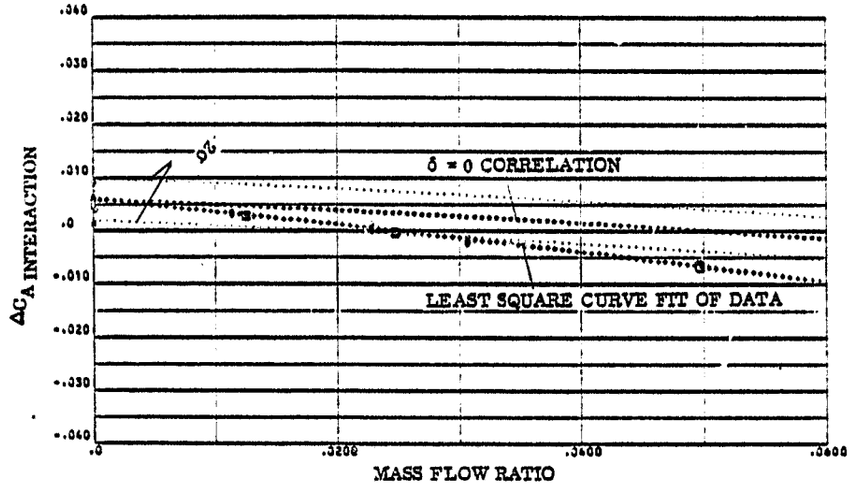

FIGURE 3-41b. : YAW RCS INCREMENTAL EFFECTS DUE TO +10 DEGREE ELEVON DEFLECTION FROM -5 TO 0 DEGREES ANGLE OF ATTACK; AXIAL FORCE

SYMBOLS	NOZZLE NUMBER	TEST NUMBER
○	N51	MA 22
□	N65	MA 22

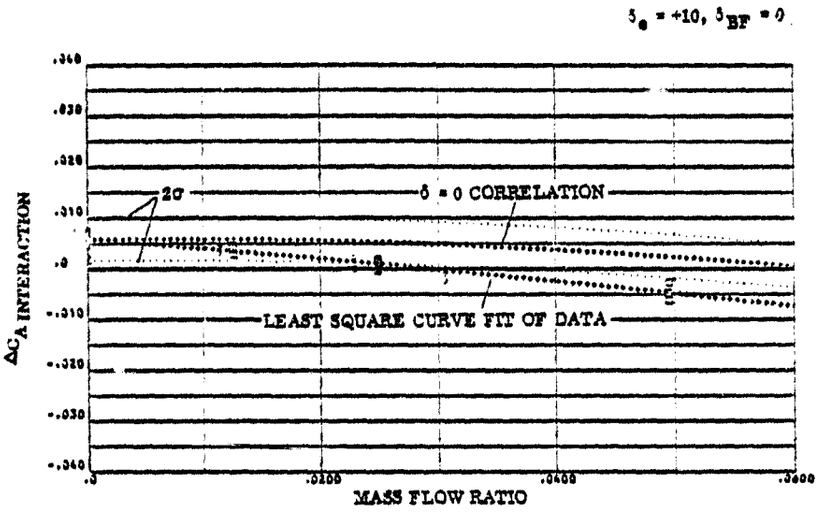

FIGURE 3-41c. : YAW RCS INCREMENTAL EFFECTS DUE TO +10 DEGREE ELEVON DEFLECTION FROM 0 TO 5 DEGREES ANGLE OF ATTACK; AXIAL FORCE

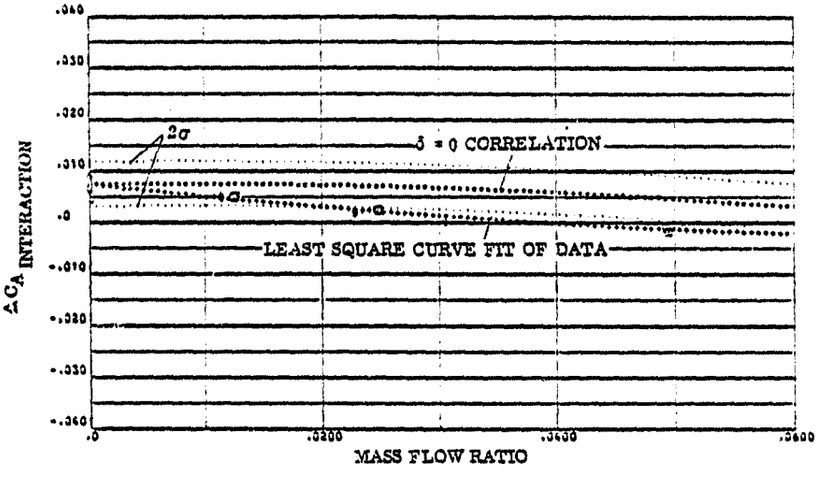

FIGURE 3-41d. : YAW RCS INCREMENTAL EFFECTS DUE TO +10 DEGREE ELEVON DEFLECTION FROM 5 TO 10 DEGREES ANGLE OF ATTACK; AXIAL FORCE

SYMBOLS	NOZZLE NUMBER	TEST NUMBER
0	N61	MA 22
□	N85	MA 22

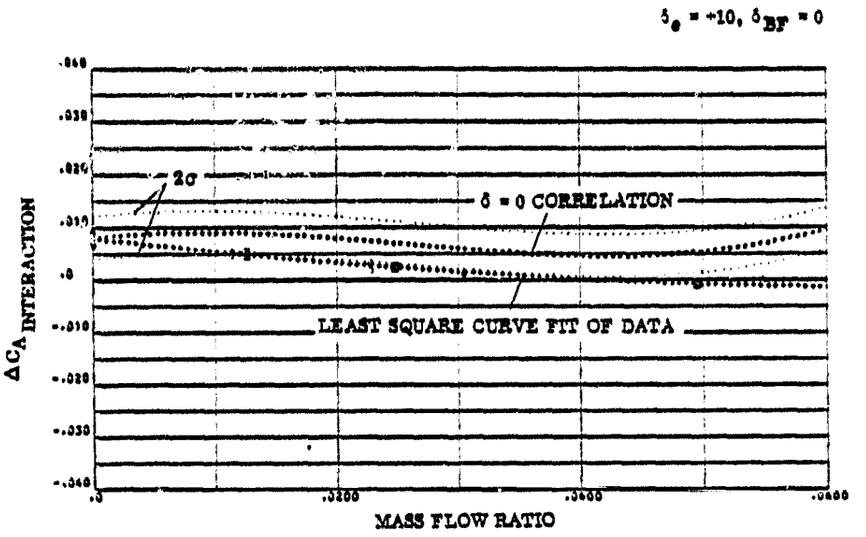

FIGURE 3-41e. : YAW RCS INCREMENTAL EFFECTS DUE TO +10 DEGREE ELEVON DEFLECTION FROM 10 TO 15 DEGREES ANGLE OF ATTACK; AXIAL FORCE

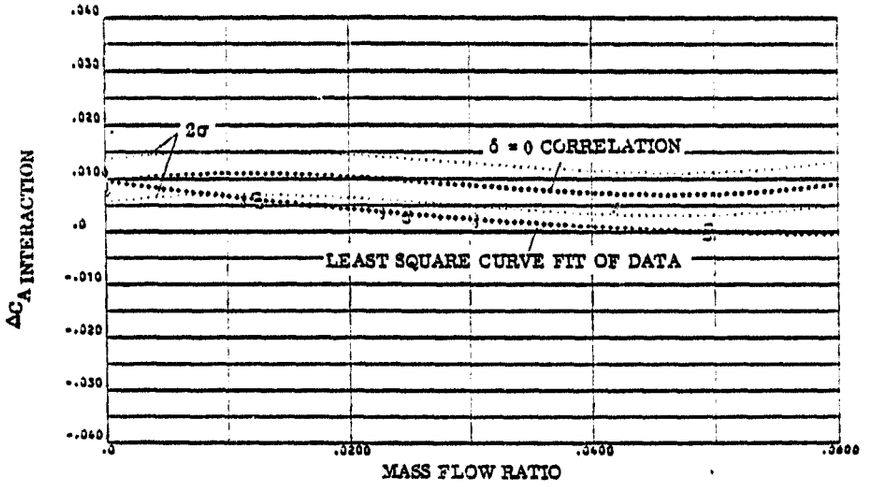

FIGURE 3-41f. : YAW RCS INCREMENTAL EFFECTS DUE TO +10 DEGREE ELEVON DEFLECTION FROM 15 TO 20 DEGREES ANGLE OF ATTACK; AXIAL FORCE

SYMBOLS	NOZZLE NUMBER	TEST NUMBER
0	N51	MA 22
□	N85	MA 22

$\delta_e = +10, \delta_{BF} = 0$

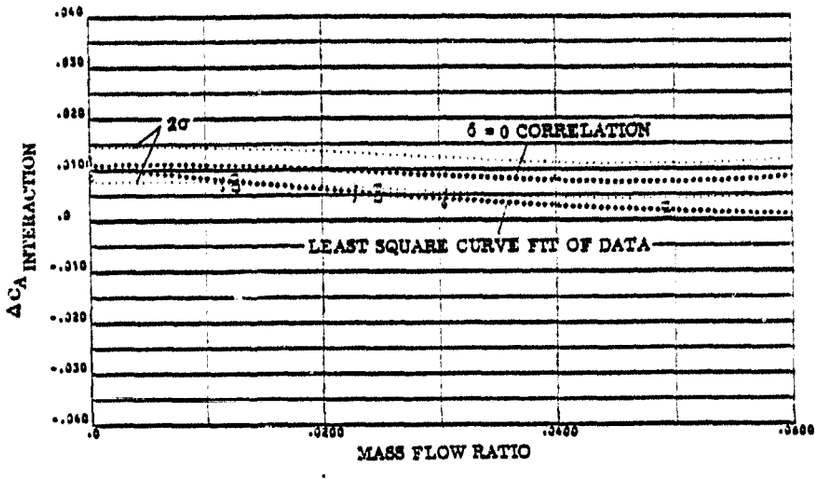

FIGURE 3-41g. : YAW RCS INCREMENTAL EFFECTS DUE TO +10 DEGREE ELEVON DEFLECTION FROM 20 TO 25 DEGREES ANGLE OF ATTACK; AXIAL FORCE

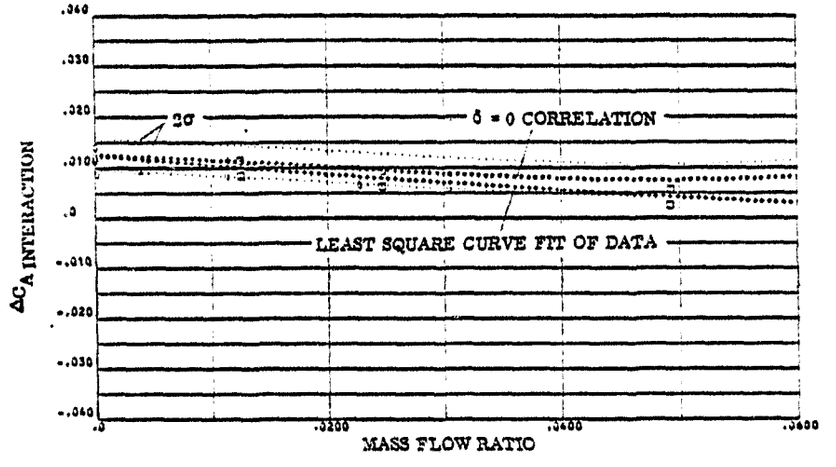

FIGURE 3-41h. : YAW RCS INCREMENTAL EFFECTS DUE TO +10 DEGREE ELEVON DEFLECTION FROM 25 TO 30 DEGREES ANGLE OF ATTACK; AXIAL FORCE

SYMBOLS	NOZZLE NUMBER	TEST NUMBER
0	N51	MA 22
□	N85	MA 22

$\delta_e = +10, \delta_{BF} = 0$

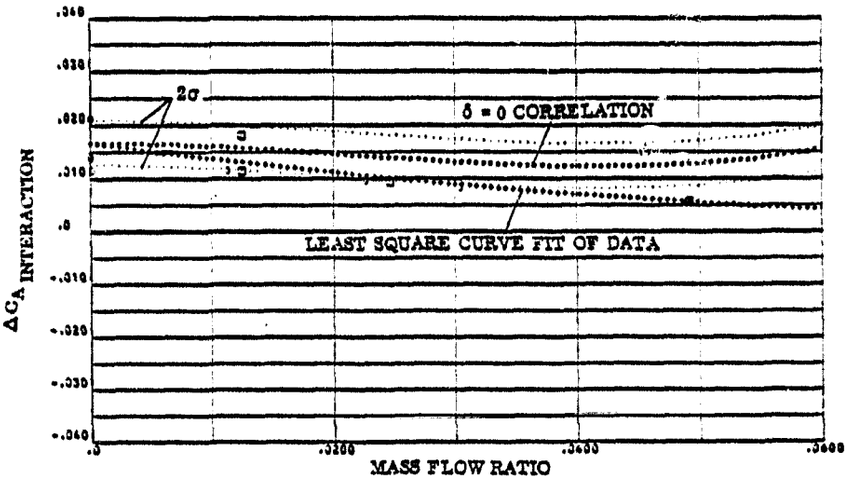

FIGURE 3-411. : YAW RCS INCREMENTAL EFFECTS DUE TO DEGREE ELEVON DEFLECTION FROM 30 TO 35 DEGREES ANGLE OF ATTACK; AXIAL FORCE

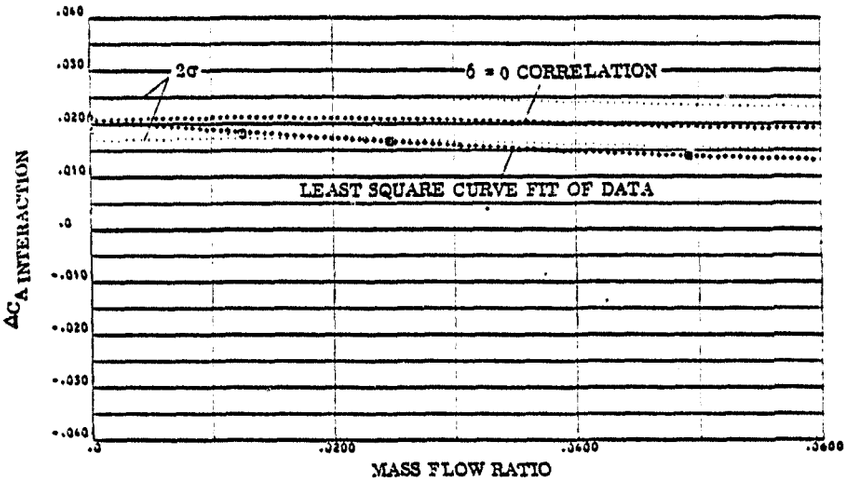

FIGURE 3-41j. : YAW RCS INCREMENTAL EFFECTS DUE TO DEGREE ELEVON DEFLECTION FROM 35 TO 42.5 DEGREES ANGLE OF ATTACK; AXIAL FORCE

SYMBOLS	NOZZLE NUMBER	TEST NUMBER
○	N51	MA 22
□	N85	MA 22

$\delta_e = +10, \delta_{BF} = 0$

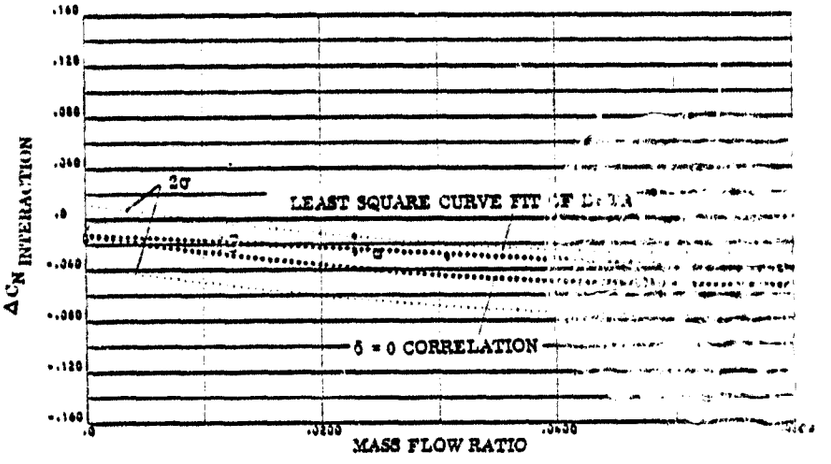

FIGURE 3-42a. : YAW RCS INCREMENTAL EFFECTS DUE TO +10 DEGREE ELEVON DEFLECTION FROM -10 TO -6 DEGREES ANGLE OF ATTACK; NORMAL FORCE

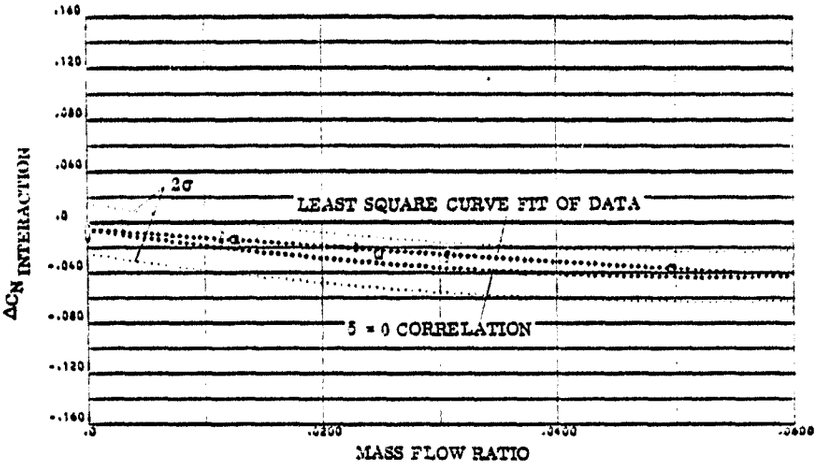

FIGURE 3-42b. : YAW RCS INCREMENTAL EFFECTS DUE TO +10 DEGREE ELEVON DEFLECTION FROM -5 TO 0 DEGREES ANGLE OF ATTACK; NORMAL FORCE

SYMBOLS	NOZZLE NUMBER	TEST NUMBER
0	N51	MA 22
□	N86	MA 28

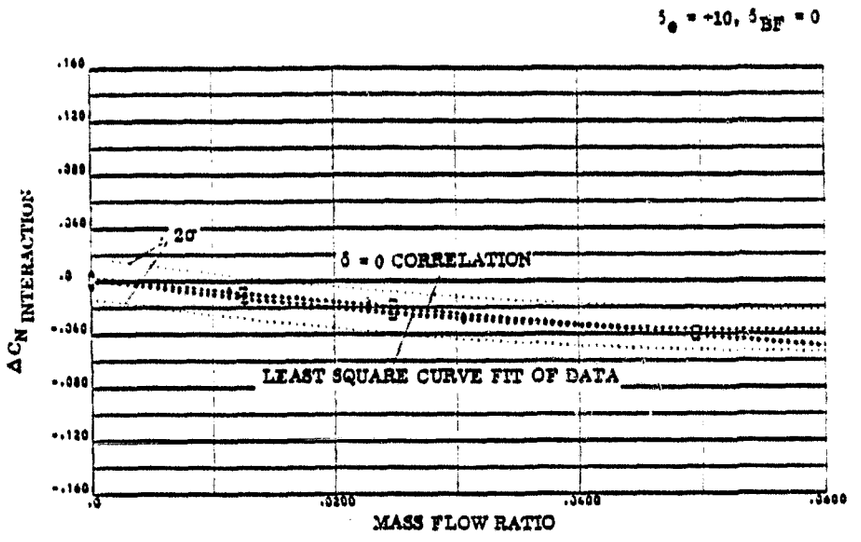

FIGURE 3-42c. : YAW RCS INCREMENTAL EFFECTS DUE TO +10 DEGREE ELEVON DEFLECTION FROM 0 TO 5 DEGREES ANGLE OF ATTACK; NORMAL FORCE

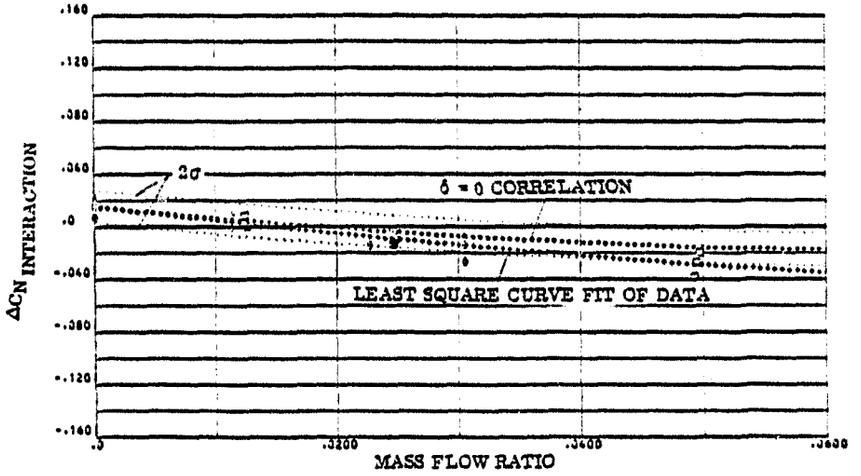

FIGURE 3-42d. : YAW RCS INCREMENTAL EFFECTS DUE TO +10 DEGREE ELEVON DEFLECTION FROM 5 TO 10 DEGREES ANGLE OF ATTACK; NORMAL FORCE

SYMBOLS	NOZZLE NUMBER	TEST NUMBER
0	N81	MA 22
□	N85	MA 22

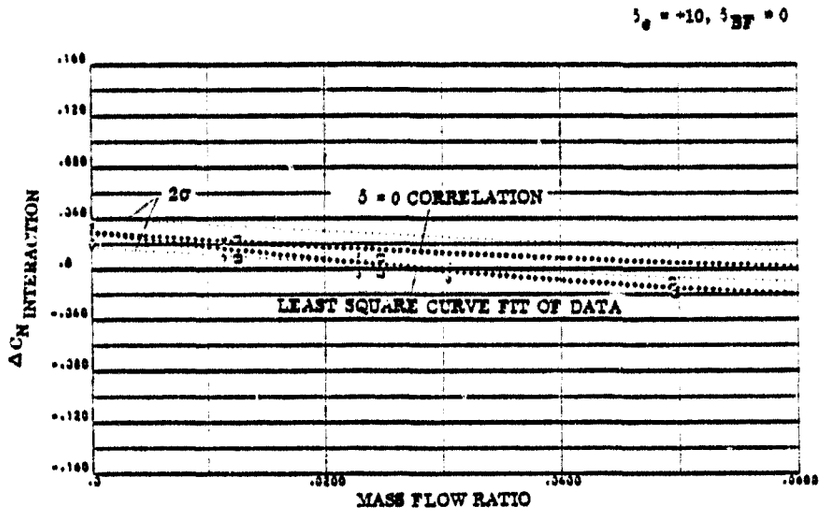

FIGURE 3-42e. : YAW RCS INCREMENTAL EFFECTS DUE TO +10 DEGREE ELEVON DEFLECTION FROM 10 TO 15 DEGREES ANGLE OF ATTACK; NORMAL FORCE

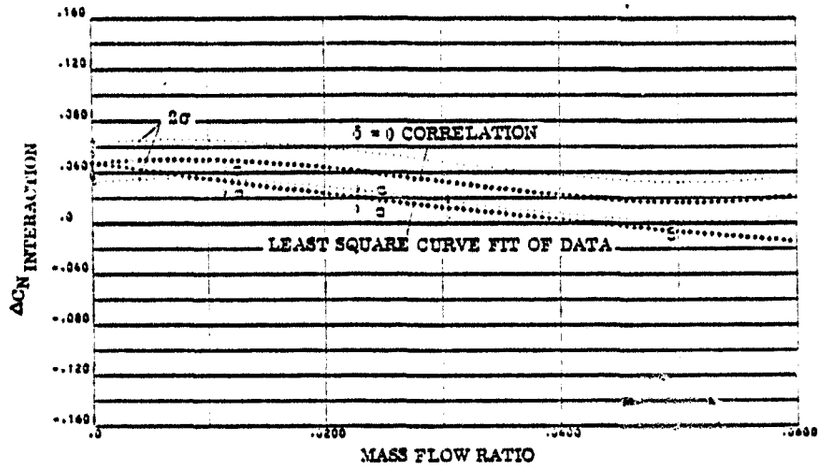

FIGURE 3-42f. : YAW RCS INCREMENTAL EFFECTS DUE TO +10 DEGREE ELEVON DEFLECTION FROM 15 TO 20 DEGREES ANGLE OF ATTACK; NORMAL FORCE

SYMBOLS	NOZZLE NUMBER	TEST NUMBER
0	N51	MA 22
□	N85	MA 22

$\delta_e = +10, \delta_{BF} = 0$

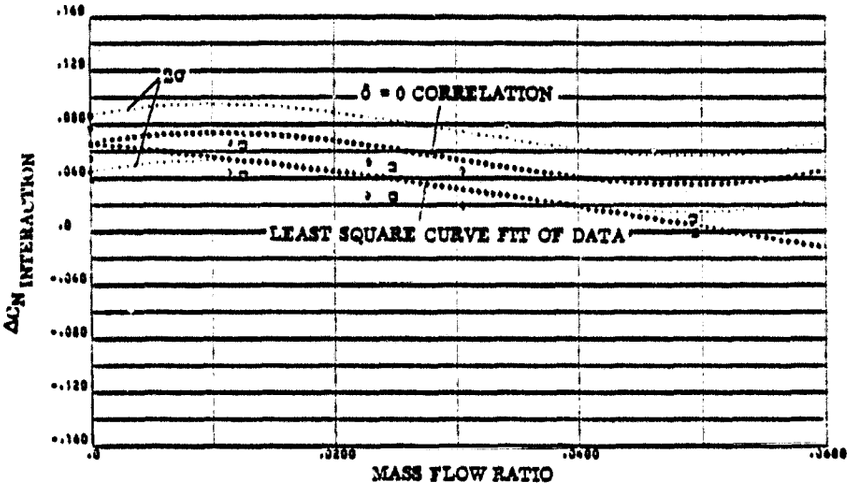

FIGURE 3-42g. : YAW RCS INCREMENTAL EFFECTS DUE TO +10 DEGREE ELEVON DEFLECTION FROM 20 TO 25 DEGREES ANGLE OF ATTACK; NORMAL FORCE

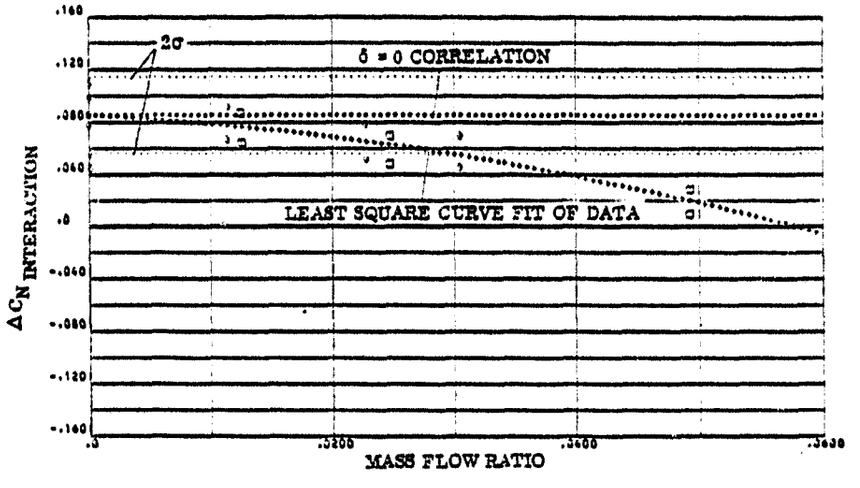

FIGURE 3-42h. : YAW RCS INCREMENTAL EFFECTS DUE TO +10 DEGREE ELEVON DEFLECTION FROM 25 TO 30 DEGREES ANGLE OF ATTACK; NORMAL FORCE

SYMBOLS	NOZZLE NUMBER	TEST NUMBER
0	N81	MA 22
□	N86	MA 22

$\delta_e = +10, \delta_{EF} = 0$

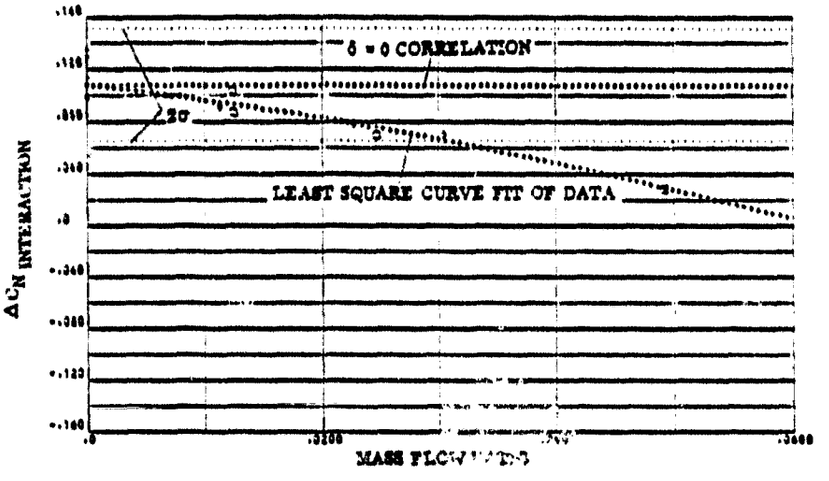

FIGURE 3-421. : YAW RCS INCREMENTAL EFFECTS DUE TO DEGREE ELEVON DEFLECTION FROM 30 TO 35 DEGREES ANGLE OF ATTACK; NORMAL FORCE

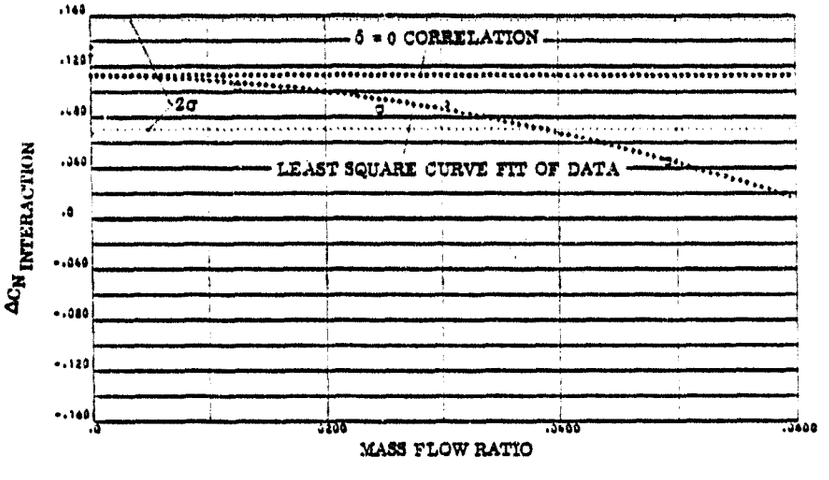

FIGURE 3-421. : YAW RCS INCREMENTAL EFFECTS DUE TO DEGREE ELEVON DEFLECTION FROM 35 TO 42.5 DEGREES ANGLE OF ATTACK; NORMAL FORCE

SYMBOLS	NOZZLE NUMBER	TEST NUMBER
○	N61	MA 22
□	N65	MA 22

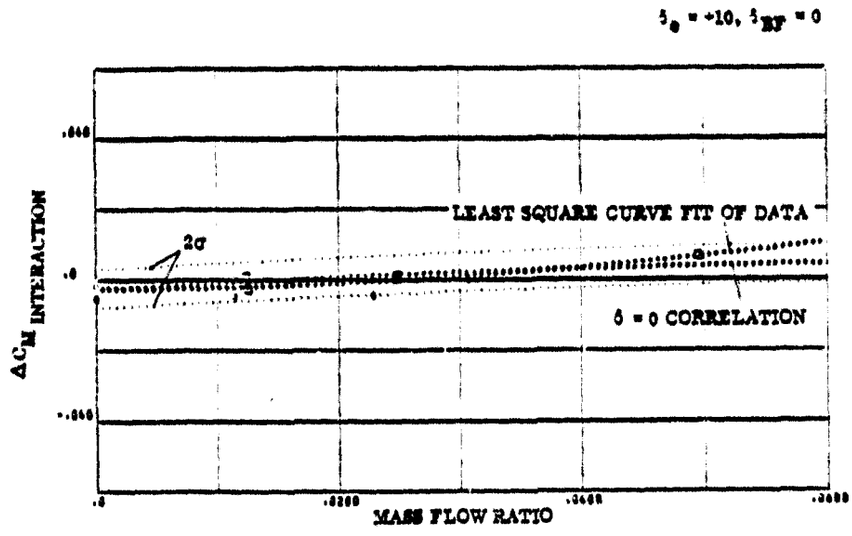

FIGURE 3-43a. : YAW RCS INCREMENTAL EFFECTS DUE TO +10 DEGREE ELEVON DEFLECTION FROM -10 TO -5 DEGREES ANGLE OF ATTACK; PITCHING MOMENT

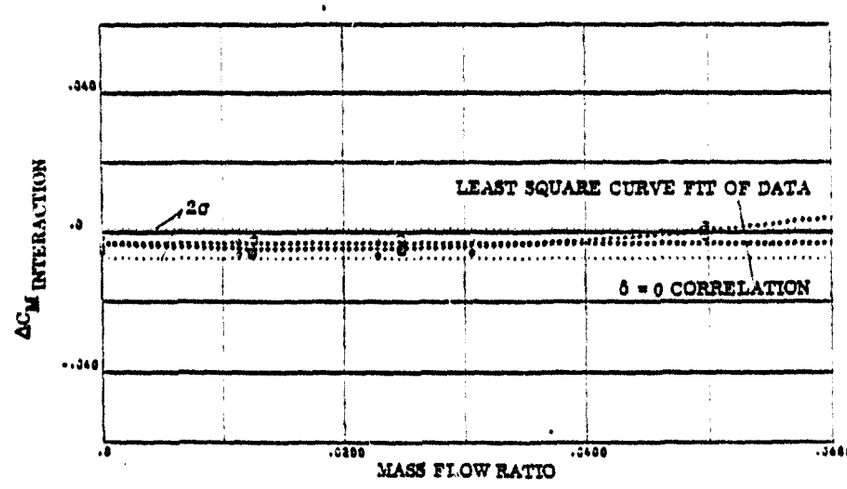

FIGURE 3-43b. : YAW RCS INCREMENTAL EFFECTS DUE TO +10 DEGREE ELEVON DEFLECTION FROM -5 TO 0 DEGREES ANGLE OF ATTACK; PITCHING MOMENT

SYMBOLS	NOZZLE NUMBER	TEST NUMBER
○	N81	MA 22
□	N85	MA 22

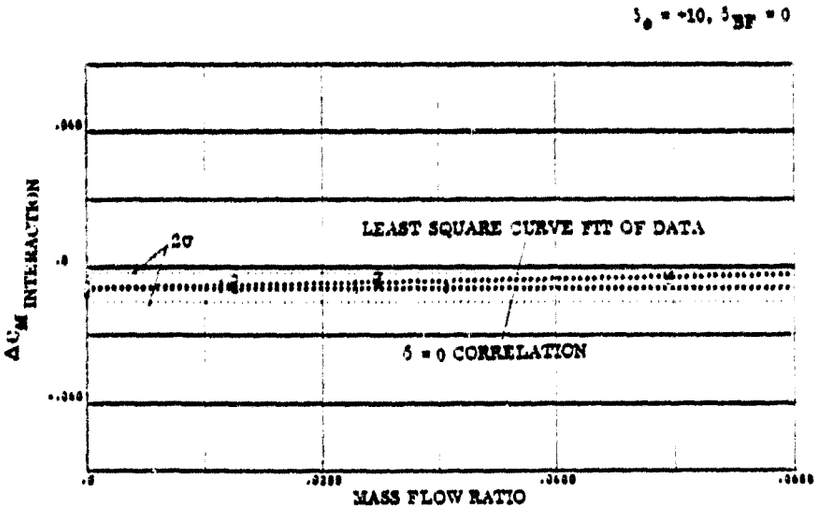

FIGURE 3-43c. : YAW RCS INCREMENTAL EFFECTS DUE TO +10 DEGREE ELEVON DEFLECTION FROM 0 TO 5 DEGREES ANGLE OF ATTACK; PITCHING MOMENT

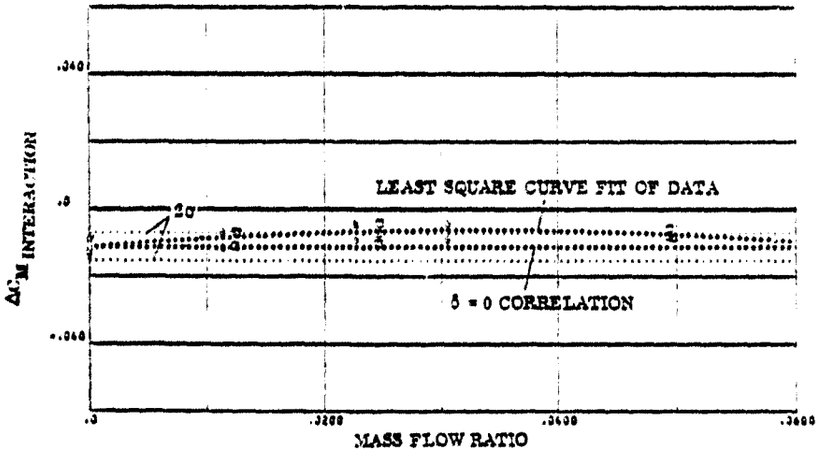

FIGURE 3-43d. : YAW RCS INCREMENTAL EFFECTS DUE TO +10 DEGREE ELEVON DEFLECTION FROM 5 TO 10 DEGREES ANGLE OF ATTACK; PITCHING MOMENT

SYMBOLS	NOZZLE NUMBER	TEST NUMBER
0	N61	MA 22
□	N65	MA 22

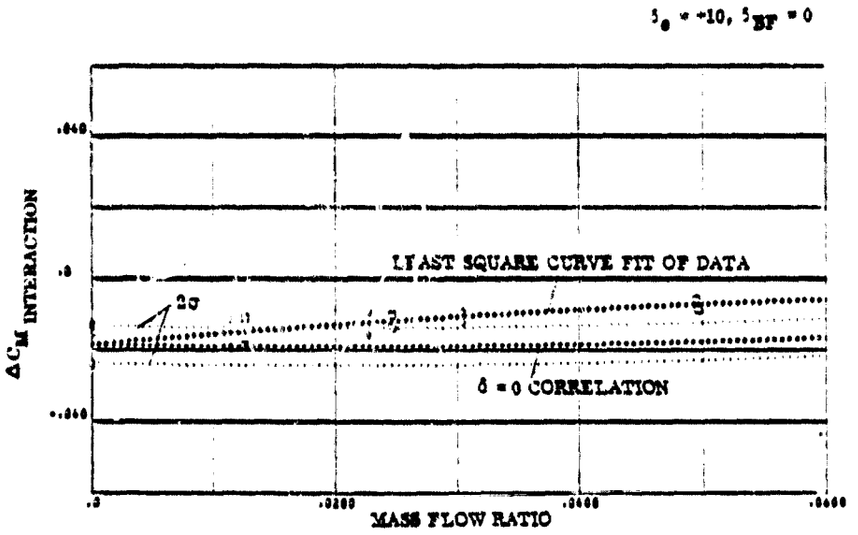

FIGURE 3-43e. : YAW RCS INCREMENTAL EFFECTS DUE TO +10 DEGREE ELEVON DEFLECTION FROM 10 TO 15 DEGREES ANGLE OF ATTACK: PITCHING MOMENT

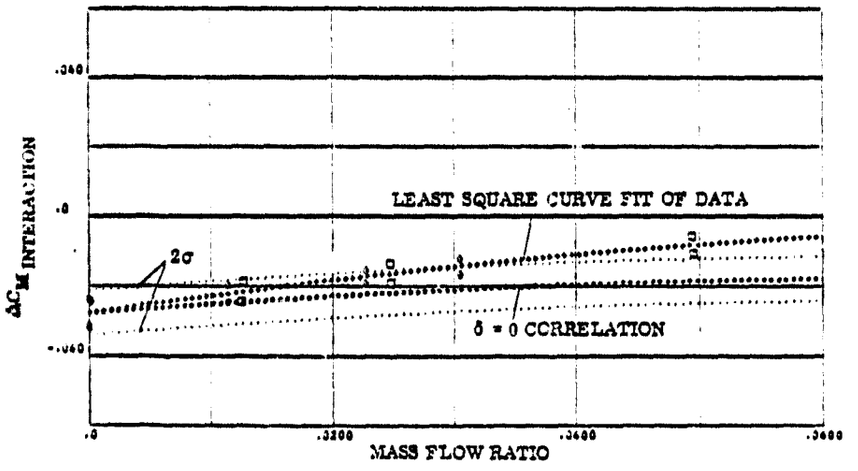

FIGURE 3-43f. : YAW RCS INCREMENTAL EFFECTS DUE TO +10 DEGREE ELEVON DEFLECTION FROM 15 TO 20 DEGREES ANGLE OF ATTACK: PITCHING MOMENT

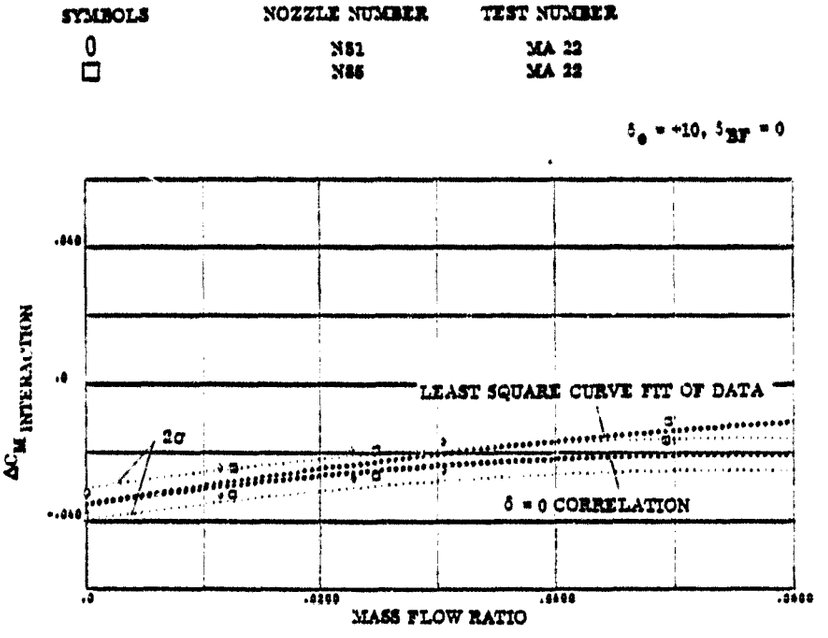

FIGURE 3-43g. : YAW RCS INCREMENTAL EFFECTS DUE TO +10 DEGREE ELEVON DEFLECTION FROM 20 TO 25 DEGREES ANGLE OF ATTACK; PITCHING MOMENT

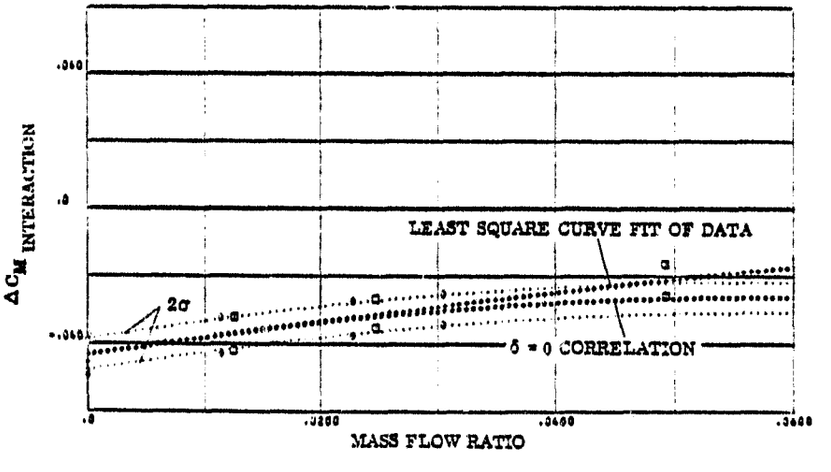

FIGURE 3-43h. : YAW RCS INCREMENTAL EFFECTS DUE TO +10 DEGREE ELEVON DEFLECTION FROM 25 TO 30 DEGREES ANGLE OF ATTACK; PITCHING MOMENT

SYMBOLS	NOZZLE NUMBER	TEST NUMBER
0	N51	MA 22
□	N55	MA 22

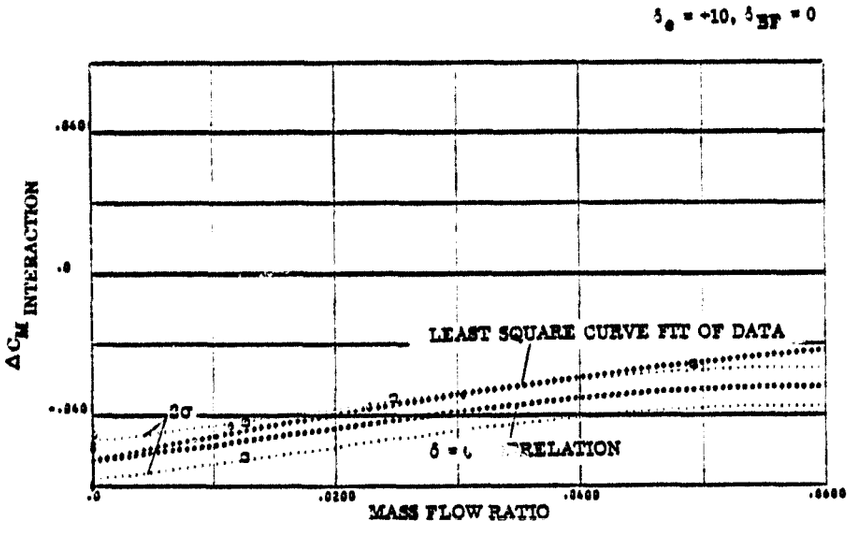

FIGURE 3-431. : YAW RCS INCREMENTAL EFFECTS DUE TO +10 DEGREE ELEVON DEFLECTION FROM 30 TO 35 DEGREES ANGLE OF ATTACK; PITCHING MOMENT

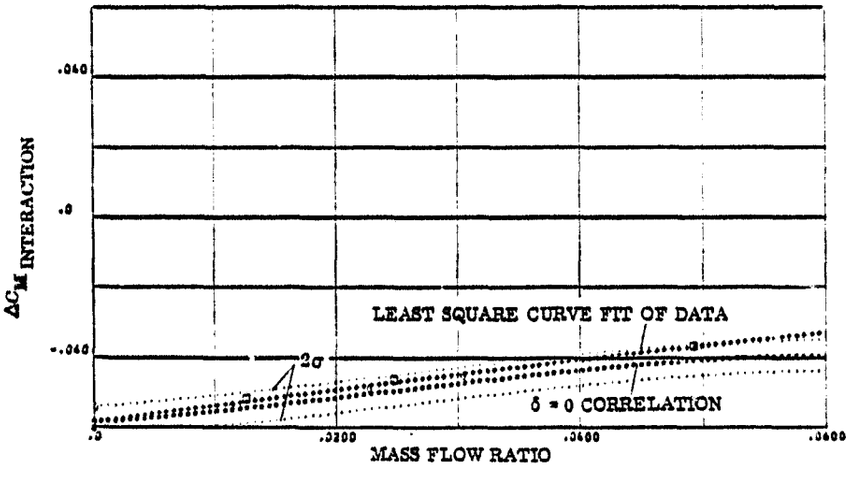

FIGURE 3-432. : YAW RCS INCREMENTAL EFFECTS DUE TO +10 DEGREE ELEVON DEFLECTION FROM 35 TO 42.3 DEGREES ANGLE OF ATTACK; PITCHING MOMENT

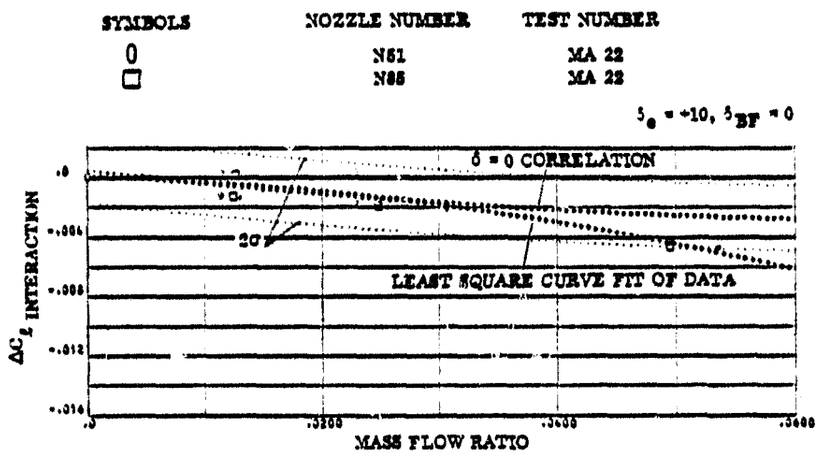

FIGURE 3-44a : YAW RCS INCREMENTAL EFFECTS DUE TO
+10 DEGREE ELEVON DEFLECTION FROM -10 TO
-5 DEGREES ANGLE OF ATTACK; ROLLING MOMENT

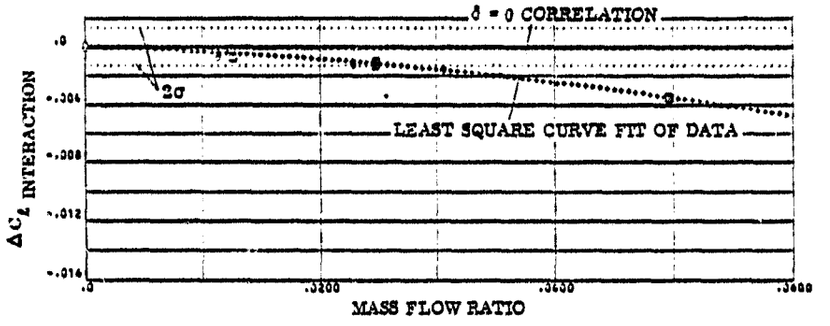

FIGURE 3-44b : YAW RCS INCREMENTAL EFFECTS DUE TO
+10 DEGREE ELEVON DEFLECTION FROM -5 TO
0 DEGREES ANGLE OF ATTACK; ROLLING MOMENT

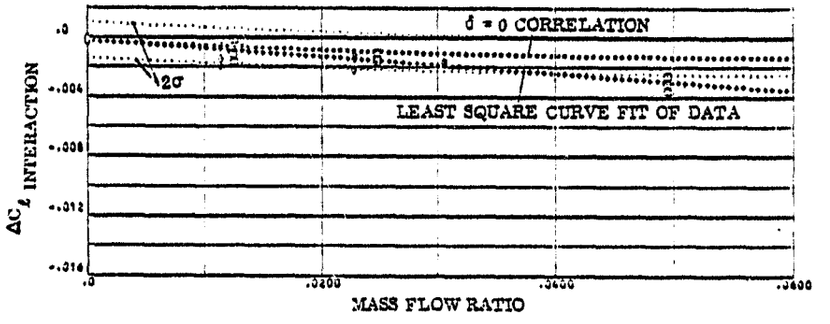

FIGURE 3-44c : YAW RCS INCREMENTAL EFFECTS DUE TO
+10 DEGREE ELEVON DEFLECTION FROM 0 TO
5 DEGREES ANGLE OF ATTACK; ROLLING MOMENT

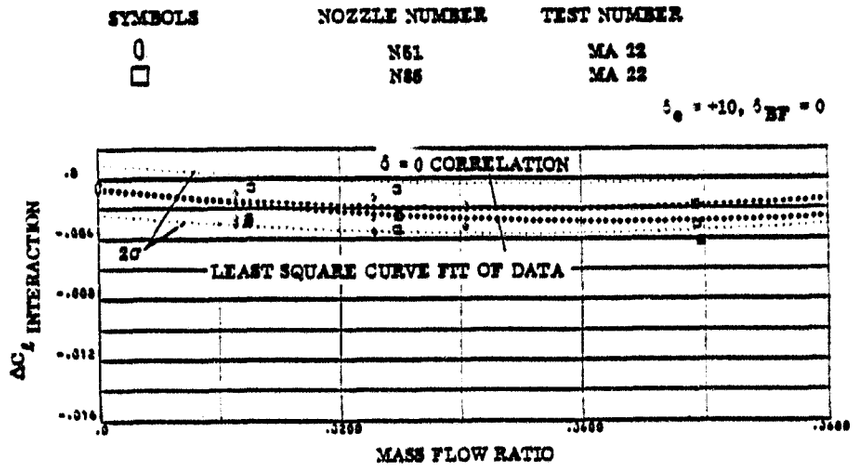

FIGURE 3-44d : YAW RCS INCREMENTAL EFFECTS DUE TO +10 DEGREE ELEVON DEFLECTION FROM 5 TO 10 DEGREES ANGLE OF ATTACK; ROLLING MOMENT

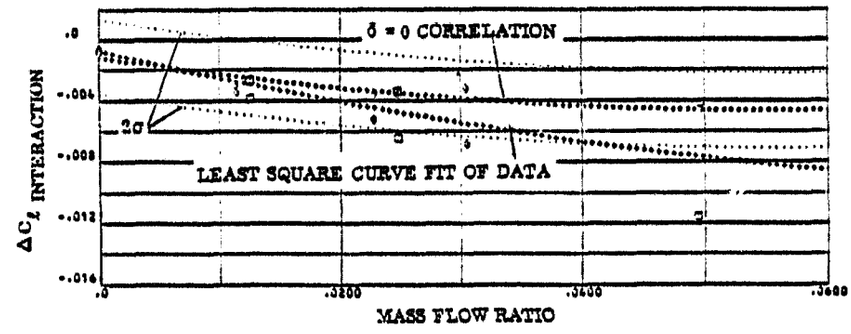

FIGURE 3-44e : YAW RCS INCREMENTAL EFFECTS DUE TO +10 DEGREE ELEVON DEFLECTION FROM 10 TO 15 DEGREES ANGLE OF ATTACK; ROLLING MOMENT

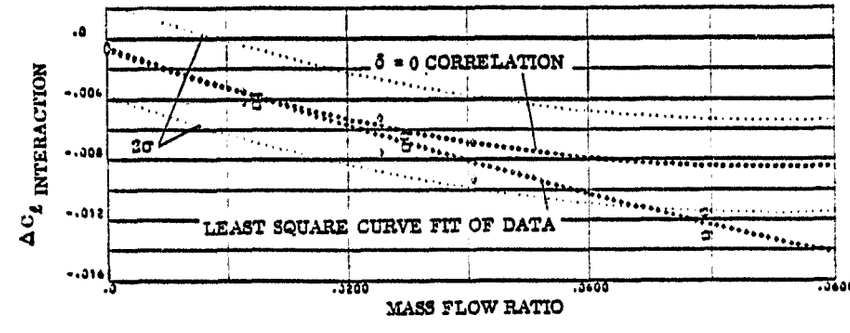

FIGURE 3-44f : YAW RCS INCREMENTAL EFFECTS DUE TO +10 DEGREE ELEVON DEFLECTION FROM 15 TO 20 DEGREES ANGLE OF ATTACK; ROLLING MOMENT

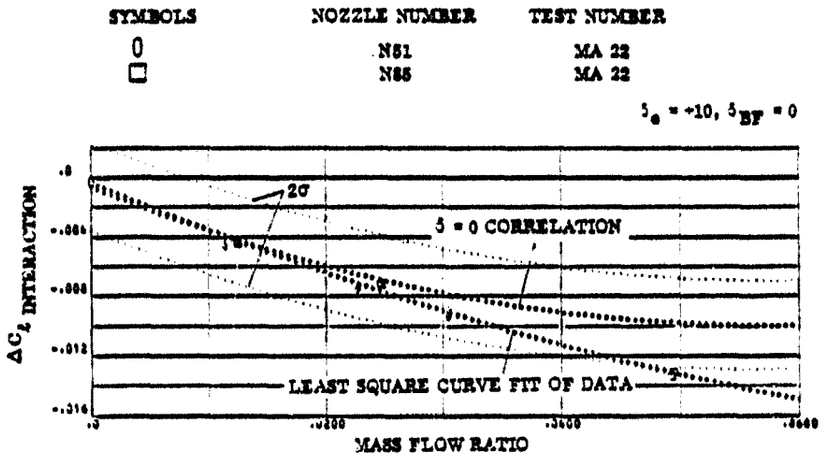

FIGURE 3-44g : YAW RCS INCREMENTAL EFFECTS DUE TO +10 DEGREE ELEVON DEFLECTION FROM 20 TO 25 DEGREES ANGLE OF ATTACK;

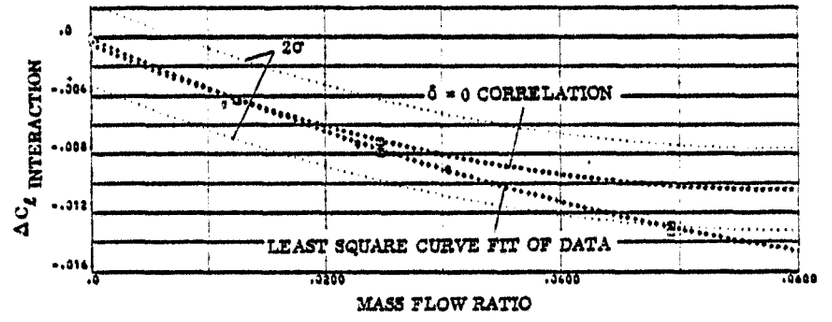

FIGURE 3-44h : YAW RCS INCREMENTAL EFFECTS DUE TO +10 DEGREE ELEVON DEFLECTION FROM 25 TO 30 DEGREES ANGLE OF ATTACK;

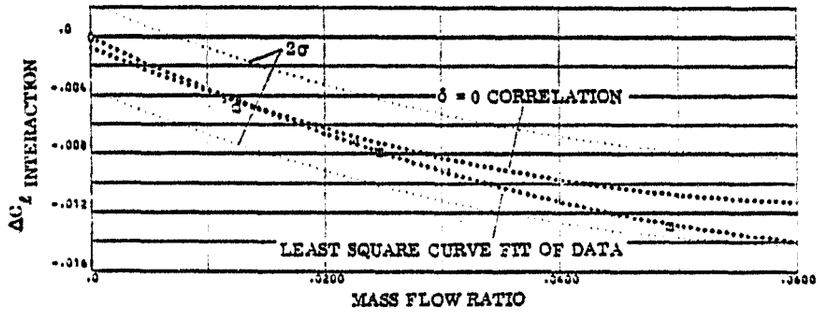

FIGURE 3-44i : YAW RCS INCREMENTAL EFFECTS DUE TO +10 DEGREE ELEVON DEFLECTION FROM 30 TO 35 DEGREES ANGLE OF ATTACK;

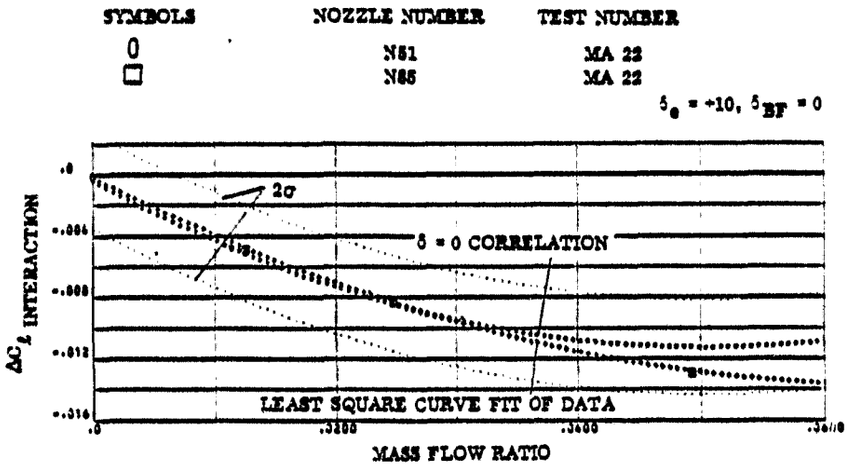

FIGURE 3-44j : YAW RCS INCREMENTAL EFFECTS DUE TO +10 DEGREE ELEVON DEFLECTION FROM 35 TO 42.5 DEGREES ANGLE OF ATTACK; ROLLING MOMENT

4

ANALYTIC MODEL DEVELOPMENT

4.1 GENERAL DESCRIPTION

The analytic model was initially developed and reported in Reference 3. The data analysis described in Section 3 refines the basic model in a number of ways but the basic approach remains the same. In general the total control effectiveness of a given control is defined as the sum of a number of parts as shown in Equation 1.

$$C_{M_{total}} = C_{M_{thrust}} + C_{M_{impingement}} + C_{M_{interaction}} + C_{M_{cross\ coupling}} \quad (1)$$

where

C_M = RCS force or moment component

and the resulting control effectiveness called control amplification is defined as an amplification factor which is the total control moment divided by the thrust moment

$$K_M = C_{M_{Total}} / C_{M_{thrust}} \quad (2)$$

where

K_M = RCS force or moment amplification factor

In addition to the effects in the thrust direction, the RCS controls induce out of plane forces and moments which are the sum of some terms given in Equation 1. The data of Section 3 showed that each time any reaction control thruster is fired measurable aerodynamic interactions occur in all 6 force and moment components which change the total effect on the vehicle. The 6 aerodynamic forces and moment components induced by either interaction or impingement must be added together on each axis to determine the total value of the induced moments.

The data was obtained and correlated in a normal force (C_N) - axial force (C_A) body axis system. The analytic model, however, has converted these coefficients to a true body axis system as shown in Figure 4-1 where the vertical force is C_Z and longitudinal force is given as C_X which are positive in the directions shown in this figure.

One basic assumption which relates to all parts of the reaction control system model is that if a discharge coefficient is defined it is always applied to the nozzle chamber pressure as a correction as given in Section 2 Equation 4.

The components of thrust used in Equations 1 and 2 are computed using the reaction control system nozzle geometry, operating characteristics, its location relative to the vehicle reference moment center, and the mounting angles of the nozzle relative to the vehicle axis system.

The thrust was computed as

$$T = N_N \left(P'_{o_j} A_T \sqrt{\frac{2\gamma^2}{\gamma-1}\left(\frac{2}{\gamma+1}\right)^{\frac{\gamma+1}{\gamma-1}}\left(1-\left(\frac{P_N}{P_o}\right)^{\frac{\gamma-1}{\gamma}}\right)} + A_N(P_N - P_\infty) \right) \quad (3)$$

where

T = Thrust of cluster

N_N = Number of nozzles firing in a cluster

$P_{oj} = C_D P_{oj}$ = Effective chamber pressure

C_D = Nozzle discharge coefficient (Section 2, Equation 3)

P_{oj} = Nozzle chamber pressure

$$P_N = P'_{oj} \left(1 + \frac{\gamma_j - 1}{2} M_j^2\right)^{-\frac{\gamma}{\gamma-1}} \quad (4)$$

P_N = Pressure at nozzle exit

γ_j = Nozzle gas specific heat ratio

P_∞ = Ambient pressure

A_T = Nozzle throat area

A_N = Nozzle exit area

and thrust coefficient as

$$C_T = \frac{T}{q\, S_{ref}} \quad (5)$$

where

q = Freestream dynamic pressure

S_{ref} = Reference (wing) area

4.2 INTERACTION COMPONENTS

4.2.1 Zero Deflection Computations

Tables 3-1 to 3-22 present the coefficients for the zero control deflection curve fit equations. The equations are evaluated in the form:

$$\Delta C_M = a_o + a_1 x + a_2 x^2 + a_3 x^3 \quad (6)$$

where

ΔC_M = Any RCS interaction force or moment coefficient

a_o to a_3 = Curve fit coefficients

x = Independent parameter for force or moment being fitted

In addition to the coefficients of the fit, each table has a specified minimum and maximum value of the independent variable. These values are used to limit the range of extrapolation of the curve fit and if x is greater than x_{max} then x_{max} is used to compute the interaction and the same is true on the minimum value. These maximum and minimum values were chosen as maximum or minimum points of the curve fit equations if such occur in or near the measured data range. If there are no maximum or minimum points the limits are generally set to the limits of the measured data range.

Each curve fit expression was developed for a given range of angle of attack which was usually a 5 degree interval. The question of how to treat different angles of attack within a given interval was treated by assuming that the curve fit represents the best fit for the angle of attack in the middle of the interval and linear interpolation is performed for other angles between curve fits. For example if $\alpha = 15°$

$$\Delta C_{M_{15}} = \Delta C_{M_{12.5}} + (\Delta C_{M_{17.5}} - \Delta C_{M_{12.5}}) \frac{15 - 12.5}{17.5 - 12.5} \quad (7)$$

where

$\Delta C_{M_{15}}$ = RCS interaction at 15 degrees

$\Delta C_{M_{12.5}}$ = RCS interaction curve fit result at 12.5 degrees

$\Delta C_{M_{17.5}}$ = RCS interaction curve fit result at 17.5 degrees

The data was obtained in 5 degree increments at the higher angles of attack and this fitting of data at the mid-points of such intervals meant that 2 sets of data were incorporated into each fit increasing the sample size for the fit. This approach also results in smoother interpolation between angles of attack since each angle of attack sample was used in two fits one above and one below the nominal measured angle. No extrapolation for angle is made above the midpoint of the last interval (37.5°) but extrapolations are made below the midpoint of the lowest interval.

4.2.2 Control Deflection Corrections

Tables 3-23 to 3-38 give the coefficients for the corrections to the interaction terms generated in Section 3. Control deflection curves were generated as the difference between the zero deflection curve fit and a curve fit through the data with the control deflected. Thus, the equation is

$$\Delta C_M = \Delta C_{M_{\delta_e=0}} + \Delta C_{M_{\delta_e}} \left(\frac{\delta_e}{\delta_{e_{REF}}} \right)^{.75} + \Delta C_{M_{\delta_{BF}}} \left(\frac{\delta_{BF}}{\delta_{BF_{REF}}} \right)^{.75} \quad (8)$$

where

ΔC_M = RCS interaction force or moment

$\Delta C_{M_{\delta_e=0}}$ = RCS interaction correction for zero control deflection

$\Delta C_{M_{\delta_e}}$ = RCS interaction correction for elevon deflection

$\Delta C_{M_{\delta_{BF}}}$ = RCS interaction correction for body flap deflection

δ_e = Elevon deflection

δ_{BF} = Body flap deflection

$\delta_{e_{REF}}$ = +10° or -30° depending on sign of δ_e

$\delta_{BF_{REF}}$ = +13.75° or -14.25° depending on sign of δ_{BF}

The ratio of elevon angle and body flap angle to reference conditions is needed to account for angles other than those tested which are the reference angles listed above. The .75 power shape of the interpolation for angle is based largely on jet-off data of elevator effectiveness such as Figure 4-2 which shows that the elevator effect is nonlinear.

4.3 INTERACTION CROSS COUPLING COMPONENTS

The present model of interaction has eliminated all cross-coupling interactions between RCS units except for the symmetric down firing RCS case. This correction was also generated as a difference in curve fits between the one side firing data and the symmetric case so that the effect of each side alone is computed and then the cross-coupling correction added separately.

The case of 2 nonequal numbers of down firing nozzles being used is taken into account by using the average momentum ratio between the sides to compute the correction.

4.4 PLUME IMPINGEMENT INCREMENTS

Figure 2-4 showed a view of the space shuttle orbiter which emphasizes the closeness of the rear RCS packages to the base area of the vehicle. It is evident that the aft RCS engines may impinge on the vehicle wing, vertical tail, body flap, main propulsion engine nozzles, and possible fuselage sides, depending on the nozzle set fired and on the altitude and other flight conditions affecting plume size. Reference 3 showed that plume impingement was a sizeable term in the earlier analytic model while Reference 7 shows the same for the present configuration based on a vacuum chamber test (Rockwell Test OA99) and impingement predictions for the vacuum case.

Two models of plume impingement were developed for the earlier analytic model of Reference 3 and have been refined for this updated model. Both are included in the prediction computer program presented in Section 5. The first model was developed from the OA99 vacuum chamber test and represents fits of measured impingement test data. It is limited in that control deflection effects are not included nor are free-stream effects on the plume. The second is an analytic prediction technique which computes impingement forces on a flat plate representation of the vehicle using a simple plume model to generate the local plume flow characteristics on each plate. It can handle control surface deflection but is limited in accuracy by the number of plates used and free stream distortion of the plume is only approximated.

4.4.1 Vacuum Test Data Model

The first model developed is based on the assumption that the range of interest of flight conditions for full scale RCS estimation is sufficiently close to the vacuum case that the test data amplification factors from test OA99 reported in Reference 7 can be used directly from the thrust and thrust moments. Converting the data into coefficient form, the impingement increments from the pitch up jets are given in Equations 9 to 14 in body axis form:

$$\Delta C_Z = .00086\, C_{T_{PU}}\, QF \tag{9}$$

$$\Delta C_X = .00266\, C_{T_{PU}}\, QF \tag{10}$$

$$\Delta C_Y = .06238\, C_{T_{PU}}\, QF \tag{11}$$

$$\Delta C_m = -.00078\, C_{T_{PU}}\, \frac{x_{PU}}{\bar{c}}\, QF \tag{12}$$

$$\Delta C_n = .0593\, C_{T_{PU}}\, \frac{x_{PU}}{B_{ref}}\, QF \tag{13}$$

$$\Delta C_\ell = -.13\, C_{T_{PU}}\, \frac{Y_{PU}}{B_{ref}}\, QF \tag{14}$$

where

$C_{T_{PU}}$ = (total thrust of pitch up engines)/(q S_{ref}) (15)

X_{PU} = X location of cluster relative to moment center

Y_{PU} = Y location of cluster relative to moment center

$QF = (1 - \frac{q_\infty}{20})$ (16)

q = Freestream dynamic pressure in PSF

The QF factor defined in Equation 16 was added to the vacuum model as an empirical approximation of the decay in impingement due to increasing flight dynamic pressure during entry. The 20 PSF cut off was developed from the predictions of Reference 3 using the analytic model which showed no impingement at dynamic pressures higher than that. All signs shown in these equations reflect in RCS unit being fired on the left side of the vehicle and X, Y and Z distances are negative numbers.

The pitch down reaction control jet impingement increments are given by Equation 17 to 22 where QF comes from Equation 16.

$$\Delta C_Z = .27389\, C_{T_{P_D}} QF \quad (17)$$

$$\Delta C_X = .10709\, C_{T_{P_D}} QF \quad (18)$$

$$\Delta C_Y = .00077\, C_{T_{P_D}} QF \quad (19)$$

$$\Delta C_m = -.00873\, C_{T_{P_D}} \frac{X_{P_D}}{\bar{c}} QF \quad (20)$$

$$\Delta C_n = .0013\, C_{T_{P_D}} \frac{X_{P_D}}{B_{ref}} QF \quad (21)$$

$$\Delta C_\ell = -.003477\, C_{T_{P_D}} \frac{Z_{P_D}}{B_{ref}} QF \quad (22)$$

where

$C_{T_{P_D}}$ = Total pitch down thrust coefficient of cluster

X_{P_D} = X location of pitch down RCS cluster relative to moment center

Z_{P_D} = Y location of pitch down RCS cluster relative to moment center

The yaw reaction control impingement equations are:

$$\Delta C_Z = .01634\, C_{T_Y}\, QF \tag{23}$$

$$\Delta C_X = .00288\, C_{T_Y}\, QF \tag{24}$$

$$\Delta C_Y = .00077\, C_{T_Y}\, QF \tag{25}$$

$$\Delta C_m = -.00873\, C_{T_Y} \frac{X_Y}{\bar{c}}\, QF \tag{26}$$

$$\Delta C_n = .0013\, C_{T_Y} \frac{X_Y}{B_{ref}}\, QF \tag{27}$$

$$\Delta C_\ell = -.03477\, C_{T_Y} \frac{Z_Y}{B_{ref}}\, QF \tag{28}$$

where

C_{T_Y} = Total yaw RCS thrust coefficient of engines in cluster

X_Y = X location of yaw thruster cluster relative to moment center

Z_Y = Z location of yaw thruster cluster relative to moment center

This model could not account for the difference in impingement due to nozzle geometry changes in the wind tunnel data and was not used to make the impingement corrections in that data. Because of this another model was developed to analytically predict the impingement components in the wind-tunnel data and to correct for it when deriving the interaction components.

4.4.2 Analytic Plume Impingement Model

The plume impingement model developed in Reference 3 and which was refined for this expanded analysis of the wind tunnel data consists of 4 parts which are

a) Equivalent nozzle plume centerline decay model

b) Off-center line shape

c) Plume pressure model

d) Surface pressure integration

This discussion will concentrate primarily on the changes to that model.

4.4.2.1 Equivalent Nozzle Plume Centerline Decay Model

The plume model developed in Reference 3 used a vacuum plume source flow approximation for the nozzle density distribution far from the nozzle:

$$\frac{\rho}{\rho_o} = B \left(\frac{x}{d^*}\right)^{-2} f(\theta) \tag{29}$$

where:

X = Distance from nozzle exit

d* = Nozzle throat diameter

$f(\theta)$ = Off-centerline model

where the constant B was shown to be principally a function of plume limiting turning angle.

$$B = \frac{(1.24 - .0040894\,\theta_\infty)}{2\gamma_j^2\,(1 - \cos\,\theta_\infty)} \tag{30}$$

where

γ_j = Jet exhaust plume gas specific heat ratio

θ_∞ = plume limiting turning angle at nozzle

A cluster of more than one nozzle firing was treated by an equivalent nozzle approach in which the throat diameter (d*) was computed from the sum of the throat areas of the nozzles in operation.

Examination of the test data shown in Reference 3 shows that the impingement appeared to be over-predicted at the higher nozzle pressures and the Mach 6 data analysis confirmed this. A re-examination of the plume model resulted in a change in the expression of the constant B which became

$$B = \frac{(.99 - .000016\,\theta_\infty^2)}{2\gamma_j^2\,(1 - \cos\,\theta_\infty)} \tag{31}$$

The equivalent nozzle assumption also appeared not to work well for a line of nozzles lying in a stream-wise direction.

A modified equivalent nozzle definition was chosen such that

$$d_e^* = \sqrt{\frac{4}{\pi} A^* \sqrt{N_N}} \tag{32}$$

where

d_e^* = Equivalent nozzle throat diameter

A^* = Single nozzle throat area

N_N = Number of nozzles operating in a cluster

4.4.2.2 Off -Centerline Plume Shape

The plume characteristics off the centerline of the nozzle were modeled in Reference 3 using Simon's model which defined $f(\theta)$ in Equation 29 as:

$$f(\theta) = \cos^{10}(\pi\theta/250);\ 0 < \theta < 60° \tag{33}$$

$$f(\theta) = 0.0438\,(e^{-0.064\,(\theta - 60°)});\ 60° < \theta \tag{34}$$

where

θ is angle from nozzle centerline in degrees

Reduction of the wind tunnel data showed that the plume limiting turning angle (θ_∞) did not in a number of cases exceed 60 degrees, so a correction was generated to the fixed 60 degree limitation given for the vacuum model

$$f(\theta) = \cos^{10}(\pi\theta/250) \text{ for } 0 < \theta < \theta' \tag{35}$$

$$f(\theta) = 0.0438\,(e^{-.064(\theta - \theta')} \text{ for } \theta' < \theta \tag{36}$$

$$\theta' = .8\,\theta_\infty \text{ for } 0 < \theta_\infty < 60° \tag{37}$$

$$\theta' = 60 \text{ for } 60° < \theta_\infty \tag{38}$$

where θ_∞ = plume limit turning angle

4.4.2.3 Plume Impingement Limits

The plume is assumed to stop in all cases when it will no longer interact with the external stream. This condition is computed as the condition where the

$$(P + q)_{plume} \leq (P_\infty + q_\infty) \tag{39}$$

local values of ambient pressure and dynamic pressure in the plume equal those of the free-stream. The effect of this limiting condition is most apparent for the plume exhausting upward past the fin (pitch up RCS) and outboard over the wing (yaw RCS) in terminating the plume before the most distant plates are reached. As dynamic pressure increases, this limit reduces the plume to the point where it no longer impinges on any surface and impingement ceases. As the vacuum case is approached, the limit disappears and only the plates not exposed to the plume see no impingement. A further check on this limit is made in computation of impingement pressure coefficients. If the impingement pressure is less than free stream ambient, the plume is terminated and zero pressure coefficient is assumed.

4.4.2.4 Plume Impingement Forces

The highly underexpanded flow from the nozzle expands very quickly to high Mach numbers at small distances from the exit and this supersonic flow will be undistrubed by an impingement surface until it is close to the surface. A detached shock wave would be formed by the high Mach number flow impinging on the surface with a region of subsonic flow between the strong shock and the surface where the flow is turned to a direction paralleling the plate. The pressure on the surface of the vehicle was assumed to be related only to the plume conditions at the point in question and to the local slope between the surface at that point and the plume flow vector emanating from the point source at the nozzle exit (radial flow approximation). It was also assumed in Reference 3 that the surface pressure could be predicted by a modified Newtonian pressure law because of the high plume Mach numbers and large turning angles.

$$P_{w_i} = C_{P_S} \frac{\gamma_j}{2} P_{j_i} M_{j_i}^2 \cos^2 \theta_i + P_{j_i} \tag{40}$$

where

P_{w_i} = Plume impingement pressure at ith point on body

P_{j_i} = Plume ambient pressure at point i

M_{j_i} = Plume Mach number at point i

θ_i = Local slope between plume flow and surface at point i

γ_j = Plume exhaust gas specific heat ratio

$$C_{P_S} = \frac{\gamma_j + 3}{\gamma_j + 1}\left(1 - \frac{2}{(\gamma_j + 3)\, M_j^2}\right) = \text{Lee's stagnation pressure approximation} \quad (41)$$

If the local slope is negative, a limited hypersonic flow expansion law approximation from Reference 9 is used:

$$P_{w_i} = \frac{\gamma}{.2436}\, P_{j_i} \sin \theta_i + P_{j_i} \quad (42)$$

Here the limiting check on local pressure being less than free-stream will terminate the pressure computations before the slope becomes large.

The local plume impingement pressure is then converted into a pressure coefficient related to ambient flight conditions to put it into the same reference as the vehicle aerodynamic coefficients and is integrated to obtain vehicle force and moment coefficients resulting from impingement.

The integration of impingement pressures was approximated in the analytic model by breaking elements of the vehicle into flat plates of known centroid location, area, and local slope, the plume impingement pressures at each point were computed, the local force and moment coefficients computed by applying the impingement pressure across the area, and the total vehicle values obtained by summing the local values. Only one side of the vehicle is represented to increase the accuracy by having a larger number of plates which will have impingement but to reduce the computation time for plates not affected. Reference 3 presented sketches of the plates used in this model. The method of computation was revised to keep track of the flat plates representing the elevon and body flap and rotation of these around their hinge lines was added to account for the effects of control deflection.

This solution was checked against the OA99 test data and a method of characteristics solution in Reference 3 and close agreement was obtained.

4.5 ERROR ESTIMATION

The analysis performed in Section 3 resulted from least square curved fits being generated through relatively large numbers of data points. In addition to the curve fit coefficients being generated, the root-mean-square error of all of the points to the curve fit was generated. When the number of points is large it is expected that the RMS error is a good measure of the standard deviation of the data error and these values were retained with each curve as the basis for the estimation of the error.

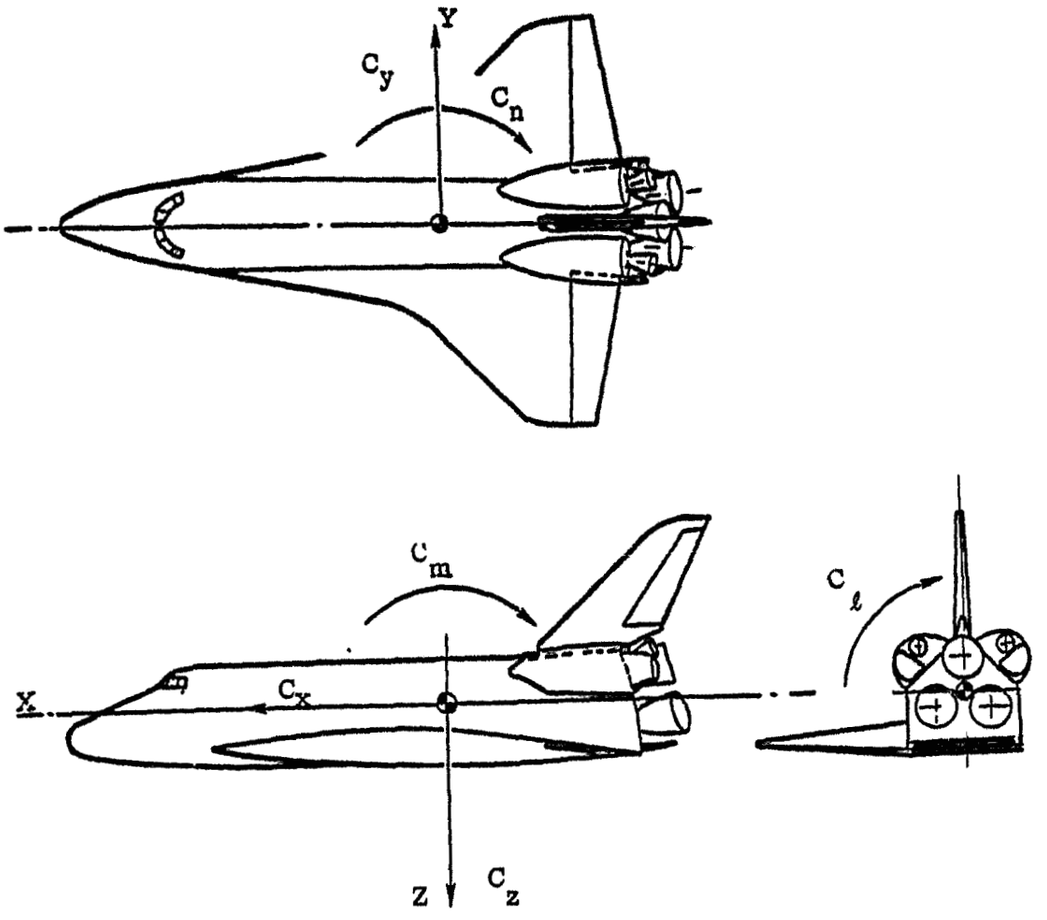

$C_N = -C_z$

$C_A = -C_x$

Figure 4-1. Body Axis Sign Convention

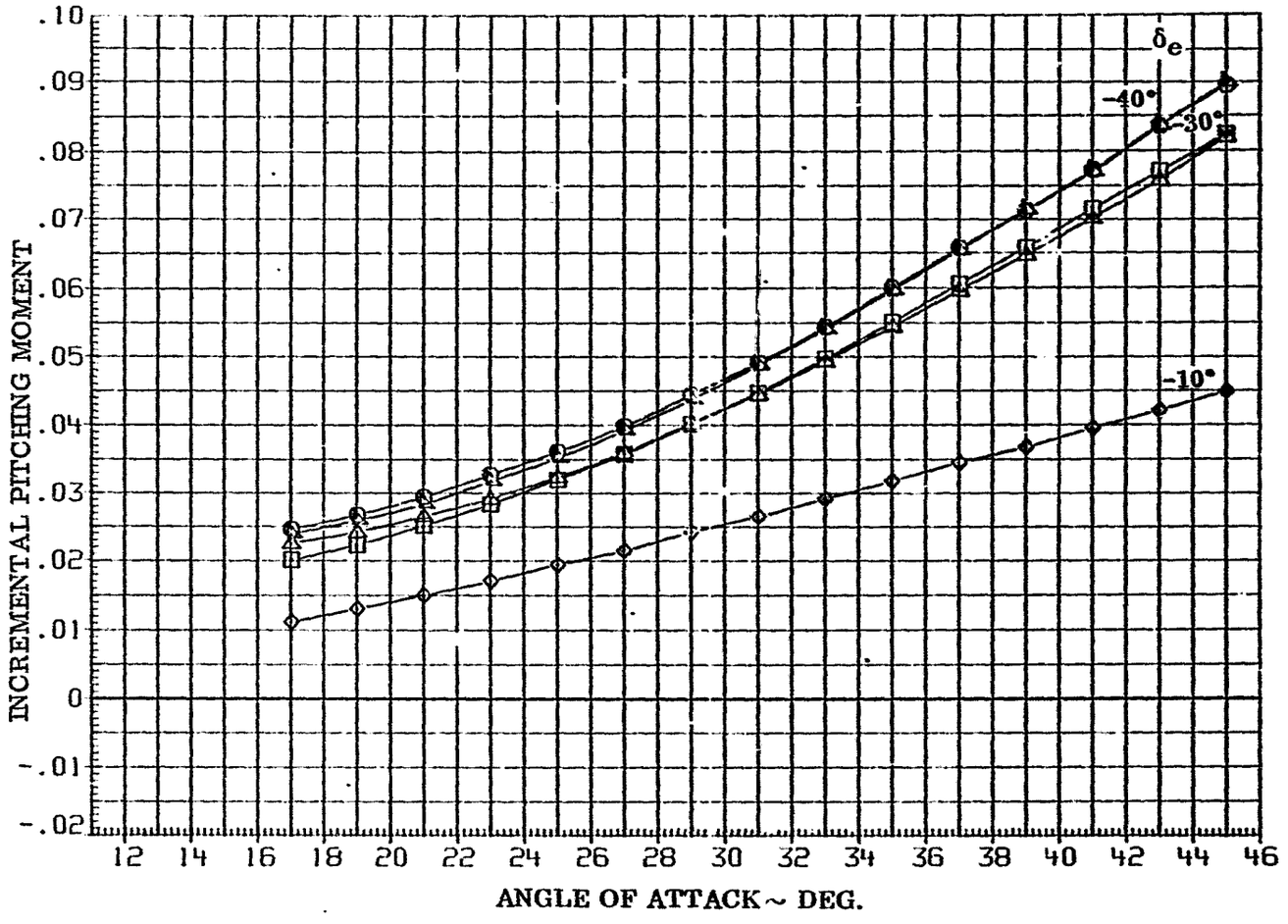

FIGURE 4-2. TEST OA77 ELEVATOR EFFECTIVENESS AT MACH 6 WITH NO RCS

5

ANALYTIC COMPUTER PROGRAM

5.1 GENERAL DESCRIPTION

An anlytic computer prediction model for rear mounted reaction control system effectiveness was developed and reported in Reference 3 . This computer program was completely revised based on the data correlations of Section 3 and the resulting changes to the analytic model discussed in Section 4.

This digital computer program named PRED will predict reaction control system effectiveness on a space shuttle type vehicle for any combination of Rear RCS engines firing at any angle of attack and flight condition up to the vacuum case. Numbers of RCS Engine, engine size, engine operating conditions, exhaust gas properties, and nozzle geometry can be varied as input parameters. Engine location on the rear of the vehicle and cant angles can also be varied, however, the analytic models were developed from one configuration (Figure 2-1) and large departures from these RCS locations will invalidate the models of interaction and cross coupling terms.

Figure 5-1 presents a flow diagram of the program which consists of a main program and 14 subroutines. The program was divided into this large number of subroutines so that modification of any part could be more easily accomplished without disrupting the whole program. The names of the subroutines are:

1. INPUTT	6. THR	11. DEFL
2. JET	7. IMPINGE	12. NEWT
3. PARCEO	8. VACPLU	13. CCOUPL
4. ATMOS	9. INTER	14. AMPL
5. EXPAN	10. CUBIC	

The name of the main program is PRED and FORTRAN listings of all parts of the program are contained in Appendix A. Each subroutine will be briefly discussed in the sections below with the input subroutine and input key presented last.

5.2 MAIN PROGRAM PRED

Figure 5-1 shows that the function of the main program is to drive the subroutines in an orderly fashion first to obtain the input to start the problem, to define the equivalent nozzles firing upward, downward, and side ways, to define the flight conditions and resulting nozzle flow parameters for a single nozzle and then proceed to define the various components of total RCS effectiveness for each set of equivalent nozzles fixing up, down, and sideways. The program proceeds to do

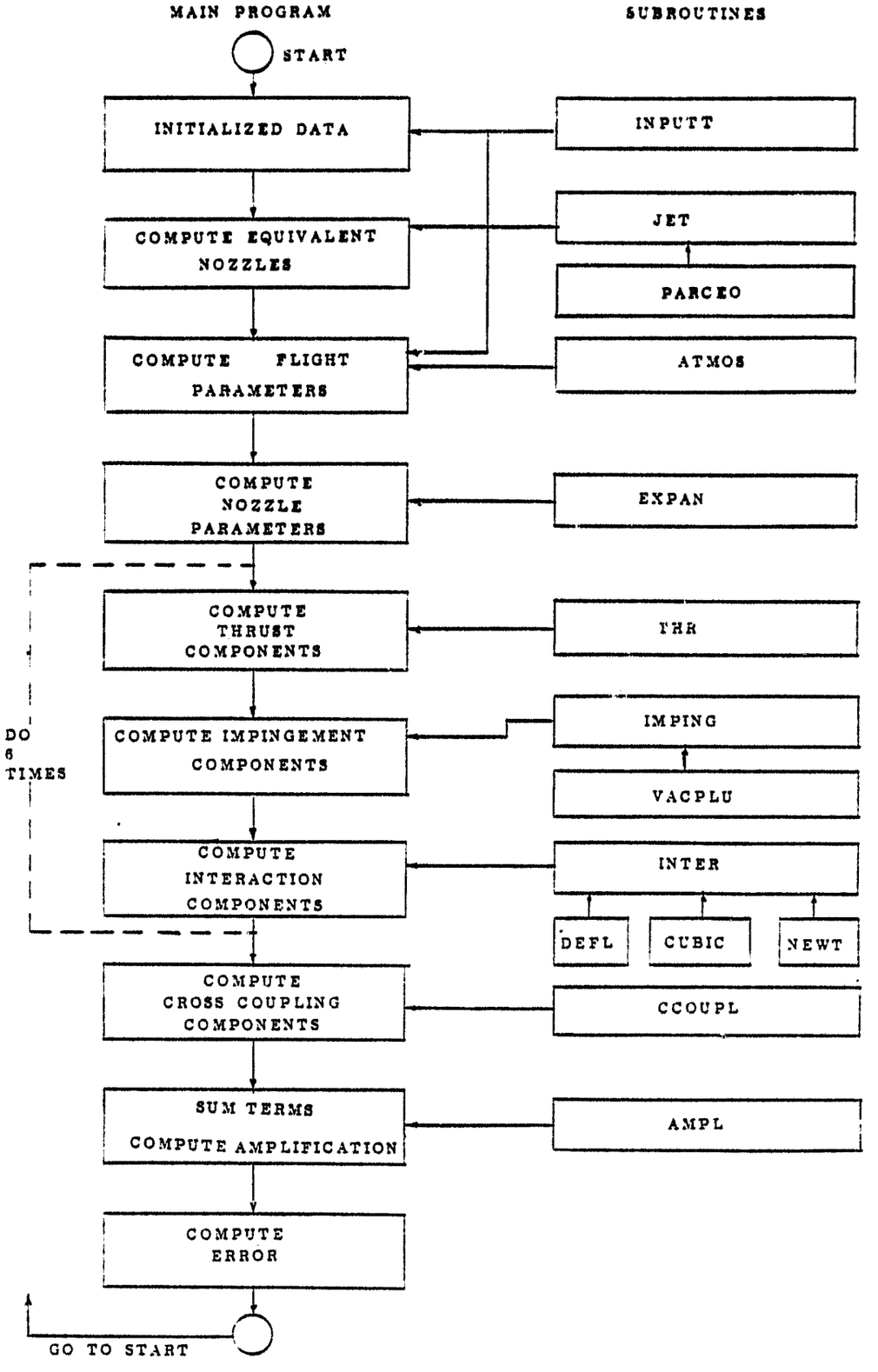

FIGURE 5-1: PRED PROGRAM SCHEMATIC

all remaining computations up to 6 times as required in the following order:

1. Pitch up left side nozzle terms
2. Pitch up right side nozzle terms
3. Pitch down left side nozzle terms
4. Pitch down right side nozzle terms
5. Yaw left side nozzle terms
6. Yaw right side nozzle terms

where the numbers of nozzles and their location in each plane are defined in the input. Checks are made for the number of nozzles in each group to avoid the non-firing sets and to minimize computation time. The data from the right and left sides for each type are summed into total for that type (i.e., pitch up). The cross coupling terms are then determined and all of the components of data are summed into the 6 total RCS aerodynamic force and moment coefficients and the amplification factors determined. The 2 sigma errors are estimated for each component sum and the program returns to the beginning to start the next case. All input comes into the program through the INPUTT subroutine, but the main program handles most of the output printing at various stages throughout its length.

The program is set up to assume all RCS nozzles are on the left side of the vehicle when viewed from the rear looking forward in order to standardize the data for the impingement calculation and to set the signs of the interaction models. The signs of the data for nozzles on the right side of the vehicle are corrected when the right and left components are summed for each control axis (i.e., pitch up). The axis system used is a body axis system shown in Figure 4-2 and the component data has these designations CX, CY, CZ, CL, CM, CN as the first two letters of the variable name where CN refers to yawing moment. Finally where the component force or moment is derived from is specified by the two middle letters of the variable names and IM is an impingement force or moment component, IN is an component, and CC is a cross-coupling component. The thrust terms have no component designation and thus are 3 letter variable names while the others are 5 letter names. The RCS directions are designated by the last letter of a variable name in the listing, where upward firing has a U as the last letter, downward firing is designated by a D as the last letter, and side firing designated by a Y as the last letter. The program always assumes that there are some upward, downward, and side firing nozzles in each problem so that all of the components are computed for all three sets before the summation of terms is made.

A typical example of a variable name is CMIMU which is the pitching moment induced by plume impingement of the upward firing nozzles. Figure 5-2 shows that the program assumes that a downward firing set, an upward firing set, and a side firing set exist for a given problem. A set of nozzles is defined in this program as the actual number firing in a given cluster on one side of the vehicle. It is not the total number available to fire on one side nor the total number firing on

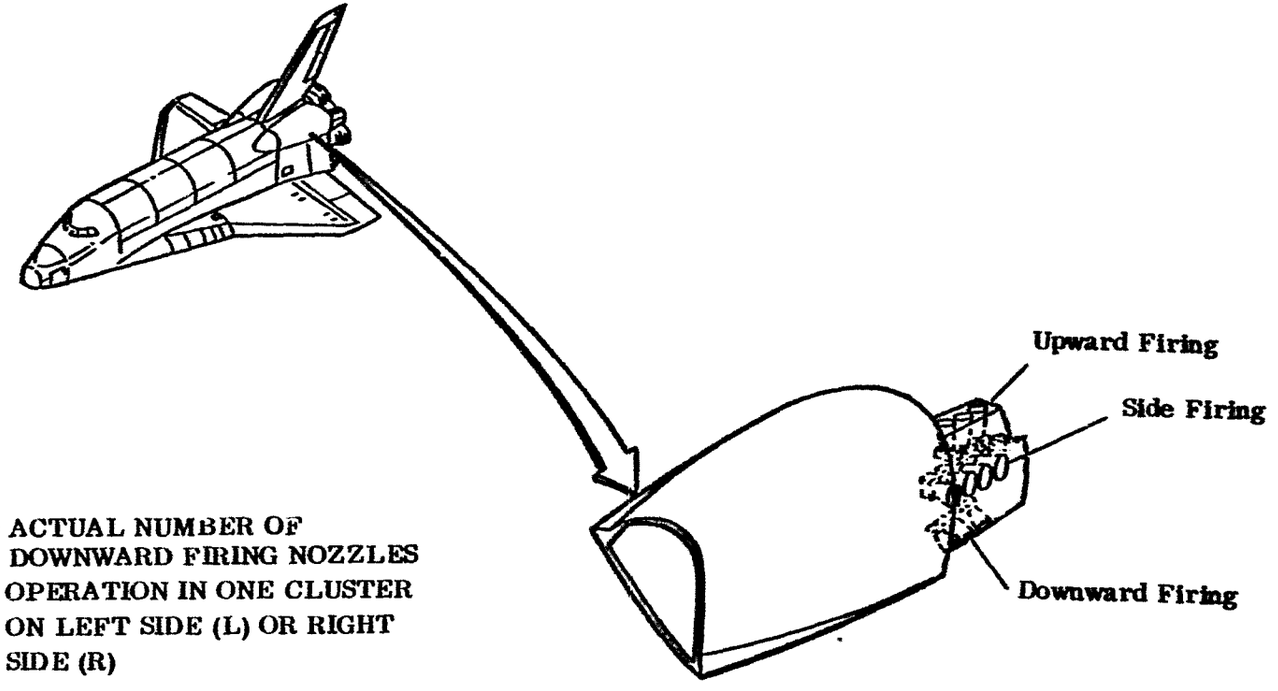

NONOZDL
NONOZDR = ACTUAL NUMBER OF DOWNWARD FIRING NOZZLES OPERATION IN ONE CLUSTER ON LEFT SIDE (L) OR RIGHT SIDE (R)

NONOZUL
NONOZUR = ACTUAL NUMBER OF UPWARD FIRING NOZZLES, ETC.

NONOZYL
NONOZYR = ACTUAL NUMBER OF SIDE FIRING NOZZLES, ETC.

FIGURE 5-2 NOZZLE SET CONVENTION

both sides in a symmetric firing case. Six numbers must be input for each colution:

a) NONOZUR = number of nozzles firing in pitch up cluster on right side
b) NONOZUL = number of nozzles firing in pitch up cluster on left side
c) NONOZDR = number of nozzles firing in pitch down cluster on right side
d) NONOZDL = number of nozzle firing in pitch down cluster on left side
e) NONOZYR = number of nozzles firing in yaw cluster on right side
f) NONOZYL = number of nozzles firing in yaw cluster on left side

The input data required for a first case is all of the data defining the vehicle, RCS units, and flight conditions, however, once this has been defined only the parameters which are to be changed need be input for additional cases. The data must all be input for a full scale vehicle but the program will rescale the solution to any model scale if desired.

The main program computes the mass flow and momentum ratio parameters for each set of nozzles and drives the solution through the thrust, impingement, interaction, and cross coupling routines to obtain the individual components of each generated by the pitch up nozzles, pitch down nozzles, and yaw nozzles and which are printed out. When all of these components are obtained a summation is made of the total values of the 6 aerodynamic force and moment coefficients resulting from the reaction control system operation and these are printed out.

Provisions have also been made to estimate the error associated with each of the components of the total aerodynamic forces and moments in terms of a standard deviation. These then are totaled as for each aerodynamic coefficient as

$$\sigma_{\text{total}_{C_M}} = \sqrt{\Sigma\, \sigma^2_{\text{component}_{C_M}}} \qquad (1)$$

where

$\sigma_{\text{component}_{C_M}}$ = Standard deviation of any aerodynamic force or moment from an individual nozzle cluster

$\sigma_{\text{total}_{C_M}}$ = Standard deviation of total RCS aerodynamic force or moment.

A limited set of amplification factors are computed and printed out and the last thing the main program does is to compute and print the 95% (2σ) error band of each aerodynamic force and moment coefficient. The program then proceeds to the next case.

A general description of each subroutine and its function to the main program will now be presented.

5.3 COMPUTE JET EXIT MACH NUMBER (SUBROUTINES JET AND PARCEO)

After the program has received input defining the reaction control system engine in terms of nozzle expansion ratio (A/A*), effective chamber pressure (P'_{oj}) chamber temperature (T_{oj}), and exhaust gas specific heat ratio (γ), the subroutine JET is called to determine the nozzle exit conditions for this engine. The exit conditions are exit Mach Number (M_j), static pressure (P_j) and static temperature (T_j).

Exit Mach number is computed by solving the Prandtl Meyer expansion ratio Mach number relationship (Ref. [3]).

$$A/A^* = \left(\frac{\gamma_j + 1}{2}\right)^{\frac{\gamma_j + 1}{2(\gamma_j - 1)}} M_j \left(1 + \frac{\gamma_j - 1}{2} M_j^2\right)^{\frac{\gamma_j + 1}{2(\gamma_j - 1)}} \quad (2)$$

Jet solves this expression by computing expansion ratio for increasing jet Mach numbers until the correct expansion ratio has been passed saving the last 3 values of each. When the correct expansion ratio is passed, JET calls the subroutine PARCEO to put a quadratic curve fit through the expansion ratio-jet Mach points and PARCEO returns the coefficients of the equation which JET then solves for jet Mach number. With jet exit Mach number determined the jet exit static pressure and temperature are computed from isontropic flow relations. In addition JET computes some constants which are related to specific heat ratio, pressure ratio, and thrust from the flow through the nozzle throat for use in later routines.

Equation 4 in Section 2 defined the effective chamber pressure as the actual pressure multiplied by the nozzle discharge coefficient. Since it was desirable to compute both wind tunnel results and flight results this correction is used in the INPUTT subroutine and all computations based on chamber pressure have this correction in them.

PARCEO is a standard quadratic curve jet routine which will give the coefficients for a curve through any 3 sets of points defined in the call statement. The main program defines the throat diameters of the single equivalent nozzles for each cluster of upward (DSTARUL, DSTARUR) downward, (DSTARDL, DSTARDR), and side (DSTARYL, DSTARYR) firing sets and the equivalent nozzle exist area (AEXUL, etc.) before proceeding to the definition of flight conditions.

5.4 COMPUTE FLIGHT PARAMETERS (SUBROUTINE ATMOS)

The input subroutine provides data required by the program at this point to define the flight conditions in one of four allowable ways defined by an input parameter (IOPT):

a) IOPT = 1 altitude, Mach, and angle of attack specified

b) IOPT = 2 altitude, velocity, and angle of attack specified

c) IOPT = 3 altitude, freestream dynamic pressure, and angle of attack specified

d) IOPT = 4 Mach, ambient pressure, ambient temperature, and angle of attack specified

The first 3 options require an atmosphere model to define ambient pressure and ambient temperature and the program currently contains a subroutine ATMOS which provides these data from the 1962 US Standard atmosphere model. The fourth option is a means of expressing an arbitrary flight condition from some other atmosphere model or for a wind tunnel test.

Subroutine ATMOS can provide a number of flight parameters not currently used in this program including local gravity for an oblate earth model, atmosphere density, local speed of sound, dynamic pressure, absolute viscosity, kinematic viscosity, and stagnation temperature on a reference sphere. The program consists of curve fits of atmospheric properties from sea level to 230,000 meters (754,600 ft) and all conditions are set to zero above this altitude.

The vacuum case ($P_\infty = q = 0$) is treated in a special way in the program to avoid division by zero. A flag is set in the program and dynamic pressure (q) is set equal to .00001 PSF. The interaction terms are not computed for the vacuum case nor are cross coupling terms which are not related to impingement. The force and moment coefficients printed are based on a q of 1×10^{-5} PSF while the amplification factors are independent of q.

With the flight conditions defined, all the required data is in the program and the RCS effectiveness computed. In order to do this the RCS nozzle parameters must be computed.

5.5 COMPUTE SINGLE NOZZLE PARAMETERS (SUBROUTINE EXPAN)

The nozzle parameters necessary to compute the RCS effectiveness include RCS engine thrust coefficient (TCOEF), jet exit momentum ratio parameter (RMFS), and jet mass flow parameter (FMR). These are all computed for a single nozzle and then multiplied by the number of nozzles in each set to obtain parameters for the six nozzle clusters within the main program where the equivalent nozzle effective jet exit momentum ratio is defined in Section 3, Equation 5 and the mass flow parameter is defined in Section 3, Equation 7. Momentum ratio relationships are used for pitch up and pitch down nozzles exclusively while the mass flow parameter is used for yaw RCS only.

Plume limit turning angle (TURN) is also required to define the plume decay characteristics as well as the extent of the plume for impingement calculations, it however is not related to the number of nozzles but rather to jet exit and free-stream conditions. The limit turning angle is computed in subroutine EXPAN based on Prandtl-meyer expansion of the flow from RCS chamber conditions to freestream ambient pressure minus the expansion in the nozzle plus the nozzle exit angle.

The program prints the flight conditions as well as a larger number of nozzle parameters for the single RCS unit at this point in the main program winding up with the important nozzle interaction parameters for the six clusters.

5.6 COMPUTE THRUST TERMS (SUBROUTINE THR)

The thrust for a single RCS nozzle was computed when the other nozzle parameters were computed and the aerodynamic coefficients of thrust moment for the three RCS directions are now computed using the subroutine THR. The main program goes through a three step do loop to do pitch up, pitch down, and yaw components in turn. Subroutine THR is called 3 times and contains within itself a two step loop which computes the data for the left side thrust cluster then the right side cluster. The 6 aerodynamic forces and moments from both left and right sides are summed before the subroutine returns to the main program on each pass. The values of all coefficients are first set to zero to remove the data from previous cases prior to the call for THR. Subroutine THR computes the thrust coefficients for each RCS firing direction and multiplies these by the direction cosines of the thrust vectors to obtain the thrust force coefficients. The program assumes that the nozzle clusters are all on the left side of the vehicle in determining the direction cosines of the thrust vectors and appropriate sign corrections are made when the right and left side data are summed. The nozzles are allowed an outboard and an aft cant angle in the computation of direction cosines. These are defined in Figure 5-3. The direction cosines are the angles of a unit vector along the centerline of the plume in the body axis system. The thrust moments are then computed about the body reference moment center accounting for cant angles and position relative to that moment center.

The pitch up, pitch down, and yaw contributions are all saved as components and the program moves on to impingement prediction.

5.7 COMPUTE IMPINGEMENT INCREMENTS (SUBROUTINES IMPING AND VACPLU)

The main program first sets the impingement components to zero to remove any from a previous case and then proceeds into a 3 step do loop which calls the impingement routine for the pitch up cases, pitch down cases, and yaw cases

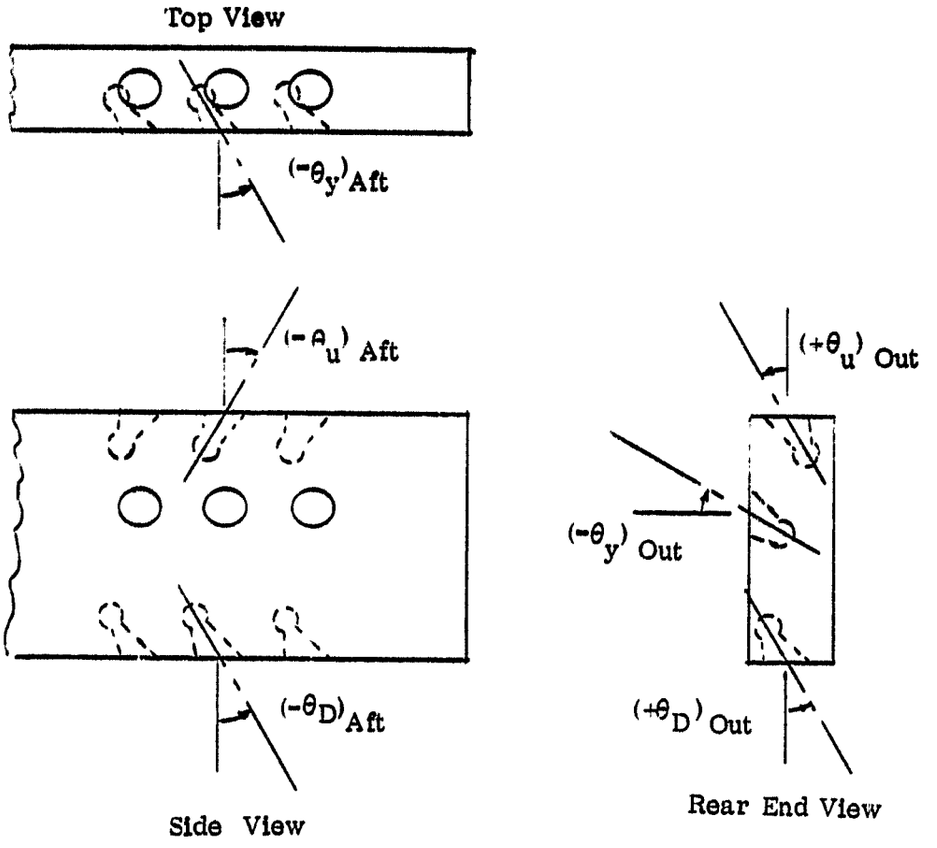

Left Side RCS Pod

FIGURE 5-3 NOZZLE CANT ANGLES

in that order. Within the impingement routine another do loop performs the left side and right side computations for each of the control directions and sums them prior to returning to the main program.

Three choices of plume impingement computation are available within the plume impingement routine based on an input parameter IIMP.

a) No impingement
b) Modified vacuum data from OA99
c) Plume impingement model.

The first option simply sets the impingement terms to zero and proceeds to the interaction computation. The second choice is a computation based on the modified OA99 test equations given in Section 4 as Equation 9 to 28 and compute the impingement increments as functions of thrust coefficient and free-stream dynamic pressure.

The third choice causes the program to make its own prediction of plume impingement by computing the pressures on the vehicle from the six nozzle cluster plume separately and integrating each pressure distribution to obtain the 6 component impingement increments. No plume/plume interaction is accounted for the three directions of RCS firing from the same cluster.

The flat plate description of the vehicle entered into the program in the INPUTT routine is used to make these computations and the cards are listed in Appendix A. These plates are different than those of Reference 3 because the order of the plates is extremely important for the first 23. Plates number 1 to 18 are the upper surface of the left elevon while plates 19 to 23 are the left half of the body flap. The subroutine proceeds through each plate in turn first rescaling it to model scale if required and in the case of the elevon and body flap rotating them about their respective hinge lines to the correct deflection angles. Both right and left elevon angles are input so that both elevator and aileron control deflections are accounted for.

IMPING selects the correct dimensions for the nozzle set being used, zeros the total coefficients and proceeds to use VACPLU to predict the plume pressures on a set of flat plates representing the left side of the vehicle. The plume local static and dynamic pressures are used to compute the local surface pressure through the pressure laws defined in Section 4, Equation 40 to 42 , and the local pressure is converted to a pressure coefficient based on freestream conditions. The pressure coefficient is multiplied by the local area and the direction cosines of the plate to obtain incremental force coefficients. The local force coefficients are used to compute local plate moments about the moment reference center and all of the local values are summed up to obtain total vehicle values.

Since this integration is accomplished by summing up local values for a series of plates, a large number of plates is desirable for good accuracy as well as to

minimize the pressure change on a plate. This is one of the principal reasons for confining all predictions to one side of the plane of symmetry of the vehicle. Reference 3 shows the spacing of approximately 280 plates representing the left side of the orbiter. Each plate is defined by 7 variables which are the location of the plate centroid from the moment reference center (X, Y, Z), the local area (SLOC), and the direction cosines of the outer unit normal vector from the plate with respect to the body axis system as is shown in Figure 5-4. The direction cosines define the local slope of the plate which combined with the angle of the plate to the nozzle determines the local slope of the surface to the flow and the pressure at that point from the pressure laws Equations 40 to 42 in Section 4.

IMPING depends on subroutine VACPLU for its definition of plume characteristics at a given point on the vehicle by sending VACPLU the location of the point in a nozzle based ordinate system by in terms of distance from the nozzle exit plane and the angle from the centerline as well as the equivalent nozzle thrust size and the engine operating characteristics. VACPLU then computes the plume local ambient pressure, dynamic pressure, and Mach number using the model defined in Reference 3 with modifications described in Section 4.4.2, and by assuming isentropic flow relations. If the angle from the centerline of the plume is greater than the limit turning angle, the plume pressures are set to zero and the limits of the extent of the plume are described in Sections 4.4.2.3 and 4.4.2.4.

5.8 COMPUTE INTERACTION INCREMENTS (SUBROUTINES INTER, DEFL, NEWT, CUBIC)

As in the earlier terms the main program zeros the interaction increments from a previous case and then performs a 3 step do loop to compute the interaction coefficients for the pitch up RCS units, pitch down RCS units and yaw RCS units respectively. Each step results in a call to the subroutine INTER which then performs a two step loop to define the left and right components of each control direction and sums them up.

All of the zero deflection curve fit data are stored within the INTER subroutine in DATA statements and are computed using the CUBIC subroutine to evaluate them. Control deflection corrections are made in INTER by calls to the subroutine DEFL. Since the pitch up lateral directional data is based on a peak model rather than curve fits for intervals of angle of attack the subroutine NEWT is called to evaluate these data from INTER.

5.8.1 Pitch Up RCS Interactions

The first entry into the subroutine INTER is to obtain pitch-up RCS interaction terms. The routine computes the upper and lower subscripts for the angle of attack interval in which the angle of attack occurs and a check is made on angle of attack to see

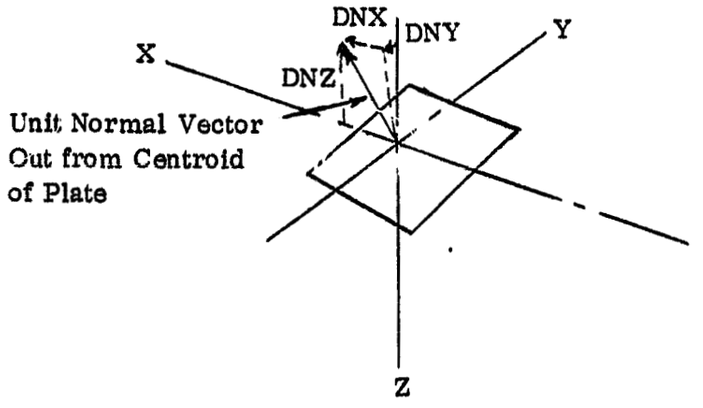

FIGURE 5-4 DIRECTION COSINES OF PLATE ON VEHICLE SURFACE

whether the angle is above or below the peak value regime. if the angle of attack is below 15 degrees the subroutine NEWT is used to predict the lateral-directional interaction components and the curve fit routine to evaluate the longitudinal components. When the angle of attack is high all interaction terms are computed using the curve fit routine (CUBIC). There are no control deflection effects computed and interpolation for angle of attack as defined in Section 4, occurs in CUBIC.

The wind tunnel data was computed in a normal force body axis system so that the sign of the normal force increment must be reversed for all RCS directions. The upward firing pitch nozzle data was generated on the right side of the vehicle in the tests and the lateral-directional increments must be reversed to the left side convention used in this program.

5.8.2 Pitch Down RCS Interactions

The second entry into the surbroutine INTER is to obtain the pitch down RCS interaction terms first for the left side units then for the right side and sums them up. All pitch down data at zero control deflection data are curve fits for intervals of angle of attack as functions of momentum ratio. These are evaluated by computing the indexs of the curve fits above and below the present value of angle of attack and by calling CUBIC to evaluate and interpolate for angle of attack.

After evaluating the zero control deflection interactions the corrections for deflection are generated using the curve fits stored in the surbroutine DEFL first for body flap effects than for elevon angle effects.

5.8.3 Yaw RCS Interactions

The third entry into INTER is to compute the yaw RCS interactions. The approach is the same as for the pitch down RCS case with the exception that the mass flow parameter is the curve fit parameter.

5.8.4 Subroutine CUBIC

All curve fits are defined by seven coefficients. The first four are the coefficients of the cubic expression defined in Section 3, Equation 6. The fifth value is the maximum value of the independent variable for which the curve fit applies while the sixth in the minimum value. The seventh value is the standard deviation of the curve fit as determined from the analysis of Section 3. This routine is called and given the name of dependent variable curves, the value of the independent variable, two subscripts defining the two curves to be evaluated and interpolation factor to be applied to both. Each curve fit is checked to see that the independent parameter lies within is applicable range or that it is made to and is then evaluated. A linear

interpolation is then made using the interpolating factor given in the input. The standard deviation is evaluated also and interpolated between the angle of attack ranges.

5.8.5 Subroutine NEWT

The subroutine NEWT contains the equations of the pitch up RCS peak value lateral-directional models defined in Section 3. Peak side force, rolling moment, and yawing moment are defined as functions of equivalent nozzle effective momentum ratio and are evaluated directly. The first entry into the routine results in the computation of peak yawing moment. An inverse solution of the peak yawing moment versus angle of attack curve is made to determine the angle of attack at which this peak value occurs. If the present angle of attack is greater than the peak angle. All three lateral-directional components are computed as functions of angle of attack only. If the present angle of attack is lower than the peak, the peak values of side force, and rolling moment are computed and returned to INTER which applies the below peak model defined in Section 3.

5.8.6 Subroutine DEFL

The control deflection correction models defined in Section 4.2.2, for the pitch down RCS and yaw RCS are contained in this subroutine. The coefficients of the curve fit equations are all stored in this subroutine through the use of data statements and are applied by calls to the CUBIC subroutine. The curve fits are broken into:

a) Body flap trailing edge up for pitch down RCS
b) Elevon trailing edge up for pitch down RCS
c) Elevon trailing edge down for pitch down RCS
d) Elevon trailing edge up for yaw RCS
e) Elevon trailing down for yaw RCS

The interpolation factor defined in Section 4.2.2, is also computed in this subroutine and allows no extrapolation at deflections angles above those for which the models were formulated. Interpolation for angle of attack between fits is done in CUBIC.

5.9 COMPUTE CROSS COUPLING INCREMENTS (SUBROUTINE CCOUPL)

The final incremental terms needed to complete the RCS effectiveness prediction are the cross coupling terms which are computed in CCOUPL. This subroutine has only the symmetric pitch down model defined in Section 4.3 since all other data correlation showed that no coupling existed within the measured data accuracy.

5.10 SUM COMPONENTS AND COMPUTE AMPLIFICATION FACTORS (SUBROUTINE AMPL)

The principal product of this computer program are the total RCS aerodynamic coefficients as computed as the sum of the increments from all sets of nozzles and printed out by the main program. Since it is also desirable for some cases to relate these total coefficients to RCS thrust, the amplification factors as defined by Equation 2 of Section 4.1 are computed in the Subroutine AMPL.

Since amplification factors can be very confusing when used to relate the out-of-plane induced forces and moments to the thrust terms needed to cancel them, this subroutine was limited to computing the amplification terms in the plane of thrust moments being generated.

This subroutine checks the summation of the thrust terms to see if a thrust components exists in a given direction (i.e., pitch up, pitch down, roll). If one exists than an amplification is computed as the total force or moment in that direction divided by the thrust force or moment.

The computations are now completed and the program returns to the place specified by input parameter INEXT either for another case or to terminate the program.

5.11 PROGRAM INPUT (SUBROUTINE INPUTT)

The preceding sections have given a summary of the program operation and given a brief outline of the data required for the program to execute. This data is loaded into the program through a subroutine called INPUTT which will be briefly described in this section while a detailed description of the input data will be given in the next section.

The input subroutine is called at three different places in the main program and provides different data at each point based on a parameter INEXT. Three types of data are required for a full loading of the program:

a) Vehicle surface plates
b) Nozzle definitions (namelist IN)
c) Flight conditions (namelist FC)

When the program is first loaded or if INEXT = 1 all of the input is required. When INEXT = 2, nozzle definitions and flight conditions changes must be input, and if INEXT = 3 only flight condition changes can be made.

The vehicle flat plate data is input using formatted read statements while the remaining data is entered through namelist. The use of namelist was made to minimize the input required for multiple cases. No input for a given variable in a namelist leaves that variable at its present value and as much as possible default values are defined by DATA declarations within INPUTT so that the full scale data of the shuttle orbiter exists within the program (except for the flat plates which must be input).

INPUTT initializes all of the data, computes the direction cosines of the nozzles, computes the discharge coefficient if a wind tunnel test nozzle is specified, corrects chamber pressure for nozzle discharge coefficient, and rescales nozzles data to model scale if required. The subroutine then provides these data to the main program.

5.12 INPUT DATA DEFINITIONS

A new problem starts with first loading the vehicle flat plate surface data as formatted data at a maximum of 8 words per card with an F10.3 format. The vehicle must be input in full scale dimensions on the left half of the vehicle.

Card	Column	Variable	Description
1 to N-1 flat plate surface cards one plate per card up to 300 allowed (at least one must be input)			
	1-10	DNX(I)	X direction cosine of flat plate I. plates are counted as input is used. See Figure 5-4 for definition of direction cosine.
	11-20	DNY(I)	Y direction cosine of flat plate I
	21-30	DNZ(I)	Z direction cosine of flat plate I
	31-40	X(I)	X distance of centroid of plate I from reference center. See Figure 4-2 for defintion of axis system. Units are feet.
	41-50	Y(I)	Y distance of centroid of plate I from moment reference center. Units are feet.
	51-60	Z(I)	Z distance of centroid of plate I from moment reference center. Units are feet.
	61-70	SLOC(I)	Area of plate I in square feet.
N	1-10	2.0	Last card of flat plate input is signified by DNX(N) being greater than 1.1. This ends flat plate input.

Order of the cards is important. The first 18 cards represent the upper surface of the left elevon. Cards 19 to 23 represent the upper surface of the body flap. All other plates are not order dependent.

The remaining input is by namelist rather than formated read and so no card need be specified. A namelist specification at Convair is made by a $ in column 2 of the first card of the list followed by the namelist name. Each variable name to be loaded must appear followed by an equal sign and the value

of the input with commas separately variable specifications. The list can extend over a number of cards and is closed by a $. The order of names within a list is not important and names can be repeated if newer data becomes available. There are two namelists within INPUTT having the names IN, and FC and they load in that order on a new job.

The namelist IN defines the RCS engine, the locations of the sets and the geometry of the firing arrangement

Namelist	Variable	Description	Default Value
IN	* RCS Engine Characteristics		
IN	GJ	Specific heat of jet	1.3
IN	ARJ	Expansion ratio of jet, exit area-to-throat area	22.
IN	POJSA	Chamber pressure of jet (PSIA)	152 PSIA
IN	RJ	Jet gas constant (R Air = 53.35)	75
IN	TOJ	Jet chamber temperature (Deg)	4873°R
IN	DEXIO	Jet exit diameter (Ft)	.8013 Ft.
IN	THETA	Nozzle exit angle (angle of bell mouth nozzle wall) (Deg)	12°
IN	DCOEF	Nozzle discharge coefficient	1.
IN	NOZNO	Nozzle number (input if Tests OA82, MA22, or OA169 are to be duplicated)	-
IN	*	Nozzle locations and geometry (all sets must be input and left side locations specified if default values not used)	
IN	SCALE	Scale of model for test simulations	1.
IN	XREUM	X coordinate of upward firing nozzles, exit plane reference center of left cluster (Ft)	-37.69
IN	YREUM	Y coordinate of upward firing nozzle exit	-11.
IN	ZREUM	Z coordinate of upward firing nozzle exit from moment reference of left cluster (Ft)	-9.864
IN	XREUS, YREUS ZREUS	Coordinates of upward firing nozzle cluster on right side	

Namelist	Variable	Description	Default Value
IN	XREDM, XREDS	X coordinate of left/right side downward firing nozzle cluster	-37.69
IN	YREDM, YREDS	Y coordinate of left/right down firing cluster	-9.25
IN	XREDM, XREDS	Z coordinate	-5 417
IN	XREYM, XREYS	X coordinate of left/right yaw clusters	-37.69
IN	YREYM, YREYS	Y coordinate	-12.4625
IN	ZREYM, ZREYS	Z coordinate	-7.003

The moment reference center is all specified to $X_{CG} = 1076.7$, $Y_{CG} = 0.$, $Z_{CG} = 375.$

IN	*	Nozzle angles see Figure 5-3 for positive directions	
IN	THAFTU	Aft cant angle of upward firing nozzle (Deg)	0°
IN	THAFTD	Aft cant angle of downward firing nozzle (Deg)	-12°
IN	THAFTY	Aft cant angle of sideway firing nozzle (Deg)	0°
IN	THOUTU	Outboard cant angle of upward firing nozzle (Deg)	0°
IN	THOUTD	Outboard cant angle of downward firing nozzle (Deg)	-20°
IN	THOUTY	Upward cant angle of sideway firing nozzle (Deg)	0°
IN	*	Nozzle set definitions	
IN	NONOZUL	Number of upward firing nozzles (causing pitch up) operating in a set on left side of vehicle	0
IN	NONOZUR	Same as above on right side	0
IN	NONOZDL, NONOZDR	Number of downward firing nozzles (causing pitch down) operating in a set on left/right side of vehicle	0

Namelist	Variable	Description	Default Value
IN	NONOZYL NONOZYR	Number of downward firing nozzles (causing pitch down) operating in a set on left/right side of vehicle	0
IN	*	Impingement Model Selector	
IN	IIMP	Defines the type of mathematical model to be used, = 1, Use the empircal impingement model, = 2, No impingement model used, = 3, Use the semi-empirical impingement model (Modified Newtonian pressures plus vacuum plume model) IIMP = 3 is the default value	

The final namelist in is called FC and contains the control deflections, flight conditions and an indicator which determines the input options on multiple cases.

FC	IOPT	Defines the flight conditions to be read = 1, Mach number, angle of attack (Deg) and altitude (Ft) must be input, all others are not used = 2, Velocity (FPS), altitude (Ft), and angle of attack (Deg) must be input = 3, Dynamic pressure (PSF), altitude (Ft), and angle of attack (Deg) must be input = 4, Ambient pressure (PSF), temperature (Deg F), Mach number and angle of attack (Deg) must be input. This is default value.	4
FC	MINF	Free stream Mach number	none given
FC	PINF	Free stream ambient pressure (PSIA)	none given
FC	TINF	Free stream ambient temperature (Deg F)	none given
FC	QI	Free stream dynamic pressure (PSF)	none given
FC	ALPH	Angle of Attack (Deg)	0°
FC	HI	Altitude (Ft)	none given
FC	VINF	Velocity (FPS)	none given

Namelist	Variable	Description	Default Value
FC	DELTEL	Elevon angle of left elevon (- trailing edge up) Deg.	0°
FC	DELTER	same as above - right elevon	0°
FC	DELTBF	Body flap deflection angle (- trailing edge up) Deg.	0°
FC	INEXT	Defines content of next set of data	4
		= 1, All data are to be read	
		= 2, Nozzle definitions and flight conditions (namelists IN and FC) must be read	
		= 3, Flight conditions only (namelist FC) are to be read	
		= 4, No more data will be read in, program stops	

5.13 OUTPUT DATA DEFINITIONS

The data printed out from a sample run is shown in Figure 5-5. Not shown in this figure is the listings of input which occur because of the use of the namelist input option and the names are defined in the preceding section. The output starts with a definition of the characteristics of the solution in lines 1 and 2.

Output Line	Word	Description
1	SCALE	Scale of solution (1= full scale)
2	REFERENCE AREA	Reference area used in this solution in Ft^2
2	REF SPAN	Reference length for lateral directional moment in Ft.
2	REF CHORD	Reference length in pitching moment in Ft.
3-5	Nozzle Characteristics	Single RCS nozzle data
3	EXIT DIA	RCS nozzle exit diameter in feet (input as DEXIO)
3	EXPANSION RATIO	RCS nozzle exit to throat area ratio (input as ARJ)

```
LINE
     XXXXXXXXXXXXXXXXXXXXXXXXXXXXXXXXXXXXXXXXXXXXXXXXXXXXXX
  1  THE SCALE OF THIS SOLUTION IS        1.0000000000
  2  REFERENCE AREA=   2690.0000000SQ FT      REF SPAN =     78.0530059FT        REF CHORD =     39.5700619FT
     XXXXXXXXXXXXXXXXXXXXXXXXXXXXXXXXXXXXXXXXXXXXXXXXXXXXXX
      NOZZLE CHARACTERISTICS
  3   EXIT DIA       .8813 EXPANSION RATIO     22.0000 EXIT ANGLE     12.0000 NOZZLE MACH        4.2951
  4   THRUST        879.88127525 CHAMBER PRESS    152.0000 EXIT PRESS          .40499712 EXHAUST GAMMA     1.3000
  5   NOZZLE DISCHARGE COEFFICIENT IS         1.0000000000
     XXXXXXXXXXXXXXXXXXXXXXXXXXXXXXXXXXXXXXXXXXXXXXXXXXXXXX
      FREE STREAM CONDITIONS
     XXXXXXXXXXXXXXXXXXXXXXXXXXXXXXXXXXXXXXXXXXXXXXXXXXXXXX
  6   MACH NO =       25.00000
  7   ANGLE OF ATTACK =      0.0000000
     XXXXXXXXXXXXXXXXXXXXXXXXXXXXXXXXXXXXXXXXXXXXXXXXXXXXXX
  8  ELEVON ANGLES,LEFT =      0.0000000  RIGHT =       0.0000000
     XXXXXXXXXXXXXXXXXXXXXXXXXXXXXXXXXXXXXXXXXXXXXXXXXXXXXX
  9  BODY FLAP DEFLECTION =      0.0000000
     XXXXXXXXXXXXXXXXXXXXXXXXXXXXXXXXXXXXXXXXXXXXXXXXXXXXXX
 10   P INFINITY          .00003010 MACH INF     25.0000 GAMMA      1.4000ANGLE OF ATTACK      0.0000
 11  PRESSURE RATIO    4049971.23458159 MOMENTUM RATIO        24.92060035 THRUST COEFF        51.91958933
 12   RT RATIO          3.79197207 POJ/PINF 152000000.0000000FREE STREAM DYNAMIC PRESS         .6063030.0
 13  (R*TOJ)/(R*TINF)     14.28530
     XXXXXXXXXXXXXXXXXXXXXXXXXXXXXXXXXXXXXXXXXXXXXXXXXXXXXX
 14   PITCH UP LEFT NOZZLES =      3.         MOMENTUM RATIO        74.76286584          THRUST COEF(1SOFT)  418991.603458
 15   PITCH UP RGHT NOZZLES =      0.         MOMENTUM RATIO         0.00000000          THRUST COEF(1SOFT)       0.000000
```

FIGURE 5-5 SAMPLE OUTPUT

LINE

16 PITCH ON LEFT NOZZLES = 3. MOMENTUM RATIO 74.76236504 THRUST COEF(1SQFT) 418991.883458

17 PITCH ON RGHT NOZZLES = 0. MOMENTUM RATIO 0.83688886 THRUST COEF(1SQFT) 0.000003

18 YAW LEFT NOZZLES = 3. MASS FLOW RAT 35.24689487 THRUST COEF(1SQFT) 418991.883458

19 YAW RIGHT NOZZLES = 0. MASS FLOW RAT 35.24689487 THRUST COEF(1SQFT) 0.000000

XXXXXXXXXXXXXXXXXXXXXXXXXXXXXXXXXXXXXXXXXXXXXXXXXXXXXXXX

BODY AXES FORCE AND MOMENT COEFFICIENTS ARE OUTPUT

SIGN CONVENTION*POSITIVE FWD *Z POSITIVE DOWN *Y POSITIVE RIGHT
PITCH + NOSE UP *ROLL + RIGHT WING DWN*YAW + NOSE RIGHT

MOMENT REF CENTER*X=1376.7 Z=375.

	THRUST TERMS	(A) ROLLING MOMENT	(B) PITCHING MOMENT	(C) YAWING MOMENT	(D) X FORCE	(E) Y FORCE	(F) Z FORCE
20	PITCH UP	-21.951065	148.358553	0.000000	0.000000	0.000000	155.750767
21	PITCH DOWN	13.384874	-132.534575	-21.618335	38.530293	52.248732	-143.530288
22	YAW	-13.974046	3.000000	-75.212329	0.000000	155.750767	0.000000

XXXXXXXXXXXXXXXXXXXXXXXXXXXXXXXXXXXXXXXXXXXXXXXXXXXXXXXX

IMPINGEMENT FORCES

		ROLLING MOMENT	PITCHING MOMENT	YAWING MOMENT	X FORCE	Y FORCE	Z FORCE
23	PITCH UP	2.452845	-.220745	-3.914722	-.179383	7.834907	-.212719
24	PITCH DOWN	-4.652617	48.106579	-9.848589	-13.338334	16.788464	46.955455
25	YAW	0.000000	0.000000	0.000000	0.000000	0.000000	0.000000

XXXXXXXXXXXXXXXXXXXXXXXXXXXXXXXXXXXXXXXXXXXXXXXXXXXXXXXX

INTERACTION TERMS

		ROLLING MOMENT	PITCHING MOMENT	YAWING MOMENT	X FORCE	Y FORCE	Z FORCE
26	PITCH UP	.013604	-.002628	-.017672	.012498	.338418	.848401
27	PITCH DOWN	-.012454	.050553	-.382543	.022365	.016864	.122869
28	YAW	-.000641	0.000000	-.005343	.000231	.016345	.033790

FIGURE 5-5 SAMPLE OUTPUT

LINE		(A)	(B)	(C)	(D)	(E)	F
	XXXXXXXXXXXXXXXXXXXXXXXXXXXXXXXXXXXXXXXXXXXXXXXXXXXXXXX						
	CROSS COUPLING TERMS						
		ROLLING MOMENT	PITCHING MOMENT	YAWING MOMENT	X FORCE	Y FORCE	Z FORCE
29	PITCH UP	0.000000	0.000000	0.000000	0.000000	0.000000	0.000000
30	PITCH DOWN	0.000000	0.000000	0.000000	0.000000	0.000000	0.000000
31	YAW	0.000000	0.000000	0.000000	0.000000	0.000000	0.000000
	XXXXXXXXXXXXXXXXXXXXXXXXXXXXXXXXXXXXXXXXXXXXXXXXXXXXXXX						
	TOTAL VALUES						
		ROLLING MOMENT	PITCHING MOMENT	YAWING MOMENT	X FORCE	Y FORCE	Z FORCE
32		-24.744181	55.749734	-118.611453	16.975471	232.614137	53.176335
	XXXXXXXXXXXXXXXXXXXXXXXXXXXXXXXXXXXXXXXXXXXXXXXXXXXXXXX						
33	STD DEV OF CX = .0049744						
34	STD DEV OF CZ = .0116293						
35	STD DEV OF CM = .0337156						
36	STD DEV OF CL = .0015439						
37	STD DEV OF CN = .0022360						
38	STD DEV OF CY = .0067165						
	AMPLIFICATION IS COMPUTED FOR THRUST COMPONENTS ONLY						
	+1 IS NO AMPLIFICATION 0 IS THRUST CANCELLATION						
	THERE ARE 22 POSSIBLE RCS CONTROL COMBINATIONS						
	THIS COMBINATION INCLUDES A PITCH UP OR DOWN COMPONENT						
39	NORMAL FORCE AMP = 4.34856473 PITCHING MOM AMP = 3.52311747						
	THIS COMBINATION INCLUDES A ROLL LEFT OR RIGHT COMP						
40	ROLL AMPLIFICATION = 2.00838716						
	THIS COMBINATION INCLUDES A YAW LEFT OR RIGHT COMPONET						

FIGURE 5-5 SAMPLE OUTPUT

```
LINE
41  SIDE FORCE AMP =     1.4934256YAW MOMENT AMP =     1.47865587
    AMPLIFICATION FACTORS
                              KL              KM              KN              KX              KY              KZ
42  AMPLIFICATION          2.8883872       3.5231175       1.4786559       0.0000000       1.4934256       4.3485648
    XXXXXXXXXXXXXXXXXXXXXXXXXXXXXXXXXXXXXXXXXXXXXXXXXXXXXXXXXXXXXX
    XXXXXXXXXXXXXXXXXXXXXXXXXXXXXXXXXXXXXXXXXXXXXXXXXXXXXXXXXXXXXXX
    THE 2 SIGMA ERROR BAND RESULTS IN THE FOLLOWING COEFS
     +2  SIGMA COEF FIRST THEN -2 SIGMA DATA ARE PRESENTD
                    ROLLING MOMENT   PITCHING MOMENT     YAWING MOMENT        X   FORCE          Y  FORCE         Z   FORCE
43                     -24.741813        55.757165       -118.686993        16.985428       232.627578       53.199594
    XXXXXXXXXXXXXXXXXXXXXXXXXXXXXXXXXXXXXXXXXXXXXXXXXXXXXXXXXXXXXX
                    ROLLING MOMENT   PITCHING MOMENT     YAWING MOMENT        X   FORCE          Y  FORCE         Z   FORCE
44                     -24.747188        55.742382       -118.615913        16.965522       232.688784       53.153876
    XXXXXXXXXXXXXXXXXXXXXXXXXXXXXXXXXXXXXXXXXXXXXXXXXXXXXXXXXXXXXX
    XXXXXXXXXXXXXXXXXXXXXXXXXXXXXXXXXXXXXXXXXXXXXXXXXXXXXXXXXXXXXXX
    XXXXXXXXXXXXXXXXXXXXXXXXXXXXXXXXXXXXXXXXXXXXXXXXXXXXXXXXXXXXXXX
```

FIGURE 5-5 SAMPLE OUTPUT

Output Line	Word	Description
3	EXIT ANGLE	RCS nozzle exit lip angle in degrees (input as THETA)
3	NOZZLE MACH	Computed nozzle exit Mach number
4	THRUST	Computed RCS nozzle thrust in pounds
4	CHAMBER PRESSURE	RCS effective chamber pressure in PSIA
4	EXIT PRESS	Computed static pressure at nozzle exit plane in PSIA
4	EXHAUST GAMMA	Specific heat ratio of nozzle gases (input as GJ)
5	NOZZLE DISCHARGE COEFFICIENT	Input or computed nozzle discharge coefficient (ratio of actual thrust to ideal)
6	MACH NO	Input or computed freestream Mach number
7	ANGLE OF ATTACK	Angle of attack of this solution INPUT as ALPH degrees
8	ELEVON ANGLES	Wing mounted elevon angles input for this solution as DELTEL and DELTER in degrees
9	BODY FLAP DEFLECTION	Body flap deflection input for this solution as DELBF in degrees
10	P INFINITY	Ambient pressure at flight condition either input or defined by standard atmosphere in PSIA (limited printout resolution)
10	MACH INF	Freestream Mach number
10	GAMMA	Freestream specific heat ratio
10	ANGLE OF ATTACK	Input angle of attack (ALPH) in degrees
11	PRESSURE RATIO	Single RCS nozzle jet exit pressure ratioed to freestream pressure (P_j/P_∞)
11	MOMENTUM RATIO	Single RCS Nozzle momentum ratio (ratioed using wing area (Φ_j/Φ_∞)
11	THRUST COEFF	Single RCS nozzle thrust ratioed by dynamic pressure and wing area = T/qS

Output Line	Word	Description
12	RT RATIO	$(R_J T_J / R_\infty T_\infty)$; RCS ambient temperature ratio to freestream
12	POJ/PINF	RCS chamber pressure (P_{oj}) ratioed to freestream ambient pressure (P_∞)
13	FREESTREAM DYNAMIC PRESSURE	$q_\infty = 0.7\ P_\infty\ M_\infty^2$ in PSF
13	R*TOJ)/R*TINF)	$(R_J T_{OJ})/R_\infty T_\infty)$; RCS chamber temperature ratioed to freestream ambient temperature - Thayer's parameter
14-19	NOZZLES	Number of nozzles firing in each cluster is defined here
14-17	MOMENTUM RATIO	Total momentum ratio of cluster used to compute interactions
14-19	THRUST COEFFICIENT	Total thrust coefficient of cluster using 1 Ft^2 as reference area
18-19	MASS FLOW RAT	Mass flow parameter used to compute yaw RCS interactions

The program now begins a printout of all terms which are combined into total control moments and amplification. This printout is in a systematic form in which any pitch up nozzle contributions are listed first (lines 20, 23, 26, and 29); then pitch down nozzles) lines 21, 24, 27, and 30) and finally yaw nozzle contributions (lines 22, 25, 28, and 31). The data is all presented in aerodynamic coefficient form so that the force terms are non dimensionalized by dividing by dynamic pressure and wing area and additionally the moment terms by the appropriate reference length. Column A presents rolling moment (C_L), column B presents pitching moment (C_M), Column C presents yawing moment (C_N), Column D presents body axis axial force (C_X), Column E presents side force (C_Y), and Column F presents vertical force (C_Z) where Figure 4-1 defines the sign convention of the force and moment coefficients.

The thrust terms are computed first and are presented first in lines 20 through 22. These thrust terms have all nozzle cant angles included in their computation. The plume impingement terms are presented in lines 23 through 25. If the input option is selected to ignore impingement a comment will be printed but output will still be listed. The interaction terms are presented in lines 26 to 28 and

the cross coupling terms in lines 29 to 31. The summation of all components (Equation 1 of Section 4) listed in lines 20 to 31 are then obtained and printed in line 32.

Lines 33 to 38 then present the standard deviations of the total aerodynamic forces and moments. Lines 39 to 42 present the amplification factors for the case computed where the thrust terms used are defined in lines 20 to 22. Lines 43 and 44 present the total coefficients (line 32) plus and minus 2 sigma where sigma is defined in lines 33 to 38 and represent the best estimated of the 95 percent confidence band within which the true value of data will occur.

6

DATA COMPARISONS

The analytic model of Sections 4 and 5 resulted from the data analysis of Section 3 and modifies it to a certain degree. The curve fits generated in Section 3 showed varying degrees of correlation with the test data, some correlations were strong while others were not so strong. Thus the question arises how well will the computer model reproduce the test data results. The scatter within the test data itself would make it unlikely that a single given run could be reproduced point for point, however, the comparison can still be useful to show the strong and weak parts of the model and to show the expected data scatter.

The approach taken to make this comparison then was to compare the analytic model results for 3 nominal examples of data at zero control deflection in which a number of repeat runs were made. The comparison was made on a jet-on minus jet-off basis so that both impingement and interaction terms are included.

6.1 NOZZLE N49 PITCH DOWN RCS COMPARISONS

Figure 6-1 to 6-6 present the analytic model results compared to six runs of nozzle N49 data at the same nominal value of momentum ratio. The 2 standard deviation error bands are plotted on the moment data correlations. The test data scatter is shown in all plots and is particularily bad in the vertical force component at high angles of attack. The agreement of the prediction with the trends of the data appears good. The model appears to overpredict the yawing moment slightly at higher angles of attack but all the data falls well within the 2 sigma error band.

6.2 NOZZLE N52 PITCH-UP RCS COMPARISON

Figures 6-7 to 6-12 compare ten runs of data obtained from nozzle N52 at the same nominal momentum ratio (.015) with the analytic model results. The longitudinal data (C_X, C_Z, C_m) where the correlations were weak show considerable scatter in the data. This is in part due to the low value of momentum ratio being correlated here. The pitching moment follows the trend of the data fairly well inspite of the scatter as does vertical force at low angles of attack. The lateral-directional data shows very good agreement between the model and test data even through the peak value region and at angles below the peak value where the curve was fitted through large amounts of scatter.

6.3 NOZZLE N85 YAW DATA COMPARISONS

Data for 6 data runs obtained using yaw nozzle block N85 are compared with analytic model predictions in Figures 6-13 through 6-18. The axial force (6-13), rolling moment (6-16), and pitching moment (6-17) show excellent agreement between the model and the test data. The vertical force data in Figure 6-14 shows only good agreement of angles of attack from 0 degrees to 20 degrees. Above 20 degrees the data scatter becomes very large (as was the case in all correlations) and the model stays close to the MA22 test data. At negative angles, Figures 3-17a and 3-17b show that the scatter again was large and the model was faired between the N85 data shown on these comparisons and N51 data which pulled the curve down. The side force comparison shown in Figure 6-15 shows good agreement above 5 degrees angle of attack and the data scatter shown at -9 degrees in this figure results in the model being kept low at the negative angles. Figures 3-21a to 3-21j present the anglysis data for the yawing moment comparison of Figure 6-18. The scatter in low angle of attack data again results in some difference between model and data around zero angle of attack.

Comparisons of these plots with the error bands on Figures 3-17 to 3-21 will show that all differences are well within the expected error band.

$\Delta C_X = C_{X\ \text{JET ON}} - C_{X\ \text{JET OFF}}$

- - - PROGRAM PREDICTION

DATA	TEST	RUN
□	MA22	200
◇	MA22	3
○	MA22	6
◇	MA22	10
◇	MA22	206
◁	OA82	61

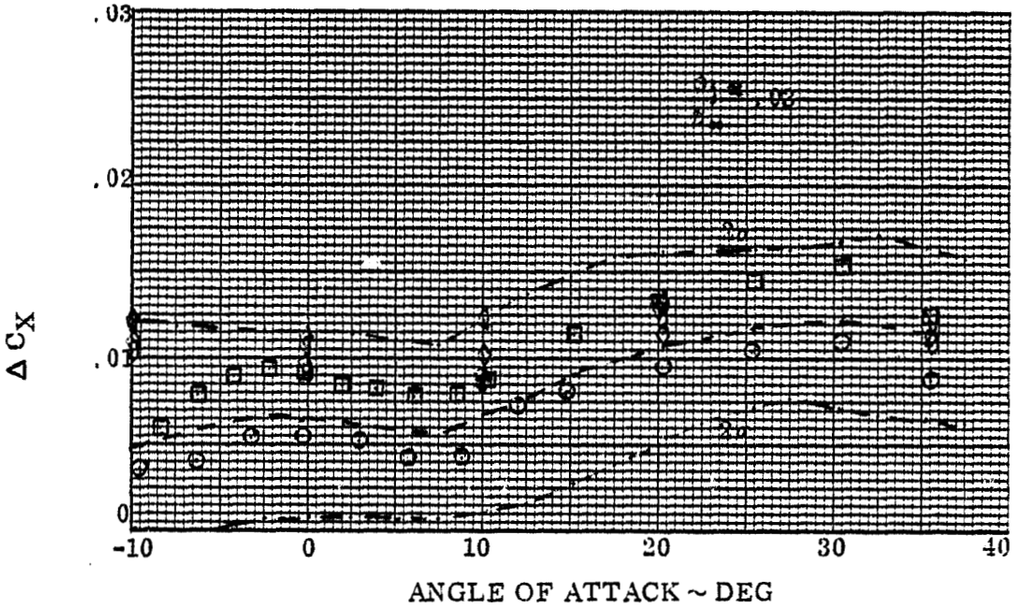

FIGURE 6-1 A COMPARISON OF TEST DATA FOR NOZZLE N49 WITH PREDICTION PROGRAM RESULTS: LONGITUDINAL FORCE COEFFICIENT

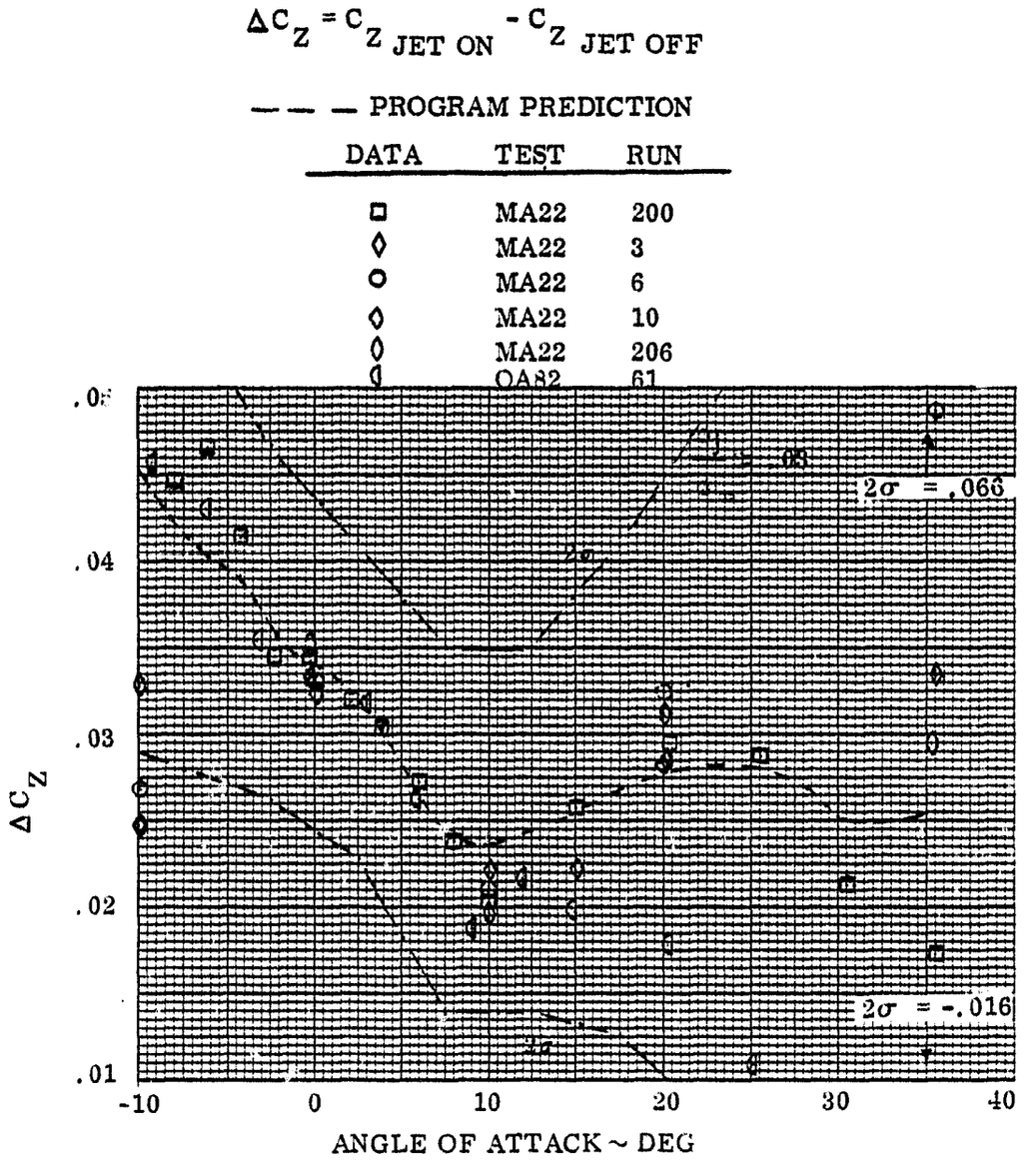

FIGURE 6-2 A COMPARISON OF TEST DATA FOR NOZZLE N49 WITH PREDICTION PROGRAM RESULTS: VERTICAL FORCE COEFFICIENT

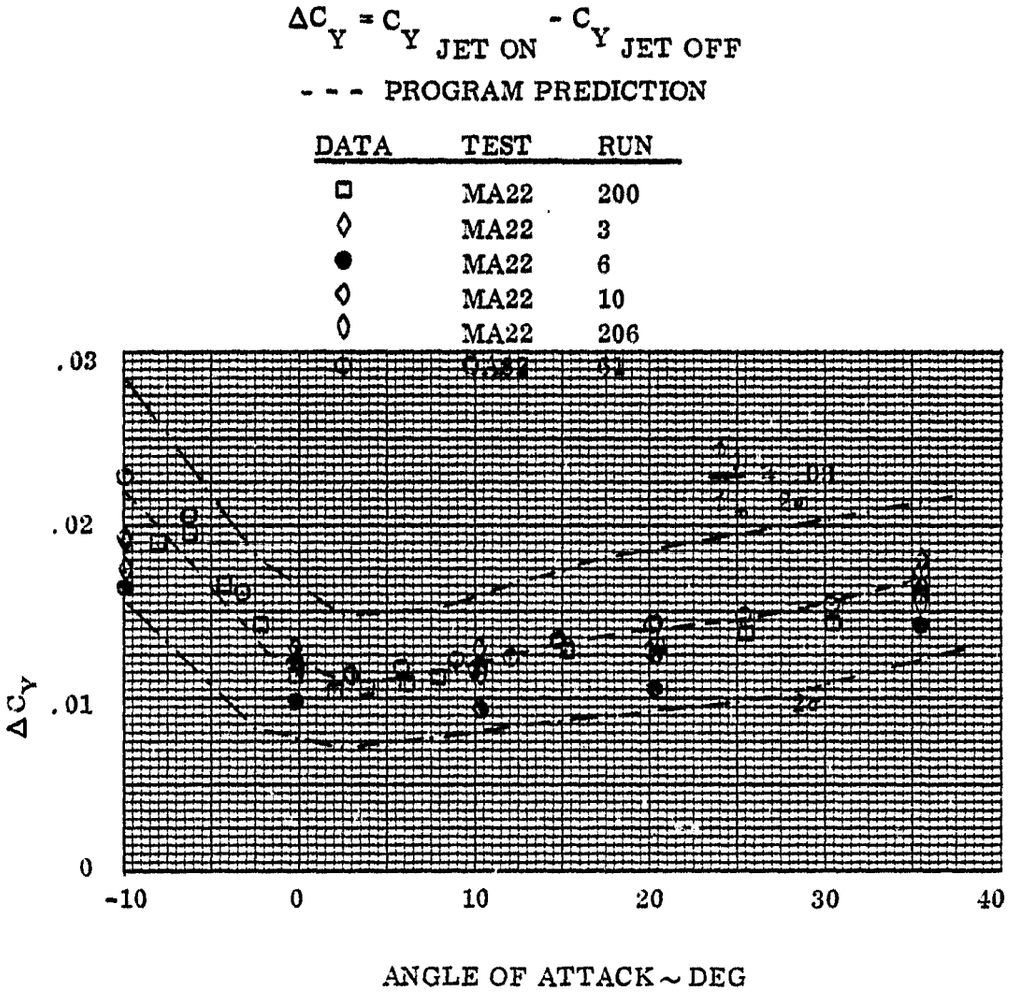

FIGURE 6-3 A COMPARISON OF TEST DATA FOR NOZZLE N49 WITH PREDICTION PROGRAM RESULTS: SIDE FORCE COEFFICIENT

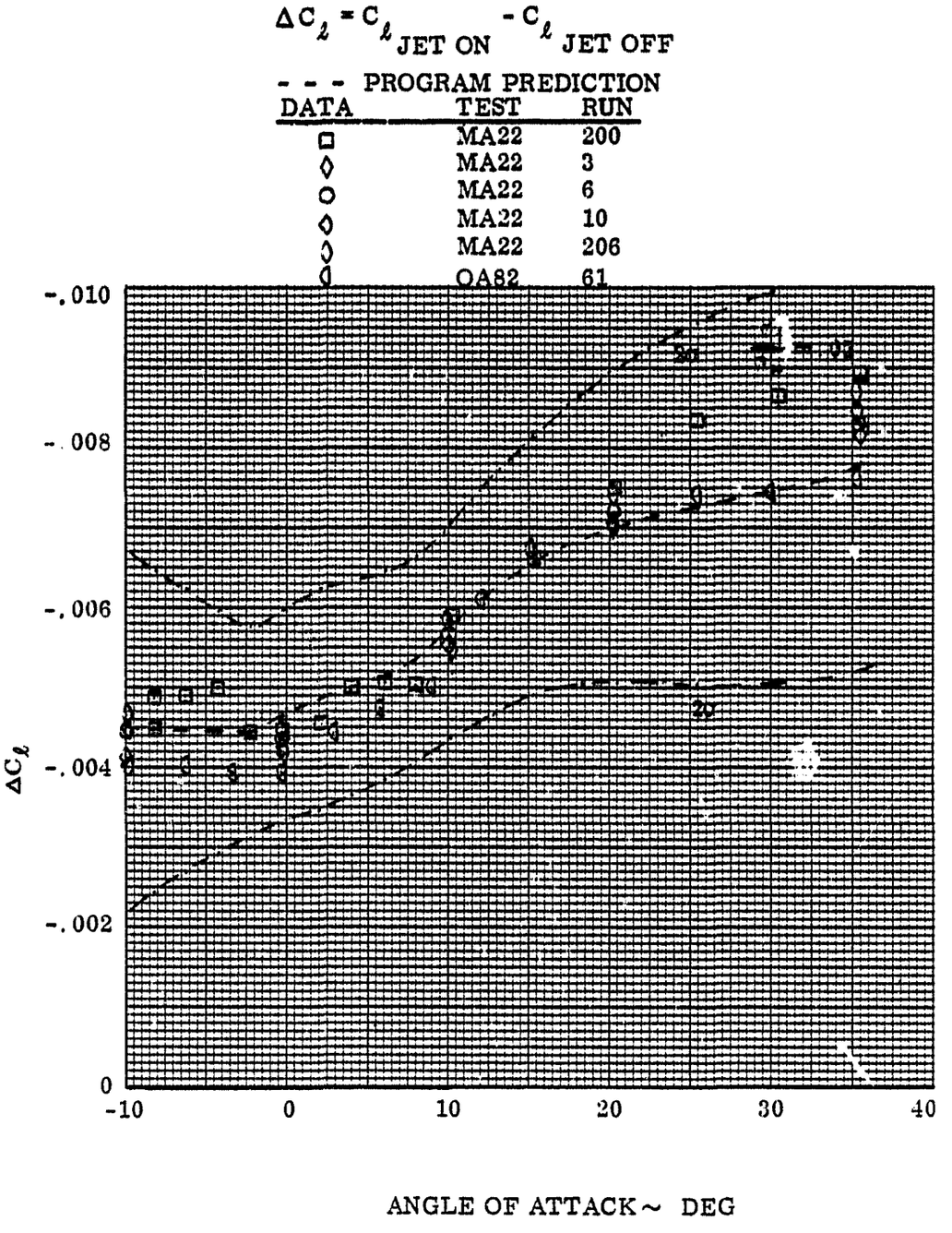

FIGURE 6-4 A COMPARISON OF TEST DATA FOR NOZZLE N49 WITH PREDICTION PROGRAM RESULTS: ROLLING MOMENT COEFFICIENT

$\Delta C_m = C_{m\ \text{JET ON}} - C_{m\ \text{JET OFF}}$

- - - PROGRAM PREDICTION

DATA	TEST	RUN
□	MA22	200
◇	MA22	3
○	MA22	6
◇	MA22	10
◇	MA22	206
◐	OA82	61

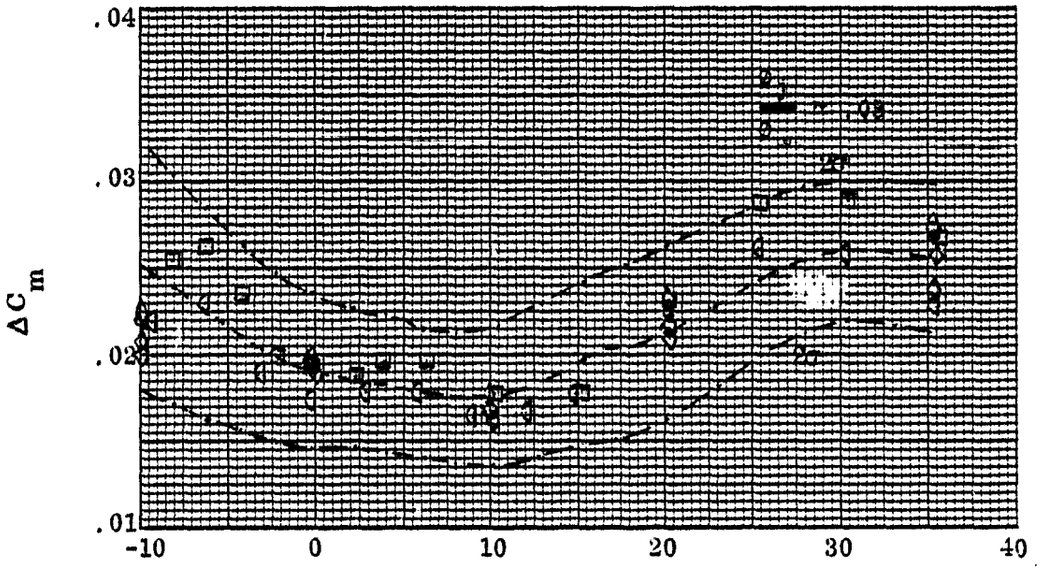

FIGURE 6-5 A COMPARISON OF TEST DATA FOR NOZZLE N49 WITH PREDICTION PROGRAM RESULTS: PITCHING MOMENT COEFFICIENT

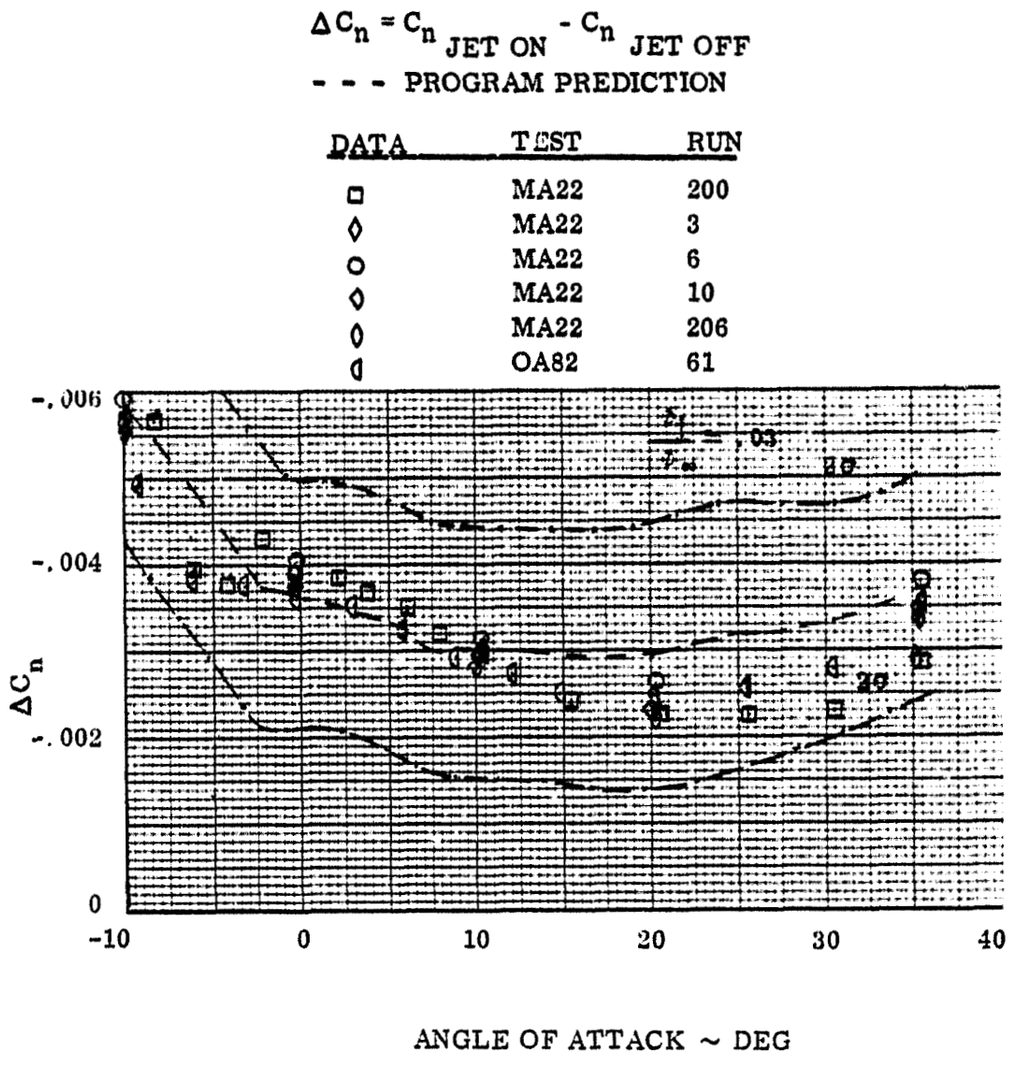

FIGURE 6-6 A COMPARISON OF TEST DATA FOR NOZZLE N49 WITH PREDICTION PROGRAM RESULTS: YAWING MOMENT COEFFICIENT

$$\Delta C_X = C_{X_{JET\ ON}} - C_{X_{JET\ OFF}}$$

— — — PROGRAM PREDICTION

DATA	TEST	RUN
△	OA82	15
○	OA82	29
●	OA82	34
□	OA82	36
◇	OA82	67
◇	OA82	72
◁	OA82	73
▽	OA82	79
◇	MA22	164
●	MA22	155

$\frac{p_j}{p_\infty} \approx .015$

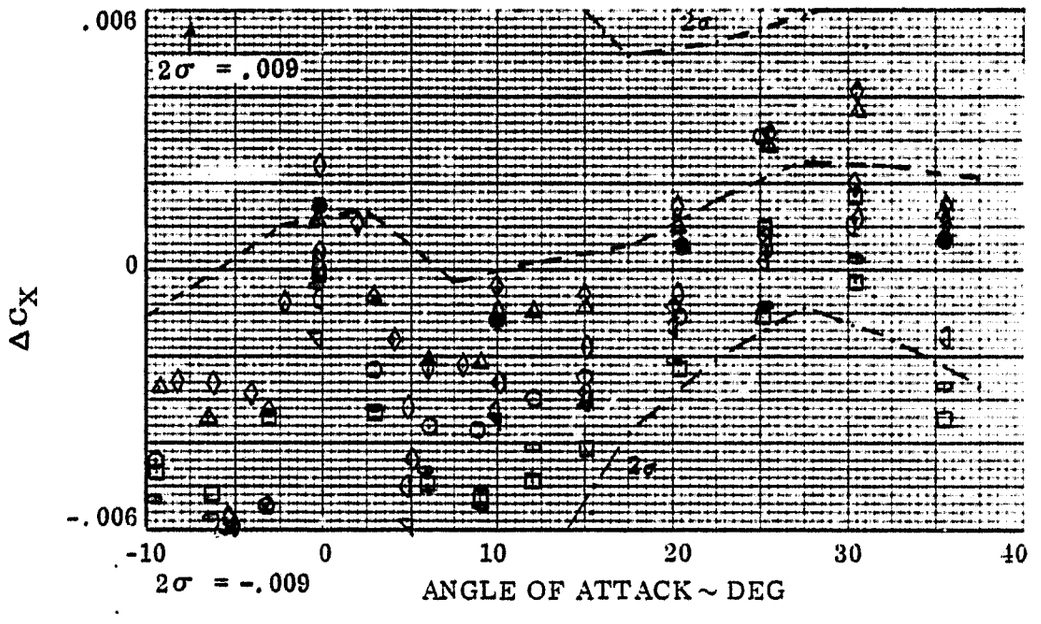

FIGURE 6-7 A COMPARISON OF TEST DATA FOR NOZZLE N52 WITH PREDICTION PROGRAM RESULTS: LONGITUDINAL FORCE COEFFICIENT

$$\Delta C_Z = C_{Z\,\text{JET ON}} - C_{Z\,\text{JET OFF}}$$

— — — PROGRAM PREDICTION

DATA	TEST	RUN
△	OA82	15
○	OA82	29
●	OA82	34
□	OA82	36
◇	OA82	67
◇	OA82	[illegible]
◁	OA82	[illegible]
▽	OA82	79
◇	MA22	164
●	MA22	155

$\frac{\sigma_j}{\sigma_\infty} \approx .015$

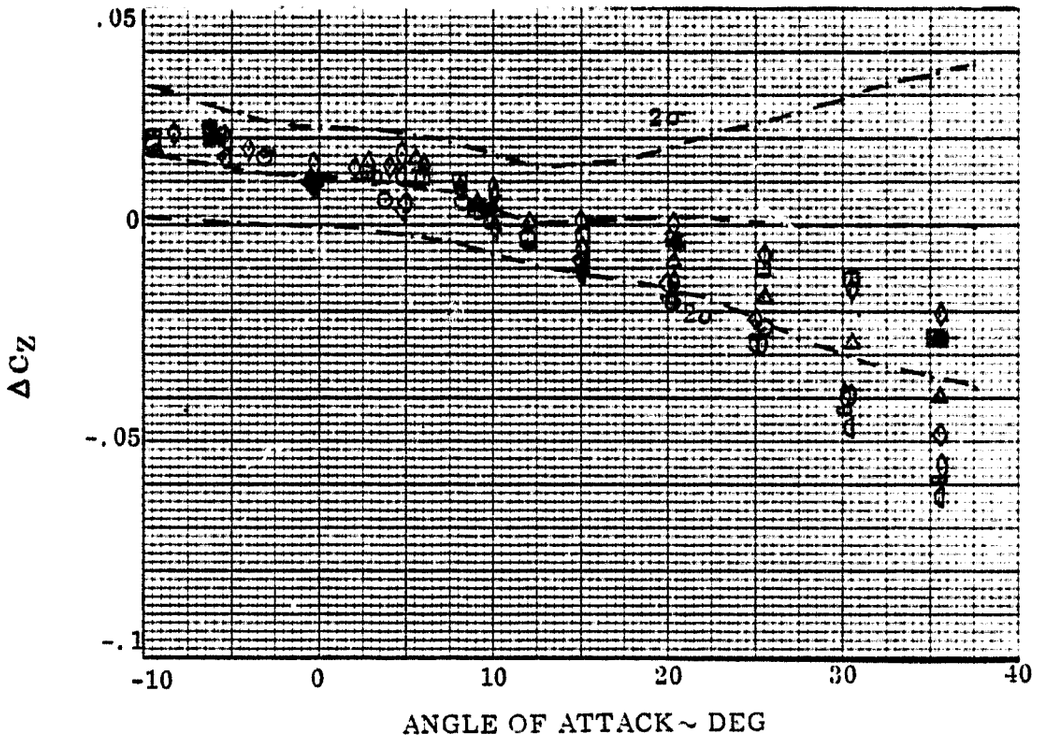

FIGURE 6-8 A COMPARISON OF TEST DATA FOR NOZZLE N52 WITH PREDICTION PROGRAM RESULTS: VERTICAL FORCE COEFFICIENT

$$\Delta C_Y = C_Y \text{ JET ON} - C_Y \text{ JET OFF}$$

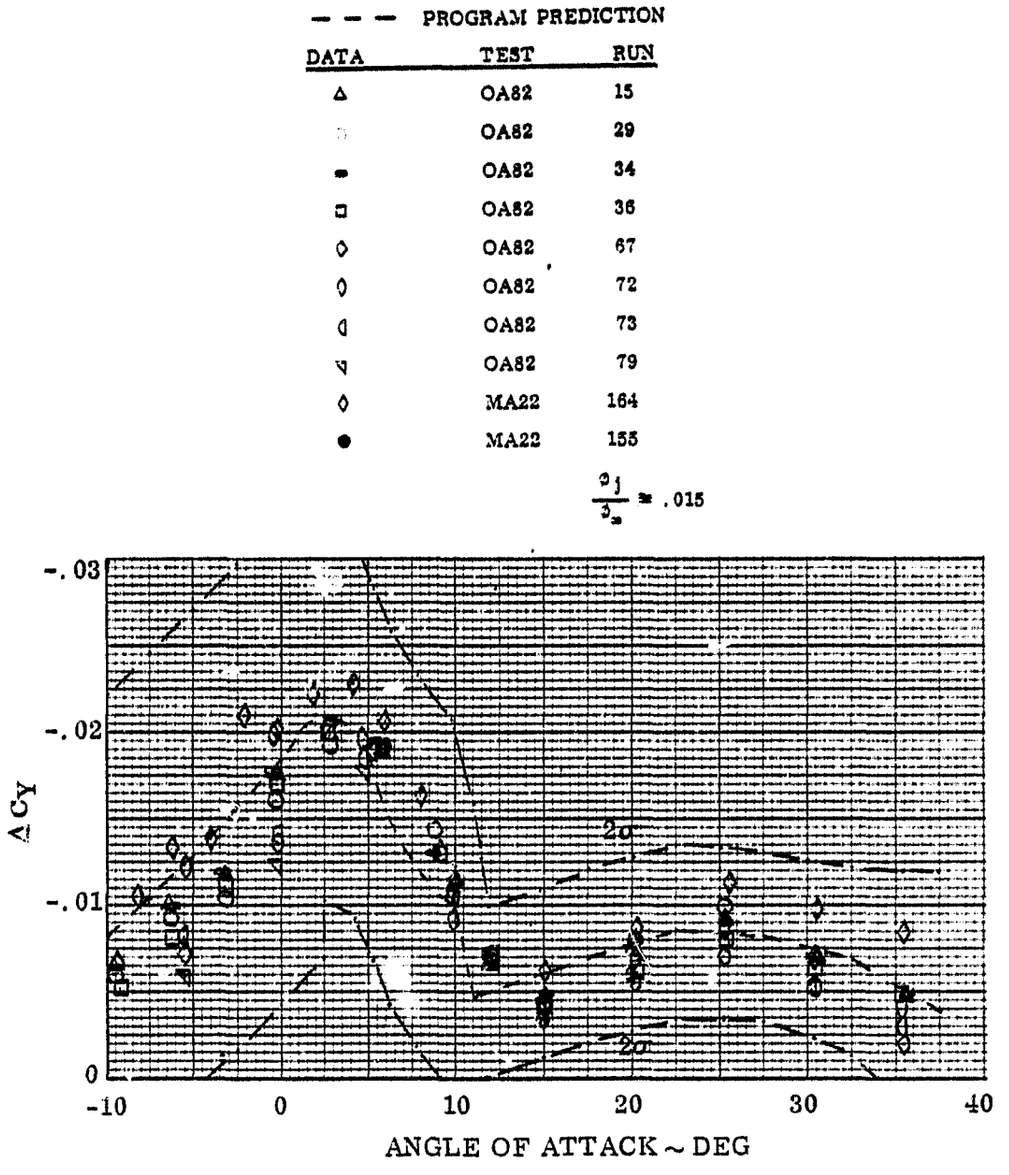

FIGURE 6-9 A COMPARISON OF TEST DATA FOR NOZZLE N52 WITH PREDICTION PROGRAM RESULTS: SIDE FORCE COEFFICIENT

$$\Delta C_\ell = C_\ell \text{ JET ON} - C_\ell \text{ JET OFF}$$

— — — PROGRAM PREDICTION

DATA	TEST	RUN
△	OA82	15
○	OA82	29
▬	OA82	34
□	OA82	36
◇	OA82	67
◇	OA82	72
◁	OA82	73
▽	OA82	79
◇	MA22	164
●	MA22	155

$\frac{p_j}{p_\infty} \cong .015$

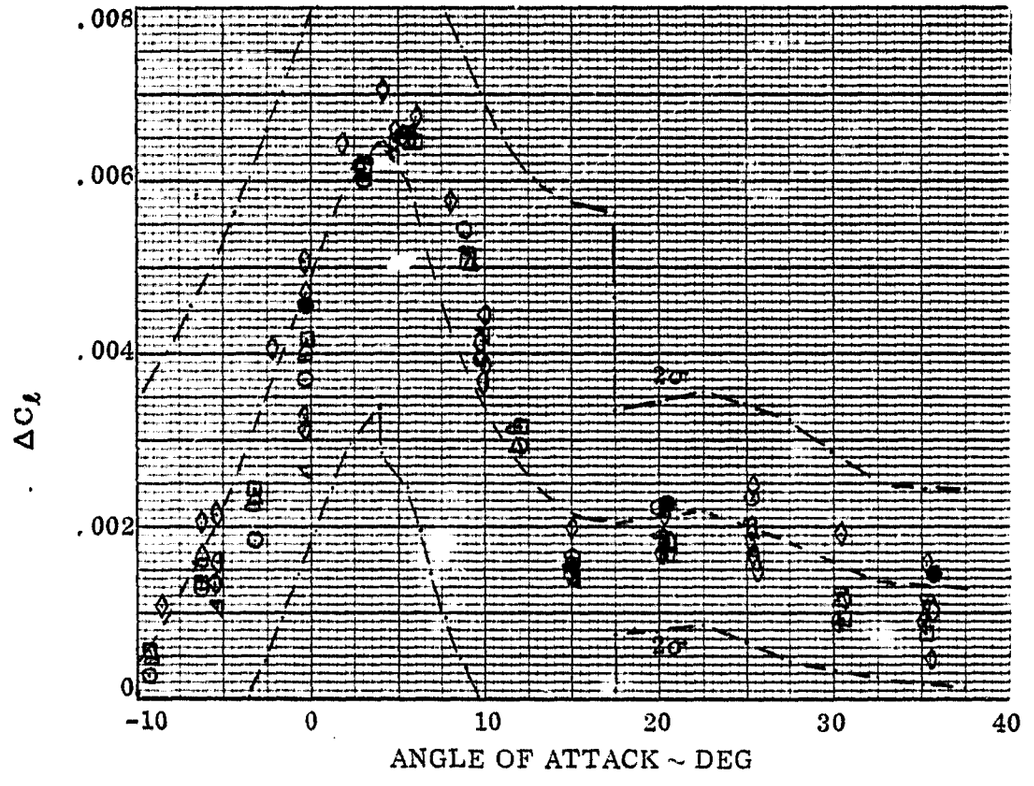

FIGURE 6-10 A COMPARISON OF TEST DATA FOR NOZZLE NS[illegible]E PREDICTION PROGRAM RESULTS: ROLLING MOM[illegible] COEFFICIENT

$$\Delta C_m = C_{m\,\text{JET ON}} - C_{m\,\text{JET OFF}}$$

— — — PROGRAM PREDICTION

DATA	TEST	RUN
△	OA82	15
○	OA82	29
▬	OA82	34
□	OA82	36
◇	OA82	67
◊	OA82	72
◖	OA82	73
▽	OA82	79
◇	MA22	164
●	MA22	155

$\frac{\Phi_j}{\Phi_a} = .015$

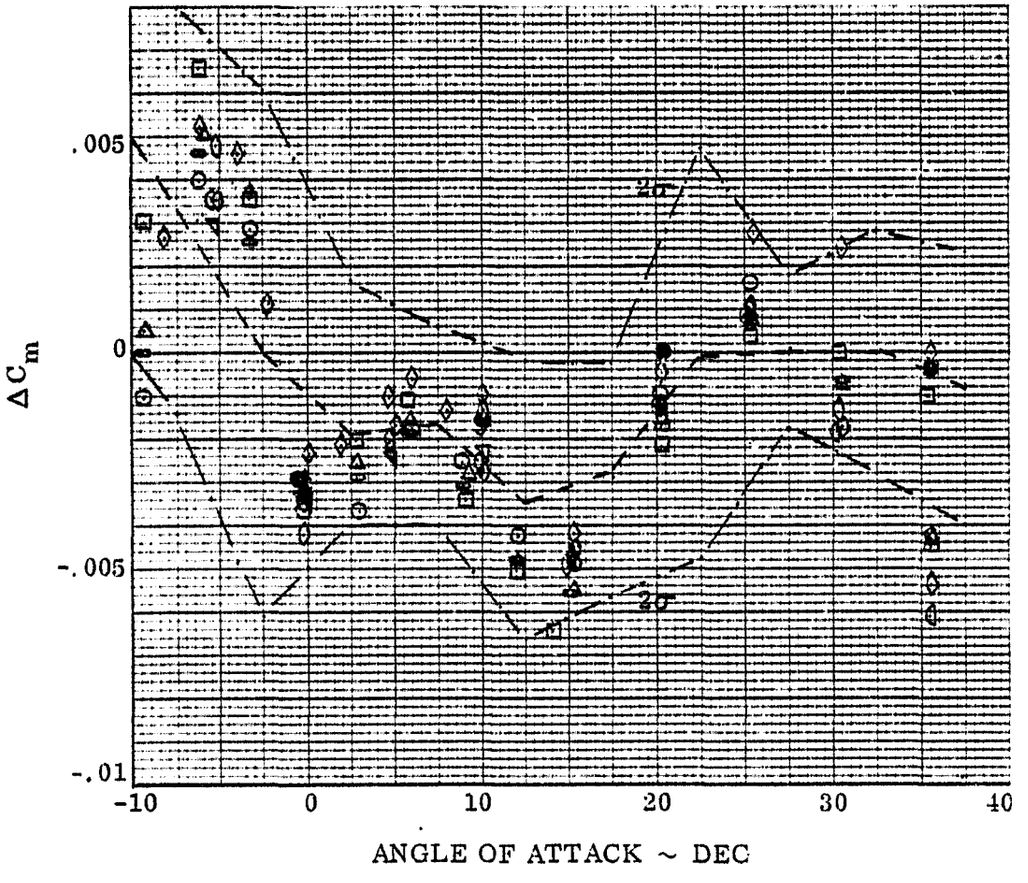

FIGURE 6-11 A COMPARISON OF TEST DATA FOR NOZZLE N52 WITH PREDICTION PROGRAM RESULTS: PITCHING MOMENT COEFFICIENT

$$\Delta C_n = C_{n\ \text{JET ON}} - C_{n\ \text{JET OFF}}$$

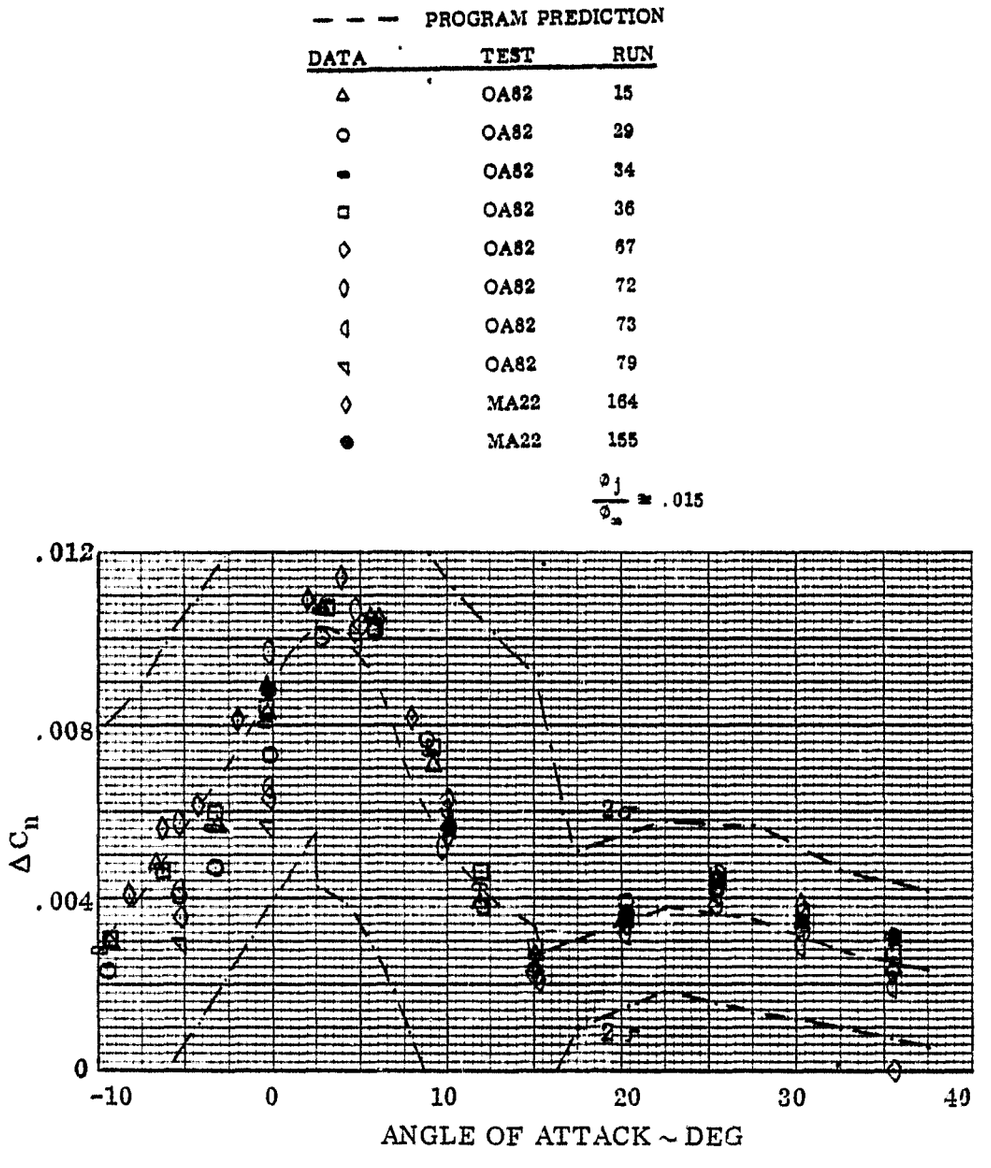

FIGURE 6-12 A COMPARISON OF TEST DATA FOR NOZZLE N52 WITH PREDICTION PROGRAM RESULTS: YAWING MOMENT COEFFICIENT

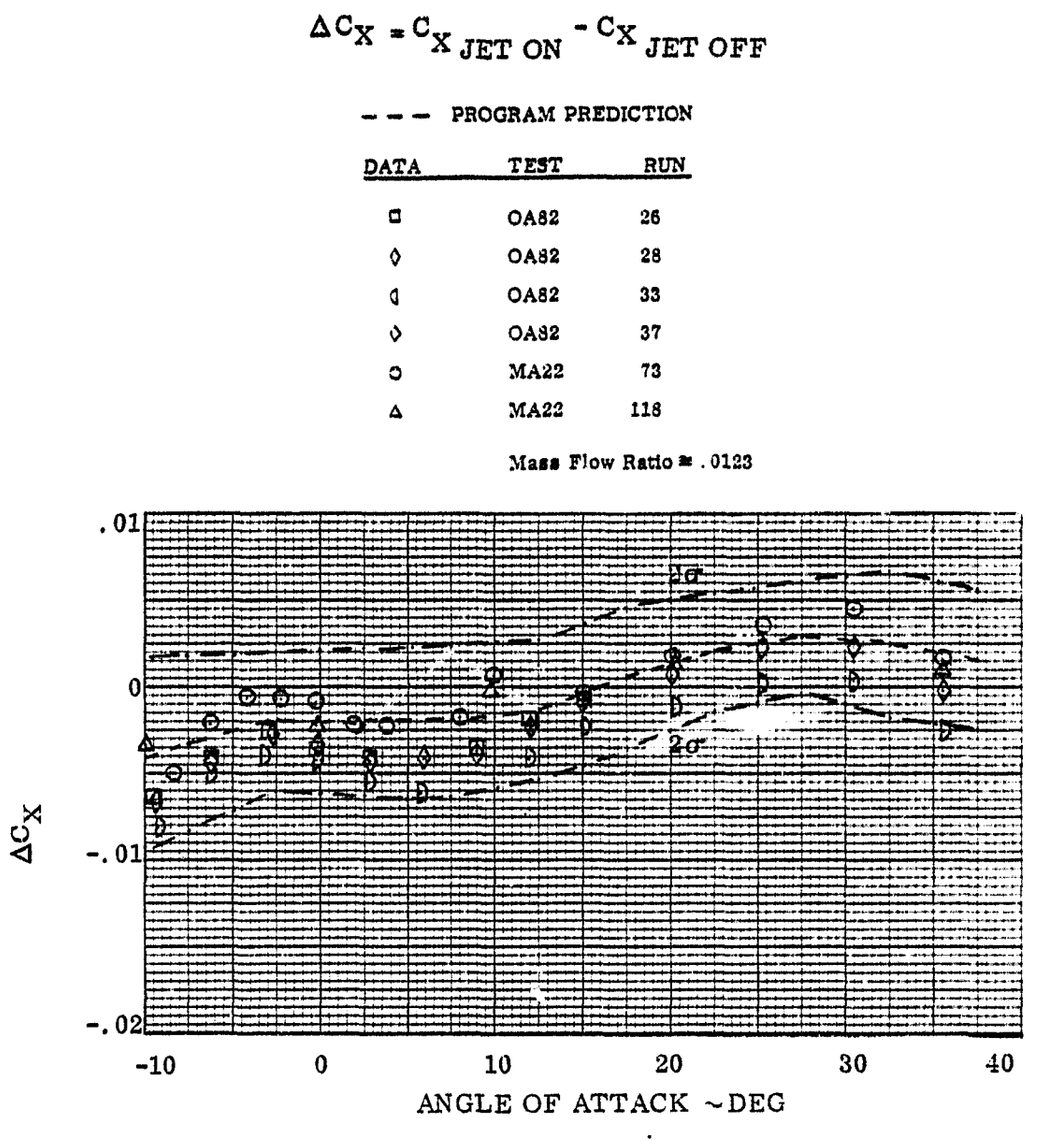

FIGURE 6-13 A COMPARISON OF TEST DATA FOR NOZZLE N85 WITH PREDICTION PROGRAM RESULTS: LONGITUDINAL FORCE COEFFICIENT

$$\Delta C_Z = C_{Z\ \text{JET ON}} - C_{Z\ \text{JET OFF}}$$

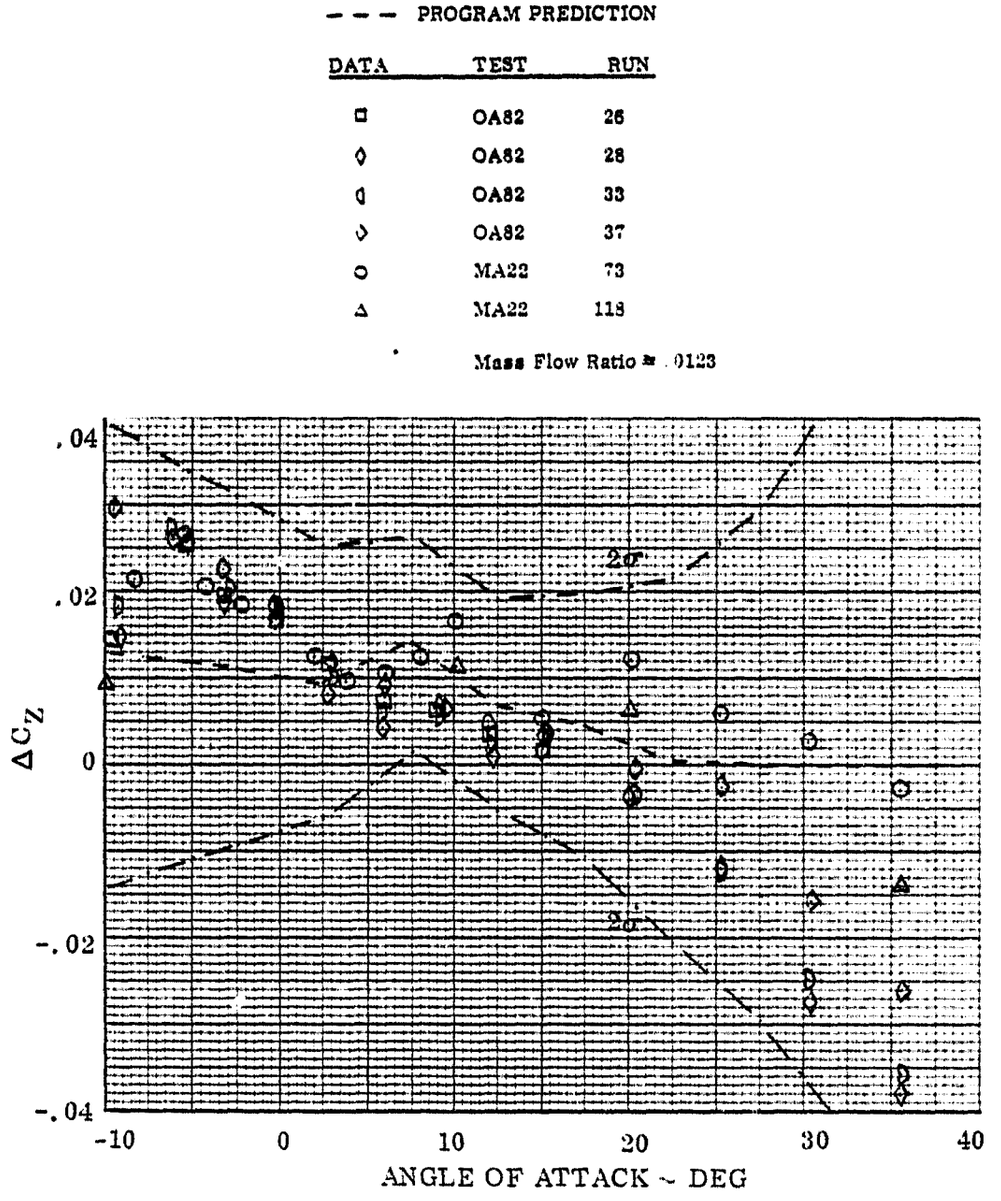

FIGURE 6-14 A COMPARISON OF TEST DATA FOR NOZZLE N85 WITH PREDICTION PROGRAM RESULTS: VERTICAL FORCE COEFFICIENT

$$\Delta C_Y = C_{Y\ \text{JET ON}} - C_{Y\ \text{JET OFF}}$$

– – – PROGRAM PREDICTION

DATA	TEST	RUN
□	OA82	26
◊	OA82	28
◁	OA82	33
◇	OA82	37
○	MA22	73
△	MA22	118

Mass Flow Ratio = .0123

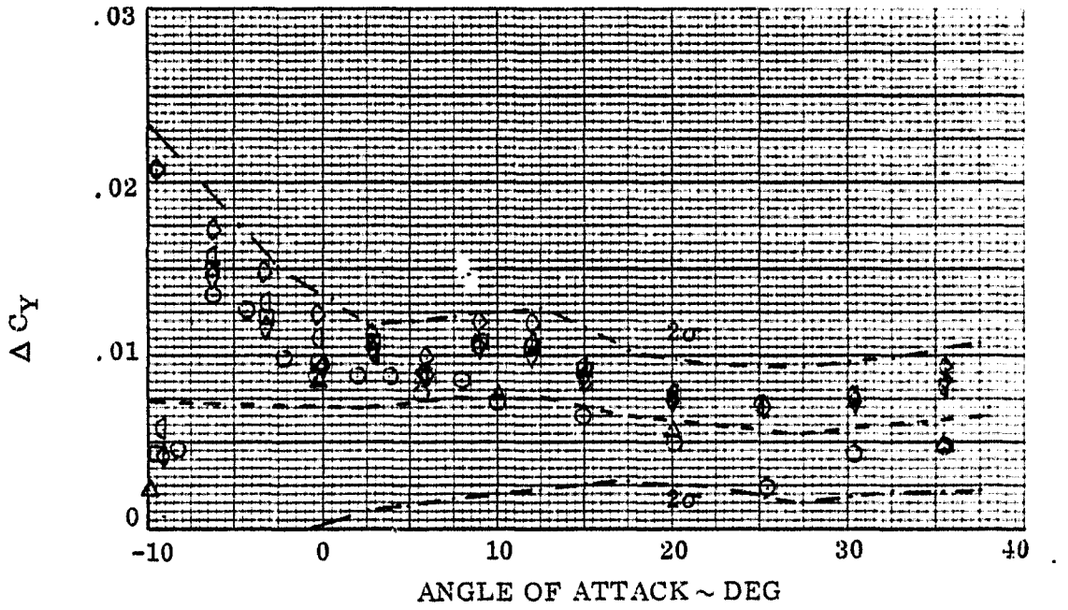

FIGURE 6-15 A COMPARISON OF TEST DATA FOR NOZZLE N85 WITH PREDICTION PROGRAM RESULTS: SIDE FORCE COEFFICIENT

$\Delta C_\ell = C_\ell$ JET ON $- C_\ell$ JET OFF

— — — PROGRAM PREDICTION

DATA	TEST	RUN
□	OA82	26
◇	OA82	28
◁	OA82	33
◇	OA82	37
○	MA22	73
△	MA22	118

Mass Flow Ratio = .0123

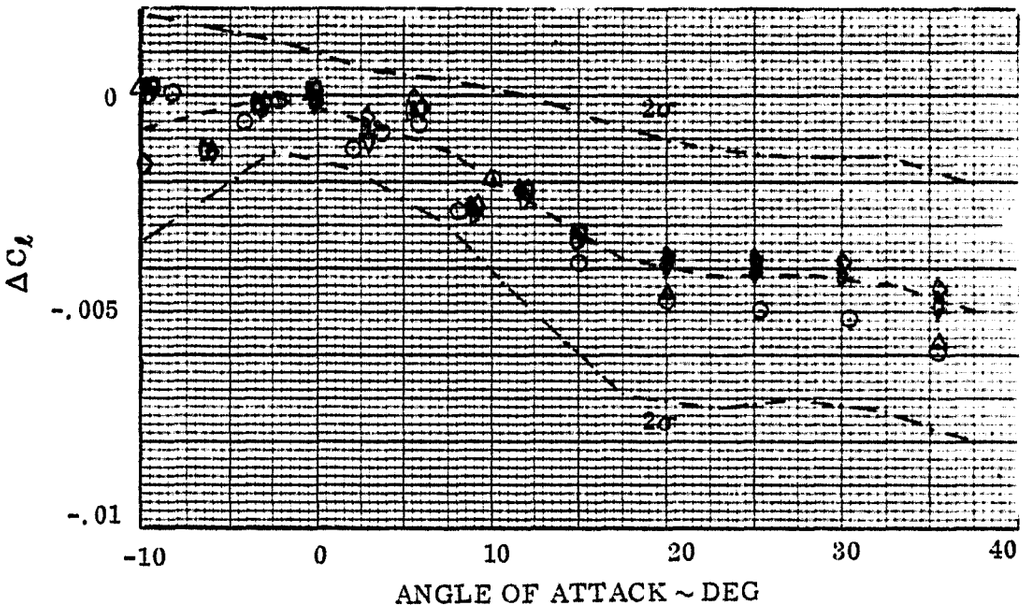

FIGURE 6-16 A COMPARISON OF TEST DATA FOR NOZZLE N85 WITH PREDICTION PROGRAM RESULTS: ROLLING MOMENT COEFFICIENT

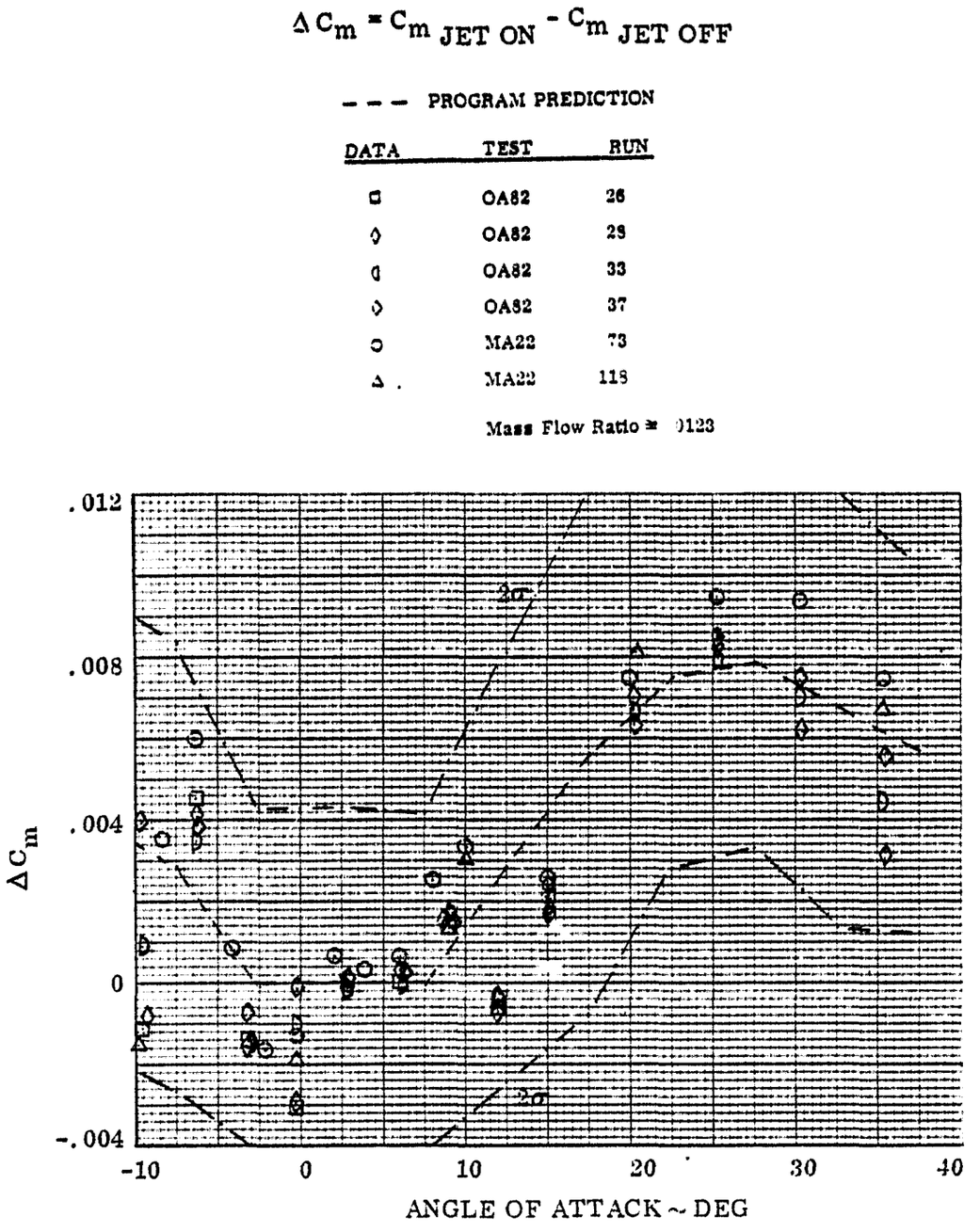

FIGURE 6-17 A COMPARISON OF TEST DATA FOR NOZZLE N85 WITH PREDICTION PROGRAM RESULTS: PITCHING MOMENT COEFFICIENT

$$\Delta C_n = C_{n\ \text{JET ON}} - C_{n\ \text{JET OFF}}$$

– – – PROGRAM PREDICTION

DATA	TEST	RUN
□	OA82	26
◊	OA82	28
◁	OA82	33
◊	OA82	37
○	MA22	73
△	MA22	118

Mass Flow Ratio = .0123

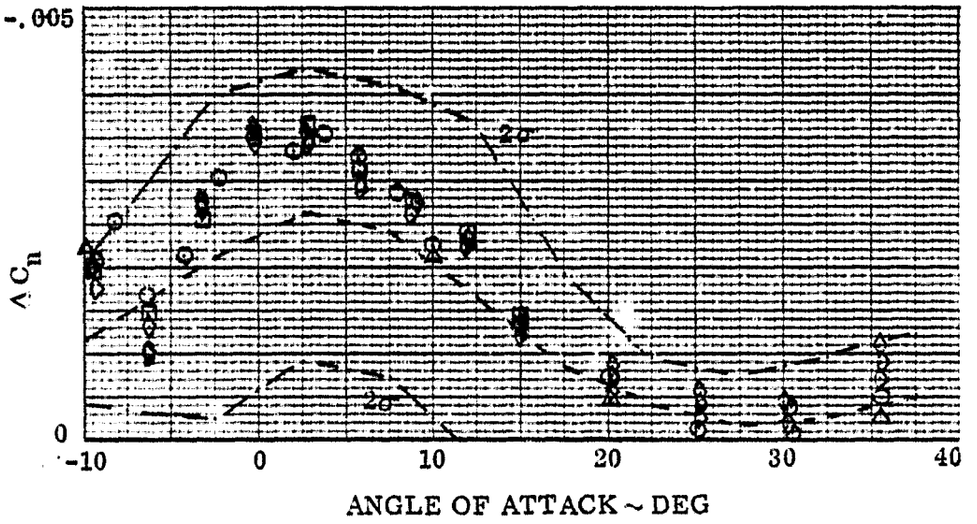

FIGURE 6-18 A COMPARISON OF TEST DATA FOR NOZZLE N85 WITH PREDICTION PROGRAM RESULTS: YAWING MOMENT COEFFICIENT

7

FULL SCALE CONFIDENCE

Sections 3 to 5 develop a prediction model for determining reaction control system effectiveness based on numerous wind tunnel data. Section 6 showed that the model will reproduce the wind-tunnel results. But such a model is of little use unless it can be extended to the flight regime with some degree of confidence. This section will attempt to address this question for the re-entry case only.

7.1 TEST TO TEST VARIATION ERRORS

The test to test variation between the Mach 10 tests OA82 and MA22 were carried over into the incremental jet data by using one jet-off run (MA22 run 5) for both sets of data. Thus all differences between these tests are accounted for in the curve fits of Section 3 and are computed into the estimates of data scatter given on each plot.

The average jet-off differences for the mean of all of the Mach 10 jet-off data compared to the mean jet-off run from OA169 is shown in Figure 7-1a to 7-1f. This difference which may be due to Mach number and/or test and models differences was too large compared to the RCS data to be left in and was removed from the data by using OA169 jet-off runs to obtain RCS increments for Mach 6. Section 3 shows that the OA169 incremental effects generally all fall within the error boundaries of the Mach 10 data. Therefore there seems to be no test to test variation of induced RCS effect has which has not been accounted for.

7.2 MEAN VALUE DIFFERENCES

There were 6 jet-off runs during test OA82 and 28 more obtained during test MA22. Since the data presented in Reference 2 showed there were measurable differences in the jet-off runs, the question can be raised as to whether all of this has been accounted for in the data sample and true mean difference curves obtained. This aspect of the problem was investigated by Chrysler DATAMAN (Reference 10) in which all jet-off data runs were used to take differences with all jet-on runs for a sample case. In this case nozzle N49 at nozzle pressures of 150, 300 and 600 psia. When all the differences were taken for all jet-on minus all jet-off runs at a given pressure and angle of attack an average value and standard deviation were computed.

Figures 7-2a and 7-2b present samples of the mean curves compared with the model results. The model accounts for many other nozzles and pressures so that the agreement is not perfect, but it appears close enough to verify that the model does a good job of representing the true mean value of the difference.

7.3 STANDARD DEVIATION OF DATA SAMPLE

The derivation of mean values discussed above also resulted in estimates of the standard deviation of error for nozzle N49 at the three supply pressures. Figure 7-3 present the computed values of the standard deviations for all of the jet-on runs at the three supply pressures minus all of the jet-off runs as computed in Reference 10 . The close agreement between them at each angle of attack shows that they are good estimates of the true data scatter. In addition the root-mean-square error from the analytic model agrees quite well with them. The RMS value contains within it other nozzle data and OA169 data averaged over 5 degree intervals and is slightly larger at all angles of attack. In addition the standard deviations of the jet-off runs for OA82 and MA22 are shown on this plot and these again show that the RMS error of the analytic curve fits contain them. Thus it is concluded that the RMS values for the analytic curve fits are good estimates of the true standard deviation of error of the population of reaction control incremental data.

7.4 MACH SCALING UNCERTAINTY

The wind-tunnel data used in this analysis was obtained at Mach numbers of 6 and 10. while the entry flight condition simulated is Mach 25. The question arises then whether the wind tunnel data is valid or needs to be scaled for Mach effects.

The nozzle flow parameters (momentum ratio and mass flow ratio) have already been tested to full scale for nominal entry conditions as low as a q of 5 PSF for a 3 nozzle case and proportionally lower for fewer nozzles. A nominal condition of 280,000 feet at 26,100 feet per second is approximately 5 PSF and represents a momentum ratio of .0954 for a 3 nozzle case while MA 22 test data was obtained to a momentum ratio of approximately .12. The mass flow parameter at this nominal entry case is .0437 while test data was obtained to .05. Thus the nozzle simulation does not need to be scaled.

Figures 7-4 a to 7-4 c show Mach effect data for the jet-off conditions obtained from orbiter test OA77/78. The only data to show a consistent Mach trend is the pitching moment data, however, the difference between Mach 8 and 10 is shown to be within the OA82-MA22 test to test variation and the OA169/MA22 difference cuts across both. Test to test variation, thus, must be larger than any Mach effect.

The OA169 data was shown in Section 3 to fit within the Mach 10 error band and thus test to test variation is accounted for. In addition, data from Reference 1 showed that there was no Mach effect on RCS interaction at Mach numbers from 2.5 to 4.5. Thus it appears that no further scaling is required for Mach number.

7.5 REYNOLDS NUMBER SCALING UNCERTAINTY

Most of the wind tunnel data was obtained at a nominal Reynolds Number of 1×10^6. The nominal entry condition value for 280,000 feet and 26,100 feet per second

velocity is 1.6×10^5 based on vehicle length.

A limited number of runs were made during test OA82 to determine whether there is a Reynolds number effect, but, all measurable changes are within the data scatter of the nominal data. Since the data was limited it was decided to replot the data at each angle of attack to compare trends just of these runs forgetting that they are all within the expected error. Figures 7-5 a to 7-5 d present the results for pitch down nozzle N49 at the one common value of momentum ratio obtained. No consistent trend can be discussed so a "worst case" was chosen from the angle of attack that showed the most slope and "worst case" approximations computed

$$\Delta C_{M_{Re}} = \Delta C_{M_{(Re=1\times10^6)}} (1 + F (13.88 - \log_e(R_e'))) \qquad (1)$$

where

$\Delta C_{M_{Re}}$ = Any RCS interaction force or moment at flight Reynolds number

$\Delta C_{M_{(Re=1\times10^6)}}$ = Predicted interaction force or moment from model

Re = Flight Reynolds number based on vehicle length

F = "Worst case" slope

The N52 nozzle data is presented in Figure 7-6 a to 7-6 c and the values of F for each component are:

I Nozzle N49

ΔC_N	F = .6634277
ΔC_A	F = .253966
ΔC_m	F = .0276764
ΔC_ℓ	F = .0547855

II Nozzle N52

ΔC_Y	F = .1787406
ΔC_ℓ	F = .4176398
ΔC_n	F = .0998407

Figure 7-7 presents the "worst case" Reynolds scaling effect on two cases; a 3 jet pitch up case and a 3 jet pitch down case. Reynolds number scaling principally changes the roll control power. This adverse change principally occurs on the pitch up fin interaction with the fin and was derived from the data at 15 to 20 degrees angle of attack (Figure 7-6 c). Since entry is to be made at angles of attack above 35 degrees, it is concluded that Reynolds scaling will not appreciably change the entry control effectiveness. RTLS roll control effects, however, need to be examined in the light of this "worst case" effect.

7.6 VEHICLE C.G. UNCERTAINTY

Figures 7-8 to 7-10 present the effect of CG misalignments in RCS effectiveness in the sample cases of 3 jets in pitch-up and pitch down at nominal entry conditions. If the center of gravity is higher than predicted there will be some loss in roll effectiveness from the pitch down jet cluster due to the sizeable amount that results from nozzle cant generated side force,on the order of 5% of the thrust moment for 1 foot of error. The error in lateral C.G. location will also change the roll component as is shown in Figure 7-10. However, a pure roll application will be self-compensating since the jets clusters will be on opposite sides rather than the same side as computed in Figure 7-10.

7.7 ATMOSPHERE UNCERTAINTY

All predictions shown in this section and made by the analytic program are done using a 1962 standard atmosphere condition. The seasonal high and low means and 1% extreme values for temperature and density obtained from the 1976 standard atmosphere (Reference 11), were used to change the standard day conditions for the entry test case at 280,000 ft. and the entry test case was recomputed. Figure 7-11 shows that seasonal means result in a variation in entry dynamic pressure at the altitude from 2.9 to 6 pounds per square foot and the two standard deviation extremes increase the range of dynamic pressure from a low of 1.7 PSF to a high of 7.3 PSF. The 3 jet on one side case momentum ratio at the standard atmosphere condition has a value of .0945 so that there is no extrapolation of interaction data. The lowest temperature/lowest density conditions result in lower dynamic pressures and an increasing momentum ratio to a value of .27 at the lowest extreme. The limiting parameters on the interaction curves fits, however, keep the interaction terms relatively constant and the thrust begins to predominate. Thus the control amplification shown in Figure 7-11 increases at the lower dynamic pressures. The higher temperature/high density conditions result in an increasing free stream dynamic pressure and a reduction in momentum ratio to a value of .064. There is no extrapolation in the interaction curve fits moving in this direction, but the interaction terms are becoming more important as shown by the declining control amplification.

The cross-coupling term which comes into play in the symmetric pitch case shown in Figure 7-11 is subject to considerable extrapolation since the limiting momentum ratio is .03 which is exceeded by all conditions at this altitude. It causes about a 10% reduction in pitch amplification using the present .03 limit on the curve.

Confidence that the predicted value and the error band are cor. . . improves with increasing dynamic pressure since there is no extrapolation of data involved. This curve points to the RTLS case as the case of lowest RCS control power and the desirability of staging at as low a dynamic pressure as possible under that condition. This curve shows that a large variation of roll controll amplification will result in flight if standard day performance is used to make predictions fuel requirements. Similar comparisons of yaw control yaw amplification showed essentially no effect.

7.8 EXTRAPOLATION UNCERTAINTY

The flight data of the preceding section section showed that no extrapolation of single side data was required at the standard day 5 PSF entry condition but that it was required for lower dynamic pressures. The analytic program was modified to remove all constraints on curve extrapolation and the case of Section 7.7 was repeated. The results of allowing unlimited extrapolation are shown in Figure 7-12 where no problem is seen down to a dynamic pressure of 2 PSF. The roll amplification curves start to break at 2 PSF as the interaction terms grow in an unbounded manner. The vacuum solution will be an amplification of negative infinity for these unbounded solutions which the OA99 vacuum data shows is unreasonable. The higher dynamic pressure cases where the extrapolation is limited to the symmetric pitch down cross-coupling remain the more critical in terms of lowest control amplification. The cross-coupling term for symmetric pitch down cuts the pitch amplifcation by nearly 25% of the thrust moment and this points out the need for better symmetric pitch simulation especially for the higher dynamic pressure RTLS case.

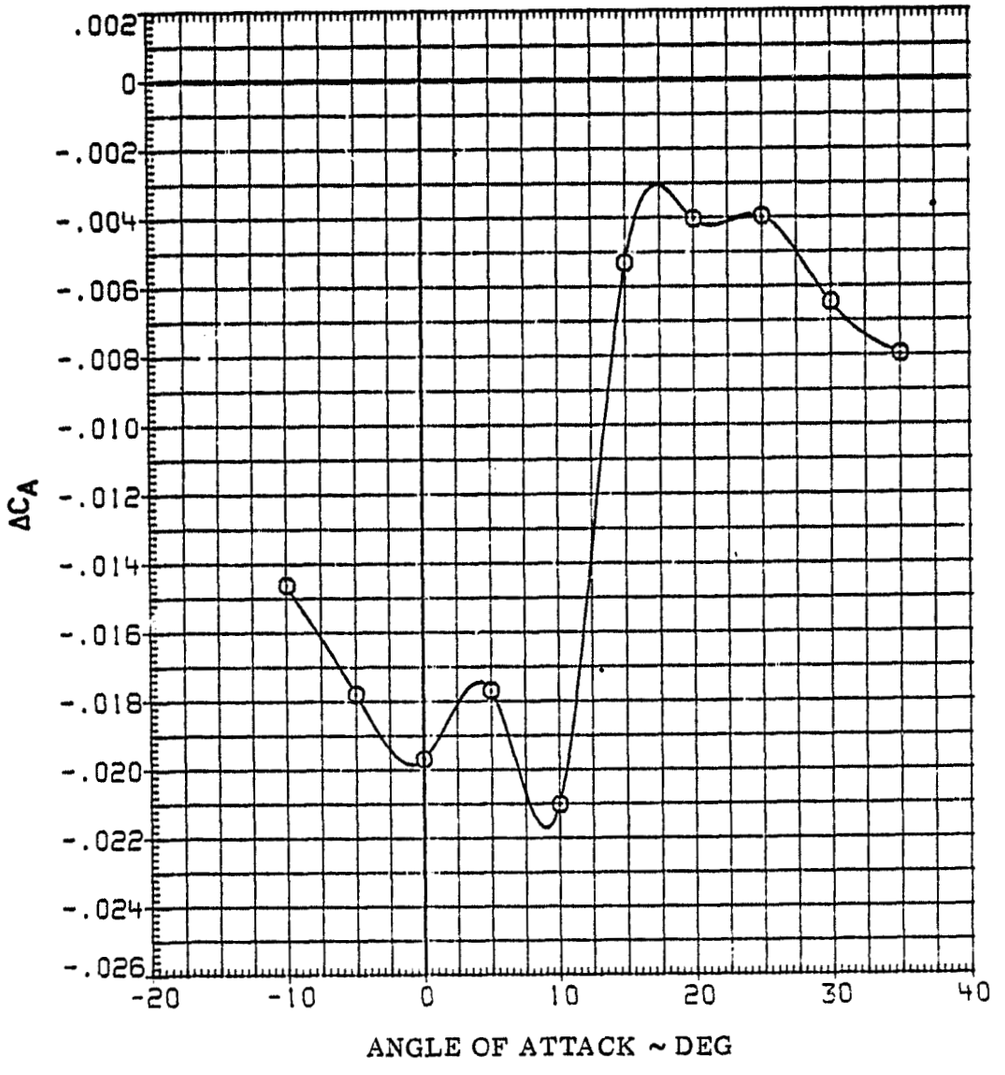

FIGURE 7-1a. DIFFERENCE OF AVERAGED DATA (MA22/0A82-0A169) AXIAL FORCE COEFFICIENT

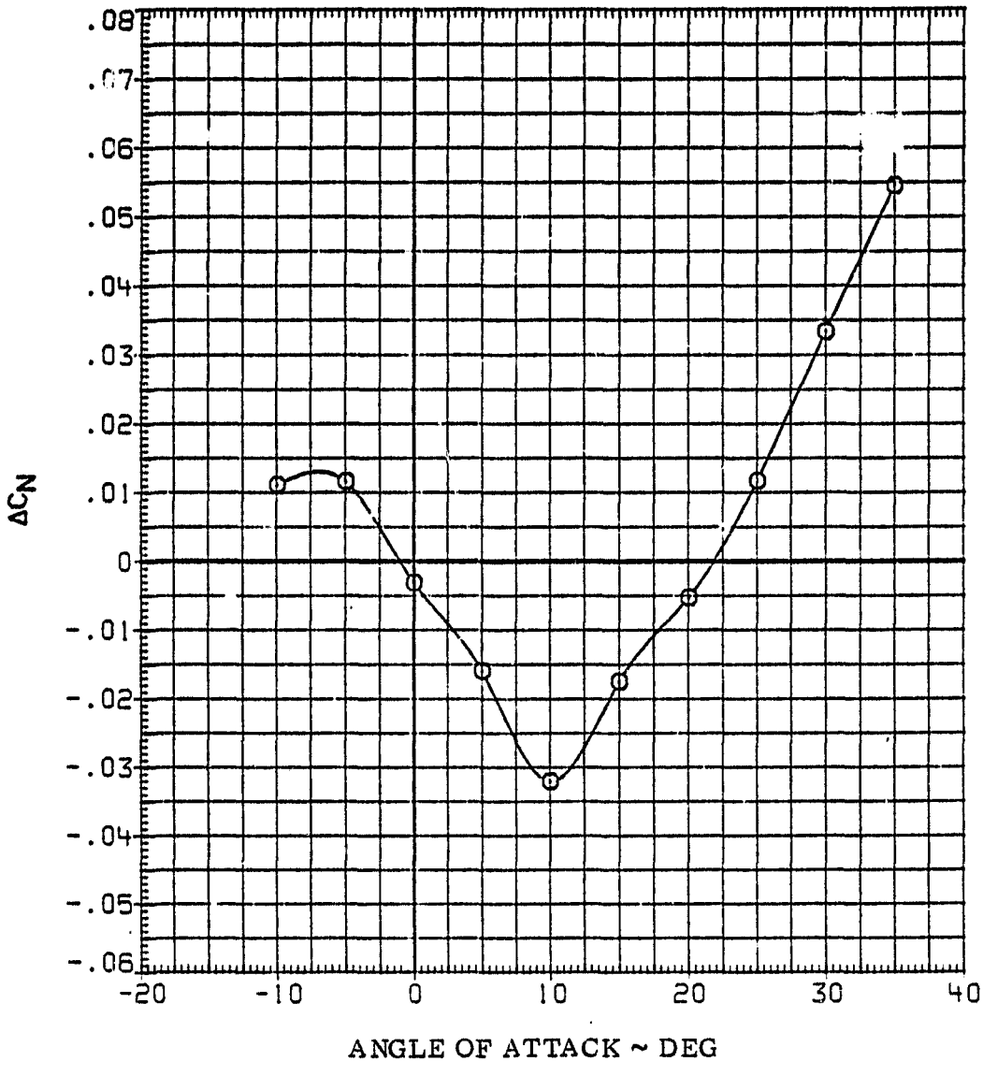

FIGURE 7-1b DIFFERENCE OF AVERAGED DATA (MA22/0A82-0A169)
NORMAL FORCE COEFFICIENT

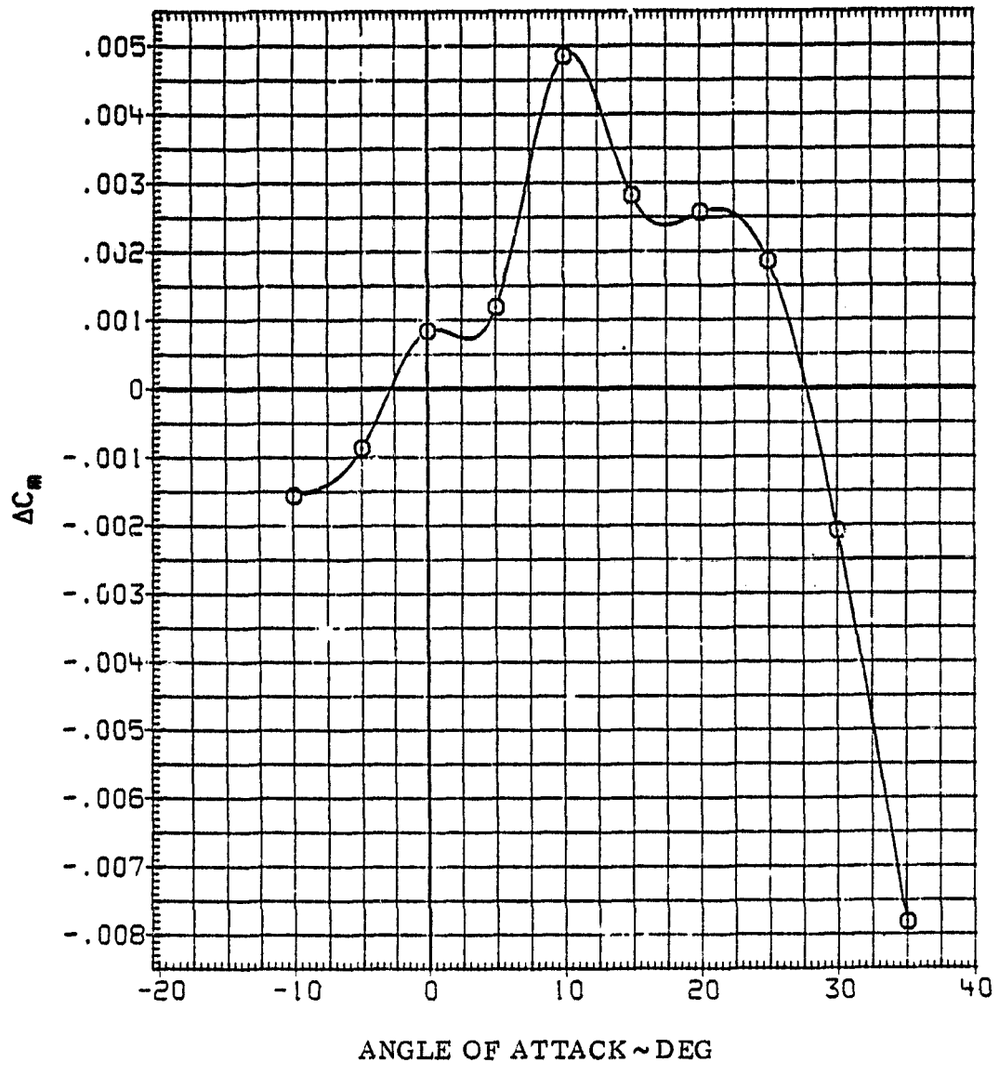

FIGURE 7-1c DIFFERENCE OF AVERAGED DATA (MA22/0A82-0A169)
PITCHING MOMENT COEFFICIENT

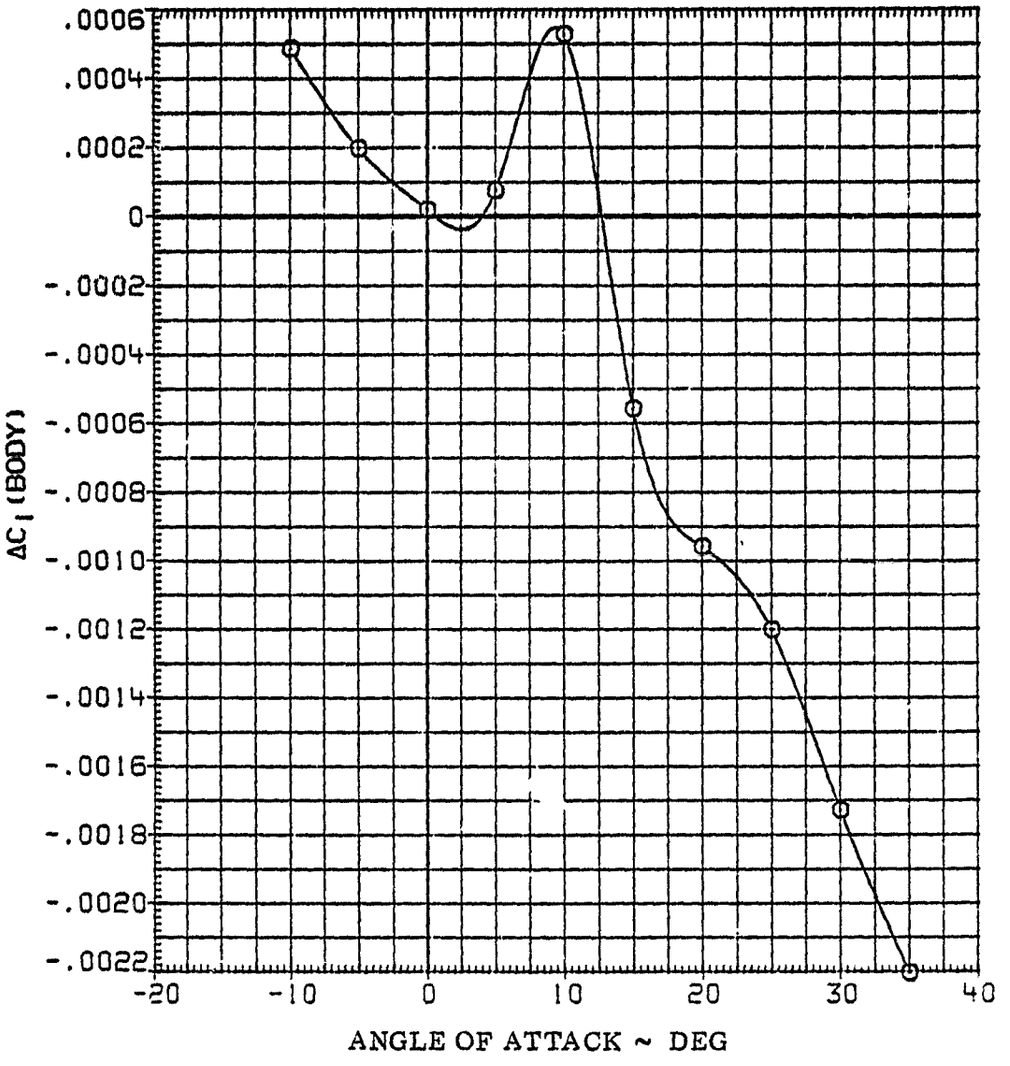

FIGURE 7-1d DIFFERENCE OF AVERAGED DATA (MA22/0A82-0A169)
ROLLING MOMENT COEFFICIENT

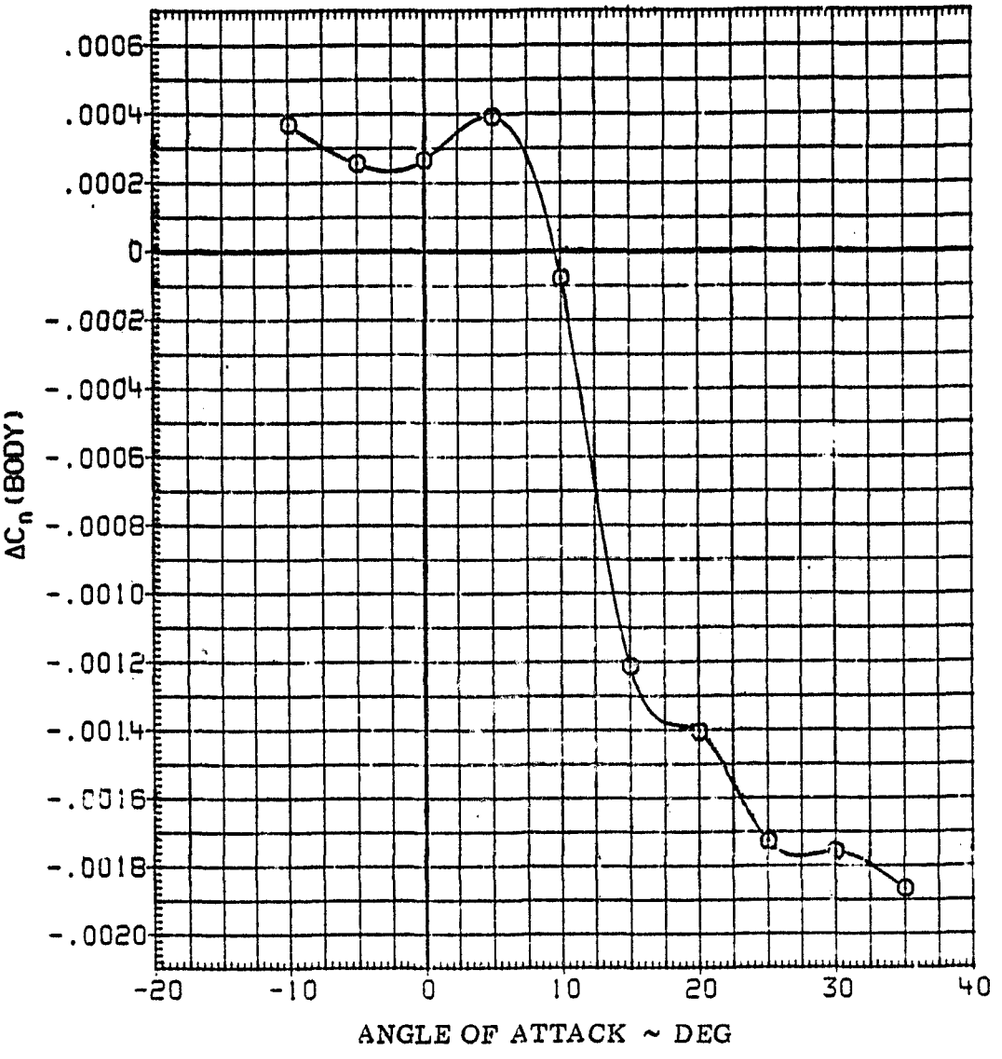

FIGURE 7-1e DIFFERENCE OF AVERAGED DATA (MA22/0A82 - 0A169) YAWING MOMENT COEFFICIENT

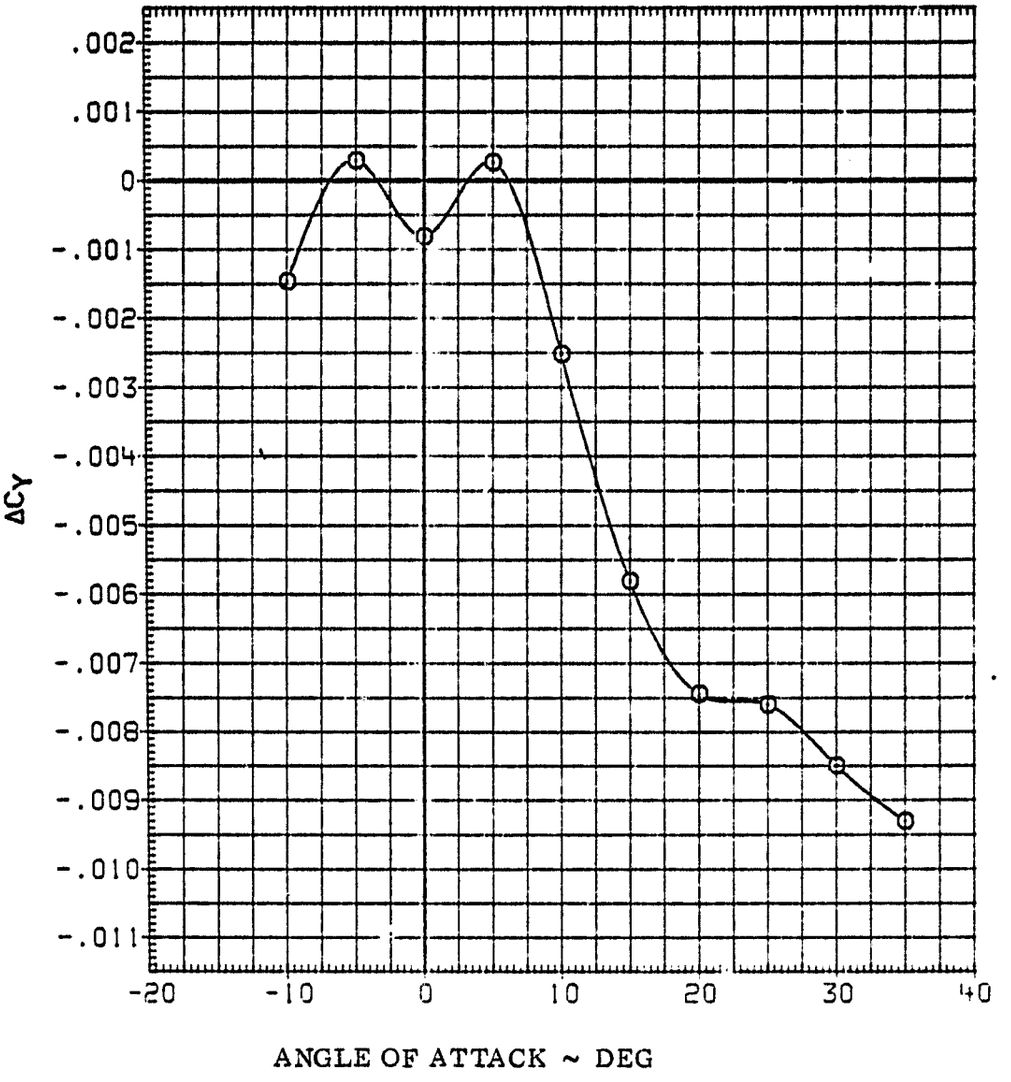

FIGURE 7-1f DIFFERENCE OF AVERAGED DATA (MA22/0A82-0A169)
SIDE FORCE COEFFICIENT

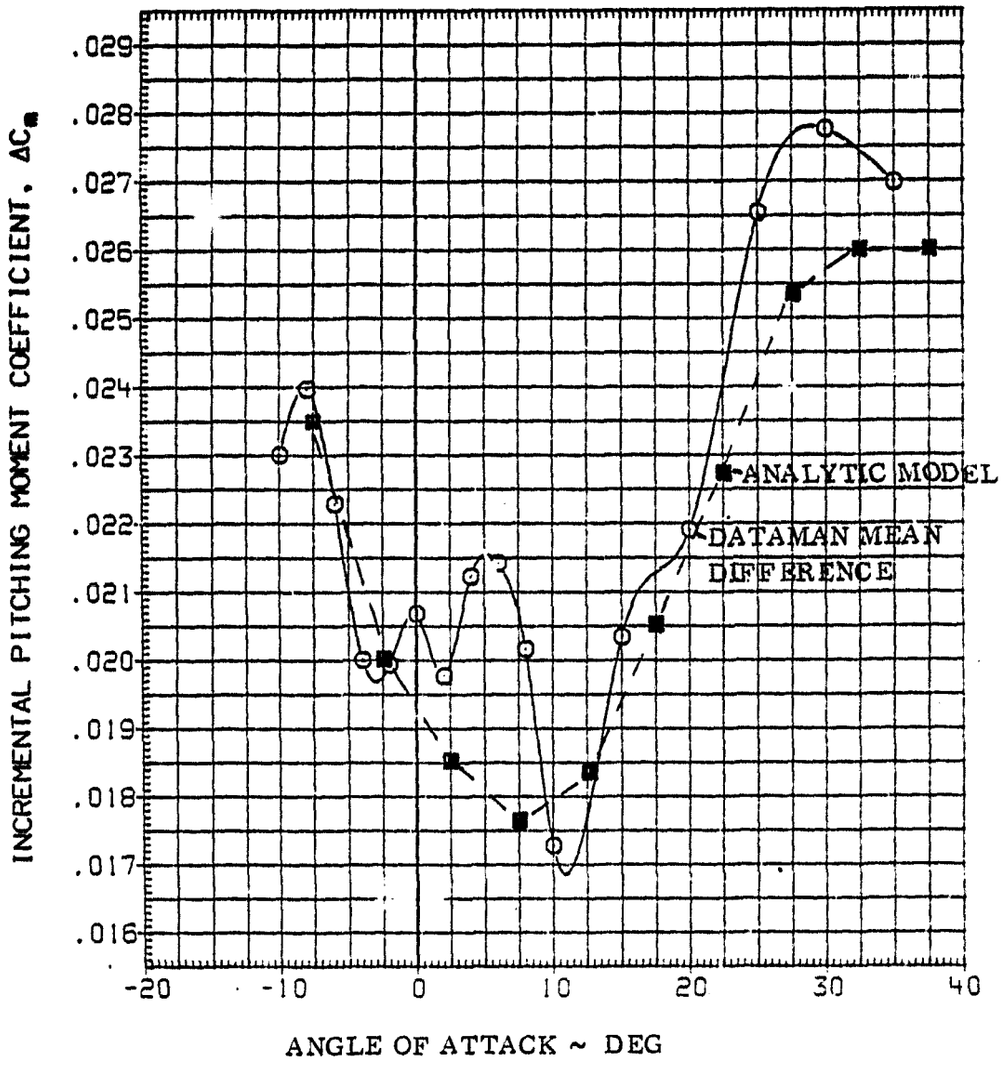

FIGURE 7-2a NOZZLE N49 MEAN INCREMENTAL DATA FOR 300 PSIA NOZZLE PRESSURE: PITCHING MOMENT

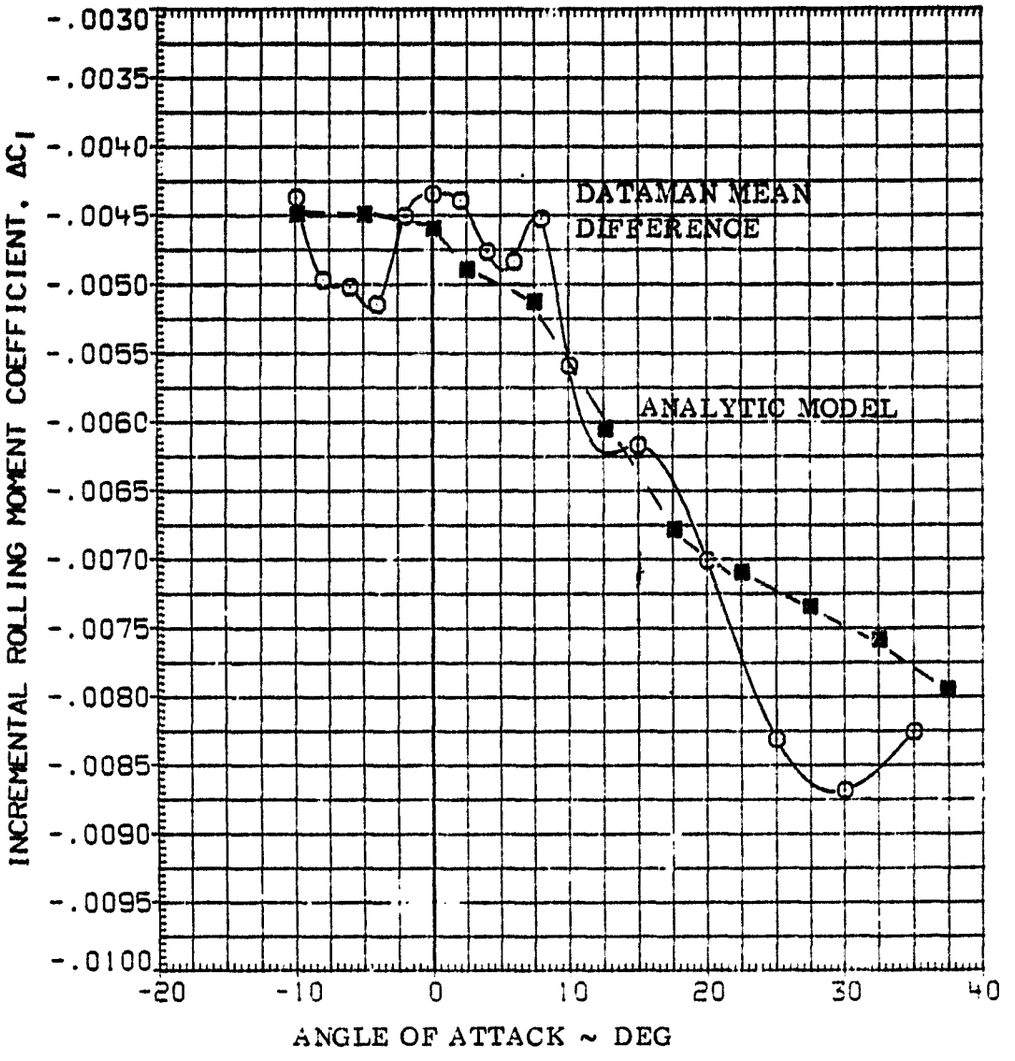

FIGURE 7-2b NOZZLE N49 MEAN INCREMENTAL DATA FOR 300 PSIA NOZZLE PRESSURE: ROLLING MOMENT

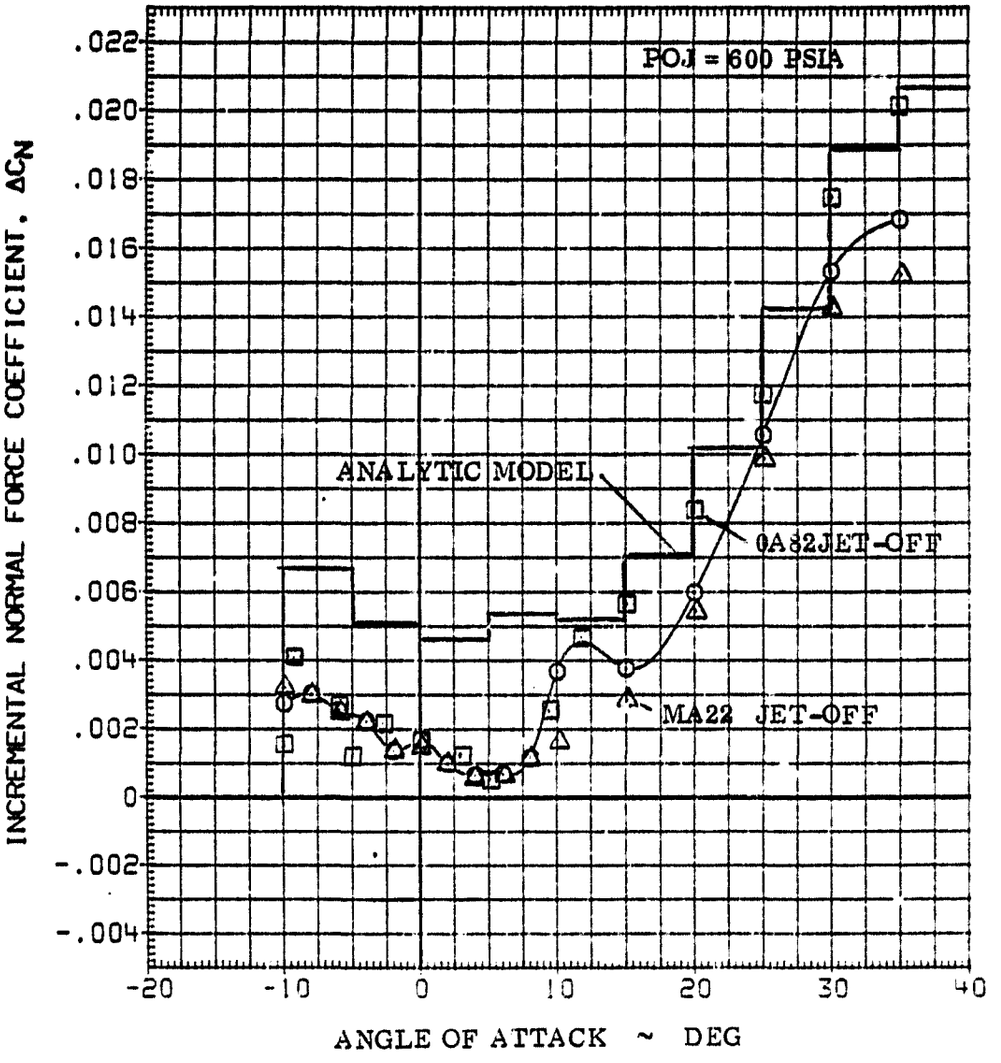

FIGURE 7-3a NOZZLE N49 STANDARD DEVIATION OF TEST INCREMENTS

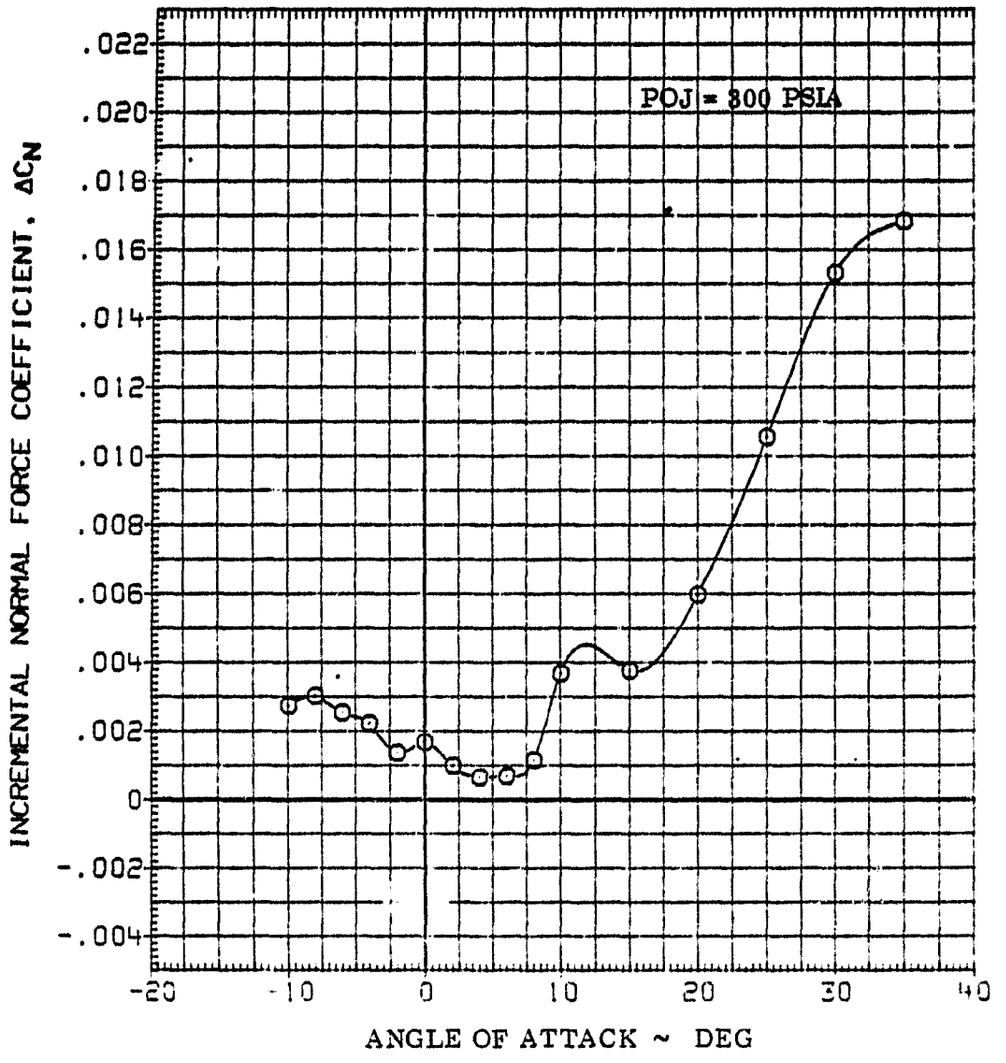

FIGURE 7-3b NOZZLE N49 STANDARD DEVIATION OF TEST INCREMENTS

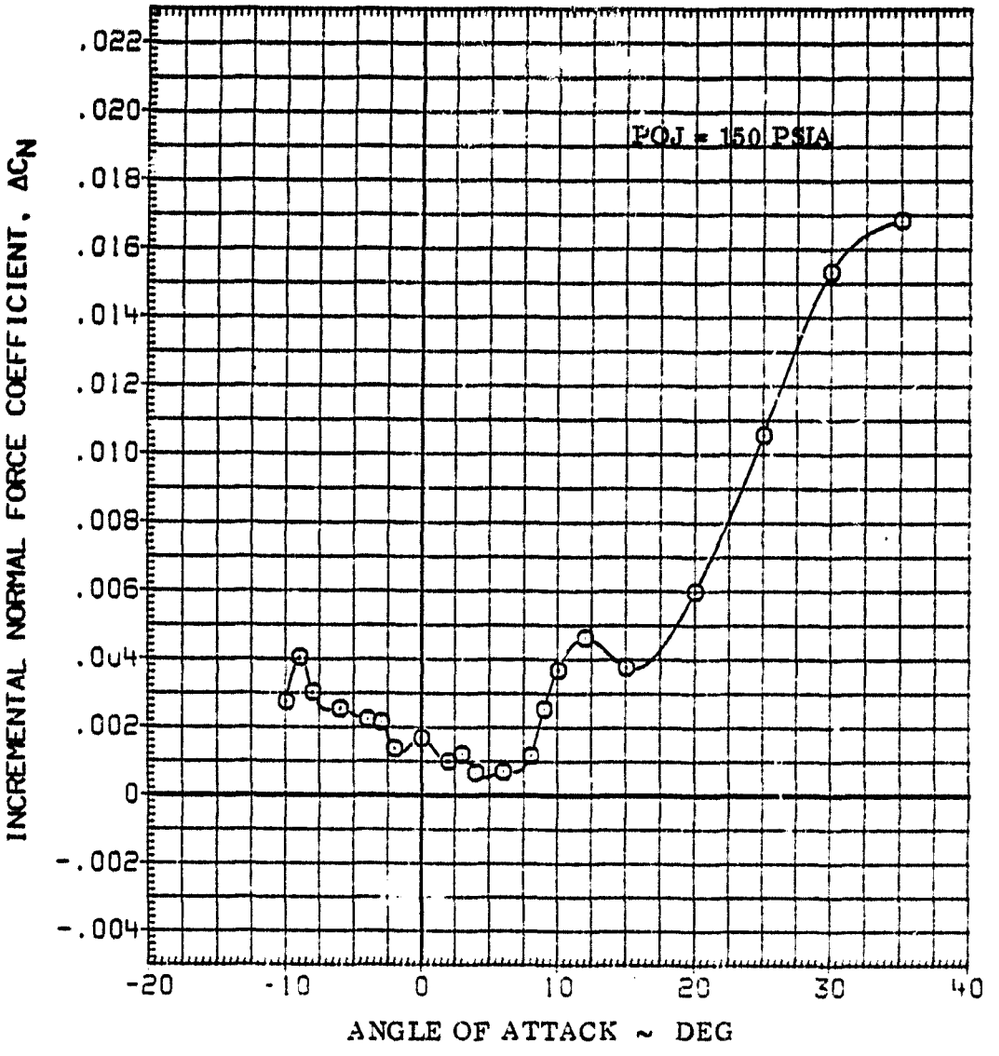

FIGURE 7-3c NOZZLE N49 STANDARD DEVIATION OF TEST INCREMENTS

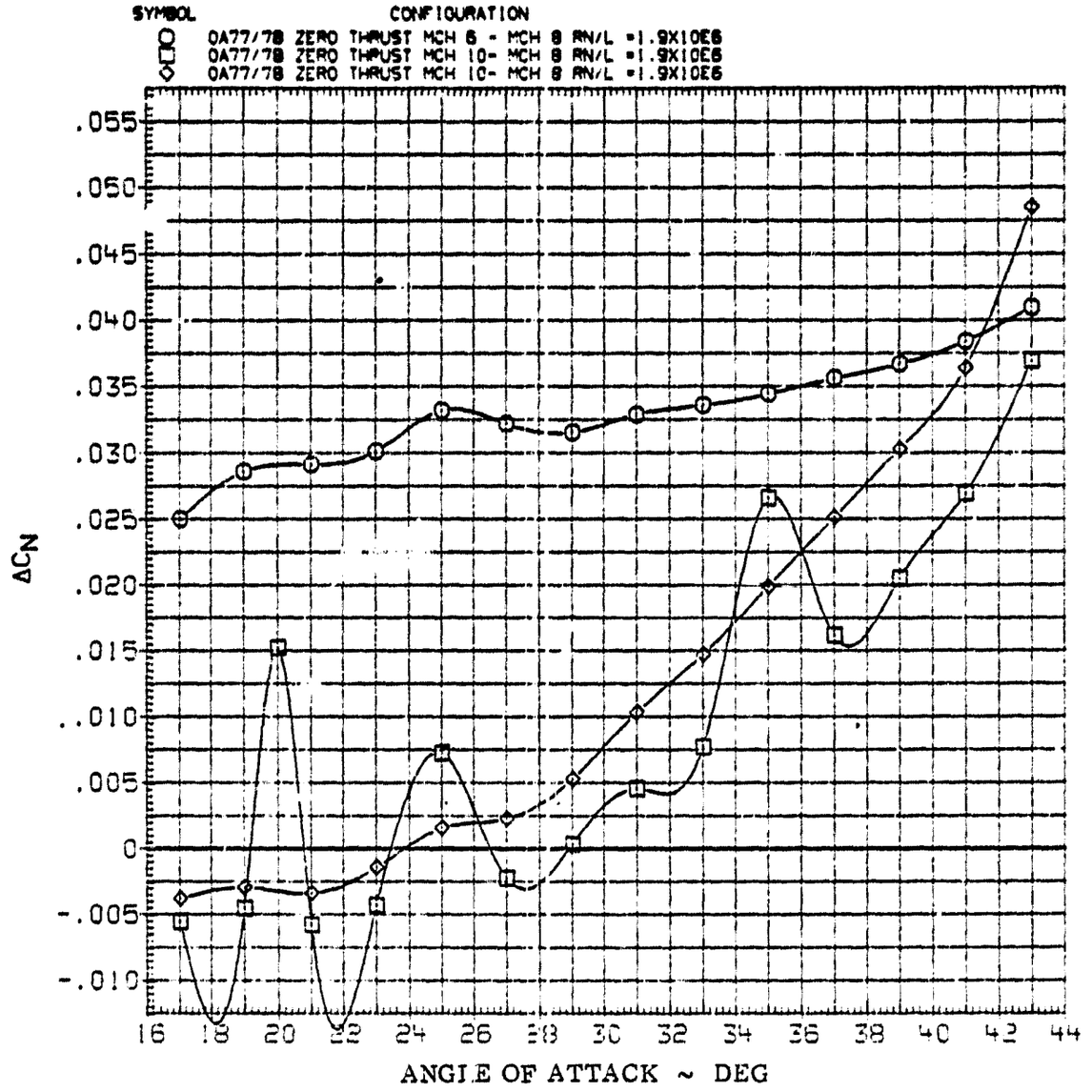

FIGURE 7-4a 0A77/78 DIFFERENCES DUE TO MACH NUMBER

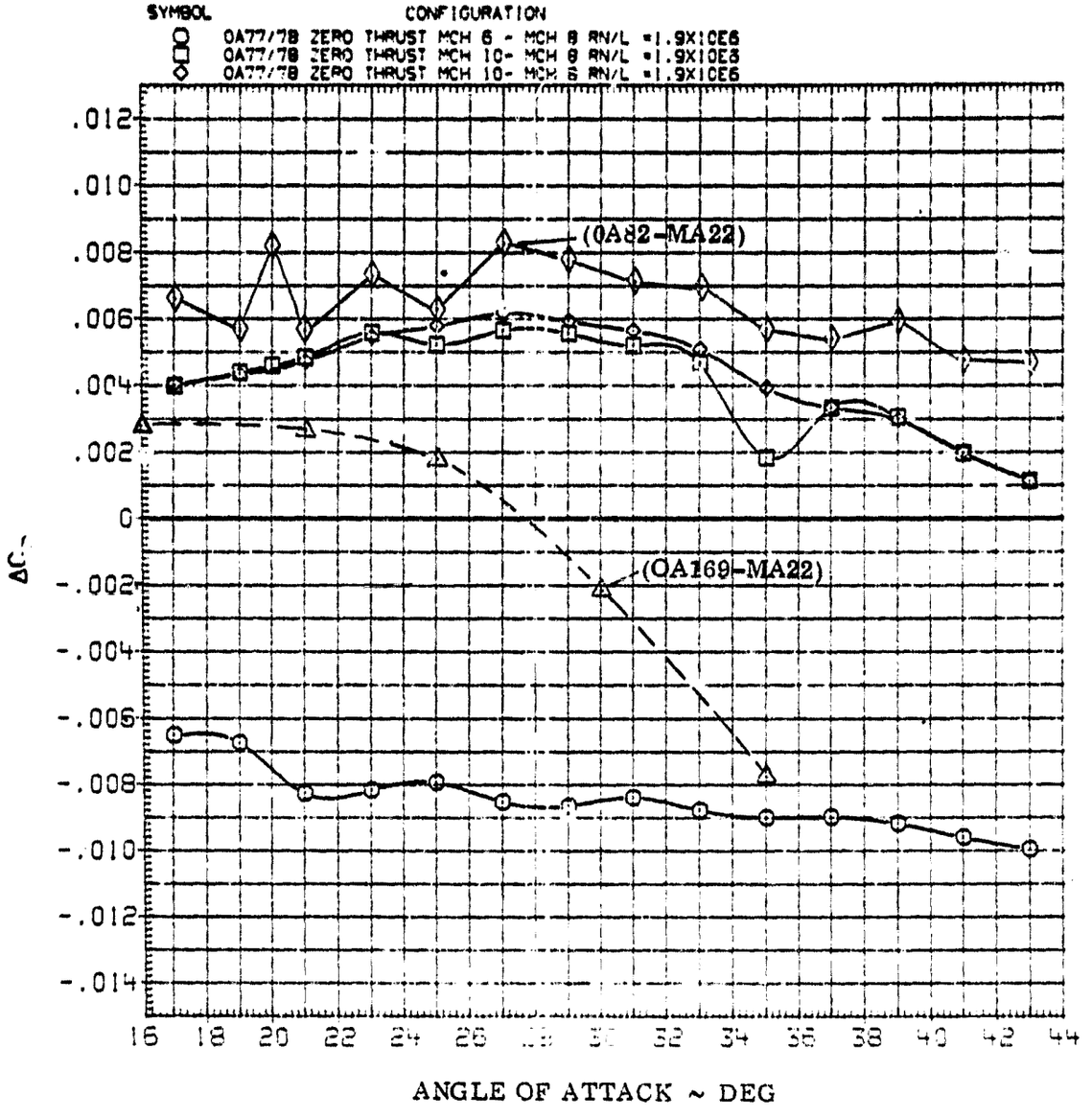

FIGURE 7-4b 0A77/78 DIFFERENCES DUE TO MACH NUMBER

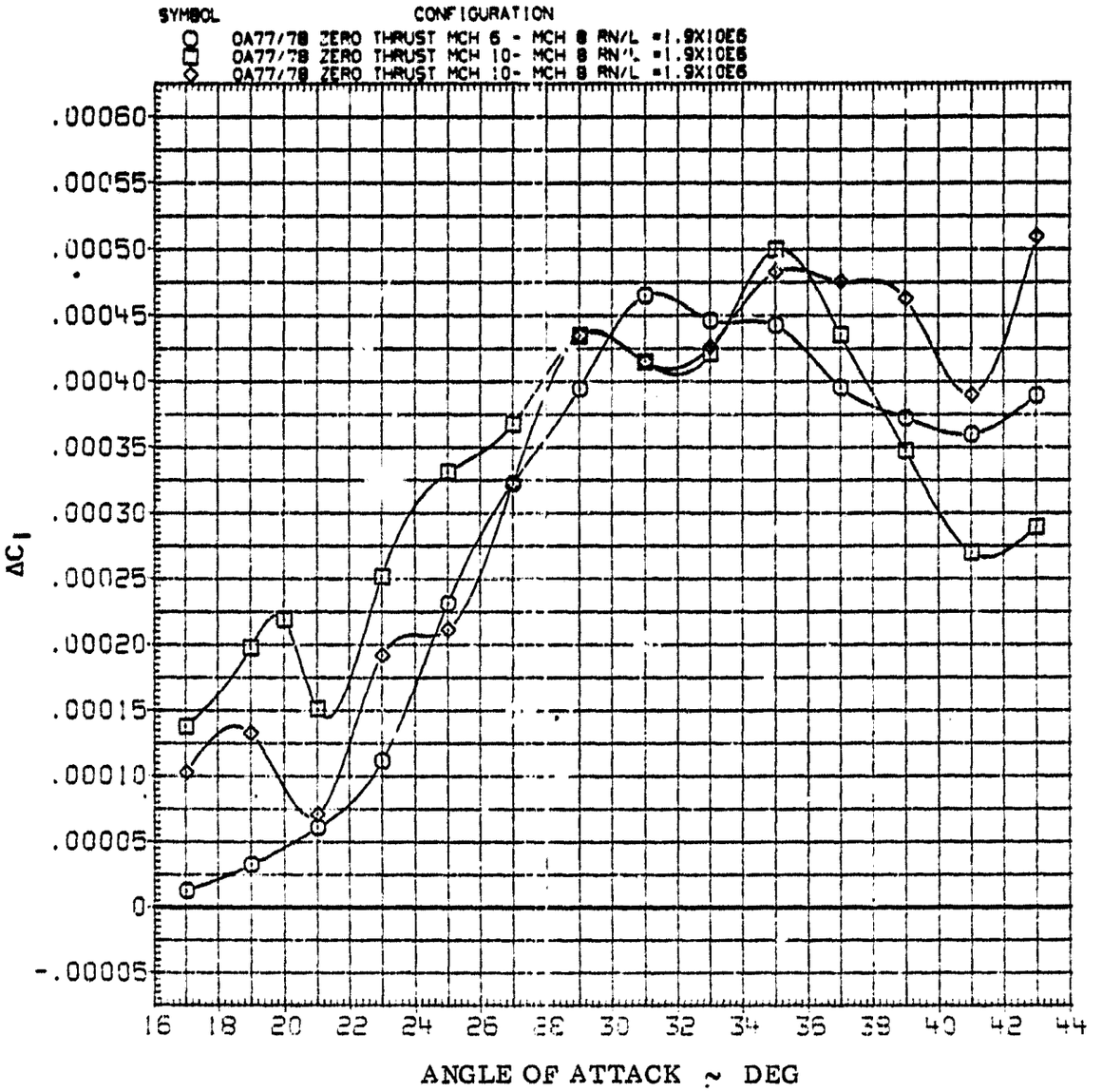

FIGURE 7-4c 0A77/78 DIFFERENCES DUE TO MACH NUMBER

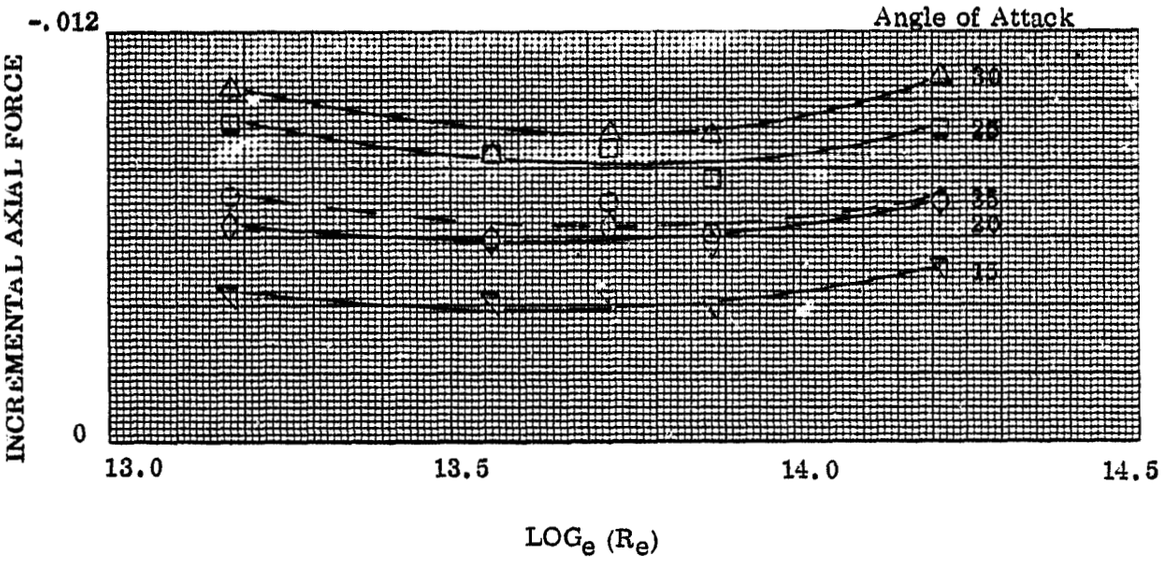

FIGURE 7-5a NOZZLE N49 AXIAL FORCE CHANGE DUE TO REYNOLDS NUMBER

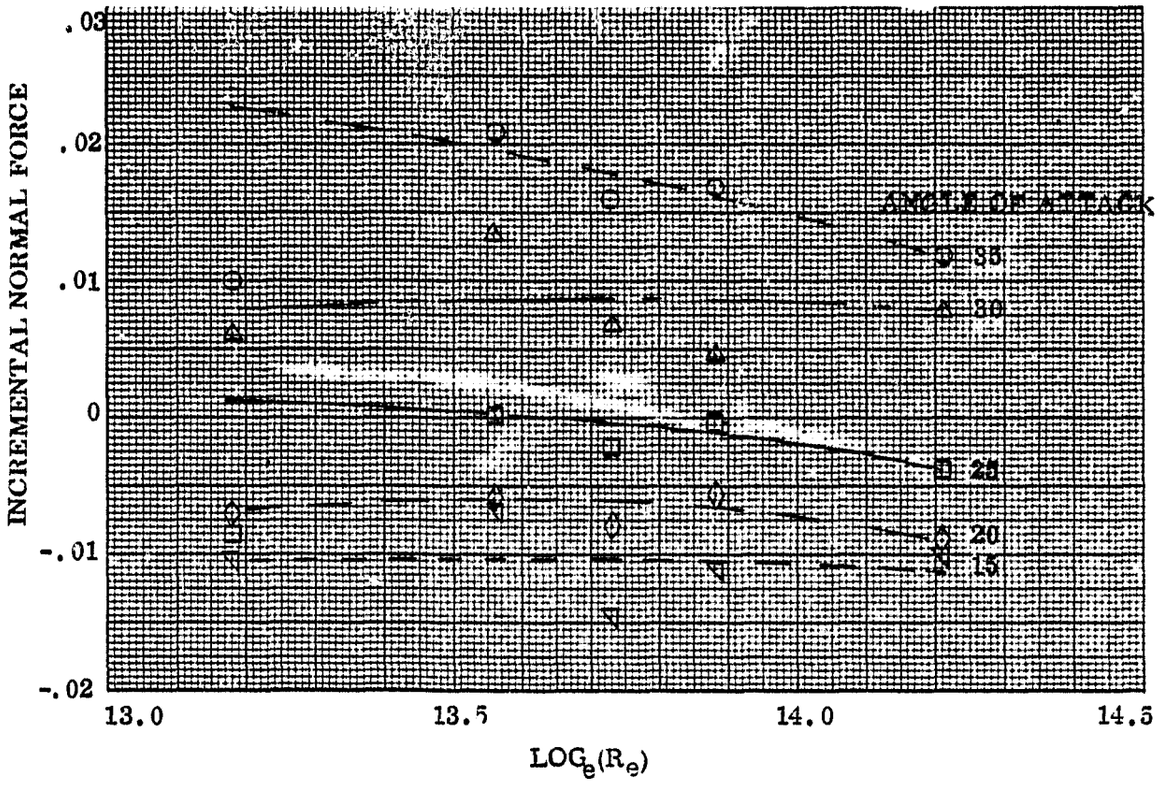

FIGURE 7-5b NOZZLE N49 NORMAL FORCE CHANGE DUE TO REYNOLDS NUMBER

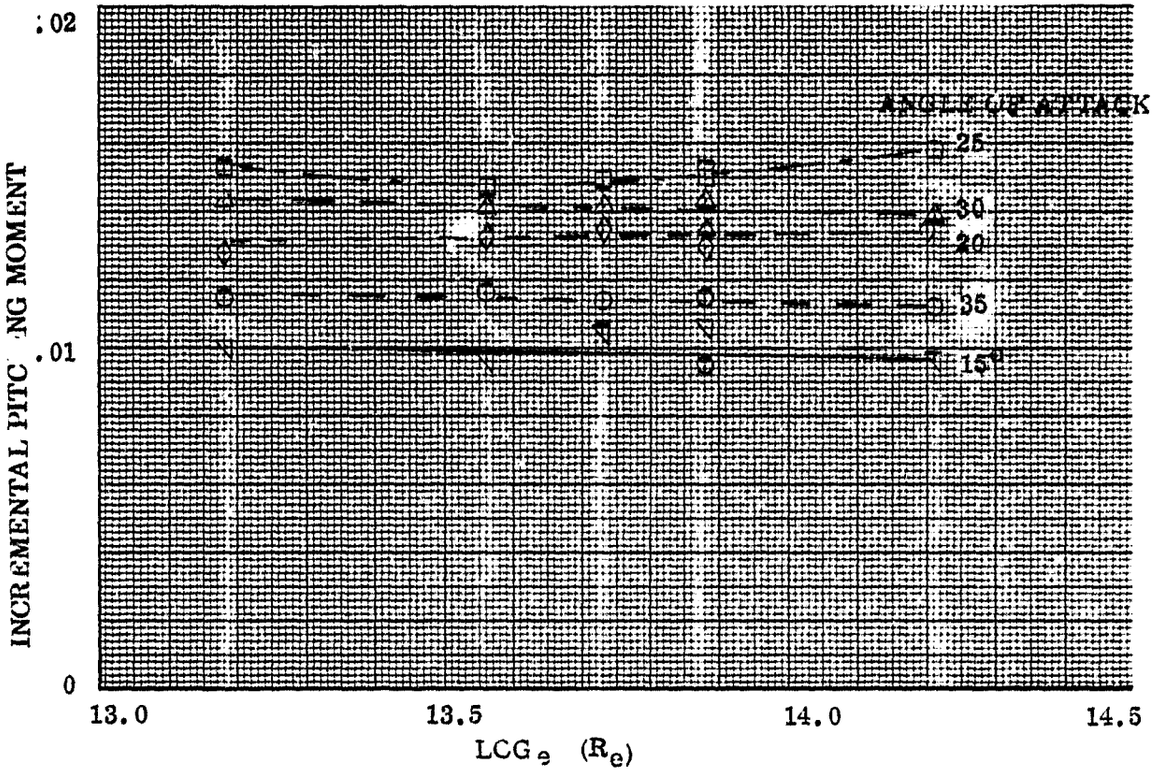

FIGURE 7-5c NOZZLE N49 PITCHING MOMENT CHANGE DUE TO REYNOLDS NUMBER

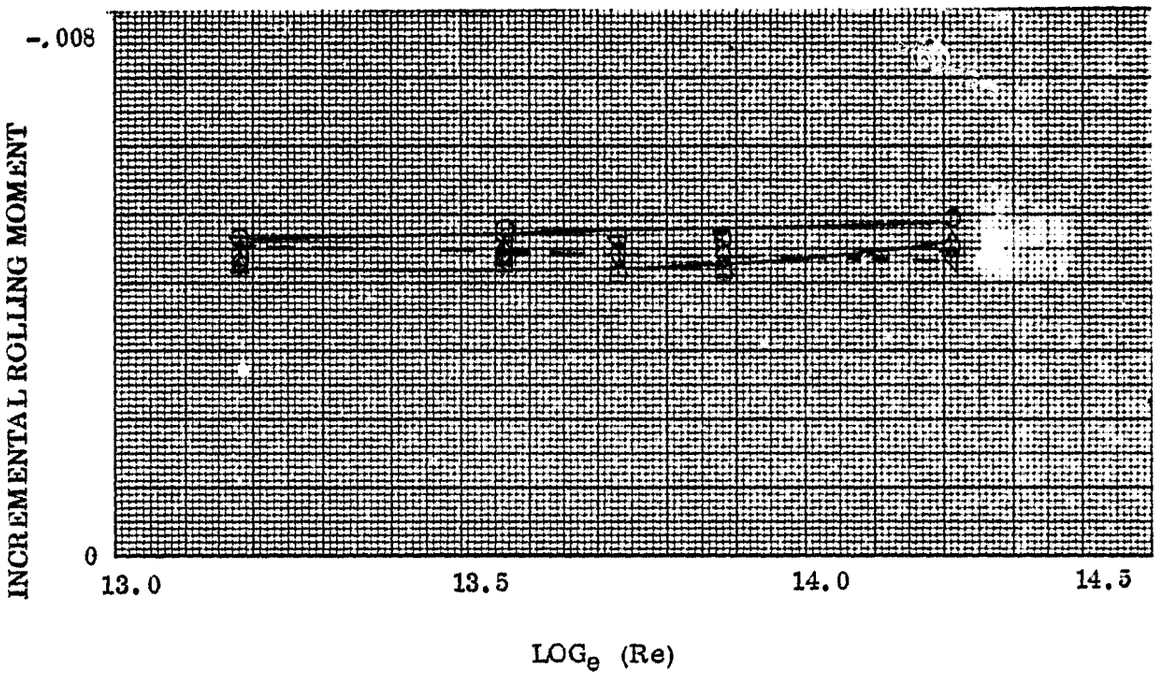

FIGURE 7-5d NOZZLE N49 ROLLING MOMENT CHANGE DUE TO REYNOLDS NUMBER

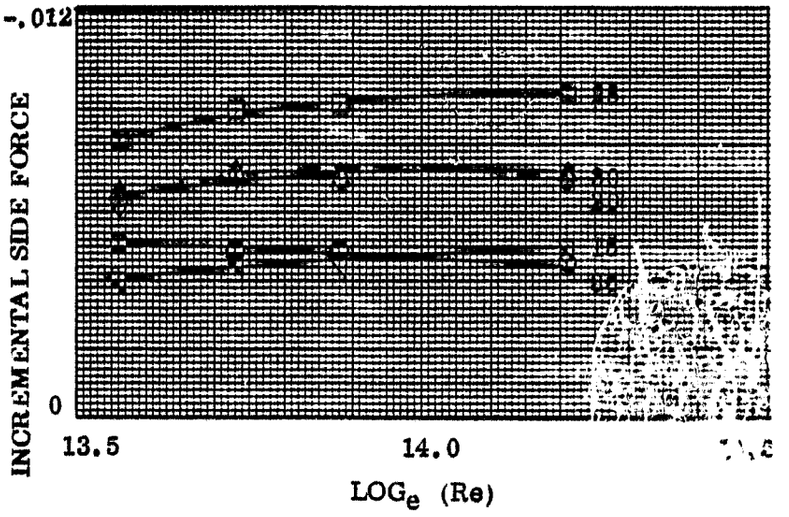

FIGURE 7-6a NOZZLE N52 SIDE FORCE CHANGE DUE TO REYNOLDS NUMBER

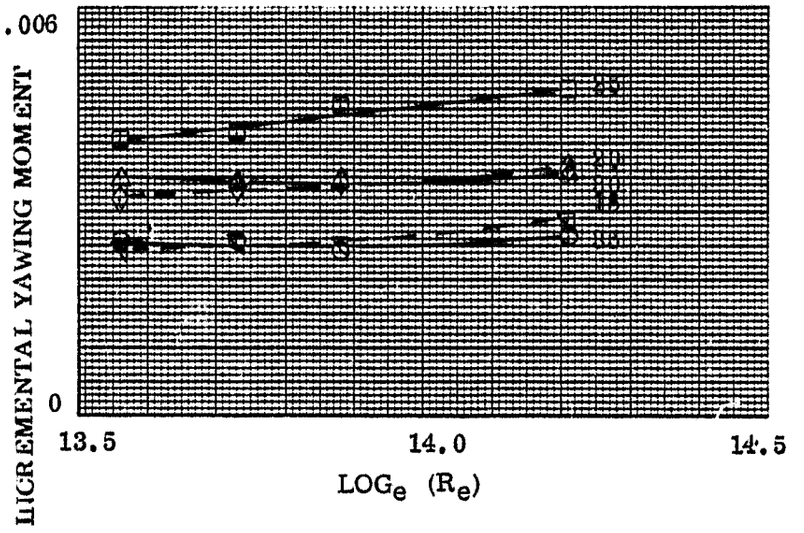

FIGURE 7-6b NOZZLE N52 YAWING MOMENT CHANGE DUE TO REYNOLDS NUMBER

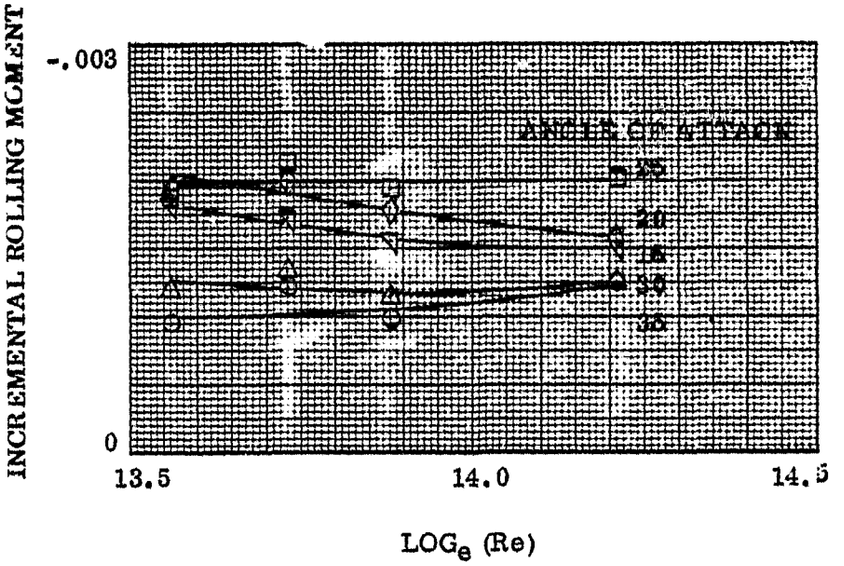

FIGURE 7-6c NOZZLE N52 ROLLING MOMENT CHANGE DUE TO REYNOLDS NUMBER

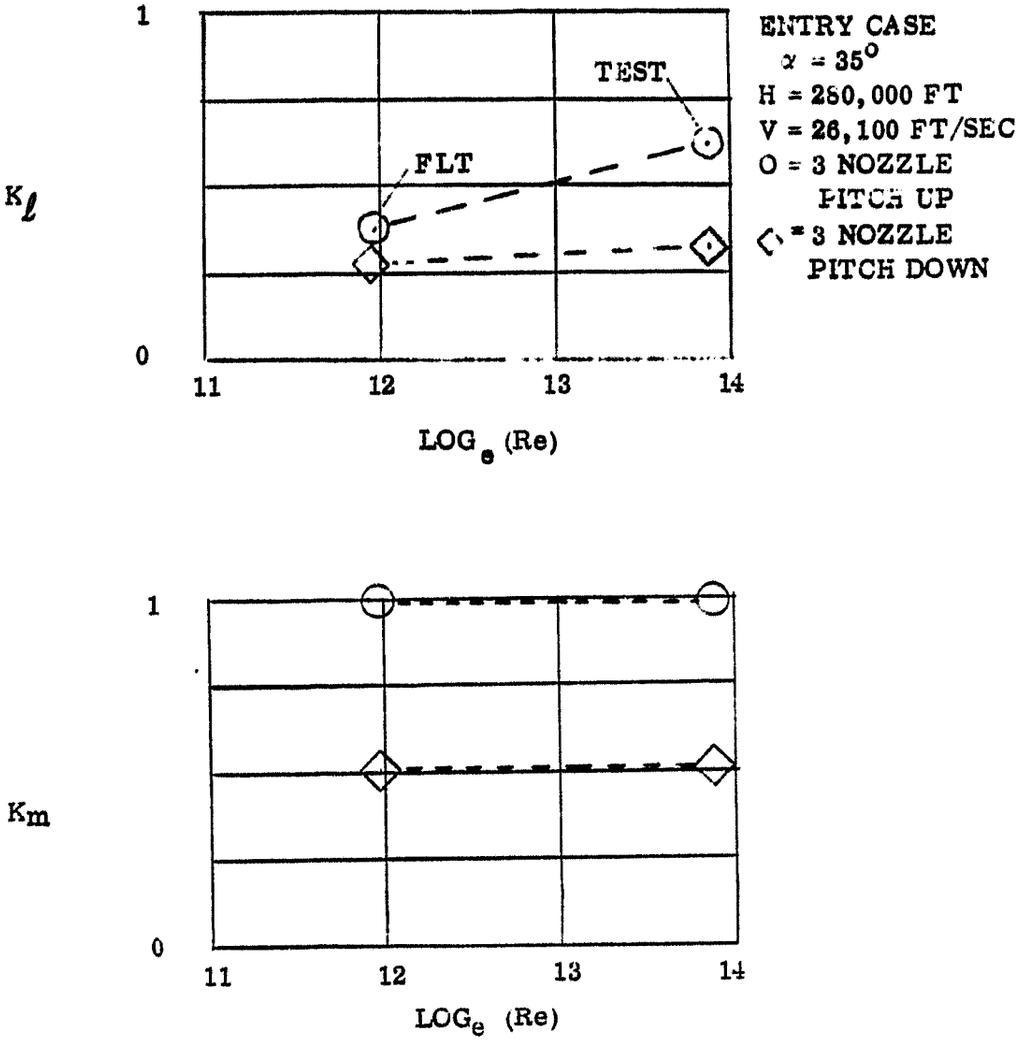

FIGURE 7-7 EFFECT OF WORST CASE REYNOLDS NUMBER TREND

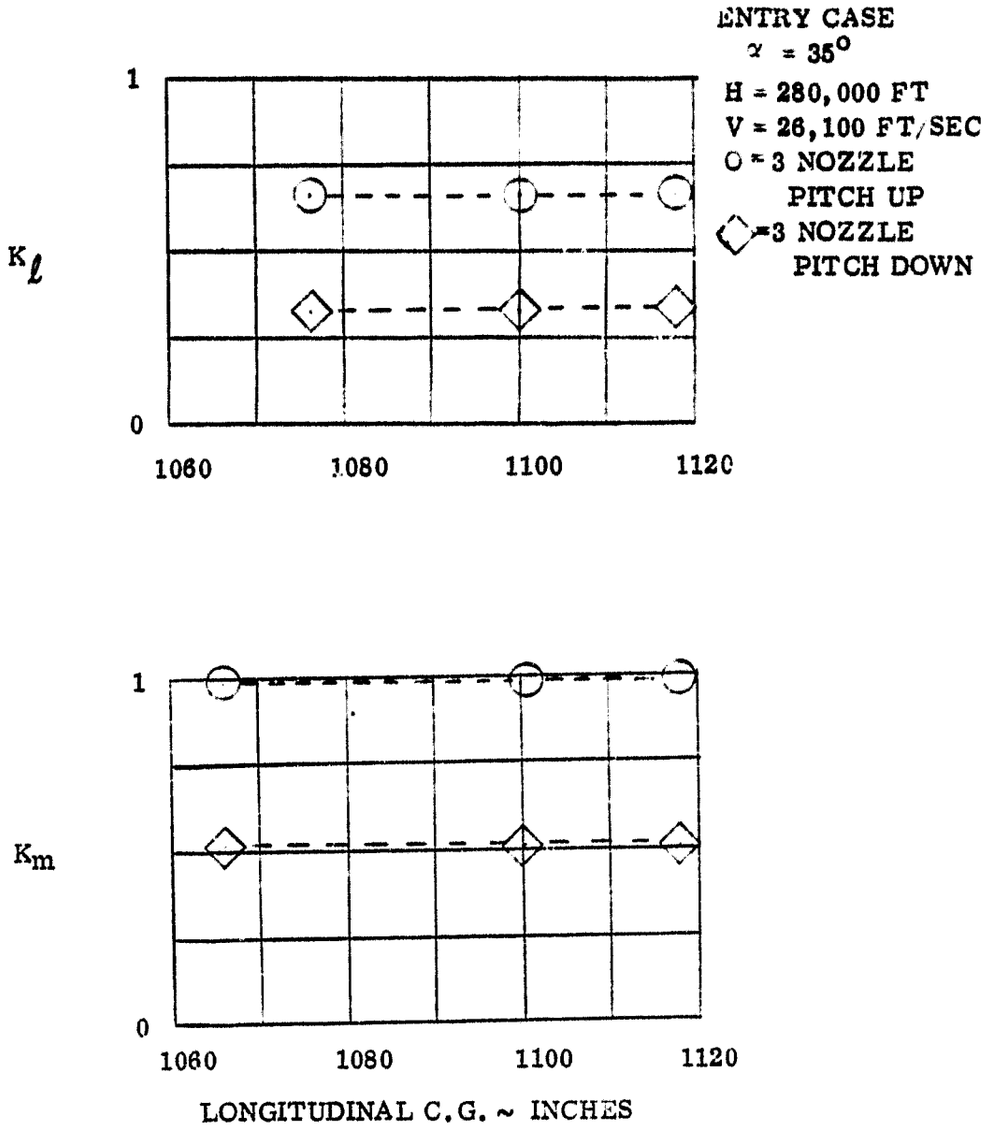

FIGURE 7-8: EFFECT OF LONGITUDINAL C.G. VARIATION

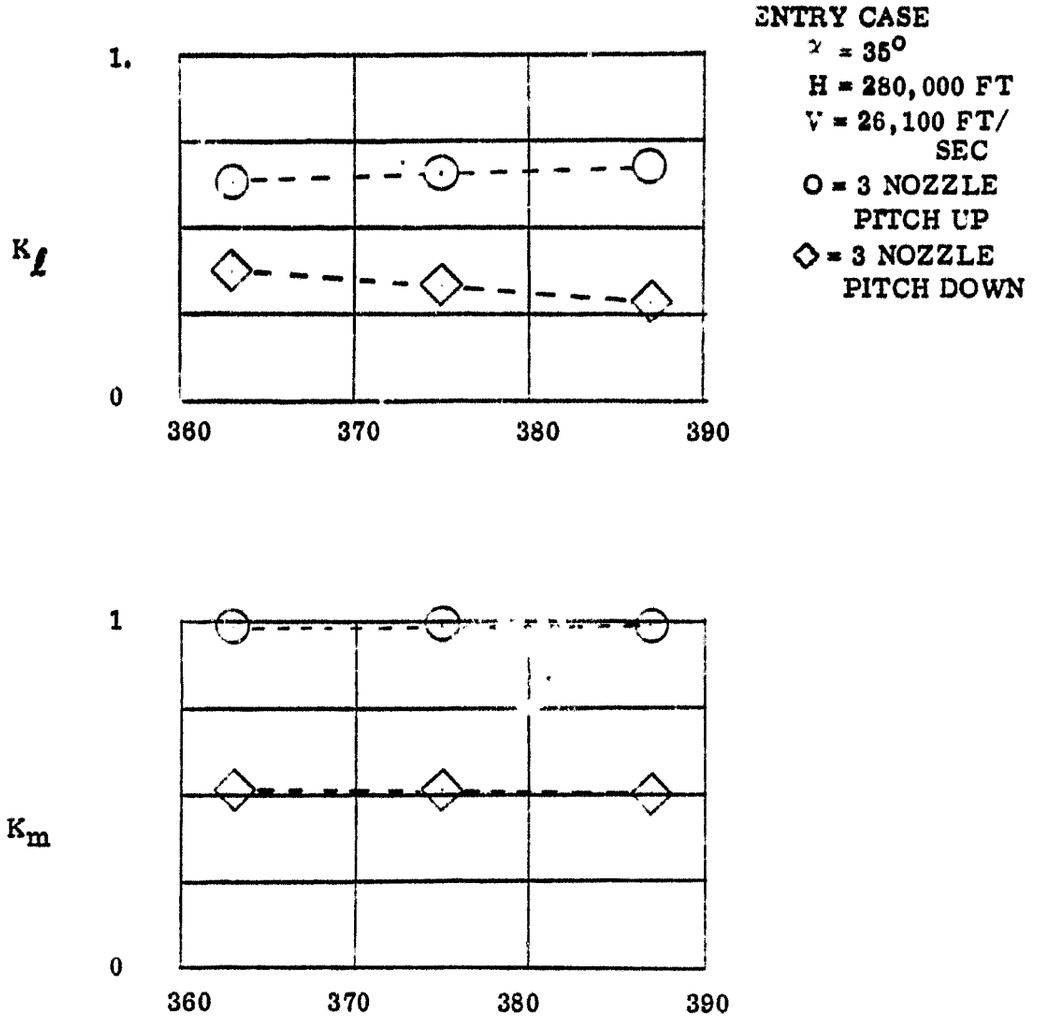

FIGURE 7-9: EFFECT OF VERTICAL C.G. ERROR

ENTRY CASE
$\alpha = 35^{o}$
H = 280,000 FT
V = 26,100 FT/SEC
O = 3 NOZZLE PITCH UP
◇ = 3 NOZZLE PITCH DOWN
BOTH SETS ON LEFT SIDE

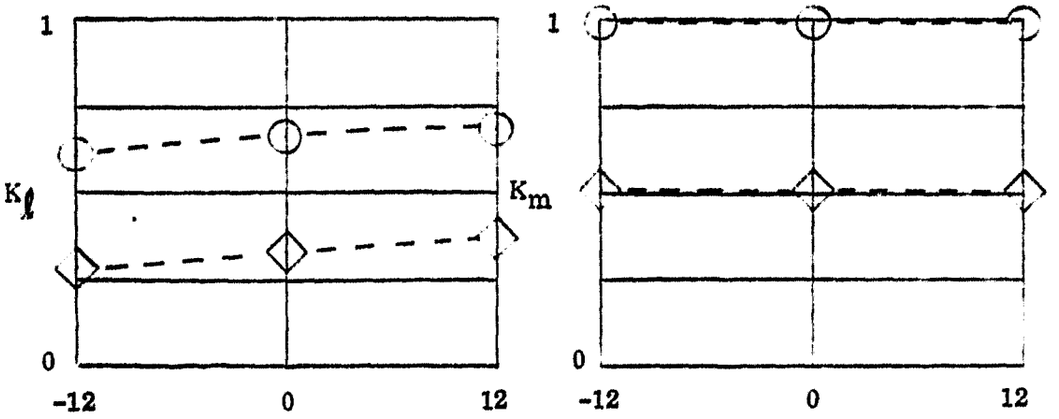

FIGURE 7-10: EFFECT OF LATERAL C.G. ERROR

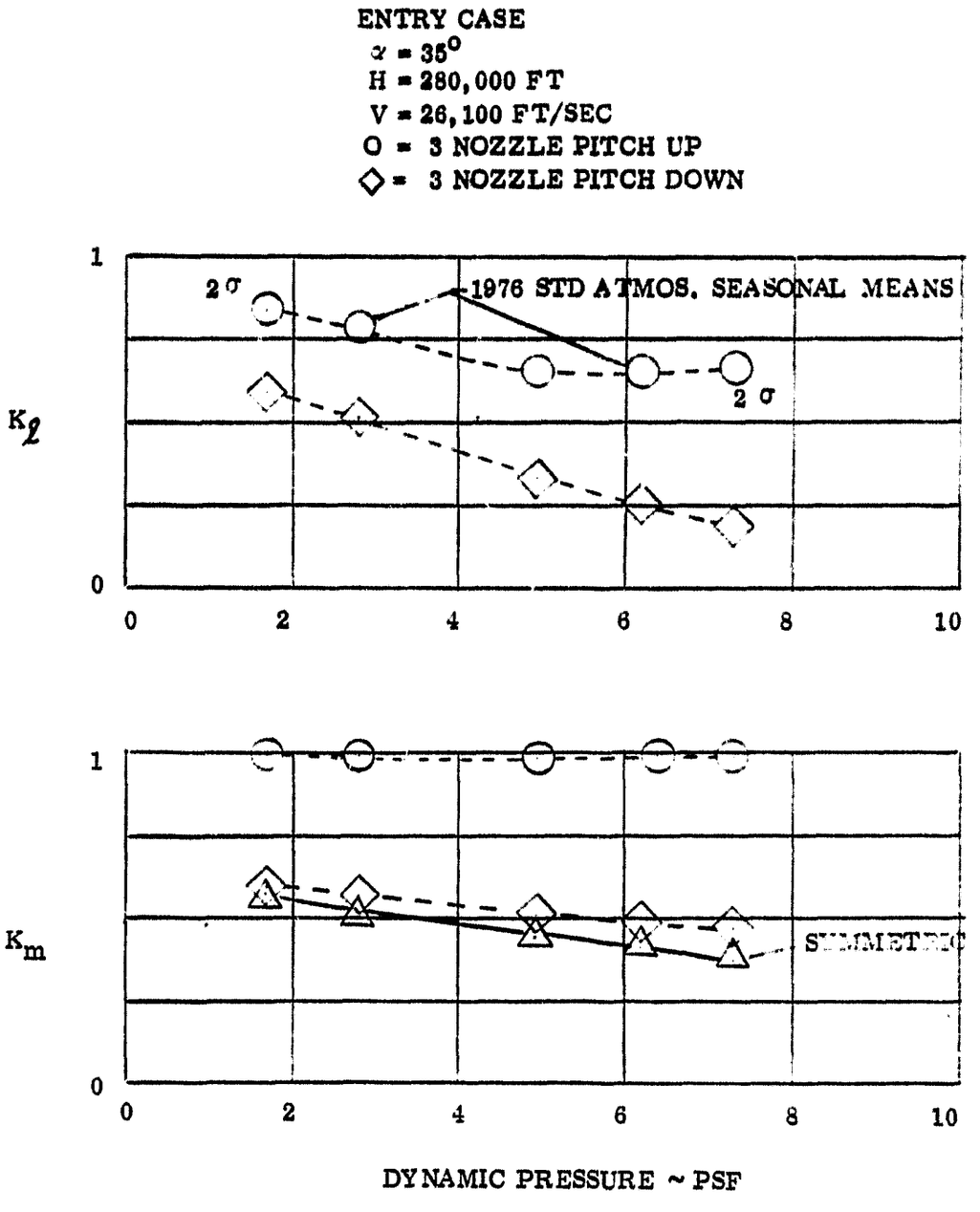

FIGURE 7-11: EFFECT OF ATMOSPHERIC VARIATION ON RCS EFFECTIVENESS

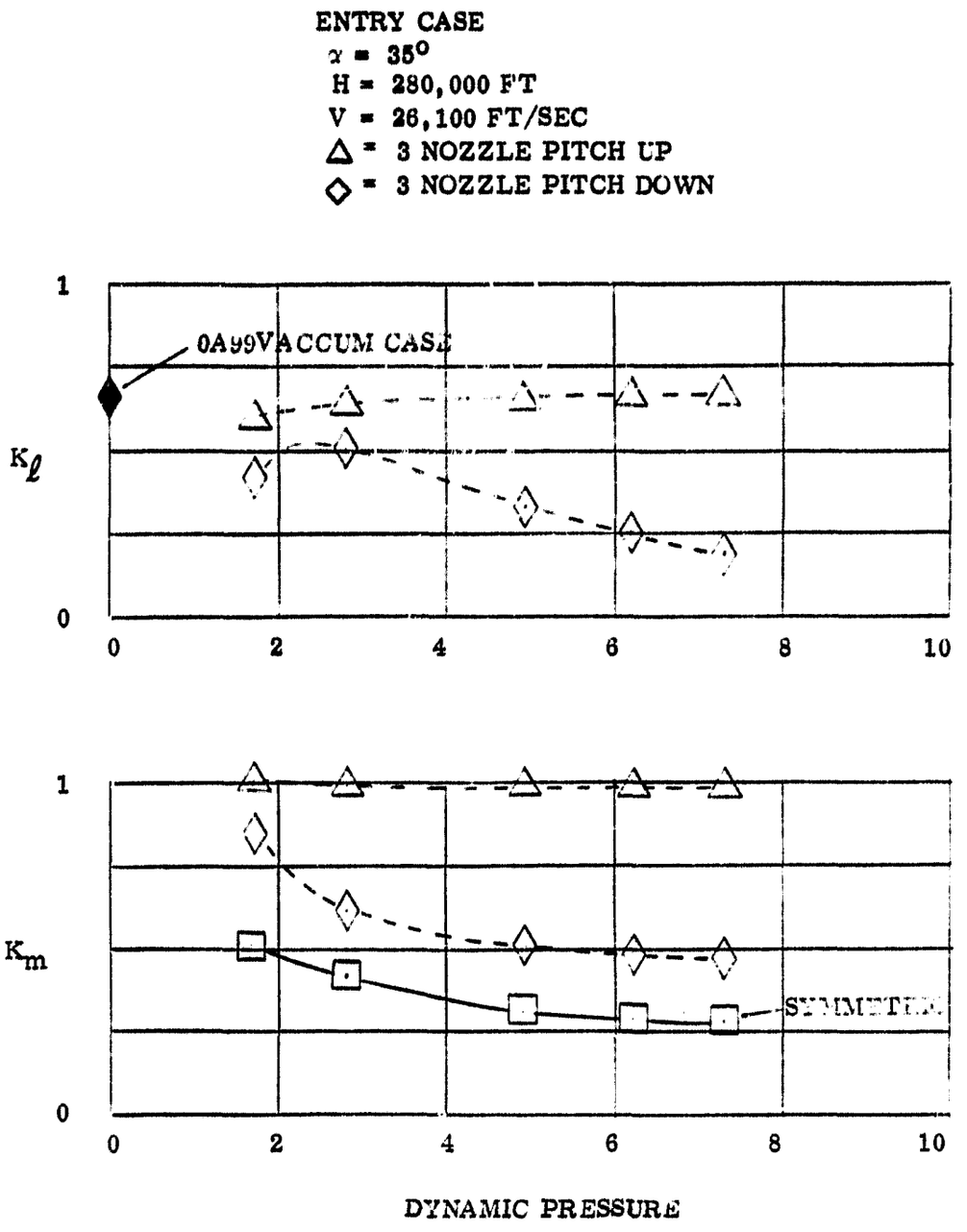

FIGURE 7-12: EFFECT OF EXTRAPOLATION OF DATA ON RCS EFFECTIVENESS

8

CONCLUSIONS

Analysis of wind tunnel data has shown that the aerodynamic interference between the aft mounted reaction control system plumes and the flow over the vehicle is sufficiently large to adversely affect vehicle control during low dynamic pressure flight. The data was analyzed to show that the interference terms could be related to nozzle flow simulation parameters and a prediction model was developed. This model predicts the total RCS control moment as the sum of the thrust term, an impingement term, an interaction term, and a cross coupling term. A program which incorporates this model has been written and is documented in this report.

8.1 STUDY CONCLUSIONS

1. Interactions between the pitch down jets and the external flow over the vehicle are shown to correlate best with an equivalent nozzle momentum ratio.

2. Data from many different geometry nozzles could be correlated together when the momentum ratio paramoter accounted for each nozzle discharge coefficient.

3. The pitch down interaction data correlated well when broken in 5 degree angle of attack intervals and this eliminated any discontinuities in the model.

4. The OA169 data correlated well with the MA22/OA82 data eliminating Mach as a parameter.

5. The pitch up interaction data correlated best with the momentum ratio parameter.

6. No peak value was found at low angles of attack for the pitch up longitudinal plane data.

7. Peak values were found in the pitch up lateral-directional data.

8. The peak values correlated well with momentum ratio and occur below 15° angle of attack.

9. The longitudinal pitch up increments and the lateral-directional data above 15° were broken into 5° angle of attack intervals which were correlated to momentum ratio.

10. The OA169 test data for pitch up interaction agrees well with the MA22/OA82 data.

11. The yaw jet interactions correlated best with a mass flow parameter in which number of nozzles in a cluster is not a part but the nozzle exit angle is a part.

12. The OA169 test data and yaw interactions agreed well with the MA22/OA82 test data.

13. The yaw data was broken into 5° angle of attack intervals for correlation.

14. Trailing edge up deflection of the body flap results in increasing pitch interaction for the pitch down reaction control.

15. Trailing edge down deflection of body flap resulted in no measurable change in RCS interaction.

16. Trailing edge up deflection of the elevon decreased the RCS pitch and roll interactions for pitch down and yaw RCS.

17. Trailing edge down deflection of the elevon increased pitch and roll interactions for the pitch down and yaw RCS.

18. The only measurable cross-coupling between RCS controls was for the symmetric pitch down case.

19. Possible sting interference effects need to be resolved in the pitch down cross coupling data.

20. Symmetric pitch down cross coupling needs more data to refine the model since data was only obtained over a limited range of momentum ratios.

21. Error bands were established for all data correlations and were shown to agree with error bands for all possible difference combinations.

22. No Mach Number effects could be found in the RCS data.

23. Reynolds Number effects were shown to be slight for the entry case but of possible importance for RTLS.

24. Uncertainty in vehicle center of gravity was shown to be not important.

25. Atmosphere uncertainty must be considered in determining propellant requirements for the entry case and will result in considerable changes in the expected control response.

26. The RTLS abort maneuver appears to provide the most adverse flight conditions for RCS effectiveness and atmospheric uncertainty may be very important for this condition.

27. With the exception of symmetric pitch down cross-coupling, the most critical case of high dynamic pressure involves no extrapolation of the test data giving high confidence that the data correlation will predict the true flight value.

8.2 STUDY RECOMMENDATIONS

1. A blade mounted model be built with a better representation of base geometry to evaluate sting interference.

2. A vacuum chamber test of symmetric pitch down RCS be performed with a good base geometry representation (no sting) to evaluate symmetric pitch down cross-coupling in the base region.

9

REFERENCES

1. Rausch, J. R. and Roberge, A. M., "RCS Jet-Flow Interaction Effects on the Aerodynamics of the Space Shuttle Orbiter," Convair Report CASD-NAS-73-020, November 1973

2. Rausch, J. R. and Shih, K. T., "Space Orbiter Reaction Control System Jet Interaction Study Interim Report," Convair Report CASD-NSC-74-009, November 1974

3. Rausch, J. R., "Space Shuttle Orbiter Reaction Control System Jet Interaction Study Final Report," Convair Report CASD-NSC-75-002, June 1975

4. Chrysler DATAMAN: "Results of Test MA22 in the NASA/LaRC 31-inch CFHT On An 0.10-scale Model (32-0) of the Space Shuttle Configuration 3 to Determine RCS Jet Flow Field Interaction," Chrysler DATAMAN DMS-DR-2267, NASA CR-147,604-7, May 1976

5. Chrysler DATAMAN: DMS-DR-2320, Test OA169, to be published

6. Daileda, J. J., "Pretest Information for RTLS Abort Separation Tests IA22/OA169 Using the .0125 Scale SSV Model In the AEDC VKF Tunnel B," Rockwell Report SD75-SH-0256, 16 February 1976

7. Hayman, L. O., "Aft RCS Impingement Estimates and Comparison with OA99 Test Data," NASA Johnson Space Center Aerodynamics Memorandum 5437, 20 August 1974

8. Chrysler DATAMAN: "Results of Investigations (OA77 and OA78) On An 0.015-scale 140A/B Configuration Space Shuttle Vehicle Orbiter Model 49-0 In the AEDC VKF B and C Wing Tunnels," Chrysler DATAMAN DMS-DR-2134, NASA CR-134,429, January 1975

9. Rausch, J. R. Hearn, E. B., "Experimental Aerodynamic Characteristics of a Lifting Entry Spacecraft Configuration," General Dynamics Convair Report GDC-ERR-1408, March 1970

10. Klug. G., "Special Request Documentation OA77/78, OA82, MA22, OA169 Statistical Analysis," Chrysler DATAMAN SPRT-I2-2, February 1977

11. Anon "U.S. Standard Atmosphere, 1976," National Oceanic and Atmospheric Administration NOAA S/T76-1562, October 1976

APPENDIX A

PROGRAM LISTING

ORIGINAL PAGE IS
OF POOR QUALITY

```
      PROGRAM PREJ(INPUT,OUTPUT,TAPE5=INPUT,TAPE6=OUTPUT,TAPE4A)
C
C
      REAL MINF
      REAL NONOZU,NONOZD,NONOZY,NONOZUL,NONOZUR,NONOZDL,NONOZDR,NONOZYL,
     1NONOZYR
      DIMENSION SIGTO(6)
      COMMON/CONST/PIE,RADIAN,GI,RI,GO
      COMMON/GRP2/DNX(300),DNY(300),DNZ(300),X(300),Y(300),Z(300),SLOC(3
     100),J
      COMMON/ERROR/SIG,SIGM(2,6),SIGIN(3,6),SIGIM(3,6),SIGTH(3,6)
      COMMON/UP/NONOZU,NONOZUL,NONOZUR,DSTARUR,DSTARUL,AEXUL,AEXUR,
     1RMFSUL,RMFSUR,DXNOZU,DYNOZU,DZNOZU,
     2XREUL,XREUR,YREUL,YREUR,ZREUL,ZREUR
      COMMON/DWN/NONOZD,NONOZDL,NONOZDR,DSTARDL,DSTARDR,AEXDL,AEXDR,
     1RMFSDL,RMFSDR,DXNOZD,DYNOZD,DZNOZD,
     2XREDL,XREDR,YREDL,YREDR,ZREDL,ZREDR
      COMMON/SIDE/NONOZY,NONOZYL,NONOZYR,DSTARYL,DSTARYR,AEXYL,AEXYR,
     1      RMRYL,RMRYR,DXNOZY,DYNOZY,DZNOZY,
     2XREYL,XREYR,YREYL,YREYR,ZREYL,ZREYR
      COMMON/FLT/MINF,PINF,TINF,ALPH,IOPT,GI,HI,VINF,THRUST,INEXT
      COMMON/REF/SREF,C,B,SCALE,XRE,YRE,ZRE,DXNOZ,DYNOZ,DZNOZ,DXNOZZ,
     1DYNOZZ,DZNOZZ
      COMMON/NOZ/XMJ,GJ,ARJ,AJE,POJ,RJ,TOJ,TURN,DSTAR,AN,THETA,DEXIT,
     1IIMP,DCOEF
      COMMON/A/POW,POW1,PRT,T1,PZT
      COMMON/CONTR/DELTER,DELTEL,XELV,ZELV,XFLA,ZFLA,
     1DELDF
      COMMON/THCOEF/ CXU,CZU,CYU,CMU,CNU,CLU,CXD,CZD,CYD,CMD,CND,CLD,
     1              CXY,CZY,CYY,CMY,CNY,CLY
      COMMON/TOCOEF/ CXT,CZT,CYT,CMT,CNT,CLT
      COMMON/FITS/ CZIDL(10,7),CAIDL(10,7),CMIDL(10,7),CLIDL(10,7),
     1 CNIDL(10,7),CYIDL(10,7), CZIYL(10,7),CAIYL(10,7),CMIYL(10,7),
     2 CLIYL(10,7),CNIYL(10,7),CYIYL(10,7),CZIUH(10,7),CAIUH(10,7),
     3 CMIUH(10,7),CLIUH(10,7),CNIUH(10,7),CYIUH(10,7),
     4CUPB(5,7)
      COMMON/DEFLECT/CLP30(10,7),CZP30(10,7),CMP30(10,7),CAP30(10,7),
     1          CZP10(10,7),CLP10(10,7),CMP10(10,7),CAP10(10,7),CMPB(10,7
     2),CZPB(10,7),CMY10(10,7),CAY10(10,7),CZY10(10,7),CLY10(10,7),
     3CZY30(10,7),CAY30(10,7),CLY30(10,7),CMY30(10,7)

      DATA GI/1.4/,RINF/53.3/,PIE/3.1415926/,RI/53.3/,GI/1.4/,ORC/0./,
     1RADIAN/57.2958/,GO/32.174049/,TLAT/0./,IN/5/,IIN/1/
  100 CONTINUE
      CALL INPUTT(IIN)
      IIN=2
  101 CONTINUE
      CALL INPUTT(IIN)
      AN = .7854*DEXIT**2
      CALL JET(GJ,ARJ,POJ,PJ,TOJ,TJ,XMJ,AN)
      AEXUL=AN*NONOZUL
      AEXUR=AN*NONOZUR
      AEXDL=AN*NONOZDL
      AEXDR=AN*NONOZDR
      AEXYL=AN*NONOZYL
      AEXYR=AN*NONOZYR
      DSTAR=SQRT(4./PIE*AN/ARJ)
      DSTARUL=DSTAR*SQRT(NONOZUL)
      DSTARUR=DSTAR*SQRT(NONOZUR)
      DSTARDL=DSTAR*SQRT(NONOZDL)
```

```
      DSTARUR=DSTAR*SQRT(NONOZDR)
      DSTARYL=DSTAR*SQRT(NONOZYL)
      DSTARYR=DSTAR*SQRT(NONOZYR)
C
      IIN=5
    1 CONTINUE
C
      PRINT 4000
 4000 FORMAT (1H1)
      CALL INPUTT(IIN)
C
      GO TO (66,67,68,69),IOPT
   66 CONTINUE
      CALL ATMOS(HI,TT,PINF,RH,SOS,AO,100.,DUM1,A8,A9,G,GO,TS,TLAT,ORC)
      PINF=PINF/144.
      TINF=TT
      VINF=MINF*SOS
      GO TO 69
   67 CONTINUE
      CALL ATMOS(HI,TT,PINF,RH,SOS,AO,VINF,MINF,A8,A9,G,GO,TS,TLAT,ORC)
      PINF=PINF/144.
      MINF=VINF/SOS
      TINF=TT
      GO TO 69
   68 CONTINUE
      CALL ATMOS(HI,TT,PINF,RH,SOS,AO,100.,DUM1,A8,A9,G,GO,TS,TLAT,ORC)
      PINF=PINF/144.
      QI=QI/144.
      MINF=SQRT(QI/(0.7*PINF))
      TINF=TT
   69 CONTINUE
      QI=0.7*144.*PINF*MINF**2
      IQ=0
      IF(QI.EQ.0.)IQ=1
      IF(QI.EQ.0.)QI=0.00001
      IF(PINF.EQ.0.)PINF=QI/(0.7*144.*MINF**2)
      CALL EXPAN (GJ,POJ,PINF,XMJ,THETA,TURN)
      PR=PJ/PINF
      PRFS=PR
C  JET MOMENTUM RATIO
      RMFS=GJ*PJ*XMJ**2*AIJ/GINF/PINF/MINF/MINF/SREF
      RMFSUL=RMFS*NONOZUL
      RMFSUR=RMFS*NONOZUR
      RMFSDL=RMFS*NONOZDL
      RMFSDR=RMFS*NONOZDR
      THRUST = PZI+AN*(PJ-PINF)*144.0
      TCOEF=THRUST/QI/SREF
      PRINT 3006
      PRINT6001,SCALE
 6001 FORMAT(31H0THE SCALE OF THIS SOLUTION IS ,F20.10)
      PRINT6888,SREF,B,C
 6888 FORMAT(10H0REFERENCE AREA=,F15.7,21H SQ FT       REF SPAN =,F15.7,22
     1HFT          REF CHORD =,F15.7,2HFT)
      PRINT 3006
      PRINT 4001
 4001 FORMAT(1H0,23H NOZZLE CHARACTERISTICS)
      PRINT4002,DEXIT,ARJ,THETA,XMJ
 4002 FORMAT(1H0,9H EXIT DIA,F12.4,16H EXPANSION RATIO,F12.4,11H EXIT AN
     1GLE,F12.4,13H NOZZLE MACH ,F15.4)
      PPJ=PJ/PCOEF
```

ORIGINAL PAGE IS
OF POOR QUALITY

```
      PRINT4003,THRUST,PPJ,PJ,GJ
4003 FORMAT(1H0,7H THRUST,F20.8,14H CHAMBER PRESS,F12.4,11H EXIT PRESS,
     1F20.8,14H EXHAUST GAMMA,F12.4)
      PRINT6002,DCOEF
6002 FORMAT(34H0 NOZZLE DISCHARGE COEFFICIENT IS ,F20.10)
      PRINT 3006
      PRINT 4004
4004 FORMAT(1H0,23H FREE STREAM CONDITIONS)
      PRINT 3006
8884 FORMAT(1H0,11H VELOCITY =,F15.5)
8885 FORMAT(1H0,16H DYNAMIC PRESS =,F15.6)
8886 FORMAT(1H0,10H MACH NO =,F15.5)
8887 FORMAT(1H0,11HALTITUDE = ,F15.5)
      IF(IOPT.LT.4)PRINT8887,HI
      IF(IOPT.EQ.1.OR.IOPT.EQ.4)PRINT8886,MINF
      IF(IOPT.EQ.3)PRINT8885,QI
      IF(IOPT.EQ.2)PRINT8884,VINF
      PRINT7000,ALPH
7000 FORMAT(19H0 ANGLE OF ATTACK =,F15.7)
      PRINT 3006
      PRINT7001,DELTEL,DELTER
7001 FORMAT(21H0ELEVON ANGLES,LEFT =,F15.7,10H  RIGHT = ,F15.7)
      PRINT 3006
      PRINT7002,DELBF
7002 FORMAT(23H0BODY FLAP DEFLECTION =,F15.7)
      PRINT 3006
      PRINT4005,PINF,MINF,GINF,ALPH
4005 FORMAT(1H0,11H P INFINITY,F20.8,9H MACH INF,F12.4,6H GAMMA,F12.4,
     115HANGLE OF ATTACK,F12.4)
      PRINT4006,PR,RMFS,TCOEF
4006 FORMAT(1H0,14HPRESSURE RATIO,F20.8,15H MOMENTUM RATIO,F20.8,13H TH
     1RUST COEFF,F20.8)
      RTRAT=RJ*TJ/(RI*TINF)
      RTORTI=TOJ*RTRAT/TJ
      POJPIN=POJ/PINF
      PRINT4007,RTRAT,POJPIN,QI
4007 FORMAT(10H0 RT RATIO,F20.8,9H POJ/PINF,F20.8,25HFREE STREAM DYNAMI
     1C PRESS,F20.8)
      PRINT4008,RTORTI
4008 FORMAT(17H0(R*TOJ)/(R*TINF),F13.5)
      FMR=(GJ/GI*RI/RJ*TINF/TJ*(((PJ*XMJ*AN)/(PINF*MINF*SREF))**2)*
     1SIN(THETA/RADIAN))
      FMR=SQRT(FMR)
      FMRYL=FMR
      FMRYR=FMR
      PRINT 3006
      ARCS=THRUST*NONOZUL/QI/(SCALE**2)
      PRINT 5001,NONOZUL,RMFSUL,ARCS
      ARCS=THRUST*NONOZUR/QI/(SCALE**2)
      PRINT 5002,NONOZUR,RMFSUR ,ARCS
      ARCS=THRUST*NONOZDL/QI/(SCALE**2)
      PRINT 5003,NONOZDL,RMFSDL,ARCS
      ARCS=THRUST*NONOZDR/QI/(SCALE**2)
      PRINT 5004,NONOZDR,RMFSDR,ARCS
      ARCS=THRUST*NONOZYL/QI/(SCALE**2)
      PRINT 5005,NONOZYL,FMRYL ,ARCS
      ARCS=THRUST*NONOZYR/QI/(SCALE**2)
      PRINT 5006,NONOZYR,FMRYR,ARCS
5001 FORMAT(25H0 PITCH UP LEFT NOZZLES =,F8.0,10X,14HMOMENTUM RATIO,F20
     1.8,10X,19H THRUST COEF(ISOFT) ,F15.6)
```

```
 5002 FORMAT(25H0 PITCH UP RGHT NOZZLES =,F8.0,10X,14HMOMENTUM RATIO,F20
     1.8,10X,19H THRUST COEF(1SQFT) ,F15.6)
 5003 FORMAT(25H0 PITCH DN LEFT NOZZLES =,F8.0,10X,14HMOMENTUM RATIO,F20
     1.8,10X,19H THRUST COEF(1SQFT) ,F15.6)
 5004 FORMAT(25H0 PITCH DN RGHT NOZZLES =,F8.0,10X,14HMOMENTUM RATIO,F20
     1.8,10X,19H THRUST COEF(1SQFT) ,F15.6)
 5005 FORMAT(25H0 YAW      LEFT NOZZLES =,F8.0,10X,14HMASS FLOW RAT ,F20
     1.8,10X,19H THRUST COEF(1SQFT) ,F15.6)
 5006 FORMAT(25H0 YAW     RIGHT NOZZLES =,F8.0,10X,14HMASS FLOW RAT ,F20
     1.8,10X,19H THRUST COEF(1SQFT) ,F15.6)
      PRINT5006
      PRINT5050
      PRINT5051
      PRINT5052
      PRINT5053
 5050 FORMAT(55H0 BODY AXES FORCE AND MOMENT COEFFICIENTS ARE OUTPUT   )
 5051 FORMAT(66H0 SIGN CONVENTION*XPOSITIVE FWD *Z POSITIVE DOWN *Y POSI
     1TIVE RIGHT )
 5052 FORMAT(57H0 PITCH + NOSE UP *ROLL + RIGHT WING DWN*YAW + NOSE RIGH
     1T)
 5053 FORMAT(38H0MOMENT REF CENTER*X=1076.7    Z=375. )
C        COMPUTE THRUST MOMENTS
      CLU=0.
      CLD=0.
      CLY=0.
      CMU=0.
      CMD=0.
      CMY=0.
      CNU=0.
      CND=0.
      CNY=0.
      CXU=0.
      CXD=0.
      CXY=0.
      CYU=0.
      CYD=0.
      CYY=0.
      CZU=0.
      CZD=0.
      CZY=0.
      DO771I=1,3
      PINF   = PINF*144.0
      CALL THR(IT,CXT,CYT,CZT,CLT,CMT,CNT)
      PINF   = PINF/144.0
      IF(IT.NE.1)GO TO 75
   74 CLU=CLT
      CMU=CMT
      CNU=CNT
      CXU=CXT
      CYU=CYT
      CZU=CZT
      GO TO 77
   75 IF(IT.EQ.3)GO TO 76
      CLD=CLT
      CMD=CMT
      CND=CNT
      CXD=CXT
      CYD=CYT
      CZD=CZT
      GO TO 77
```

```
   76 CLY=CLT
      CMY=CMT
      CNY=CNT
      CXY=CXT
      CYY=CYT
      CZY=CZT
   77 CONTINUE
C     COMPUTE PLUME IMPINGEMENT MOMENTS
      CLIMU=0.
      CLIMD=0.
      CLIMY=0.
      CMIMU=0.
      CMIMD=0.
      CMIMY=0.
      CNIMU=0.
      CNIMD=0.
      CNIMY=0.
      CXIMU=0.
      CXIMD=0.
      CXIMY=0.
      CYIMU=0.
      CYIMD=0.
      CYIMY=0.
      CZIMU=0.
      CZIMD=0.
      CZIMY=0.
      DO189IT=1,3
      CALL IMPING(IT,CXT,CYT,CZT,CLT,CMT,CNT)
      IF(IT.NE.1)GO TO 187
  186 CLIMU=CLT
      CMIMU=CMT
      CNIMU=CNT
      CXIMU=CXT
      CYIMU=CYT
      CZIMU=CZT
      GO TO 189
  187 IF(IT.EQ.3)GO TO 188
      CLIMD=CLT
      CMIMD=CMT
      CNIMD=CNT
      CXIMD=CXT
      CYIMD=CYT
      CZIMD=CZT
      GO TO 189
  188 CLIMY=CLT
      CMIMY=CMT
      CNIMY=CNT
      CXIMY=CXT
      CYIMY=CYT
      CZIMY=CZT
  189 CONTINUE
  190 CONTINUE
      CLINU=0.
      CLIND=0.
      CLINY=0.
      CMINU=0.
      CMIND=0.
      CMINY=0.
      CNIND=0.
      CNINU=0.
```

```
      CNINY=0.
      CXINU=0.
      CXIND=0.
      CXINY=0.
      CYINU=0.
      CYIND=0.
      CYINY=0.
      CZINU=0.
      CZIND=0.
      CZINY=0.
C  COMPUTE PLUME  INTERACTION MOMENTS
      IF(IQ.EQ.1)GO TO 204
      DO203IT=1,3
      CALL INTER(IT,CXB,CYB,CZB,CLB,CMB,CNB)
      IF(IT.NE.1)GO TO 201
  200 CLINU=CLB
      CMINU=CMB
      CNINU=CNB
      CXINU=CXB
      CYINU=CYB
      CZINU=CZB
      GO TO 203
  201 IF(IT.EQ.3)GO TO 202
      CLIND=CLB
      CMIND=CMB
      CNIND=CNB
      CXIND=CXB
      CYIND=CYB
      CZIND=CZB
      GO TO 203
  202 CLINY=CLB
      CMINY=CMB
      CNINY=CNB
      CXINY=CXB
      CYINY=CYB
      CZINY=CZB
  203 CONTINUE
  204 CONTINUE
  210 CONTINUE
C COMPUTE MULTIPLE AXES CROSSCOUPLING  TERMS
      CXCCU=0.
      CXCCD=0.
      CXCCY=0.
      CYCCU=0.
      CYCCD=0.
      CYCCY=0.
      CZCCU=0.
      CZCCD=0.
      CZCCY=0.
      CLCCU=0.
      CLCCD=0.
      CLCCY=0.
      CMCCU=0.
      CMCCD=0.
      CMCCY=0.
      CNCCU=0.
      CNCCD=0.
      CNCCY=0.
      CALL CCOUPL (2,CXCCD,CZCCD,CYCCD,CMCCD,CNCCD,CLCCD)
  211 CONTINUE
```

ORIGINAL PAGE IS
OF POOR QUALITY


```
C COMPUTE TOTAL FORCES AND MOMENTS
      CXT=CXU+CXD+CXY+CXIMU+CXIMD+CXIMY+CXINU+CXIND+CXINY+CXCCU+
     1CXCCD+CXCCY
      CYT=CYU+CYD+CYY+CYIMU+CYIMD+CYIMY+CYINU+CYIND+CYINY+CYCCU+
     1CYCCD+CYCCY
      CZT=CZU+CZD+CZY+CZIMU+CZIMD+CZIMY+CZINU+CZIND+CZINY+CZCCU+
     1CZCCD+CZCCY
      CLT=CLU+CLD+CLY+CLIMU+CLIMD+CLIMY+CLINU+CLIND+CLINY+CLCCU+
     1CLCCD+CLCCY
      CMT=CMU+CMD+CMY+CMIMU+CMIMD+CMIMY+CMINU+CMIND+CMINY+CMCCU+
     1CMCCD+CMCCY
      CNT=CNU+CND+CNY+CNIMU+CNIMD+CNIMY+CNINU+CNIND+CNINY+CNCCU+
     1CNCCD+CNCCY
      PRINT 3001
 3001 FORMAT(14H0 THRUST TERMS)
      PRINT 3002
 3002 FORMAT(1H0,17X,14HROLLING MOMENT,3X,15HPITCHING MOMENT,5X,13HYAWIN
     1G MOMENT,7X,11H  X   FORCE,8X,10H  Y  FORCE,8X,12H   Z   FORCE)
      PRINT 3003, CLU,CMU,CNU,CXU,CYU,CZU
      PRINT 3004, CLD,CMD,CND,CXD,CYD,CZD
      PRINT 3005, CLY,CMY,CNY,CXY,CYY,CZY
 3003 FORMAT(14H0 PITCH UP     ,6F18.6)
 3004 FORMAT(14H0 PITCH DOWN   ,6F18.6)
 3005 FORMAT(14H0 YAW          ,6F18.6)
      PRINT 3006
 3006 FORMAT(55H0XXXXXXXXXXXXXXXXXXXXXXXXXXXXXXXXXXXXXXXXXXXXXXXXXXXX)
      PRINT 3007
 3007 FORMAT(21H0 IMPINGEMENT FORCES )
      PRINT 3002
      PRINT 3003, CLIMU,CMIMU,CNIMU,CXIMU,CYIMU,CZIMU
      PRINT 3004, CLIMD,CMIMD,CNIMD,CXIMD,CYIMD,CZIMD
      PRINT 3005, CLIMY,CMIMY,CNIMY,CXIMY,CYIMY,CZIMY
      PRINT 3006
      PRINT 3008
 3008 FORMAT(19H0 INTERACTION TERMS)
      PRINT 3002
      PRINT 3003, CLINU,CMINU,CNINU,CXINU,CYINU,CZINU
      PRINT 3004, CLIND,CMIND,CNIND,CXIND,CYIND,CZIND
      PRINT 3005, CLINY,CMINY,CNINY,CXINY,CYINY,CZINY
      PRINT 3006
      PRINT 3009
 3009 FORMAT (22H0 CROSS COUPLING TERMS)
      PRINT 3002
      PRINT 3003, CLCCU,CMCCU,CNCCU,CXCCU,CYCCU,CZCCU
      PRINT 3004, CLCCD,CMCCD,CNCCD,CXCCD,CYCCD,CZCCD
      PRINT 3005, CLCCY,CMCCY,CNCCY,CXCCY,CYCCY,CZCCY
      PRINT 3006
      PRINT 3010
 3010 FORMAT(14H0 TOTAL VALUES)
      PRINT 3002
      PRINT 3011, CLT,CMT,CNT,CXT,CYT,CZT
 3011 FORMAT (1H0,13X,6F18.6)
      PRINT 3006
      DO600ICOM=1,6
      SIG=0.
      DO500IAXIS=1,3
      SIG=SIG+SIGIN(IAXIS,ICOM)**2+SIGIM(IAXIS,ICOM)**2+SIGTN(IAXIS,ICOM
     1)**2
  500 CONTINUE
      SIGTO(ICOM)=SQRT(SIG)
```

```
      GOTO(591,592,593,594,595,596),ICOM
  591 PRINT5991,SIGTO(ICOM)
 5991 FORMAT(1H0,16HSTD DEV OF CX = ,F15.7)
      GO TO 600
  592 PRINT5992,SIGTO(ICOM)
 5992 FORMAT(1H0,16HSTD DEV OF CZ = ,F15.7)
      GO TO 600
  593 PRINT5993,SIGTO(ICOM)
 5993 FORMAT(1H0,16HSTD DEV OF CM = ,F15.7)
      GO TO 600
  594 PRINT5994,SIGTO(ICOM)
 5994 FORMAT(1H0,16HSTD DEV OF CL = ,F15.7)
      GO TO 600
  595 PRINT5995,SIGTO(ICOM)
 5995 FORMAT(1H0,16HSTD DEV OF CN = ,F15.7)
      GO TO 600
  596 PRINT5996,SIGTO(ICOM)
 5996 FORMAT(1H0,16HSTD DEV OF CY = ,F15.7)
  600 CONTINUE
C     CALCULATE AMPLIFICATION FACTORS
      CALL AMPL (1,AKXU,AKZU,AKYU,AKMU,AKNU,AKLU)
      PRINT 3012
 3012 FORMAT (23HU AMPLIFICATION FACTORS)
      PRINT 3013
 3013 FORMAT (1H0,29X2HKL,16X2HKM,16X2HKN,16X2HKX,16X2HKY,16X2HKZ)
      PRINT 3043, AKLU,AKMU,AKNU,AKXU,AKYU,AKZU
 3043 FORMAT(1H0,*AMPLIFICATION*,10X,6F18.7)
      PRINT 3006
      PRINT 3006
C ERROR ANALYSIS OF DATA BASED ON 2 SIGMA ERRORS
      PRINT9000
      PRINT9001
 9000 FORMAT(55H0 THE 2 SIGMA ERROR HAND RESULTS IN THE FOLLOWING COEFS)
 9001 FORMAT(55H0  +2  SIGMA COFF FIRST THEN -2 SIGMA DATA ARE PRESENTD)
      DO660IER=1,2
      W=2.
      IF(IER.GT.1)W=-4.
      CXT=CXT+W*SIGTO(1)
      CZT=CZT+W*SIGTO(2)
      CMT=CMT+W*SIGTO(3)
      CLT=CLT+W*SIGTO(4)
      CNT=CNT+W*SIGTO(5)
      CYT=CYT+W*SIGTO(6)
      PRINT 3002
      PRINT 3011, CLT,CMT,CNT,CXT,CYT,CZT
      PRINT 3006
  660 CONTINUE
      PRINT 3006
      PRINT 3006
      IIN=INEXT
      GO TO (100,101,1,61),IIN
   61 CALLEXIT
      END
```

```
      SUBROUTINE VACPLU(THET,RAD,XMP,PLOC,QLOC,THAT)

      COMMON/NOZ/XMJ,GJ,ARJ,AJE,POJ,RJ,TOJ,TURN,DSTAR,AM,THETA,DEXIT,
     1IIMP,DCDEF

      IF(THET.GT.TURN)GO TO 100
      PIE=3.14159
      RED=1.
      POH=POJ*144.
      DSTAR=SQRT(AJE/ARJ*4./PIE)
      RHORHE=((1.+(GJ-1.)/2.*XMJ**2)**(-1./(GJ-1.)))
      BGJF   = (0.99-0.000016*TURN**2)/(2.0*(GJ**2)*(1.0-COS(TURN/
     1          57.2958)))
      XDLIM2=BGJF/RHORHE
      XDLIM3=SQRT(XDLIM2)
      XDLIM=XDLIM2**0.667
      DCLINE=RAD/DSTAR
      EXPON  = (DCLINE/XDLIM2)**2
      IF (EXPON.GT.675.0)  GO TO 2
      FTHAT  = EXP(-EXPON)
      GO TO 3
    2 FTHAT  = 0.0
    3 THAT   = THET+RED*ASIN(1.0/XMJ)*FTHAT
    4 IF(THAT.GT.TURN)GO TO 100
      TC=0.8*TURN
      IF(TC.GT.60.)TC=60.
      TTTTT=PIE*TC/0.75396
      FTHET  = (COS(PIE*THAT/TTTTT))**10.0
      IF(THAT.LE.TC) GO TO 5
      EXPON=0.064*(THAT-TC)
      FTHETA = EXP(-EXPON)
      FTHET  = 0.042572*FTHETA
    5 CONTINUE
      POW=2.
      DCLINE = RAD/DSTAR
      IF(DCLINE.GE.XDLIM2)GO TO 10
      IF(DCLINE.LE.XDLIM3)GO TO 6
      IF(DCLINE.LE.XDLIM)GO TO 7
      RHORAT=FTHET*0.5*(RHORHE/DCLINE+BGJF/DCLINE**2)
      GO TO 11
    6 CONTINUE
      POW=0.5
      BGJF=RHORHE
      GO TO 10
    7 RHORAT=RHORHE*FTHET*0.5*(1./(SQRT(DCLINE))+1./DCLINE)
      GO TO 11
   10 CONTINUE
      RHORAT=BGJF*(DCLINE**(-POW))*FTHET
   11 IF(RHORAT.GT.RHORHE)RHORAT=RHORHE
      XMP=SQRT((2./(GJ-1.)*((RHORAT**(1.-GJ))-1.)))
      PLOC=POH*((1.+(GJ-1.)/2.*XMP**2)**(GJ/(1.-GJ)))
      QLOC=GJ/2.*PLOC*XMP**2
      GO TO 101
  100 XMP=100.
      PLOC=0.
      QLOC=0.
  101 RETURN
      END
```

```
      SUBROUTINE JET(GAMN,ARN,PONOZ,PNOZ,TEE,TEX,MNOZ,AN)
      DIMENSION PM(3),ZM(3),COE(3)
      COMMON/A/POW,POW1,PRT,T1,PZT
      REAL MNOZ
      PM(1)=1.
      PM(2)=1.
      ZM(1)=1.
      ZM(2)=1.
      MNOZ=1.
      DM=.1
      POW=(GAMN+1.)/(2.*(GAMN-1.))
      DO111IF=1,100
      MNOZ=MNOZ+DM
      AAST=((GAMN+1.)/2.)**POW
      AAST=AAST*MNOZ/((1.+0.5*(GAMN-1.)*MNOZ**2)**POW)
      AAST=1./AAST
      ZM(1)=ZM(2)
      ZM(2)=ZM(3)
      ZM(3)=MNOZ
      PM(1)=PM(2)
      PM(2)=PM(3)
      PM(3)=AAST
      IF(AAST.GE.ARN)GO TO 112
  111 CONTINUE
  112 CALL PARCEO(PM,ZM,COE)
      MNOZ=COE(1)+COE(2)*ARN+COE(3)*ARN**2
      AAST=((GAMN+1.)/2.)**POW
      AAST=AAST*MNOZ/((1.+0.5*(GAMN-1.)*MNOZ**2)**POW)
      AAST=1./AAST
      PNOZ=PONOZ/((1.+0.5*(GAMN-1.)*MNOZ**2)**(GAMN/(GAMN-1.)))
      POW=2.*POW
      POW1=(GAMN-1.)/GAMN
      PRT=(PNOZ/PONOZ)**POW1
      PRT=1.-PRT
      T1=((2./(GAMN+1.))**POW)*2.*GAMN**2/(GAMN-1.)
      PZT=AN/AAST*PONOZ*SQRT(T1*PRT)*144.
      TEX=TEE/(1.+0.5*(GAMN-1.)*MNOZ*MNOZ)
      RETURN
      END
```

```
      SUBROUTINE CUBIC(X,C,Y,I,J,XFA)
      DIMENSION C(10,1)
      COMMON/ERROR/SIG,SIGM(2,6),SIGIN(3,6),SIGIM(3,6),SIGTH(3,6)
C CUBIC CURVE EQUATION WHERE C(I,5)=LARGEST VALUUE ALLOWED
      X1=X
      IF(X.LT.C(I,6))X1=C(I,6)
      IF(X.GT.C(I,5))X1=C(I,5)
      Y=C(I,1)+X1*(C(I,2)+X1*(C(I,3)+X1*C(I,4)))
      IF(J.EQ.I)GO TO 10
      X1=X
      IF(X.LT.C(J,6))X1=C(J,6)
      IF(X.GT.C(J,5))X1=C(J,5)
      Y=Y*(1.-XFA)+XFA*(C(J,1)+X1*(C(J,2)+X1*(C(J,3)+X1*C(J,4))))
   10 SIG=C(I,7)*(1.-XFA)+XFA*C(J,7)
      RETURN
      END
```

```
      SUBROUTINE PARCEO(Y,D,COEF)
      DIMENSION Y(3), D(3), COEF(3)
C-----GIVES COEFFICIENTS FOR A PARABOLIC FIT
      X1 = Y(1)
      X2 = Y(2)
      X3 = Y(3)
      D1 = D(1)
      D2 = D(2)
      D3 = D(3)
      FACTOR  = X2*X3*X3 - X2*X2*X3 - X1*X3*X3 + X1*X2*X2 + X1*X1*X3
     *        - X1*X1*X2
      A1      = X2*X3*X3 - X2*X2*X3
      A2      = X3*X1*X1 - X1*X3*X3
      A3      = X1*X2*X2 - X2*X1*X1
      B1      = X2*X2 - X3*X3
      B2      = X3*X3 - X1*X1
      B3      = X1*X1 - X2*X2
      C1      = X3 - X2
      C2      = X1 - X3
      C3      = X2 - X1
      COEF(1) = (D1*A1 + D2*A2 + D3*A3)/ FACTOR
      COEF(2) = (D1*B1 + D2*B2 + D3*B3) / FACTOR
      COEF(3) = (D1*C1 + D2*C2 + D3*C3) / FACTOR
      RETURN
      END
```

```
      SUBROUTINE EXPAN(G,PT,PIT,XM,THETNO,TURN)
      IF(PT.LE.PIT)GO TO 300
      TURN=0.
      G1=(G-1.)/G
      G2=2./(G-1.)
      G3=SQRT((G+1.)/(G-1.))
      G4=SQRT((G-1.)/(G+1.))
      IF(PIT.EQ.0.)GO TO 5
      XME=SQRT(G2*((PT/PIT)**G1-1.))
      X1=SQRT(XME**2-1.)
      TURN=57.2958*(G3*ATAN(G4*X1)-ATAN(X1))
      GO TO 6
    5 TURN=90.*(G3-1.)
    6 CONTINUE
      TURNL=TURN
      XME=XM
      X1=SQRT(XME**2-1.)
      TURN=57.2958*(G3*ATAN(G4*X1)-ATAN(X1))
      TURN=TURNL-TURN+THETNO
      RETURN
  300 TURN=THETNO
      RETURN
  400 FORMAT(1H0,5F20.5)
      END
```

```
      SUBROUTINE THR(I,CX,CY,CZ,CL,CM,CN)
      COMMON/ERROR/SIG,SIGM(2,6),SIGIN(3,6),SIGIM(3,6),SIGTH(3,6)
      COMMON/UP/NONOZU,NONOZUL,NONOZUR,DSTARUR,DSTARUL,AEXUL,AEXUR,
     1RMFSUL,RMFSUR,DXNOZU,DYNOZU,DZNOZU,
     2XREUL,XREUR,YREUL,YREUR,ZREUL,ZREUR
      COMMON/DWN/NONOZD,NONOZDL,NONOZDR,DSTARDL,DSTARDR,AEXDL,AEXDR,
     1RMFSDL,RMFSDR,DXNOZD,DYNOZD,DZNOZD,
     2XREDL,XREDR,YREDL,YREDR,ZREDL,ZREDR
      COMMON/SIDE/NONOZY,NONOZYL,NONOZYR,DSTARYL,DSTARYR,AEXYL,AEXYR,
     1      FMRYL,FMRYR,DXNOZY,DYNOZY,DZNOZY,
     2XREYL,XREYR,YREYL,YREYR,ZREYL,ZREYR
      COMMON/ALT/MINF,PINF,TINF,ALPH,IOPT,QI,HI,VINF,THRUST,INEXT
      COMMON/REF/SREF,C,B,SCALE,XRE,YRE,ZRE,DXNOZ,DYNOZ,DZNOZ,DXNOZZ,
     1DYNOZZ,DZNOZZ
      COMMON/NOZ/XMJ,GJ,ARJ,AJE,POJ,RJ,TOJ,TURN,DSTAR,AN,THETA,DEXIT,
     1IIMP,DCOEF
      REAL NONOZU,NONOZD,NONOZY,NONOZUL,NONOZUR,NONOZDL,NONOZDR,NONOZYL,
     1NONOZYR
      REAL MINF
   99 DO 7 J=1,2
      CT1=THRUST/QI/SREF
      IF(I.NE.1)GO TO 2
      IF(J.EQ.2)GO TO 111
   11 NONOZU=NONOZUL
      X=XREUL
      Y=YREUL
      Z=ZREUL
      GO TO 1111
  111 NONOZU=NONOZUR
      X=XREUR
      Y=YREUR
      Z=ZREUR
 1111 IF(NONOZU.EQ.0.) GO TO 5
      CT=CT1*NONOZU
      DX=DXNOZU
      DY=DYNOZU
      DZ=DZNOZU
      GO TO 4
    2 IF(I.EQ.3)GO TO 3
      IF(J.EQ.2)GO TO 222
   22 NONOZU=NONOZUL
      X=XREDL
      Y=YREDL
      Z=ZREDL
      GO TO 2222
  222 NONOZU=NONOZUR
      X=XREDR
      Y=YREDR
      Z=ZREDR
 2222 IF(NONOZU.EQ.0.) GO TO 5
      CT=CT1*NONOZU
      DX=DXNOZU
      DY=DYNOZU
      DZ=DZNOZU
      GO TO 4
    3 IF(J.EQ.2)GO TO 333
   33 NONOZY=NONOZYL
      X=XREYL
      Y=YREYL
      Z=ZREYL
      GO TO 3333
  333 NONOZY=NONOZYR
      X=XREYR
      Y=YREYR
      Z=ZREYR
 3333 IF(NONOZY.EQ.0.) GO TO 5
      CT=CT1*NONOZY
      DX=DXNOZY
```

```
      DY=DYN0ZY
      DZ=DZN0ZY
    4 CX=-CT*DX
      CY=-CT*DY
      CZ=-CT*DZ
      CL=(CZ*Y+CY*Z)/B
      CM=(CX*Z+CZ*X)/C*(-1.)
      CN=(CY*X-CX*Y)/B
      GO TO 6
    5 CX=0.
      CY=0.
      CZ=0.
      CL=0.
      CM=0.
      CN=0.
    6 IF(J.EQ.2) GO TO 66
      CX1=CX
      CY1=CY
      CZ1=CZ
      CL1=CL
      CM1=CM
      CN1=CN
      GO TO 7
   66 CX=CX1+CX
      CY=CY1-CY
      CZ=CZ1+CZ
      CL=CL1-CL
      CM=CM1+CM
      CN=CN1-CN
    7 CONTINUE
      RETURN
      END
```

ORIGINAL PAGE IS
OF POOR QUALITY

```
      SUBROUTINE IMPING(L,CXB,CYB,CZB,CLB,CMB,CNB)

      COMMON/CONST/PIE,RADIAN,GI,RI,GO
      COMMON/GRP2/DNX(300),DNY(300),DNZ(300),X(300),Y(300),Z(300),SLOC(3
     100),J
      COMMON/ERROR/SIG,SIGM(2,6),SIGIN(3,6),SIGIM(3,6),SIGTH(3,6)
      COMMON/UP/NONOZU,NONOZUL,NONOZUR,DSTARUR,DSTARUL,AEXUL,AEXUR,
     1RMFSUL,RMFSUR,DXNOZU,DYNOZU,DZNOZU,
     2XREUL,XREUR,YREUL,YREUR,ZREUL,ZREUR
      COMMON/DWN/NONOZD,NONOZDL,NONOZDR,DSTARDL,DSTARDR,AEXDL,AEXDR,
     1RMFSUL,RMFSUR,DXNOZD,DYNOZD,DZNOZD,
     2XREDL,XREDR,YREDL,YREDR,ZREDL,ZREDR
      COMMON/SIDE/NONOZY,NONOZYL,NONOZYR,DSTARYL,DSTARYR,AEXYL,AEXYR,
     1      RMRYL,RMRYR,DXNOZY,DYNOZY,DZNOZY,
     2XREYL,XREYR,YREYL,YREYR,ZREYL,ZREYR
      COMMON/FLT/MINF,PINF,TINF,ALPH,IOPT,QI,HI,VINF,THRUST,INEXT
      COMMON/REF/SREF,C,B,SCALE,XRE,YRE,ZRE,DXNOZ,DYNOZ,DZNOZ,DXNOZZ,
     1DYNOZZ,DZNOZZ
      COMMON/NOZ/XMJ,GJ,ARJ,AJE,POJ,RJ,TOJ,TURN,DSTAR,AN,THETA,DEXIT,
     1IIMP,DCOEF
      COMMON/CONTR/DELTER,DELTEL,XELV,ZELV,XFLA,ZFLA,
     1DELDF

      REAL NONOZU,NONOZD,NONOZY,NONOZUL,NONOZUR,NONOZDL,NONOZDR,NONOZYL,
     1NONOZYR,NONOZ
      DATAXFLA,ZFLA/-37.94,9.42/,XELV,ZELV/-25.858,11.554/,CCC/.0915172/
 1900 FORMAT(1H0,2I5,8F14.6)
      DO 18001Q=1,2
      IF(IIMP.NE.1)GO TO 180
C VACUUM PLUME IMPINGEMENT MODEL
      QFACT=1.-QI/20.
      IF(QFACT.LE.0.)GO TO 2000
C A DYNAMIC PRESSURE DECAY IS FACTORED IN SO THAT THERE IS NO IMP IF Q
C IS GREATER THAN 20 PSF ON THE VACUUM MODEL
  170 TCO=THRUST/SREF/QI*QFACT
      IF(L.NE.1)GO TO 1720
C PITCH UP NOZZLE MODEL
  171 IF(IQ.EQ.2)GO TO 1711
      IF(NONOZUL.EQ.0.)GO TO 2000
      YRE=YREUL
      XRE=XREUL
      CZT=TCO*NONOZUL
      GO TO 1712
 1711 IF(NONOZUR.EQ.0.)GO TO 2000
      YRE=YREUR
      XRE=XREUR
      CZT=TCO*NONOZUR
 1712 CZB=+.00086*CZT
      CXB=.00266*CZT
      CMB=-.00078*CZT*XRE/C
      CLB=-.13*CZT*YRE/B
      CYB=+.00238*CZT
      CNB=+.0093*CZT*XRE/B
      GO TO 1700
 1720 IF(L.EQ.3)GO TO 173
  172 IF(IQ.EQ.2)GO TO 1721
C PITCH DOWN NOZZLE MODEL
      IF(NONOZDL.EQ.0.)GO TO 2000
      XRE=XREDL
      YRE=YREDR
      CZT=-TCO*NONOZDL
      GO TO 1722
 1721 IF(NONOZDR.EQ.0.)GO TO 2000
      XRE=XREDR
      YRE=YREDR
      CZT=-TCO*NONOZDR
 1722 CZB=-.27389*CZT
      CXB=-.10709*CZT
      CYB=-.01937*CZT
```

```
      CMB=+.3018*CZT*XRE/C
      CLB=-.2512*CZT*YRE/B
      CNB=-.01657*CZT*XRE/B
      GO TO 1700
  175 IF(IW.EQ.2)GO TO 1731
C  YAW NOZZLE MODEL
      IF(NONOZYL.EQ.0.)GO TO 2000
      XRE=XREYL
      ZRE=ZREYL
      CZT=-1CC*NONOZYL
      GO TO 1732
 1731 IF(NONOZYR.EQ.0.)GO TO 2000
      XRE=XREYR
      ZRE=ZREYR
      CZT=-1CC*NONOZYR
 1732 CXB=-.00268*CZT
      CZB=-.01534*CZT
      CYB=-.00077*CZT
      CLB=+.03477*CZT*ZRE/B
      CMB=+.00873*CZT*XRE/C
      CNB=-.0013*CZT*XRE/B
      GO TO 1700
  180 IF(IIMP.NE.2)GO TO 185
C NO IMPINGEMENT COMPUTED
      GO TO 2000
  185 CONTINUE
C    NEWTONIAN IMPACT IMPINGEMENT MODEL
      IF(L.NE.1)GO TO 2
    1 CONTINUE
      DXNOZ=DXNOZU
      DYNOZ=DYNOZU
      DZNOZ=DZNOZU
      DXNOZZ=1.
      DYNOZZ=1.
      DZNOZZ=-1.
      XRE=XREUL
      YRE=YREUL
      ZRE=ZREUL
      DSTAR=DSTARUL
      AJE=AEXUL
      DELTAE=DELTLL
      NONOZ=NONOZUL
      IF(IW.LT.2) GO TO 4
      XRE=XREUR
      YRE=YREUR
      ZRE=ZREUR
      AJE=AEXUR
      DSTAR=DSTARUR
      DELTAE=DELTER
      NONOZ=NONOZUR
      GO TO 4
    2 IF(L.EQ.3)GO TO 3
      DZNOZZ=1.
      DYNOZZ=1.
      DXNOZZ=1.
      DZNOZ=DZNOZU
      DYNOZ=DYNOZU
      DXNOZ=DXNOZU
      XRE=XREUL
      YRE=YREUL
      ZRE=ZREUL
      AJE=AEXUL
      DSTAR=DSTARUL
      DELTAE=DELTLL
      NONOZ=NONOZUL
      IF(IW.LT.2) GO TO 4
      XRE=XREUR
      YRE=YREUR
      ZRE=ZREUR
```

```
      AJE=AEXOR
      DSTAR=DSTAROR
      DELTAE=DELTER
      NONOZ=NONOZOR
      GO TO 4
    3 CONTINUE
      DZNOZZ=1.
      DYNOZZ=1.
      DXNOZZ=1.
      DZNOZ=DZNOZY
      DYNOZ=DYNOZY
      DXNOZ=DXNOZY
      XRE=XREYL
      YRE=YREYL
      ZRE=ZREYL
      AJE=AEXYL
      DSTAR=DSTARYL
      DELTAE=DELTEL
      NONOZ=NONOZYL
      IF(IU.LT.21 GO TO 4
      XRE=XREYR
      YRE=YREYR
      ZRE=ZREYR
      AJE=AEXYR
      DSTAR=DSTARYR
      DELTAE=DELTER
      NONOZ=NONOZYR
    4 IF(NONOZ.LE.0.)GO TO 2000
      AJE=AJE/SQRT(NONOZ)
      CXB=0.
      CYB=0.
      CZB=0.
      CLB=0.
      CMB=0.
      CNB=0.
C     BEGIN CALCULATIONS OF COEFFICIENTS AND DERIVATIVES
      DO1150IU=1,J
  630 I = IU
      XXIX=X(I)*SCALE
      YYIY=Y(I)*SCALE
C CORRECTION TO NEW VERTICAL CG
      ZZIZ=(Z(I)-2.08333)*SCALE
      SLOCC=  SLOC(I)*SCALE*SCALE
      DNXXIX=DNX(I)
      DNZZIZ=DNZ(I)
      IF(IU.GT.23)GO TO 23
      IF(IU.GE.19)GO TO 19
C ELEVON DEFLECTION CORRECTION
      IF(DELTAE.EQ.0.)GO TO 23
      DELE=DELTAE/57.2958
      XHC=XELV*SCALE
      ZHC=(ZELV+CCC*  Y(IU))*SCALE
      GO TO 22
C BODY FLAP CORRECTION
   19 IF(DELBF.EQ.0.)GO TO 23
      DELE=DELBF/57.2958
      XHC=XFLA*SCALE
      ZHC=ZFLA*SCALE
   22 DHL=SQRT((  X(IU)*SCALE-XHC)**2+(  Z(IU)*SCALE-ZHC)**2)
      XXIX=XHC-DHL*COS(DELE)
      ZZIZ=ZHC+DHL*SIN(DELE)
C CORRECTION TO NEW VERTICAL CG
      ZZIZ=ZZIZ-2.08333*SCALE
      DNXXIX=DNX(IU)*COS(DELE)+DNZ(IU)*SIN(DELE)
      DNZZIZ=DNZ(IU)*COS(DELE)-DNX(IU)*SIN(DELE)
   23 CONTINUE
      YQ=YYIY
      DNQ = DNY(I)
  660 XB = XXIX / B
```

```
      XC=XX1X/C
      YB=YQ  /B
      ZB=ZZ1Z/B
      ZC=ZZ1Z/C
      SRATIO=SLOCC  /SREF
      DX=XX1X-XRE
      DY=YQ-YRE
      DZ=ZZ1Z-ZRE
      DIST=SQRT(DX**2+DY**2+DZ**2)
      IF(DIST.EQ.0.)GO TO 1150
      IF(DZ.GE.0.)GO TO 6
      IF(DZNOZZ.GT.0.)GO TO 1150
      GO TO 7
    6 IF(DZNOZZ.LT.0.)GO TO 1150
    7 CONTINUE
      DXTOT=DX/DIST
      DYTOT=DY/DIST
      DZTOT=DZ/DIST
      CETA=DXTOT*DXNOZ+DYTOT*DYNOZ+DZTOT*DZNOZ
      THETA=ACOS(CETA)*RADIAN
      IF(THETA.GE.TURN)GO TO 1150
      CALL VACPLU (THETA,DIST,XMPLUM,PLOC,QLOC,THAT)
      DXTOTP = -DXTOT
      DYTOTP = -DYTOT
      DZTOTP = -DZTOT
      IF (THAT.EQ.THETA)  GO TO 10

C     FIND DIRECTION COSINES OF NEW JET FLOW DIRECTION

      X1     = DXNOZ
      Y1     = DYNOZ
      Z1     = DZNOZ
      D2     = 1.0/CETA
      X2     = D2*DXTOT
      Y2     = D2*DYTOT
      Z2     = D2*DZTOT
      S      = SQRT((X2-X1)*(X2-X1)+(Y2-Y1)*(Y2-Y1)+(Z2-Z1)*(Z2-Z1))
      DXS    = (X2-X1)/S
      DYS    = (Y2-Y1)/S
      DZS    = (Z2-Z1)/S
      S3     = TAN(THAT/RADIAN)
      X3     = X1+S3*DXS
      Y3     = Y1+S3*DYS
      Z3     = Z1+S3*DZS
      D3     = 1.0/COS(THAT/RADIAN)
      DXTOTP = -X3/D3
      DYTOTP = -Y3/D3
      DZTOTP = -Z3/D3

   10 CETA2  = DXTOTP*DNXXIX+DYTOTP*DNQ+DZTOTP*DNZZIZ
      PIZF=PINF*144.
      IF(CETA2.LE.0.)GO TO 1050
      CPLOC  = (GJ+3.0)/(GJ+1.0)*(1.0-2.0/(XMPLUM*XMPLUM*(GJ+3.0)))*
     1         CETA2*CETA2
      GO TO 1051
 1050 CPLOC=CETA2/XMPLUM/XMPLUM/.1218
 1051 CONTINUE
      PTJJ=PLOC+QLOC
      PTINF=PIZF+QI
      IF(PTJJ.LT.PTINF)GO TO 1150
      IF (QLOC.LT.1.0)  GO TO 1150
      CPLOC=(CPLOC*QLOC+PLOC-PIZF)/QI
      IF(CPLOC.LE.0.)GO TO 1150
      DELCP=-CPLOC*SRATIO
 1008 DELCX=DELCP*DNXXIX
      DELCY=DELCP*DNQ
      DELCZ=DELCP*DNZZIZ
      DELCL=DELCZ*YB-DELCY*ZB
      DELCM=DELCX*ZC-DELCZ*XC
```

```
      DELCN=DELCY*XB-DELCX*YB
      CXB=CXB+DELCX
      CYB=CYB+DELCY
      CZB=CZB+DELCZ
      CLB=CLB+DELCL
      CMB=CMB+DELCM
      CNB=CNB+DELCN
 1150 CONTINUE
 1500 CONTINUE
      GO TO 1700
 2000 CXB=0.
      CYB=0.
      CZB=0.
      CLB=0.
      CMB=0.
      CNB=0.
 1700 IF(IQ.GT.1) GO TO 1750
C LEFT SIDE DATA SAVED
      CXB1=CXB
      CYB1=CYB
      CZB1=CZB
      CLB1=CLB
      CMB1=CMB
      CNB1=CNB
      GO TO 1800
 1750 CONTINUE
C LEFT SIDE ADDED TO RIGT SIDE DATA
      CXB=CXB1+CXB
      CYB=CYB1-CYB
      CZB=CZB1+CZB
      CLB=CLB1-CLB
      CMB=CMB1+CMB
      CNB=CNB1-CNB
 1800 CONTINUE
      RETURN
      END
```

```
      SUBROUTINE INPUTT(I1)
C     READS INPUT DATA

      DIMENSION KNOZ(34),TD(34),FD(34),FK(34),XM(34)
      REAL NONOZU,NONOZD,NONOZY,NONOZUL,NONOZUR,NONOZDL,NONOZDR,NONOZYL,
     1NONOZYR
      REAL MINF
      COMMON/CONST/PIE,RADIAN,GI,RI,GO
      COMMON/GRP2/DNX(300),DNY(300),DNZ(300),X(300),Y(300),Z(300),SLOC(3
     100),J
      COMMON/UP/NONOZU,NONOZUL,NONOZUR,DSTARUR,DSTARUL,AEXUL,AEXUR,
     1RMFSUL,RMFSUR,DXNOZU,DYNOZU,DZNOZU,
     2XREUL,XREUR,YREUL,YREUR,ZREUL,ZREUR
      COMMON/DWN/NONOZD,NONOZDL,NONOZDR,DSTARDL,DSTARDR,AEXDL,AEXDR,
     1RMFSUL,RMFSUR,DXNOZD,DYNOZD,DZNOZD,
     2XREDL,XREDR,YREDL,YREDR,ZREDL,ZREDR
      COMMON/SIDE/NONOZY,NONOZYL,NONOZYR,DSTARYL,DSTARYR,AEXYL,AEXYR,
     1     FMRYL,FMRYR,DXNOZY,DYNOZY,DZNOZY,
     2XREYL,XREYR,YREYL,YREYR,ZREYL,ZREYR
      COMMON/FLT/MINF,PINF,TINF,ALPH,IOPT,GI,HI,VINF,THRUST,INEXT
      COMMON/REF/SREF,C,B,SCALE,XRE,YRE,ZRE,DXNOZ,DYNOZ,DZNOZ,DXNOZZ,
     1DYNOZZ,DZNOZZ
      COMMON/NOZ/XMJ,GJ,ARJ,AJE,POJ,RJ,TOJ,TURN,DSTAR,AN,THETA,DEXIT,
     1IIMP,DCOEF
      COMMON/A/POW,POW1,PRT,T1,PZT
      COMMON/CONTR/DELTER,DELTEL,XELV,ZELV,XFLA,ZFLA,
     1DELBF
      NAMELIST/IN/GJ,ARJ,RJ,TOJ,DCOEF,DEXIO,THETA,SCALE,POJSA,
     1THAFTU,THAFTD,THAFTY,THOUTU,THOUTD,THOUTY,IIMP,
     2NONOZUL,XREUM,YREUM,ZREUM,NONOZUR,XREUS,YREUS,ZREUS,
     3NONOZDL,XREDM,YREDM,ZREDM,NONOZDR,XREDS,YREDS,ZREDS,
     4NONOZYL,XREYM,YREYM,ZREYM,NONOZYR,XREYS,YREYS,ZREYS,NOZNO
      NAMELIST/FC/MINF,PINF,TINF,ALPH,IOPT,GI,HI,VINF,INEXT
     1,DELTER,DELTEL,DELBF
      DATA KNOZ/31,32,33,34,35,36,37,38,60,61,43,44,46,47,48,49,50,52,
     1          51,45,42,78,79,98,99,82,83,81,85,84,100,96,97,95/
      DATA TD/3*0.0921,5*0.052,7*0.0465,4*0.067,2*0.0465,10*0.067,
     1 3*0.03871/
      DATA ED/3*0.099,5*0.0878,4*0.129,3*0.117,4*0.1413,2*0.129,
     1        10*0.1413,3*0.1368/
      DATA FK/3*0.00792,              0.00266,0.0027,0.00261,0.003,
     1        0.0027,0.0024,0.00221,0.0025,0.00245,0.00222,2*0.00237,
     2        0.0046,0.00412,0.0046,0.00405,0.0024,0.00237,0.0045,
     3        2*0.0046,0.0045,4*0.00452,0.00443,0.00452,
     4 .0013165,.0012258,.001647/
      DATA XM/2*1.466,1.472,5*2.584,4*3.635,3*3.425,4*3.047,2*3.635,
     1        10*3.047,4.172,4.172,4.172/
      DATAGJ/1.3/,TOJ/4873./,POJSA/152./,ARJ/22./,THETA/12./,DEXIO/.8013
     1/,THAFTU/0./,THOUTU/0./,THAFTD/-12./,THOUTD/-20./,THAFTY/0./,THOUT
     2Y/0./,XREUM/-37.69/,XREUS/-37.69/,YREDM/-37.69/,XREDS/-37.69/,
     3YREUM/-11./,YREUS/-11./,YREDM/-9.25/,YREDS/-9.25/,YREYM/-12.4625/,
     4YREYS/-12.4625/,ZREUM/-9.865/,ZREUS/-9.865/,ZREDM/-5.417/,ZREDS/-5
     5.417/,ZREYM/-7.003/,ZREYS/-7.003/,RJ/75./,XREYM/-37.69/,XREYS/-37.
     669/
      DATADELTER,DELTEL,DELBF/0.,0.,0./
      DATASREF,CO,BO/2690.,39.57,78.053/
      DATA DCOEF/1.0/
      DATANOZNO/0/
C **********************   INPUT DEFINITIONS     ********************************
C  ALL GEOMETRY DATA MUST BE INPUT IN FULL SCALE WITH UNITS OF FEET
C ALL DATA IS SPECIFIED TO A MOMENT REFERENCE CENTER  AT,
C                              XCG = 1076.7
C                              YCG = 0.
C                              ZCG = 375.
C               FROM THE CENTER OF GRAVITY, X POSITIVE FORWARD,
C               Y POSITIVE TO THE RIGHT, Z POSITIVE DOWNWARD
C ALL DATA HAS SIGNS FOR LEFT SIDE BECAUSE THE PROGRAM DOES ALL COMPUTATIONS
C ON THIS SIDE AND CORRECTS TO RIGHT SIDE
```

```
C*****************************************************************************
C                FORMATTED INPUT
C      DNX, DNY, DNZ     ARRAY OF DIRECTION COSINES OF THE FLAT PLATE
C                        SIMULATION AREAS
C      X, Y, Z   ARRAY OF CENTROIDS OF THE FLAT PLATE SIMULATION AREAS
C      SLOC      ARRAY OF LOCAL FLAT PLATE SIMULATION AREAS (SQ FT)
C NOTE THE ORDER OF FLAT PLATES IS IMPORTANT THE FIRST 18 ARE LEFT ELEVON
C UPPER SURFACE
C  THE NEXT 5 ARE UPPER LEFT SURFACE OF THE BODY FLAP

C*****************************************************************************
C                NAMELIST IN (NOZZLE DESCRIPTIONS)
C  NOZZLE   DESCRIPTION
C  DEXIO = FULL SCALE EXIT DIA IN FT ** DEFAULT VALUE = .8013 FT
C  ARJ = NOZZLE EXPANSION RATIO      ** DEFAULT VALUE = 22.
C  THETA = NOZZLE EXIT ANGLE IN DEG  ** DEFAULT VALUE = 12. DEG
C   GJ = EXIT GAS SPECIFIC HEAT RATIO** DEFAULT VALUE = 1.3
C  TOJ = NOZ TOTAL TEMP. IN DEG RANKINE  DEFAULT VALUE = 4873.
C  POJSA = NOZ TOTAL PRESSURE IN PSIA    DEFAULT VALUE =152.
C     RJ = EXHAUST GAS GAS CONSTANT  ** DEFAULT VALUE = 75.
C  DCOEF = NOZ DISCHARGE COEFF           DEFAULT VALUE =  1.000
C NOZZLES CANT ANGLES IN X-Z PLANE ARE THAFTU FOR UP NOZ , THAFTD FOR DOWN NOZ
C  AND  THAFTY FOR YAW NOZ
C   NOZZLE CANT  ANGLES IN Y-Z PLANE ARE THOUTU,THOUTD,THOUTY
C ALL DEFAULT VALUES ARE 0. EXCEPT FOR THAFTD = -12. AND THOUTD = -20.
C NOZZLE LOCATION DATA IS GIVEN BY THE VARIABLES XRE--,YRE--,ZRE--
C   THE FIRST - IS U FOR UP , D FOR DOWN OR Y FOR YAW
C   THE SECOND - IS M FOR LEFT SIDE DATA AND S FOR RIGHT SIDE DATA
C DEFAULT VALUES
C              XREUM =XREUS = -37.69
C              XREDM = XREDS = -37.69
C              XREYM = XREYS = -37.69
C              YREUM = YREUS = -11.
C              YREDM = YREDS = -9.25
C              YREYM = YREYS = -12.4625
C              ZREUM = ZREUS =-9.864
C              ZREDM = ZREDS =-5.417
C              ZREYM = ZREYS =-7.003
C     NONOZU   NUMBER OF UPWARD FIRING NOZZLES (CAUSING PITCH UP)
C              OPERATING IN A SET
C NONOZUL = LEFT SIDE  NONOZUR = RIGHT SIDE
C     NONOZD   NUMBER OF DOWNWARD FIRING NOZZLES (CAUSING PITCH DOWN)
C              OPERATING IN A SET
C NONOZDL= LEFT SIDE  NONOZDR = RIGHT SIDE
C     NONOZY   NUMBER OF SIDEWAY FIRING NOZZLES (CAUSING YAW)
C              OPERATING IN A SET
C   NONOZYL = LEFT SIDE   NONOZYR = RIGHT SIDE
C     SCALE    SCALE FACTOR FOR THE FLAT PLATE SIMULATION DATA
C     IIMP     DEFINES THE TYPE OF MATHEMATICAL MODEL TO BE USED,
C            = 1, USE THE EMPIRICAL IMPINGMENT MODEL,
C            = 2, NO IMPINGMENT MODEL USED,
C            = 3, USE THE SEMI-EMPIRICAL IMPINGMENT MODEL (MODIFIED
C                 NEWTONIAN PRESSURES PLUS VACUUM PLUME MODEL)
C    NOZNO IS NOZZLE CODE NUMBER IF WT TEST RESULTS ARE TO BE COMPUTED

C**********  ****************************************,**********************
C                NAMELIST FC (FLIGHT CONDITIONS)
C      ALPH     ANGLE OF ATTACK (DEG)
C      MINF     FREE STREAM MACH NUMBER
C      PINF     FREE STREAM AMBIENT PRESSURE (PSIA)
C      TINF     FREE STREAM AMBIENT TEMPERATURE (DEG R)
C      QI       FREE STREAM DYNAMIC PRESSURE (PSF)
C      HI       ALTITUDE (FT)
C      VINF     VELOCITY (FPS)
C    DELTER = RIGHT ELEVON DEFLECTIO  - TRAILING EDGE UP
C DELTEL = LEFT ELEVON DEFLECTION - TRAILING EDGE UP
C  DELBF = BODY FLAP DEFLECTION - TRAILING EDGE UP
C      IOPT     DEFINES THE FLIGHT CONDITIONS BEING INPUTTED,
```

```
C             = 1, MACH NUMBER, ANGLE OF ATTACK (DEG) AND ALTITUDE (FT)
C                  ARE INPUTTED,
C             = 2, VELOCITY (FPS), ALTITUDE (FT), AND ANGLE OF ATTACK
C                  (DEG) ARE INPUTTED,
C             = 3, DYNAMIC PRESSURE (PSF), ALTITUDE (FT), AND ANGLE OF
C                  ATTACK (DEG) ARE INPUTTED,
C             = 4, AMBIENT PRESSURE (PSI), TEMPERATURE (DEG R), MACH
C                  NUMBER AND ANGLE OF ATTACK (DEG) ARE INPUTTED
C     INEX1   DEFINES CONTENT OF NEXT SET OF DATA,
C             = 1, ALL TYPES OF DATA ARE TO BE INPUTTED,
C             = 2, NOZZLE DEFINITIONS AND FLIGHT CONDITIONS (NAMELISTS IN
C                  AND FC) ARE TO BE INPUTTED,
C             = 3, FLIGHT CONDITIONS ONLY (NAMELIST FC) ARE TO BE
C                  INPUTTED,
C             = 4, NO MORE DATA WILL BE READ IN , PROGRAM STOPS
C*************************************************************************
      IF(II.NE.1)GO TO 2
    1 CONTINUE
 2080 FORMAT(8E10.3)
      J=0
  120 J=J+1
      I=J
      READ (5,2080) DNX(I),DNY(I),DNZ(I),X(I),Y(I),Z(I),SLOC(I)
      IF(DNX(I).LT.1.1)GO TO 120
      J=J-1
      RETURN
    2 IF(II.EQ.3)GO TO 3
      READ(5,IN)
      IF(IIMP.LE.0)IIMP=3
      IF(IIMP.GT.3)IIMP=3
      IF(SCALE.EQ.0.)SCALE=1.
      TATAFT=TAN(THAFTU/RADIAN)
      TATOUT=TAN(THOUTU/RADIAN)
      DZNOZ=-1.*COS(ATAN(SQRT(TATAFT**2+TATOUT**2)))
      DXNOZ=-1.*DZNOZ*TATAFT
      DYNOZ=-1.*DZNOZ*TATOUT
      DXNOZU=DXNOZ
      DYNOZU=DYNOZ
      DZNOZU=DZNOZ
      TATAFT=TAN(THAFTD/RADIAN)
      TATOUT=TAN(THOUTD/RADIAN)
      DZNOZ=+1.*COS(ATAN(SQRT(TATAFT**2+TATOUT**2)))
      DXNOZ=+1.*DZNOZ*TATAFT
      DYNOZ=+1.*DZNOZ*TATOUT
      DXNOZD=DXNOZ
      DYNOZD=DYNOZ
      DZNOZD=DZNOZ
      TATAFT=TAN(THAFTY/RADIAN)
      TATOUT=TAN(THOUTY/RADIAN)
      DYNOZ=-1.*COS(ATAN(SQRT(TATAFT**2+TATOUT**2)))
      DXNOZ=-1.*DYNOZ*TATAFT
      DZNOZ=-1.*DYNOZ*TATOUT
      DXNOZY=DXNOZ
      DYNOZY=DYNOZ
      DZNOZY=DZNOZ
      GSA=GO
      IF(NOZNO.EQ.0)GO TO 2222
      N=NOZNO
C COMPUTE DISCHARGE COEF FOR TEST NOZZLES
      XMI=MINF
      POJ=POJSA
      DO100K=1,34
      K2=K
      IF(N.EQ.KNOZ(K))GO TO 200
  100 CONTINUE
      CF=1.
      GO TO 2222
  200 IF(POJ.EQ.0.)POJ=164.43
```

```
      GJ      = 1.4
      F       = 2.0*GJ*GJ/(GJ-1.0)
      F1      = (2.0/(GJ+1.0))**((GJ+1.0)/(GJ-1.0))
      DT      = TD(K2)
      DE      = ED(K2)
      FKI     = FK(K2)
      XMJ     = XM(K2)
      AT      = 0.7854*DT*DT
      AJ      = 0.7854*DE*DE
      PN      = POJ*(1.0+(GJ-1.0)/2.0*XMJ*XMJ)**(-1.0/(GJ-1.0))
      F2      = 1.0-(PN/POJ)**((GJ-1.0)/GJ)
      FS      = SQRT(F*F1*F2)
      IF(XMI.EQ.0.)XMI=10.
      PI      =          QI/GI*2.0/XMI/XMI/144.0
      IF(QI.EQ.0.)PI=.028336
      CT      = (FKI-AJ/POJ*(PN-PI  ))/(AT*FS)
 2222 CONTINUE
      DCOEF=C1
      IF(DCOEF.LE.0.)DCOEF=1.
      GJ=GJSA
C ADJUST CHAMBER PRESSURE FOR DISCHARGE COEFFICIENT
      POJ=POJSA*DCOEF
C ALL DATA IS RESCALED TO MODEL SCALE
C     SREF      REFERENCE AREA (SQ FT)
      SREF=SREF*SCALE*SCALE
C     B         WING SPAN (REFERENCE LENGTH) (FT)
      B=BO*SCALE
C     C         MEAN AERODYNAMIC CHORD (REFERENCE LENGTH) (FT)
      C=CO*SCALE
      DEXIT=DEXIT*SCALE
      XREUL=XREUM*SCALE
      XREUR=XREUS*SCALE
      XREDL=XREDM*SCALE
      XREDR=XREDS*SCALE
      XREYL=XREYM*SCALE
      XREYR=XREYS*SCALE
      YREUL=YREUM*SCALE
      YREUR=YREUS*SCALE
      YREDL=YREDM*SCALE
      YREDR=YREDS*SCALE
      YREYL=YREYM*SCALE
      YREYR=YREYS*SCALE
      ZREUL=ZREUM*SCALE
      ZREUR=ZREUS*SCALE
      ZREDL=ZREDM*SCALE
      ZREDR=ZREDS*SCALE
      ZREYL=ZREYM*SCALE
      ZREYR=ZREYS*SCALE
   33 CONTINUE
      AJE=.7854*DEXIT**2
      RETURN
    3 CONTINUE
      READ(5,FC)
      IF(INEXT.LE.0)INEXT=4
      IF(INEXT.GT.4)INEXT=4
      IF(IOPT.LE.0)IOPT=4
      IF(IOPT.GE.4)IOPT=4
      WRITE(6,IN)
      WRITE(6,FC)
      RETURN
      END
```

ORIGINAL PAGE IS
OF POOR QUALITY


```
      SUBROUTINE INTER(IT,CXB,CYB,CZB,CLB,CMB,CNB)
C     COMPUTES PLUME INTERACTION COEFFICIENTS

      DIMENSION RATIO(3)
      COMMON/FITS/ CZIDL(10,7),CAIDL(10,7),CMIDL(10,7),CLIDL(10,7),
     1 CNIDL(10,7),CYIDL(10,7), CZIYL(10,7),CAIYL(10,7),CMIYL(10,7),
     2 CLIYL(10,7),CNIYL(10,7),CYIYL(10,7),CZIUH(10,7),CAIUH(10,7),
     3 CMIUH(10,7),CLIUH(10,7),CNIUH(10,7),CYIUH(10,7),
     4CUPB(3,7)
      COMMON/DEFLECT/CLP30(10,7),CZP30(10,7),CMP30(10,7),CAP30(10,7),
     1        CZP10(10,7),CLP10(10,7),CMP10(10,7),CAP10(10,7),CMPR(10,7
     2),CZPB(10,7),CMY10(10,7),CAY10(10,7),CZY10(10,7),CLY10(10,7),
     3CZY30(10,7),CAY30(10,7),CLY30(10,7),CMY30(10,7)
      COMMON/COMP/IC,LC,ARAT,RMFSD,FMRY
      COMMON/CONST/PIE,RADIAN,GI,RI,GO
      COMMON/ERROR/SIG,SIGM(2,6),SIGIN(3,6),SIGIM(3,6),SIGTH(3,6)
      COMMON/FLT/MINF,PINF,TINF,ALPH,IOPT,GI,HI,VINF,THRUST,INEXT
      COMMON/NOZ/XMJ,GJ,ARJ,AJE,POJ,RJ,TOJ,TURN,DSTAR,AN,THETA,DEXIT,
     1IIMP,DCDCF
      COMMON/A/POW,POW1,PRT,T1,PZ1
      COMMON/CONTR/DELTER,DELTEL,XELV,ZELV,XFLA,ZFLA,
     1DELBF
      COMMON/UP/NONOZU,NONOZUL,NONOZUR,DSTARUR,DSTARUL,AEXUL,AEYUR,
     1RMFSUL,RMFSUR,DXNOZU,DYNOZU,DZNOZU,
     2XREUL,XREUR,YREUL,YREUR,ZREUL,ZREUR
      COMMON/DWN/NONOZD,NONOZDL,NONOZDR,DSTARDL,DSTARDR,AEXDL,AEXDR,
     1RMFSDL,RMFSDR,DXNOZD,DYNOZD,DZNOZD,
     2XREDL,XREDR,YREDL,YREDR,ZREDL,ZREDR
      COMMON/SIDE/NONOZY,NONOZYL,NONOZYR,DSTARYL,DSTARYR,AEXYL,AEXYR,
     1     FMRYL,FMRYR,DXNOZY,DYNOZY,DZNOZY,
     2XREYL,XREYR,YREYL,YREYR,ZREYL,ZREYR
      REAL NONOZU,NONOZD,NONOZY,NONOZUL,NONOZUR,NONOZDL,NONOZDR,NONOZYL,
     1NONOZYR
      REAL MINF
C     ****  C--DL IS  PITCH DOWN LEFT SIDE CURVE FITS
C ***** PITCH DOWN INDEPENDENT PARAMETER IS MOMENTUM RATIO
C **********  C--UH IS PITCH UP RIGHT SIDE DATA CURVE FITS
C ***** PITCH UP INDEPENDENT PARAMETER IS MOMENTUM RATIO
C *********  C--YL IS YAW  DATA LEFT SIDE  CURVE FITS
C ***** YAW INDEPENDENT PARAMETER IS MASS FLOW RATIO
C ***** C----(I,1) TO C----(I,4) ARE COEFFICIENT S OF A CUBIC CURVE
C*****C----(I,5) IS MAX VALUE OF X FOR FIT
C***** C(I,6) IS MIN VALUE OF X FOR FIT
C***** C----(I,7) IS STD DEV OF FIT
C ALL CURVES ARE FITTED IN 5 DEG INCREMENTS
C ***** LINEAR INTERPOLATION IS DONE ON ALPHA
      DATA(CZIDL(1,I),I=1,7)/-.003578175E-,-1.3252434,1.8262287,0.,
     1 .13,0.,.006721/
      DATA(CAIDL(1,I),I=1,7)/.008119224,-.57281949,2.255663,2.659706,
     1 .11,.015,.005177/
      DATA(CMIDL(1,I),I=1,7)/-.0026167640,.97960279,-3.8857783,0.,
     1 .126,0.,.003239/
      DATA(CLIDL(1,I),I=1,7)/.001045451,-.16934446,-.862314,11.861382,
     1 .10,.005,.000866/
      DATA(CNIDL(1,I),I=1,7)/-.004,0.,0.,0.,.10,0.,.000963/
      DATA(CYIDL(1,I),I=1,7)/.0024493900,.59508919,-3.3693275,0.,
     1 .09,0.,.0030004/
      DATA(CZIDL(2,I),I=1,7)/-.00091927427,-1.1969597,1.1705735,0.,
     1 .13,0.,.005081/
      DATA(CAIDL(2,I),I=1,7)/.0067533831,-.5785186,2.6606857,1.5467384,
     1 .10,.012,.002732/
      DATA(CMIDL(2,I),I=1,7)/-.0017074711,.80419637,-3.0904617,0.,
     1 .13,0.,.002467/
      DATA(CLIDL(2,I),I=1,7)/.0002625382,-.1307714,-1.254691,13.318271,
     1 .10,.0025,.000829/
      DATA(CNIDL(2,I),I=1,7)/-.0025,0.,0.,0.,.10,0.,.000644/
      DATA(CYIDL(2,I),I=1,7)/.004170530,.27382076,-1.5025533,0.,
     1 .09,0.,.002482/
      DATA(CZIDL(3,I),I=1,7)/-.003413075,-.7379121,-0.097693,64.447924,
```

ORIGINAL PAGE IS
OF POOR QUALITY

```
1 .13E,0.,.0045787
 DATA(CA1DL(5,I),I=1,7)/.006659158,-.56F0699,3.067603,-2.4254496,
1 .11,.012,.0042661/
 DATA(CM1DL(5,I),I=1,7)/-.0020585775,.76115482,-2.7562347,0.,
1 .13E,0.,.0020033/
 DATA(CL1DL(5,I),I=1,7)/-.000095447037,-.17971984,.63221810,0.,
1 .14,0.,.0007033/
 DATA(CN1DL(5,I),I=1,7)/-.0013022764,-.0403915E0,.31668833,0.,
1 .0E,0.,.00060E8/
 DATA(CY1DL(5,I),I=1,7)/.00409155E0,.17177915,-.52919510,0.,
1 .12,0.,.0019207/
 DATA(CZ1DL(4,I),I=1,7)/.0000594E5,-.0456804,-6.565167,43.737769,
1 .12,0.,.0053033/
 DATA(CA1DL(4,I),I=1,7)/.006352837,-.5116206E,2.0792274,2.4822579,
1 .10,.013,.0025097/
 DATA(CM1DL(4,I),I=1,7)/-.0007390E721,.67186097,-2.3644230,0.,
1 .142,0.,.0018995/
 DATA(CL1DL(4,I),I=1,7)/-.0016220048,-.12366976,-.056961137,4.309143
1,.10,0.,.0007347/
 DATA(CN1DL(4,I),I=1,7)/-.0012290902,-.022937711,.12178972,0.,
1 .10,0.,.0006537/
 DATA(CY1DL(4,I),I=1,7)/.004430916E4,.17440759,-.45905824,0.,
1 .12,0.,.0018627/
 DATA(CZ1DL(5,I),I=1,7)/-.00241811,-.565491,-5.139405,36.014229,
1 .12,0.,.0052547/
 DATA(CA1DL(5,I),I=1,7)/.00180809,-.38329,.3147143,10.74809,
1 .10,.005,.0030005/
 DATA(CM1DL(5,I),I=1,7)/.0010742638,.63443672,-2.6484171,0.,
1 .12,0.,.0021047/
 DATA(CL1DL(5,I),I=1,7)/-.0016938,-.18779,1.27817,-2.6.3793,
1 .12,0.,.0007087/
 DATA(CN1DL(5,I),I=1,7)/-.0005073493,-.076025E,1.51248,-9.0837746,
1 .04,0.,.0007127/
 DATA(CY1DL(5,I),I=1,7)/.0040394700,.24188801,-1.0085301,0.,
1 .12,0.,.0020797/
 DATA(CZ1DL(6,I),I=1,7)/-.0015918E,-.862021,-.14723614,18.818404,
1 .12,0.,.0070807/
 DATA(CA1DL(6,I),I=1,7)/-.0004702835E,-.4415E615,2.0930306,0.,
1 .10,0.,.0030157/
 DATA(CM1DL(6,I),I=1,7)/.0012286037,.76797273,-3.7259380,0.,
1 .10,0.,.0026052/
 DATA(CL1DL(6,I),I=1,7)/-.0011580353,-.22933375,1.3295553,0.,
1 .09,0.,.0007E65/
 DATA(CN1DL(6,I),I=1,7)/-.0000607E6,-.1037E39,2.0792968,-12.055484,
1 .04,0.,.0006899/
 DATA(CY1DL(6,I),I=1,7)/.0034298420,.5123289E,-1.5445693,0.,
1 .10,0.,.0023067/
 DATA(CZ1DL(7,I),I=1,7)/.000993E3,-1.0118165,.4592628,25.1E0138,
1 .11,0.,.0102107/
 DATA(CA1DL(7,I),I=1,7)/-.0014697E,-.412E163,1.255279,5.7341E13,
1 .10,0.,.0025E06/
 DATA(CM1DL(7,I),I=1,7)/-.0012751066,.88163818,-4.2850148,0.,
1 .10,0.,.0023E08/
 DATA(CL1DL(7,I),I=1,7)/-.00081171129,-.2537E530,1.4259182,0.,
1 .09,0.,.0007791/
 DATA(CN1DL(7,I),I=1,7)/-.0001123E1,-.1032412,2.02777,-11.E10639,
1 .04,0.,.0010257/
 DATA(CY1DL(7,I),I=1,7)/.0033707E26,.3334573E,-1.E159087,0.,
1 .10,0.,.0023E68/
 DATA(CZ1DL(E,I),I=1,7)/.0020583734,-1.0371776,1.1E0E121,19.727744,
1 .12,0.,.0142167/
 DATA(CA1DL(E,I),I=1,7)/-.001638172,-.446219,1.706198,3.833255,
1 .10,0.,.0021857/
```

```
 DATA(CMIDL(8,I),I=1,7)/.0007614405S,.00068403,-4.972S607,0.,
1 .10,0.,.001414/
 DATA(CL1DL(8,I),I=1,7)/-.000379466,-.3007144,2.4398586,-6.846879,
1 .12,0.,.000739/
 DATA(CN1DL(8,I),I=1,7)/-.00006123667,-.1296327,2.51692,-14.102086,
1 .04,0.,.001293/
 DATA(CY1DL(8,I),I=1,7)/.0029564353,.39863291,-2.1873767,0.,
1 .09,0.,.002411/
 DATA(C21DL(9,I),I=1,7)/-.000960869,-.5688283,-8.8023067,83.41719,
1 .095,0.,.018895/
 DATA(CA1DL(9,I),I=1,7)/-.0012341B4,-.512663S,3.540908,-7.7873735,
1 .12,0.,.002638/
 DATA(CM1DL(9,I),I=1,7)/.00066166776,.97128770,-4.53S9956,0.,
1 .105,0.,.002071/
 DATA(CL1DL(9,I),I=1,7)/-.0006645465,-.2890016,2.109604,-5.0808823,
1 .12,0.,.000624/
 DATA(CN1DL(9,I),I=1,7)/.00013892S,-.1568336,2.7970658,-14.902663,
1 .02,0.,.001226/
 DATA(CY1DL(9,I),I=1,7)/.0024542023,.45838338,-2.5668342,0.,
1 .09,0.,.002322/
 DATA(C21DL(10,I),I=1,7)/-.00056136878,-.98676745,4.2378887,0.,
1 .12,0.,.020753/
 DATA(CA1DL(10,I),I=1,7)/-.00185607,-.4086227,1.847751,2.1262878,
1 .10,0.,.002367/
 DATA(CM1DL(10,I),I=1,7)/.00055591734,.93723610,-4.1921034,0.,
1 .11,0.,.002163/
 DATA(CL1DL(10,I),I=1,7)/-.000847837,-.2936418,2.010513,-4.545096,
1 .12,0.,.000672/
 DATA(CN1DL(10,I),I=1,7)/-.000001955,-.19391S,3.355843,-17.116039,
1 .02,0.,.001331/
 DATA(CY1DL(10,I),I=1,7)/.0025220313,.52801444,-3.1718149,0.,
1 .08,0.,.002319/
 DATA(C21YL(1,I),I=1,7)/.0032702044,-1.4354405,12.806984,0.,
1 .06,0.,.012259/
 DATA(CA1YL(1,I),I=1,7)/.0033388762,.027432974,-2.0489098,0.,
1 .055,0.,.002578/
 DATA(CM1YL(1,I),I=1,7)/.000063570804,.19699183,-1.3005521,0.,
1 .06,0.,.002753/
 DATA(CL1YL(1,I),I=1,7)/.00049644244,-.088258694,.57105188,0.,
1 .06,0.,.001090/
 DATA(CN1YL(1,I),I=1,7)/.00006750841,-.14366869,1.4157109,0.,
1 .06,0.,.000577/
 DATA(CY1YL(1,I),I=1,7)/-.0024513299,.88000484,-7.0176860,0.,
1 .06,0.,.006692/
 DATA(C21YL(2,I),I=1,7)/.0041409843,-1.4090787,13.206927,0.,
1 .06,0.,.010019/
 DATA(CA1YL(2,I),I=1,7)/.0030389246,-.083256282,-.63857132,0.,
1 .05,0.,.002013/
 DATA(CM1YL(2,I),I=1,7)/0.,0.,0.,0.,.06,0.,.002141/
 DATA(CL1YL(2,I),I=1,7)/0.,0.,0.,0.,.06,0.,.000652/
 DATA(CN1YL(2,I),I=1,7)/.00015714701,-.20931584,2.0280340,0.,
1 .06,0.,.000941/
 DATA(CY1YL(2,I),I=1,7)/-.00038106379,.70259959,-7.0662578,0.,
1 .06,0.,.005996/
 DATA(C21YL(3,I),I=1,7)/.0052374878,-1.3338312,11.130794,0.,
1 .06,0.,.007848/
 DATA(CA1YL(3,I),I=1,7)/.0021116066,.025275694,-1.8870194,0.,
1 .05,0.,.002144/
 DATA(CM1YL(3,I),I=1,7)/0.,0.,0.,0.,.06,0.,.002159/
 DATA(CL1YL(3,I),I=1,7)/-.00016250169,-.038748113,.33467152,0.,
1 .06,0.,.000606/
 DATA(CN1YL(3,I),I=1,7)/-.00012742867,-.23542177,2.5365194,0.,
1 .045,0.,.000845/
```

ORIGINAL PAGE IS
OF POOR QUALITY

```
 DATA(CYIYL(3,I),I=1,7)/-.00016339430,.67321891,-7.1003986,0.,
1 .045,0.,.002705/
 DATA(CZIYL(4,I),I=1,7)/-.0038216065,-.42590104,6.2993438,0.,
1 .06,0.,.006199/
 DATA(CAIYL(4,I),I=1,7)/+.0019908037,.031449239,-1.7329775,0.,
1 .045,0.,.002172/
 DATA(CMIYL(4,I),I=1,7)/0.,0.,0.,0.,.06,0.,.002091/
 DATA(CLIYL(4,I),I=1,7)/-.00072107788,-.073978808,1.0560601,0.,
1 .035,0.,.000838/
 DATA(CNIYL(4,I),I=1,7)/-.00010941856,-.21107940,1.9920371,0.,
1 .05,0.,.000850/
 DATA(CYIYL(4,I),I=1,7)/.00061094204,.65106053,-6.5599346,0.,
1 .05,0.,.002652/
 DATA(CZIYL(5,I),I=1,7)/.00031879143,-.62650797,2.8398293,0.,
1 .06,0.,.006052/
 DATA(CAIYL(5,I),I=1,7)/.00015063235,.28186338,-18.950500,
1 246.34760,.045,0.,.002018/
 DATA(CMIYL(5,I),I=1,7)/.0033500641,-.059385419,1.5668712,0.,
1 .06,0.,.002639/
 DATA(CLIYL(5,I),I=1,7)/-.0011278857,-.12337774,1.0857623,0.,
1 .05,0.,.001234/
 DATA(CNIYL(5,I),I=1,7)/.00019366269,-.17333227,1.7849972,0.,
1 .04,0.,.000988/
 DATA(CYIYL(5,I),I=1,7)/.00062267197,.65514122,-7.1471735,0.,
1 .05,0.,.002639/
 DATA(CZIYL(6,I),I=1,7)/-.0071455546,.96431099,-72.633196,
1 827.26421,.05,.01,.007573/
 DATA(CAIYL(6,I),I=1,7)/-.0022047408,.28969745,-15.964851,
1 184.43640,.045,.01,.002031/
 DATA(CMIYL(6,I),I=1,7)/.0023669280,.28859677,-2.1141551,0.,
1 .06,0.,.003203/
 DATA(CLIYL(6,I),I=1,7)/-.00068297887,-.27986258,2.5155903,0.,
1 .055,0.,.001534/
 DATA(CNIYL(6,I),I=1,7)/.00029592129,-.11654945,1.8446555,
1 -.96759609,.035,0.,.000544/
 DATA(CYIYL(6,I),I=1,7)/.0010122592,.51411814,-5.5159605,0.,
1 .05,0.,.001895/
 DATA(CZIYL(7,I),I=1,7)/-.0087101578,1.8493792,-112.78191,
1 1277.3926,.05,.01,.010572/
 DATA(CAIYL(7,I),I=1,7)/-.0020497229,.071553366,-7.3647072,
1 92.465680,.05,.005,.001713/
 DATA(CMIYL(7,I),I=1,7)/.0017533997,.52368116,-4.6631665,0.,
1 .06,0.,.002349/
 DATA(CLIYL(7,I),I=1,7)/-.00056833042,-.32374633,2.7968741,0.,
1 .06,0.,.001498/
 DATA(CNIYL(7,I),I=1,7)/.000189807,-.043820856,-.57021348,
1 20.848859,.035,0.,.000287/
 DATA(CYIYL(7,I),I=1,7)/.0012629695,.44075727,-4.1943874,0.,
1 .05,0.,.001798/
 DATA(CZIYL(8,I),I=1,7)/0.,0.,0.,0.,.06,0.,.014774/
 DATA(CAIYL(8,I),I=1,7)/-.0016900386,-.067370039,-3.4182848,
1 56.342650,.05,0.,.001556/
 DATA(CMIYL(8,I),I=1,7)/.0013210578,.59692937,-5.2062245,0.,
1 .055,0.,.002286/
 DATA(CLIYL(8,I),I=1,7)/-.00044359890,-.33774549,2.8614639,0.,
1 .06,0.,.001399/
 DATA(CNIYL(8,I),I=1,7)/.00012927304,-.00025741787,-2.5218212,
1 37.794705,.045,0.,.000283/
 DATA(CYIYL(8,I),I=1,7)/.00094977196,.41586129,-3.4208285,0.,
1 .06,0.,.0019235/
```

```
 DATA(CZ1YL(9,I),I=1,7)/0.,0.,0.,0.,.06,0.,.021512/
 DATA(CA1YL(9,I),I=1,7)/-.0015480294,.0067151618,-7.8046554,
1 125.63158,.045,0.,.002099/
 DATA(CM1YL(9,I),I=1,7)/.0012917244,.40459572,4.5215123,
1 -93.323704,.055,0.,.002700/
 DATA(CL1YL(9,I),I=1,7)/-.00068816496,-.32564394,2.4882146,0.,
1 .06,0.,.0014821/
 DATA(CN1YL(9,I),I=1,7)/.00024515912,-.029196155,-1.0389104,
1 12.495974,.06,.0075,.000358/
 DATA(CY1YL(9,I),I=1,7)/.00070530046,.481855e3,-4.1995683,0.,
1 .06,0.,.001906/
 DATA(CZ1YL(10,I),I=1,7)/0.,0.,0.,0.,.06,0.,.021653/
 DATA(CA1YL(10,I),I=1,7)/-.0020593017,.0869710380,-3.6662959,
1 31.622778,.045,0.,.002003/
 DATA(CM1YL(10,I),I=1,7)/.0015784903,.27141860,.2202993,
1 -90.247616,.06,0.,.002226/
 DATA(CL1YL(10,I),I=1,7)/-.00034787615,-.43184256,4.2899613,0.,
1 .05,0.,.001553/
 DATA(CN1YL(10,I),I=1,7)/.00021431192,-.055138734,-.44508055,
1 9.9558416,.06,.005,.000355/
 DATA(CY1YL(10,I),I=1,7)/.00028691536,.57002619,-5.4858448,0.,
1 .05,0.,.002112/
 DATA CZ1UH(1,I),I=1,7)/-.0101992e4,-.25004168,-2.8889915,
1 0.,.12,0.,.006911/
 DATA(CA1UH(1,I),I=1,7)/.0033246301,-.1891426?,-.38758593,
1 0.,.12,.015,.004584/
 DATA(CM1UH(1,I),I=1,7)/.0020691696,.078414997,.25498217,
1 0.,.12,0.,.002352/
 DATA(CL1UH(1,I),I=1,7)/-.0011379249,-.050739927,-.54467691,
1 0.,.1,0.,.000650/
 DATA(CN1UH(1,I),I=1,7)/+.0016783900,.083783238,.88916133,
1 0.,.1,0.,.001026/
 DATA(CY1UH(1,I),I=1,7)/-.0036263451,-.20951531,-.97696821,
1 0.,.1,0.,.002503/
 DATA(CZ1UH(2,I),I=1,7)/-.0021597353,-.67917598,2.2030149,
1 0.,.12,0.,.005710/
 DATA(CA1UH(2,I),I=1,7)/.00084467717,-.11755e86,-.20560750,
1 0.,.12,0.,.003828/
 DATA(CM1UH(2,I),I=1,7)/0.,0.,0.,0.,.12,0.,.003061/
 DATA(CL1UH(2,I),I=1,7)/-.0013664026,-.04901406?,-.39853918,
1 0.,.1,0.,.000674/
 DATA(CN1UH(2,I),I=1,7)/.0020467295,.10582929,.64847448,
1 0.,.1,0.,.001001/
 DATA(CY1UH(2,I),I=1,7)/-.0043476172,-.27230722,-.85583024,
1 0.,.1,0.,.002501/
 DATA(CZ1UH(3,I),I=1,7)/.00095569189,-.83975463,3.5949048,
1 0.,.12,0.,.005623/
 DATA(CA1UH(3,I),I=1,7)/-.0014178126,.019088997,-1.0550313,
1 0.,.12,.01,.003433/
 DATA(CM1UH(3,I),I=1,7)/-.0018290780,-.0010959327,-.29746119,
1 0.,.12,0.,.001032/
 DATA(CL1UH(3,I),I=1,7)/-.00068987812,-.074837736,-.11617501,
1 0.,.1,0.,.000698/
 DATA(CN1UH(3,I),I=1,7)/.0013629073,.13651789,.44586858,
1 0.,.1,0.,.001074/
 DATA(CY1UH(3,I),I=1,7)/-.0031605811,-.32308172,-.89652575,
1 0.,.1,0.,.002450/
 DATA(CZ1UH(4,I),I=1,7)/-.00018203725,-.50650366,.17492840,
1 0.,.12,0.,.005677/
 DATA(CA1UH(4,I),I=1,7)/.0017723453,-.068957909,-.13636109,
```

ORIGINAL PAGE IS
OF POOR QUALITY

```
     1 0.,.12,.02,.003556/
      DATA(CM1UH(4,I),I=1,7)/-.0013541272,-.017396436,-.36738946,
     1 0.,.12,0.,.001135/
      DATA(CL1UH(4,I),I=1,7)/-.0001230839S,-.0821b9773,-.15834899,
     1 0.,.1,0.,.000557/
      DATA(CN1UH(4,I),I=1,7)/.00051078035,.14588312,.43107917,
     1 0.,.1,0.,.000913/
      DATA(CY1UH(4,I),I=1,7)/-.0015919561,-.34167782,-.55079590,
     1 0.,.1,0.,.002077/
      DATA(CZ1UH(5,I),I=1,7)/.00094173140,-.18718384,-2.8674166,
     1 0.,.12,0.,.006365/
      DATA(CA1UH(5,I),I=1,7)/.0011059299,-.087115893,.058179381,
     1 0.,.12,.01,.003413/
      DATA(CM1UH(5,I),I=1,7)/-.0027289361,-.048914860,.097267140,
     1 0.,.12,0.,.001600/
      DATA(CL1UH(5,I),I=1,7)/.00002380332b,-.081991177,-.37175052,
     1 1.3644941,.1,0.,.000582/
      DATA(CN1UH(5,I),I=1,7)/.00013393436,.13628298,.71300937,
     1 -.57405296,.1,0.,.000905/
      DATA(CY1UH(5,I),I=1,7)/.00073074507,-.27243329,-2.8394416,
     1 14.148681,.1,0.,.003962/
      DATA(CZ1UH(6,I),I=1,7)/.00051959765,.20847718,-18.913730,
     1 140.54675,.08,.02,.007031/
      DATA(CA1UH(6,I),I=1,7)/-.000066071509,-.0082030530,-1.8698173,
     1 10.9[illegible]383,.12,0.,.002171/
      DATA(CM1UH(6,I),I=1,7)/-.0011051556,-.11603847,.71362241,
     1 0.,.09,0.,.001475/
      DATA(CZ1UH(7,I),I=1,7)/.0012511790,.39042663,-22.149902,
     1 168.86056,.08,.025,.009566/
      DATA(CA1UH(7,I),I=1,7)/-.00028348979,-.0841996B9,-.19822264,
     1 0.,.1,0.,.001816/
      DATA(CM1UH(7,I),I=1,7)/-.00000798914d2,.024358474,-2.4396543,
     1 19.087992,.08,.015,.002382/
      DATA(CZ1UH(8,I),I=1,7)/0.,0.,0.,0.,.1,0.,.012899/
      DATA(CA1UH(8,I),I=1,7)/-.00068327005,-.12187716,.058610876,
     1 0.,.1,0.,.001680/
      DATA(CM1UH(8,I),I=1,7)/0.,0.,0.,0.,.1,0.,.000881/
      DATA(CZ1UH(9,I),I=1,7)/0.,0.,0.,0.,.1,0.,.016174/
      DATA(CA1UH(9,I),I=1,7)/-.00071967288,-.11483830,-.011504877,
     1 0.,.1,0.,.002006/
      DATA(CM1UH(9,I),I=1,7)/0.,0.,0.,0.,.1,0.,.001597/
      DATA(CZ1UH(10,I),I=1,7)/0.,0.,0.,0.,.1,0.,.018516/
      DATA(CA1UH(10,I),I=1,7)/-.00080542253,-.085743779,-.050942977,
     1 0.,.1,0.,.002383/
      DATA(CM1UH(10,I),I=1,7)/.00009086288,-.061026137,.28931719,
     1 0.,.1,0.,.001550/
      DATA(CUPB(1,I),I=1,7)/1.038182,.08081425,-.3901599E-3,
     1-.8940111E-4,0.,-18.,0./
      DATA(CUPB(2,I),I=1,7)/1.0367126,.05025877,-.1751849E-2,
     1-.9876866E-4,0.,-20.,0./
      DATA(CUPB(3,I),I=1,7)/1.0266617,.039196,-.1823657E-2,
     1-.947253E-4,0.,-20.,0./
      DATA(CUPB(I,7),I=1,3)/.13606,.14238,.18157B/
      DATA ALPHBK/15.0/

C     RMFSD     MOMENTUM RATIO FOR DOWNWARD FIRING JETS
C     RMFSU     MOMENTUM RATIO FOR UPWARD FIRING JETS
C     RMFSY     MOMENTUM RATIO FOR SIDEWAY FIRING JETS
C     FMRD      MASS FLOW RATIO FOR DOWNWARD FIRING JETS
C     FMRU      MASS FLOW RATIO FOR UPWARD FIRING JETS
```

```
C     FMRY      MASS FLOW RATIO FOR SIDEWAY FIRING JETS
      DO 99 IQ=1,2
      CXB=0.
      CYB=0.
      CZB=0.
      CLB=0.
      CMB=0.
      CNB=0.
      XIC=(ALPH+7.5)/5.
      IC=IFIX(XIC)
      XIC= FLOAT(IC)*5.-7.5
      IC=IC+1
      IF(IC.GT.10)IC=10
      IF(IC.LE.0)IC=1
      LC=IC+1
      IF(LC.GT.10)LC=10
      ARAT=(ALPH-XIC)/5.
      DELTE=DELTEL
      IF(IQ.EQ.2)DELTE=DELTER
      IF(II.NE.1)GO TO 64
C  PITCH UP DATA
   10 NONOZU=NONOZUL
      RMFSU=RMFSUL
      IF (IQ.LT.2) GO TO 13
      NONOZU=NONOZUR
      RMFSU=RMFSUR
   13 IF(NONOZU.LE.0.) GO TO 85
      XIC=(ALPH-17.5)/5.
      JC=IFIX(XIC)
      XIC= FLOAT(JC)*5.+17.5
      JC=JC+1
      IF(JC.LT.1)JC=1
      IF(JC.GT.5)JC=5
      KC=JC+1
      IF(KC.GT.5)KC=5
      ARAL=(ALPH-XIC)/5.
      IF (ALPH.GT.ALPHBK)  GO TO 60
C LOW ANGLE OF ATTACK
      CALL NEWT(2,RMFSU,CNB,ALPEAK,ALPH)
      SIGM(IQ,4)=SIG
      CALL NEWT(1,RMFSU,CLB,ALPEAK,ALPH)
      SIGM(IQ,5)=SIG
      IF(ALPH.LT.10.958)GO TO 16
      CALL CUBIC(RMFSU,CYIUH,CYB,JC,KC,ARAL)
      GO TO 17
   16 CONTINUE
      CALL NEWT(3,RMFSU,CYB,ALPEAK,ALPH)
   17 CONTINUE
      SIGM(IQ,6)=SIG
      IF(ALPH.GT.ALPEAK) GO TO 55
      XALPH=ALPH-ALPEAK
      DO30II=1,3
      IF(XALPH.LT.CUPB(II,6))XALPH=CUPB(II,6)
      IF(XALPH.GT.CUPB(II,5))XALPH=CUPB(II,5)
      RATIO(II)=CUPB(II,1)+XALPH*(CUPB(II,2)+XALPH*(CUPB(II,3)+XALPH*
     1CUPB(II,4)))
   30 CONTINUE
      SIGM(IQ,4)=SQRT((CUPB(1,7)*CLB)**2+SIG**2)
      SIGM(IQ,5)=SQRT((CUPB(2,7)*CNB)**2+SIG**2)
      SIGM(IQ,6)=SQRT((CUPB(3,7)*CYB)**2+SIG**2)
```

```
      CLB=CLB*RATIO(1)
      CNB=CNB*RATIO(2)
      CYB=CYB*RATIO(3)
   55 CONTINUE
   60 CONTINUE
      CALL CUBIC (RMFSU,CAIUH,CXB,IC,LC,ARAT)
      SIGM(IQ,1)=SIG
      CALL CUBIC (RMFSU,CZIUH,CZB,IC,LC,ARAT)
      SIGM(IQ,2)=SIG
      CALL CUBIC (RMFSU,CMIUH,CMB,IC,LC,ARAT)
      SIGM(IQ,3)=SIG
      IF(ALPH.LE.ALPHBK) GO TO 90
      CALL CUBIC (RMFSU,CNIUH,CNB,JC,KC,ARAL)
      SIGM(IQ,4)=SIG
      CALL CUBIC (RMFSU,CYIUH,CYB,JC,KC,ARAL)
      SIGM(IQ,6)=SIG
      CALL CUBIC (RMFSU,CLIUH,CLB,JC,KC,ARAL)
      SIGM(IQ,5)=SIG
      GO TO 90
C PITCH DOWN ANALYSIS
   64 IF(IT.EQ.3)GO TO 75
   65 NONOZD=NONOZDL
      RMFSD=RMFSDL
      IF(IQ.EQ.1) GO TO 66
      NONOZD=NONOZDR
      RMFSD=RMFSDR
   66 IF(NONOZD.LE.0.) GO TO 85
      CALL CUBIC(RMFSD,CAIDL,CXB,IC,LC,ARAT)
      SIGM(IQ,1)=SIG
      CALL CUBIC(RMFSD,CZIDL,CZB,IC,LC,ARAT)
      SIGM(IQ,2)=SIG
      CALL CUBIC(RMFSD,CMIDL,CMB,IC,LC,ARAT)
      SIGM(IQ,3)=SIG
      CALL CUBIC(RMFSD,CNIDL,CNB,IC,LC,ARAT)
      SIGM(IQ,4)=SIG
      CALL CUBIC(RMFSD,CLIDL,CLB,IC,LC,ARAT)
      SIGM(IQ,5)=SIG
      CALL CUBIC(RMFSD,CYIDL,CYB,IC,LC,ARAT)
      SIGM(IQ,6)=SIG
C CONTROL DEFLECTION CORRECTIONS
      CALL DEFL(IT,DELHF,0,CXQ,CYQ,CZQ,CLQ,CMQ,CNQ,DFQ)
C BODY FLAP CORRECTION
      CALL DEFL(IT,DELTE,2,CXC,CYC,CZC,CLC,CMC,CNC,DFL)
C ELEVATOR CORRECTION
      CXB=CXB+CXC*DFL+CXQ*DFQ
      CYB=CYB+CYC*DFL+CYQ*DFQ
      CZB=CZB+CZC*DFL+CZQ*DFQ
      CLB=CLB+CLC*DFL+CLQ*DFQ
      CMB=CMB+CMC*DFL+CMQ*DFQ
      CNB=CNB+CNC*DFL+CNQ*DFQ
      GO TO 90
C YAW ANALYSIS
   75 FMRY=FMRYL
      NONOZY=NONOZYL
      IF(IQ.EQ.1) GO TO 76
      FMRY=FMRYR
      NONOZY=NONOZYR
   76 IF(NONOZY.LE.0) GO TO 85
      CALL CUBIC (FMRY,CZIYL,CZL,IC,LC,ARAT)
      SIGM(IQ,2)=SIG
```

ORIGINAL PAGE IS
OF POOR QUALITY

```
      CALL CUBIC (FMRY,CAIYL,CXB,IC,LC,ARAT)
      SIGM(IQ,1)=SIG
      CALL CUBIC (FMRY,CMIYL,CMB,IC,LC,ARAT)
      SIGM(IQ,3)=SIG
      CALL CUBIC (FMRY,CLIYL,CLB,IC,LC,ARAT)
      SIGM(IQ,5)=SIG
      CALL CUBIC (FMRY,CNIYL,CNB,IC,LC,ARAT)
      SIGM(IQ,4)=SIG
      CALL CUBIC (FMRY,CYIYL,CYB,IC,LC,ARAT)
      SIGM(IQ,6)=SIG
C CONTROL DEFLECTION CORRECTIONS
      CALL DEFL(IT,DELTE,2,CXC,CYC,CZC,CLC,CMC,CNC,DFL)
      CXB=CXB+CXC*DFL
      CYB=CYB+CYC*DFL
      CZB=CZB+CZC*DFL
      CLB=CLB+CLC*DFL
      CMB=CMB+CMC*DFL
      CNB=CNB+CNC*DFL
      GO TO 90
   85 CYB    = 0.0
      CZB    = 0.0
      CMB    = 0.0
      CNB    = 0.0
      CLB    = 0.0
      CXB=0.
      DO855ISI=1,6
  855 SIGM(IQ,ISI)=0.
   90 CONTINUE
C     THE FOLLOWING DATA MUST BE REVERSED IN SIGN SO AS TO CORREC3L8
C     CORRELATE THE BUILT-IN CURVE FIT COEFFICIENT DATA (BASED ON WIND
C     TUNNEL TEST DATA) WITH BODY AXES CONVENTION.
      CZB    = -CZB
      CXB=-CXB
      IF(IT.NE.1) GO TO 97
      CYB    = -CYB
      CNB    = -CNB
      CLB    = -CLB
   97 IF(IQ.GT.1) GO TO 98
      CX1=CXB
      CY1=CYB
      CZ1=CZB
      CL1=CLB
      CM1=CMB
      CN1=CNB
      GO TO 99
   98 CXB=CX1+CXB
      CYB=CY1-CYB
      CZB=CZ1+CZB
      CLB=CL1-CLB
      CMB=CM1+CMB
      CNB=CN1-CNB
      DO999ISI=1,6
  999 SIGIN(IT,ISI)=SQRT(SIGM(1,ISI)**2+SIGM(2,ISI)**2)
   99 CONTINUE
      RETURN
      END
```

```
      SUBROUTINE NEWT(J,X,YMAX,XA,ALPHA)
      COMMON/ERROR/SIG,SIGM(2,6),SIGIN(3,6),SIGIM(3,6),SIGTH(3,6)
      DIMENSION C(6,7)
C C(1,I)=PEAK ROLLING MOMENT AS A FUNCTION OF MOMENTUM RATIO
      DATA(C(1,I),I=1,6)/-.10311266E-02,-.4028187,1.4107644,
     1-9.5493416,.12,0./
C C(2,I)=PEAK  YAWING MOMENT AS A FUNCTION OF MOMENTUM RATIO
      DATA(C(2,I),I=1,6)/.1053117E-02,.6719102,-1.1489908,
     17.2895142,.12,0./
C C(3,I)=PEAK SIDE   FORCE   AS A FUNCTION OF MOMENTUM RATIO
      DATA(C(3,I),I=1,6)/-.2266176E-02,-1.189385,-9.6859178,
     196.800641,.10551,0./
C C(4,I)=PEAK ROLLING MOMENT AS A FUNCTION OF ALPHA
      DATA(C(4,I),I=1,6)/-.01060376,.1094004E-02,-.4258494E-04,.4827789
     119E-06,0.,17.41484/
C C(5,I)=PEAK  YAWING MOMENT AS A FUNCTION OF ALPHA
      DATA(C(5,I),I=1,6)/.017671924,-.19821074E-02,.82349374E-04,
     1-.9126B003E-06,0.,16.6353/
C C(6,I)=PEAK SIDE   FORCE   AS A FUNCTION OF ALPHA
      DATA(C(6,I),I=1,6)/-.038418188,.490538E-02,-.1708478E-03,
     1-.32170623E-05,0.,10.95834/
      DATA(C(1,7),I=1,6)/.0019976,.001069,.005389,.001417,.00234,.00424/
C COMPUTE PEAK VALUE
      IF(X.GT.C(J,5))X=C(J,5)
      YMAX=C(J,1)+X*(C(J,2)+X*(C(J,3)+X*C(J,4)))
      SIG=C(J,7)
      IF(J.NE.2)GO TO 20
C YAWING MOMENT CURVE IS USED TO COMPUTE ANGLE OF ATTACK OF PEAK VALUE
C BY NEWTON-RAPHSON ITERATION SO J = 2 IS DONE FIRST
C COMPUTE PEAK ALPHA
      ICNT=0
      XA=0.
      ERROR=.001
      K=J+3
      GUESS=(YMAX-C(K,1))/C(K,2)
    5 A=XA+GUESS
      IF(A.GE.C(K,6))GUESS=(C(K,6)-XA)/2.
      ICNT=ICNT+1
      XA=XA+GUESS
      GUESS=(YMAX-(C(K,1)+XA*(C(K,2)+XA*(C(K,3)+XA*C(K,4)))))/
     1(C(K,2)+2.*C(K,3)*XA+3.*C(K,4)*XA*XA)
      IF(ABS(GUESS).GT.ERROR)GO TO 5
      IF(ICNT.GE.100)GO TO 15
      IF(XA.GT.C(K,6))XA=C(K,6)
      IF(ALPHA.LE.XA)RETURN
      GO TO 21
   15 PRINT2000,ICNT,XA
 2000 FORMAT(41H0 TROUBLE IN PEAK VALUE ITERATION IN NEWT,I5,F20.7)
      XA=15.
      RETURN
C COMPUTE PEAK VALUE AS A FUNCTION OF ANGLE OF ATTACK BECAUSE ANGLE IS
C ABOVE PEAK VALUE
   20 IF(ALPHA.LE.XA)RETURN
   21 K=J+3
      YMAX=C(K,1)+ALPHA*(C(K,2)+ALPHA*(C(K,3)+ALPHA*C(K,4)))
      RETURN
      END
```

```
      SUBROUTINE DEFL(I,DEL,IFLAP,CX,CY,CZ,CL,CM,CN,DFL)
      COMMON/COMP/IC,LC,ARAT,RMFSD,FMRY
      COMMON/DEFLECT/CLP30(10,7),CZP30(10,7),CMP30(10,7),CAP30(10,7),
     1          CZP10(10,7),CLP10(10,7),CMP10(10,7),CAP10(10,7),CMPB(10,7
     2),CZPB(10,7),CMY10(10,7),CAY10(10,7),CZY10(10,7),CLY10(10,7),
     3CZY30(10,7),CAY30(10,7),CLY30(10,7),CMY30(10,7)
C  C--PB ARE BODY FLAP DATA
      DATA(CMPB(1,I),I=1,7)/0.,0.,0.,0.,.12,0.,0./
      DATA(CMPB(2,I),I=1,7)/0.,-.0308183,1.709049,0.,.088,.03,0./
      DATA(CMPB(3,I),I=1,7)/0.,.011613,1.217626,0.,.088,0.,0./
      DATA(CMPB(4,I),I=1,7)/0.,.06899,.495664,0.,.088,0.,0./
      DATA(CMPB(5,I),I=1,7)/0.,.1277447,.0032869,0.,.088,0.,0./
      DATA(CMPB(6,I),I=1,7)/0.,.1386713,-.300274,0.,.088,0.,0./
      DATA(CMPB(7,I),I=1,7)/0.,.0854596,-.526711,0.,.088,0.,0./
      DATA(CMPB(8,I),I=1,7)/0.,.0080933,.946782,0.,.088,0.,0./
      DATA(CMPB(9,I),I=1,7)/0.,.0168753,1.197332,0.,.088,0.,0./
      DATA(CMPB(10,I),I=1,7)/0.,.080233,.593376,0.,.088,0.,0./
      DATA(CZPB(1,I),I=1,7)/0.,0.,0.,0.,.12,0.,0./
      DATA(CZPB(2,I),I=1,7)/0.,0.,0.,0.,.12,0.,0./
      DATA(CZPB(3,I),I=1,7)/0.,0.,0.,0.,.12,0.,0./
      DATA(CZPB(4,I),I=1,7)/0.,0.,0.,0.,.12,0.,0./
      DATA(CZPB(5,I),I=1,7)/0.,-.494498,8.081047,-36.01423,.0306,0.,0./
      DATA(CZPB(6,I),I=1,7)/0.,-.59755,7.043025,-18.818,.0424,0.,0./
      DATA(CZPB(7,I),I=1,7)/0.,-.557898,6.58894,-25.1604,.0423,0.,0./
      DATA(CZPB(8,I),I=1,7)/0.,-.38137,2.846837,-14.72774,.067,0.,0./
      DATA(CZPB(9,I),I=1,7)/0.,-.806397,12.181,-83.4172,.0331,0.,0./
      DATA(CZPB(10,I),I=1,7)/0.,-.410527,-.868257,0.,.088,0.,0./
C  C-P-- ARE PITCH DOWN RCS DATA
C  C--10 ARE +10 DEG ELEVATOR DATA
      DATA(CZP10(1,I),I=1,7)/0.,.00628336,-4.614157B,0.,.0857,0.,0./
      DATA(CZP10(2,I),I=1,7)/0.,.436209,-2.859625,0.,.0763,0.,0./
      DATA(CZP10(3,I),I=1,7)/0.,-.0998582,8.575346,-64.4979,.088,0.,0./
      DATA(CZP10(4,I),I=1,7)/0.,0.,0.,0.,.12,0.,0./
      DATA(CZP10(5,I),I=1,7)/0.,-.4540887,6.983626,-36.0142,.06,0.,0./
      DATA(CZP10(6,I),I=1,7)/0.,-.173979,1.0059981,-18.8184,.06,0.,0./
      DATA(CZP10(7,I),I=1,7)/0.,0.,0.,0.,.12,0.,0./
      DATA(CZP10(8,I),I=1,7)/0.,0.,0.,0.,.12,0.,0./
      DATA(CZP10(9,I),I=1,7)/0.,0.,0.,0.,.12,0.,0./
      DATA(CZP10(10,I),I=1,7)/0.,0.,0.,0.,.12,0.,0./
      DATA(CLP10(1,I),I=1,7)/0.,.0601934,.4924273,-11.86138,.05,0.,0./
      DATA(CLP10(2,I),I=1,7)/0.,-.0019006,1.225812,-13.31827,.05,0.,0./
      DATA(CLP10(3,I),I=1,7)/0.,0.,0.,0.,.12,0.,0./
      DATA(CLP10(4,I),I=1,7)/0.,-.0790635,1.0242953,-4.30914,.088,0.,0./
      DATA(CLP10(5,I),I=1,7)/0.,-.064398,-.027973,2.68379,.088,0.,0./
      DATA(CLP10(6,I),I=1,7)/0.,-.039249,-.165415,0.,.088,0.,0./
      DATA(CLP10(7,I),I=1,7)/0.,-.024235,-.233684,0.,.088,0.,0./
      DATA(CLP10(8,I),I=1,7)/0.,.017832,-1.24932,6.8469,.088,.022,0./
      DATA(CLP10(9,I),I=1,7)/0.,-.0043639,-.75064,5.08088,.088,0.,0./
      DATA(CLP10(10,I),I=1,7)/0.,-.0,0.,0.,.12,0.,0./
      DATA(CMP10(1,I),I=1,7)/0.,-.4772946,5.76496,0.,.041,0.,0./
      DATA(CMP10(2,I),I=1,7)/0.,-.308668,4.11828,0.,.0375,0.,0./
      DATA(CMP10(3,I),I=1,7)/0.,-.203773,2.895427,0.,.0352,0.,0./
      DATA(CMP10(4,I),I=1,7)/0.,0.,0.,0.,.12,0.,0./
      DATA(CMP10(5,I),I=1,7)/0.,.09622,.767693,0.,.088,0.,0./
      DATA(CMP10(6,I),I=1,7)/0.,.0410377,1.801176,0.,.088,0.,0./
      DATA(CMP10(7,I),I=1,7)/0.,-.101365,3.328115,0.,.088,.015,0./
      DATA(CMP10(8,I),I=1,7)/0.,0.,0.,0.,.12,0.,0./
      DATA(CMP10(9,I),I=1,7)/0.,0.,0.,0.,.12,0.,0./
      DATA(CMP10(10,I),I=1,7)/0.,0.,0.,0.,.12,0.,0./
C  C--30 ARE -30 DEG ELEVATOR DATA
      DATA(CLP30(1,I),I=1,7)/0.,.112554,.776222,-11.86138,.088,0.,0./
      DATA(CLP30(2,I),I=1,7)/0.,.0805115,.928726,-13.31827,.088,0.,0./
      DATA(CLP30(3,I),I=1,7)/0.,.1208744,-.861833,0.,.088,0.,0./
      DATA(CLP30(4,I),I=1,7)/0.,.0348942,.2175078,-4.30914,.088,0.,0./
      DATA(CLP30(5,I),I=1,7)/0.,.052602,-.690597,2.683793,.088,0.,0./
      DATA(CLP30(6,I),I=1,7)/0.,.0710422,-.460898,0.,.088,0.,0./
      DATA(CLP30(7,I),I=1,7)/0.,.0967565,-.579512,0.,.088,0.,0./
      DATA(CLP30(8,I),I=1,7)/0.,.1345912,-1.466618,6.84688,.088,0.,0./
```

ORIGINAL PAGE IS
OF POOR QUALITY


```
      DATA(CLP30(9,I),I=1,7)/0.,.118667,-.961303,5.08088,.08,0.,0./
      DATA(CLP30(10,I),I=1,7)/0.,.1245252,-.7886,4.5451,.07,0.,0./
      DATA(CZP30(1,I),I=1,7)/0.,.9057804,-3.811823,0.,.1,0.,0./
      DATA(CZP30(2,I),I=1,7)/0.,.8207267,-4.038106,0.,.1,0.,0./
      DATA(CZP30(3,I),I=1,7)/0.,.1894748,7.69125,-64.4979,.1,0.,0./
      DATA(CZP30(4,I),I=1,7)/0.,.1039182,5.669416,-43.737769,.1,0.,0./
      DATA(CZP30(5,I),I=1,7)/0.,-.11215,6.1011271,-36.01423,.09,0.,0./
      DATA(CZP30(6,I),I=1,7)/0.,.0536082,2.50097,-18.8184,.09,0.,0./
      DATA(CZP30(7,I),I=1,7)/0.,.3363512,.5857807,-25.16014,.09,0.,0./
      DATA(CZP30(8,I),I=1,7)/0.,.597206,-2.9125867,-19.72774,.09,0.,0./
      DATA(CZP30(9,I),I=1,7)/0.,.0439123,8.483934,-83.41719,.09,0.,0./
      DATA(CZP30(10,I),I=1,7)/0.,.3754955,-3.4756065,0.,.09,0.,0./
      DATA(CMP30(1,I),I=1,7)/0.,-.5524307,4.166181,0.,.09,0.,0./
      DATA(CMP30(2,I),I=1,7)/0.,-.50014412,4.6953353,0.,.09,0.,0./
      DATA(CMP30(3,I),I=1,7)/0.,-.41036849,3.8207067,0.,.09,0.,0./
      DATA(CMP30(4,I),I=1,7)/0.,-.24082413,2.3301214,0.,.09,0.,0./
      DATA(CMP30(5,I),I=1,7)/0.,-.1470361,1.75829358,0.,.085,0.,0./
      DATA(CMP30(6,I),I=1,7)/0.,-.1954625,2.1214309,0.,.09,0.,0./
      DATA(CMP30(7,I),I=1,7)/0.,-.27780826,1.99743797,0.,.09,0.,0./
      DATA(CMP30(8,I),I=1,7)/0.,-.45264811,4.0059764,0.,.09,0.,0./
      DATA(CMP30(9,I),I=1,7)/0.,-.35552212,2.5261263,0.,.09,0.,0./
      DATA(CMP30(10,I),I=1,7)/0.,-.27300927,1.2353699,0.,.09,0.,0./
      DATA(CAP30(1,I),I=1,7)/0.,0.,0.,0.,.12,0.,0./
      DATA(CAP30(2,I),I=1,7)/0.,0.,0.,0.,.12,0.,0./
      DATA(CAP30(3,I),I=1,7)/0.,0.,0.,0.,.12,0.,0./
      DATA(CAP30(4,I),I=1,7)/0.,0.,0.,0.,.12,0.,0./
      DATA(CAP30(5,I),I=1,7)/0.,-.1735844,2.509746,-10.74809,.1,0.,0./
      DATA(CAP30(6,I),I=1,7)/0.,-.18284168,1.153831,0.,.1,0.,0./
      DATA(CAP30(7,I),I=1,7)/0.,-.206174,1.96794,-5.734161,.1,0.,0./
      DATA(CAP30(8,I),I=1,7)/0.,-.1549924,1.1465491,-3.833255,.1,0.,0./
      DATA(CAP30(9,I),I=1,7)/0.,-.1026336,-.83891469,7.787374,.1,0.,0./
      DATA(CAP30(10,I),I=1,7)/0.,-.2747671,1.3246952,-2.126288,.1,0.,0./
C  C-Y-- ARL YAW RCS DATA
      DATA(CLY10(1,I),I=1,7)/0.,.0651217,-1.93635,0.,.05,.033,0./
      DATA(CLY10(2,I),I=1,7)/0.,-.0272225,-.8984637,0.,.05,0.,0./
      DATA(CLY10(3,I),I=1,7)/0.,-.0151378,-.38125675,0.,.05,0.,0./
      DATA(CLY10(4,I),I=1,7)/0.,-.0297554,.1362836,0.,.05,0.,0./
      DATA(CLY10(5,I),I=1,7)/0.,-.0630139,-.1460194,0.,.05,0.,0./
      DATA(CLY10(6,I),I=1,7)/0.,.0060522,1.753304,0.,.05,.003,0./
      DATA(CLY10(7,I),I=1,7)/0.,-.0126222,-1.251029,0.,.05,0.,0./
      DATA(CLY10(8,I),I=1,7)/0.,-.0173344,-.9783852,0.,.05,0.,0./
      DATA(CLY10(9,I),I=1,7)/0.,-.0514681,-.0790533,0.,.05,0.,0./
      DATA(CLY10(10,I),I=1,7)/0.,.0253333,-1.254912,0.,.05,.02,0./
      DATA(CMY10(1,I),I=1,7)/0.,0.,0.,0.,.05,0.,0./
      DATA(CMY10(2,I),I=1,7)/0.,0.,0.,0.,.05,0.,0./
      DATA(CMY10(3,I),I=1,7)/0.,.067611,-.0247677,0.,.05,0.,0./
      DATA(CMY10(4,I),I=1,7)/0.,.3064222,-4.6270487,0.,.0331,0.,0./
      DATA(CMY10(5,I),I=1,7)/0.,.3766199,-3.295248,0.,.05,0.,0./
      DATA(CMY10(6,I),I=1,7)/0.,.2335367,-.484581,0.,.05,0.,0./
      DATA(CMY10(7,I),I=1,7)/0.,.06002697,1.655791,0.,.05,0.,0./
      DATA(CMY10(8,I),I=1,7)/0.,-.0735547,3.72785,0.,.05,.0197,0./
      DATA(CMY10(9,I),I=1,7)/0.,.3109171,-7.83852,93.3237,.05,0.,0./
      DATA(CMY10(10,I),I=1,7)/0.,.2235781,-7.366294,90.24762,.03,0.,0./
      DATA(CAY10(1,I),I=1,7)/0.,-.135835,-1.6009645,0.,.05,0.,0./
      DATA(CAY10(2,I),I=1,7)/0.,-.1431525,.09176022,0.,.05,0.,0./
      DATA(CAY10(3,I),I=1,7)/0.,-.2054548,1.2000865,0.,.05,0.,0./
      DATA(CAY10(4,I),I=1,7)/0.,-.28414775,3.2769264,0.,.0433,0.,0./
      DATA(CAY10(5,I),I=1,7)/0.,-.555291,20.9274477,-246.3476,.02,0.,0./
      DATA(CAY10(6,I),I=1,7)/0.,-.6029302,18.390013,-184.436,.025,0.,0./
      DATA(CAY10(7,I),I=1,7)/0.,-.35201358,9.319685,-92.466,.025,0.,0./
      DATA(CAY10(8,I),I=1,7)/0.,-.1403738,4.223294,-56.3426,.03,0.,0./
      DATA(CAY10(9,I),I=1,7)/0.,-.3191362,9.550405,-123.6316,.03,0.,0./
      DATA(CAY10(10,I),I=1,7)/0.,-.2771056,4.852895,-31.62278,.05,0.,0./
      DATA(CZY10(1,I),I=1,7)/0.,.9616367,-13.529153,0.,.035,0.,0./
      DATA(CZY10(2,I),I=1,7)/0.,.69781676,-11.5633015,0.,.0302,0.,0./
      DATA(CZY10(3,I),I=1,7)/0.,0.,0.,0.,.05,0.,0./
      DATA(CZY10(4,I),I=1,7)/0.,-.1845058,-1.8070644,.0,.05,0.,0./
      DATA(CZY10(5,I),I=1,7)/0.,-.5933273,3.7516572,0.,.05,0.,0./
      DATA(CZY10(6,I),I=1,7)/0.,-2.238434,76.76023,-827.26,.025,0.,0./
```

```
      DATA(CZY10(7,I),I=1,7)/0.,-2.789925E-6,106.6892,-1277.39,.02,0.,0./
      DATA(CZY10(8,I),I=1,7)/0.,-.48753865,-17.27032,0.,.05,0.,0./
      DATA(CZY10(9,I),I=1,7)/0.,-1.069881,-10.95358,0.,.05,0.,0./
      DATA(CZY10(10,I),I=1,7)/0.,-.17183747,-24.38131,0.,.05,0.,0./
      DATA(CZY30(1,I),I=1,7)/0.,.4465306,-.8089369,0.,.05,0.,0./
      DATA(CZY30(2,I),I=1,7)/0.,.5942164,-8.917269,2,0.,.0333,0.,0./
      DATA(CZY30(3,I),I=1,7)/0.,.7167401,-15.28057,4,0.,.0234,0.,0./
      DATA(CZY30(4,I),I=1,7)/0.,0.,0.,0.,.05,0.,0./
      DATA(CZY30(5,I),I=1,7)/0.,-.0637588,-3.835024,0.,.05,0.,0./
      DATA(CZY30(6,I),I=1,7)/0.,-1.6478765,72.46641,-827.26,.015,0.,0./
      DATA(CZY30(7,I),I=1,7)/0.,-2.193,103.6645,-1277.39,.015,0.,0./
      DATA(CZY30(8,I),I=1,7)/0.,.2068325,-19.70335,0.,.05,0.,0./
      DATA(CZY30(9,I),I=1,7)/0.,.4118046,-25.0111146,0.,.05,0.,0./
      DATA(CZY30(10,I),I=1,7)/0.,.3652593,-21.84501,0.,.05,0.,0./
      DATA(CAY30(1,I),I=1,7)/0.,-.1027983,-.2553071,0.,.05,0.,0./
      DATA(CAY30(2,I),I=1,7)/0.,0.,0.,0.,.05,0.,0./
      DATA(CAY30(3,I),I=1,7)/0.,-.2399972,3.6730053,0.,.0327,0.,0./
      DATA(CAY30(4,I),I=1,7)/0.,-.2991048,4.9136785,0.,.0356,0.,0./
      DATA(CAY30(5,I),I=1,7)/0.,-.576255,22.58203,-246.375,.015,0.,0./
      DATA(CAY30(6,I),I=1,7)/0.,-.5933965,19.74591,-184.436,.02,0.,0./
      DATA(CAY30(7,I),I=1,7)/0.,-.353379,10.53229,-92.466,.02,0.,0./
      DATA(CAY30(8,I),I=1,7)/0.,0.,0.,0.,.05,0.,0./
      DATA(CAY30(9,I),I=1,7)/0.,0.,0.,0.,.05,0.,0./
      DATA(CAY30(10,I),I=1,7)/0.,-.2287461,3.427166,-31.6228,.05,0.,0./
      DATA(CLY30(1,I),I=1,7)/0.,0.,0.,0.,.05,0.,0./
      DATA(CLY30(2,I),I=1,7)/0.,.06582136,-1.363924,0.,.0241,0.,0./
      DATA(CLY30(3,I),I=1,7)/0.,.15920629,-2.6356227,0.,.0302,0.,0./
      DATA(CLY30(4,I),I=1,7)/0.,.18161066,-3.06518,0.,.0296,0.,0./
      DATA(CLY30(5,I),I=1,7)/0.,.11935401,-2.79648478,0.,.0213,0.,0./
      DATA(CLY30(6,I),I=1,7)/0.,.1574292,-3.4092864,0.,.0231,0.,0./
      DATA(CLY30(7,I),I=1,7)/0.,.14585808,-2.773725,0.,.0268,0.,0./
      DATA(CLY30(8,I),I=1,7)/0.,.154335,-2.576349,0.,.03,0.,0./
      DATA(CLY30(9,I),I=1,7)/0.,.13079182,-1.8875066,0.,.0346,0.,0./
      DATA(CLY30(10,I),I=1,7)/0.,.12984339,-1.2315626,0.,.05,0.,0./
      DATA(CMY30(1,I),I=1,7)/0.,-.1583872,.2749334,0.,.05,0.,0./
      DATA(CMY30(2,I),I=1,7)/0.,-.4110916,3,7.277437,0.,.0282,0.,0./
      DATA(CMY30(3,I),I=1,7)/0.,-.35528426,6.0390632,0.,.0294,0.,0./
      DATA(CMY30(4,I),I=1,7)/0.,-.14289157,2.14623779,0.,.0353,0.,0./
      DATA(CMY30(5,I),I=1,7)/0.,.05040218,.60594117,0.,.05,0.,0./
      DATA(CMY30(6,I),I=1,7)/0.,0.,0.,0.,.05,0.,0./
      DATA(CMY30(7,I),I=1,7)/0.,-.2176282,3.1811784,0.,.0342,0.,0./
      DATA(CMY30(8,I),I=1,7)/0.,-.2481885,3.921589,0.,.0316,0.,0./
      DATA(CMY30(9,I),I=1,7)/0.,-.1237619,-6.19504,93.324,.05,0.,0./
      DATA(CMY30(10,I),I=1,7)/0.,.1000102,-9.991185,90.2476,.05,0.,0./
      DFL=0.
      CX=0.
      CY=0.
      CZ=0.
      CL=0.
      CM=0.
      CN=0.
      IF(I.NE.2)GO TO 190
C PITCH DOWN CORRELATION
C IFLAP = 0 IS BODY FLAP COMPUTATION
C IFLAP = 2 IS ELEVON COMPUTATION
  100 IF(IFLAP.GT.1)GO TO 150
C BODY FLAP CORRECTIONS FOR - DEFLECTIONS ONLY
      IF(DEL.GE.0.)RETURN
      DFL=(DEL/(-14.25))**.75
      IF(DFL.GT.1.)DFL=1.
      CALL CUBIC (RMFSD,CZPB,CZ,IC,LC,ARAT)
      CALL CUBIC (RMFSD,CMPB,CM,IC,LC,ARAT)
      RETURN
  150 IF(DEL)160,300,175
C ELEVATOR DEFLECTION CORRECTIONS
  160 DFL=(DEL/(-30.))**.75
      IF(DFL.GT.1.)DFL=1.
C TRAILING EDGE UP CORRECTION
      CALL CUBIC(RMFSD,CZP30,CZ,IC,LC,ARAT)
```

```
      CALL CUBIC(RMFSD,CAP30,CX,IC,LC,ARAT)
      CALL CUBIC(RMFSD,CMP30,CM,IC,LC,ARAT)
      CALL CUBIC(RMFSD,CLP30,CL,IC,LC,ARAT)
      RETURN
  175 CONTINUE
C TRAILING EDGE DOWN
      DFL=(DEL/10.)**.75
      IF(DFL.GT.1.)DFL=1.
      CALL CUBIC(RMFSD,CZP10,CZ,IC,LC,ARAT)
      CALL CUBIC(RMFSD,CMP10,CM,IC,LC,ARAT)
      CALL CUBIC(RMFSD,CLP10,CL,IC,LC,ARAT)
      RETURN
  190 IF(I.NE.3)GO TO 300
  200 IF(IFLAP.LT.1)RETURN
C YAW CORRECTION FOR ELEVON ONLY
      IF(DEL)210,300,250
  210 DFL=(DEL/(-30.))**.75
      IF(DFL.GT.1.)DFL=1.
C TRAILING EDGE UP CORRECTIONS
      CALL CUBIC(FMRY,CZY30,CZ,IC,LC,ARAT)
      CALL CUBIC(FMRY,CAY30,CX,IC,LC,ARAT)
      CALL CUBIC(FMRY,CMY30,CM,IC,LC,ARAT)
      CALL CUBIC(FMRY,CLY30,CL,IC,LC,ARAT)
      RETURN
  250 DFL=(DEL/10.)**.75
      IF(DFL.GT.1.)DFL=1.
C TRAILING EDGE DOWN CORRECTIONS
      CALL CUBIC(FMRY,CZY10,CZ,IC,LC,ARAT)
      CALL CUBIC(FMRY,CMY10,CM,IC,LC,ARAT)
      CALL CUBIC(FMRY,CAY10,CX,IC,LC,ARAT)
      CALL CUBIC(FMRY,CLY10,CL,IC,LC,ARAT)
  300 RETURN
      END
```

```
      SUBROUTINE CCOUPL (IT,CXC,CZC,CYC,CMC,CNC,CLC)
C     CALCULATES CROSS COUPLING NOZZLE INTERACTION COEFFICIENTS
      REAL NONOZU,NONOZD,NONOZY,NONOZUL,NONOZUR,NONOZDL,NONOZDR,NONOZYL,
     1NONOZYR
      COMMON/UP/NONOZU,NONOZUL,NONOZUR,DSTARUR,DSTARUL,AEXUL,AEXUR,
     1RMFSUL,RMFSUR,DXNOZU,DYNOZU,DZNOZU,
     2XREUL,XREUR,YREUL,YREUR,ZREUL,ZREUR
      COMMON/DWN/NONOZD,NONOZDL,NONOZDR,DSTARDL,DSTARDR,AEXDL,AEXDR,
     1RMFSDL,RMFSDR,DXNOZD,DYNOZD,DZNOZD,
     2XREDL,XREDR,YREDL,YREDR,ZREDL,ZREDR
      COMMON/SIDE/NONOZY,NONOZYL,NONOZYR,DSTARYL,DSTARYR,AEXYL,AEXYR,
     1      RMRYL,RMRYR,DXNOZY,DYNOZY,DZNOZY,
     2XREYL,XREYR,YREYL,YREYR,ZREYL,ZREYR
      IF(IT.NE.2)GO TO 60
C PITCH + YAW COMB HAVE NO COUPLING
C PITCH UP + PITCH DOWN ( SYMM ROLL ) HAVE NO COUPLING
   50 CONTINUE
      IF(NONOZUL.EQ.0.0.OR.NONOZDR.EQ.0.)GO TO 60
      RMFSD=(RMFSDL+RMFSDR)/2.
C SYMM PITCH DOWN HAS COUPLING
      CYC=0.
      CNC=0.
      CLC=0.
      XMR=RMFSD
      IF(XMR.GT.0.03)XMR=.03
      CXC=-.4596321*XMR
      CZC=.399782*XMR
      CMC=.3468713*XMR
      CXC=-CXC
      GO TO 70
   60 CXC    = 0.0
      CZC    = 0.0
      CYC    = 0.0
      CMC    = 0.0
      CNC    = 0.0
      CLC    = 0.0
   70 RETURN
      END
```

```
      SUBROUTINE AMPL (I,AKX,AKZ,AKY,AKM,AKN,AKL)
C     CALCULATES AMPLIFICATION FACTORS
      COMMON/REF/SREF,C,B,SCALE,XRE,YRE,ZRE,DXNOZ,DYNOZ,DZNOZ,DXNOZZ,
     1DYNOZZ,DZNOZZ
      COMMON/THCOEF/ CXU,CZU,CYU,CMU,CNU,CLU,CXD,CZD,CYD,CMD,CND,CLD,
     1               CXY,CZY,CYY,CMY,CNY,CLY
      COMMON/TOCOEF/ CXT,CZT,CYT,CMT,CNT,CLT
      AKX=0.
      AKY=0.
      AKZ=0.
      AKL=0.
      AKM=0.
      AKN=0.
      PRINT1000
 1000 FORMAT(55H0AMPLIFICATION IS COMPUTED FOR THRUST COMPONENTS ONLY  )
      PRINT1001
 1001 FORMAT(55H0+1 IS NO AMPLIFICATION 0 IS THRUST CANCELLATION      )
      PRINT1002
 1002 FORMAT(55H0THERE ARE 22 POSSIBLE RCS CONTROL COMBINATIONS       )
      CMP=CMU+CMD
      CMTEST=.0809*CMU
      CMA=ABS(CMP)
      IF(CMA.LE.CMTEST)GO TO 10
      CZP=CZU+CZD
      PRINT1003
 1003 FORMAT(55H0THIS COMBINATION INCLUDES A PITCH UP OR DOWN COMPONENT)
      AKZ=CZT/CZP
      AKM=CMT/CMP
      PRINT1004,AKZ,AKM
 1004 FORMAT(20H0NORMAL FORCE AMP = ,F15.8,17HPITCHING MOM AMP ,F15.8)
      GO TO 11
   10 CONTINUE
      PRINT1005
 1005 FORMAT(55H0 NO PITCH COMPONENT IS CONTAINED IN THIS COMBINATION  )
   11 CLP=CLU+CLD
      CLTEST=.0809*CLU
      CLA=ABS(CLP)
      IF(CLA.LE.CLTEST)GO TO 12
1     PRINT1006
 1006 FORMAT(55H0THIS COMBINATION INCLUDES A ROLL LEFT OR RIGHT COMP   )
      AKL=CLT/CLP
      PRINT1007,AKL
 1007 FORMAT(25H0 ROLL AMPLIFICATION = ,F15.8)
      GO TO 13
   12 CONTINUE
      PRINT1008
 1008 FORMAT(55H0 NO ROLL COMPONENT IS INCLUDED IN THIS COMBINATION    )
   13 CNP=CNY
      CNA=ABS(CNP)
      CNTEST=-.0809*CMD/B*C
      IF(CNA.LE.CNTEST)GO TO 14
      CYP=CYY
 1009 FORMAT(55H0THIS COMBINATION INCLUDES A YAW LEFT OR RIGHT COMPONET)
      PRINT1009
      AKN=CNT/CNP
      AKY=CYT/CYP
      PRINT1011,AKY,AKN
 1011 FORMAT(18H0 SIDE FORCE AMP =,F15.8,16HYAW MOMENT AMP =,F15.8)
      GO TO 15
   14 CONTINUE
 1010 FORMAT(55H0NO YAW COMPONENT IN THIS COMBINATION                  )
      PRINT1010
   15 CONTINUE
      RETURN
      END
```

```
      SUBROUTINE ATMOS(Z,TT,P,RHO,C,Q,V,AM,AMU,ANU,G,GO,TS,THET,OBC)
C     LATEST COMPILATION DATED     6-27-72
C     U.S. STANDARD ATMOSPHERE,1962
      ZM=Z*0.3048
      ABAR=-3.085462E-04
      BBAR=7.254E-11
      CBAR=-1.517E-17
C     GRAVITATIONAL FORCE DETERMINED FROM SMITHSONIAN POLYNOMIAL
      IF (OBC) 10,20,10
   10 THETP=90.0-THET
      THETPR=THETP/57.29578
      GO=980.665*(1.0-.0026376*COS(2.0*THETPR)+.0000059*(COS(2.0*THETPR)
     1)**2)
      DBAR=-2.27E-07
      EBAR=1.0E-13
      FBAR=0.0E-20
      G=.01*(GO+(ABAR+DBAR*COS(2.0*THETPR))*ZM+(BBAR+EBAR*COS(2.0*THETPR
     1))*ZM**2+(CBAR+FBAR*COS(2.0*THETPR))*ZM**3)
      GO TO 30
   20 GO = GO*30.48
      G=0.01*(GO+ABAR*ZM+BBAR*ZM*ZM+CBAR*ZM*ZM*ZM)
   30 HM=(GO*ZM+ABAR*ZM*ZM/2.0+BBAR*ZM*ZM*ZM/3.0+CBAR*ZM*ZM*ZM*ZM/4.0)/G
     10
      GOE=GO/30.48
      AMO=28.9644
      RSM=8.31432
      IF (HM-11000.0) 40,40,50
   40 PA=1013.25
      DH=HM
      TA=288.15
      DTDH=-6.5
      GO TO 190,
   50 IF (HM-20000.0) 60,60,70
   60 PA=226.32
      TA=216.65
      DTDH=0.0
      DH=HM-11000.0
      GO TO 190
   70 IF (HM-32000.0) 80,80,90
   80 PA=54.7487
      TA=216.65
      DTDH=1.0
      DH=HM-20000.0
      GO TO 190
   90 IF (HM-47000.0) 100,100,110
  100 PA=8.68014
      TA=228.65
      DTDH=2.8
      DH=HM-32000.0
      GO TO 190
  110 IF (HM-52000.0) 120,120,130
  120 PA=1.10905
      TA=270.65
      DTDH=0.0
      DH=HM-47000.0
      GO TO 190
  130 IF (HM-61000.0) 140,140,150
  140 PA=0.590005
      TA=270.65
      DTDH=-2.0
      DH=HM-52000.0
      GO TO 190
  150 IF (HM-79000.0) 160,160,170
  160 PA=0.182099
      TA=252.65
      DTDH=-4.0
      DH=HM-61000.0
      GO TO 190
  170 IF (HM-88743.0) 180,180,230
```

```
180 PA=0.010577
    TA=180.65
    DTDH=0.0
    DH=HM-79000.0
    GO TO 190
190 CONTINUE
    TM=TA+DTDH*DH/1000.0
    IF (DTDH) 210,200,210
200 PPA=EXP(-GO*AMO*DH/(100000.0*RSM*TA))
    GO TO 220
210 PPA=(TA/TM)**(GO*AMO/(100.0*RSM*DTDH))
220 CONTINUE
    TE=TM*1.8
    TT= TE
    B = 7.3025E-07
    P = PA*PPA*2.0885468
    RHO=AMO*P/(1545.31*GOE*TE)
    AMU=B*TE**1.5/(198.72+TE)/GOE
    ANU=AMU/RHO
    C=SQRT(1.4*1545.31*GOE*TE/AMO)
    AM = V/C
    Q = 0.7*P*AM*AM
    TS = (4.56E+16*SQRT(RHO/0.00238)*(V/26000.0)**3.15)**0.25
    G=G/0.3048
    GO = GO/30.48
    RETURN
230 IF (ZM-100000.0) 240,240,250
240 TMB=180.65
    ALM=3.0
    ZBK=90.0
    PBM = 1.6436E-03
    AMB=28.9644
    GM=-.00844
    GO TO 400
250 IF (ZM-110000.0) 260,260,270
260 TMB=210.65
    ALM=5.0
    ZBK=100.0
    PBM=3.0075E-04
    AMB=28.88
    GM=-.032
    GO TO 400
270 IF (ZM-120000.0) 280,280,290
280 TMB=260.65
    ALM=10.0
    ZBK=110.0
    PBM=7.3544E-05
    AMB=28.56
    GM=-.049
    GO TO 400
290 IF (ZM-150000.0) 300,300,310
300 TMB=360.65
    ALM=20.0
    ZBK=120.0
    PBM=2.5217E-05
    AMB=28.07
    GM=-.0383333
    GO TO 400
310 IF (ZM-160000.0) 320,320,330
320 TMB=960.65
    ALM=15.0
    ZBK=150.0
    PBM=5.0617E-06
    AMB=26.92
    GM=-.026
    GO TO 400
330 IF (ZM-170000.0) 340,340,350
340 TMB=1110.65
```

```
      ALM=10.0
      ZBK=160.
      PBM=5.6943E-06
      AMB=26.00
      GM=-.026
      GO TO 400
  350 IF (ZM-190000.0) 360,360,370
  360 TMB=1210.65
      ALM=7.0
      ZBK=170.0
      PBM=2.7926E-06
      AMB=26.4
      GM=-.0275
      GO TO 400
  370 IF (ZM-230000.0) 380,380,390
  380 TMB=1350.65
      ALM=5.0
      ZBK=190.0
      PBM=1.6852E-06
      AMB=26.85
      GM=-.02875
      GO TO 400
  390 CONTINUE
      Q = 0.0
      P = 0.0
      G = G/0.3048
      GO = GO/30.48
      RETURN
  400 CONTINUE
C     COMPUTE KINETIC TEMPERATURE
      ZK=ZM/1000.0
      AMRAT=((AMB+GM*(ZK-ZBK))/28.9644)
      TMOL=TMB+ALM*(ZK-ZBK)
      TT=TMOL*AMRAT*1.80
  410 CONTINUE
C     COMPUTE STATIC PRESSURE
      AP=(TMB/ALM)-ZBK
      PARTA=(ZK-ZBK)*(.625E-06*(ZK+ZBK)-.125E-05*AP-.00325)
      PARTB=(.125E-05*AP*AP+.00325*AP+9.818)*ALOG((ZK+AP)/(ZBK+AP))
      AMO=28.9644
      RSTAR=8.31432
      COEF = -ALM*RSTAR/AMO
      PRLOG=(PARTA+PARTB)/COEF
      P=2.0885468*PBM*EXP(PRLOG)
  420 CONTINUE
C     COMPUTE DENSITY, SPEED OF SOUND, DYNAMIC PRESSURE
      RHO = P*AMRAT*28.9644/(1545.31*TT*GOE)
      C=SQRT(1.4*P/RHO)
      Q=0.5*RHO*V*V
  430 CONTINUE
C     COMPUTE MACH NUMBER, GRAVITATIONAL FORCE, VISCOSITY + KIN. VISC'TY
      AM=V/C
      G = (0.125E-05)*ZK*ZK-.00325*ZK+9.818
      BETA = 7.3025E-07
      SUTH = 198.72
      AMU = BETA*SQRT(TT**3.0)/(TT+SUTH)
      ANU=AMU/RHO/GOE
      AMU=AMU/GOE
      TS = (4.56E+16*SQRT(RHO/0.00238)*(V/26000.0)**3.15)**0.25
      G=G/0.3048
      GO = GO/30.48
      RETURN
  440 FORMAT (32H0  UPPER ALTITUDE LIMIT EXCEEDED)
      END
```

ORIGINAL PAGE IS
OF POOR QUALITY

APPENDIX B

ORIGINAL PAGE IS
OF POOR QUALITY

SAMPLE INPUT

```
R
-2.207E-01 3.145E-02-9.748E-01-3.086E+01-1.243E+01 9.501E+00 6.137E+00
-2.060E-01 4.984E-03-9.785E-01-3.249E+01-1.156E+01 9.871E+00 6.575E+00
-2.332E-01 3.357E-02-9.718E-01-3.072E+01-1.456E+01 9.416E+00 4.121E+00
-2.208E-01 4.182E-03-9.753E-01-3.226E+01-1.394E+01 9.785E+00 4.353E+00
-2.253E-01-2.094E-02-9.745E-01-3.047E+01-1.701E+01 9.359E+00 5.739E+00
-2.334E-01-6.077E-03-9.724E-01-3.197E+01-1.610E+01 9.700E+00 5.992E+00
-2.169E-01 2.781E-03-9.762E-01-3.007E+01-2.014E+01 9.273E+00 6.546E+00
-2.234E-01 9.893E-03-9.747E-01-3.155E+01-1.903E+01 9.615E+00 6.993E+00
-2.095E-01-1.533E-02-9.777E-01-2.970E+01-2.358E+01 9.216E+00 6.413E+00
-2.169E-01-7.936E-03-9.762E-01-3.106E+01-2.242E+01 9.501E+00 6.882E+00
-2.059E-01 2.974E-02-9.781E-01-2.933E+01-2.731E+01 9.074E+00 6.366E+00
-2.094E-01 3.258E-02-9.773E-01-3.061E+01-2.603E+01 9.387E+00 7.042E+00
-1.789E-01 5.833E-03-9.839E-01-2.887E+01-3.121E+01 8.904E+00 5.618E+00
-2.060E-01 2.351E-02-9.783E-01-3.007E+01-2.990E+01 9.160E+00 6.506E+00
-1.644E-01-1.333E-02-9.863E-01-2.850E+01-3.462E+01 8.847E+00 4.098E+00
-1.789E-01-2.417E-03-9.839E-01-2.953E+01-3.357E+01 9.017E+00 4.519E+00
-2.249E-01 1.922E-03-9.744E-01-2.808E+01-3.789E+01 8.818E+00 3.789E+00
-1.643E-01-5.670E-02-9.858E-01-2.904E+01-3.678E+01 8.989E+00 4.321E+00
 1.822E-01 0.        -9.833E-01-4.066E+01-5.366E+00 8.192E+00 6.760E+00
 1.822E-01 0.        -9.833E-01-4.066E+01-6.368E+00 8.192E+00 6.760E+00
 1.822E-01 0.        -9.833E-01-4.066E+01-7.371E+00 8.192E+00 6.760E+00
 1.822E-01 0.        -9.833E-01-4.066E+01-8.374E+00 8.192E+00 6.760E+00
 1.822E-01 0.        -9.833E-01-3.954E+01-9.501E+00 8.192E+00 6.328E+00
-1.703E-01-9.535E-01 2.486E-01-3.465E+01-1.067E+00-1.075E+01 2.085E+00
-5.405E-02-9.945E-01 9.008E-02-3.180E+01-1.209E+00-1.075E+01 6.569E+00
 2.567E-01-7.706E-03-9.665E-01-4.104E+01-5.984E+00-0.8224    4.464E+00
 3.068E-01-1.665E-01-9.371E-01-4.088E+01-6.499E+00-0.7272    4.464E+00
 3.546E-01 3.181E-01-8.792E-01-41.20     -5.517    -0.54      4.464E+00
 3.068E-01 1.665E-01-9.371E-01-41.04     -6.008    -0.7272    4.464E+00
 3.546E-01-3.181E-01-8.792E-01-4.072E+01-6.990E+00-0.54      4.464E+00
 3.986E-01-4.578E-01-7.947E-01-4.058E+01-7.442E+00-0.266     4.464E+00
 3.986E-01 4.578E-01-7.947E-01-41.34     -5.065    -0.266     4.464E+00
 4.376E-01-5.813E-01-6.860E-01-4.046E+01-7.843E+000.087      4.464E+00
 4.376E-01 5.813E-01-6.860E-01-41.46     -4.664    0.087      4.464E+00
 4.703E-01-6.850E-01-5.565E-01-4.035E+01-8.179E+000.506      4.464E+00
 4.703E-01 6.850E-01-5.565E-01-41.57     -4.336    0.506      4.464E+00
 4.957E-01-7.656E-01-4.100E-01-4.027E+01-8.440E+000.981      4.464E+00
 4.957E-01 7.656E-01-4.100E-01-41.65     -4.077    0.981      4.464E+00
 5.131E-01-8.208E-01-2.511E-01-4.021E+01-8.619E+001.496      4.464E+00
 5.131E-01 8.208E-01-2.511E-01-41.71     -3.898    1.496      4.464E+00
 5.219E-01-8.488E-01-8.455E-02-4.018E+01-8.710E+002.036      4.464E+00
 5.219E-01-8.488E-01 8.455E-02-4.018E+01-8.710E+002.584      4.464E+00
 5.219E-01 8.488E-01-8.455E-02-41.74     -3.807    2.036      4.464E+00
 5.131E-01-8.208E-01 2.511E-01-4.021E+01-8.619E+002.584      4.464E+00
 4.703E-01-6.850E-01 5.565E-01-4.035E+01-8.179E+004.114      4.464E+00
 4.957E-01-7.656E-01 4.100E-01-4.027E+01-8.440E+003.639      4.464E+00
 4.376E-01-5.813E-01 6.860E-01-4.046E+01-7.843E+004.533      4.464E+00
 3.986E-01-4.578E-01 7.947E-01-4.058E+01-7.442E+004.886      4.464E+00
 2.567E-01-7.706E-03 9.665E-01-4.104E+01-5.984E+005.442      4.464E+00
 3.068E-01-1.665E-01 9.371E-01-4.088E+01-6.499E 005.347      4.464E+00
 3.546E-01-3.181E-01 8.792E-01-4.072E+01-6.990E+005.16       4.464E+00
 1.839E-01-2.456E-02-9.826E-01-3.668E+01-8.335E+00-10.73     1.160E+00
 2.418E-01-1.837E-01-9.528E-01-3.661E+01-8.549E+00-10.663    1.160E+00
 2.971E-01-3.355E-01-8.940E-01-3.653E+01-8.754E+00-10.583    1.160E+00
 3.440E-01-4.754E-01-8.080E-01-3.646E+01-8.942E+00-10.468    1.160E+00
 3.930E-01-5.992E-01-6.975E-01-3.640E+01-9.109E+00-10.319    1.160E+00
 4.308E-01-7.031E-01-5.658E-01-3.635E+01-9.248E+00-10.142    1.160E+00
 4.602E-01-7.838E-01-4.169E-01-3.631E+01-9.357E+00-9.941     1.160E+00
```

ORIGINAL PAGE IS
OF POOR QUALITY

4.804E-01	8.391E-01	2.553E-01	-3.628E+01	-9.431E+00	-9.724	1.160E+00
4.906E-01	8.572E-01	8.597E-02	-3.627E+01	-9.469E+00	-9.496	1.160E+00
4.906E-01	8.572E-01	8.597E-02	-3.627E+01	-9.469E+00	-9.265	1.160E+00
4.804E-01	8.391E-01	2.553E-01	-3.628E+01	-9.431E+00	-9.037	1.160E+00
4.602E-01	7.838E-01	4.169E-01	-3.631E+01	-9.357E+00	-8.819	1.160E+00
4.308E-01	7.051E-01	5.658E-01	-3.635E+01	-9.248E+00	-8.619	1.160E+00
3.930E-01	5.992E-01	6.975E-01	-3.640E+01	-9.109E+00	-8.442	1.160E+00
3.480E-01	4.754E-01	8.080E-01	-3.646E+01	-8.942E+00	-8.293	1.160E+00
2.971E-01	3.355E-01	8.940E-01	-3.653E+01	-8.754E+00	-8.177	1.160E+00
2.418E-01	1.837E-01	9.528E-01	-3.661E+01	-8.549E+00	-8.098	1.160E+00
1.839E-01	2.456E-02	9.826E-01	-3.668E+01	-8.335E+00	-8.058	1.160E+00
0.	-1.000E+00	0.	-7.680E+00	-8.192E+00	5.063E+00	2.185E+01
0.	-1.000E+00	0.	-3.413E+00	-8.192E+00	3.926E+00	1.311E+01
0.	-1.000E+00	0.	-7.680E+00	-8.192E+00	2.162E+00	2.075E+01
0.	-1.000E+00	0.	-3.413E+00	-8.192E+00	1.081E+00	2.075E+01
0.	-9.989E-01	-4.757E-02	-7.680E+00	-8.164E+00	-5.974E-01	1.148E+01
0.	-9.989E-01	-4.757E-02	-3.413E+00	-8.135E+00	-1.195E+00	1.148E+01
0.	-9.524E-01	-3.048E-01	-7.680E+00	-7.879E+00	-2.503E+00	1.434E+01
0.	-9.524E-01	-3.048E-01	-3.413E+00	-7.652E+00	-3.214E+00	1.434E+01
0.	-7.568E-01	-6.536E-01	-7.680E+00	-6.884E+00	-4.551E+00	1.588E+01
0.	-7.568E-01	-6.536E-01	-3.413E+00	-6.343E+00	-5.177E+00	1.588E+01
0.	-6.347E-01	-7.727E-01	-7.680E+00	-5.006E+00	-6.457E+00	1.979E+01
0.	-6.347E-01	-7.727E-01	-3.413E+00	-4.210E+00	-7.111E+00	1.979E+01
0.	-2.195E-01	-9.756E-01	-7.680E+00	-2.276E+00	-8.022E+00	2.239E+01
0.	-2.195E-01	-9.756E-01	-3.413E+00	-1.138E+00	-8.278E+00	2.239E+01
6.652E-02	-9.978E-01	0.	-1.715E+01	-8.534E+00	6.941E+00	3.284E+00
6.652E-02	-9.978E-01	0.	-1.459E+01	-8.363E+00	5.518E+00	1.314E+01
6.652E-02	-9.978E-01	0.	-1.715E+01	-8.534E+00	5.006E+00	5.912E+00
6.652E-02	-9.978E-01	0.	-1.459E+01	-8.363E+00	2.788E+00	1.248E+01
6.652E-02	-9.978E-01	0.	-1.715E+01	-8.534E+00	2.475E+00	1.084E+01
5.225E-02	-9.975E-01	-4.750E-02	-1.459E+01	-8.335E+00	1.707E-01	6.899E+00
7.754E-02	-9.970E-01	0.	-1.715E+01	-8.505E+00	3.129E-01	7.231E+00
-1.397E-02	-9.523E-01	-3.047E-01	-1.459E+01	-8.079E+00	-1.764E+00	8.603E+00
7.484E-02	-9.947E-01	-1.575E-01	-1.715E+01	-8.164E+00	-1.735E+00	8.320E+00
4.900E-01	-7.446E-01	4.533E-01	-1.715E+01	-7.908E+00	-3.726E+00	1.012E+01
4.616E-01	-8.798E-01	1.135E-01	-1.715E+01	-8.420E+00	-5.262E+00	1.155E+01
4.708E-01	-8.559E-01	-2.140E-01	-1.715E+01	-8.306E+00	-7.055E+00	1.225E+01
4.091E-01	-5.520E-02	-9.108E-01	-1.715E+01	-7.140E+00	-8.022E+00	1.187E+01
1.238E-01	-9.874E-01	-9.874E-02	-2.375E+01	-9.245E+00	7.851E+00	2.618E+00
1.258E-01	-9.921E-01	0.	-2.173E+01	-8.960E+00	7.254E+00	2.606E+00
1.127E-01	-9.902E-01	-6.252E-02	-2.375E+01	-9.160E+00	6.599E+00	6.266E+00
9.812E-02	-9.952E-01	0.	-2.173E+01	-8.904E+00	5.774E+00	4.676E+00
9.538E-02	-9.947E-01	-3.826E-02	-2.375E+01	-9.074E+00	4.665E+00	6.757E+00
8.421E-02	-9.964E-01	0.	-2.173E+01	-8.875E+00	3.584E+00	8.562E+00
7.652E-02	-9.960E-01	-4.527E-02	-2.375E+01	-9.017E+00	2.361E+00	5.710E+00
7.025E-02	-9.975E-01	0.	-2.173E+01	-8.847E+00	1.394E+00	5.702E+00
5.853E-02	-9.959E-01	-6.868E-02	-2.375E+01	-8.932E+00	2.845E-01	7.528E+00
7.930E-02	-9.843E-01	-1.575E-01	-2.173E+01	-8.676E+00	-7.680E-01	6.566E+00
1.379E-01	-8.805E-01	4.536E-01	-2.375E+01	-9.245E+00	-2.190E+00	9.689E+00
1.051E-01	-8.495E-01	5.171E-01	-2.173E+01	-9.444E+00	-3.072E+00	7.000E+00
1.314E-01	-9.721E-01	1.944E-01	-2.375E+01	-1.030E+01	-4.637E+00	7.979E+00
1.636E-01	-9.784E-01	1.262E-01	-2.173E+01	-1.013E+01	-5.462E+00	8.191E+00
1.590E-01	-9.085E-01	3.866E-01	-2.375E+01	-1.001E+01	-7.709E+00	1.338E+01
5.457E-02	-9.687E-01	2.422E-01	-2.173E+01	-9.444E+00	-8.591E+00	8.540E+00
2.165E-01	-1.746E-01	9.605E-01	-2.375E+01	-7.965E+00	-1.018E+01	1.184E+01
2.873E-01	-5.795E-02	9.561E-01	-2.173E+01	-7.026E+00	-9.785E+00	8.923E+00
3.271E-01	4.589E-01	8.261E-01	-2.375E+01	-4.750E+00	-9.899E+00	1.127E+01
1.497E-01	-9.766E-01	1.542E-01	-2.970E+01	-1.016E+01	8.420E+00	4.808E+00
1.427E-01	-9.848E-01	9.848E-02	-2.773E+01	-9.785E+00	7.879E+00	2.551E+00
1.429E-01	-9.863E-01	8.219E-02	-2.970E+01	-9.984E+00	6.912E+00	6.114E+00

ORIGINAL PAGE IS
OF POOR QUALITY

1.429E-01	-9.883E-01	-8.219E-02	2.773E+01	-9.643E+00	6.230E+00	6.114E+00
1.433E-01	-9.889E-01	-5.804E-02	2.970E+01	-9.842E+00	4.807E+00	6.605E+00
1.433E-01	-9.889E-01	-3.804E-02	2.773E+01	-9.529E+00	4.068E+00	6.605E+00
1.433E-01	-9.887E-01	-4.494E-02	2.970E+01	-9.757E+00	2.702E+00	5.591E+00
1.433E-01	-9.887E-01	-4.494E-02	2.773E+01	-9.444E+00	2.077E+00	5.591E+00
1.431E-01	-9.874E-01	-6.809E-02	2.970E+01	-9.643E+00	6.258E-01	7.379E+00
1.431E-01	-9.874E-01	-6.809E-02	2.773E+01	-9.302E+00	-1.991E-01	7.379E+00
1.278E-01	-8.817E-01	4.542E-01	2.970E+01	-1.001E+01	-1.963E+00	9.404E+00
1.278E-01	-8.817E-01	4.542E-01	2.773E+01	-1.021E+01	-2.901E+00	9.404E+00
1.407E-01	-9.708E-01	1.942E-01	2.970E+01	-1.115E+01	-4.694E+00	7.764E+00
1.407E-01	-9.708E-01	1.942E-01	2.773E+01	-1.104E+01	-5.547E+00	7.764E+00
1.322E-01	-9.121E-01	-3.881E-01	2.970E+01	-1.092E+01	-7.737E+00	1.295E+01
1.322E-01	-9.121E-01	-3.881E-01	2.773E+01	-1.007E+01	-9.074E+00	1.295E+01
2.711E-02	-1.870E-01	-9.820E-01	2.970E+01	-8.591E+00	-1.064E+01	1.075E+01
3.110E-02	-1.788E-01	-9.834E-01	2.773E+01	-7.055E+00	-1.087E+01	1.124E+01
-6.674E-02	3.838E-01	-9.210E-01	2.970E+01	-4.779E+00	-1.052E+01	1.309E+01
0.	4.856E-01	-8.742E-01	2.773E+01	-3.413E+00	-9.956E+00	1.035E+01
3.618E-02	-9.989E-01	-3.121E-02	-3.416E+01	-1.067E+01	9.046E+00	5.133E+00
6.944E-02	-9.838E-01	-1.553E-01	-3.291E+01	-1.052E+01	8.135E+00	3.094E+00
9.023E-02	-9.925E-01	-8.271E-02	-3.416E+01	-1.050E+01	6.912E+00	3.874E+00
9.023E-02	-9.925E-01	-8.271E-02	-3.291E+01	-1.033E+01	6.230E+00	3.874E+00
9.047E-02	-9.952E-01	-3.828E-02	-3.416E+01	-1.035E+01	4.807E+00	4.186E+00
9.047E-02	-9.952E-01	-3.828E-02	-3.291E+01	-1.021E+01	4.068E+00	4.186E+00
9.044E-02	-9.949E-01	-4.522E-02	-3.416E+01	-1.027E+01	2.702E+00	3.543E+00
9.044E-02	-9.949E-01	-4.522E-02	-3.291E+01	-1.013E+01	2.077E+00	3.543E+00
9.032E-02	-9.936E-01	-6.852E-02	-3.416E+01	-1.016E+01	6.258E-01	4.676E+00
9.032E-02	-9.936E-01	-6.852E-02	-3.291E+01	-9.984E+00	-1.991E-01	4.676E+00
8.855E-02	-8.861E-01	4.565E-01	-3.416E+01	-1.052E+01	-1.963E+00	5.967E+00
8.855E-02	-8.861E-01	4.565E-01	-3.291E+01	-1.089E+01	-2.901E+00	5.967E+00
8.879E-02	-9.767E-01	1.953E-01	-3.416E+01	-1.166E+01	-4.694E+00	4.921E+00
8.879E-02	-9.767E-01	1.953E-01	-3.291E+01	-1.172E+01	-5.547E+00	4.921E+00
8.336E-02	-9.170E-01	-3.902E-01	-3.416E+01	-1.144E+01	-7.737E+00	8.212E+00
8.336E-02	-9.170E-01	-3.902E-01	-3.291E+01	-1.075E+01	-9.074E+00	8.212E+00
1.701E-02	-1.871E-01	-9.822E-01	-3.416E+01	-9.103E+00	-1.064E+01	6.851E+00
1.701E-02	-1.871E-01	-9.822E-01	-3.291E+01	-7.794E+00	-1.087E+01	6.851E+00
-5.262E-02	3.588E-01	-9.328E-01	-3.416E+01	-5.234E+00	-1.052E+01	8.931E+00
0.	3.846E-01	-9.231E-01	-3.291E+01	-3.755E+00	-9.956E+00	8.331E+00
5.015E-02	-2.491E-01	-9.672E-01	1.428E+01	-1.243E+01	6.770E+00	3.151E+01
3.951E-02	-9.096E-02	-9.951E-01	7.197E+00	-1.155E+01	6.315E+00	4.572E+01
-1.302E-01	2.427E-02	-9.912E-01	-8.761E+00	-1.243E+01	6.429E+00	1.560E+01
-1.171E-01	-4.334E-02	-9.922E-01	-1.274E+01	-1.155E+01	6.912E+00	1.832E+01
-1.080E-01	-4.249E-02	-9.932E-01	-1.986E+01	-1.243E+01	7.766E+00	1.046E+01
-1.227E-01	-0.	-9.924E-01	-2.247E+01	-1.155E+01	8.050E+00	1.012E+01
-1.738E-01	-0.	-9.848E-01	-2.645E+01	-1.243E+01	8.619E+00	5.846E+00
-1.923E-01	3.194E-02	-9.808E-01	-2.791E+01	-1.155E+01	8.904E+00	5.869E+00
6.824E-02	-3.892E-01	-9.186E-01	6.230E+00	-1.456E+01	6.855E+00	1.526E+01
5.134E-02	-1.297E-01	-9.902E-01	1.735E+00	-1.394E+01	6.429E+00	2.184E+01
-1.168E-01	1.814E-14	-9.932E-01	-1.030E+01	-1.456E+01	6.543E+00	1.097E+01
-1.297E-01	9.432E-02	-9.871E-01	-1.371E+01	-1.394E+01	6.998E+00	1.112E+01
-1.299E-01	9.445E-02	-9.870E-01	-2.022E+01	-1.456E+01	7.794E+00	6.168E+00
-1.081E-01	-0.	-9.941E-01	-2.239E+01	-1.394E+01	8.079E+00	7.413E+00
-1.580E-01	-0.	-9.874E-01	-2.643E+01	-1.456E+01	8.591E+00	4.056E+00
-1.737E-01	3.684E-02	-9.841E-01	-2.788E+01	-1.394E+01	8.847E+00	4.151E+00
8.400E-02	-1.803E-01	-9.800E-01	7.965E-01	-1.701E+01	6.969E+00	1.665E+01
7.361E-02	-1.125E-01	-9.909E-01	-2.560E+00	-1.610E+01	6.571E+00	2.058E+01
-1.159E-01	1.759E-02	-9.931E-01	-1.158E+01	-1.701E+01	6.656E+00	1.408E+01
-1.168E-01	2.190E-02	-9.929E-01	-1.482E+01	-1.610E+01	7.055E+00	1.596E+01
-1.275E-01	2.390E-02	-9.916E-01	-2.085E+01	-1.701E+01	7.766E+00	8.226E+00
-1.304E-01	3.097E-02	-9.910E-01	-2.284E+01	-1.610E+01	8.050E+00	8.936E+00
-1.880E-01	3.068E-02	-9.817E-01	-2.634E+01	-1.701E+01	8.562E+00	5.579E+00

```
-1.580E-01-1.481E-02-9.873E-01-2.776E+01-1.610E+01 8.818E+00 5.901E+00
 7.823E-02-8.224E-02-9.935E-01-2.788E+00-2.014E+01 7.055E+00 1.815E+01
 8.487E-02-1.117E-01-9.901E-01-5.604E+00-1.903E+01 8.713E+00 2.008E+01
-1.263E-01 3.987E-02-9.912E-01-1.328E+01-2.014E+01 6.799E+00 1.461E+01
-1.159E-01 4.245E-03-9.933E-01-1.590E+01-1.903E+01 7.140E+00 1.716E+01
-1.322E-01 8.472E-03-9.912E-01-2.131E+01-2.014E+01 7.794E+00 8.596E+00
-1.275E-01-0.        -9.918E-01-2.301E+01-1.903E+01 8.022E+00 1.002E+01
-1.829E-01-0.        -9.831E-01-2.623E+01-2.014E+01 8.505E+00 6.211E+00
-1.881E-01 5.894E-03-9.821E-01-2.756E+01-1.903E+01 8.761E+00 6.796E+00
 6.003E-02-8.283E-02-9.940E-01-5.917E+00-2.358E+01 7.197E+00 1.741E+01
 7.760E-02-1.510E-01-9.855E-01-8.392E+00-2.242E+01 6.884E+00 1.924E+01
-1.431E-01 4.653E-03-9.897E-01-1.519E+01-2.358E+01 7.055E+00 1.252E+01
-1.263E-01-4.171E-02-9.911E-01-1.727E+01-2.242E+01 7.311E+00 1.536E+01
-9.939E-02-4.848E-02-9.939E-01-2.187E+01-2.358E+01 7.908E+00 7.611E+00
-1.322E-01-0.        -9.912E-01-2.330E+01-2.242E+01 8.050E+00 9.037E+00
-1.961E-01-0.        -9.806E-01-2.614E+01-2.358E+01 8.505E+00 6.090E+00
-1.829E-01-1.338E-02-9.830E-01-2.736E+01-2.242E+01 8.733E+00 6.530E+00
 3.993E-02-4.457E-02-9.982E-01-4.444E+00-2.731E+01 7.311E+00 1.641E+01
 5.986E-02-1.114E-01-9.920E-01-1.132E+01-2.603E+01 7.111E+00 1.916E+01
-1.482E-01 4.610E-02-9.879E-01-1.730E+01-2.731E+01 7.254E+00 9.952E+00
-1.430E-01 3.496E-02-9.891E-01-1.869E+01-2.603E+01 7.510E+00 1.375E+01
-1.271E-01 3.107E-02-9.914E-01-2.247E+01-2.731E+01 7.993E+00 6.446E+00
-9.950E-02-0.        -9.950E-01-2.358E+01-2.603E+01 8.135E+00 8.234E+00
-1.601E-01-0.        -9.871E-01-2.606E+01-2.731E+01 8.448E+00 6.142E+00
-1.960E-01 3.049E-02-9.801E-01-2.719E+01-2.603E+01 8.676E+00 6.697E+00
 1.149E-02-1.124E-02-9.999E-01-1.356E+01-3.121E+01 7.396E+00 1.457E+01
 3.980E-02-9.257E-02-9.949E-01-1.462E+01-2.990E+01 7.282E+00 1.684E+01
-1.764E-01 5.860E-02-9.826E-01-1.949E+01-3.121E+01 7.453E+00 6.648E+00
-1.483E-01 1.397E-02-9.888E-01-2.028E+01-2.990E+01 7.623E+00 1.016E+01
-1.414E-01 1.230E-02-9.899E-01-2.310E+01-3.121E+01 8.022E+00 4.738E+00
-1.272E-01-0.        -9.919E-01-2.389E+01-2.990E+01 8.135E+00 6.586E+00
-1.498E-01-0.        -9.887E-01-2.594E+01-3.121E+01 8.420E+00 5.590E+00
-1.601E-01 7.539E-03-9.871E-01-2.700E+01-2.990E+01 8.591E+00 6.279E+00
 1.333E-02-1.441E-02-9.998E-01-1.627E+01-3.462E+01 7.396E+00 1.011E+01
 1.149E-02-8.697E-03-9.999E-01-1.761E+01-3.357E+01 7.367E+00 1.172E+01
-4.236E-01 5.206E-01-8.472E-01-2.145E+01-3.462E+01 7.623E+00 3.180E+00
-1.765E-01-3.681E-02-9.836E-01-2.176E+01-3.357E+01 7.823E+00 5.342E+00
-5.244E-02-6.803E-02-9.963E-01-2.367E+01-3.462E+01 8.135E+00 2.569E+00
-1.414E-01-0.        -9.899E-01-2.421E+01-3.357E+01 8.164E+00 3.811E+00
-1.644E-01-0.        -9.864E-01-2.586E+01-3.462E+01 8.420E+00 4.098E+00
-1.498E-01-1.215E-02-9.886E-01-2.680E+01-3.357E+01 8.562E+00 4.497E+00
-5.281E-01 6.373E-01-6.973E-01-2.031E+01-3.789E+01 7.766E+00 3.462E+00
 1.281E-02-2.781E-01-9.605E-01-2.017E+01-3.678E+01 7.680E+00 1.109E+01
-4.465E-01 5.724E-02-8.930E-01-2.301E+01-3.678E+01 7.936E+00 3.181E+00
 0.        -2.715E-01-9.624E-01-2.307E+01-3.789E+01 7.965E+00 7.377E-01
 0.        -2.563E-02-9.997E-01-2.412E+01-3.789E+01 8.249E+00 1.705E+00
-5.256E-02-0.        -9.986E-01-2.446E+01-3.678E+01 8.249E+00 2.702E+00
-1.521E-01-0.        -9.884E-01-2.574E+01-3.789E+01 8.392E+00 3.736E+00
-1.644E-01 8.430E-03-9.864E-01-2.660E+01-3.678E+01 8.534E+00 4.319E+00
 0.        -1.000E+00 1.335E-08-2.765E+01-1.280E+00-9.643E+00 4.970E+00
 0.        -1.000E+00 1.335E-08-2.751E+01-1.280E+00-1.075E+01 9.941E+00
 0.        -9.960E-01-6.397E-02-3.109E+01-1.209E+00-9.643E+00 5.692E+00
 0.        -1.000E+00 1.335E-08-2.392E+01-1.280E+00-9.643E+00 3.692E+00
 0.        -1.000E+00 1.335E-08-2.261E+01-1.280E+00-1.075E+01 1.079E+01
 0.        -1.000E+00 1.335E-08-2.034E+01-1.280E+00-9.643E+00 3.408E+00
-1.320E-01-9.897E-01-5.461E-02-3.891E+01-5.689E-01-1.351E+01 4.801E+00
-1.756E-01-9.832E-01-4.965E-02-3.715E+01-8.676E-01-1.269E+01 1.504E+00
-1.378E-01-9.878E-01-7.248E-02-3.601E+01-9.814E-01-1.351E+01 4.597E+00
-5.427E-02-9.985E-01 2.994E-03-3.422E+01-1.180E+00-1.269E+01 4.865E+00
 8.124E-02-9.952E-01-7.655E-02-3.163E+01-1.109E+00-1.351E+01 8.897E+00
```

ORIGINAL PAGE IS
OF POOR QUALITY

```
 0.        -9.855E-01-1.699E-01-2.907E+01-1.138E+00-1.269E+01 7.501E+00
 5.344E-02-9.753E-01-2.142E-01-2.571E+01-8.818E-01-1.351E+01 7.904E+00
 0.        -9.551E-01-2.964E-01-2.284E+01-1.024E+00-1.269E+01 8.403E+00
-1.299E-01-9.899E-01 5.600E-02-4.184E+01-3.200E-01-1.764E+01 8.533E+00
-1.320E-01-9.897E-01 5.546E-02-3.985E+01-4.907E-01-1.599E+01 9.602E+00
-1.402E-01-9.883E-01 5.975E-02-3.837E+01-7.894E-01-1.764E+01 7.906E+00
-1.379E-01-9.8  5E-01 6.005E-02-3.630E+01-9.814E-01-1.599E+01 9.186E+00
 5.783E-02-9.964E-01-6.166E-02-3.450E+01-1.017E+00-1.764E+01 1.187E+01
 5.131E-02-9.963E-01-6.045E-02-3.163E+01-9.458E-01-1.599E+01 1.378E+01
 5.145E-02-9.973E-01-5.281E-02-2.927E+01-7.183E-01-1.764E+01 1.334E+01
 5.464E-02-9.972E-01-5.181E-02-2.591E+01-6.258E-01-1.599E+01 1.546E+01
-1.273E-01-9.900E-01 6.119E-02-4.412E+01-2.987E-01-2.224E+01 6.604E+00
-1.299E-01-9.897E-01 6.060E-02-4.227E+01-4.480E-01-2.077E+01 7.653E+00
-1.433E-01-9.873E-01 6.844E-02-4.110E+01-7.040E-01-2.224E+01 5.945E+00
-1.402E-01-9.878E-01 6.854E-02-3.920E+01-8.747E-01-2.077E+01 7.093E+00
 5.085E-02-9.967E-01-6.395E-02-3.778E+01-9.103E-01-2.224E+01 9.309E+00
 5.783E-02-9.964E-01-6.219E-02-3.516E+01-8.605E-01-2.077E+01 1.064E+01
 4.535E-02-9.976E-01-5.189E-02-3.322E+01-6.756E-01-2.224E+01 1.044E+01
 5.145E-02-9.974E-01-5.046E-02-3.021E+01-6.045E-01-2.077E+01 1.196E+01
-1.028E-01-9.937E-01 4.497E-02-4.620E+01-2.560E-01-2.645E+01 5.101E+00
-1.274E-01-9.910E-01 4.070E-02-4.460E+01-3.840E-01-2.509E+01 6.173E+00
-1.284E-01-9.909E-01 4.129E-02-4.361E+01-5.689E-01-2.645E+01 4.763E+00
-1.435E-01-9.888E-01 4.120E-02-4.196E+01-7.396E-01-2.509E+01 5.480E+00
 5.161E-02-9.969E-01-7.233E-02-4.079E+01-7.595E-01-2.645E+01 7.188E+00
 5.084E-02-9.964E-01-6.829E-02-3.852E+01-7.595E-01-2.509E+01 8.595E+00
 2.549E-02-9.985E-01-4.776E-02-3.689E+01-6.173E-01-2.645E+01 8.227E+00
 4.536E-02-9.980E-01-4.442E-02-3.422E+01-5.831E-01-2.509E+01 9.632E+00
-1.035E-01-9.935E-01 4.760E-02-4.824E+01-2.418E-01-3.066E+01 4.398E+00
-1.028E-01-9.936E-01 4.762E-02-4.676E+01-3.271E-01-2.924E+01 5.314E+00
-1.079E-01-9.929E-01 5.051E-02-4.608E+01-4.694E-01-3.066E+01 4.217E+00
-1.284E-01-9.903E-01 5.245E-02-4.452E+01-5.831E-01-2.924E+01 4.964E+00
 1.514E-02-9.991E-01-3.966E-02-4.372E+01-6.258E-01-3.066E+01 6.013E+00
 5.167E-02-9.987E-01-3.932E-02-4.164E+01-6.315E-01-2.924E+01 7.474E+00
 1.282E-02-9.996E-01-2.425E-02-4.051E+01-5.604E-01-3.066E+01 7.103E+00
 2.552E-02-9.994E-01-2.450E-02-3.803E+01-5.462E-01-2.924E+01 8.562E+00
-5.298E-02-9.957E-01 4.023E-02-4.981E+01-2.276E-01-3.396E+01 2.896E+00
-1.035E-01-9.940E-01 3.514E-02-4.867E+01-2.987E-01-3.303E+01 2.901E+00
-1.167E-01-9.923E-01 4.157E-02-4.796E+01-4.125E-01-3.396E+01 2.059E+00
-1.080E-01-9.933E-01 4.188E-02-4.685E+01-4.978E-01-3.303E+01 2.782E+00
 0.        -9.995E-01-3.029E-02-4.600E+01-5.405E-01-3.396E+01 3.486E+00
 1.514E-02-9.995E-01-2.708E-02-4.443E+01-5.547E-01-3.303E+01 3.967E+00
 0.        -9.999E-01-1.515E-02-4.364E+01-5.262E-01-3.396E+01 2.524E+00
 1.282E-02-9.998E-01-1.709E-02-4.179E+01-5.262E-01-3.303E+01 4.687E+00
 1.305E-01-9.914E-01 0.        -3.541E+01-1.075E+01 8.534E-01 2.895E+00
 1.305E-01-9.914E-01 0.        -3.610E+01-1.075E+01 2.645E+00 2.452E+00
 1.305E-01-9.914E-01 0.        -3.669E+01-1.075E+01 6.656E+00 5.790E+00
 1.305E-01-9.914E-01 0.        -3.576E+01-1.075E+01 4.608E+00 4.916E+00
 1.305E-01-9.914E-01 0.        -3.576E+01-1.075E+01 9.131E+00 5.790E+00
 5.0       0.        0.        0.        0.        0.        0.
 $IN
    GJ=1.3,POJSA=152.,RJ=75.,SCALE=1,IIMP=3,NONOZD. ',,
 NONOZUL=3.,NONOZYL=3.,
 $
P$FC IOPT=4,PINF=1.E-7,MINF=25.,TINF=480.,ALPH=0.,
 DELTEL=0.,
 INEXT=3$
P$FC
 DELTEL=-30.,
 $
```